THE EFFECT OF NANOSCALE PARTICLES AND IONOMER ARCHITECTURE ON THE CRYSTALLIZATION BEHAVIOR OF SULFONATED SYNDIOTACTIC POLYSTYRENE

Sonya Denese Benson

Dissertation submitted to the faculty of the Virginia Polytechnic Institute and State University in partial fulfillment of the requirements for the degree of

DOCTOR OF PHILOSOPHY

in

Macromolecular Science and Engineering

Robert B. Moore, Chair
Judy S. Riffle
S. Richard Turner
Donald G. Baird
Sergei Nazarenko

January 24, 2010
Blacksburg, Virginia

Keywords: ionomer, semicrystalline ionomer, nanocomposites, polymer crystallization, polymer microstructure

THE EFFECT OF NANOSCALE PARTICLES AND IONOMER ARCHITECTURE ON THE CRYSTALLIZATION BEHAVIOR OF SULFONATED SYNDIOTACTIC POLYSTYRENE

Sonya Denese Benson

ABSTRACT

Semicrystalline ionomers are an important class of polymers that are utilized in a wide range of applications. The particular end-use applications of these materials are determined by their chemical, physical, and thermomechanical properties which are directly related to their crystallization behavior. It is therefore critical to identify structure-property relationships for these materials. Sulfonated syndiotactic polystyrene (SsPS) is used as a model semicrystalline ionomer and two approaches are utilized to control the rate of crystallization of the SsPS ionomer in the presence of ionic aggregates.

The first approach investigates the effect of the incorporation of nanoscale particles, montmorillonite clay, on the crystallization behavior of SsPS. The morphology of the ionomer clay hybrids were studies via TEM and WAXD while the crystallization behavior of SsPS in the presence of the clay was evaluated using DSC. It was found that the SsPS matrix containing 5 wt.% organically-modified clay crystallized more rapidly than the sPS homopolymer containing the same clay content. This behavior is attributed to the presence of homogenously dispersed nanoscale clay platelets that act as nucleation sites distributed throughout the ionomer matrix.

The second approach that employed involved the manipulation of SsPS ionomer architecture via a controlled placement of the ionic sulfonate groups along the polymer backbone. A post-polymerization sulfonation technique was developed to place the sulfonate

groups along the homopolymer backbone in a non-random fashion leading to a pseudo-block ionomer architecture. The crystallization behavior of the non-randomly sulfonated SsPS ionomer is compared to randomly sulfonated SsPS using differential scanning calorimetry. The morphologies of the two ionomers were studied using SALLS and SAXS. We have found that the non-randomly sulfonated SsPS ionomer crystallizes much more rapidly than the randomly sulfonated ionomer. The more rapid crystallization behavior of the non-random ionomer to the presence of longer sequences of unsulfonated homopolymer that are able to readily organize into crystalline structures than the random SsPS ionomer containing the same ionic content.

ACKNOWLEDGEMENTS

I certainly did not make it to the finish line alone. It has been a group effort designed and orchestrated by a loving Creator. I am so very thankful for every person that supported, encouraged, and sacrificed to help me chase my dream and reach this accomplishment.

I lovingly acknowledge my parents, Chester and Joyce Benson, who taught me very early on about the value of hard work and education and I will always be grateful for all of the sacrifices they made on my behalf. I want to thank my sister Nicole Davis and my sister-friends Dr. Kelley Haynes Mendez and Dr. Leigh Haynes, who laughed, cried, and celebrated with me sometimes all in one conversation. The love and support of these ladies was invaluable. Though one may be overpowered, two can defend themselves. A cord of three strands is not quickly broken. I thank each of you for lending yourselves to create a lasting and loving cord of friendship. I also want to thank my children Sidnei and David Benson for encouraging me with their smiles, hugs, and giggles. I am so grateful to parent such wonderful, loving, and inquisitive children. I hope that I can instill in them the same passion for learning that my parents did for me.

I am so thankful for the love and support that I received at Pilgrim Valley Missionary Baptist Church (Fort Worth, Texas), Mount Olive Baptist Church (Hattiesburg, Mississippi), St. Paul African Methodist Episcopal Church (Blacksburg, Virginia), Victorious Life and Covenant Community Christian Churches (Roanoke, Virginia), and the Bible study time that I shared with Andrea Abiyounes, Juanita Morris, Ona Reeder, and friends. I learned so much about the love of God through the teaching and the actions of the people at each of these places.

It has been wonderful to have the opportunity to study at two great universities - the University of Southern Mississippi and Virginia Tech. I want to acknowledge and thank the faculty, staff, and students within the School of Polymers and High Performance Materials at the University of Southern Mississippi. During my time there, many people went out of their way to offer support and encouragement including Machell Haynes, Dr. Douglas Wicks, Dr. Joe Whitehead, Dr. Charles Hoyle, Dr. William Jarrett, and Dr. Steve Curry. I will always remember their kind words and actions.

I greatly valued the opportunity to study at Virginia Tech. The people and the place are both remarkable. Both students and faculty welcomed the Moore Research Group to the university and helped make the transition easy. My committee members: Dr. Judy Riffle, Dr. Don Baird, and Dr. Richard Turner were so nice when I was in the process of forming a new committee and I appreciate their willingness to serve and share their knowledge and expertise with me. I also want to thank LaShonda Cureton Williams (Turner Research Group) for her support and friendship and Justin Spano (Wii Research Group) for his encouraging words.

I want to thank all of the members of the Moore Research Group for their support and friendship. I spent five years with an outstanding group of people and I will always remember the work and the play that we had in the lab. I want to specifically thank Gilles Divoux from the MoRG for his friendship.

I finally want to express a most sincere thank you to my advisor Dr. Robert Moore. Thank you so much for simply giving me a chance. You gave me an opportunity at a time when I really needed it and I will forever be grateful. Your enthusiasm and energy for what you do is contagious. It was hard not be excited about physical polymer science in the MoRG!

William Arthur Ward said, “The mediocre teacher tells. The good teacher explains. The superior teacher demonstrates. The great teacher inspires.” Thank you Dr. Moore for inspiring me. I hope to inspire others as well.

TABLE OF CONTENTS

LIST OF FIGURES

Figure

LIST OF TABLES

Table

CHAPTER I

INTRODUCTION TO IONOMERS AND RESEARCH OBJECTIVES

Ionomers are polymers that contain less than 15 mol% of ionic groups incorporated into a hydrophobic polymer [1-7]. Functionalization of a hydrophobic polymer through the incorporation of a comonomer or post-polymerization modification a homopolymer allows these functionalized polymers to be utilized in a greater number of applications than their monofunctional counteparts. Ionomers may aid in increasing the miscibility between two different polymers of differing hydrophobicity by acting as a compatibilization agent [8-24]. Ionomers may also be utilized in applications where adhesion is necessary as the ionic content increases the surface energy of otherwise hydrophobic polymers leading to improved interfacial interaction between the ionomer and the substrate [25-29]. Ionomers are also are en extremely important class of materials in the fuel cell arena as they are a critical component within a fuel cell that allows the transport or water and ions through the membrane necessary to produce electrical current [30-37].

Ionomers are used in numerous advanced applications, but their fundamental properties and behavior have been studied providing insight into their structure/property relationships. The fundamental structure/property research drives the future design and synthesis of ionomers with specific properties for high performance applications. Due to the incorporation of the ionic content, these ion-containing polymers exhibit properties and behavior drastically different from their non-ionic counterparts in both the solution [38-52] and bulk states [53-65].

Ionomer Morphological Models

The behavior of ion-containing polymers both in the solution and bulk states has been attributed to the phase separation of the ionic component from the hydrophobic backbone with the ion pairs forming electrostatic crosslinks. Several factors affect the aggregation of the ionic component such as the type and concentration of the ionic group, the size of the neutralizing counterion, glass transition temperature of the polymer, rigidity of the polymer backbone, position of the ionic group relative to the hydrophobic backbone, addition of plasticizers, and thermal processing. Several morphological models have been proposed to describe the morphological arrangement of the ionic groups within the hydrocarbon matrix [66-68].

One of the most widely accepted ionomer morphological models was proposed by Eisenberg, Hird, and Moore in 1990 [69] often referred to as the EHM model shown in Figure I-1.

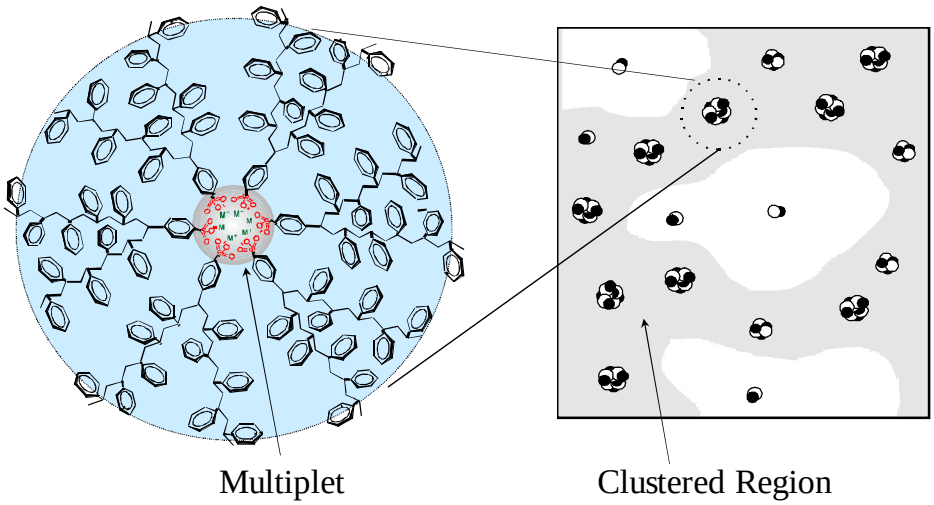

Figure I-1. Eisenberg Hird Moore morphological model. Reprinted from Macromolecules, 23(18), 4098. Copyright 1990 American Chemical Society.

This model which describes the morphology of random ionomers was developed using data and information gathered from morphological studies that included small angle X-ray scattering studies and studies of the viscoelastic behavior of random ionomers through dynamic mechanical analysis. The EHM model proposes that ion pairs aggregate/assemble into structures called multiplets. The multiplets act as multifunctional electrostatic crosslinks that have a tremendous effect on the behavior and properties of the ionomer. Polymer chains that emanate directly from surface of the multiplet structure experience a significant reduction in chain mobility. The motions of the polymer chains that radiate directly from the multiplet surface are hindered significantly. Eisenberg and coworkers suggested that the thickness of the region of restricted chain motion near the surface of the multiplet is in the range of the persistence length of the polymer. Beyond the region very close to the multiplet surface, polymer chain mobility increases, but is still sluggish due to presence of the multiplet structures. The EHM model proposed that polymer chains outside of the region of restricted mobility display segmental chain mobility similar to non-ionized crosslinked polymers.

The formation of multiplets depends on a number of polymer properties as aforementioned, but the concentration of the ionic component has a significant effect on the size and number of multiplets formed. As the ionic content is increased, the multiplets increase in size and the region radiating from the multiplet surface also grows. As the multiplets and regions surrounding the multiplets grow, the individual multiplet structures begin to overlap and form contiguous regions of restricted mobility. The overlapping, contiguous regions of restricted mobility are called clusters. The cluster phase often exhibits phase separated behavior and may

have a glass transition temperature different from that of regions of the ionomer that do not contain a large concentration of ionic content.

Ion Hopping

Ion hopping is the process by which ion pairs migrate from one multiplet to another [70] . This dynamic process has been observed in a number of different ionomers [71-76] and considered to be the mechanism by which long range mobility and flow occurs for the polymer chains within an ionomer. Ion hopping is a very important mechanism within ionomers because it explains how polymer chains can be mobile in the presence of stable ionic domains.

Eisenberg and coworkers proposed that at temperatures below the glass transition temperature of the matrix phase of the ionomer, that chain mobility is severely restricted. As the temperature is raised above the T_g of the matrix phase, chain mobility increases. A continued increase in the temperature results in enhanced mobility of polymer chains and the elastic forces associated with the movement of the polymer chains induces the movement of ion pairs.

Elastic forces associated with polymer chain mobility have the ability to influence the actual glass transition temperature of the cluster phase in addition to the mechanism of ion-hopping. Upon moving through the glass transition of the cluster phase, the stability of the physical crosslinks within the multiplet structures decreases which is often observed as a decrease in the modulus of an ionomer during a DMA experiment. The migration of ion-pairs from one multiplet to another leads to destabilization of the electrostatic network created by the multiplets and decreases the mechanical and thermal properties of the material. Liebler and coworkers proposed that the mobility of polymer chains is affected by both the concentration and the lifetime of the physical crosslinks of the multiplet structures [77].

Ionomer Architecture

The placement of ionic groups along the polymer backbone results in different polymer architectures. Random, linear telechelic, branched telechelic, graft, and block ionomers have been produced and characterized. The placement of the ionic groups along the polymer backbone is shown in Figure I-2.

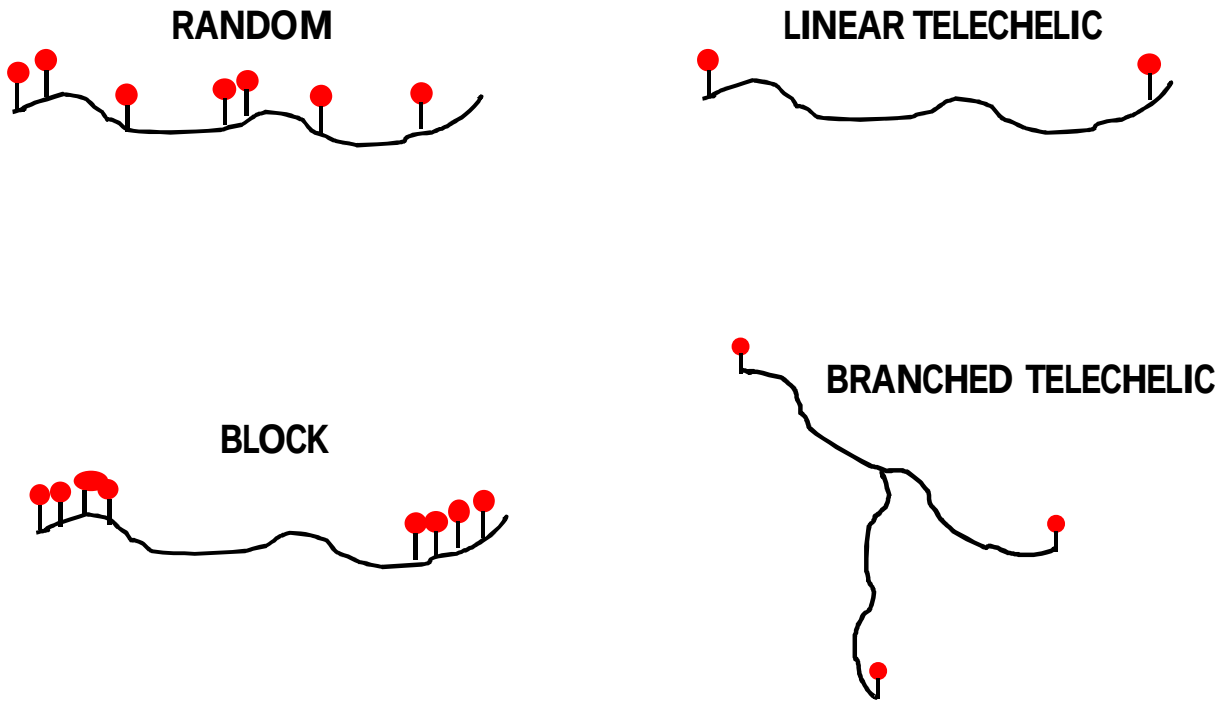

Figure I-2. Schematic of various ionomer architectures. Black lines represent the hydrophobic polymer backbone. Red circles represent ionic groups incorporated onto hydrophobic backbone via copolymerization or post-polymerization modification.

Random ionomers contain the ionic species placed along the polymer backbone in a random manner. Random ionomers have been synthesized via various copolymerization methods [78-86] and through the post-polymerization modification of homopolymers [87-95].

The effect of the placement of the ionic group along the polymer backbone within poly(ethylene-co-acrylic acid) zinc-neutralized ionomers was studied by Seitz and coworkers using Small angle X-ray scattering (SAXS), DSC, and scanning transmission electron microscopy (STEM) [96]. In their study, linear poly(ethylene-co-acrylic acid) ionomers with random or precisely placed comonomers were prepared using ring-opening metathesis polymerization (ROMP) and acyclic diene methathesis (ADMET), respectively.

Figure I-3 contains the plots of scattering intensity versus q for PE_pAA_{13}-Zn0, PE_pAA_{13}-Zn82, PE_rAA_{13}-Zn0, and $PErAA_{13}$-Zn81. The PE_xAA_y-ZnZ nomenclature denotes the placement of the comonomer along the polymer backbone with x identifying the microstructure of the ionomer with p=precise and r=random, the y represents the mol% acid content, and the Z identifies the extent of acid neutralization with zinc. The scattering patterns in Figure I-3 were obtained as 120 °C while the poly(ethylene acrylic acid) ionomers were in the amorphous state. It can be seen that both the unneutralized random and the precise poly(ethylene acrylic acid) ionomers do not exhibit any significant scattering in the q range between 2 -14 nm^{-1}. The neutralization of the random and precise poly(ethylene acrylic acid) ionomers with zinc results in sharpening of the low-angle ionomer peak with the ionomer peak being significantly sharper for the precise poly(ethylene acrylic acid) ionomer than the random poly(ethylene acrylic acid) ionomer. The strong intensity and narrow breadth of the ionomer peak for PE_pAA_{13}-Zn82 is attributed to the presence of ionic aggregates with a more uniform spatial distribution than the ionic aggregates of the random ionomer.

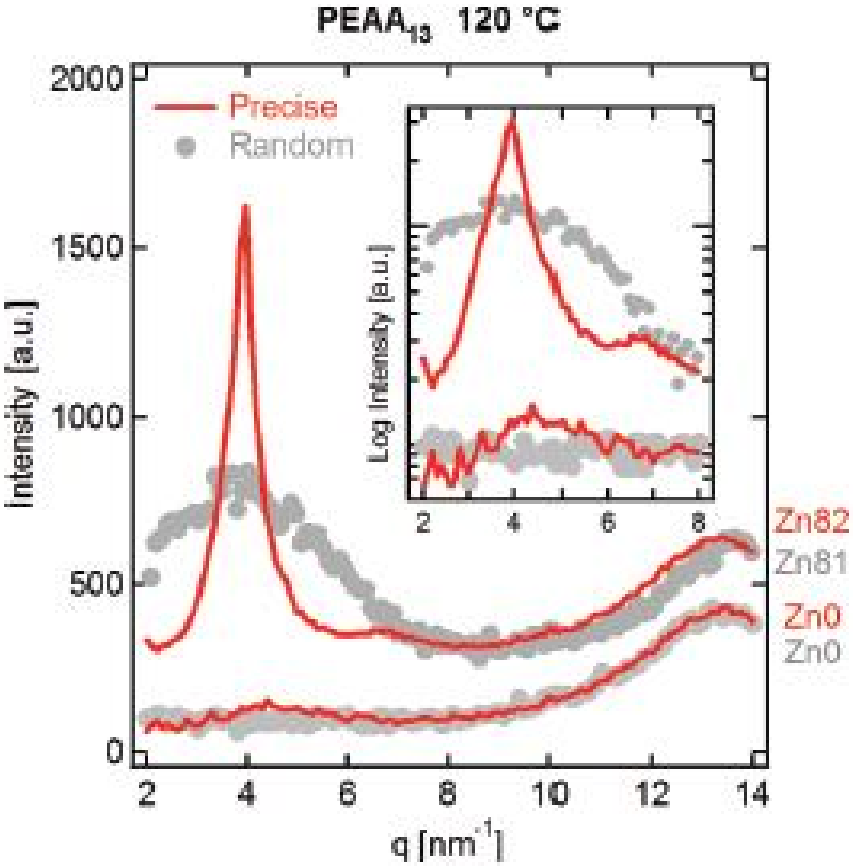

Figure I-3. Scattering intensity versus q for PE_pAA_{13}-Zn0, PE_pAA_{13}-Zn82, PE_rAA_{13}-Zn0, and PE_rAA_{13}-Zn81 at 120 °C plotted on a linear scale. The inset shows the low q features on a log scale. Moving from an ionomer with a pseudorandom acid distribution to a precise distribution dramatically increases the intensity of the ionomer peak. The more intense and well-defined peak indicates that the spatial distribution of the ionic aggregates is vastly more uniform in precise ionomers. Reprinted from Journal of the American Chemical Society 123(23) 8165. Copyright 2010 American Chemical Society.

Okamura and coworkers prepared poly(styrene-*ran*-styrenesulfonic acid) and poly(styrene-*block*-styrene sulfonic acid) via nitroxide-mediated living radical polymerization [86]. The thermal stability and solution behavior of the ionomers were evaluated. They found that the poly(styrene-*ran*-styrenesulfonic acid) ionomers were more thermally stable than the poly(styrene-*block*-styrene sulfonic acid) of similar sulfonic acid content. The percent decomposition of the ionomer versus heating time is shown in Figure I-3. Okamura and

coworkers monitored the changes in the thermal decomposition of the ionomers using the time at which 50% of the starting material is lost. The decomposition times for PSSPen, P(St(62)-*block*-PEN(38)), and P(St(57)-*ran*-PEN(43)) were 15, 20, and 70 minutes, respectively. It was suggested that the shorter decomposition time of the block ionomer was to due to the degradation of sulfonate ester groups into sulfonic acid groups which then rapidly catalyzes the decomposition of neighboring sulfonate ester groups within the poly(styrene-*block*-styrene sulfonic acid) ionomer. This process thus resulted in a more rapid decomposition rate within the block ionomer than the random ionomer. Okamura and coworkers also observed that the decomposition rate increased with increasing ionic content and that poly(styrene-*block*-styrene sulfonic acid) ionomers decomposed more quickly than the poly(styrene-*ran*-styrene sulfonic acid) ionomer at every ionic concentration studied.

The solution behavior of the poly(styrene-*ran*-styrene sulfonic acid) ionomer and poly(styrene-*block*-styrene sulfonic acid) ionomers were studied in hexane, toluene, benzene, THF, chloroform, acetone, DMF, methanol, and water by Okamura and coworkers [86]. The architecture of the ionomers had a profound effect on the solution behavior of the ionomers at room temperature in chloroform. It was found that the random polystyrene ionomers were not soluble in chloroform, but the block ionomers in the acid form were soluble in chloroform.

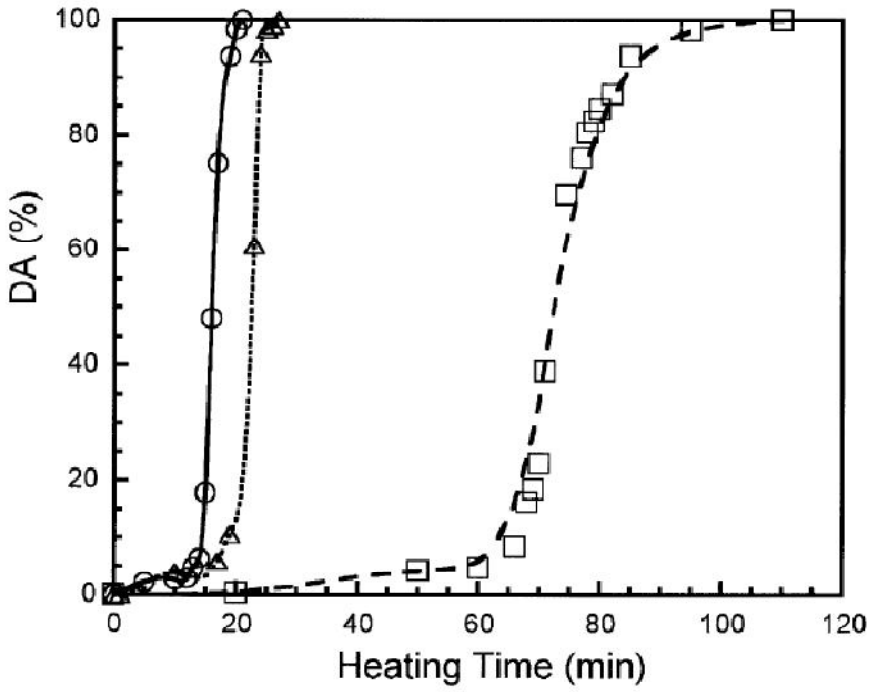

Figure I-4. Decomposition properties of sulfonate esters of PSSPen (open circles), P(St(62)-*block*-PEN(38)) (open triangles), and P(St(57)-*ran*-PEN(43)) (open squares). Reprinted from Polymer, Vol 43, Issue 11, Haruyuki Okamura, Yusuke Takatori, Masahiro Tsunooka and Masamitsu Shirai, Synthesis of random and block copolymers of styrene and styrenesulfonic acid with low polydispersity using nitroxide-mediated living radical polymerization technique, 3155-3162, Copyright 2002, with permission from Elsevier.

Telechelic ionomers have the ionic groups placed at the end of the polymer chain [97-113] and therefore, the ionic content is inversely proportional to the molecular weight of the polymer. Although the telechelic ionomer architecture contains the ionic groups at the end of the polymer chain, the polymer chain may be linear, branched, or a star with the ionic content located at the ends of each of these structures resulting in even more elaborate architecture.

Telechelic poly(lactic acid) ionomers were prepared by Ro and coworkers through transesterification of commercial poly(lactic acid) (PLA) yielding hydroxy-terminated PLA

[110]. Itaconic anhydride was reacted with the hydroxy-terminated PLA to form terminal carboxylic acid groups. The thermal properties and crystallization behavior of the telechelic ionomers were studied as a function of neutralizing counterion and ionic content.

The effect of the concentration of ionic groups on the crystallization behavior of telechelic PLA ionomers was studied using non-isothermal DSC crystallization experiments. Figure I-5 provides a plot of the fractional crystallinity, X_t, versus time for HPLA3.4 and HPLA13.0 telechelic ionomers within only one carboxylate chain end prepared using 2-hydroxyethyl methacrylate with molecular weights of 3.4 and 13.0 kg/mol, respectively. The plot also contains data for the EPLA8.9 telechelic ionomer prepared using ethylene glycol with a molecular weight of 8.9 kg/mol possessing two carboxylate chain ends. It can be seen from the plot of Figure I-5 that the crystallization half-time increases within increasing molecular weight for the HPLA ionomers despite the decrease in ionic content as a result of the higher molecular weight. Also, the presence of two functionalized chains ends on the lower molecular weight EPLA8.9 telechelic ionomer results in a decreased rate of crystallization compared to the HPLA telechelic ionomers.

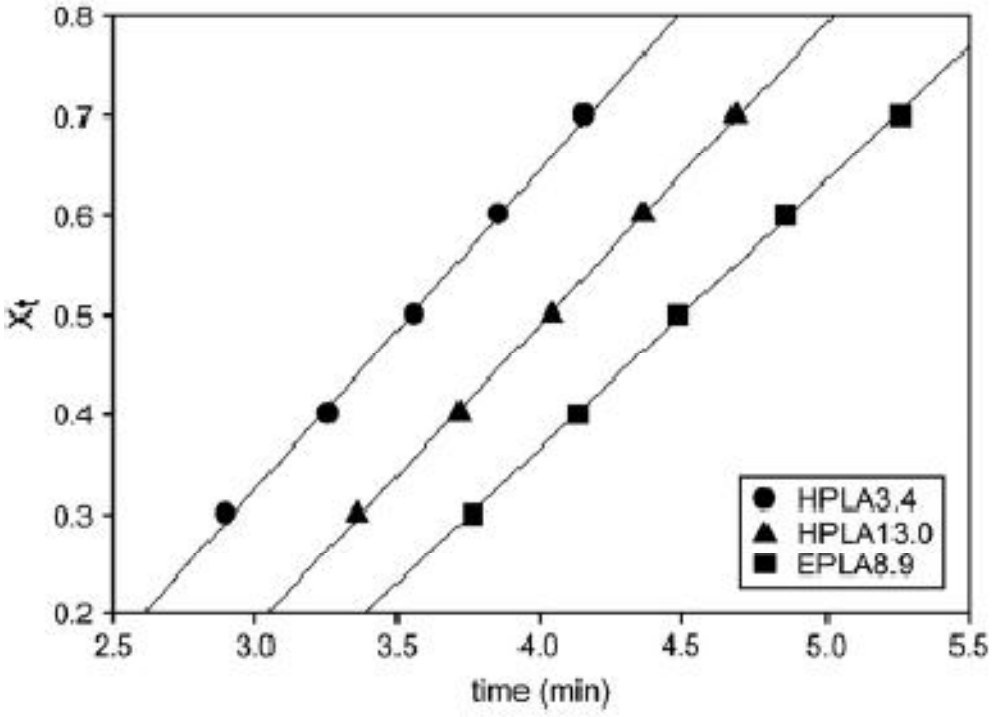

Figure I-5. Fractional crystallization versus time profiles for $HPLA_x$ and $EPLA_x$ ionomers calculated from non-isothermal crystallization studies. Reprinted from Polymer, Vol 49, Issue 2, Andrew J. Roa, Samuel J. Huanga, and R.A. Weiss, Synthesis and thermal properties of telechelic poly(lactic acid) ionomers, 422-431, Copyright 2008, with permission from Elsevier.

In addition to random and telechelic ionomers, block ionomers of many types have been prepared. Diblock [114-121], triblock [119, 122-129], and multiblock ionomers [130-138] are microstructural possibilities. Multiblock ionomers may have the blocks of ionic content arranged randomly throughout the copolymer or as alternating or segmented blocks of ionic content.

Increasing costs for fossil based fuels has generated a significant amount of interest in improving fuel cell technology with a tremendous amount of attention focused on understanding and improving the morphology and properties of the proton exchange membrane (PEM) of the fuel cell. Researchers have focused on ascertaining the relationship between the microstructure

of PEM and PEM properties such as water uptake and proton conductivity [133, 135-136, 138-151]. In a review of sulfonated aromatic hydrocarbon polymers as PEMs, Higashihara and coworkers identified many of the different polymer microstructures and architectures that have been reported in the literature as shown in Figure I-6. Although the microstructures of the ion-containing polymers vary significantly in the placement and sequence length of the ionic functionality, the goal for each system is to produce a PEM with moderate to high ion exchange capacity (IEC) to achieve proton conduction through the membrane via ionic channels created through the phase separation of the hydrophilic and hydrophobic domains of the ionomer.

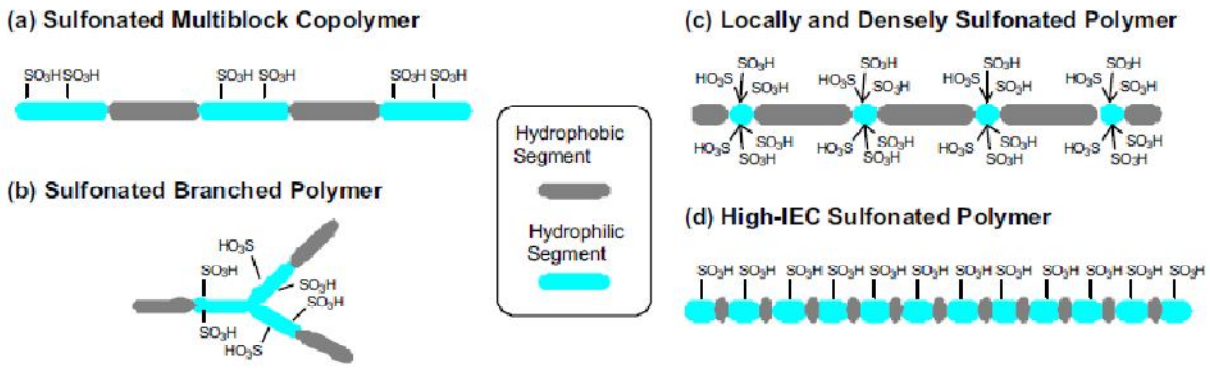

Figure I-6. Illustrations of several polymer architectures for PEMs. Reprinted from Polymer, Vol 50, Issue 23, Tomoya Higashiharaa, Kazuya Matsumotoa and Mitsuru Ueda, Sulfonated aromatic hydrocarbon polymers as proton exchange membranes for fuel cells, 5341-5357, Copyright 2009, with permission from Elsevier.

The effect of the length of the hydrophilic block on the water uptake and proton conductivity of diblock copolymers of sulfonated copolyimides was investigated by Li and coworkers [137]. Figure I-7 shows the plots of water uptake and proton conductivity versus the length of the hydrophilic block of sulfonated copolyimides for different IEC values where the

hydrophilic block of the block copolyimides were composed of sulfonated dianhydride and sulfonated diamines. It can be seen in Figure I-7a of water uptake versus hydrophilic block length that the water uptake increases with increasing hydrophilic block length at IEC values of 2.01 and 2.69 mequiv/g reaching plateau at a hydrophilic block length of 20. However, the water uptake versus hydrophilic block length at IEC=1.50 mequiv/g does not change with the length of the hydrophilic block. Figure I-7b shows the proton conductivity of the block copolymers of sulfonated polyimides versus hydrophilic block length at room temperature in water.

Li and coworkers compared the proton conductivity and water uptake behaviors of the sulfonated block polyimides to random sulfonated polyimides as shown in Figure I-8. Their research demonstrated that the microstructure of the ionomer has an impact on the water uptake and proton conductivity of the membrane. It can be seen according to their reports that the sulfonated copolyimides exhibited improved proton conductivity behavior as a function of water uptake than the random sulfonated copolyimides.

There has been a tremendous amount of work done to both synthesize and characterize the ionomers of varying architecture. It is clear that continued focus in the area of structure/property relationship will prove to be extremely variable in creating advanced materials that meet the often very specific needs of high performance applications.

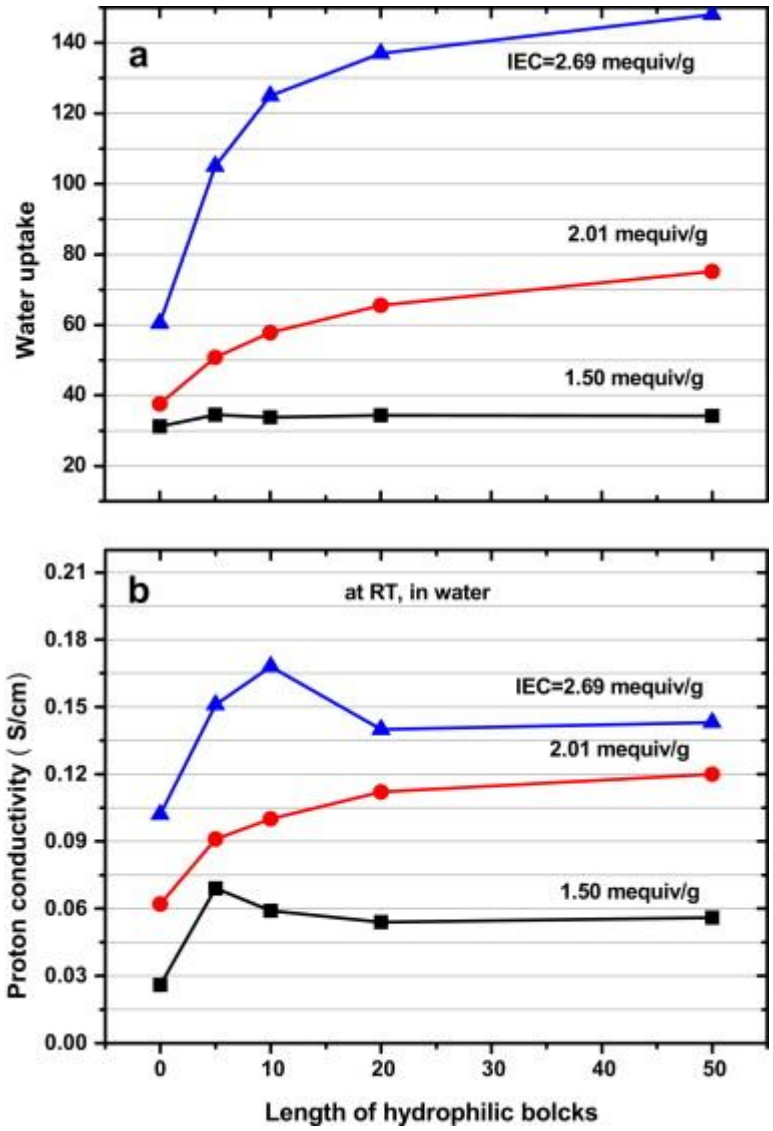

Figure I-7. Plots of (a) water uptake versus length of hydrophilic blocks, (b) proton conductivity at 20 °C in water versus length of hydrophilic blocks. Reprinted from Polymer, Vol 50, Issue 19, Nanwen Lia, Jia Liua, Zhiming Cuib, Suobo Zhanga, and Wei Xing, Novel hydrophilic-hydrophobic multiblock copolyimides as proton exchange membranes: Enhancing the proton conductivity, 4505-4511, Copyright 2009, with permission from Elsevier.

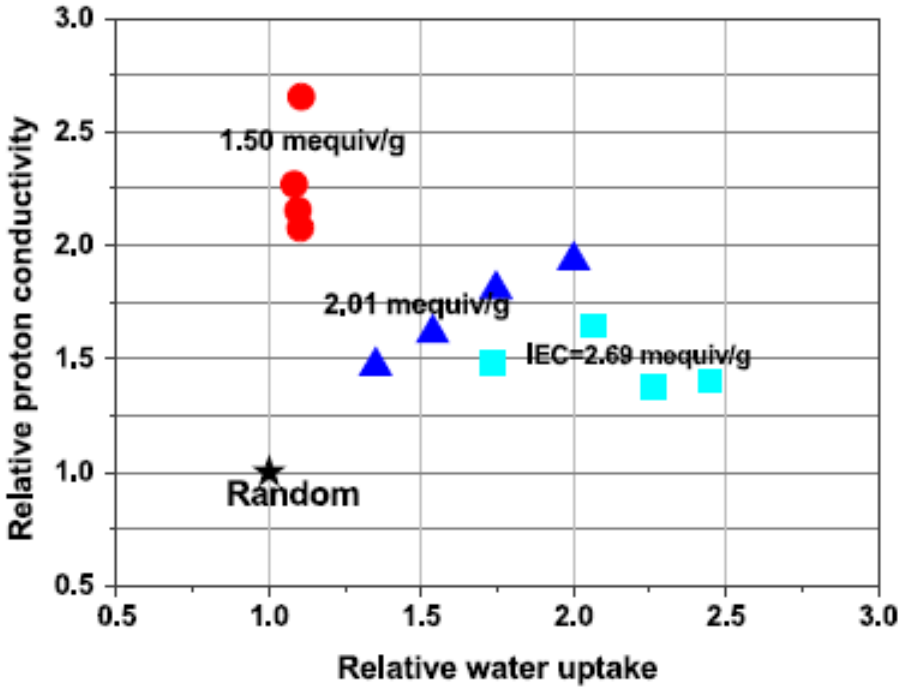

Figure I-8. The relative water uptake as a function of the relative proton conductivity. Reprinted from Polymer, Vol 50, Issue 19, Nanwen Lia, Jia Liua, Zhiming Cuib, Suobo Zhanga, and Wei Xing, Novel hydrophilic-hydrophobic multiblock copolyimides as proton exchange membranes: Enhancing the proton conductivity, 4505-4511, Copyright 2009, with permission from Elsevier.

Influence of Polymer Backbone on Ionic Aggregation

The greater the difference in the polarity between the hydrophobic backbone and the ionic group of the ionomer, the greater the driving force for the phase separation of the two copolymer components [69].

The degree of flexibility of the hydrophobic backbone of the ionomer has a strong influence on morphology of the ion-containing polymer through the development of ionic aggregates and phase separated domains. Hickner and Pivovar highlighted the potential morphological differences between ionomers used as PEMs such as Nafion® and BPSH as shown in Figure I-9 [151]. They attribute the differences in the phase separation of Nafion® and

BPSH to differences in the backbone structures of the ionomers. The sulfonic acid groups of Nafion® are located at the ends of long, flexible side chains which allows a greater degree of phase separation from the poly(tetrafluoroethylene) (PTFE) backbone. Additionally, the PTFE backbone of the Nafion® ionomer is very flexible. In contrast, the morphology of biphenol sulphone (BPSH) PEMs with two sulfonic acid groups in close proximity to the BPSH repeat unit would result in the formation of a larger degree of microphase separation of the ionic content from the hydrophobic backbone. Also, the BPSH backbone does not have the flexibility of the PTFE backone of Nafion® which leads to a different degree and type of phase separated morphology as shown in Figure I-9.

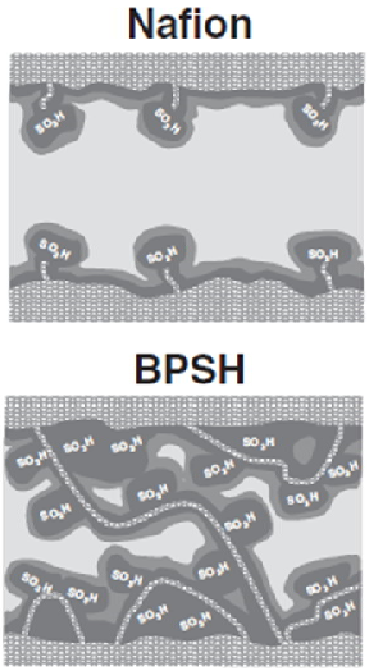

Figure I-9. Schematic of proposed domain structures of Nafion® and BPSH PEMs. M.A. Hickner and B.S. Pivovar, The Chemical and Structural Nature of Proton Exchange Membrane Fuel Cell Properties. Fuel Cells Special Special Issue: Polymer Membranes I, 2005, Volume 5, Issue 2, 213-229, Copyright Wiley-VCH Verlag GmbH & Co. KGaA. Reproduced with permission.

Influence of Acid Group on Ionic Aggregation

Ionomers have been prepared through the incorporation of different ionic groups including sulfonate [152-160], carboxylate [152, 161-166], and phosphate [167-169]. The nature of the ionic group has a direct influence on the morphology and properties of the resulting ionomer [70, 170-174].

The strength of the electrostatic interactions in ionomers containing sulfonate groups have been reported to be stronger than ionomers of the same hydrophobic backbone containing carboxylate groups. Investigations into the properties of ionomers using DMA and mechanical testing have demonstrated the greater strength of ionic aggregates consisting of sulfonate groups versus carboxylate groups [70, 106, 175]. Model polyurethane ionomers were prepared that contained either sulfonate or carboxylate groups by Visser and Cooper [176]. They studied the thermomechanical properties of the polyurethane ionomers using DMA, DSC, and mechanical testing. The polyurethane ionomers containing sulfonate groups exhibited higher stress at break and elongation at break than carboxylate-containing polyurethane ionomers as shown in Figure I-10. The improved mechanical behavior of sulfonate containing ionomers over carboxylate ionomers have been reported for other polyurethane-based ionomers [171] as well.

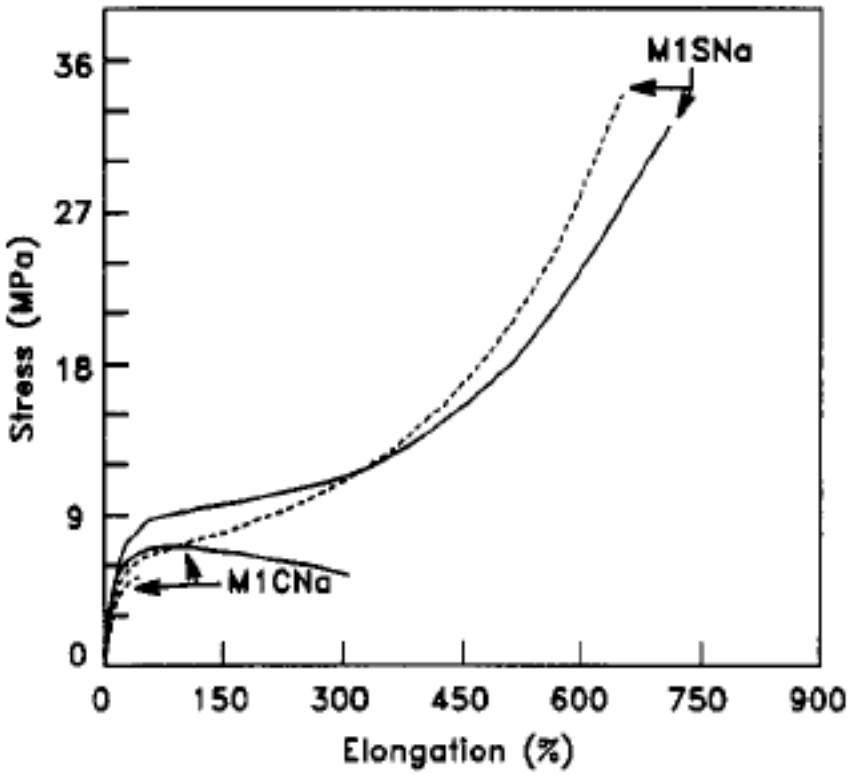

Figure I-10. Uniaxial stress-strain results for solution-cast and compression-molded ionomers based on l000 molecular weight PTMO. Solution cast samples are represented with solid lines, and compression molded samples are shown as the dashed curves. Reprinted from Macromolecules 24(9), 2576 .Copyright 1991 American Chemical Society.

Ionomers have also been prepared with mixed ionic functionality. Hensley and Way reported the synthetic methodology used to prepare Nafion® with both carboxylate and sulfonate ionic groups from the sulfonyl fluoride Nafion® precursor [177-178]. They evaluated the effect of the carboxylate content on the water permeability and proton conductivity behavior of the mixed acid group Nafion ionomer® as shown in Figure I-11. The incorporation of carboxylate groups into Nafion® has a negative effect on the transport properties of the membrane. The proton conductivity decreases rapidly with increasing carboxylate content as expected. Although the transport properties of the mixed carboxylate/sulfonate ionomer decrease, it is very interesting that the proton conductivity decrease does not occur as rapidly as the decrease in

water permeability. Hensley and Way suggest that this behavior may be a result of the development of a different morphological structure and proton conduction mechanism than Nafion ionomer® containing only sulfonic acid groups.

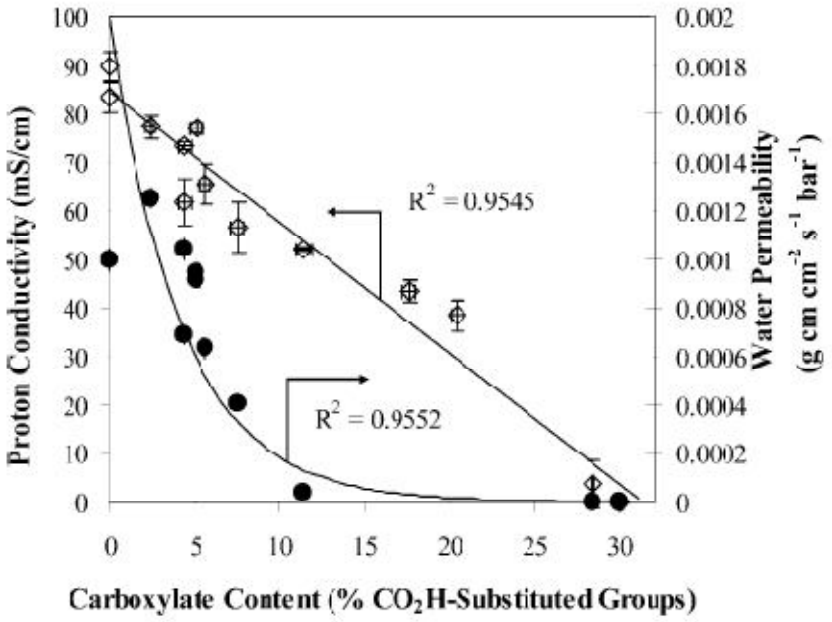

Figure I-11. Water permeability at 35 °C and proton conductivity at room temperature and 100% relative humidity in c/s films. All measurements were taken with films in the acid form. Solid lines are least-squares fits of linear and exponential functions for conductivity and permeability data, respectively. Reprinted from Chemistry of Materials 19(18), 4576. Copyright 2007 American Chemical Society.

Influence of Counterion Type on Ionic Aggregation

The effect of the counterion on the behavior and properties of ionomers has been studied in detail. Experimental evidence clearly demonstrates that the strength of the electrostatic interactions between ion pairs is dependent upon the size and valency of the neutralizing counterion of the ionomer [54, 87, 89, 179-192].

Taylor and coworkers studied the effect of the neutralizing counterion used for Nafion® on the crystallization behavior of Nafion®/PVDF blends. A fundamental portion of their

investigation involved evaluating the effect of the neutralizing counterion on the dynamic mechanical behavior of Nafion® as shown in Figure I-12. It can be seen from the plot of tan δ versus temperature that there is a shift in the tan δ to lower temperatures with increasing counterion size. The shift in the tan δ peak attributed to the glass transition temperature of the ionomer to lower temperatures is attributed to a weakening of the electrostatic network with increasing size of the counterion. The counterion size increases in the order of $TBA^+ > TPA^+ > TEA^+ > TMA^+ > Na^+$.

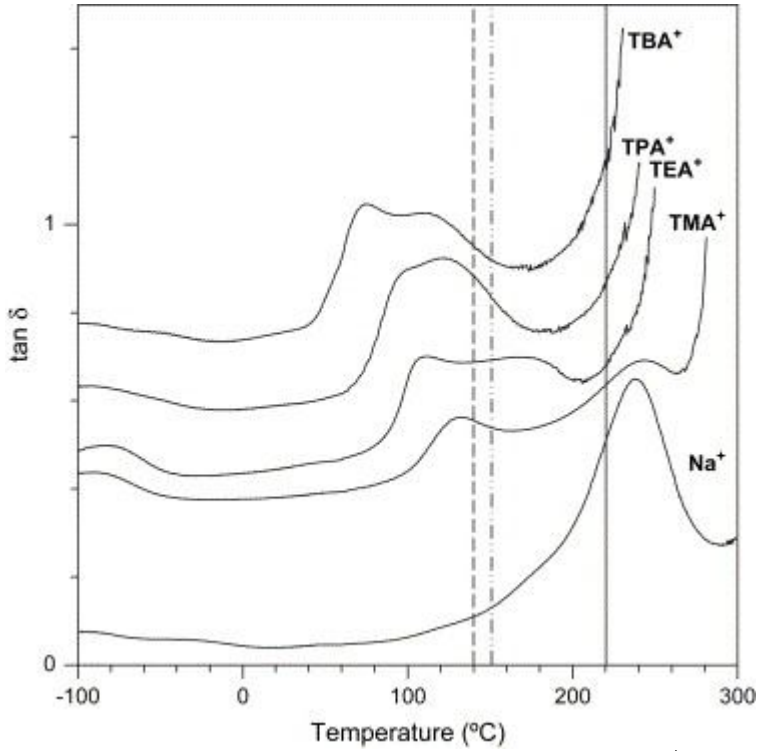

Figure I-12. Dynamic mechanical tan δ versus temperature plots for Na^+-, TMA^+-, TEA^+-, TPA^+- and TBA^+-form 1100 EW Nafion®. Curves are offset vertically for clarity. Reprinted from Polymer, Vol 47, Issue 21, Eric P. Taylor, Forrest A. Landisa, Kirt A. Page and Robert B. Moore, Counterion dependent crystallization kinetics in blends of a perfluorosulfonate ionomer with poly(vinylidene fluoride), 7425-7435, Copyright 2006, with permission from Elsevier.

The fundamental work done to understand the effect of the counterion type of the behavior of ionomers has led to researchers demonstrating that the choice of the neutralizing counterion of the ionomer can be used as a method to control, process, and tune the properties of the ionomer for specific applications.

Landis and Moore demonstrated that the neutralizing counterion used for the perfluorosulfonated ionomer Nafion® could be used to control the miscibility of blends prepared with poly(vinylidene fluoride) (PVDF) [181]. By changing the neutralizing cation of Nafion® from the alkali metal Na^+ to a significantly larger organic cation, tetrabutylammonium (TBA^+), PVDF and Nafion® are both miscible in the melt and in the solid state as well and do not exhibit large-scale phase separation as seen in the PVDF/ Na^+-neutralized Nafion® blends.

The effect of valency on the properties of ionomers has been investigated [49, 194-195]. Bellinger and coworkers studied the effects of the neutralizing counterion on the deformation and tensile fracture behavior of sulfonated atactic polystyrene (SaPS) ionomers [186]. Their mechanical investigations of the deformation behavior of SaPS ionomers neutralized with monovalent sodium and divalent calcium revealed that Ca^{2+} SaPS ionomers exhibited crazing and shear deformation at lower sulfonate concentrations than SaPS ionomers neutralized with Na^+. The improved mechanical performance of the SaPSCa^{2+} ionomers was attributed to a more stable electrostatic network in the presence of the divalent calcium cations.

An exception to the general trend of higher valency counterions forming stronger electrostatic networks is observed for Zn^{2+} cations. Bagrodia and Wilkes suggested that the divalent zinc cations formed weaker electrostatic networks than monovalent cations because the divalent zinc cation may form more covalent bonds than ionic bonds leading to a less stable

electrostatic network [196]. Lefelar and Weiss alos suggested that monovalent Na^+ cations have a higher number of interactions with the anion within ionomers derived from atactic polystyrene. Using SAXS results, they proposed that monovalent Na^+ forms a greater number of interactions with the anion of atactic polystyrene ionomer whether the anion is a sulfonate or carboxylate group than than the divalent Zn^{2+} cations [197].

Influence of Degree of Neutralization on Ionic Aggregation

The degree of neutralization has been shown to have a profound influence on the ionic aggregation of ionomers and their resulting morphology and properties [198-203]. Zhou and coworkers studied the melt rheology of SaPS ionomers neutralized with different counterions and varying levels of neutralization [49] as shown in Table I-1.

Table I-1. Relaxation Times for PS, P(S-SS0.019), and P(S-SS0.019)-M as a Function of Cation and Neutralization Level at 170 °C.

M	Neutralization level (%)	Relaxation time (s)
PS	0	0.1
P(S-SS0.019)	0	0.4
Na	25	0.5
Zn	25	0.6
Na	125	42
Zn	125	53

It can be seen from the data in Table I-1 that the relaxation times are affected by the counterion type and the degree of neutralization. Upon increasing the degree of neutralization of

both the Na^+ and Zn^{2+}-neutralized SaPS ionomers containing 0.019 mol% of sulfonate groups, there is an order of magnitude increase in the relaxation time of the SaPS ionomers. The data clearly demonstrates the strong effect of the degree of neutralization on the rheological properties of the SaPS ionomers.

Kim and Eisenberg showed that under neutralization of styrene co-sodium methacrylate ionomers lowered the ionic plateau modulus and the temperature at which terminal flow begins [204]. They suggested that under neutralization results in the formation of fewer ionic crosslinks and a less stable electrostatic network. Neutralization of the styrene co-sodium methacrylate ionomers at levels greater than 200% resulted in a significant increase in the modulus and ionic plateau of the ionomers. The significant increase in the mechanical behavior of the styrene co-sodium methacrylate ionomers at high levels of over neutralization was attributed to the external crystallization of excess salt outside of the ionic multiplets. Similar behavior was also reported for ethylene-methacrylic acid ionomers [205].

Influence of Plasticizers on Ionic Aggregation

The study of the incorporation of various molecules into the matrices of different ionomers has been studied [161, 206-216]. Early work by Lundberg and coworkers showed that different regions of SaPS ionomers could be selectively plasticized through the utilization of polar or nonpolar plasticizers [209]. They showed the polar plasticizers were quite effective in lowering the melt viscosity of SaPS ionomers and attributed the effectiveness of the polar plasticizers to the selective interaction of the molecule with the ionic domains of the SaPS ionomers. The interaction of the polar plasticizers with the ionic domains resulted in a

weakening/destabilization of the electrostatic network and the resultant observed decrease in the melt viscosity of the SaPS ionomers containing polar plasticizers such as glycerol.

Kim and coworkers investigated the effect of polar and nonpolar plasticizers on the mechanical properties and morphology of cobalt and sodium neutralized poly(ethyl acrylate-co-acrylate) ionomers [217]. Figure I-13 shows the plots of the loss tangent versus temperature for cobalt-neutralized poly(ethyl acrylate-co-acrylate) ionomers containing 4-decylaniline (4-DA) and glycerol as the nonpolar and polar plasticization agents, repsectively. As the concentration of 4-DA increases in the ionomer, the loss tangent (lower temperature peak) associated with the matrix phase of the ionomer decreases to lower temperatures and also decreases in intensity. The decrease in the loss tangent/glass transition temperature of the matrix phase is attributed to the increase in the mobility of the polymers chains of the matrix phase in the presence of 4-DA. The loss tangent attributed to the ion-rich cluster phase (high temperature peak) shifts to lower temperatures, but increases in intensity. There is no significant change in the position or peak intensity of the loss tangent associated with the matrix phase of the poly(ethyl acrylate-co-acrylate) ionomer upon incorporating increasing concentrations of glycerol. However, there is a very gradual shift in the higher temperature cluster transition to lower temperatures attributed to the interaction of glycerol with the ionic domains.

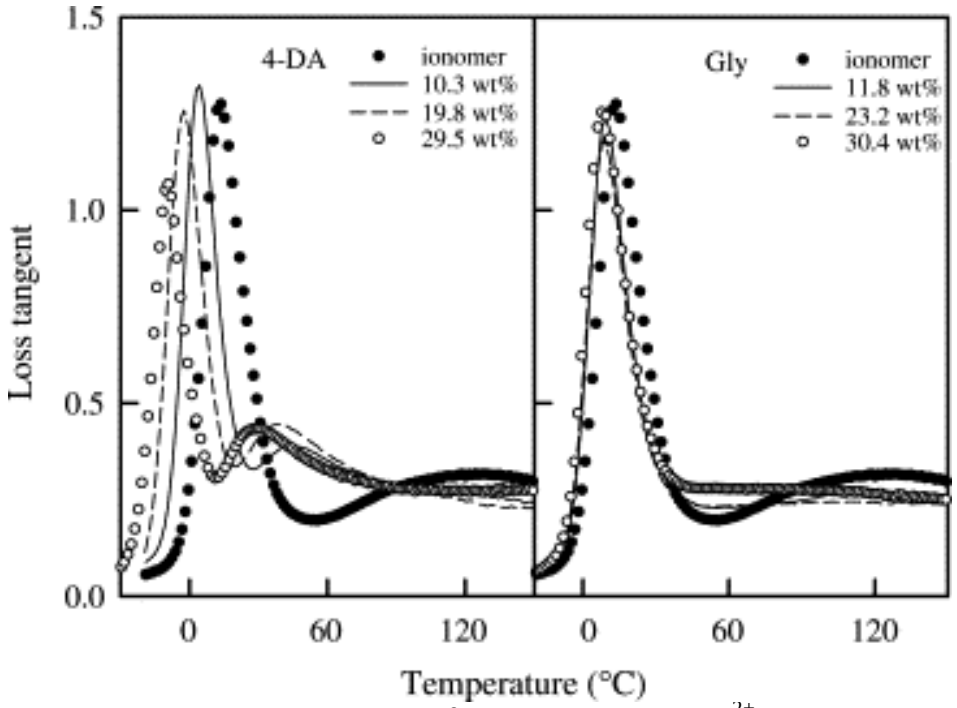

Figure I-13. Loss tangents vs. temperature for the P(EA-7.0-ACo^{2+}) ionomers containing various amounts of 4-decylaniline (4-DA) (left) and for the ionomers containing various amounts of glycerol (Gly) (right), measured at 1 Hz. Reprinted from Polymer, Vol 47, Issue 3, Jung-Won Kim, Ju-Myung Song, Youn-Jeong Cho, Joon-Seop Kim, and Jeong-A Yu, Plasticization effects on the mechanical properties and morphology of cobalt and sodium neutralized poly(ethyl acrylate-co-acrylate) ionomers, 871-877, Copyright 2006, with permission from Elsevier.

Varley and coworkers evaluated the effect of polar plasticization agents on the self-healing properties of poly(ethylene-co-methacrylic acid) ionomers [218]. They evaluated the effectiveness of three different dicarboxylic acids – oxalic acid, adipic acid, and sebacic acid on the disruption of the electrostatic network and the resulting mechanical and morphological properties of the poly(ethylene-co-methacrylic acid) ionomer with attention given to the self-healing behavior of the ionomer. Figure I-14 shows the SEM micrographs of unmodified poly(ethylene-co-methacrylic acid) ionomers and poly(ethylene-co-methacrylic acid) ionomers containing 10 wt.% of oxalic, adipic, or sebacic acid at 130 °C. The SEM images clearly show that the poly(ethylene-co-methacrylic acid) ionomers containing the dicarboxylic acid

plasticizers exhibit self-healing behavior at the impact site which is seen within the center of the sample. Varley and coworkers attribute the improved self-healing behavior of the plasticized ionomers to the disruption of ion pairs within the cluster phase which increases the dynamic behavior of the electrostatic network providing increased mobility to polymer chains necessary for self-healing of the polymer to occur after ballistic impact.

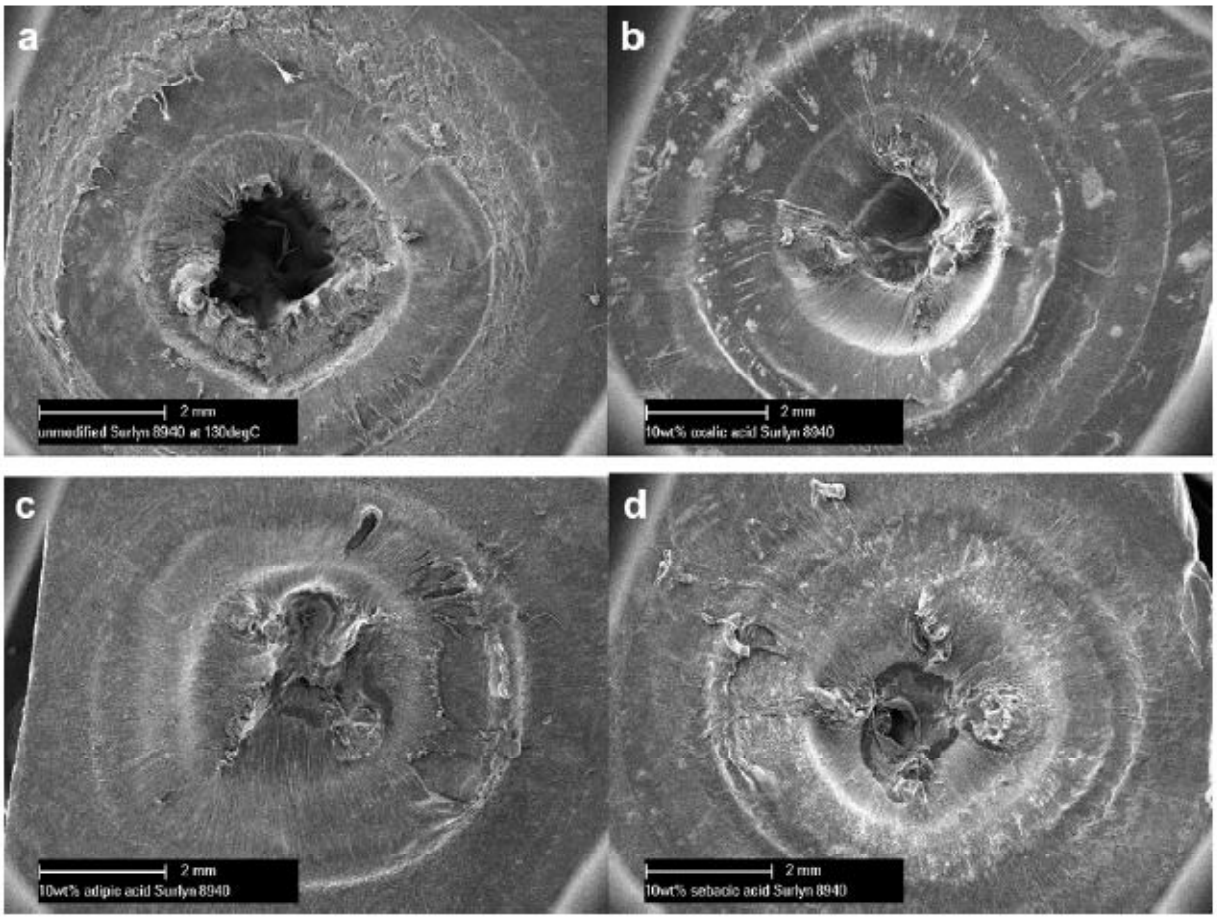

Figure I-14. Scanning electron micrographs comparing the impact site of a) unmodified Surlyn 8940® with b) oxalic acid, c) adipic acid and d) sebacic acid modified Surlyn 8940® at 130 °C. Reprinted from Polymer, Vol 51, Issue 3, Russell John Varley, Shirley Shen and Sybrand van der Zwaag, The effect of cluster plasticisation on the self healing behaviour of ionomers, 679-686, Copyright 2010, with permission from Elsevier.

Morphological Classes of Ionomers

Ionomers can be divided into different classes depending upon the nature of the hydrophobic matrix, the type of ionic content, and the placement of the ionic groups along the polymer backbone. Ionomers can also be readily divided into two major classes based upon the ability of the matrix phase to organize into crystalline structures [7]. Amorphous ionomers are comprised of a two-phase morphology that contains the matrix phase and ionic domains distributed throughout the hydrophobic polymer matrix as shown in Figure I-15.

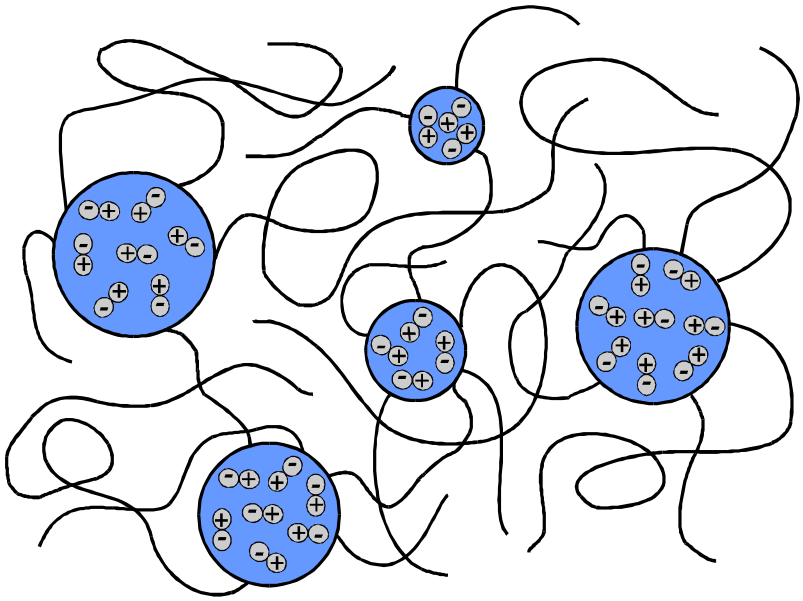

Figure I-15. Schematic of ionic domains dispersed throughout an amorphous polymer matrix.

As the degree of ion content increases, the number and size of ionic domains increase until an ion-rich cluster phase is formed. The matrix phase of amorphous ionomers is made of the hydrophobic polymer chains that do not exhibit any type of long-range structural order.

SaPS has been one of the most widely studied amorphous ionomers due to the simplicity of the polymer backbone and relatively simple method of preparing random SaPS through post-functionalization of the aPS homopolymer [219-220]. Other amorphous ionomers that have

synthesized and characterized include amorphous ionomers based on poly(methyl methacrylate) [221-222], polyimides [223-224], polyethers [225], poly(ethyl acrylate) [226], and poly(styrene-co-sodium methacrylate) [227].

Semicrystalline ionomers are widely used in a wide array of commercial applications such as food packaging [228], biodegradable materials and biological applications [229-230], filtration membranes [231-232], various types of chemical and electrical sensors [233-235], and proton exchange membranes [30, 236]. Semicrystalline ionomers are comprised of a more complex morphology compared to amorphous ionomers due to the ability of the polymer matrix to form crystalline structures. Semicrystalline ionomers may adopt a three-phase morphology that consists of ionic domains, amorphous polymer chains, and crystalline domains as well. The relative amount of polymer chains making up the amorphous and crystalline domains is highly dependent upon the nature of the hydrophobic matrix (i.e. backbone stiffness/rigidity), the type and concentration of the ionic group, and the neutralizing counterion. A depiction of the three-phase morphology of semicrystalline ionomers is shown in Figure I-16.

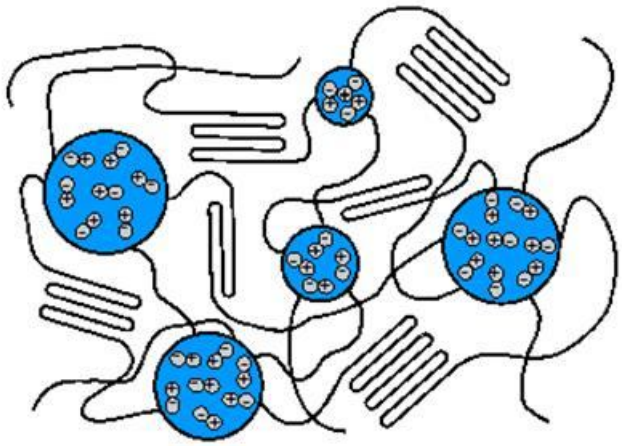

Figure I-16. Schematic of the morphology of a semicrystalline ionomer. Adapted from Nature 218(5136),85. R Longworth and DJ. Vaughan, Physical Structure of Ionomers, Nature Publishing Group.

Longworth and Vaughn proposed the morphological model for semicrystalline ionomers shown in Figure I-16 based upon WAXD diffraction data for ethylene methacrylic acid ionomers [237]. The level of complexity increases in the three-phase morphology of semicrystalline ionomers because one polymer chain may traverse each structural domain of the ionomer. Therefore, the ionic interactions may also have a direct impact on the development of the crystalline domains.

Two of the most widely used semicrystalline ionomers are Nafion® and Surlyn® ionomers which have two different hydrophobic backbones and different ionic groups. Nafion® is a perfluorosulfonate ionomer with a poly(tetrafluoroethylene) backbone while Surlyn® is an ethylene methacrylic acid ionomer. Although the chemical structures of these two ionomers are significantly different as shown in Figure I-17, their physical, chemical, and thermomechanical properties are both affected by the quantity, and distribution of their respective ionic groups within the poly(tetrafluoroethylene) and poly(ethylene) backbones.

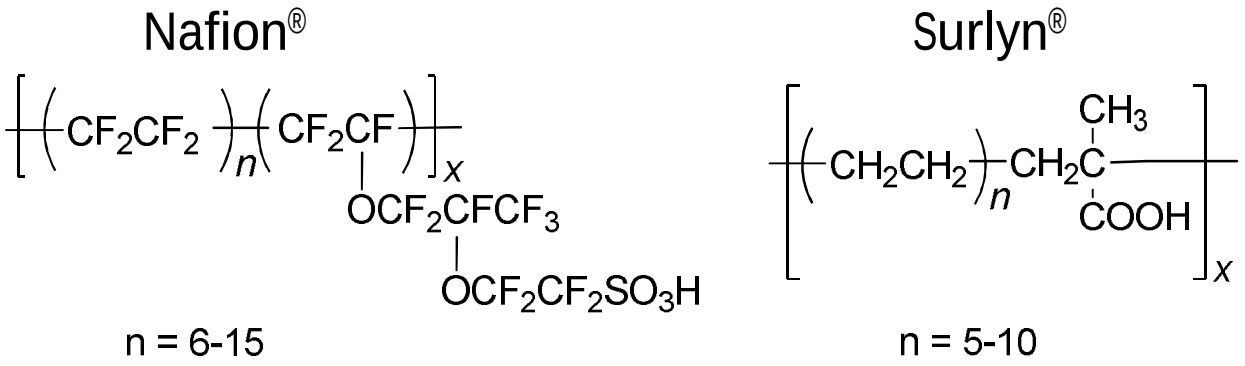

Figure I-17. Chemical structures of Nafion® and Surlyn®.

Generally, it has been found that as the degree of ionic content increases that the glass transition temperature associated with the matrix phase and the cluster phase increases, but the overall degree of crystallinity and rate of crystallization decrease regardless of the nature of the hydrophobic backbone [157]. Upon introducing sufficient ionic content to the semicrystalline either through copolymerization of post-polymerization modification, the ability of the polymer chains to crystallize on a readily-observable time scale can be completely eliminated.

Nafion® and Surlyn® have been studied quite extensively because of their implementation and interest as materials for high performance applications. However, in addition to these two very important ionomers, semicrystalline ion-containing polymers have been prepared based on polyesters such as poly(ethylene) and poly(butylene) [154, 159, 238-246], poly(lactic acid), and sulfonated poly(aryl ether ether ketone) [247-251].

Lim and Kim studied the effect of ionic content on the crystallization and mechanical properties of poly(oxyethylene-b-butylene adipate) ionomers [252]. The structure of the semicrystalline ionomer is shown in Figure I-18. The poly(oxyethylene-b-butylene adipate) ionomers (POBAi) were synthesized via a two-step polycondensation reaction.

\

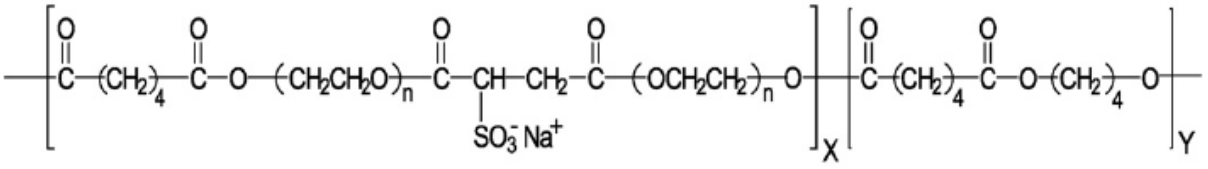

Figure I-18. Chemical structure of poly(oxyethylene-b-butylene adipate) ionomers.

The authors determined the molecular weight of the pure POBA polymer to be 30,000 g/mol via size exclusion chromatography (SEC), but were unable to determine the size of the POBA ionomers via SEC because of negative interaction of the ionomers with the column material. Therefore, solution viscosity measurements were used as an indirect measure of the molecular weights of the polymer and the ionomers. The inherent viscosities of the pure POBA polymer and the POBA ionomers were found to be between 0.75 and 0.78 g dL^{-1} via solution viscosity measurements. The crystallization half-times were determined via non-isothermal crystallization experiments and the crystallization half-times of the POBA ionomers containing 2.5 and 5 mol% of the sulfonated comonomer were higher than the pure POBA homopolymer. The crystallization half-time for the pure POBA homopolymer and POBA ionomers containing 2.5 mol% of the sulfonated comonomer at a cooling rate of 2.5 °C/min were 1.25 and 1.62 min, respectively. The decrease in the rate of crystallization upon adding 2.5 mol% of ionic content to the homopolymer via copolymerization is attributed to the formation of ionic aggregates that restrict polymer chain mobility upon cooling from the melt.

The tensile properties of POBA and the POBA ionomers were evaluated. The tensile properties of the homopolymer and ionomers are summarized in Table I-2.

Table I-2. Tensile Properties of POBA and POBA ionomers.
Reprinted from Materials Science and Engineering:A Vol 527, Issues 18-19, Jung Seop Lim, and Jong Hoon Kim, Effects of ionic substitution on physical properties, and crystallization rates of, poly(oxyethylene-b-butylene adipate) ionomers, 4641-4645, Copyright 2010, with permission from Elsevier.

Samples	Stress at Break (MPa)	Elongation at Break (%)	Modulus (MPa)
POBA-2.5	23.0 ± 0.35	400 ± 6.1	160 ± 2.4
POBA-2.5	32.9 ± 0.46	599 ± 8.4	155 ± 2.2
POBA-5	17.9 ± 0.32	209 ± 3.8	125 ± 2.3

There is an increase in the stress at break, elongation at break, and modulus of the ionomer containing 2.5 mol% of the comonomer. However, upon increasing the concentration of ionic content to 5 mol%, the tensile properties decrease to values below that of the POBA homopolymer. The improvement in the tensile properties at the lower ionic content of 2.5 mol% is attributed to the development of physical crosslinks that provide additional mechanical integrity to the system. Lim and Kim report that the decrease in the tensile properties of the 5 mol% POBA ionomer suggests that above a critical ionomer concentration that the physical crosslinks created through ion pair associations do not provide additional mechanical strength to the overall semicrystalline ionomer system. However, it must be noted that mechanical properties are directly affected by the molecular weight of the polymer and any changes in the mechanical properties of the polymer may be attributed to differences in molecular weight. Although the Lim and Kim utilized viscosity measurements as an indirect measure of molecular weight, the differences in the mechanical behavior of the ionomers may potentially be due to changes in molecular weight as well.

Sulfonated Syndiotactic Polystyrene as a Model Semicrystalline Ionomer

Many of the commercially-available semicrystalline ionomers such as Nafion® and Surlyn® as well as polyester based ionomers are produced via copolymerization and as a result it is very difficult to control the molecular weight of the ionomers as the ionic content is varied. Therefore, it is challenging to utilize many of these systems as model semicrystalline ionomers within investigations to determine the effect of ionic aggregation on the crystallization behavior of the ionomers. Orler and coworkers circumvented this problem by utilizing randomly sulfonated syndiotactic polystyrene as a model semicrystalline ionomer [253]. They suggested that ionomers based upon syndiotactic polystyrene (sPS) would be ideal candidates for fundamental semicrystalline ionomer studies due to the simplicity of the structure of the hydrophobic backbone, the rapid crystallization rate of the sPS homopolymer, high melting temperature, and well-defined and readily characterized crystalline nature of the homopolymer. Moreover, the most attractive incentive to using sPS as a model semicrystalline ionomer was that a very mild post-polymerization sulfonation method had been developed for atatic polystyrene which maintained both the molecular weight and molecular weight distribution of the parent homopolymer [254-255]. Therefore, the ionic content can be systematically varied without degradation of the homopolymer. Additionally, because a significant amount of research had been completed on the properties and behavior of sulfonated atactic polystyrene (SaPS), it would be very interesting to compare the differences in the morphologies and properties of the amorphous ionomer to the semicrystalline ionomer.

Orler and coworkers conducted a series of studies that explored the effect of the degree of sulfonation [253] and choice of neutralizing counterion [89] and plasticization agent [88] on the

ionic aggregation and crystallization behavior of SsPS ionomers. The reaction scheme for the sulfonation of sPS is shown in Figure I-19.

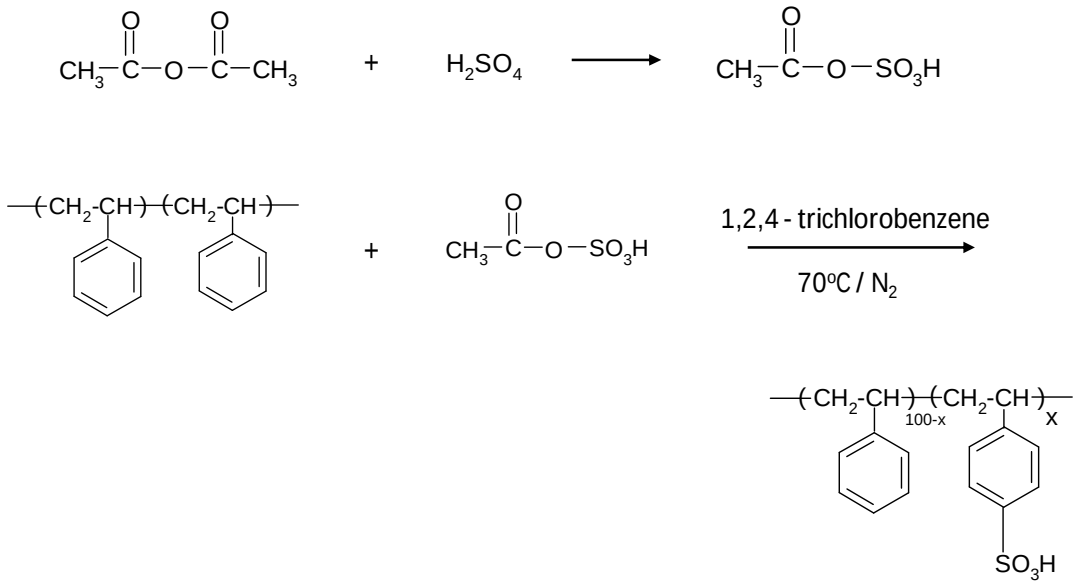

Figure I-19. Post-polymerization sulfonation of syndiotactic polystyrene using acetic acid and sulfuric acid.

It was found the incorporation of the small concentrations of sulfonate groups dramatically affected the thermal properties and crystallization of sPS as shown in Table I-3.

Table I-3. Thermal Properties of sPS and SsPS Ionomers
Reprinted from Macromolecules 26(19), 5157. Copyright 1993 American Chemical Society.

Sample	T_g (°C)	T_m (°C)	ΔH_f (J/g)	X_c (%)	T_c (°C)	ΔH_c (J/g)
pure sPS	99	269	22.4	27	-----	-----
0.5 mol% SsPS	102	264	20	24	-----	-----
2.0 mol% SsPS	101	254	17.7	21	177	13.5
3.4 mol% SsPS	104	249	10.3	12	194	9.6

The evaluation of the thermal properties of lightly sulfonated SsPS ionomers via DSC reveal that with increasing ionic content that there is an increase in the glass transition and decreases in the melting temperature and degree of crystallinity. The decrease in the melting temperature of the SsPS ionomers is directly attributed to the formation of ionic aggregates which inhibit chain mobility during the crystallization process and result in the formation of smaller crystallites which melt at lower temperatures than the corresponding homopolymer. The increase in the glass transition of the matrix of the SsPS ionomers is attributed to the formation of ionic aggregates as well which restrict chain mobility as one polymer chain may traverse both ionic and amorphous regions of the ionomer.

The crystallization kinetics of sPS is also significantly altered by the incorporation of ionic groups and choice of neutralizing counterion. Orler and Moore studied the isothermal crystallization kinetics of sPS and SsPS neutralized with different alkali metal counterions and found that the crystallization half-time significantly increased with increasing degree of sulfonation and decreasing counterion size [89]. The crystallization half-time for the sPS homopolymer at 235 °C was 1.3 min while the crystallization half-time increased for SsPS

containing 2 mol% of sulfonate groups. The crystallization half-time for SsPS containing 2.0 mol% sulfonate groups neutralized with cesium and potassium alkali metal counterions was found to be 19 and 40 minutes, respectively. The drastic decrease in the rate of crystallization of the ionomers compared to the sPS homopolymer is attributed to the electrostatic interactions within the ionic aggregates that restrict chain mobility during crystallization from the melt state. The much slower crystallization kinetics of the potassium neutralized SsPS ionomer as compared to the cesium neutralized ionomer is attributed to the presence of stronger electrostatic interactions between the smaller potassium counterion and the SO^{3-} group. Moreover, Orler and coworkers noticed that the ability of sPS chains to crystallize on a readily observable timescale was essentially destroyed at degrees of sulfonation above 3.4 mol%.

Research Objectives

The profound reduction of the ability of sPS to crystallize in the presence of low concentrations of ionic content can be considered to be somewhat of a negative drawback to utilizing sPS to prepare a semicrystalline ionomer. There are many cases when it is desirable to introduce ionic functionality to a hydrophobic polymer to render the polymer hydrophilic, but yet maintain the ability of the polymer to crystallize as it is generally accepted and known that the presence of a crystalline component may add mechanical and thermal stability to a polymer and enhanced properties in other areas as well.

Therefore, there is a need to explore methods to partially restore the ability of SsPS ionomers to crystallize in the presence of ionic aggregates. Two approaches will be employed to enhance the rate of crystallization and increase the overall degree of crystallinity of SsPS ionomers.

The first method that will be explored to enhance the rate of crystallization of SsPS ionomers is through the incorporation of an external component to the SsPS matrix using montmorillonite clay. The incorporation of the clay has a two-fold purpose: (1) to disrupt the electrostatic network (2) and to increase chain mobility in addition to acting heterogeneous nucleation sites within the ionomer matrix to increase the rate of crystallization of the SsPS ionomer. We will utilize nanoscale montmorillonite clay platelets as a means to disrupt the electrostatic network and provide points of attachment for polymer chains to begin to crystallize upon cooling from the molten state. Montmorillonite clay platelets have been studied in great detail and have been incorporated within many different polymer matrices in order to improve a wide array of polymer properties. The goal is to incorporate small concentrations of pristine montmorillonite clay and organically-modified clay into lightly sulfonated sPS and evaluate the effect of clay type, concentration, and degree of dispersion on the rate of crystallization and crystallization mechanisms of SsPS using differential scanning calorimetry, wide-angle X-ray diffraction, transmission electron microscopy, polarized light microscopy, and small angle laser light scattering.

The second method will be to conduct an internal modification of the SsPS ionomer itself through a manipulation of the SsPS ionomer architecture. The post-polymerization sulfonation of sPS while in a homogeneous solution state utilized by Orler and coworkers results in the formation of a random SsPS containing the sulfonic acid groups located in a random manner along the sPS backbone [253]. It is proposed that a blocky type of SsPS ionomer architecture which maintains long sequences of unsulfonated homopolymer will crystallize more rapidly than randomly sulfonated sPS. However, most block ionomers are produced using complex

copolymerization techniques and it is often difficult to control the molecular weight and polydispersity of the ionomer when varying the ionic content.

A post-polymerization sulfonation of sPS while it is in the gel state will be conducted in order to prepare an SsPS ionomer with a non-random, pseudo-block architecture that contains relatively longer sequences of unsulfonated sPS chains that may readily pack into crystalline structures at a much more rapid rate than randomly sulfonated sPS. Figure I-21 contains a schematic of the non-random sulfonation process.

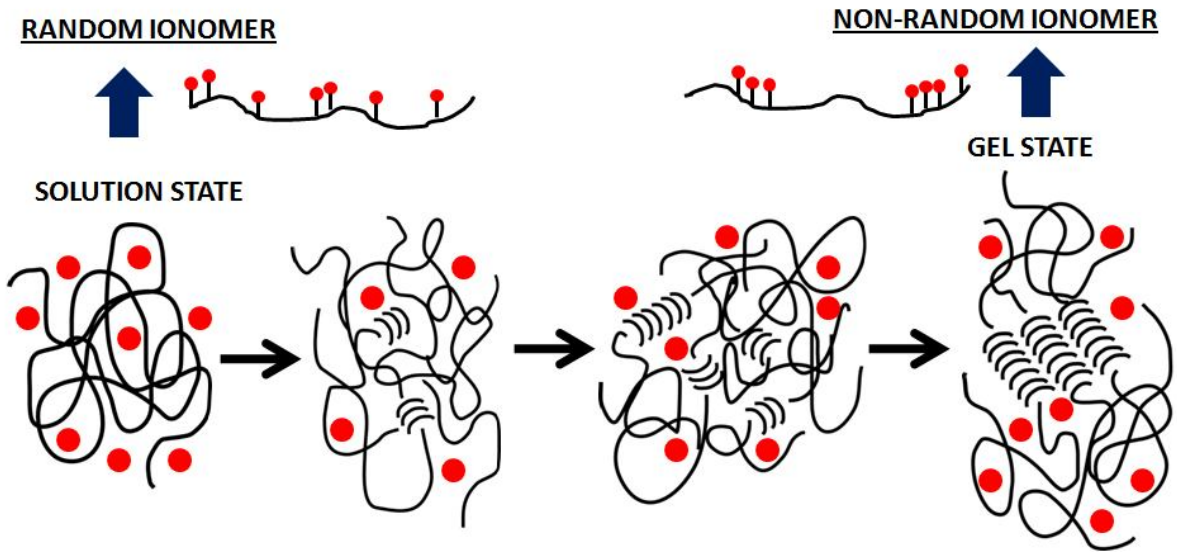

Figure I-20. Schematic of post-polymerization sulfonation of sPS in the homogeneous solution state (far right) and upon crystallization into the physical gel state (far right). The red circles represent sulfonic acid groups.

Conducting the sulfonation process while sPS in the physical gel state results in the exclusion of the acetyl sulfate reagent from the crystalline domains because the reagent is too large to be accommodated in the crystalline regions thereby resulting in the preferential sulfonation of the amorphous regions.

The crystallization behavior and morphology of sPS sulfonated in the solution and gel states will be characterized using DSC, PLM, and SALLS.

REFERENCES

1. Eisenberg A and Kim J. Introduction to ionomers: Wiley, 1998.
2. Tant M, Mauritz K, and Wilkes G. Ionomers: synthesis, structure, properties, and applications: Blackie Academic & Professional, 1997.
3. Pineri M, Eisenberg A, and Division NATOSA. Structure and properties of ionomers: D. Reidel Pub. Co., 1987.
4. Schlick S. Ionomers: characterization, theory, and applications: CRC Press, 1996.
5. Capek I. Advances in Colloid and Interface Science 2004;112(1-3):1-29.
6. Capek I. Advances in Colloid and Interface Science 2005;118(1-3):73-112.
7. Grady BP. Polymer Engineering & Science 2008;48(6):1029-1051.
8. Lee J-W, Kim C-H, Park J-K, and Hwang T-S. Polymer International 1998;45(1):47-54.
9. Kalfoglou NK, Skafidas DS, and Sotiropoulou DD. Polymer 1994;35(17):3624-3630.
10. Retolaza A, Eguiazábal JI, and Nazábal J. Journal of Applied Polymer Science 2003;87(8):1322-1328.
11. Dutta D, Weiss RA, and He J. Polymer 1996;37(3):429-435.
12. Gemeinhardt GC, Moore AA, and Moore RB. Polymer Engineering & Science 2004;44(9):1721-1731.
13. Son Y and Weiss RA. Journal of Applied Polymer Science 2003;87(3):564-568.
14. Abad MJ, Ares A, Barral L, and Eguiazábal JI. Polymer International 2005;54(4):673-678.
15. Leewajanakul P, Pattanaolarn R, Ellis JW, Nithitanakul M, and Grady BP. Journal of Applied Polymer Science 2003;89(3):620-629.
16. Bhattacharyya AR, Ghosh AK, and Misra A. Polymer 2003;44(5):1725-1732.
17. Gemeinhardt GC and Moore RB. Macromolecules 2005;38(7):2813-2819.

18. Shelat KJ, Dutta NK, and Choudhury NR. Langmuir 2008;24(10):5464-5473.

19. Papadopoulou CP and Kalfoglou NK. Polymer 1998;39(26):7015-7021.

20. Papadopoulou CP and Kalfoglou NK. Polymer 1999;40(4):905-911.

21. Samios CK and Kalfoglou NK. Polymer 1999;40(17):4811-4819.

22. Vallejo FJ, Eguiazábal JI, and Nazábal J. Polymer 2000;41(16):6311-6321.

23. Bazuin CG, Rancourt L, Villeneuve S, and Soldera A. Journal of Polymer Science Part B: Polymer Physics 1993;31(10):1431-1440.

24. Iyer S and Schiraldi DA. Journal of Polymer Science Part B: Polymer Physics 2006;44(15):2091-2103.

25. Elley–Bristow DM, Bellinger MA, Sauer JA, and Hara M. Journal of Polymer Science Part B: Polymer Physics 1999;37(18):2705-2710.

26. Belfiore LA, Shah RJ, and Cheng C. Polymer Composites 1989;10(2):122-133.

27. Compston P and Cantwell WJ. Journal of Materials Science Letters 2001;20(6):509-512.

28. Gao Y, Choudhury NR, and Dutta NK. Journal of Applied Polymer Science 2010;117(6):3395-3405.

29. Parent JS, Liskova A, and Resendes R. Polymer 2004;45(24):8091-8096.

30. Smitha B, Sridhar S, and Khan AA. Journal of Membrane Science 2005;259(1-2):10-26.

31. Barbir F. PEM Fuel Cells. In: Sammes N, editor. Fuel Cell Technology: Springer London, 2006. pp. 27-51.

32. Kerres JA. Journal of Membrane Science 2001;185(1):3-27.

33. Neburchilov V, Martin J, Wang H, and Zhang J. Journal of Power Sources 2007;169(2):221-238.

34. DeLuca NW and Elabd YA. Journal of Polymer Science Part B: Polymer Physics 2006;44(16):2201-2225.

35. Jagur-Grodzinski J. Polymers for Advanced Technologies 2007;18(10):785-799.

36. Peighambardoust SJ, Rowshanzamir S, and Amjadi M. International Journal of Hydrogen Energy 2010;35(17):9349-9384.

37. Zaidi SMJ and Matsuura T. Polymer Membranes for Fuel Cells. New York: Spring Science + Business Media, LLC, 2009.

38. Aldebert P, Dreyfus B, and Pineri M. Macromolecules 1986;19(10):2651-2653.

39. Batra A, Cohen C, and Duncan TM. Macromolecules 2006;39(6):2398-2404.

40. Bodycomb J and Hara M. Macromolecules 1994;27(25):7369-7377.

41. Bodycomb J and Hara M. Macromolecules 1995;28(24):8190-8197.

42. Hara M and Jar PY. Macromolecules 1988;21(11):3187-3190.

43. Hara M, Wu J, and Lee AH. Macromolecules 1988;21(7):2214-2218.

44. Hara M, Wu J, and Lee AH. Macromolecules 1989;22(2):754-757.

45. Hara M and Wu JL. Macromolecules 1988;21(2):402-407.

46. Natansohn A and Eisenberg A. Macromolecules 1987;20(2):323-329.

47. Nomula S and Cooper SL. Macromolecules 2001;34(8):2653-2659.

48. Wu C, Woo K, and Jiang M. Macromolecules 1996;29(16):5361-5367.

49. Zhou NC, Burghardt WR, and Winey KI. Macromolecules 2007;40(17):6401-6405.

50. Zhou Z, Chu B, Wu G, and Peiffer DG. Macromolecules 1993;26(11):2968-2973.

51. Parent JS, Penciu A, Guillén-Castellanos SA, Liskova A, and Whitney RA. Macromolecules 2004;37(20):7477-7483.

52. Wu JL, Wang YM, Hara M, Granville M, and Jerome RJ. Macromolecules 1994;27(5):1195-1200.

53. Hara M, Jar PY, and Sauer JA. Macromolecules 1988;21(11):3183-3186.

54. Hara M, Jar P, and Sauer JA. Macromolecules 1990;23(20):4465-4469.

55. Hara M, Jar P, and Sauer JA. Macromolecules 1990;23(23):4964-4969.

56. Weiss RA and Yu W-C. Macromolecules 2007;40(10):3640-3643.

57. Douglas EP, Waddon AJ, and MacKnight WJ. Macromolecules 1994;27(15):4344-4352.

58. Barbi V, Funari SS, Gehrke R, Scharnagl N, and Stribeck N. Polymer 2003;44(17):4853-4861.

59. Kusoglu A, Karlsson AM, and Santare MH. Polymer 2010;51(6):1457-1464.

60. Scogna RC and Register RA. Polymer 2009;50(2):585-590.

61. Takahashi T, Watanabe J, Minagawa K, and Koyama K. Polymer 1994;35(26):5722-5728.

62. Termonia Y. Polymer 2007;48(5):1435-1440.

63. Xie H and Feng Y. Polymer 1988;29(7):1216-1220.

64. Oh S-H, Kim J-S, and Shin K. Polymer 2004;45(10):3313-3319.

65. He L, Fujimoto CH, Cornelius CJ, and Perahia D. Macromolecules 2009;42(18):7084-7090.

66. Yarusso DJ and Cooper SL. Macromolecules 1983;16(12):1871-1880.

67. Macknight WJ, Taggart WP, and Stein RS. Journal of Polymer Science: Polymer Symposia 1974;45(1):113-128.

68. Eisenberg A. Macromolecules 1970;3(2):147-154.

69. Eisenberg A, Hird B, and Moore RB. Macromolecules 1990;23(18):4098-4107.

70. Hird B and Eisenberg A. Macromolecules 1992;25(24):6466-6474.

71. Tierney NK and Register RA. Macromolecules 2002;35(6):2358-2364.

72. Weiss RA, Sen A, Pottick LA, and Willis CL. Polymer 1991;32(15):2785-2792.

73. Page KA, Cable KM, and Moore RB. Macromolecules 2005;38(15):6472-6484.

74. Kim J-S, Hong M-C, and Nah YH. Macromolecules 2001;35(1):155-160.

75. Kim S-H and Kim J-S. Macromolecules 2003;36(7):2382-2386.

76. Kim J-S, Hwa Nah Y, and Jarng S-S. Polymer 2001;42(13):5567-5571.

77. Leibler L, Rubinstein M, and Colby RH. Macromolecules 1991;24(16):4701-4707.

78. Wang F, Hickner M, Kim YS, Zawodzinski TA, and McGrath JE. Journal of Membrane Science 2002;197(1-2):231-242.

79. O'Gara JF, Williams DJ, Macknight WJ, and Karasz FE. Journal of Polymer Science Part B: Polymer Physics 1987;25(7):1519-1536.

80. Roy A, Hickner MA, Einsla BR, Harrison WL, and McGrath JE. Journal of Polymer Science Part A: Polymer Chemistry 2009;47(2):384-391.

81. Ro AJ, Huang SJ, and Weiss RA. Polymer 2009;50(5):1134-1143.

82. Weiss RA, Lundberg RD, and Turner SR. Journal of Polymer Science: Polymer Chemistry Edition 1985;23(2):549-568.

83. Turner SR, Weiss RA, and Lundberg RD. Journal of Polymer Science: Polymer Chemistry Edition 1985;23(2):535-548.

84. Weiss RA, Turner SR, and Lundberg RD. Journal of Polymer Science: Polymer Chemistry Edition 1985;23(2):525-533.

85. Wang F, Hickner M, Ji Q, Harrison W, Mecham J, Zawodzinski TA, and McGrath JE. Macromolecular Symposia 2001;175(1):387-396.

86. Okamura H, Takatori Y, Tsunooka M, and Shirai M. Polymer 2002;43(11):3155-3162.

87. Orler EB, Calhoun BH, and Moore RB. Macromolecules 1996;29(18):5965-5971.

88. Orler EB, Gummaraju RV, Calhoun BH, and Moore RB. Macromolecules 1999;32(4):1180-1188.

89. Orler EB and Moore RB. Macromolecules 1994;27(17):4774-4780.

90. Benson SD and Moore RB. Polymer 2010;51(23):5462-5472.

91. Borriello A, Lavorgna M, Malagnino N, Mensitieri G, Napoletano T, and Nicolais L. Macromolecular Symposia 2004;218(1):293-302.

92. Li H-M, Shen Z-G, Zhu F-M, and Lin S-A. European Polymer Journal 2002;38(6):1255-1263.

93. Su Z, Hsu SL, and Li X. Macromolecules 1994;27(1):287-291.

94. Borriello A, Agoretti P, Ambrosio L, Fasano G, Pellegrino M, Venditto V, and Guerra G. Chemistry of Materials 2009;21(14):3191-3196.

95. Li H-M, Liu J-C, Zhu F-M, and Lin S-A. Polymer International 2001;50(4):421-428.

96. Seitz ME, Chan CD, Opper KL, Baughman TW, Wagener KB, and Winey KI. Journal of the American Chemical Society 2010;132(23):8165-8174.

97. Stadler FJ, Pyckhout-Hintzen W, Schumers J-M, Fustin C-A, Gohy J-Fo, and Bailly C. Macromolecules 2009;42(16):6181-6192.

98. Stadler FJ, Still T, Fytas G, and Bailly C. Macromolecules 2010;43(18):7771-7778.

99. Atthoff B, Nederberg F, Hilborn J, and Bowden T. Macromolecules 2006;39(11):3907-3913.

100. Xue H, Bhowmik P, and Schlick S. Macromolecules 1993;26(13):3340-3343.

101. Fontaine F, Ledent J, Sobry R, Francois E, Jerome R, and Teyssie P. Macromolecules 1993;26(6):1480-1482.

102. Charlier P, Jerome R, Teyssie P, and Utracki LA. Macromolecules 1992;25(10):2651-2656.

103. Charlier P, Jerome R, Teyssie P, and Utracki LA. Macromolecules 1992;25(2):617-624.

104. Eicke HF, Gauthier M, Hilfiker R, Struis RPWJ, and Xu G. The Journal of Physical Chemistry 1992;96(12):5175-5179.

105. Register RA, Cooper SL, Thiyagarajan P, Chakrapani S, and Jerome R. Macromolecules 1990;23(11):2978-2983.

106. Venkateshwaran LN, Tant MR, Wilkes GL, Charlier P, and Jerome R. Macromolecules 1992;25(15):3996-4001.

107. Atiqur Rahman S, Kitao H, and Nemoto N. Polymer 2004;45(13):4523-4532.

108. Bagrodia S, Tant MR, Wilkes GL, and Kennedy JP. Polymer 1987;28(13):2207-2226.

109. Essahli M, Colomines G, Monge S, Robin J-J, Collet A, and Boutevin B. Polymer 2008;49(21):4510-4518.

110. Ro AJ, Huang SJ, and Weiss RA. Polymer 2008;49(2):422-431.

111. Vlaic G, Williams CE, Jérome R, Tant MR, and Wilkes GL. Polymer 1988;29(1):173-176.

112. Mahesh GN, Philip TG, and Radhakrishnan G. Polymer Bulletin 1996;37(6):737-742.

113. Berti C, Colonna M, Binassi E, Fiorini M, Karanam S, and Brunelle DJ. Reactive and Functional Polymers 2010;70(6):366-375.

114. Nguyen D, Zhong X-F, Williams CE, and Eisenberg A. Macromolecules 1994;27(18):5173-5181.

115. Yoshikawa K, Desjardins A, Dealy JM, and Eisenberg A. Macromolecules 1996;29(4):1235-1243.

116. Zhang G, Liu L, Wang H, and Jiang M. European Polymer Journal 2000;36(1):61-68.

117. Nguyen D, Varshney SK, Williams CE, and Eisenberg A. Macromolecules 1994;27(18):5086-5089.

118. Ma Y, Wu G, and Yang W. Journal of Polymer Science Part A: Polymer Chemistry 2003;41(18):2755-2764.

119. Fang Z, Wang S, Wang SQ, and Kennedy JP. Journal of Applied Polymer Science 2003;88(6):1516-1525.

120. Kabanov AV, Bronich TK, Kabanov VA, Yu K, and Eisenberg A. Journal of the American Chemical Society 1998;120(38):9941-9942.

121. Xu S, Tang T, Chen B, and Huang B. Polymer 1999;40(9):2239-2247.

122. Venkateshwaran LN, York GA, DePorter CD, McGrath JE, and Wilkes GL. Polymer 1992;33(11):2277-2286.

123. Elabd YA, Napadensky E, Sloan JM, Crawford DM, and Walker CW. Journal of Membrane Science 2003;217(1-2):227-242.

124. Lu X, Steckle WP, and Weiss RA. Macromolecules 1993;26(24):6525-6530.

125. Loveday D, Wilkes GL, Deporter CD, and McGrath JE. Macromolecules 1995;28(23):7822-7830.

126. Elabd YA and Napadensky E. Polymer 2004;45(9):3037-3043.

127. Xie H-Q, Liu D-G, and Xie D. Journal of Applied Polymer Science 2005;96(4):1398-1404.

128. Sangeetha D. European Polymer Journal 2005;41(11):2644-2652.

129. Weiss RA, Sen A, Willis CL, and Pottick LA. Polymer 1991;32(10):1867-1874.

130. Badami Anand S, Lee H-S, Li Y, Roy A, Wang H, and McGrath James E. Molecular Weight Effects on Poly(arylene ether sulfone)-Based Random and Multiblock Copolymers Characteristics for Fuel Cells. Fuel Cell Chemistry and Operation, vol. 1040: American Chemical Society, 2010. pp. 65-81.

131. Bae B, Miyatake K, and Watanabe M. Macromolecules 2010;43(6):2684-2691.

132. Bai Z, Yoonessi M, Juhl SB, Drummy LF, Durstock MF, and Dang TD. Macromolecules 2008;41(23):9483-9486.

133. Ghassemi H, Ndip G, and McGrath JE. Polymer 2004;45(17):5855-5862.

134. Higashihara T, Matsumoto K, and Ueda M. Polymer 2009;50(23):5341-5357.

135. Lee H-S, Roy A, Lane O, Dunn S, and McGrath JE. Polymer 2008;49(3):715-723.

136. Lee M, Park JK, Lee H-S, Lane O, Moore RB, McGrath JE, and Baird DG. Polymer 2009;50(25):6129-6138.

137. Li N, Liu J, Cui Z, Zhang S, and Xing W. Polymer 2009;50(19):4505-4511.

138. Roy A, Lee H-S, and McGrath JE. Polymer 2008;49(23):5037-5044.

139. Takimoto N, Wu L, Ohira A, Takeoka Y, and Rikukawa M. Polymer 2009;50(2):534-540.

140. Roy A, Yu X, Dunn S, and McGrath JE. Journal of Membrane Science 2009;327(1-2):118-124.

141. Badami AS, Lane O, Lee H-S, Roy A, and McGrath JE. Journal of Membrane Science 2009;333(1-2):1-11.

142. Badami AS, Roy A, Lee H-S, Li Y, and McGrath JE. Journal of Membrane Science 2009;328(1-2):156-164.

143. Dwight DW, McGrath JE, Riffle JS, Smith SD, and York GA. Journal of Electron Spectroscopy and Related Phenomena 1990;52:457-473.

144. Ghassemi H, McGrath JE, and Zawodzinski JTA. Polymer 2006;47(11):4132-4139.

145. Lee H-S, Lane O, and McGrath JE. Journal of Power Sources 2010;195(7):1772-1778.

146. Li Y, Roy A, Badami AS, Hill M, Yang J, Dunn S, and McGrath JE. Journal of Power Sources 2007;172(1):30-38.

147. Risch BG, Rodrigues DE, Lyon K, McGrath JE, and Wilkes GL. Polymer 1996;37(7):1229-1242.

148. Robeson LM, Hwu HH, and McGrath JE. Journal of Membrane Science 2007;302(1-2):70-77.

149. Roy A, Hickner MA, Lane O, and McGrath JE. Journal of Power Sources 2009;191(2):550-554.

150. Takimoto N, Takamuku S, Abe M, Ohira A, Lee H-S, and McGrath JE. Journal of Power Sources 2009;194(2):662-667.

151. Hickner MA and Pivovar BS. Fuel Cells 2005;5(2):213-229.

152. Lundberg R D and Makowski H S. A Comparison of Sulfonate and Carboxylate Ionomers. Ions in Polymers, vol. 187: AMERICAN CHEMICAL SOCIETY, 1980. pp. 21-36.

153. Gil M, Ji X, Li X, Na H, Eric Hampsey J, and Lu Y. Journal of Membrane Science 2004;234(1-2):75-81.

154. Gorda KR and Peiffer DG. Journal of Polymer Science Part B: Polymer Physics 1992;30(3):281-292.

155. Chisholm BJ, Sisti L, Soloveichik S, and Gillette G. Polymer 2003;44(6):1903-1910.

156. Chisholm BJ, Richards WD, Banach TE, Soloveichik S, Kelley JF, Bradtke GR, and Dhawan S. Journal of Applied Polymer Science 2006;100(6):4762-4771.

157. Lim JS, Lee Y, and Im SS. Journal of Polymer Science Part B: Polymer Physics 2008;46(10):925-937.

158. Timm DA and Hsieh Y-L. Journal of Polymer Science Part B: Polymer Physics 1993;31(12):1873-1883.

159. Gaona O, Kint DPR, MartInez de Ilarduya A, Alla A, Bou J, and Muñoz-Guerra S. Polymer 2003;44(24):7281-7289.

160. Iojoiu C, Maréchal M, Chabert F, and Sanchez JY. Fuel Cells 2005;5(3):344-354.

161. Navratil M and Eisenberg A. Macromolecules 1974;7(1):84-89.

162. Robila G, Buruiana T, and Buruiana EC. European Polymer Journal 1999;35(7):1305-1311.

163. Hensley JE and Way JD. Chemistry of Materials 1980;19(18):4576-4584.

164. Tierney NK, Trzaska ST, and Register RA. Macromolecules 1980;37(26):10205-10207.

165. Li M, Jiang M, Zhu L, and Wu C. Macromolecules 1997;30(7):2201-2203.

166. Poppe D, Frey H, Kreuer KD, Heinzel A, and Mülhaupt R. Macromolecules 2002;35(21):7936-7941.

167. Kakati DK and George MH. Polymer 1993;34(20):4319-4324.

168. Jayakumar R, Nanjundan S, and Prabaharan M. Reactive and Functional Polymers 2006;66(3):299-314.

169. Wu Q and Weiss RA. Polymer 2007;48(26):7558-7566.

170. Bazuin CG and Eisenberg A. Journal of Polymer Science Part B: Polymer Physics 1986;24(5):1137-1153.

171. Okkema AZ and Cooper SL. Biomaterials 1991;12(7):668-676.

172. Suchocka-Gałaś K. Journal of Applied Polymer Science 2005;96(2):268-275.

173. Hourston DJ, Williams GD, Satguru R, Padget JC, and Pears D. Journal of Applied Polymer Science 1999;74(3):556-566.

174. Doyle M, Lewittes ME, Roelofs MG, and Perusich SA. The Journal of Physical Chemistry B 2001;105(39):9387-9394.

175. Kim J-S, Yoshikawa K, and Eisenberg A. Macromolecules 1994;27(22):6347-6357.

176. Visser SA and Cooper SL. Macromolecules 1991;24(9):2576-2583.

177. Hensley JE and Way JD. Chemistry of Materials 2007;19(18):4576-4584.

178. Hensley JE and Way JD. Journal of Power Sources 2007;172(1):57-66.

179. Weiss RA, Agarwal PK, and Lundberg RD. Journal of Applied Polymer Science 1984;29(9):2719-2734.

180. Cable KM, Mauritz KA, and Moore RB. Journal of Polymer Science Part B: Polymer Physics 1995;33(7):1065-1072.

181. Landis FA and Moore RB. Macromolecules 2000;33(16):6031-6041.

182. Hara M, Lee AH, and Wu J. Journal of Polymer Science Part B: Polymer Physics 1987;25(7):1407-1418.

183. Agarwal PK, Garner RT, and Graessley WW. Journal of Polymer Science Part B: Polymer Physics 1987;25(10):2095-2111.

184. Ng CWA and MacKnight WJ. Macromolecules 1996;29(7):2421-2429.

185. Phillips AK and Moore RB. Journal of Polymer Science Part B: Polymer Physics 2006;44(16):2267-2277.

186. Bellinger MA, Sauer JA, and Hara M. Polymer 1994;35(25):5478-5482.

187. Batra A, Cohen C, Kim H, Winey KI, Ando N, and Gruner SM. Macromolecules 2006;39(4):1630-1638.

188. Chen Y and Chen Y-L. Journal of Applied Polymer Science 1992;46(3):435-443.

189. Yang J-E, Kong J-S, Park S-W, Lee D-J, and Kim H-D. Journal of Applied Polymer Science 2002;86(9):2375-2383.

190. Ohtani N, Inoue Y, Kaneko Y, and Okumura S. Journal of Polymer Science Part A: Polymer Chemistry 1995;33(14):2449-2454.

191. Nishiyama Y and Satoh M. Macromolecular Rapid Communications 2000;21(4):174-177.

192. Atorngitjawat P and Runt J. Macromolecules 2007;40(4):991-996.

193. Taylor EP, Landis FA, Page KA, and Moore RB. Polymer 2006;47(21):7425-7435.

194. Hirasawa E, Yamamoto Y, Tadano K, and Yano S. Journal of Applied Polymer Science 1991;42(2):351-362.

195. Feng Y, Karim A, Weiss RA, Douglas JF, and Han CC. Macromolecules 1998;31(2):484-493.

196. Bagrodia S and Wilkes GL. Polymer Bulletin 1984;12(5):389-392.

197. Lefelar JA and Weiss RA. Macromolecules 1984;17(6):1145-1148.

198. O'Connell EM, Root TW, and Cooper SL. Macromolecules 1994;27(20):5803-5810.

199. Nanda AK and Wicks DA. Polymer 2006;47(6):1805-1811.

200. Kim H. The Journal of Physical Chemistry B 2009;113(28):9359-9363.

201. Tsujita Y, Yasuda M, Takei M, Kinoshita T, Takizawa A, and Yoshimizu H. Macromolecules 2001;34(7):2220-2224.

202. Wang W, Chan T-T, Perkowski AJ, Schlick S, and Winey KI. Polymer 2009;50(5):1281-1287.

203. Nanda AK, Wicks DA, Madbouly SA, and Otaigbe JU. Journal of Applied Polymer Science 2005;98(6):2514-2520.

204. Kim J-S and Eisenberg A. Journal of Polymer Science Part B: Polymer Physics 1995;33(2):197-209.

205. Bonotto S and Bonner EF. Macromolecules 1968;1(6):510-515.

206. Bazuin CG. Plasticization Studies of Ionomers. Multiphase Polymers: Blends and Ionomers, vol. 395: American Chemical Society, 1989. pp. 476-502.

207. Kim JS, Roberts SB, Eisenberg A, and Moore RB. Macromolecules 1993;26(19):5256-5258.

208. Kim J-S, Hong M-C, and Nah YH. Macromolecules 1980;35(1):155-160.

209. Lundberg R D, Makowski H S, and Westerman L. The Dual Plasticization of Sulfonated Polystyrene Ionomer. Ions in Polymers, vol. 187: AMERICAN CHEMICAL SOCIETY, 1980. pp. 67-76.

210. Orler EB, Gummaraju RV, Calhoun BH, and Moore RB. Macromolecules 1980;32(4):1180-1188.

211. Ma X, Sauer JA, and Hara M. Polymer 1997;38(17):4425-4431.

212. Wakabayashi K and Register RA. Polymer 2006;47(8):2874-2883.

213. Mandal UK, Tripathy DK, and De SK. Polymer 1996;37(25):5739-5742.

214. Bazuin CG, Eisenberg A, and Kamal M. Journal of Polymer Science Part B: Polymer Physics 1986;24(5):1155-1169.

215. Tong X and Bazuin CG. Journal of Polymer Science Part B: Polymer Physics 1992;30(4):389-399.

216. Luqman M, Song J-M, Kim J-S, Kwon YJ, Jarng S-S, and Shin K. Polymer 2008;49(7):1871-1878.

217. Kim J-W, Song J-M, Cho Y-J, Kim J-S, and Yu J-A. Polymer 2006;47(3):871-877.

218. Varley RJ, Shen S, and van der Zwaag S. Polymer 2010;51(3):679-686.

219. Register RA and Cooper SL. Macromolecules 1990;23(1):310-317.

220. Hara M, Jar P, and Sauer JA. Polymer 1991;32(9):1622-1626.

221. Ma X, Sauer JA, and Hara M. Macromolecules 1995;28(11):3953-3962.

222. Ma X, Sauer JA, and Hara M. Macromolecules 1995;28(16):5526-5534.

223. Essafi W, Gebel G, and Mercier R. Macromolecules 2003;37(4):1431-1440.

224. Iojoiu C, Chabert F, Maréchal M, Kissi NE, Guindet J, and Sanchez JY. Journal of Power Sources 2006;153(2):198-209.

225. Miyatake K, Chikashige Y, Higuchi E, and Watanabe M. Journal of the American Chemical Society 2007;129(13):3879-3887.

226. Tong X and Bazuin CG. Chemistry of Materials 1992;4(2):370-377.

227. Ma X, Sauer JA, and Hara M. Polymer 1996;37(21):4739-4745.

228. Mensitieri G, Del Nobile MA, and Manfredi C. Packaging Technology and Science 1996;9(4):225-236.

229. Han S-I, Yoo Y, Kim DK, and Im SS. Macromolecular Bioscience 2004;4(3):199-207.

230. Lim J and Kim J. Journal of Materials Science 2009;44(23):6398-6403.

231. Xu T. Journal of Membrane Science 2005;263(1-2):1-29.

232. Bowen WR, Doneva TA, and Yin H. Desalination 2002;145(1-3):39-45.

233. Shahinpoor M and et al. Smart Materials and Structures 1998;7(6):R15.

234. Ugo P, Moretto LM, and Vezzà F. ChemPhysChem 2002;3(11):917-925.

235. Bonomo C and et al. Smart Materials and Structures 2006;15(3):749.

236. Rikukawa M and Sanui K. Progress in Polymer Science 2000;25(10):1463-1502.

237. Longworth R and Vaughan DJ. Nature 1968;218(5136):85-87.

238. Ishida K, Han S-I, Im S-S, and Inoue Y. Macromolecular Chemistry and Physics 2007;208(2):146-154.

239. Wang W, Liu W, Tudryn GJ, Colby RH, and Winey KI. Macromolecules 2010;43(9):4223-4229.

240. Kang H, Lin Q, Armentrout RS, and Long TE. Macromolecules 2002;35(23):8738-8744.

241. Pilati F, Manaresi P, Ruperto MG, Bonora V, Munari A, and Fiorini M. Polymer 1993;34(11):2413-2421.

242. Fragiadakis D, Dou S, Colby RH, and Runt J. The Journal of Chemical Physics 2009;130(6):064907-064911.

243. Lu M, Runt J, and Painter P. Macromolecules 2009;42(17):6581-6587.

244. Connelly RW, McConkey RC, Noonan JM, and Pearson GH. Journal of Polymer Science: Polymer Physics Edition 1982;20(2):259-268.

245. Berti C, Fiorini M, Marchese P, and Sisti L. European Polymer Journal 2007;43(9):3943-3952.

246. Bandiera M, Manaresi P, Munari A, Borghini MC, and Mastragostino M. European Polymer Journal 1997;33(10-12):1679-1683.

247. Xing P, Robertson GP, Guiver MD, Mikhailenko SD, Wang K, and Kaliaguine S. Journal of Membrane Science 2004;229(1-2):95-106.

248. Liu B, Robertson GP, Kim D-S, Guiver MD, Hu W, and Jiang Z. Macromolecules 2007;40(6):1934-1944.

249. Bailly C, Williams DJ, Karasz FE, and MacKnight WJ. Polymer 1987;28(6):1009-1016.

250. Gao Y, Robertson GP, Guiver MD, Mikhailenko SD, Li X, and Kaliaguine S. Macromolecules 2005;38(8):3237-3245.

251. Hickner MA, Ghassemi H, Kim YS, Einsla BR, and McGrath JE. Chemical Reviews 2004;104(10):4587-4612.

252. Lim JS and Kim JH. Materials Science and Engineering: A 2010;527(18-19):4641-4645.

253. Orler EB, Yontz DJ, and Moore RB. Macromolecules 1993;26(19):5157-5160.

254. Makowski HS, Lundberg RD, and Singhal GH. FLEXIBLE POLYMERIC COMPOSITIONS COMPRISING A NORMALLY PLASTIC POLYMER SULFONATED TO ABOUT 0.2 TO ABOUT 10 MOLE % SULFONATE. vol. 3,870,841, 1975.

255. Thaler WA. Macromolecules 1983;16(4):623-628.

CHAPTER II

SYNDIOTACTIC POLYSTYRENE

FROM ENGINEERING THERMOPLASTIC TO ADVANCED FUNCTIONAL MATERIAL

Since the production of syndiotactic polystyrene (sPS) in 1985, there has been a tremendous amount of research focused on the synthesis and characterization of this stereoregular polymer [1-8]. The drive for the investigation of the behavior and properties of sPS is due to the high melting temperature, rapid crystallization rate which is several orders of magnitude higher than isotactic polystyrene [9], solvent resistance, and good electrical properties [10-11]. Since sPS is the base homopolymer that is utilized to produce sulfonated syndiotactic polystyrene ionomers, it is important to review the basic properties of this semicrystalline polymer with emphasis placed on its crystalline structure and morphology.

Research into the crystallization behavior of syndiotactic polystyrene has revealed that sPS exhibits an extremely complex polymorphic behavior that is highly dependent upon processing conditions. There are two main types of crystalline structures that have been identified. The all-trans crystal structure (T_4) is obtained under melt processing conditions while the helical crystal structure (T_2G_2) is formed as a result of solvent induced crystallization. Figure II-1 depicts the arrangement of sPS in the all-trans, planar zig-zag structure (T_4) and the helical (T_2G_2) polymorph which are formed as a result of thermal or solvent induced crystallization, respectively.

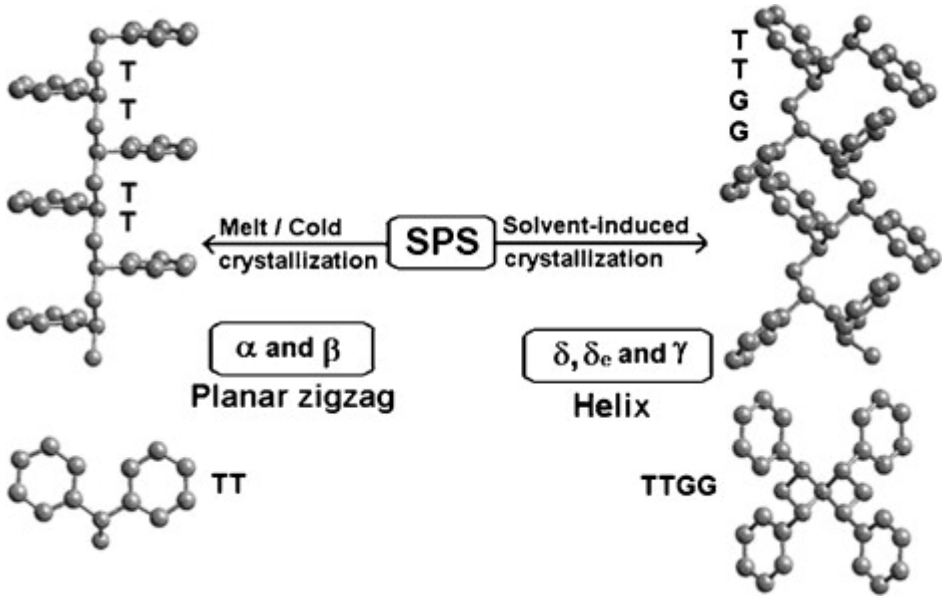

Figure II-1. Molecular chain conformations of the crystalline phases of sPS. Reprinted from Progress in Polymer Science, Vol 34, Issue 3, E. Bhoje Gowda, Kohji Tashiroa, and C. Ramesh, Structural phase transitions of syndiotactic polystyrene, 280-315, Copyright 2009, with permission from Elsevier.

A total of five different crystalline polymorphs have been identified: α, β, δ, γ, and ε. the α- and β-crystal polymorphs are obtained under melt processing conditions while the δ- and γ-crystal polymorphs are obtained as a result of solvent induced crystallization. The δ and ε-forms of sPS are clathrate or co-crystalline phases that are able to accommodate small molecules within nanopores of the crystalline lattices created by the chains.

Under certain thermal processing conditions, the presence of either the α-crystal or the β-crystal may dominate, but both the α- and β-crystal structures may coexist in one sample when sPS is processed under certain conditions [5]. The coexistence of the two different crystalline structures is often observed as multiple melting endotherms in the thermal analysis of sPS by differential scanning calorimetry (DSC). Figure II-2 shows the various conversion and processing routes that have been identified for the different sPS polymorphs.

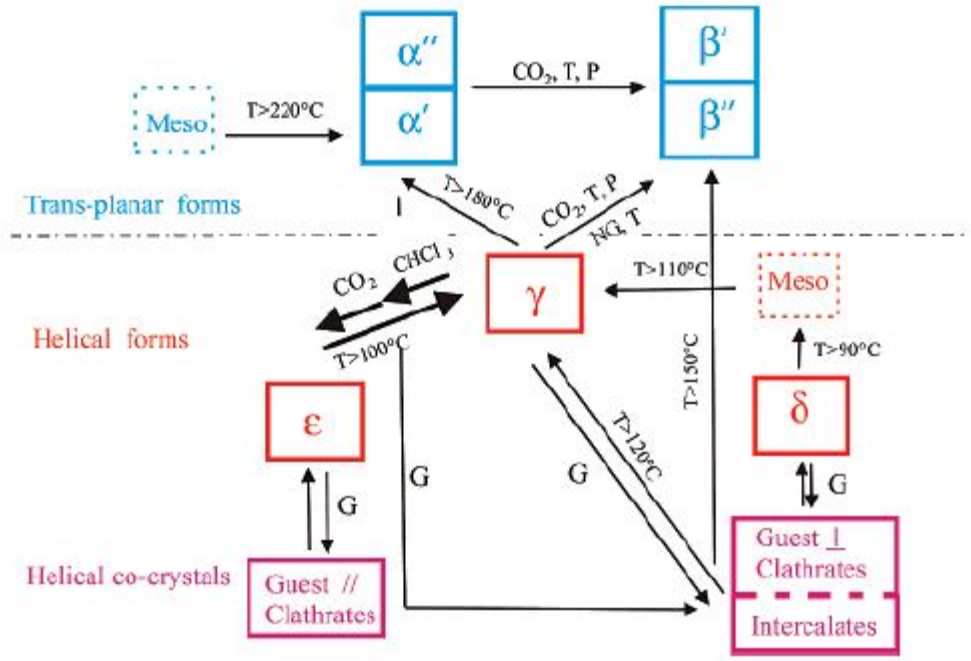

Figure II-2. Schematic representation of the main interconversion conditions for the polymorphic crystalline forms of syndiotactic polystyrene. G and NG stand for molecules which are guests or nonguests of δ- and ε-phases. T and P indicate increases of temperature and pressure, respectively. Reprinted from Macromolecules 40(26), 9470. Copyright 2007 American Chemical Society.

Melt Induced Crystallization of sPS

Two all-trans, planar zig-zag crystalline polymorphs termed the α-crystal and the β-crystal have been identified when sPS is crystallized from the melt state. Thermal history parameters such as maximum melting temperature, residence time in the melt, crystalline form of the starting material, cooling rate from the melt, and crystallization temperature strongly influence the development of crystalline structures of sPS chains and determine which all-trans planar polymorph will be formed [5, 13-14]. The α-crystal form of sPS has also been of significant interest due to the low density of this crystalline form. The α-crystal density is lower than that of the amorphous phase of sPS being 1.033 [15] and 1.046 g/cm^3 [16], respectively.

The lower density of the α-crystal than the amorphous phase is due to the arrangement of the chains which results in unoccupied space that has been proposed to be present as channels or cylinders depending on the α-crystal model [16].

Melt Induced Crystallization of sPS: α-form Crystal Structure

Two models have been proposed for the α-crystal form of sPS. Figure II-3 shows the hexagonal model proposed by Greis and coworkers [17] while Figure II-4 contains the trignoal model for the α-phase proposed by DeRosa and coworkers. There are also two sub-modifications of the α-crystal [18]. There is the limit-ordered sub-modification identified as the α″-modification and the limit-disordered structure that is identified as the α′–modification. Models for the sub-modifications of the α-form proposed by DeRosa are shown in Figure II-5 [19-20]. Schematic A and B of Figure II-5 contain models of the limit-ordered α″-modification while Schematic C of Figure II-5 is a model of the α′–modification.

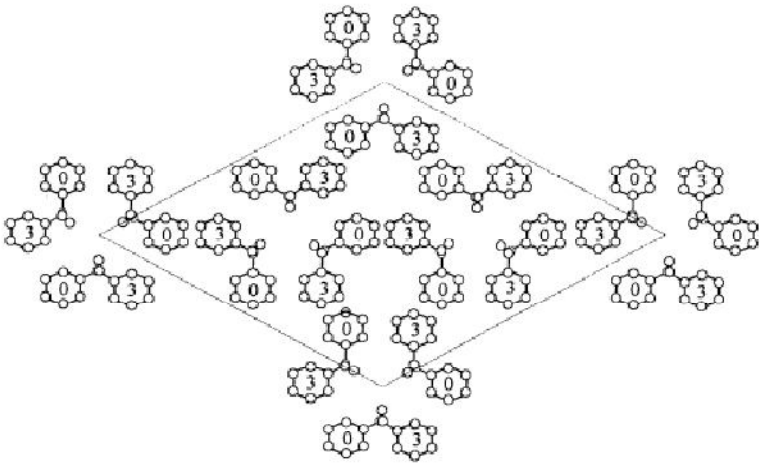

Figure II-3. Hexagonal model of the α-crystal proposed by Greis and coworkers. Reprinted from Progress in Polymer Science, Vol 26, Issue 6, E. M. Woo, Y. S. Sun, and C.P. Yang, Polymorphism, thermal behavior, and crystal stability in syndiotactic polystyrene vs. its miscible blends, 945-983, Copyright 2001, with permission from Elsevier.

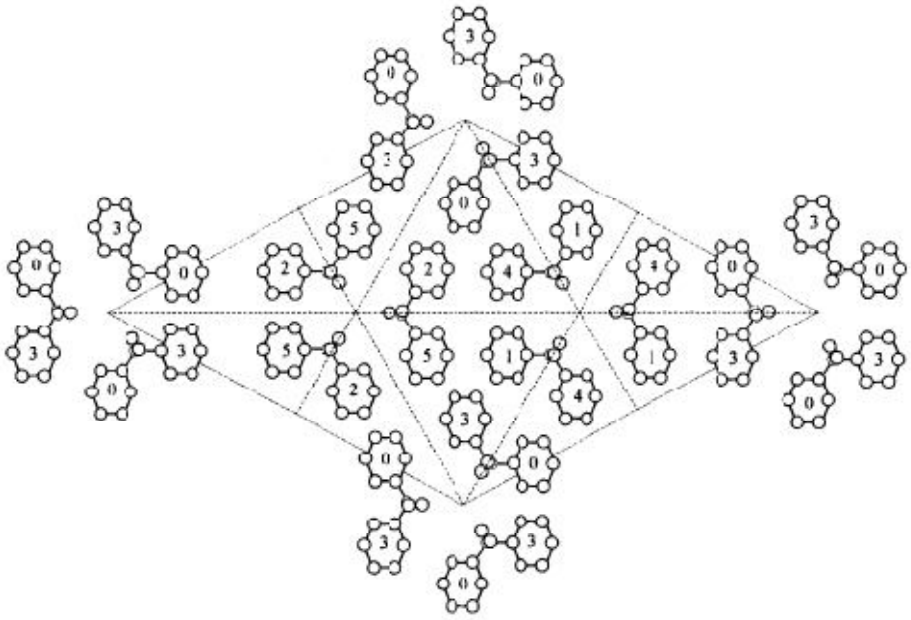

Figure II-4. Trigonal model of the α-crystal structure proposed by De Rosa and coworkers. Reprinted from Polymer Journal Volume 23, Issue 12, 1435-1142, C. DeRosa, G. Guerra, V. Petraccone, and P Corradini, Crystal structure of the α-form of syndiotactic polystyrene with permission from Nature Publishing Group.

The thermally-induced formation of the α-crystal within sPS occurs primarily under the three following conditions: (1) slow cooling from the melt state, (2) crystallization temperatures lower than 230°C, and (3) cold crystallization from the amorphous state [5]. At intermediate isothermal crystallization temperatures between 230 and 260°C, it has been found that both the α and β-crystals coexist within the sPS sample.

Wang and coworkers studied the lamellar morphology and crystal stability of the sPS α-crystal using SAXS, WAXD, TEM, and DSC [21] and found that there is a significant memory effect on the crystallization behavior of sPS as reported by other researchers in the literature [22-23]. It was found that melting sPS in the α-crystal form six degrees above its melting temperature of 274.8 °C was not sufficient to completely melt the α-crystal structure which may

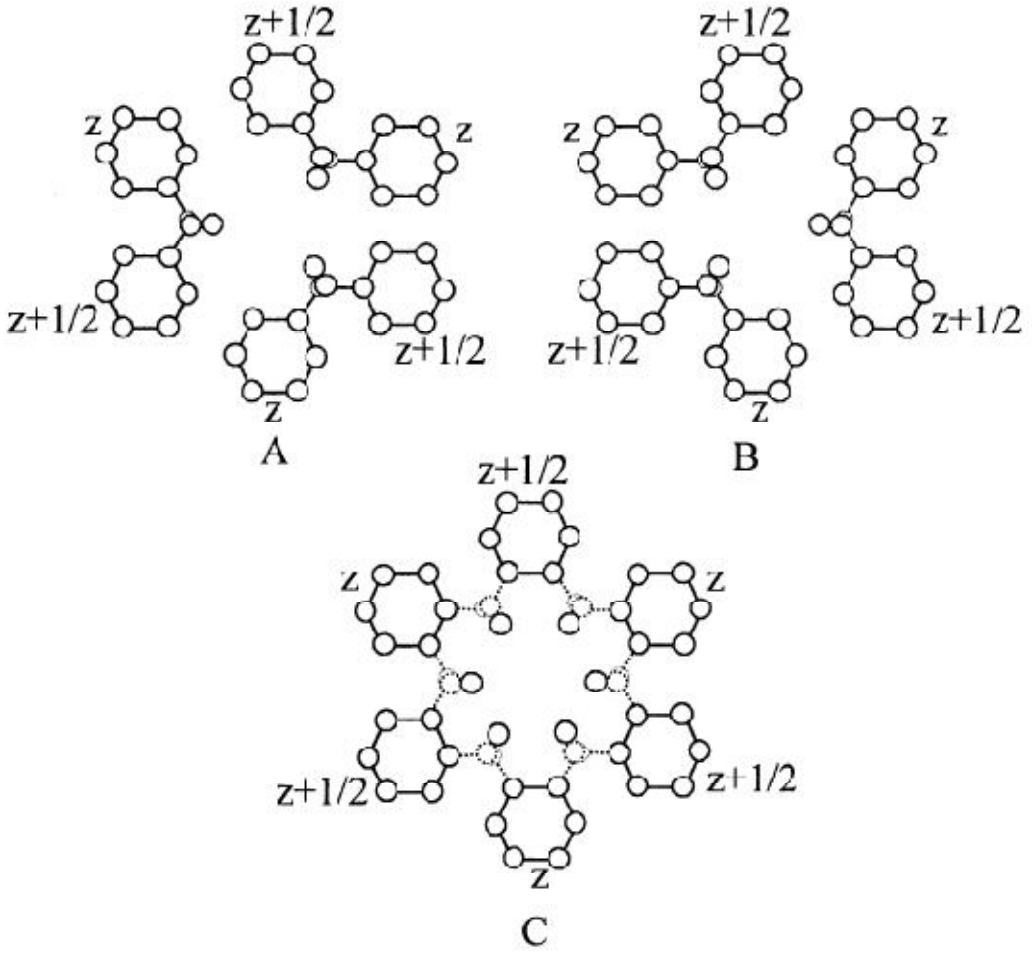

Figure II-5. Two sub-modifications of the sub-modifications for the α-crystal: a limit-ordered α″-modification and a limit-ordered α′-modification. Models for the α″-modification (schematics A and B) and α′-modification (schematic C). Reprinted from Macromolecules 29(26), 8460. Copyright1996 American Chemical Society.

result in the residual, partially-ordered clusters of sPS chains which are able to self-nucleate upon cooling from the melt state. The residual, partially-ordered clusters leads to a self-seeding nucleation process that results in the preferential formation of the α-crystal with only a trace of the β-form crystal at low crystallization temperatures of 200 °C. Upon raising the melting temperature of the initial sPS sample in the α-crystal form room temperature to 300 °C for 10 minutes, there is a greater percentage of the β-form crystal obtained upon crystallization which

suggests the higher melting temperature aids in eliminating the number and size of residual α-crystal nuclei remaining in the melt state.

The spherulitic morphology of the α-crystal was observed using polarized optical microscopy (POM) as shown in Figure II-6. The spherulites of the α-crystal isothermally crystallized at 230 and 260 °C (images a and b, respectively) are very small. Woo and coworkers attributed the smaller size of the sPS α-crystal to a heterogeneous nucleation process that occurs upon cooling from the melt leading to the formation of a higher number nuclei and therefore smaller spherulites [5].

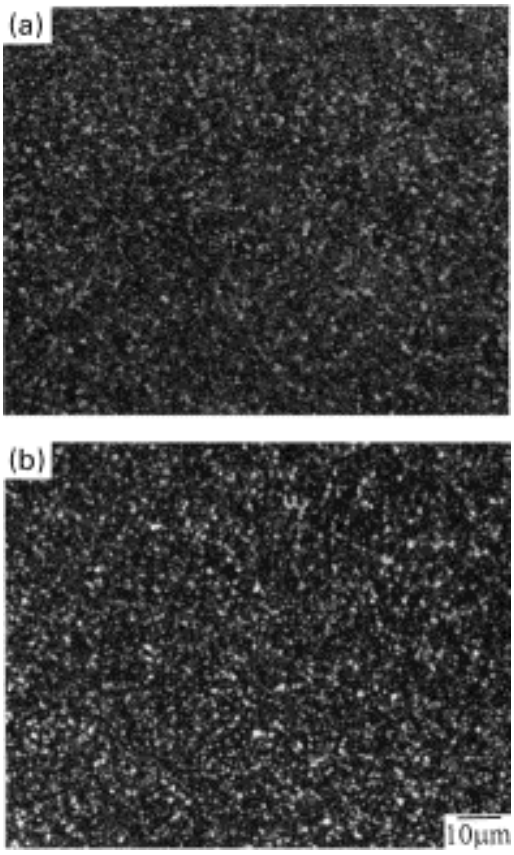

Figure II-6. Optical micrographs showing highly-nucleated, tiny spherulites in sPS of α-crystal. Reprinted from Progress in Polymer Science, Vol 26, Issue 6, E. M. Woo, Y. S. Sun, and C.P. Yang, Polymorphism, thermal behavior, and crystal stability in syndiotactic polystyrene vs. its miscible blends, 945-983, Copyright 2001, with permission from Elsevier.

Experimental data by researchers has also supported this theory and it is generally accepted that the α-crystal is the kinetically favored crystal form of sPS while the β-crystal is the thermodynamically stable crystal [24-26].

Melt Induced Crystallization of sPS: β-form Crystal Structure

The β-crystal structure of sPS is comprised of an orthorhombic unit cell with a = 8.81 Å, b = 28.82 Å, and c = 5.51 Å. As observed with the α-form of sPS, the β-form of sPS exhibits different degrees of structural order/disorder that are identified using the same nomenclature used for the different α-form sPS crystal structures. The β-form limit-ordered sub-modification is identified as the β″-modification and the limit-disordered structure that is identified as the β′–modification [14, 27]. Figure II-7 contains the proposed crystal structure of the limit-ordered sub-modification of sPS, the β″-crystal structure [27-28] and Figure II-8 shows the packing model for the β′–modification.

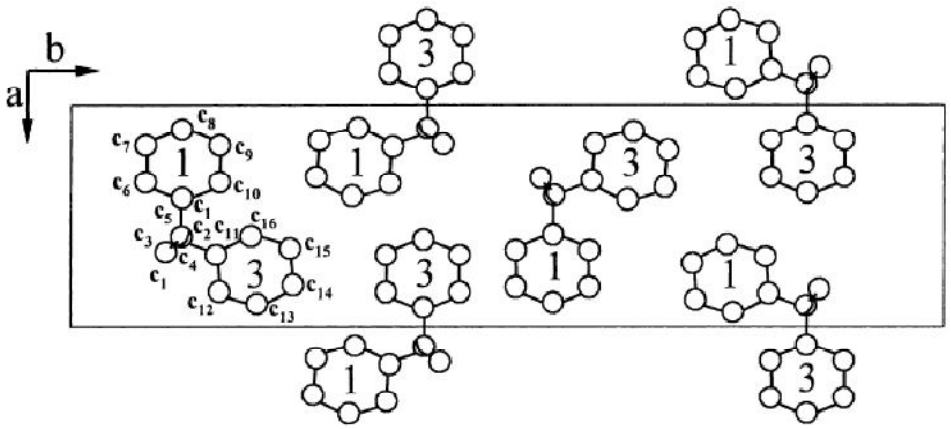

Figure II-7. Packing model of the β″-crystal structure limit-ordered sub-modification. Reprinted from Progress in Polymer Science, Vol 26, Issue 6, E. M. Woo, Y. S. Sun, and C.P. Yang, Polymorphism, thermal behavior, and crystal stability in syndiotactic polystyrene vs. its miscible blends, 945-983, Copyright 2001, with permission from Elsevier.

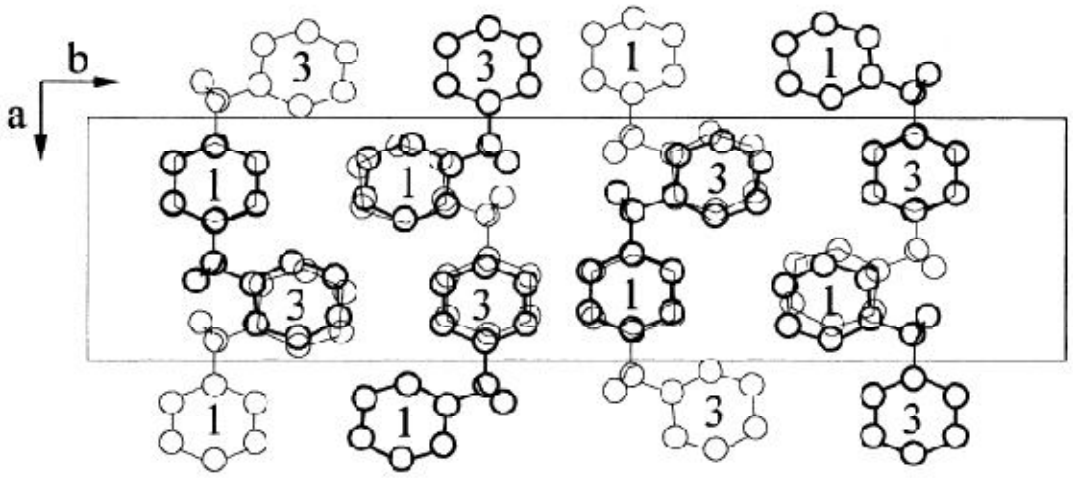

Figure II-8. Packing model of β′-crystal structure limit-disordered sub-modification. Reprinted from Progress in Polymer Science, Vol 26, Issue 6, E. M. Woo, Y. S. Sun, and C.P. Yang, Polymorphism, thermal behavior, and crystal stability in syndiotactic polystyrene vs. its miscible blends, 945-983, Copyright 2001, with permission from Elsevier.

Wang and coworkers studied the melting behavior of the α and β-crystal forms in order to determine the equilibrium melting temperatures [29] of the two different crystals using the Hoffman-Weeks (HW) approach [30] and the linear MX approach proposed by Marand [31-32]. The equilibrium melting temperatures were determined to be 281 and 291°C for the α- and β-form crystals, respectively using the linear HW approach. The equilibrium melting temperature of the α- and β-form crystals using the approach developed by Marand was 294 and 320 °C for α- and β-form crystals, respectively. Each method of determining the equilibrium melting point of the α- and β-form crystals led to a higher equilibrium melting temperature for the β-form crystal. Further investigation into the melting and crystallization behaviors of the α and β-form

crystal structures were performed utilizing simultaneous SAXS/WAXS/DSC measurements of bulk syndiotactic polystyrene which provided insight into the origin of the higher melting temperature of the β-crystal form [33]. Su and coworkers determined that the α-crystal exhibits a higher nucleation rate and crystallizes into fringed-micelle type crystals that are resistant to crystal thickening due to low basal fold energy. It was determined via the simultaneous SAXS/WAXS/DSC measurements that the β-crystal has a higher basal surface energy and higher equilibrium melting point resulting in a larger drive toward crystallization.

The spherulitic morphology of the sPS β-crystal isothermally crystallized at 230 and 260 °C was observed using POM as shown in images (a) and (b) of Figure II-8, respectively. The β-crystals are significantly larger than the α-crystals formed at the same isothermal crystallization temperatures. The spherulites of the β-crystal isothermally crystallized at 230 °C appear to be well-defined and the impingement of spherulites with other neighboring spherulites is clear.

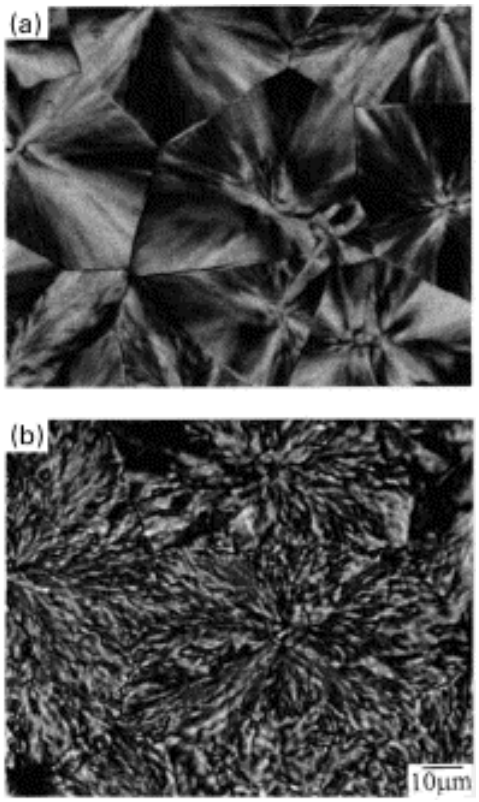

Figure II-9. Optical micrographs showing large/impinged spherulites in sPS of β-crystal. Reprinted from Progress in Polymer Science, Vol 26, Issue 6, E. M. Woo, Y. S. Sun, and C.P. Yang, Polymorphism, thermal behavior, and crystal stability in syndiotactic polystyrene vs. its miscible blends, 945-983, Copyright 2001, with permission from Elsevier.

At the higher crystallization temperatures such as 260 °C, the β-crystal suprastructure changes from the classic spherulitic structure exhibiting a Maltese cross to a more sheaf-like spherulitic structure which suggests coarsening of the sPS lamellae according to Woo and coworkers [5].

Solvent Induced Crystallization of sPS

δ-form Clathrate Phase of sPS

The δ-form of sPS is a helical host-guest structure where the arrangement of the sPS polymer chains creates nanopores that can accommodate small molecules. Due to the high sorption and selectivity behavior of sPS in δ-form, it has been considered to be a material that

could potentially be utilized as polymeric molecular sieves with behavior similar to that of zeolites [34-36] and as chemical sensors [37-41].

The solvent induced crystallization behavior of the δ-form of sPS has been studied by evaluating the crystalline morphology of sPS crystallized from the solution state [42-49] and from solid amorphous films of sPS exposed to liquid solvent or solvent vapor [50-56]. The WAXD patterns and FTIR spectra of sPS clathrates formed from different solvents differ slightly in the position and intensity of the crystalline reflections [57-59] and IR bands [54, 60-64], respectively due to the inherent molecular nature of the incorporated guest solvent into the nanopores of the sPS clathrate. In addition to hosting guest molecules within the nanopores of the sPS clathrate, the nanopores also exhibit selective uptake of guest molecules [65]. The guest molecules often exhibit a preferential orientation within the cavities of the clathrate structure [66-70]. Rizzo and coworkers have also demonstrated that guest diffusion into amorphous sPS can induce a preferential alignment of the actual polymer chains generating an oriented clathrate phase that is perpendicular to the plane of the film with the orientation of the chains remaining stable even upon heating [71].

Monoclinic and triclinic forms of the δ-form clathrate phase have been identified as two distinct forms of the δ-crystal as shown in Figure II-9 [72-73]. The sPS clathrates shown in Figure II-10 contain p-nitroaniline and p-nitrobenzene as guest molecules. The monoclinic form of the δ-form of sPS has also been identified by Petraccone and coworkers as a co-crystalline molecular complex of sPS containing bicyclo[2.2.1]hepta-2,5-diene (norbornadiene) [73] .

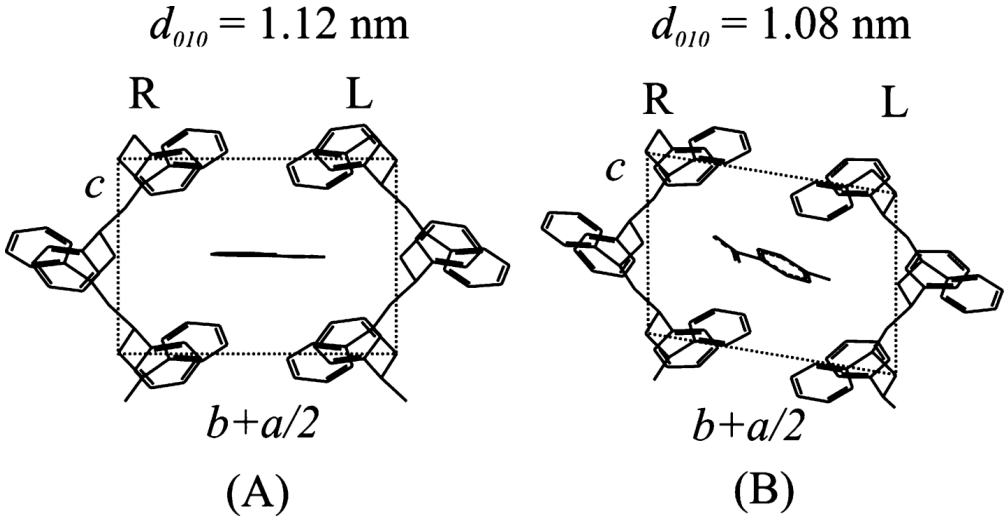

Figure II-10. Packing model proposed for the δ-clathrate structures of s-PS with p-nitrobenzene (A, monoclinic) and p-nitroaniline (B, triclinic). Only a couple of enantiomorphous polymer helices (R=right-handed; L = left-handed) that confine the guest molecule is shown. A closer distance between the ac layers is observed for the bulkier p-nitroaniline guest (B) because the guest is rather accommodated by shifting the *ac* layers along the chain axis, leading to the triclinic symmetry. Reprinted from Macromolecules 43(20), 8549. Copyright 2010 American Chemical Society.

The molecular volume of the solvent has a strong determination on whether the monoclinic or the triclinic clathrate structure is formed [72]. Based upon WAXD measurements of different sPS/solvent co-crystalline clathrates, Tarollo and Petraccone have proposed that sPS clathrates can be divided into two different classes: monoclinic or triclinic [72]. Figure II-11 contains a plot of the d_{010} versus guest volume of the solvent hosted within the sPS crystalline structure for a variety of solvents.

Monoclinic clathrates are formed through the incorporation of solvents into the sPS nanopores with a molecular volume significantly lower than that of the molecular volume of the sPS nanopore being 0.125 nm^3. Due to the small volume of the solvent molecule, the crystalline lattice of the monoclinic clathrate form is not altered significantly. According to Tarallo and Petraccone, there may be a slight increase in the *ac* layers of the enantiomorphous helices, but

the monoclinic unit cell and the $P2_1/a$ symmetry are maintained. Also, the guest molecule within the monoclinic sPS clathrate is oriented perpendicular to the chain axes.

The triclinic sPS clathrate form is obtained when the volume of the guest molecule is much greater than the volume of the nanopore of the sPS δ-form. When the molecular volume of the solvent molecule is very close to the size of the sPS nanopore of the crystalline phase, the d_{010} spacing must be determined in order to determine whether the sPS/solvent inclusion complex is of the monoclinic or triclinic form. When the d_{010} spacing is close to or lower than the d_{010} pacing of the sPS clathrate, the triclinic sPS clathrate form is predicted. When the d_{010} spacing of the sPS/solvent complex is significantly higher than the δ-phase, the structure is predicted to be a monoclinic clathrate according to Tarallo and Petraccone.

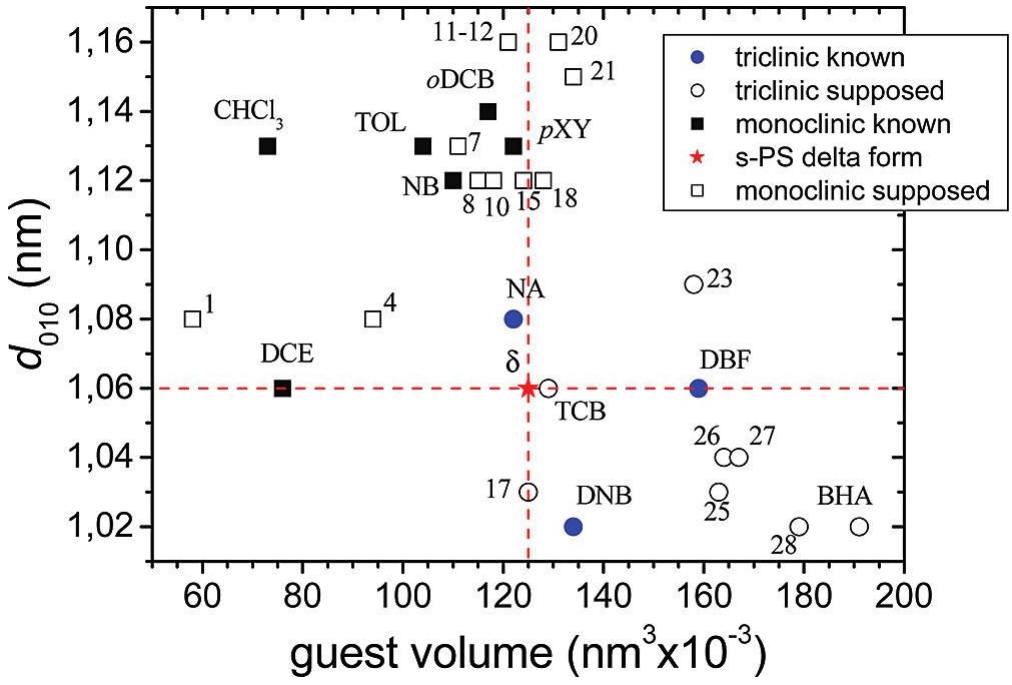

Figure II-11. d_{010} distances for the s-PS δ-clathrates versus the guest molecular volume. Supposed or known monoclinic clathrates are indicated with empty or filled squares respectively, while supposed or known triclinic ones are indicated with empty or filled circles, respectively. The red star (whose position is highlighted by the two red dashed lines) indicates the d_{010} and

volume of the cavities of the s-PS δ-form. TOL = toluene; NB = nitrobenzene; pXY = p-xylene; oDCB = o-dichlorobenzene; NA = 4-nitroaniline; DCE = 1,2-dichloroethane; DBF=dibenzofuran; TCB=1,3,5-trichlorobenzene;DNB = 1,4-dinitrobenzene; BHA = 2-tert-butyl-4-methoxyphenol. Reprinted from Macromolecules 43(20), 8549. Copyright 2010 American Chemical Society.

Ray and coworkers conducted an investigation of the crystalline suprastructure of sPS crystallized from a homogeneous solution state and from sPS crystallized via the exposure of amorphous sPS thin films to liquid solvent [74]. It was determined that the morphology of sPS was strongly dependent upon the thickness of the sPS film exposed to the liquid solvent for sPS thin films (70-250 nm thickness). AFM images of the resulting morphologies showed the development of fibrillar networks that were highly porous in nature even after exposure of the thin film to toluene for 1 hour as shown in Figure II-12. The mesh size of the fibrillar network was found to vary between 0.1 and 1 μm depending on the initial film thickness.

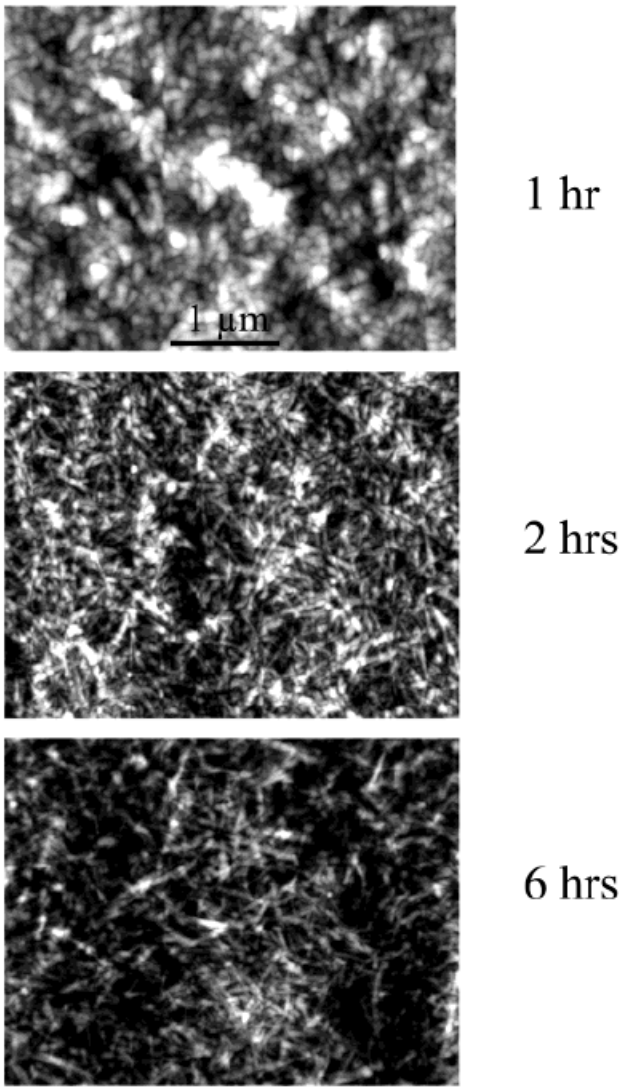

Figure II-12. AFM images of a thin sPS films (initial thickness = 0.15 μm) exposed to toluene at 75 °C for different times (as indicated). Each image corresponds to a different sample. Reprinted from Macromolecules 35(26) 9730. Copyright 2002 American Chemical Society.

Fibrillar morphological structures are obtained for solvent crystallized thin sPS films with the porosity of the fibril being dependent upon the crystallization temperature. The morphological structure of bulk crystallized sPS (0.1 mm thick films) could not be readily identified and depended greatly upon the solvent chosen for crystallization.

δ_e Emptied Clathrate Form of sPS

The δ-form of sPS can be thermally treated [75] at low temperatures to obtain an emptied clathrate crystalline structure that is free of solvent molecules or treated through stepwise solvent extraction with methanol and acetone to prepare a solvent-free crystalline structure [76-77]. The emptied clathrate form has also been obtained as an intermediate structure between the δ-form and γ-form via supercritical carbon dioxide treatment of the sPS clathrate form [78]. The emptied clathrate form has been reported to have a lower density than that of the amorphous phase of sPS as observed for the low density α-crystal of sPS. The reported density of the δ_e-crystal of sPS is 0.977 g/cm^3 compared to a density of 1.055 g/cm^3 for the amorphous phase of sPS as reported by De Rosa and coworkers [79].

The emptied clathrate structure has also been called the mesophase structure and the sorption behavior of this mesophase structure has been studied in detail [80-84]. The sorption behavior of chloroform at 35°C was monitored in sPS powders exhibiting the α, β, γ, and δ_e forms by Manfredi and coworkers as shown in Figure II-13 [80]. The sorption of chloroform in the δ_e-form of sPS is considerably higher than the α, β, and γ-forms. The sorption behavior of the δ_e-form clearly indicates that this material retains its nanoporous structures which allow the more rapid diffusion/sorption of solvent as compared to the other crystalline forms.

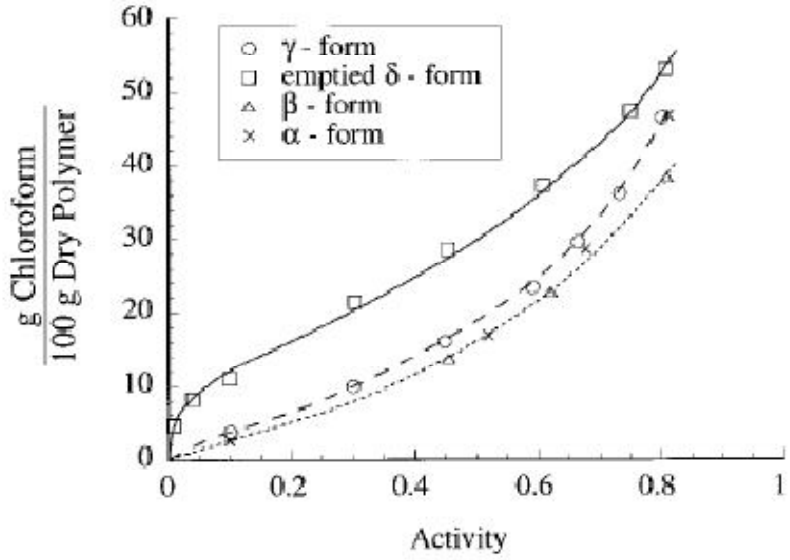

Figure II-13. Chloroform vapor sorption isotherms for different crystalline forms of s-PS at 35°C. Reprinted from Journal of Polymer Science Part B: Polymer Physics, Volume 35, Issue 1, 133. Copyright 1997 John Wiley and Sons.

The WAXD diffraction pattern of the δ_e-form crystalline structure was compared to other sPS samples by Manfredi and coworkers and is shown in Figure II-14. It can be seen that the WAXD profile of the emptied clathrate is significantly different from that of the γ-form which suggests that the crystalline structure of the mesophase/emptied clathrate is distinct from that of the solvent-free γ-phase of sPS [85].

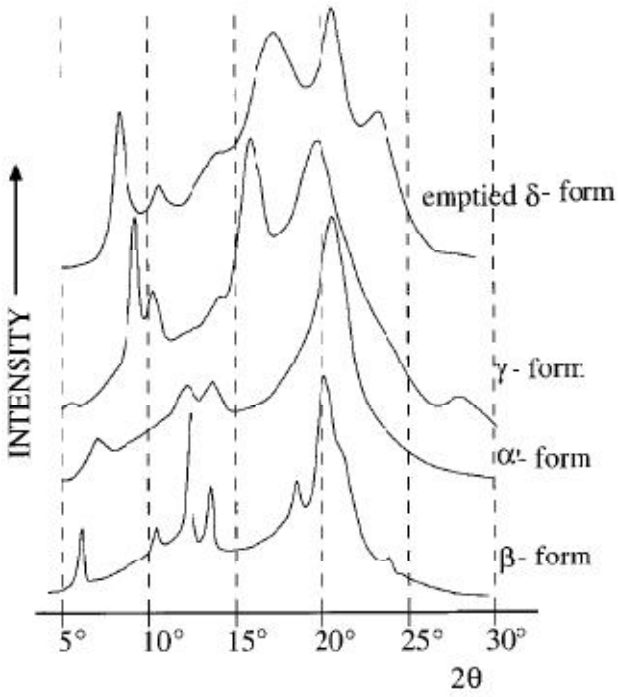

Figure II-14. X-ray diffraction patterns (CuK_α) of four different crystalline forms of s-PS. Reprinted from Journal of Polymer Science Part B: Polymer Physics, Volume 35, Issue 1, 133. Copyright 1997 John Wiley and Sons.

The IR spectra of the helical phases exhibit slight differences as shown in Figure II-154 of the δ, δ_e, and γ-forms of sPS containing toluene, chloroform, and benzene. Yoshioka and coworkers determined that because the three solvent induced crystalline structures of sPS have the same helical chain conformation that any observed differences in the IR spectra may be attributed to differences in the packing of mode of the chains or differences in intermolecular interactions between polymer chains and/or between polymer chains and the incorporated organic solvents [62].

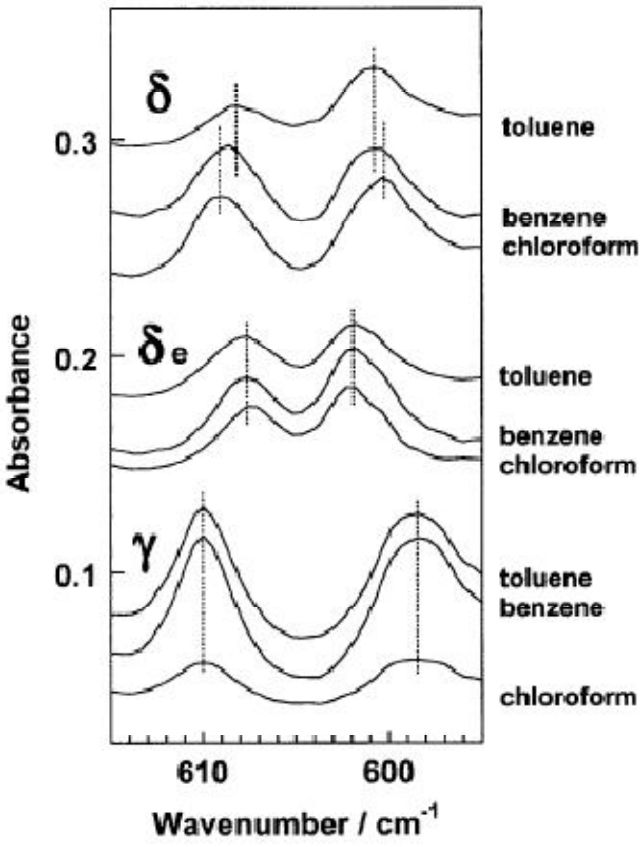

Figure II-15. Infrared spectra in the region of 595-615 cm^{-1} at room temperature for the various samples of the sPS/solvent system. Reprinted from Macromolecules 36(9), 3001. Copyright 2003 American Chemical Society.

It can be seen that there are bands that are characteristic of each of the three helical forms. The IR bands located at 608.2 and 600.8 cm^{-1} are attributed to the δ-form. The bands centered at 607.6 and 601.9 cm^{-1} associated with the δ_e-form, and the IR bands located at 610.0 and 598.5 cm^{-1} have been attributed to sPS chains packed in the γ-form. It can be seen that the positions of these bands vary slightly in each of the helical forms of sPS with the incorporation of different solvents. Yoshioka and coworkers suggest that these IR bands may be used as indicators to monitor the structural transition that occurs from one phase to another.

ε-form Channel Clathrate Crystal Structure of sPS

The ε-form of sPS known as the channel clathrate form was initially identified by Rizzo and coworkers [86]. The ε-form is also a helical structure similar to that of the δ-form of sPS, but unlike the δ-form, the ε-form is able to accommodate guest molecules larger than the limiting value of 0.25-0.26 nm^3 for the δ-form. Not only is the ε-form able to accommodate larger molecular volume guests with large hyperpolarizability, but the guest molecules are also aligned within the ε-form with their molecular planes parallel to the polymer chain axes and perpendicular to the surface of the film [86-88] as shown in Figure II-16.

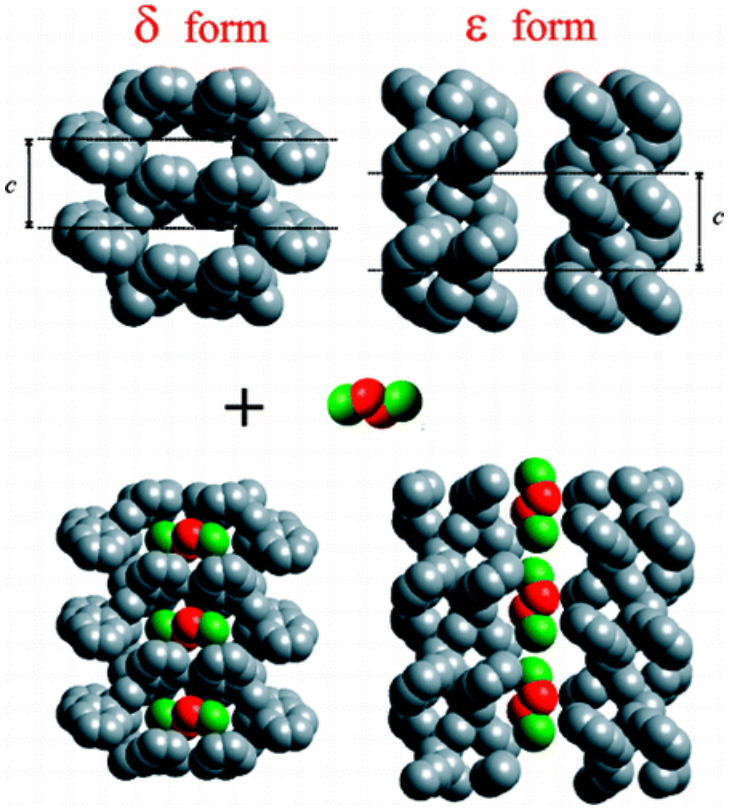

Figure II-16. Schematic presentation of the orientation of the cocrystal chain axes (c) and of solvent guest molecules δ-form and ε-form films. Reprinted from Chemistry of Materials 20(11), 3663. Copyright 2008 American Chemical Society.

Petraccone and coworkers utilize FTIR, WAXD, and electron diffraction (ED) to show that guest molecules are arranged as channels within the ε-form of sPS as shown in Figure II-17. Based upon their findings, they suggest that the ε-form consists of an orthorhombic unit cell with a=16.2 Å, b=22.0 Å, c =7.9 Å and has a calculated density of 0.98 g cm^{-3}, with four chains of s-PS in the s(2/1)2 helical conformation included in the unit cell.

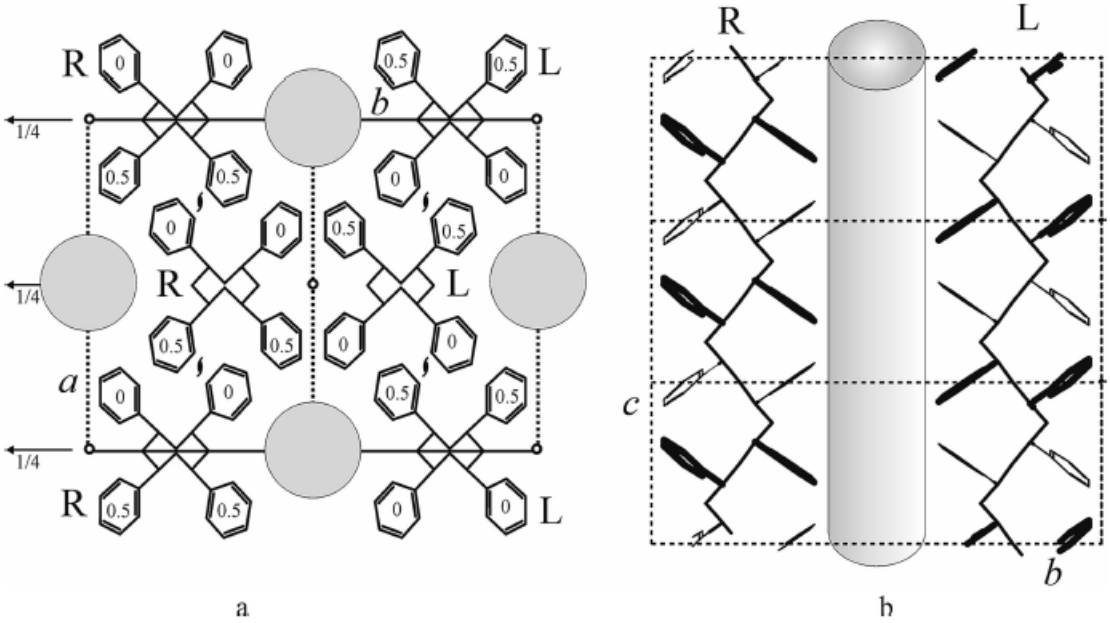

Figure II-17. Packing model of the nanoporous ε form of s-PS in the projections along c (a) and along a (b). Grey circles (a) and cylinders (b) indicate the channels where guest molecules can be hosted. In part b the phenyl rings of s-PS helical chains towards the reader are drawn with bold lines, and only a couple of polymer chains delimiting the channel are represented. Right-handed (R) and left-handed helical chains (L). Reprinted from Chemistry of Materials 20(11), 3663. Copyright 2008 American Chemical Society.

Three different uniplanar orientations can be achieved of the nanochannels of the ε-form of sPS with respect to the sPS film surface [89] shown in the Schematic of Figure II-18. The authors suggest that oriented channels may be utilized as a method to control guest diffusivity.

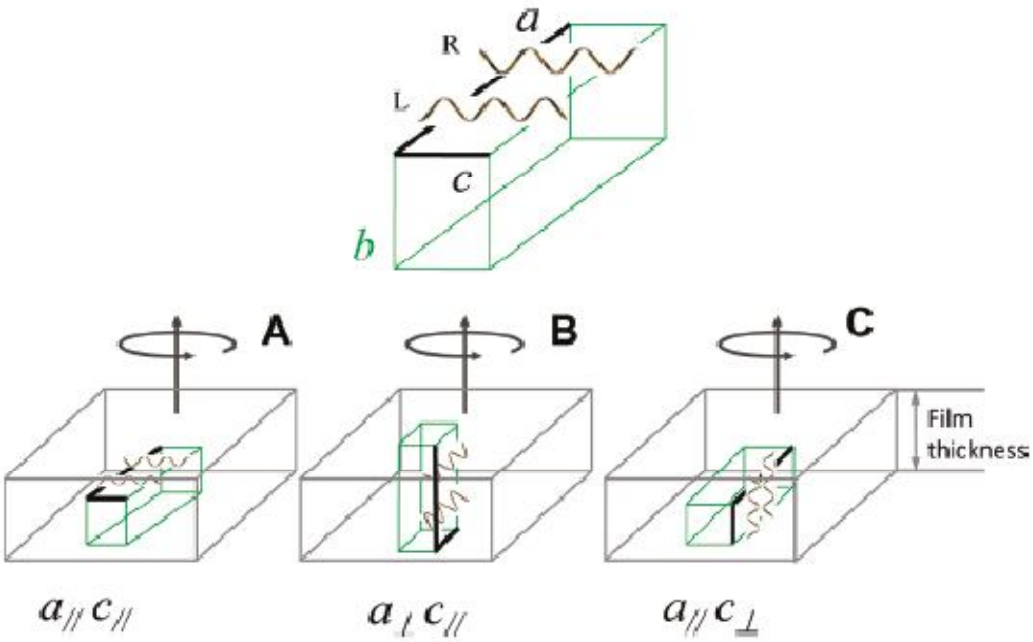

Figure II-18. Schematic presentation of the three uniplanar orientations of s-PS cocrystalline films, corresponding to the three simplest orientations of the high-planar-density ac layers with respect to the film plane. Reprinted from Chemistry of Materials 21(14), 3370. Copyright 2009 American Chemical Society.

Aerogels were prepared from the δ-form and ε-form of sPS and studied to determine their hydrogen adsorption behavior [90]. It was found that the hydrogen adsorption behavior was highly dependent upon the nature of the sPS crystalline form as shown in Figure II-19 of the H_2 uptake versus pressure of sPS in various crystalline forms.

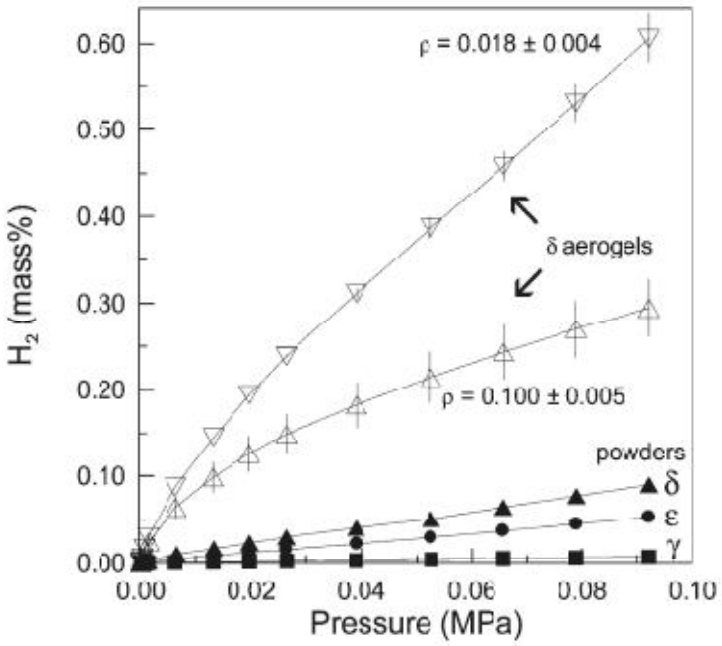

Figure II-19. H_2 gravimetric adsorption isotherms, for pressure lower than 0.1MPa at 77 K, on s-PS powders exhibiting the nanoporous δ (2), the nanoporous ε (b), and the dense γ (9) crystalline phases and for s-PS aerogels exhibiting the nanoporous δ phase and different apparent densities (4, F = 0.100 (0.005 g/cm^3; 3, F = 0.018 (0.004 g/cm^3). Reprinted from Macromolecules 43(20), 8594. Copyright 2010 American Chemical Society.

The hydrogen adsorption behavior was found to be smallest for the higher density β and γ sPS phases, intermediate for the ε-form, and the highest hydrogen adsorption behavior was observed for the δ-form of sPS. The gravimetric hydrogen adsorption measurements demonstrated that gas adsorption was dependent upon the morphology of the sPS sample. The hydrogen adsorption behavior was observed to increase in the following order: aerogels>powders>films. The hydrogen adsorption for sPS in film form was negligible while the adsorption behavior of the aerogels increased within increasing degree of porosity of the aerogel structure indicating the hydrogen adsorption behavior was dependent upon the surface area of the host structure.

The morphology of ε-form aerogels was studied by Daniel and coworkers using SEM [91]. Based upon their studies they proposed that highly porous ε-form aerogels consists of macropores due to the free volume within the aerogel structure and micropores that are the channels formed through the arrangement of the polymer chains of the sPS ε-form. Figure II-20 contains a diagram of the morphology of sPS aerogels in the ε-form.

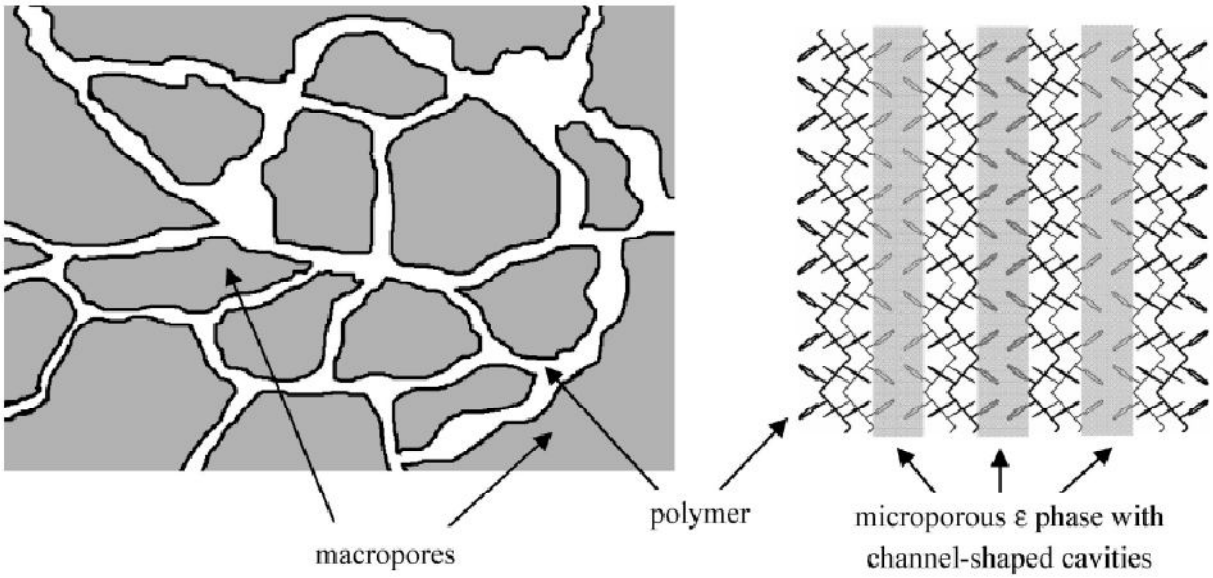

Figure II-20. Representation of the texture (left) and the microporous crystalline structure (right) of ε-aerogels. Reprinted from Chemistry of Materials 21(6), 1028. Copyright 2009 American Chemical Society.

The identification and study of the sPS ε-form exhibiting nanochannels throughout the sPS film thickness is exciting as it presents a potential method to simply control the uptake, orientation, and diffusivity of molecules throughout a polymeric membrane that is relatively inexpensive for potential use in numerous applications where guest orientation and diffusivity are critical parameters.

γ-form Crystal Structure of sPS

The formation of the γ-phase sPS helical structure has been obtained through thermal annealing of δ-form or solvent extraction [75], subjection of the sPS amorphous phase to supercritical carbon dioxide treatment [92], and via solution casting of sPS from bulky solvents [93-94]. The formation of the γ-phase of sPS is of particular interest as it the helical crystalline form that is observed before structural transition of the δ_e-form into the all-trans, planar, zigzag crystalline structures upon heating [95] or treatment with supercritical carbon dioxide. The sPS γ-form is also used to prepare the channel clathrate structure of the ε-form through solvent uptake procedures [96] making it a sPS crystalline structure of interest as well.

Gowd and coworkers studied the structural transition of the oriented sPS in the emptied clathrate form into γ-form through studies combining WAXD, FTIR, and DSC data [95]. The model constructed depicting the transition from the δ_e to the γ-form is shown in Figure II-21. Region (a) corresponds to the emptied clathrate form of sPS containing the empty nanocavities. Region (b) contains both crystalline structures in the δ_e-form and an intermediate form. There is a decrease in the number of cavities and an increase in the disorder within the system which is manifested as an endothermic peak in the DSC thermogram. In region (c) the disordered chains begin to pack into more ordered structures that eventually result in the formation of the γ-form of sPS with continued heating shown in (d).

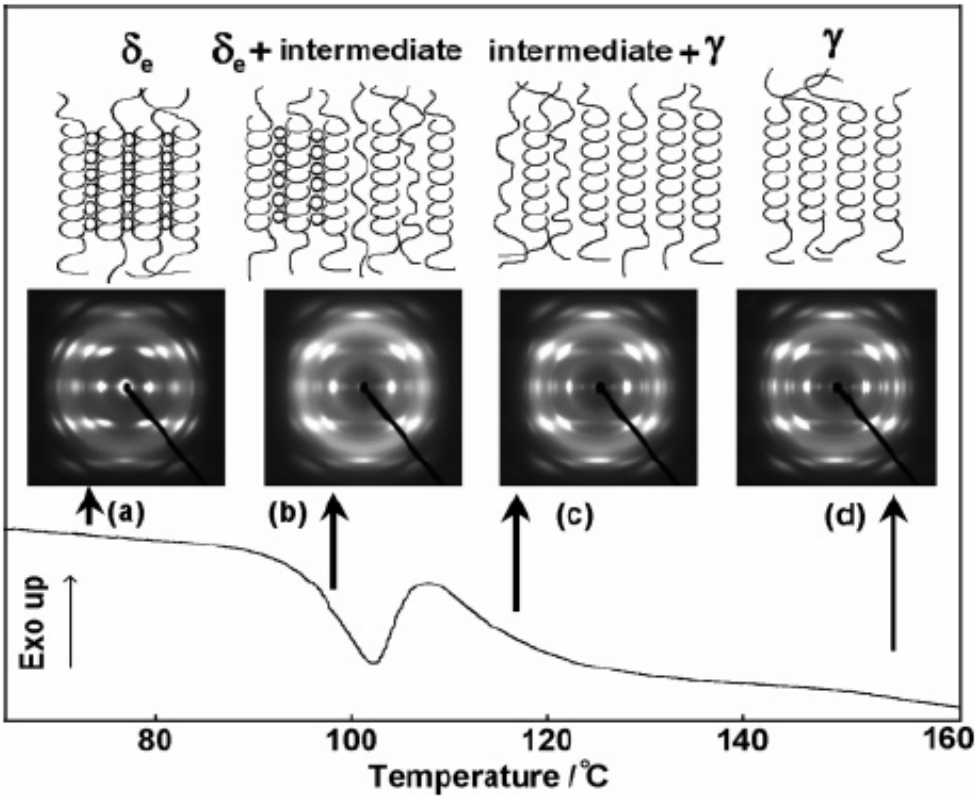

Figure II-21. Schematic illustration of the chain-packing mode at different temperatures during heating of the δ_e form sample in comparison with the observed X-ray fiber diagram and DSC thermogram. Reprinted from reference Macromolecules 39(24), 8412. Copyright 2006 American Chemical Society.

Cold Crystallization of sPS

Cold crystallization is the process of chain organization that occurs from the glassy amorphous state at temperatures above the glass transition temperature of the polymer. The study of the cold crystallization behavior of sPS is important as it provides insight in to the mechanisms of chain organization of the polymer chains with limited molecular mobility as opposed to the organization of chains into crystalline structures from the melt state where the level of molecular mobility is often significantly higher.

The organization of polymer chains from the glassy state during cold crystallization occurs via cooperative segmental motion, while crystallization from the melt state occurs through polymer chain reputation [97]. To gain insight into the behavior and chain dynamics that occur during the cold crystallization of sPS researches have studied the behavior the polymer over a wide temperature range and a utilized a number of optical, thermal, and spectroscopic techniques to study the mechanisms responsible for cold crystallization within sPS.

Researchers have found that the primary crystal structure obtained upon crystallizing sPS from the glassy state is the α-crystal polymorph. Woo and coworkers evaluated the crystalline structure of cold crystallized sPS using WAXD. Figure II-22 shows the WAXD diffractograms of sPS cold crystallized at temperatures between 120 and 252 °C. sPS cold crystallized at temperatures below 170 °C did not exhibit any strong diffraction peaks after crystallization for four hours. However, diffraction peaks begin to appear at cold crystallization temperatures of 200 °C and above and continue to increase in intensity with increasing cold crystallization temperature. The diffraction peaks located at $2\theta = 6.7$, 11.7, 13.2, 15.6, and 17.88° are indicative of the a″-form and each of the aforementioned peaks with the exception of the 17.88° peak are observed within the cold crystallized sPS samples.

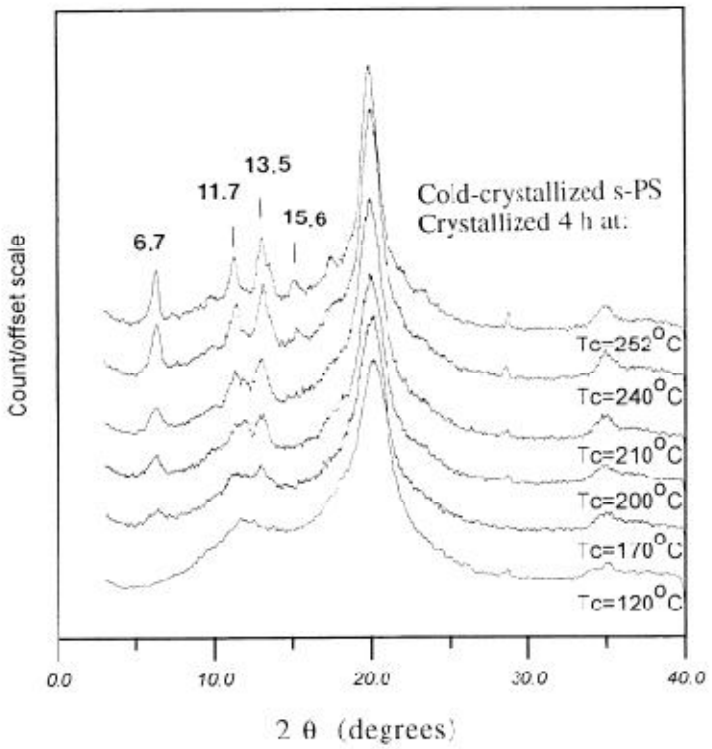

Figure II-22. X-ray diffractograms of s-PS samples cold-crystallized at several isothermal temperatures: 120, 170, 200, 210, 240 and 252 °C for 240 min. Reprinted from Polymer, Vol 40, Issue 15, E.M. Woo, Ya Sen Sun and Meng Lu Lee, Crystal forms in cold-crystallized syndiotactic polystyrene, 4425-4429, Copyright 1999, with permission from Elsevier.

The cold crystallization behavior of sPS was also studied by Yoshioka and Tashiro using time-resolved FTIR measurements [99]. The development of FTIR bands at 840 cm^{-1} and 1222 cm^{-1} associated with the amorphous and α-crystalline forms were monitored with time at different cold crystallization temperatures as shown in Figure II-23. The FTIR bands indicative of the amorphous sPS phase located at 840, 970, 1195 and 1240 cm^{-1} were observed in the initial amorphous sample, but decreased upon crystallizing sPS at cold crystallization temperature of 117 °C and above. At 117 °C, IR bands characteristic of the α-form of sPS began to appear at 850, 980, 1090, 1222 and 1333 cm^{-1}.

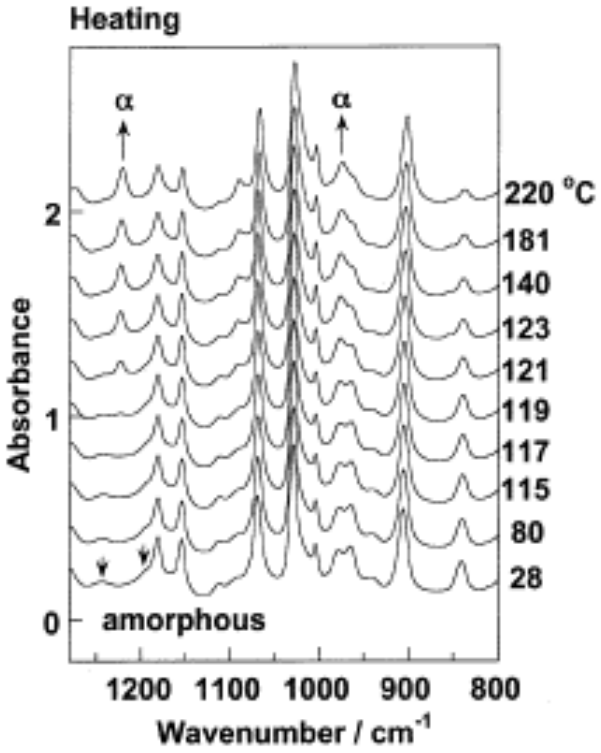

Figure II-23. Infrared spectra of sPS glass taken in the heating process from room temperature to 220 °C. Reprinted from Polymer, Vol 44, Issue 21, Akiko Yoshiokaa and Kohji Tashiro, Thermally- and solvent-induced crystallization kinetics of syndiotactic polystyrene viewed from time-resolved measurements of infrared spectra at the various temperatures (1) estimation of glass transition temperature shifted by solvent absorption, 6681-6688, Copyright 2003, with permission from Elsevier.

Woo and coworkers compared the crystallization behaviors of melt and cold crystallized sPS. Figure II-24 provides the post-isothermal crystallization DSC thermograms of sPS crystallized under three different conditions: slow cooled from the melt at 10 °C/min, melt crystallized at 240 °C for 30 minutes, and cold crystallized at 240 °\C for 30 minutes. It is readily observable that the melting behavior of the sPS crystallized under different conditions is quite different. Three melting endotherms are present for the sPS samples crystallized by slow cooling from the melt and isothermally crystallized at 240 °C. The multiple melting endotherms observed in the slow cooled and melt crystallized samples are attributed to a mixture of both the α and β-form of the sPS through the analysis of WAXD profiles of the samples.

The sPS sample cold crystallized at 240 °C exhibits one melting endotherm at 269 °C that is attributed to the melting of α-form crystal of sPS using WAXD analysis of the sPS sample prior to heating. Woo and coworkers also found that sPS cold crystallized at temperatures between 200 – 260 °C exhibited only one melting endotherm that was consistently located at 269 °C. Cold crystallization temperatures below 200 °C led to the formation of imperfect crystals that did not produce clear diffraction peaks.

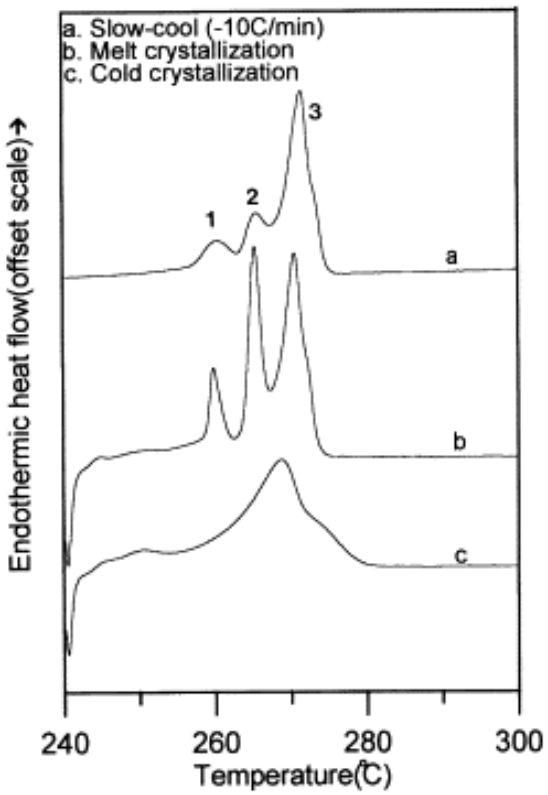

Figure II-24. Comparison of melting peaks of s-PS samples: (a) slow-cooled (−10°C/min), (b) melt-crystallized (240°C, 30 min) and (c) cold-crystallized (240°C, 30 min). Reprinted from Polymer, Vol 40, Issue 15, E.M. Woo, Ya Sen Sun and Meng Lu Lee, Crystal forms in cold-crystallized syndiotactic polystyrene, 4425-4429, Copyright 1999, with permission from Elsevier.

The cold crystallization behavior of sPS was studied by Sun and Woo using FTIR, WAXD, SEM, and POM as shown in Figure II-25. They studied the crystalline suprastructure of sPS cold crystallized over a wide temperature range between150 to 260 °C. POM and SEM analysis reveals that the size of the spherulites increases with increasing cold crystallization

temperature. The crystalline structures at low crystallization temperature are very small and granular in appearance lacking any type of lamellar structure. However, cold crystallization at higher temperatures resulted in the formation of lamellar structures surrounding a circular core.

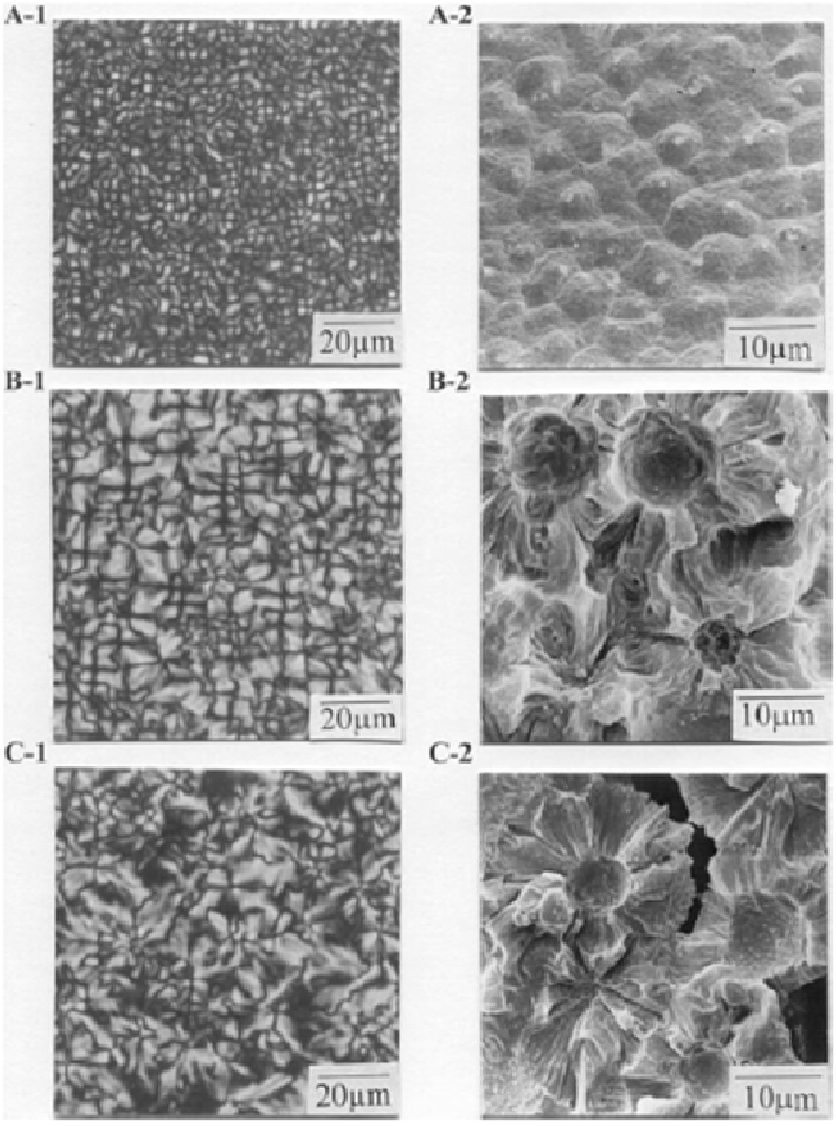

Figure II-25. POM and SEM graphs, respectively, for sPS samples: (A-1&2) cold crystallized at low T_{cc} = 150°C, (B-1&2) cold-crystallized at T_{cc} = 225°C,all for 120 min, and (C-1&2) cold-crystallized at T_{cc} = 260°C, all for 20 min. Reprinted from Polymer, Vol 42, Issue 5, Y. S. Sun and E. M. Woo, Morphology and crystal structure of cold-crystallized syndiotactic polystyrene, 2241-2245, Copyright 2001, with permission from Elsevier.

The crystalline suprastructure of sPS cold crystallized at low and high temperature was evaluated using small-angle light scattering (SALS) and polarized optical microscopy (POM) as shown in Figure II-26 [101]. The H_v and V_v SALS scattering patterns were obtained. The H_v patterns show distinct four-leaf clover patterns indicative of well-defined spherulitic structure. The size of the H_v SALS patterns decreases with increasing temperature indicating that the size of the spherulite increases with increasing cold crystallization temperatures. POM observation of the cold crystallized samples reveals the presence sPS spherulites with the majority of the spherulites being positively birefringent with a few negatively birefringent spherulites present.

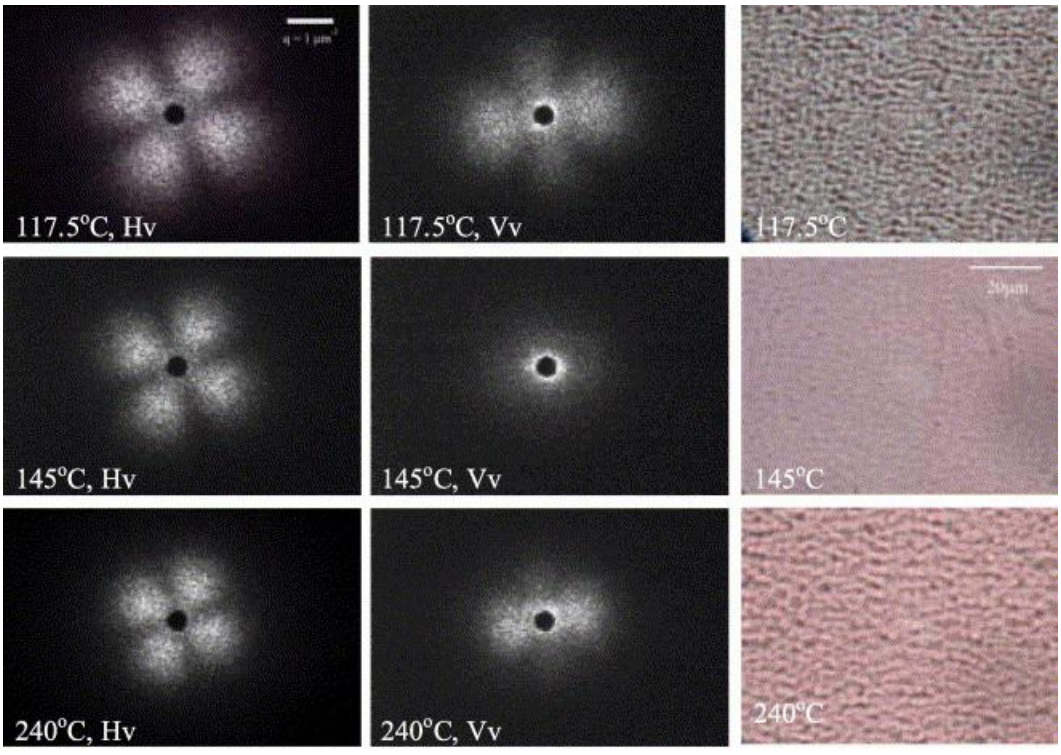

Figure II-26. (a) H_v, (b) V_v scattering patterns and (c) phase contrast micrographs of sPS cold-crystallized at various T_c. Reprinted from Polymer, Vol 46, Issue 26, Y. S. Chi Wang, Chang-Chun Lin and Chia-Ping Chu, Morphology and crystal structure of cold-crystallized syndiotactic polystyrene, 12595-12606, Copyright 2005, with permission from Elsevier.

The mechanism of cold crystallization was studied by Su and coworkers using in-Situ Small/Wide-Angle X-ray Scattering and DSC [102]. They proposed that the cold crystallization process within sPS occurs through the nucleation, growth, and coalescence of nanograins of randomly-coiled sPS. Figure II-27 shows the WAXD profiles of sPS cold crystallized from room temperature to 240 °C and the crystal thickness of associated with three different crystalline reflections as a function of temperature. Through analysis of the WAXD profiles, it can be seen that there is no long-range positional order at temperatures below 132 °C and that densification of nuclei does not lead to any diffraction. After densification of nanograins of sPS occurs, there is a rapid amount of growth that takes place at elevated temperatures as indicated by the appearance and sharpening of diffraction peaks associated with the (110), (300), and (211) reflections of the α-form of sPS.

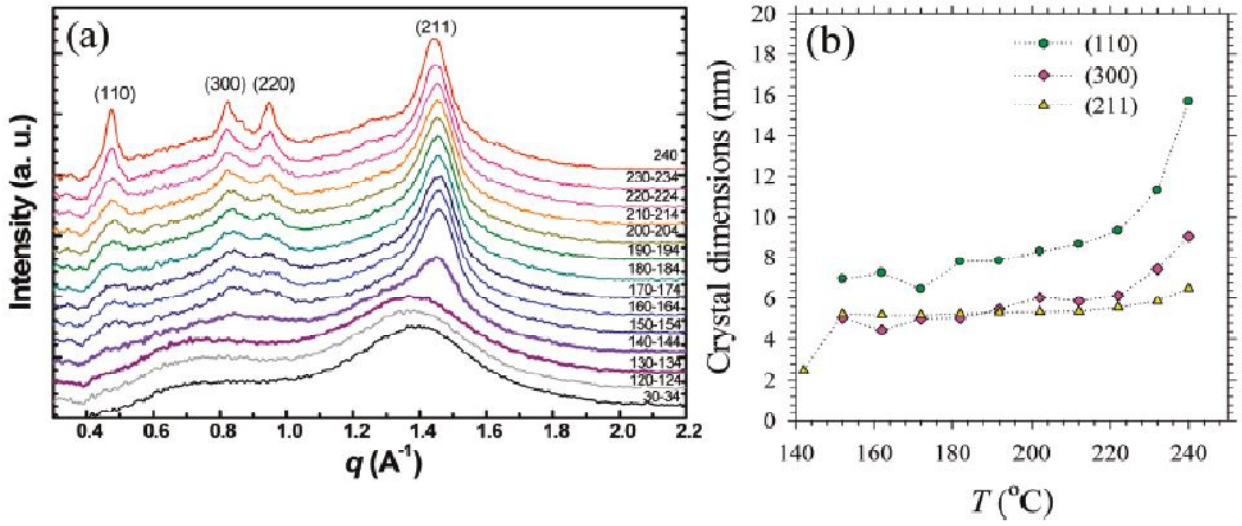

Figure II-27. (a) In-situ WAXS spectra of the sPS specimen measured with a powder X-ray diffractometer 30 to 240 °C and (b) crystallite dimensions calculated from the peak widths using the Scherrer equation. Reprinted from Macromolecules 42(17) 4244. Copyright 2009 American Chemical Society.

Processing of sPS

Due to the excellent properties exhibited by sPS combined with the relatively low cost of the material, there have been numerous investigations into processing of bulk sPS using various methods to yield sPS with specific macroscale and nanoscale morphologies.

Syndiotactic Polystyrene Nanorods

Nanorods of sPS have been prepared through the melt crystallization of sPS within porous anodic alumina oxide (AAO) templates by Wu and coworkers [103]. The morphology, orientation, and degree of crystallinity of the sPS nanorods were studied using a combination of FTIR, SEM, ED, and TEM. The morphology of the sPS nanorods obtained via crystallization within anodic alumina oxide templates are shown in the SEM micrographs of Figure II-28. The sPS nanorods appear to be uniform in diameter with nanorod lengths up to 60 μm which corresponds to the thickness of the AAO templates. The residual sPS film below the AAO template was found to be 90 μm thick. The residual sPS film that did not crystallize within the AAO template was used to study the differences between the crystalline regions of sPS that formed within the AAO template and in crystalline regions of the bulk state.

The authors utilized crystallization conditions that were previously reported within the literature to induce the formation of the α-form and β-form sPS crystal structures for the preparation of the sPS nanorods. Under crystallization at low temperature from the amorphous state which has been reported to induce the formation of the α-form, sPS nanorods and the sPS bulk material both consist of primarily the α-form crystal structure with similar degree of crystallinity.

Wu and coworkers found that the percentage of the α-form crystal obtained when crystallizing the sPS within the AAO template at 240 °C for 2 hours via FTIR measurements. The percent crystallinity of the α-form found within the sPS nanorods of 80 and 200 nm diameter and the sPS bulk material under these low temperature conditions was found to be 57.4%, 58.6%, and 61.5%, respectively. The percentage of the β-form developed under the same low temperature conditions was 6.3%, 6.6%, and 6.7%, respectively. The data obtained from FTIR indicate that both the sPS nanorods and the bulk sPS consist of the similar degrees of crystallinity and crystal structure.

High temperature processing conditions that have been reported to induce the formation of the β-form crystal polymorph of sPS were also used to process the sPS within the AAO templates by crystallizing sPS from the melt state at 260 °C for 2 hours. The crystalline structure found in both the sPS nanorod and the bulk material was essentially the β-crystal. The α-form crystal was not detected using FTIR under the higher temperature processing conditions. The percent crystallinity determined via FTIR measurements for the 80 nm sPS nanorods, 200 sPS nanorods, and bulk sPS were found to 36.2%, 49.8%, and 62.0%, respectively. The lower degree crystallinity of the sPS nanorods compared to the bulk sPS was attributed to the preferential growth of sPS chains within the AAO template with the c-axis of the sPS polymer chains oriented normal to the axial direction of the AAO template. The bulk sPS processed under the high temperature conditions does not exhibit any preferred orientation as seen in the sPS nanorods processed under the same conditions.

The orientation of the polymer chains within the sPS nanorods were evaluated using electron diffraction (ED) of sPS nanorods removed the AAO template and bulk sPS film base. Figure II-29 contains the TEM micrographs with ED pattern inserts of sPS nanorods prepared

under low temperature and high temperature processing conditions. The ED pattern of the sPS nanorod exhibiting the α-form contains one diffraction circle at (211) attributed to the α-crystal polymorph with no preferred orientation. However, the ED pattern of the sPS nanorod prepared using the high temperature processing conditions, clearly contains symmetric diffraction arcs indicating the presence of orientated polymer chains within the high-temperature processed sPS nanorod. Wu and coworkers highlight the relevance of this work to the study of the crystallization of polymers under confined conditions and also as an initial exploratory evaluation of sPS as polymeric material to construct nanodevices.

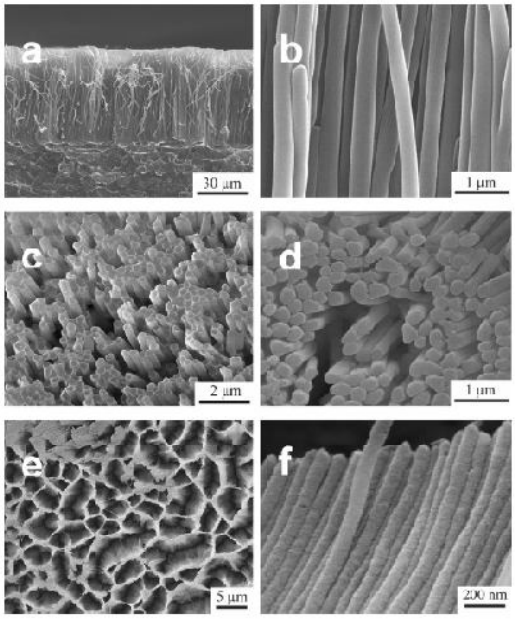

Figure II-28. FE-SEM micrographs of sPS nanorods (a, b, c, d) 200 nm; (e, f) 80 nm. (a, b, f) Cross section of the nanorod array; (c, e) top view of the nanorod array; (d) top view of the nanorod array with the tips of the nanorods removed. Reprinted from Macromolecules 40(12), 4244. Copyright 2007 American Chemical Society.

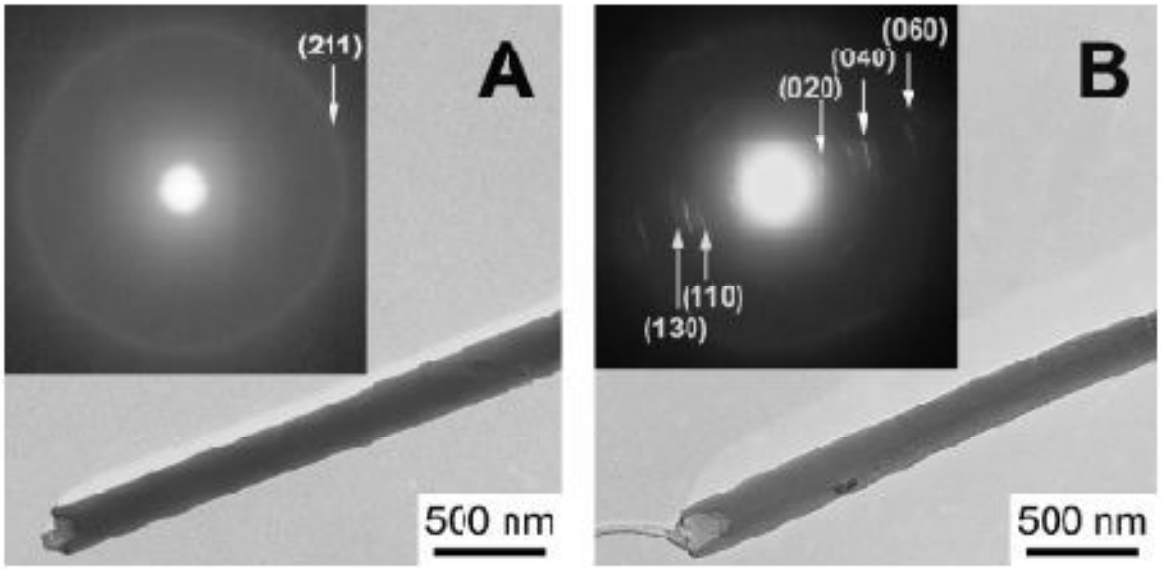

Figure II-29. TEM images of a single sPS nanorod crystallized at lower temperatures (A) and at 260 °C (B). The inset is the corresponding electron diffraction pattern. Reprinted from Macromolecules 40(12), 4244. Copyright 2007 American Chemical Society.

Multiporous Fibrillar Syndiotactic Polystyrene

A report of multiporous materials prepared through the sublimation of naphthalene from a sPS/naphthalene intercalate exhibiting fibrillar morphology was made by Malik and coworkers [104]. Analysis of the morphology of sPS after sublimation of naphthalene using atomic force microscopy (AFM) revealed the cross section of the fibrils to be 50 nm as shown in Figure II-30. Based upon mercury intrusion porosimetry measurements, it was found that the fibrillar sPS structures contained two size distributions of pores centered at 0.05 μm and 8-10 μm. FTIR analysis indicated that the crystalline phase of the multiporous fibrils were helical by the presence of the band at 571 cm^{-1} attributed to the 2_1 helical conformation.

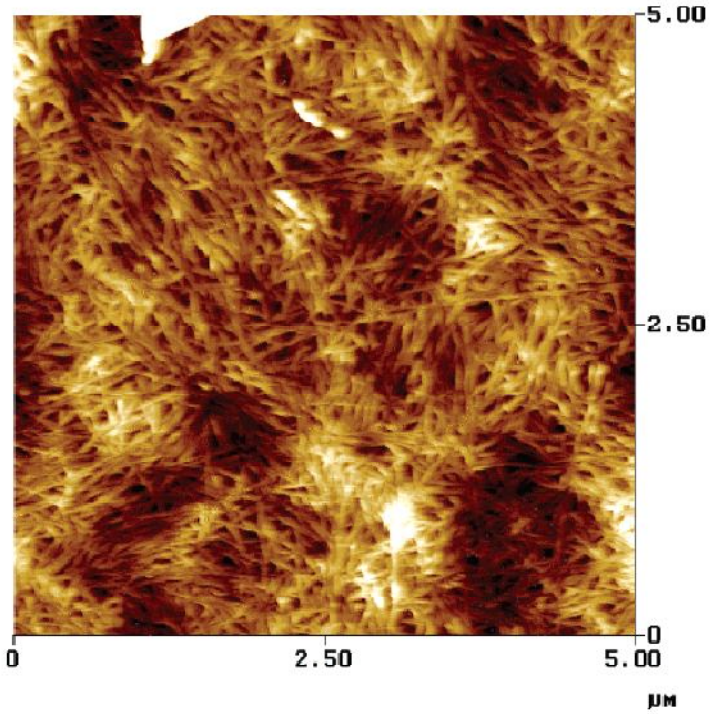

Figure II-30. AFM picture taken from a sPS/naphthalene system (C_{pol}) = 0.30 g/g) after sublimation of naphthalene through vacuum extraction for 10 days. Reprinted from Macromolecules 39(18) 5957. Copyright 2006 American Chemical Society.

Syndiotactic Polystyrene Nanofibers via Electrospinning

High-temperature electrospinning of sPS in *o*-dichlorobenzene was done by Cheng and coworkers. The as-spun fibers were amorphous as determined via WAXD analysis. Thermal annealing of the electrospun fibers resulted in the formation of the α-form of sPS. The size and morphological structure of sPS of varying concentrations in *o*-dichlorobenzene was observed using SEM as shown in Figure II-31. At low concentrations such as 7 wt.%, only beads of sPS were obtained which is lower than the critical entanglement concentration of approximately 11.6 wt%.

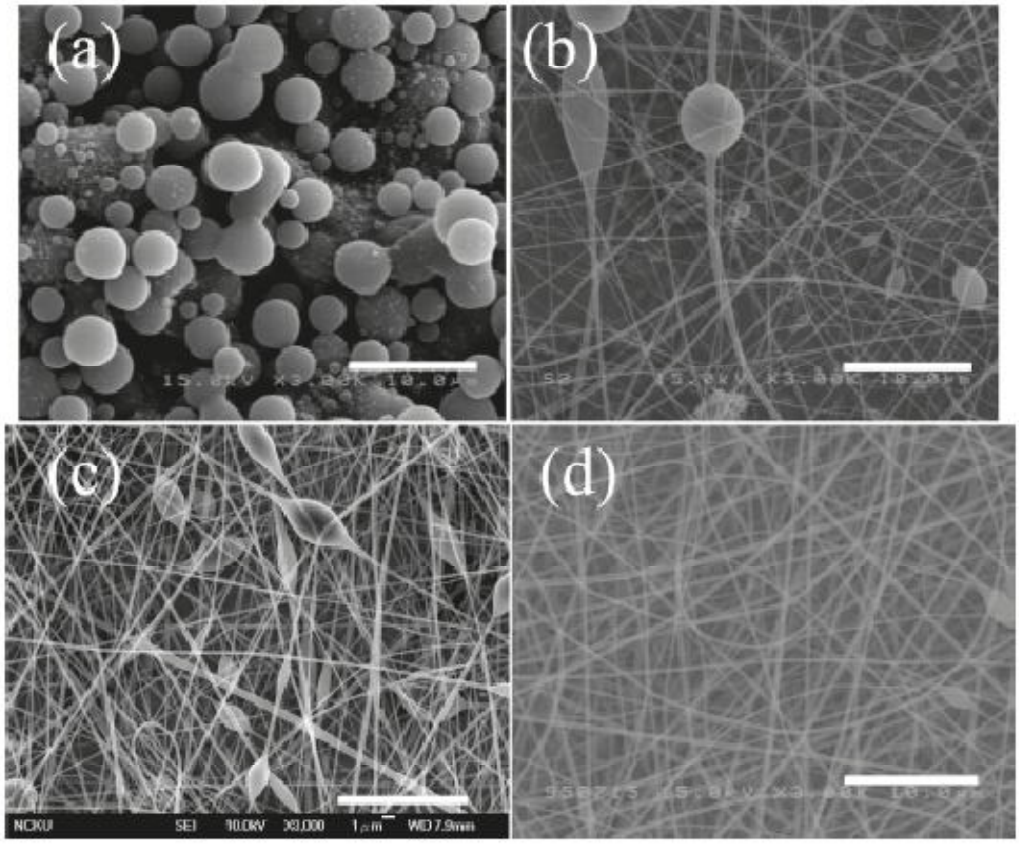

Figure II-31. Morphologies of sPS fibers electrospun from solutions of (a) 7, (b) 12, (c) 14, and (d) 14 wt. %: (a-c) obtained by IR heating and (d) by superheated o-DCB vapor to control the needle-end temperature. The scale bar is 10 μm. Reprinted from Macromolecules 43(5), 2371. Copright 2010 American Chemical Society.

Fibers with beads were formed at sPS solution concentrations near the entanglement concentration by electrospinning with IR heating. The fiber dimensions were more uniform and less beads were present when using superheated *o*-dichlorobenzene vapor to control temperature at the needle zone instead of an IR emitter.

Functionalization of Syndiotactic Polystyrene

Syndiotactic polystyrene exhibits desirable properties as an engineering thermoplastic, such as high melting temperature and chemical resistance in combination with very a unique crystallization behavior through the formation of multiple crystalline forms each with a distinctive set of properties. Despite these outstanding properties and interesting polymorphic behavior, the utilization of sPS in many engineering and technological applications has been severely limited due to the brittleness of the material, the lack of polar functionality to promote adhesion to other substrates, and high temperatures required to process sPS both in solution and in the melt [106]. In order to overcome such drawbacks, a number of researchers have modified sPS through the incorporation of functional groups. The techniques and approaches utilized to modify sPS have included copolymerization [107-111], chain transfer functionalization, polymerization of substituted styrenes [112-117], modification of sPS through grafting [118-120], and post-polymerization functionalization [121-134].

The incorporation of functional groups into sPS drastically affects the crystallization kinetics and polymorphic behavior of the semicrystalline homopolymer. Orler and coworkers study the effect of adding small concentrations of sulfonate groups onto sPS [129]. They found that the crystallization behavior was drastically reduced with the incorporation of as little as 2 mol% of sulfonate groups [129]. The degree of crystallinity of the sPS homopolymer decreased from 27% to 12% upon incorporating 3.4 mol% of sulfonate groups to the sn the degree of crystallinity and the rate of crystallization were also observed for sPS functionalized with other functional groups such as the benzoylate group [125].

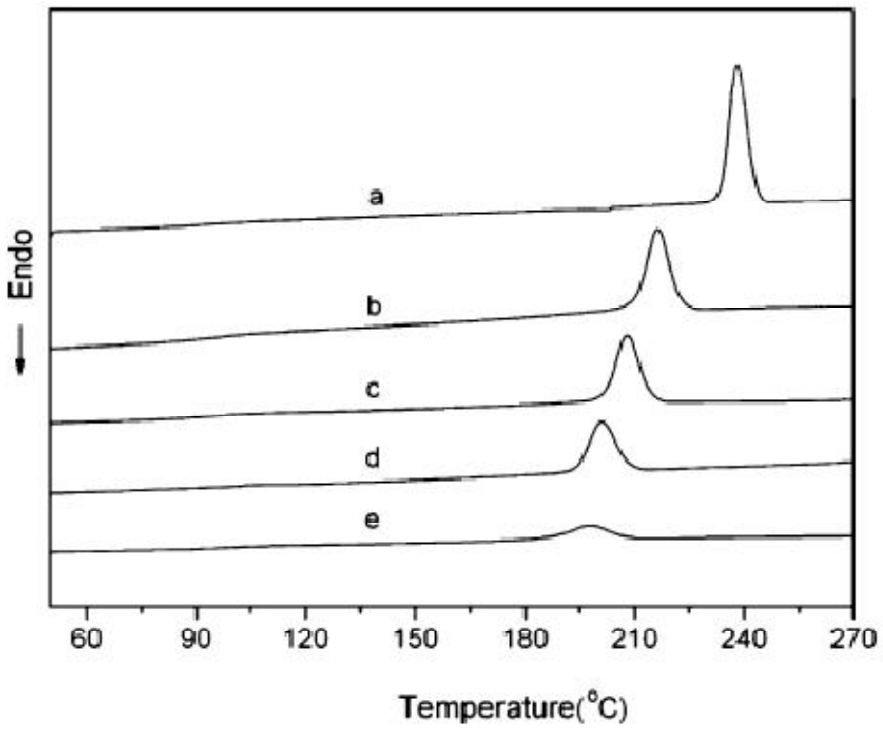

Figure II-32. DSC cooling curves of (a) sPS and benzoylated syndiotactic polystyrene with different benzoylation level, (b) 7 mol%, (c) 16.8 mol%, (d) 24.5 mol%, and (e) 33.4 mol%. Reprinted from Journal of Polymer Research 14(4), 291. Copyright 2007 Springer.

The DSC cooling curve of pure sPS and benzoylated sPS in Figure II-32 show the effect of the degree of benzoylation on the crystallization behavior of sPS upon from the melt. It can be seen that as the concentration of the benzoylate group increases that the area of the crystallization exotherm decreases and shifts to lower temperatures suggesting that the benzoylate groups retard the crystallization process.

The incorporation of a comonomer during the polymerization of sPS has an effect on the polymorphic behavior as reported by Manfredi and coworkers [109]. Using WAXD analysis, they found that the incorporation para-methylstyrene (pMS) units favors the formation of the α-form and at para-methylstyrene contents of 20 mol% that WAXD profile of the sPS/pMS copolymer exhibits only the α-form crystalline structure.

Functionalized sPS has been investigated as a material for proton exchange membranes [133] and as matrices for the formation of polymer nanocomposites [135-136]. The addition of the functional groups to the sPS homopolymer improved the performance and properties of the unfunctionalized material thereby bringing attention to this material as an inexpensive alternative for the production of advanced polymer composites.

Syndiotactic polystyrene is a very interesting semicrystalline polymer with a very complex polymorphic behavior. Each of the crystalline forms appears to have a unique set of properties that has the potential to be utilized for a specific application. The helical forms of sPS have gained considerable interest over the years due to specific arrangements of the sPS chains that can lead to the formation of nanocavities and nanochannels within the sPS crystalline phase. The potential to exploit these cavities and channels as hosts for the incorporation of different guest molecules remains to be a major research interest for the use of sPS as an inexpensive material for advanced technological applications.

REFERENCES

1. Tomotsu N, Newman TH, Takeuchi M, Campbell R, and Schellenberg J. Transition Metal Catalysts for Syndiotactic Polystyrene: John Wiley & Sons, Inc., 2009.
2. Pó R and Cardi N. Progress in Polymer Science 1996;21(1):47-88.
3. Schellenberg J and Tomotsu N. Progress in Polymer Science 2002;27(9):1925-1982.
4. Schellenberg J. Progress in Polymer Science 2009;34(8):688-718.
5. Woo EM, Sun YS, and Yang CP. Progress in Polymer Science 2001;26(6):945-983.
6. Gowd EB, Tashiro K, and Ramesh C. Progress in Polymer Science 2009;34(3):280-315.
7. Tomotsu N, Malanga M, and Schellenberg J. Synthesis of Syndiotactic Polystyrene: John Wiley & Sons, Ltd, 2003.
8. Tomotsu N and Ishihara N. Recent development of catalysts for syndiospecific polymerization of styrene. In: Hideshi H and Kiyoshi O, editors. Studies in Surface Science and Catalysis, vol. Volume 121: Elsevier, 1999. pp. 269-276.
9. Ishihara N. Macromolecular Symposia 1995;89.
10. Malanga M. Adv. Mater. 2000;12(null):1869.
11. Fiola T, Okada A, Mihara M, and Nichols K. Applications of Syndiotactic Polystyrene: John Wiley & Sons, Inc., 2009.
12. Rizzo P, D'Aniello C, De Girolamo Del Mauro A, and Guerra G. Macromolecules 2007;40(26):9470-9474.
13. Li Y, He J, Qiang W, and Hu X. Polymer 2002;43(8):2489-2494.
14. Guerra G, Vitagliano VM, De Rosa C, Petraccone V, and Corradini P. Macromolecules 1990;23(5):1539-1544.
15. Sun Z, Morgan RJ, and Lewis DN. Polymer 1992;33(3):660-661.

16. Hodge K, Prodpran T, Shenogina NB, and Nazarenko S. Journal of Applied Polymer Science 2002;83(12):2705-2715.

17. Greis O, Xu Y, Asano T, and Petermann J. Polymer 1989;30(4):590-594.

18. Corradini P, De Rosa C, Guerra G, Napolitano R, Petraccone V, and Pirozzi B. European Polymer Journal 1994;30(10):1173-1177.

19. De Rosa C. Macromolecules 1996;29(26):8460-8465.

20. DeRosa C, Guerra G, Petraccone V, and Corradini P. Polymer Journal 1991;23(12):1435-1442.

21. Wang C, Chen C-C, Hung C-H, and Lin K-S. Polymer 2004;45(19):6681-6689.

22. De Rosa C, Ruiz de Ballesteros O, Di Gennaro M, and Auriemma F. Polymer 2003;44(6):1861-1870.

23. Sorrentino A, Pantani R, and Titomanlio G. Journal of Polymer Science Part B: Polymer Physics 2007;45(2):196-207.

24. Napolitano R and Pirozzi B. Macromolecules 1993;26(26):7225-7228.

25. Wu S-C and Chang F-C. Polymer 2004;45(3):733-738.

26. Ho R-M, Lin C-P, Hseih P-Y, Chung T-M, and Tsai H-Y. Macromolecules 2001;34(19):6727-6736.

27. De Rosa C, Rapacciuolo M, Guerra G, Petraccone V, and Corradini P. Polymer 1992;33(7):1423-1428.

28. Chatani Y, Shimane Y, Ijitsu T, and Yukinari T. Polymer 1993;34(8):1625-1629.

29. Wang C, Hsu YC, and Lo CF. Polymer 2001;42(20):8447-8460.

30. Hoffman JD and Weeks J. Natl Bur Stand 1962;66A(1):13-28.

31. Marand H, Xu J, and Srinivas S. Macromolecules 1998;31(23):8219-8229.

32. Xu J, Srinivas S, Marand H, and Agarwal P. Macromolecules 1998;31(23):8230-8242.

33. Su CH, Jeng U, Chen SH, Cheng CY, Lee JJ, Lai YH, Su WC, Tsai JC, and Su AC. Macromolecules 2009;42(12):4200-4207.

34. Milano G and Guerra G. Progress in Materials Science 2009;54(1):68-88.

35. Guerra G, Milano G, Venditto V, Musto P, De Rosa C, and Cavallo L. Chemistry of Materials 2000;12(2):363-368.

36. Annunziata L, Albunia AR, Venditto V, Mensitieri G, and Guerra G. Macromolecules 2006;39(26):9166-9170.

37. Giordano M, Russo M, Cusano A, Mensitieri G, and Guerra G. Sensors and Actuators B: Chemical 2005;109(2):177-184.

38. Giordano M, Russo M, Cusano A, and Mensitieri G. Sensors and Actuators B: Chemical 2005;107(1):140-147.

39. Giordano M, Russo M, Cusano A, Cutolo A, Mensitieri G, and Nicolais L. Applied Physics Letters 2004;85(22):5349-5351.

40. Mensitieri G, Venditto V, and Guerra G. Sensors and Actuators B: Chemical 2003;92(3):255-261.

41. De Girolamo Del Mauro A, Carotenuto M, Venditto V, Petraccone V, Scoponi M, and Guerra G. Chemistry of Materials 2007;19(24):6041-6046.

42. Rizzo P, Lamberti M, Albunia AR, Ruiz de Ballesteros O, and Guerra G. Macromolecules 2002;35(15):5854-5860.

43. Chatani Y, Shimane Y, Inoue Y, Inagaki T, Ishioka T, Ijitsu T, and Yukinari T. Polymer 1992;33(3):488-492.

44. Daniel C, Menelle A, Brulet A, and Guenet J-M. Polymer 1997;38(16):4193-4199.

45. Daniel C, Avallone A, Rizzo P, and Guerra G. Macromolecules 2006;39(14):4820-4823.

46. Rizzo P, Costabile A, and Guerra G. Macromolecules 2004;37(8):3071-3076.

47. Moyses S, Sonntag P, Spells SJ, and Laveix O. Polymer 1998;39(15):3537-3544.

48. Albunia AR, Musto P, and Guerra G. Polymer 2006;47(1):234-242.

49. Rizzo P, Albunia AR, Milano G, Vendiito V, Guerra G, Mensitieri G, and Di Maio L. Macromolecular Symposia 2002;185(1):65-75.

50. Vittoria V, de Candia F, Iannelli P, and Immirzi A. Die Makromolekulare Chemie, Rapid Communications 1988;9(11):765-769.

51. Immirzi A, de Candia F, Iannelli P, Zambelli A, and Vittoria V. Makromol. Chem., Rapid Commun. 1988;9(null):761.

52. Vittoria V, Russo R, and de Candia F. Polymer 1991;32(18):3371-3375.

53. Gowd EB, Nair SS, and Ramesh C. Macromolecules 2002;35(22):8509-8514.

54. Gowd EB, Nair SS, Ramesh C, and Tashiro K. Macromolecules 2003;36(19):7388-7397.

55. Albunia AR, Graf R, Guerra G, and Spiess HW. Macromolecular Chemistry and Physics 2005;206(7):715-724.

56. Gupper A, Chan KLA, and Kazarian SG. Macromolecules 2004;37(17):6498-6503.

57. Tarallo O and Petraccone V. Macromolecular Chemistry and Physics 2005;206(6):672-679.

58. Rastogi S, Goossens JGP, and Lemstra PJ. Macromolecules 1998;31(9):2983-2998.

59. Mahesh KPO, Sivakumar M, Yamamoto Y, Tsujita Y, Yoshimizu H, and Okamoto S. Journal of Polymer Science Part B: Polymer Physics 2004;42(18):3439-3446.

60. Musto P, Manzari M, and Guerra G. Macromolecules 2000;33(1):143-149.

61. Guerra G, Musto P, Karasz FE, and MacKnight WJ. Die Makromolekulare Chemie 1990;191(9):2111-2119.

62. Yoshioka A and Tashiro K. Macromolecules 2003;36(9):3001-3003.

63. Albunia AR, Di Masi S, Rizzo P, Milano G, Musto P, and Guerra G. Macromolecules 2003;36(23):8695-8703.

64. Uda Y, Kaneko F, and Kawaguchi T. Macromolecules 2005;38(8):3320-3326.

65. Uda Y, Kaneko F, and Kawaguchi T. Macromolecular Rapid Communications 2004;25(22):1900-1904.

66. Sivakumar M, Yamamoto Y, Amutharani D, Tsujita Y, Yoshimizu H, and Kinoshita T. Macromolecular Rapid Communications 2002;23(1):77-79.

67. Venditto V, De Girolamo Del Mauro A, Mensitieri G, Milano G, Musto P, Rizzo P, and Guerra G. Chemistry of Materials 2006;18(9):2205-2210.

68. Milano G, Guerra G, and Müller-Plathe F. Chemistry of Materials 2002;14(7):2977-2982.

69. Tamai Y, Tsujita Y, and Fukuda M. Journal of Molecular Structure 2005;739(1-3):33-40.

70. Albunia AR, Grassi A, Milano G, Rizzo P, Venditto V, Musto P, and Guerra G. Macromolecular Symposia 2006;234(1):102-110.

71. Rizzo P, Della Guardia S, and Guerra G. Macromolecules 2004;37(21):8043-8049.

72. Tarallo O, Petraccone V, R. Albunia A, Daniel C, and Guerra G. Macromolecules 2010;43(20):8549-8558.

73. Petraccone V, Tarallo O, Venditto V, and Guerra G. Macromolecules 2005;38(16):6965-6971.

74. Ray B, Elhasri S, Thierry A, Marie P, and Guenet J-M. Macromolecules 2002;35(26):9730-9736.

75. Guadagno L, Baldi P, Vittoria V, and Guerra G. Macromolecular Chemistry and Physics 1998;199(12):2671-2675.

76. Rani DA, Yamamoto Y, Mohri S, Sivakumar M, Tsujita Y, and Yoshimizu H. Journal of Polymer Science Part B: Polymer Physics 2003;41(3):269-273.

77. Sivakumar M, Suzuki T, Yamamoto Y, Mahesh KPO, Yoshimizu H, and Tsujita Y. Journal of Membrane Science 2004;238(1-2):75-81.

78. Ma W, Yu J, and He J. Macromolecules 2005;38(11):4755-4760.

79. De Rosa C, Guerra G, Petraccone V, and Pirozzi B. Macromolecules 1997;30(14):4147-4152.

80. Manfredi C, Del Nobile MA, Mensitieri G, Guerra G, and Rapacciuolo M. Journal of Polymer Science Part B: Polymer Physics 1997;35(1):133-140.

81. Rani DA, Yamamoto Y, Saito A, Sivakumar M, Tsujita Y, Yoshimizu H, and Kinoshita T. Journal of Polymer Science Part B: Polymer Physics 2002;40(6):530-536.

82. Sivakumar M, Mahesh KPO, Yamamoto Y, Yoshimizu H, and Tsujita Y. Journal of Polymer Science Part B: Polymer Physics 2005;43(14):1873-1880.

83. Guerra G, Manfredi C, Musto P, and Tavone S. Macromolecules 1998;31(4):1329-1334.

84. Mahesh KPO, Sivakumar M, Yamamoto Y, Tsujita Y, Yoshimizu H, and Okamoto S. Journal of Membrane Science 2005;262(1-2):11-19.

85. Manfredi C, De Rosa C, Guerra G, Rapacciuolo M, Auriemma F, and Corradini P. Macromolecular Chemistry and Physics 1995;196(9):2795-2808.

86. Rizzo P, Daniel C, De Girolamo Del Mauro A, and Guerra G. Chemistry of Materials 2007;19(16):3864-3866.

87. Petraccone V, Ruiz de Ballesteros O, Tarallo O, Rizzo P, and Guerra G. Chemistry of Materials 2008;20(11):3663-3668.

88. Tarallo O, Schiavone MM, Petraccone V, Daniel C, Rizzo P, and Guerra G. Macromolecules 2010;43(3):1455-1466.

89. Albunia AR, Rizzo P, and Guerra G. Chemistry of Materials 2009;21(14):3370-3375.

90. Figueroa-Gerstenmaier S, Daniel C, Milano G, Vitillo JG, Zavorotynska O, Spoto G, and Guerra G. Macromolecules 2010;43(20):8594-8601.

91. Daniel C, Giudice S, and Guerra G. Chemistry of Materials 2009;21(6):1028-1034.

92. Ma W, Yu J, and He J. Macromolecules 2004;37(18):6912-6917.

93. Sun YS, Woo EM, Wu MC, and Ho R-M. Polymer 2003;44(18):5293-5302.

94. Rizzo P, Albunia AR, and Guerra G. Polymer 2005;46(23):9549-9554.

95. Gowd EB, Shibayama N, and Tashiro K. Macromolecules 2006;39(24):8412-8418.

96. Albunia AR, Annunziata L, and Guerra G. Macromolecules 2008;41(7):2683-2688.

97. Hoffman JD and Miller RL. Polymer 1997;38(13):3151-3212.

98. Woo EM, Sun YS, and Lee ML. Polymer 1999;40(15):4425-4429.

99. Yoshioka A and Tashiro K. Polymer 2003;44(21):6681-6688.

100. Sun YS and Woo EM. Polymer 2001;42(5):2241-2245.

101. Wang C, Lin C-C, and Chu C-P. Polymer 2005;46(26):12595-12606.

102. Su CH, Jeng U, Chen SH, Lin SJ, Wu WR, Chuang WT, Tsai JC, and Su AC. Macromolecules 2009;42(17):6656-6664.

103. Wu H, Wang W, Yang H, and Su Z. Macromolecules 2007;40(12):4244-4249.

104. Malik S, Roizard D, and Guenet J-M. Macromolecules 2006;39(18):5957-5959.

105. Cheng Y-W, Lu H-A, Wang Y-C, Thierry A, Lotz B, and Wang C. Macromolecules 2010;43(5):2371-2376.

106. Zinck P, Bonnet F, Mortreux A, and Visseaux M. Progress in Polymer Science 2009;34(4):369-392.

107. Luo Y, Baldamus J, and Hou Z. Journal of the American Chemical Society 2004;126(43):13910-13911.

108. Dong JY, Manias E, and Chung TC. Macromolecules 2002;35(9):3439-3447.

109. Manfredi C, Guerra G, De Rosa C, Busico V, and Corradini P. Macromolecules 1995;28(19):6508-6515.

110. De Rosa C, Buono A, Ricci A, De Luca F, and Caporaso L. Macromolecules 2003;36(17):6389-6400.

111. Chen R, Wu Q, Zhu F, and Lin S. Journal of Applied Polymer Science 2003;89(6):1596-1605.

112. Ishihara N, Kuramoto M, and Uoi M. Macromolecules 1988;21(12):3356-3360.

113. Nakatani H, Nitta K-h, Takata T, and Soga K. Polymer Bulletin 1997;38(1):43-48.

114. Thomann R, Sernetz FG, Heinemann J, Steinmann S, Mulhaupt R, and Kressler J. Macromolecules 1997;30(26):8401-8409.

115. Xu G and Chung TC. Macromolecules 2000;33(16):5803-5809.

116. Gao Y, Li S, Li H, and Wang X. European Polymer Journal 2005;41(10):2329-2334.

117. Kim Y and Do Y. Macromolecular Rapid Communications 2000;21(16):1148-1155.

118. Abbasian M, Rahmani S, Mohammadi R, and Entezami AA. Journal of Applied Polymer Science 2007;104(1):611-619.

119. Li H-M, Chen H-b, Shen Z-G, and Lin S. Polymer 2002;43(20):5455-5461.

120. Senoo K, Endo K, Tosaka M, Murakami S, and Kohjiya S. Macromolecules 2001;34(5):1267-1273.

121. Govindaiah P, Avadhani CV, and Ramesh C. Macromolecular Symposia 2006;241(1):88-94.

122. Li J and Li H-M. European Polymer Journal 2005;41(4):823-829.

123. Shin J, Jensen SM, Ju J, Lee S, Xue Z, Noh SK, and Bae C. Macromolecules 2007;40(24):8600-8608.

124. Gao Y and Li H-M. Polymer International 2004;53(10):1436-1441.

125. Gao Y, Li H-M, Liu F-S, Wang X-Y, and Shen Z-G. Journal of Polymer Research 2007;14(4):291-296.

126. Orler EB, Calhoun BH, and Moore RB. Macromolecules 1996;29(18):5965-5971.

127. Orler EB, Gummaraju RV, Calhoun BH, and Moore RB. Macromolecules 1999;32(4):1180-1188.

128. Orler EB and Moore RB. Macromolecules 1994;27(17):4774-4780.

129. Orler EB, Yontz DJ, and Moore RB. Macromolecules 1993;26(19):5157-5160.

130. Su Z, Hsu SL, and Li X. Macromolecules 1994;27(1):287-291.

131. Li H-M, Liu J-C, Zhu F-M, and Lin S-A. Polymer International 2001;50(4):421-428.

132. Lavorgna M, Fusco L, Piscitelli F, Mensitieri G, Agoretti P, Borriello A, and Mascia L. Polymer Engineering & Science 2008;48(12):2389-2399.

133. Borriello A, Lavorgna M, Malagnino N, Mensitieri G, Napoletano T, and Nicolais L. Macromolecular Symposia 2004;218(1):293-302.

134. Borriello A, Agoretti P, Ambrosio L, Fasano G, Pellegrino M, Venditto V, and Guerra G. Chemistry of Materials 2009;21(14):3191-3196.

135. Govindaiah P, Mallikarjuna SR, and Ramesh C. Macromolecules 2006;39(21):7199-7203.

136. Benson SD and Moore RB. Polymer 2010;51(23):5462-5472.

CHAPTER III
CHEMICAL MODIFICATION OF POLYMERS VIA POST-POLYMERIZATION MODIFICATION
A REVIEW OF METHODS AND CHARACTERIZATION TECHNIQUES

The chemical modification of polymers is of significant interest to achieve or enhance a range of polymer properties[1-2] including interfacial adhesion [3-7], flame retardance [8-10], hydrophilicity/wettability [11] , electrical properties [12] ,and increased biocompatibility [13-18]. The methods employed to prepare chemically-modified polymers has included both surface and bulk methods and have been explored extensively as a means to tailor polymer properties for specific applications.

Surface Modification of Polymers

Surface-modification of polymers is of considerable interest as many industrially-important engineering polymers are low surface energy materials that lack functional groups that promote adhesion [19]. As a result extensive research has focused on the surface modification of low surface energy polymers to enhance interfacial adhesion and modify other surface properties such as abrasion resistance, gloss, and weatherability. Surface modified polymers are critically important materials in numerous technological fields including the textile [20-22], aerospace , biomedical [23-27], and automotive industries. As a result, these industries have significantly driven the advancement and development of techniques of preparation and characterization surface-modified polymers.

Polymer surfaces can be modified using both physical and chemical techniques depending on the desired final properties and end-use environment for the modified polymer. The modification of a polymer surface is often desired when there is a need to retain the bulk properties of the material. A combination of both physical and chemical techniques is often utilized to modify the surface of a polymer as well.

Surface Modification of Polymer via Physical Methods

There are several physical methods currently employed and investigated to modify polymer surfaces. These methods include flame [28-30] , corona discharge [31-33], UV and gamma rays [34-36], electron and ion beams, laser [37-38], and plasma treatments [39-42]. Each of these methods has a distinct set of advantages and drawbacks in terms of the efficacy and ease of use and the selection of a physical surface modification technique depends heavily upon the desired final properties and end-use application of the material. Physical surface modification techniques are of considerable interest as these methods offer environmentally-friendly, clean processes that do not require the use of solvents to modify the polymer surface as required for chemical modification methods eliminating the costs and numerous considerations associated with the cost of solvent disposal and recycling. Physical methods of polymer surface modification are also preferred methods for many industrial processes as some physical surface modification methods are low cost and readily incorporated into the manufacturing environment.

Surface Modification of Polymers via Chemical Methods

The physical modification of polymer surfaces using methods such as plasma treatment are effective in the modification of polymer surface, but often lack the ability to provide the necessary changes in the polymer surface for specific applications. As a result, chemical

modification of the polymer surface via chemical methods is required. The modification of polymer surfaces via chemical methods has been successfully employed to introduce a wide range of chemical species to polymer surfaces such as functional groups such as hydroxyl, carboxyl [43-44], and silane [45].

The introduction of functional groups to polymer surfaces and substrates via chemical methods has been extensively explored for both relatively inert and reactive polymers. Gibson and Bailey studied the sulfonation of free standing polystyrene films with a focus on identifying techniques for the quantitative analysis of the extent of sulfonation through the polystyrene film surface, the development of conditions for reproducible controlled sulfonation, and the determination of the kinetics of the reaction [46]. Gibson and Bailey conducted the surface modification of PS films at room temperature in a dry box using 100% sulfuric acid, made from concentrated sulfuric acid and fuming sulfuric acid. They determined the extent of sulfonation through the film surface using a combination of interferometric measurements and X-ray photoelectron spectroscopy (XPS). Under the reaction conditions utilized, Gibson and Bailey found that the extent of sulfonation through the free-standing PS film thickness was greater than 2000 monolayers in depth which corresponded to a 3.5 μm thick sulfonated layer on each side of the PS film.

Poly(ethylene terepthalate) (PET) is a vital engineering thermoplastic and a core material in many different industrial applications due to its good mechanical strength, toughness, fatigue resistance, and high melting temperature. However, like many other thermoplastics, PET has a low surface energy and resultant poor adhesion and wettability. As a result, considerable attention has been given to the surface modification of PET. Unlike, many chemically- resistant fluoropolymers that are candidates for surface modification due to their hydrophobicity and low

surface energy such as poly-(tetrafluoroethylene), poly(chlorotrifluoroethylene), and poly(vinylidene fluoride), PET is more reactive due to the presence of the ester groups on the polymer backbone. The surface functionalization of PET has been investigated due to its innate chemical reactivity with careful consideration given to the prevention of polymer degradation through chain cleavage of the PET ester bonds. Chen and McCarthy utilized reduction and glycolysis reactions to introduce alcohol functionality to the surface of PET films to film depths of less than 40 Å [47]. The type of hydroxyl groups generated on the surface of PET via reduction and glycolysis are shown in Figure III-1.

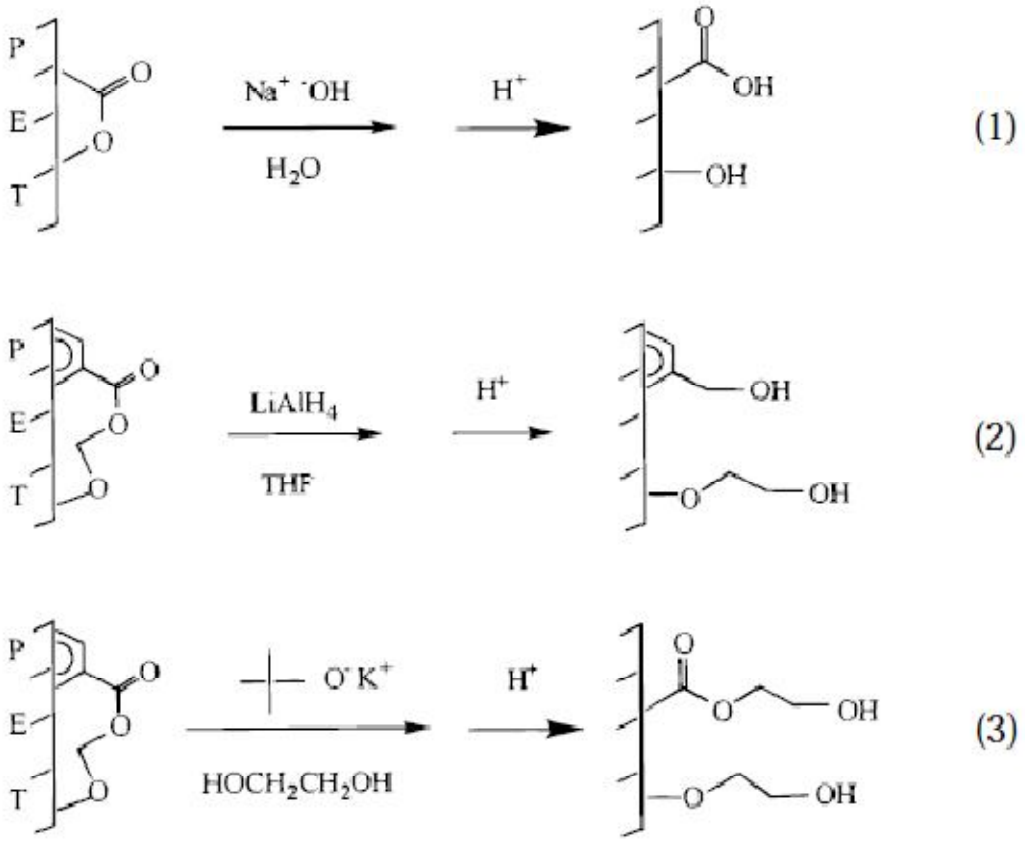

Figure III-1. Different surface-chemical structures of PET produced via (1) hydrolysis with sodium hydroxide, (2) reduction with lithium aluminum hydride, and (3) transesterification with ethylene glycol. Reprinted from Macromolecules 31(11), 3648. Copyright 1998 American Chemical Society.

They determined that PET-OH prepared via glycolysis had double the surface density of hydroxyl groups than surface-modified PET-OH prepared via reduction. Chen and McCarthy were able to increase the surface density of hydroxyl groups via reduction of the PET surface by first subjecting the PET film to solvent annealing in THF. They attributed the increase in the density of hydroxyl groups on the PET surface created through reduction to a reorientation of the PET chains during solvent annealing. The authors note that "the surface functional group density will depend on the morphology of the polymer near the surface, and, in particular, on the orientation of chains relative to the plane of the surface" [47] which does suggest controlling the morphology of the polymer may provide a method to tune or control the functionalization of the polymer surface.

Advanced methods of chemical functionalization of polymer surfaces include layer-by-layer deposition [48-51], grafting polymers from polymer substrates [52-55], growth of polymer brushes from the polymeric substrate surfaces via controlled living free radical polymerization techniques [56-59], and surface modification via click chemistry [60].

The modification of chemically-resistant thermoplastics such as fluoropolymers has been explored in depth [3, 61]. Although fluoropolymers are low surface energy materials, they possess a wide range of desirable bulk material properties such as chemical resistance and high thermal stability. Poly(tetrafluoroethylene) is a widely used engineering thermoplastic due to its many advantageous properties. However, due to the extremely low surface energy and high hydrophobicity of PTFE, surface modification is necessary for the polymer to be utilized in applications that require good adhesion or biocompatibility for medical applications. Several approaches have been taken to modify the surface such as plasma, flame, and ozone treatments. The aforementioned methods effectively lower the surface energy of PTFE, but do not provide

advanced control in creating a modified surface that contains tunable chemical moieties or moieties with advanced morphologies. Yu and coworkers, however, utilized surface-initiated RAFT and ATRP to modify the surface of PTFE with comb copolymer brushes [62]. The surface modification of PTFE first required exposing the substrate to argon plasma treatment to generate formation of peroxide and hydroperoxide species. Figure III-2 provides the reaction scheme utilized by Yu and coworkers to functionalize the PTFE surface with comb copolymer brushes. The chemical composition the modified PTFE surfaces were analyzed using XPS and the change in the hydrophobicity of the modified PTFE surfaces were monitored using static contact angle measurements using water as the solvent. The multi-step surface fucntionalization of PTFE as shown in Figure III-2 clearly demonstrates the level of complexity involved to prepare well-defined polymer brushes on the PTFE surface. Even though several steps were required to create the changes in the low energy PTFE surface, experimental data obtained via XPS and water contact angle measurements demonstrated that a significant reduction in the hydrophobicity of the surface was obtained though the polymerization of the hydrophilic monomers including ethylene glycol, methyl ether methacrylate, and sodium 4-styrenesulfonic acid.

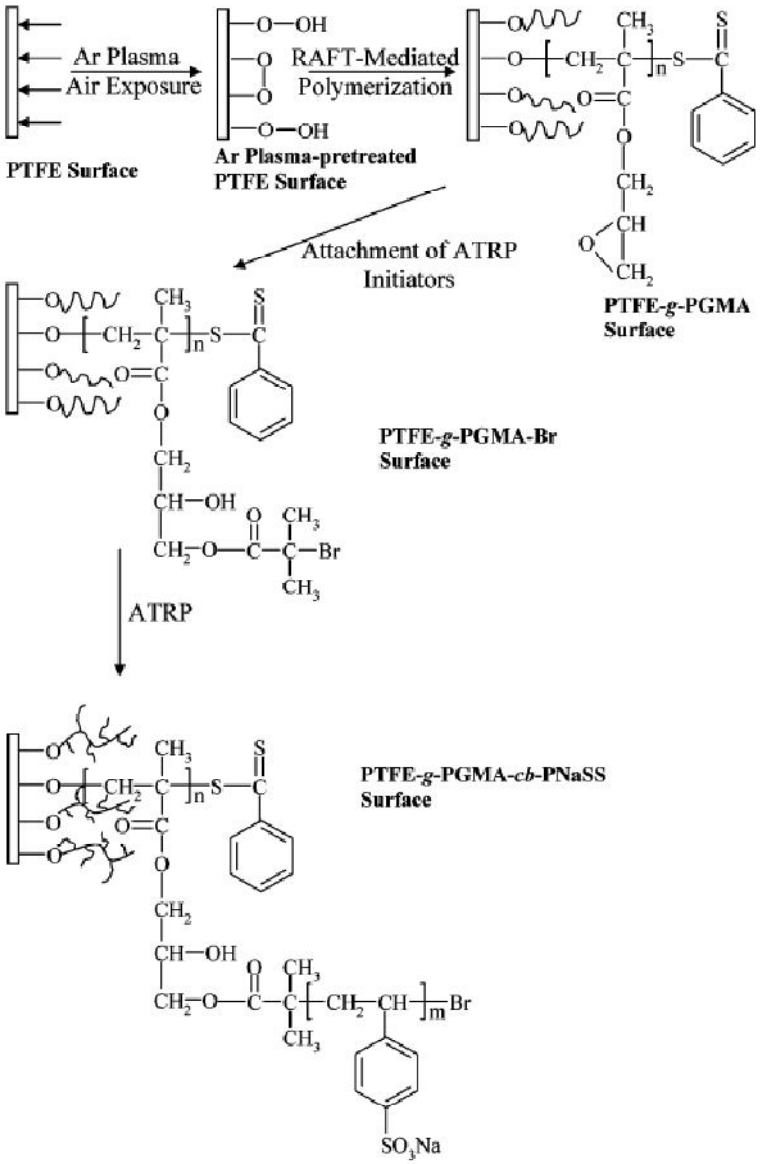

Figure III-2. Schematic diagram illustrating the processes of Ar plasma pretreatment of the PTFE surface, surface-initiated RAFT polymerization of GMA, attachment of the ATRP initiators to the PGMA brushes, and preparation of the comb copolymer brushes on the PTFE surface. Reprinted from Langmuir 21(1), 450. Copyright 2004 American Chemical Society.

.

Table III-1 provides the chemical composition of the surface determined using XPS along with the corresponding water contact angle data. It can be seen that the surface-initiated comb copolymer brushes effectively modify the hydrophobicity of PTFE. The PTFE surface modified with the comb copolymer PGMA-cb-PNaSS lowers the water contact angle from 115° for the

pristine PTFE to 25°. The study conducted by Yu and coworkers combining physical and chemical methods to modify a polymer substrate is an excellent example of the application and fusion of standard practice and cutting edge technology in the field of polymer science in regards to surface medication.

Table III-1. Chemical Composition and Water Contact Angle of the Pristine and Modified PTFE Surfaces
Reprinted from Langmuir 21(1), 450. Copyright 2004 American Chemical Society.

	chemical composition			
Sample	[O]/[C]	[F]/[C]	[C-H]/[C-O]/[O=C-O]/[CF_2]	Static WCA (± 3°)
Pristine PTFE surface	0.01	1.9		15
90-s Ar plasma-pretreated PTFE surface	0.13	1.1	0.04:0.08:0.11:1	65
PTFE-g-PGMA surface	0.37	0/18	3.6:3.0:1.0:0.7	60
PTFE-g-PGMA + surface	0.42	0.0	3.1:3.0:1.0:0	60
PTFE-g-PGMA-Br surface	0.44	0.13	4.1:2.8:1.0:1.1	58
PTFE-g-PGMA-cb-PPEGMA surface	0.47	0.0	5.1:10.7:1.0:0	35
PTFE-g-PGMA-cb-PNaSS surface	0.3	0.01	11.8:3.0:1.0:0.1	25

A similar surface grafting polymerization method was utilized by Tu and coworkers [63] to modify the surface of PTFE. The PTFE surface was prepared for surface-initiated graft polymerization through sequential hydrogen plasma and ozone treatments to generate C-H and peroxide groups on the PTFE surface, respectively. ATRP was used to create graft copolymers of PTFE and acrylamide, acrylic acid, glycidyl methacrylate, 4-styrenesulfonate (NaSS), and 2-(2-bromoisobutyryloxy) ethyl acrylate (BIEA). The change in the hydrophilicity of the PTFE surface was monitored using XPS, ATIR-FTIR, SEM, AFM, and water contact angle measurements. Modification of the PTFE surface via graft polymerization led to a drastic

reduction of the hydrophobicity of the modified polymers. Tu and coworkers reported the water contact angle measurement of pristine PTFE to be 120° while the PTFE surface modified with a graft copolymer PTFE-g-PBIEA-ar-PSSA exhibited a water contact angle of 25° thereby demonstrating the effectiveness of the graft copolymerization approach in creating a PTFE substrate with a hydrophilic surface.

The field of surface modification has always been of significant interest and continues to advance and develop as new analytical tools and synthetic methods are developed and improved. Surface modification of polymers will undoubtedly continue to be a critical area of study within the field of polymer science.

Chemical Modification of Bulk Polymer Properties

It is often necessary to change not only the polymer surface, but also to modify the bulk polymer in order to manipulate polymer properties such as modulus, tensile strength, and transport properties. The bulk modification of polymers has been accomplished by many methods including melt phase modification of preformed polymer, supercritical fluid phase post-polymerization modification, blending of multiple polymers, copolymerization, and post-polymerization modification of preformed polymer in solution. Each of these methods has certain advantages and limitations that are dependent upon the nature of the polymers/monomers, the processing parameters and variables associated with the technique, and the desired final properties of the material.

Chemical Modification of Polymers via Melt Phase Processing

The utilization of melt phase processing to chemically modify polymers has been explored for decades [64-65]. This method of utilizing twin-screw extruders as reaction vessels

to conduct polymerization and post-polymerization modification of polymers is known as reactive extrusion. Reactive extrusion combines two very important techniques into one process: polymer synthesis/modification and polymer extrusion. The advantages of approaching polymer synthesis/modification via reactive extrusion noted by Moad are that reactive extrusion requires little or no use of solvents, simple product isolation, short reaction times, offers the potential to conduct polymer synthesis and modification as one continuous process, and incurs relatively low costs [66].

Reactive extrusion has been employed to conduct both polymer synthesis and polymer functionalization. Polymer synthesis via the reactive extrusion process is centered on the use of the extruder as the reaction vessel [67]. Although the synthesis of polymer within the extruder is cited to be a more complex process than polymer synthesis that occurs within a traditional reaction vessel, the reactive extrusion technique is still extensively explored [68]. Even though complex interactions and variables such as fluid flow and heat transfer complicate the polymerization of monomers within the extruder, a variety of polymers have been synthesized by reactive extrusion including polyurethane, poly(styrene), and poly(methyl methacrylate). The modes of polymerization have included radical polymerization, ionic polymerization [69-72], metathesis polymerization, and ring opening polymerization [73-76].

Shishuang and coworkers prepared styrene-butadiene multiblock copolymers via reactive extrusion [77]. They characterized the styrene-butadiene multiblock copolymers using FTIR, NMR, TEM, and DMA. The authors noted that when styrene and butadiene are copolymerized within a conventional tank reactor that the butadiene monomer polymerizes first due to its higher reactivity. Styrene does not polymerize until the butadiene has been consumed resulting in the formation of an S-B diblock copolymer or an S-B-S triblock copolymer. In reactive extrusion,

the reaction conditions are quite different and the resulting S-B copolymer consists of a multiblock structure. The development of a multiblock copolymer structure from the styrene and butadiene monomers during reactive extrusion was attributed to the elevated barrel temperature of the extruder. The barrel temperature of the extruder is maintained at a temperature above the vaporization temperature of the butadiene monomer. As the monomer mixture is fed into the extruder reactor, a significant portion of the butadiene monomer is immediately converted to the gaseous phase occupying the unfilled portion of the extruder barrel. The small portion of liquid butadiene monomer remaining in the barrel polymerizes first once initiator is added followed by the polymerization of styrene. As the polymerization of styrene occurs, the melt viscosity of the system increases and occupies a greater portion of the extruder barrel forcing the gaseous butadiene to enter the melt phase and polymerize. Due to the strong mixing that occurs along the barrel of the extruder the gaseous butadiene enters the polymer melt in small volumes resulting in the polymerization of small blocks of butadiene and multiblock styrene-butadiene copolymer. The mechanical properties of the multiblock styrene-butadiene copolymers showed significant improvement over the pure PS homopolymer as shown in Table III-2. It can be seen from the results provided in Table III-2 that there is a significant improvement in the impact strength of the S/B multiblock copolymers compared to the pristine PS homopolymer. This method of copolymerization via reactive extrusion provides an example of a non-conventional method to prepare varied copolymer architectures. The variation in the molecular weight (MW) and molecular distribution (MWD) of the styrene-butadiene multiblock copolymers were not reported by Shishuang and coworkers, but both polymer MW and MWD have a significant impact on polymer properties and behavior. Therefore, due to the importance of molecular weight and polydispersity on polymer properties and the difficulty in controlling

the development of molecular weight via reactive extrusion, this method may not be ideal in creating model systems for the study of structure/property relationships for chemically-modified polymers.

Table III-2. Mechanical Properties of S/B Copolymers
Reprinted from Polymers for Advanced Technologies Volume 91, Issue 4, 2265-2270. Gao Shishuang, Zhang Ying, Zheng Anna, Huining Xiao, Study on nanometer-size styrene-butadiene multiblock copolymer synthesized by reactive extrusion. Copyright 2004 John Wiley and Sons.

	St content, %				
	100	91.9	85.7	81.6	68.4
Tensile strength, MPa	47.9	52.1	43.5	40.4	34.1
Flexural strength, MPa	78.8	94.3	83.9	75.8	56.8
Elongation at break, %	6.7	21.3	76.1	128.3	215.5
Simple beam impact strength					
Notched, kJ/m^2	1.35	2.56	2.68	2.85	3.79
Unnotched, kJ/m^2	6.3	---	10.1	13.7	19.5

Reactive extrusion has also been studied in great detail as a means to chemically modify preformed polymer. Chemical modification of polymers via reactive extrusion has been accomplished using a variety of chemical reactions while the polymer is in the melt state including maleation and carboxylation. Due to these very attractive advantages, reactive extrusion has been explored as a post-polymerization modification technique for many commodity polymers such as polypropylene (PP), polyethylene (PE), and polystyrene (PS) [78].

One of the most common post-polymerization modifications of preformed polymers achieved via reactive extrusion is the grafting of a functional group onto the homopolymer backbone in the presence of a free radical initiator. The grafting of maleic anhydride onto commodity polymers such as PP and PE has been studied extensively. The grafting of maleic anhydride onto PS (MPS) by reactive extrusion was completed by Jo and coworkers [79]. The PS

grafted with maleic anhydride and used to prepare blends with polyamide 6 (PA6). The effect of the maleic anhydride content on the mechanical properties of the PA6/MPS blends was monitored through the evaluation of changes in the tensile properties of the individual homopolymer and the blends. Table III-3 shows the tensile properties for the hompolymers and PA6/MPS blends. There is a readily observable improvement in the tensile modulus, tensile strength, and elongation at break with small concentrations of MPS melt blended with PA6.

Table III-3. Tensile Properties of 80/20 PA6/MPS blends.
Reprinted from Polymer, Vol 37, Issue 9, Won Ho Jo, Chan Dong Park and Moo Sung Lee, Preparation of functionalized polystyrene by reactive extrusion and its blend with polyamide 6, 1709-1714, Copyright 1996, with permission from Elsevier.

Blends	Modulus (MPa)	Strength (MPa)	Elongation (%)
PA6/PS	530 ± 30	57.8 ± 1.2	187 ± 13
PA6/MPS-0.08	574 ± 28	54.2 ± 1.4	257 ± 13
PA6/MPS-0.11	594 ± 48	56.8 ± 1.8	243 ± 10
PA6/MPS-0.18	596 ± 47	57.5 ± 2.6	238 ± 11

An additional important contribution of the work of Jo and coworkers is the observation of the changes in molecular weight of the parent PS homopolymer as a function of maleic anhydride grafting through reactive extrusion. The molecular weight data and glass transition data is provided for PA6, PS, and MPS of varying concentrations in Table III-4. The data shows that there is a decrease in the molecular weight of the MPS graft copolymers compared to the parent PS homopolymer which is an undesired result of the reactive extrusion method.

Table III-4. Properties of PA6, PS, and MPS.
Reprinted from Polymers for Advanced Technologies Volume 91, Issue 4, 2265-2270. Gao Shishuang, Zhang Ying, Zheng Anna, Huining Xiao, Study on nanometer-size styrene-butadiene multiblock copolymer synthesized by reactive extrusion. Copyright 2004 John Wiley and Sons.

Designation	M_n ($x10^3$)	M_w ($x10^3$)	Tg (°C)	MAH content (wt.%)
PS	115	306	100	---
PA6	18	---	44	---
MPS-0.08	113	300	100	0.083
MPS-0.11	113	282	99	0.113
MPS-0.18	113	288	97	0.183

Reactive extrusion provides a means to chemically modify both commodity and specialty polymers through the utilization of industry-standard equipment which makes it an economically-viable option for the production of functionalized polymers with improved properties. The drawbacks associated with reactive extrusion such as the need to achieve intimate mixing of reactants and substrates, the high reaction temperatures necessary to form a polymer melt, and the extent of polymer degradation or crosslinking that may accompany processing are significant challenges that must be addressed in order for this method to be widely accepted and routinely used within an industrial setting.

Chemical Modification of Polymers via Supercritical Fluid Processing

The utilization of supercritical fluids especially supercritical carbon dioxide ($ScCO_2$) has gained considerable and continuous growing attention within the field of polymer science and engineering since the early 1990s. $ScCO_2$ is considered a green solvent [80-82] due to the very mild reaction and processing conditions associated with its use to polymerize [83-86], chemically modify [87-90], and process[91-94] both natural and synthetic polymers. The ability

of $ScCO_2$ to plasticize a polymer thereby lowering the glass transition of the material results in the penetration and swelling of the polymer substrate and penetration of chemical species throughout the polymer under relatively mild conditions. $ScCO_2$ processing is also highly advantageous because polymer synthesis and processing can be done without harsh solvents and high temperatures that can be deleterious to the environment and the polymer, respectively.

Wang and coworkers homogeneously modified bulk polymer substrates using a combination of γ-irradiation and supercritical carbon dioxide processing to graft styrene, methylmethacrylate, N-vinylpyrrolidone, and 2-hydroxyethyl methacrylate from PP and LDPE [95] substrates. The PP and LDPE films of 5 mm thickness were first treated to γ-irradiation to produce free radicals which are trapped within the matrices. $ScCO_2$ was then used as a solvent for the desired monomer and as a swelling agent for the polymer substrate to conduct the grafting of the monomer to the PP or LDPE substrate at 35 -55 °C and 9.0 - 13.0 MPa for various time periods.

A schematic of the grafting procedure utilized by Wang and coworker is shown in Figure III-3. The authors' note the crystallinity of the PP substrate does not change as the grafting process occurs primarily in the amorphous regions of the PP matrix. Wang and coworkers attribute preferential grafting in the amorphous regions of the PP substrate to the difference in the lifetime of the radicals residing in the amorphous and crystalline regions. The radicals produced within the amorphous regions have a shorter lifetime according to Wang and coworkers because they are quickly converted to the peroxide in the presence oxygen. The radicals formed in the crystalline domains migrate to the crystalline/amorphous interfacial region and react with the vinyl monomers to form homopolymer grafts throughout the thickness of the PP substrate.

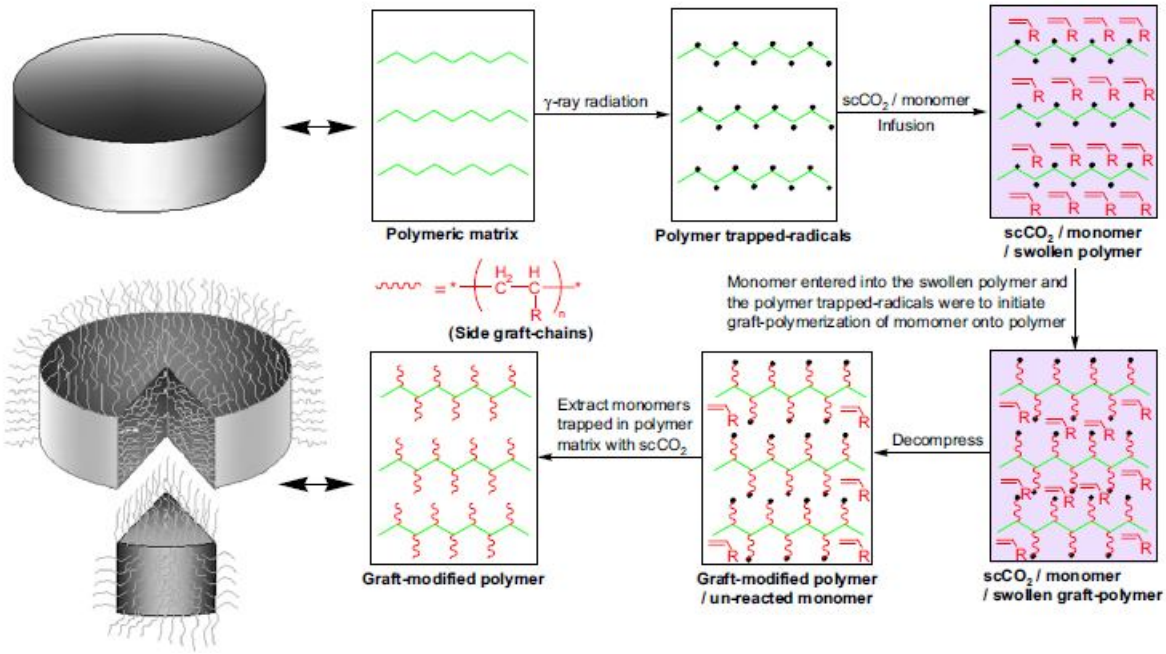

Figure III-3. Schematic representation of uniformly bulk graft modification of vinyl monomers to gamma-rays activated pre-existing polymer materials with $scCO_2$ as both solvent and swelling agent. Reprinted from The Journal of Supercritical Fluids Vol 44, Issue 1, Yi-Ming Wang, Yu Pan, Yi-Long Wang, Guang-Peng Wu, Yan-Juan Wang, Lev N. Nikitin and Xiao-Bing Lu, Bulk graft modification of polyolefin membranes by combining pre-irradiation-induced graft and supercritical CO_2-swelling polymerization, 62-70, Copyright 2008, with permission from Elsevier.

Supercritical carbon dioxide processing was used to produce a composite of polyethylene (PE) and poly(vinyl acetate) (PVAc) by Hoshi and coworkers [97]. $ScCO_2$ was used to impregnate the amorphous PE matrix with initiator and vinyl acetate monomer which is then polymerized under mild $ScCO_2$ processing conditions. Hoshi and coworkers evaluated the microstructure of the PE/PVAc composite using SAXS as shown in Figure III-4. Attention was given to monitoring changes of the long period of PE within the SAXS profiles as a function of PVAc content. Hoshi and coworkers found that the peak attributed to the long period of the PE lamella at 0.0374 $Å^{-1}$ did not change with increasing concentration of PVAc. However, upon adding increasing amounts of PVAc to PE, a small angle scattering peak was observed. The low angle scattering peak was attributed to a significant disruption of the crystalline PE lamellar. By combining the

SAXS profiles of the PE/PVAc composites with data obtained from WAXD and DSC that demonstrated the PE crystalline structure and degree of crystallinity did not change with PVAc content, Hoshi and coworkers concluded that PVAc is formed within the amorphous regions of PE between crystalline lamellae or in large amorphous regions of bulk PE.

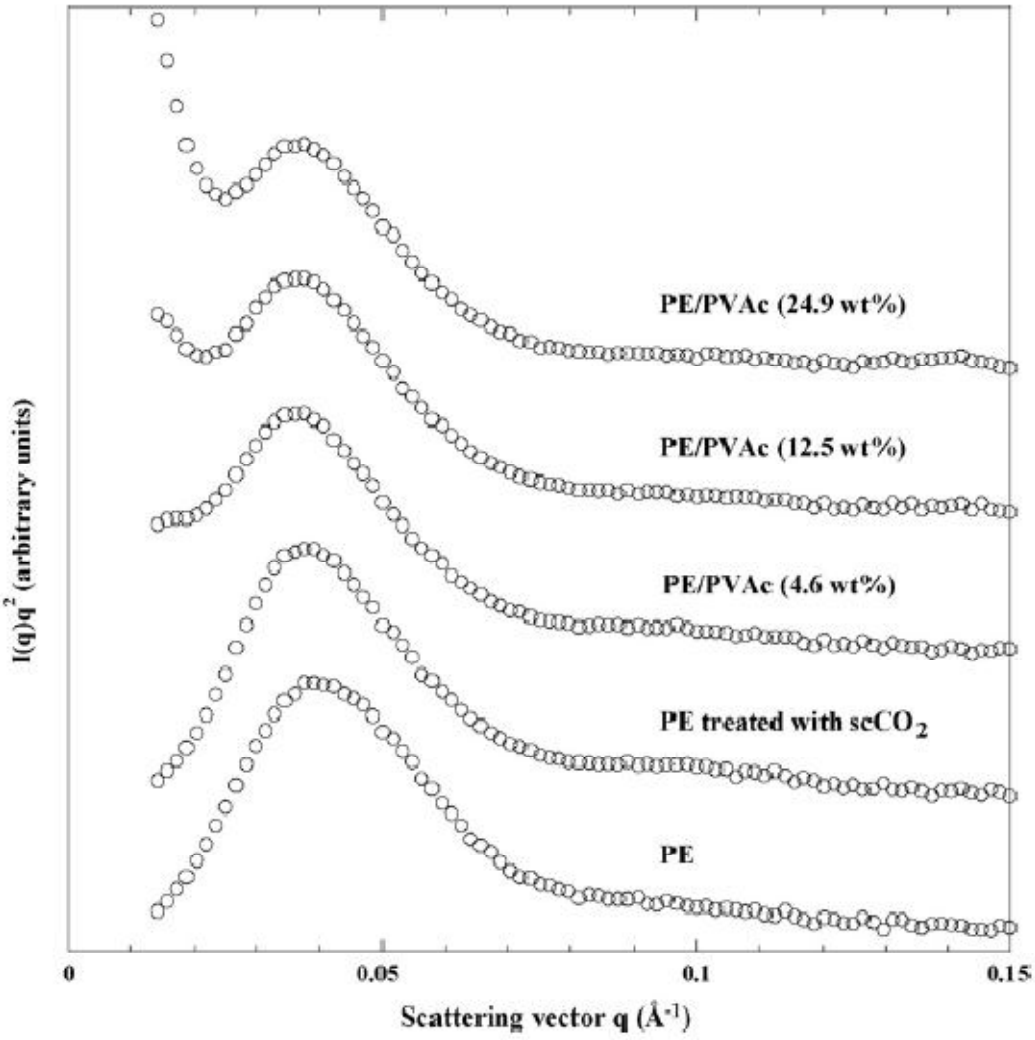

Figure III-4. Lorentz-corrected SAXS profiles of original PE, PE treated with scCO2, and PE/PVAc composites. Reprinted from The Journal of Supercritical Fluids Vol 44, Issue 3, Toru Hoshia, Takashi Sawaguchid, Ryosuke Matsunoa, Tomohiro Konnoa, Madoka Takaia, and Kazuhiko Ishihara, Polymer composite biomaterials from polyethylene/poly(vinyl acetate) prepared in supercritical carbon dioxide and their bulk and surface characterization, 391-399, Copyright 2008, with permission from Elsevier.

.

Polymer Modification Via Copolymerization

Copolymerization is studied extensively as a means to create polymers with specific properties through the proper selection of monomers and architectural design of the copolymer constituent monomers. Several investigations have focused on the properties of block copolymers as a function of monomer type and block copolymer architecture. It has been demonstrated the polymer architecture has a profound and direct influence on the morphology and properties of the copolymer. Figure III-5 shows different morphologies that may be formed through the self-organization of block copolymers.

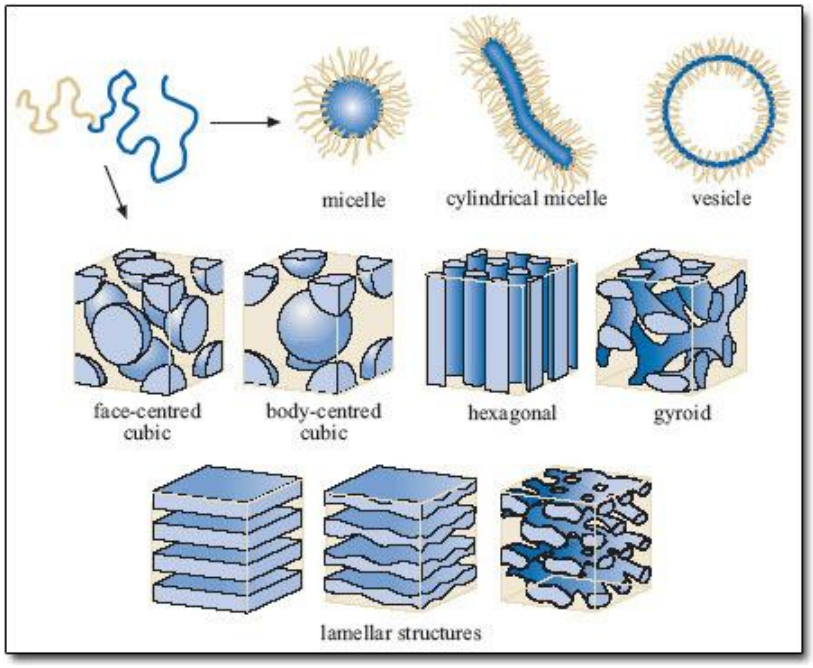

Figure III-5. Self-organization of block copolymers. Block copolymers can form spherical and cylindrical micelles, vesicles, spheres with face-centered cubic (fcc) and body-centered cubic (bcc) packing, hexagonally packed cylinders, minimal surfaces (gyroid, F surface, and P surface), simple lamellae, and modulated and perforated lamellae. Reprinted from http://openlearn.open.ac.uk/mod/oucontent/view.php?id=397881&section=2 accessed February 24, 2011.

There are many synthetic approaches than can be used to prepare block copolymers and many of the living free-radical polymerization techniques such as ATRP [99-102] and RAFT [103-108] , living anionic polymerization [109] and group transfer polymerization [110-111] have been used to prepare block copolymers and other complex polymer architectures.

There are abundant examples within the literature that demonstrate the effectiveness of living free radical polymerization techniques to produce block copolymers with varying microstructures. Du and coworkers prepared linear, amphiphilic multiblock copolymers of $(PNIPAm\text{-}PtBA\text{-}PNIPAm)_m$ using a two-step RAFT polymerization in the presence of a cyclic trithiocarbonate RAFT agent [112]. The formation of different micellar structures as a function of the initial concentration of the multiblock copolymer in solution were evaluated using TEM as shown in Figure III-6. At an initial concentration of 0.025 wt.%, the $PNIPAm\text{-}PtBA\text{-}PNIPAm)_m$ forms toroidal structures followed by the formation of cage-like structure, spherical micelles and larger aggregates as the initial concentration of $PNIPAm\text{-}PtBA\text{-}PNIPAm)_m$ in solution increases to 0.05, 0.1, and 0.25 wt.%, respectively.

There has been a strong driving force to prepare polymeric membranes for utilization within proton exchange membranes (PEMs) in cells that meet the desired requirements of the United States Department of Energy. Many of the ion-containing polymers that have been studied for use as PEMs contain sulfonate groups that are placed randomly along the polymer backbone such as Nafion®. It has been suggested that the random placement of the sulfonate groups within a copolymer results in formation of isolated sulfonate rich domains that do not sufficiently facilitate the movement of protons throughout the membrane [113]. However, recent

theoretical and experimental data suggests that block copolymers comprised of regions of well-defined sulfonate content may improve proton transport through the PEM [113-116].

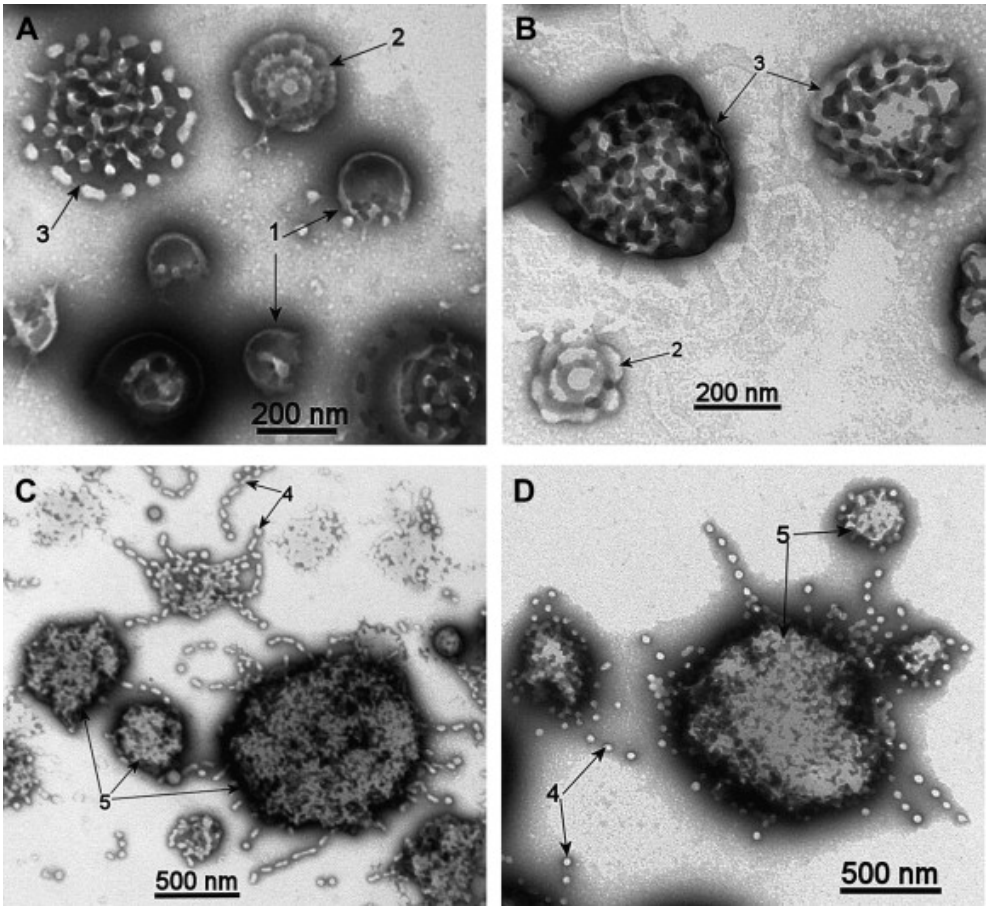

Figure III-6. TEM images of (PNIPAm-PtBA-PNIPAm)m micelles in aqueous solution. The initial concentrations of (PNIPAm-PtBA-PNIPAm)m THF solutions were (A) 0.025 wt.%, (B) 0.05 wt.%, (C) 0.1 wt.%, and (D) 0.25 wt.%, respectively. Reprinted from Polymer Vol 51, Issue 15, Binyang Du, Aixiong Mei, Yong Yang, Qinfen Zhang, Qi Wanga, Junting Xu and Zhiqiang Fa, Synthesis and micelle behavior of (PNIPAm-PtBA-PNIPAm)m amphiphilic multiblock copolymer, 3493-3502, Copyright 2010, with permission from Elsevier.

Roy and coworkers prepared hydrophilic–hydrophobic multiblock copolymers based on poly(arylene ether sulfone)s of varying sulfonate block length [116]. The multiblock copolymers were prepared by a coupling reaction between phenoxide terminated fully disulfonated

poly(arylene ether sulfone) (BPSH100) and decafluorobiphenyl (DFBP) end-capped unsulfonated poly(arylene ether sulfone) (BPS00) as hydrophilic and hydrophobic blocks, respectively. BPSH100 hydrophilic oligomers of varying block length with phenoxide end-groups were prepared via step growth polymerization. Roy and coworkers identified the BPSH and BPS copolymers using the following nomenclature, BPSH:BPS (A:B), where the A represents the hydrophilic BPSH block length in kg/mol and the B represents the hydrophobic BPS block length in kg/mol. Figure III-7 shows the proton conductivity of BPSH random copolymer, Nafion® 112, and two BPSH:BPS multiblock copolymers with unequal block lengths. It is evident in Figure III-7 that the proton conductivity of the multiblock BPSH:BPS copolymers are higher than the BPS random copolymer and Nafion® 112 especially at lower humidity levels. The authors attribute the improved proton conductivity behavior of the multiblock copolymers to the formation of co-continuous channels of sulfonate groups that provide a path for the movement of protons along with water through the membrane.

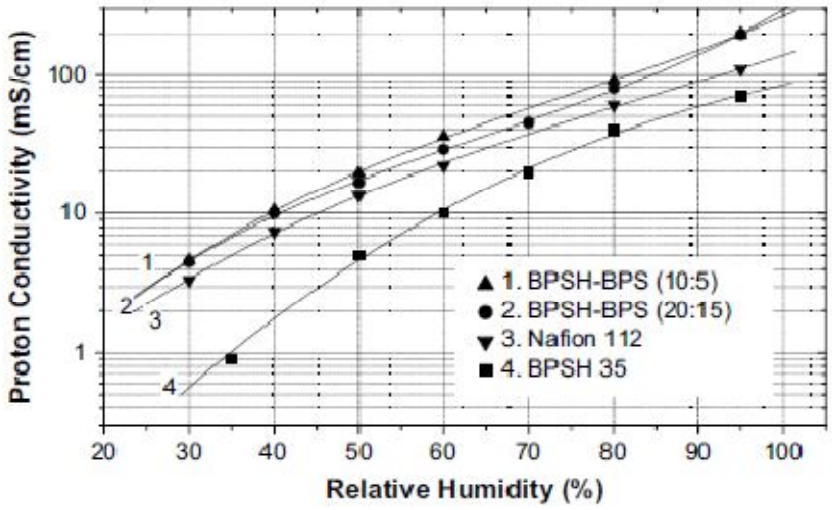

Figure III-7. Proton conductivity as a function of relative humidity for the multiblocks with higher IECs at 80 °C. Reprinted from Polymer Vol 49, Issue 23, Abhishek Roy, Hae-Seung Lee and James E. McGrath, Hydrophilic-hydrophobic multiblock copolymers based on poly(arylene ether sulfone)s as novel proton exchange membranes - Part B, 5037-5044, Copyright 2008, with permission from Elsevier.

The effects of block length and solution casting conditions on the morphology of the multiblock BPSH:BPS copolymers were evaluated using TEM and SAXS by Lee and coworkers [118]. TEM images of BPSH100:BPS0 multiblock copolymers cast from NMP at 20 °C are shown in Figure III-8. The bright regions of the TEM images are unsulfonated BPS0 while the darker regions are BPSH100 which are electron-rich due to the presence of cesium-neutralized sulfonate groups. The BPS35 random copolymer is made of sulfonate groups that randomly distributed along the backbone resulting in a homogenous distribution of sulfonate groups throughout the BPS35 film resulting in the lack of any well-defined morphological structures. However, the development of well-defined morphological features is present within the BPSH100:BPS0 multiblock copolymers. As the block length is increased from 5 to 15 kg/mol, the morphology of the multiblock copolymer changes considerably as shown in Figure III-8 demonstrating that microstructure of the copolymer strongly influences the morphological development of the system.

Although synthetic methods have been used successfully to prepare block copolymers in solution, these methods can be rather complicated and are not readily adaptable to large-scale polymer production. Therefore, it is of particular interest to identify simple methods to produce complex architectural polymeric systems.

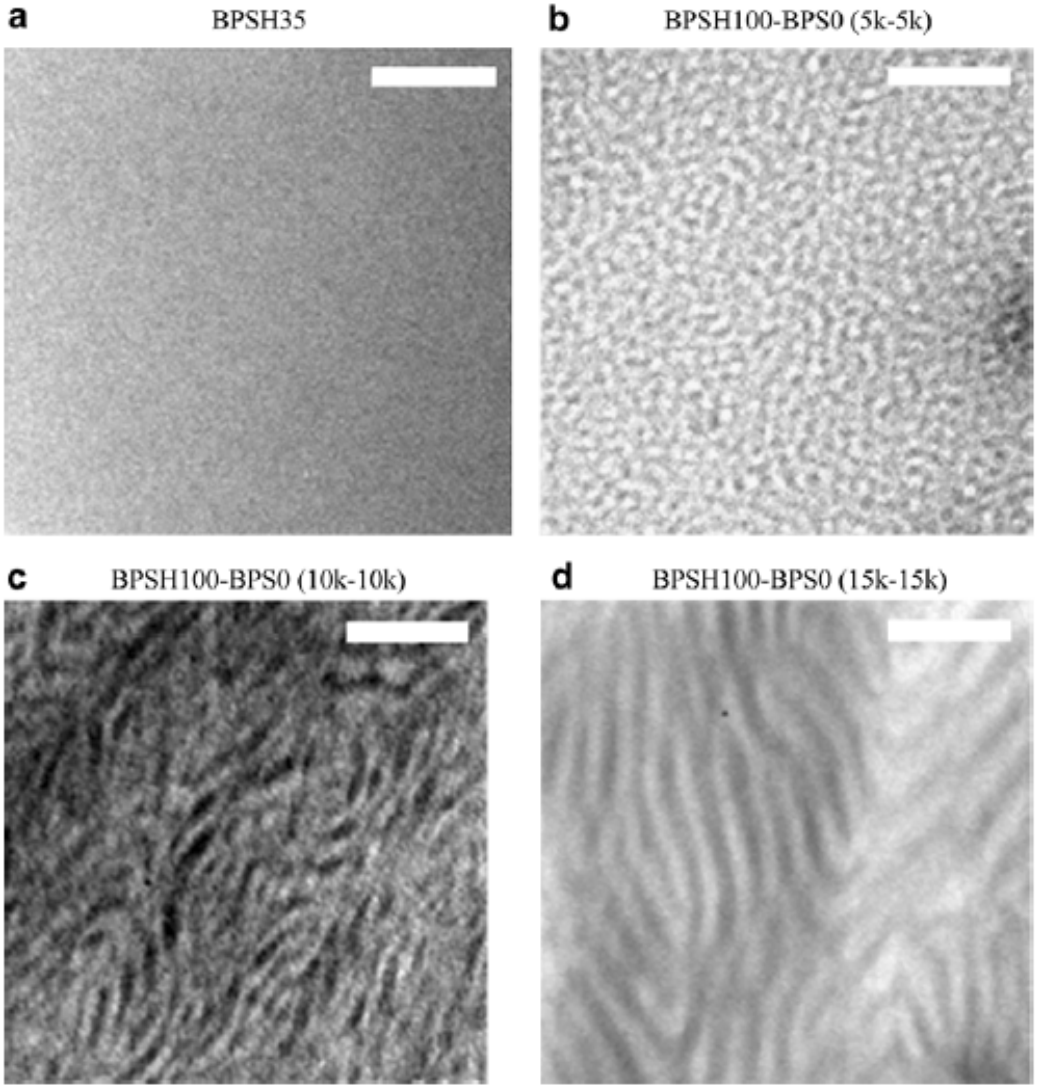

Figure III-8. TEM micrographs of the copolymer films cast with NMP and dried at 20 °C. Length of scale bar = 100 nm. Reprinted from Polymer Vol 50, Issue 25, Myoungbae Lee, Jong Keun Park, Hae-Seung Lee, Ozma Lane, Robert B. Moore, James E. McGrath and Donald G. Baird, Effects of block length and solution-casting conditions on the final morphology and properties of disulfonated poly(arylene ether sulfone) multiblock copolymer films for proton exchange membranes, 6129-6138, Copyright 2009, with permission from Elsevier.

Post -Polymerization Modification of Polymers in Solution

Post-polymerization modification of polymers in solution has been used to prepare a wide range of functionalized polymers. The modification of polymer properties through the

incorporation of ionic species has been studied for decades and has resulted in production of a very important class of polymers. Ionomers are polymers that contain less than 15 mol% of ionic content. Ionomers have been prepared both through copolymerization and post-polymerization modification of a homopolymer.

The post-polymerization modification method has been extensively used to prepare ionomers of sulfonated atactic polystyrene. Makowski developed a method to sulfonated atactic polystyrene that maintained the starting molecular weight and molecular weight distribution of the starting PS homopolymer [119]. By using a employing an acetyl sulfate complex to sulfonate the benzene ring, no significant degradation of the homopolymer is observed. The post-polymerization sulfonation of atactic PS homopolymer in solution results in the random placement of sulfonate groups along the polymer chain. The Makowski method has been used extensively to prepare sulfonated polystyrene (SPS) ionomers and study the effect of the sulfonate groups on the solution[120-122], viscoelastic [123-125], thermal, mechanical [126], and morphological [127-132] properties of the ionomer.

In 1985, Weiss, Turner, and Lundburg published a series of papers that compared the properties of sulfonated polystyrene (SPS) ionomers prepared via emulsion copolymerization and the post-polymerization modification of PS homopolymer [133-135]. The dilute solution behavior of the two different sulfonated polystyrene ionomers were previously evaluated by Lundberg and demonstrated that information regarding ion-pair interactions and intermolecular/intramolecular association can be obtained [136-137]. The dilute solution behavior of sulfonated polystyrene ionomers prepared by copolymerization and post-polymerization modification were studied and quantified using reduced viscosity measurements over a range of polymer concentrations and ionic content in 90:10 v/v toluene/methanol and

dimethylformamide [133]. The authors noted that it was not possible to definitively attribute the differences in the solution behavior of the two different sulfonate polystyrene ionomers to differences in the microstructure of the ionomers due to the differences in the molecular weight of ionomers. The SPS ionomers of different sulfonate content prepared via copolymerization also vary in molecular weight as a result of the copolymerization process and because a molecular weight determination could not be made, it was challenging to ascribe any differences in the dilute solution behavior of the SPS ionomers prepared from the different methods to differences in architecture. Although no quantitative determination of the molecular weight of the SPS ionomers prepared via copolymerization could be made, Weiss and coworkers determined that qualitatively the solution behavior the SPS ionomers prepared by copolymerization and post-sulfonation were the same.

Although the lack of a molecular weight data did not allow quantitative comparison of the solution behavior of the different SPS ionomers to be made, interesting results were obtained from water sorption isotherm measurements as seen in Figure III-9. At a lower sulfonate content of 1.6 mol%, the SPS ionomer prepared via post-polymerization modification exhibits the higher equilibrium water sorption value compared to the SPS ionomer prepared via copolymerization and the opposite behavior is seen at a higher sulfonate content of 4.1 mol%. The differences in the water sorption behavior of the two ionomers were ascribed to different morphologies that result from the random and blocky placement of sulfonate groups within the PS ionomer prepared from post-polymerization modification and copolymerization, respectively.

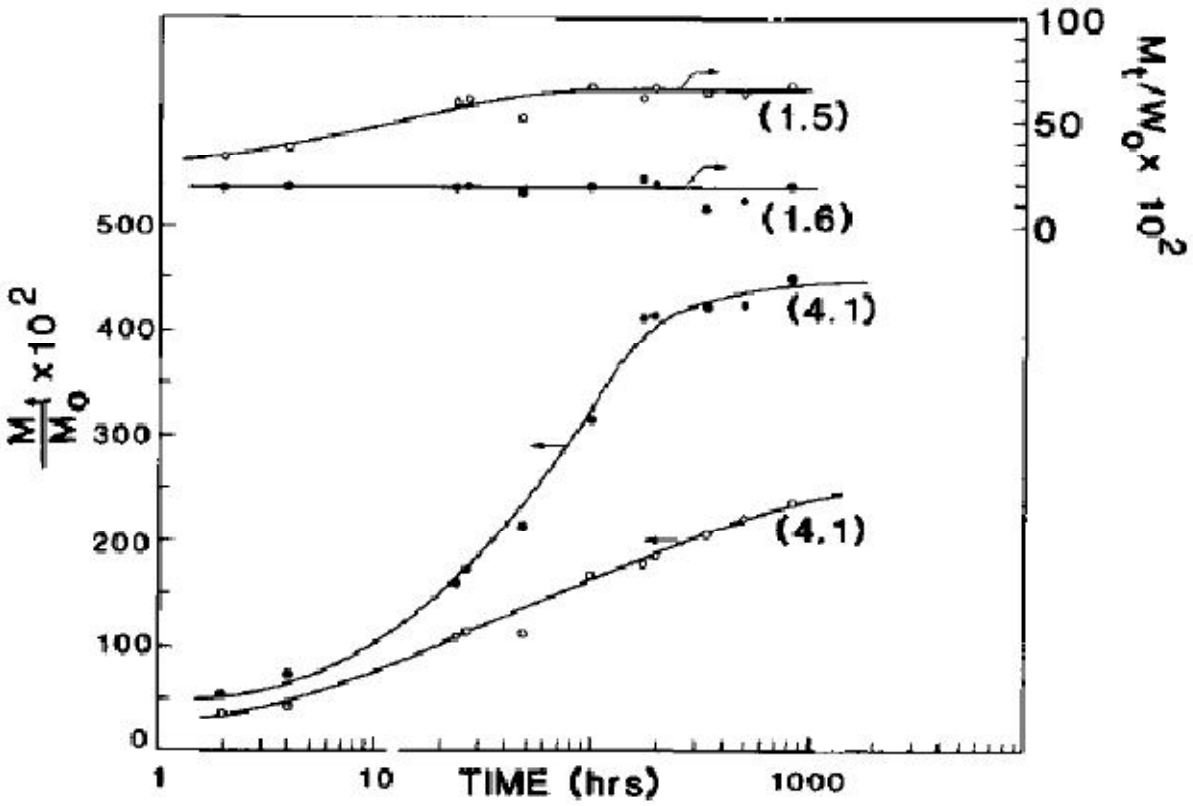

Figure III-9. Water sorption isotherms for (open circles) sulfonated polystyrenes and (closed circles) styrene-co-sodium styrene sulfonate copolymers. The numbers in parentheses represent the mol % sulfonate. Reprinted from Journal of Polymer Science: Polymer Chemistry Edition Vol 23, Issue 2, R. A. Weiss, R. D. Lundberg, S. R. Turner, Comparisons of styrene ionomers prepared by sulfonating polystyrene and copolymerizing styrene with styrene sulfonate, 549-568, Copyright 1985, with permission from John Wiley and Sons.

The differences in the thermal behavior of the SPS ionomers prepared by post-polymerization and copolymerization were significantly different as reported by Weiss and coworkers [134]. The change in the glass transition temperature of the SPS ionomers were monitored as a function of sulfonate content as shown in Figure III-10. The glass transition temperature of the SPS ionomers prepared by post-polymerization modification increases linearly as the concentration of sulfonate groups increases. However, the glass transition temperature of the SPS ionomers prepared via copolymerization do not increase linearly with increasing sulfonate concentration, but reaches a maximum at approximately 100 °C. The non-

linear behavior glass transition behavior of the SPS ionomer was attributed to a non-random distribution of sulfonate groups within the styrene-styrene sulfonate copolymer.

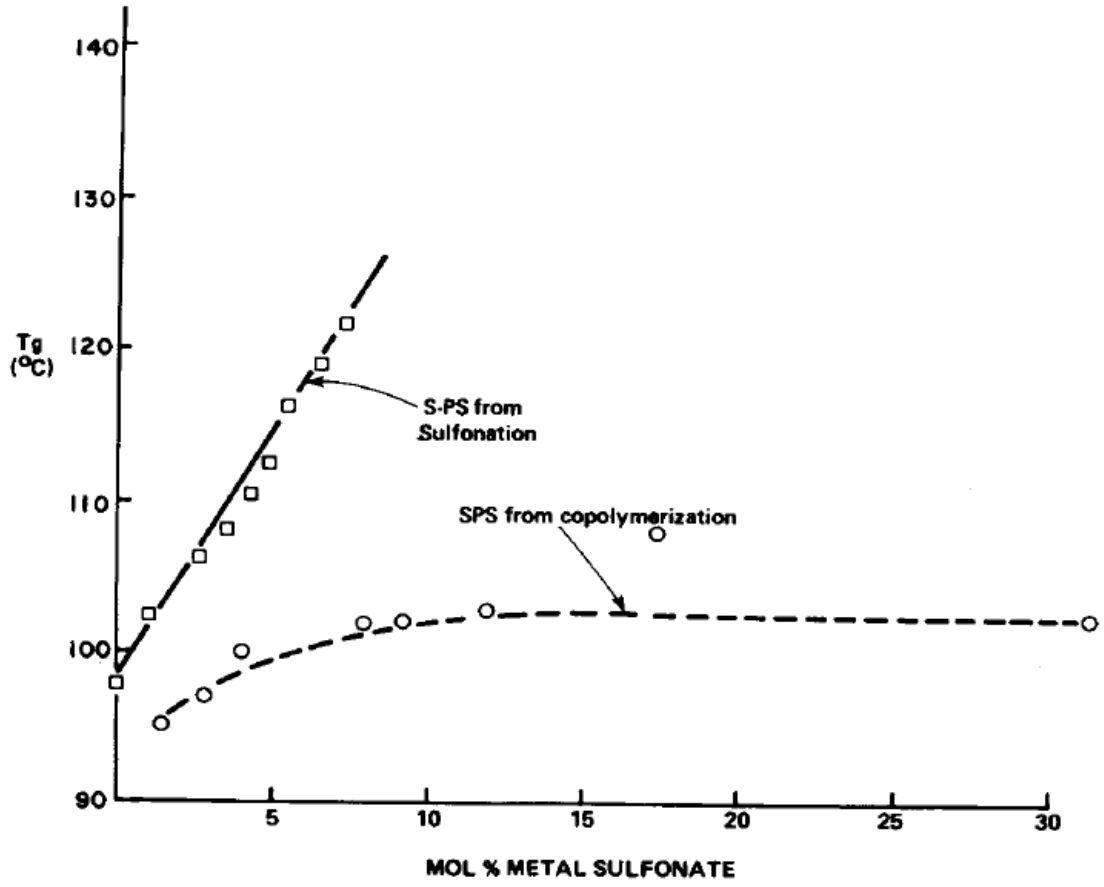

Figure III-10. Glass transition temperature versus sulfonate level for S-PS from sulfonation of polystyrene and S-PS from copolymerization. Reprinted from Journal of Polymer Science: Polymer Chemistry Edition Vol 23, Issue 2, R. A. Weiss, S. R. Turner, R. D. Lundberg, Comparisons of styrene ionomers prepared by sulfonating polystyrene and copolymerizing styrene with styrene sulfonate, 525-533, Copyright 1985, with permission from John Wiley and Sons.

Post-Polymerization Modification of Polymers in Solid State

The modification of polymers in solution is extensively employed to modify the bulk polymer properties and prepare functionalized polymers for specialized applications. Researchers have also explored methods to not only modify polymers in solution, but also to modify bulk properties while the polymers are in the solid state as well. A method that has been

used to not only functionalize bulk semicrystalline polymer in the solid state, but also results in the preferential placement of the incorporated functional groups into the polymer relies upon the inherent structure of the semicrystalline polymer. Selective reactivity based upon polymer morphology has been studied in the preparation of graft copolymers in $scCO_2$ where free radicals have been suggested to reside primarily in the amorphous regions of semicrystalline polymers, thereby leading to the formation of a semicrystalline polymer modified with grafted polymer located along the backbone in a preferential manner [96].

Exploiting the inherent two-component morphology of a semicrystalline polymer to conduct a selective chemical process where the reaction only occurs in the amorphous or the crystalline region has not been investigated in detail. Coplan and Gotz report a heterogeneous sulfonation method to sulfonate poly(ether sulfone) while the homopolymer is in a cocrystalline state in suspension [138]. They suggest that the resulting sulfonated poly(ether sulfone) "will resemble to a certain extent, that of a block copolymer with alternating regions of highly sulfonated and unsulfonated backbone sequences" [138]. Coplan and Gotz do not provide any experimental data within the patent that probes the microstructure or thermal, rheological, or morphological properties of the heterogeneously sulfonated poly(ether sulfone)s (PESs) prepared using the described process.

Nolte and coworkers prepared sulfonated poly(arylene ether sulfone) in solution and via the heterogeneous method described by Coplan and Gotz and evaluated the behavior of these materials as PEMs [139]. Nolte and coworkers prepared sulfonated poly(arylene ether sulfone)s via the heterogeneous method containing 30 – 90 mol% sulfonate groups. The authors reported that the heterogeneously sulfonated poly(arylene ether sulfone)s containing 90 mol% sulfonate groups swelled significantly in water with a measured water uptake value greater than 400%, but

did not deteriorate in water as often obtained with other highly sulfonated membranes. The stability of the highly sulfonated PES membrane in water is remarkable, but the authors did not attribute this behavior specifically to the microstructure of the material. Nolte and coworkers did not clearly correlate any improvements in the behavior or properties of the heterogeneously sulfonated PESs compared PESs prepared in solution.

A heterogeneous sulfonation method for syndiotactic polystyrene (sPS) was proposed by Borriello and coworkers that proposed the utilization of the nanoporous clathrate phase of syndiotactic polystyrene as cavities for the sulfonation of sPS [140]. The post-polymerization sulfonation of sPS by Borriello and coworkers was performed on 100 μm thick sPS films in the crystalline clathrate form using chlorosulfonic acid as the sulfonation agent. Borriello and coworkers suggest that the sulfonation will occur preferentially in the nanocavities of the sPS clathrate phase and not in the amorphous regions. The thermal properties and proton conductivity of the sulfonated sPS were evaluated. The melting temperature and degree of crystallinity for sulfonated sPS with a theoretical degree of crystallinity of 44 mol% was reported as 264 °C and 9%, respectively which are decreases in the melting temperature and degree of crystallinity of the sPS homopolymer from 271 °C and 29%, respectively. The conductivity of sulfonated sPS as a function of water content was measured and compared to that of Nafion 117® as shown in Figure III-11.

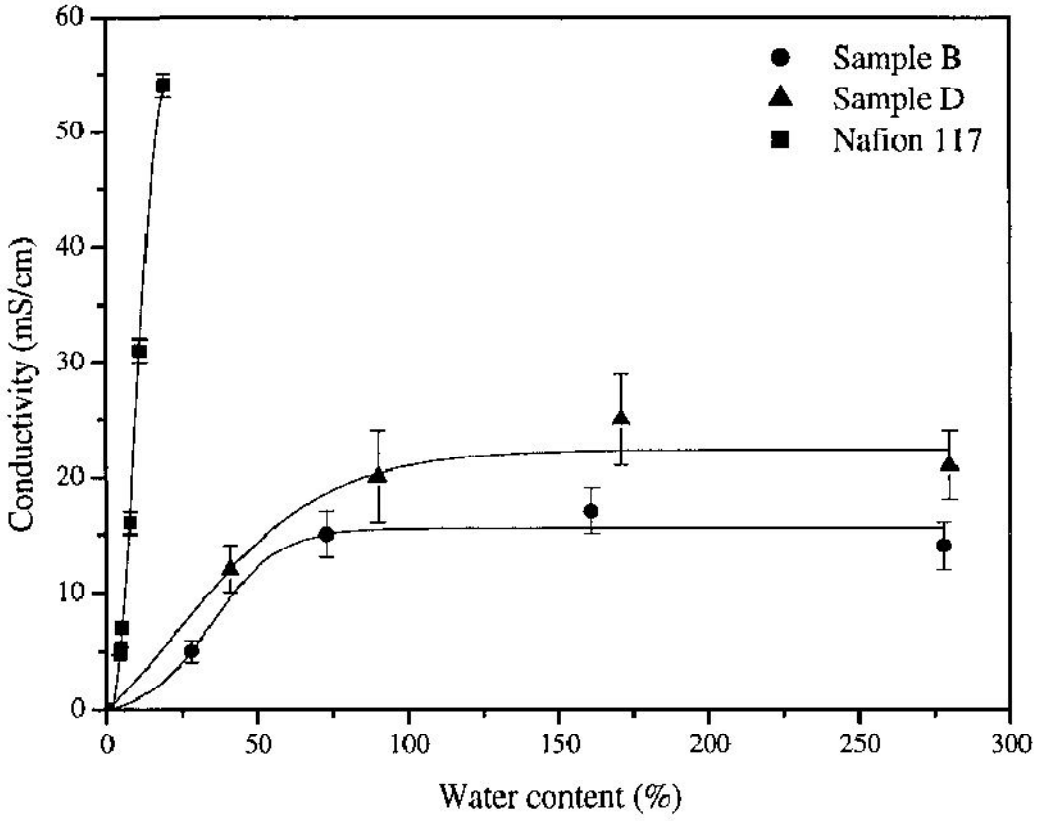

Figure III-11. Proton conductivity versus water content for Nafion® 117 and sulfonated sPS containing maximum theoretical degrees of sulfonation of 33 mol% for Sample B and 44 mol% for Sample D. A. Borriello, M. Lavorgna, N. Malagnino, G. Mensitieri, T. Napoletano, L. Nicolais, Polyelectrolyte Membranes Based on Sulfonated Syndiotactic Polystyrene in Its Clathrate Form Macromolecular Symposia 2004, Vol 218, Issue 1, 293-302, Copyright Wiley-VCH Verlag GmbH & Co. KGaA. Reproduced with permission.

The proton conductivity of Nafion® 117 is higher than that of the sulfonated sPS materials when the sulfonated sPS materials at both low and high water uptake levels. It must be noted that Borriello and coworkers did not experimentally measure the degree of sulfonation of the sulfonated sPS materials, therefore it is very difficult to properly assess the thermal and physical properties of these materials without a quantification of the degree of sulfonation.

Also, based upon the experimental data on the clathrate phase of sPS prepared via solvent-induced crystallization, it is unlikely that the sulfonation reagent will migrate into the crystalline cavity due to the size of crystalline cavity. The molecular volume of the clathrate

phase is likely smaller than the molecular volume of the chlorosulfonic acid and therefore not likely to penetrate the clathrate phase as reported for other sPS clathrate-guest systems. Although, the study conducted by Borriello and coworkers does lack experimental data critical to assessing the behavior of the sulfonated sPS materials, the notion of utilizing the morphology of the homopolymer to conduct the post-polymerization sulfonation is of fundamental interest.

Sulfonated sPS membranes containing siloxane networks were prepared by Lavorgna and coworkers [141]. They utilized the method described by Borriello and coworkers to sulfonate semicrystalline films of sPS containing the clathrate phase using chlorosulfonic acid. Lavorgna and coworkers also mention the utilization of the clathrate phase to prepare sulfonated membranes with preferential sulfonation occurring in the clathrate phase due to "reactions controlled by Fickian diffusion" in the chlathrate phases throughout the sPS membrane. The focus of this particular study was to prepare low-cost, mechanically stable membranes for methanol fuel cells. Therefore, no information was provided that compared the properties of the sPS sulfonated as swollen films to the properties of sPS sulfonated homogeneously in solution.

Films of sulfonated polystyrene were later prepared by Borriello and coworkers that claimed the sulfonation occurred in the amorphous regions rather than in the nanoporous crystalline region [142] which was in contrast to their earlier study which proposed the sulfonation reaction took place in the nanoporous clathrate regions of sPS homopolymer. The sulfonation of 100 -200 μm thick sPS films were conducted using acetyl sulfate as the sulfonation reagent instead of chlorosulfonic acid as employed in their previous study [140]. The authors demonstrate that the sulfonation process occurred through the thickness of the film using SEM and EDX as shown in Figure III-12.

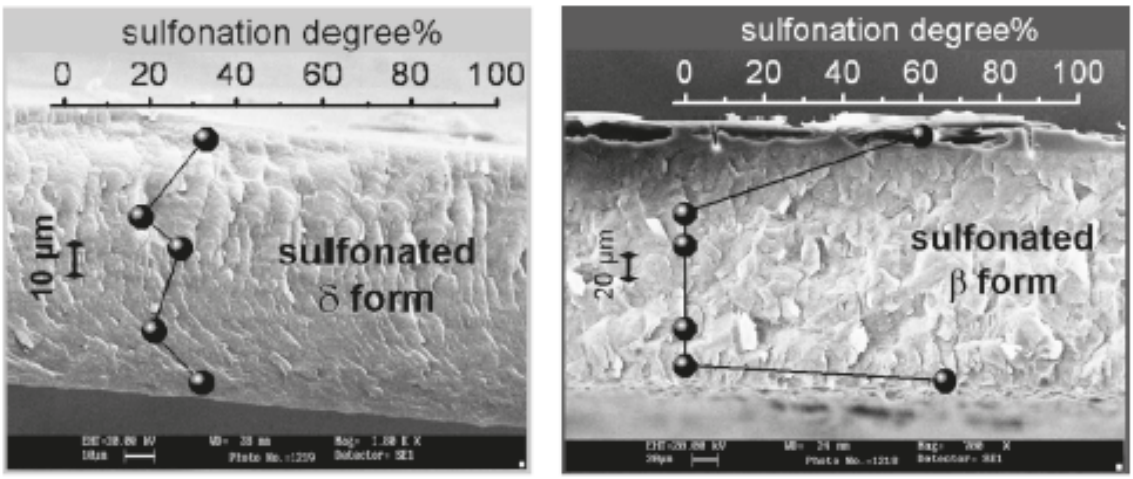

A B

Figure III-12. Scanning electron microscopy images of the section of s-PS films exhibiting the (A) nanoporous δ- and (B) β-crystalline phases. The black dots indicate the sulfonation degrees (S), as evaluated by EDS profiling analysis. Reprinted from Chemistry of Materials 21(14), 3191. Copyright 2009 American Chemical Society.

Borriello and coworkers demonstrated that sPS sulfonated in the δ-form occurred throughout the thickness of the sPS membranes while sPS sulfonated in the β-form showed a higher degree of sulfonation near the film surface. The authors attribute the differences in the distribution of sulfonation throughout the sPS films sulfonated in the δ-form and the β-form to the improved diffusion of the solvent throughout the clathrate phase of sPS which plasticizes the polymer chains in the amorphous regions and also enhances the diffusion of the reactants throughout the amorphous domains.

Copolymer Microstructure Characterization Methods

The determination of copolymer composition and architecture is paramount to constructing structure-property relationships. Precise determination of copolymer composition and microstructure is also critical to assessing the success of any synthetic method used to create the copolymer. For copolymers containing charged species such as ionomers and

polyelectrolytes, chemical titration and elemental analysis are the methods most often used to determine the quantity of charged species within the copolymer. However, these two methods only provide the average amount of the charged component and provide no insight regarding the compositional distribution of the charged units within the copolymer. The techniques available to study copolymer architecture are somewhat limited and often those techniques involve complex data interpretation or may be extremely sensitive to the sample preparation method such as NMR [143-147] and MALDI-TOF [148-151]. Therefore, it is desirable to identify copolymer microstructure characterization methods that are both readily accessible and not highly sensitive to sample preparation or involve complex data analysis.

NMR Characterization

High resolution NMR techniques such as 2D NMR have been used with a great deal of success to determine the microstructure of copolymers [152-153]. For example, 2D NMR techniques have been used in the microstructural analysis of various vinylidene chloride copolymers [143, 154-159], various methacrylate copolymers [160-164], and ethylene copolymers [165-167].

2D Heteronuclear Multiple Bond Correlation NMR

Reports of NMR methods to characterize the microstructure of ionomers in terms of characterizing the degree of randomness/block length of the ionic moiety are limited due to the strong aggregation behavior of ionomers in solution which can have an adverse impact on the NMR spectra. Two-dimensional HMBC NMR was utilized by Dickinson and coworkers to evaluate the degree of blockiness in copoly(styrene-sulfonated styrene) ionomers [147]. They

evaluated the microstructure of random sulfonated styrene containing 12 mol% of sulfonate groups that was produced via post-polymerization modification of polystyrene in solution and a block copolymer of sulfonated polystyrene containing blocks of sulfonate groups on the end of the polymer chain totaling 3 mol% of sulfonate groups. The block sulfonated polystyrene ionomer was prepared via emulsion polymerization. Dickinson and coworkers proposed that the C1 aromatic carbon of the comonomer units is the prime candidate to monitor as an indicator of the copolymer architecture. However, the C1 carbon does not appear in simple ^{13}C-^{1}H correlation spectra because there is no directly bonded proton. Therefore, they used 2D HMBC NMR to monitor the C1aromatic carbon as this method provides the correlation of a proton with carbon atoms that are located several bonds away from the proton of interest. Dickinson and coworkers identified a diagnostic coordinate set of peaks from the 2D HMBC study located at 7.45 and 153 ppm in the proton and carbon NMR spectra, respectively as shown in Figure III-13.

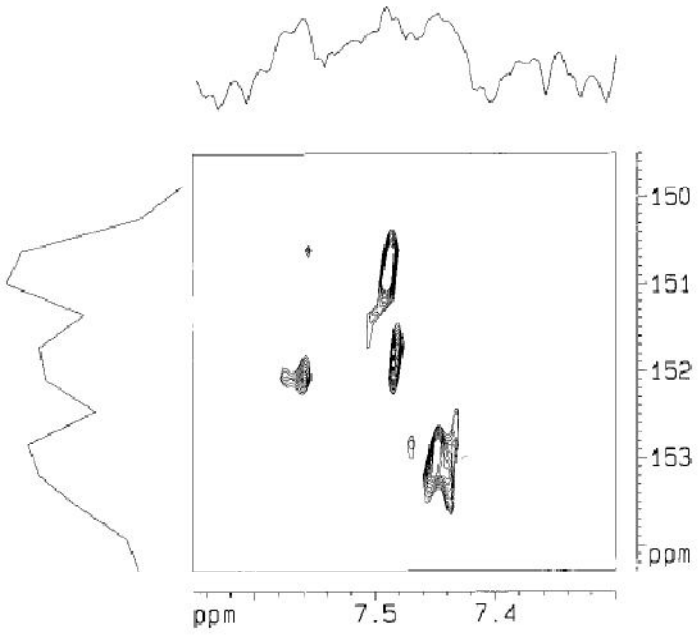

Figure III-13. ^{1}H-^{13}C HMBC of BST/3sST, sulfonated polystyrene with terminal blocks of sulfonated polystyrene amounting to 3 mol %, showing the region of correlation between the H2 proton and C1 carbon of the sulfonated aromatic ring. Reprinted from Macromolecules 34(9), 3108. Copyright 2001 American Chemical Society.

The greatest challenge experienced by the researchers was identification of suitable solvent systems for the block copolymers. Aggregation of the ionomers was observed in many solvent systems which has a detrimental effect on the signal-to-noise ratio of the NMR signal. Therefore, utilization of this particular method for sulfonated polystyrene ionomers must include detailed fundamental work on the identification of the solubility of the ionomers well.

Dickinson and coworkers suggested that this method showed potential as a tool to evaluate the degree of blockiness of sulfonated polystyrene copolymers, but stressed the need for the study of model compounds to aid in the development of the 2D HMBC method for routine use.

^{23}Na NMR Spectroscopy

^{23}Na NMR spectroscopy has been used to evaluate the distribution of lone and aggregated sodium ions within sodium-neutralized sulfonate ionomers. O'Connell and coworkers studied the effect of sample composition [131], solution casting [128], humidification and annealing [129], and molecular weight and polydispersity [130] on the ratio of isolated sodium and aggregated ions within randomly sulfonated polystyrene. ^{23}Na NMR spectroscopy is based on upon the determination of the quadrupolar coupling constant (QCC) of nuclei which is defined in the equations below:

$$QCC = \frac{e^2qQ}{h} = \frac{eQ(eq)}{h} \quad (1)$$

$$eq = V_{zz} = \frac{e}{r^3}\left(\frac{3cos^2\theta - 1}{2}\right) \quad (2)$$

The elementary charge is represented by *e*, *Q* is the electric quadrupole moment, *h* is Planck's constant, and *r* is the Na-O distance in the $S0_3^-Na^+$ group, and θ is the angle between the Na-O vector and the principal axis of the SO_3^- group.

The *QCC* is a measure of the strength of interaction of a nucleus with its surroundings. The *QC*C can be affected by the imposed electric field of the NMR experiment in addition to the structure of the surrounding molecules. The QCC is also heavily affected by the symmetry of the charge distribution that surrounds the nucleus as well.

Figure III-14 shows the three different types of sodium-sulfonate ion pairs that were identified though ^{23}Na NMR investigations by O'Connell and coworkers.

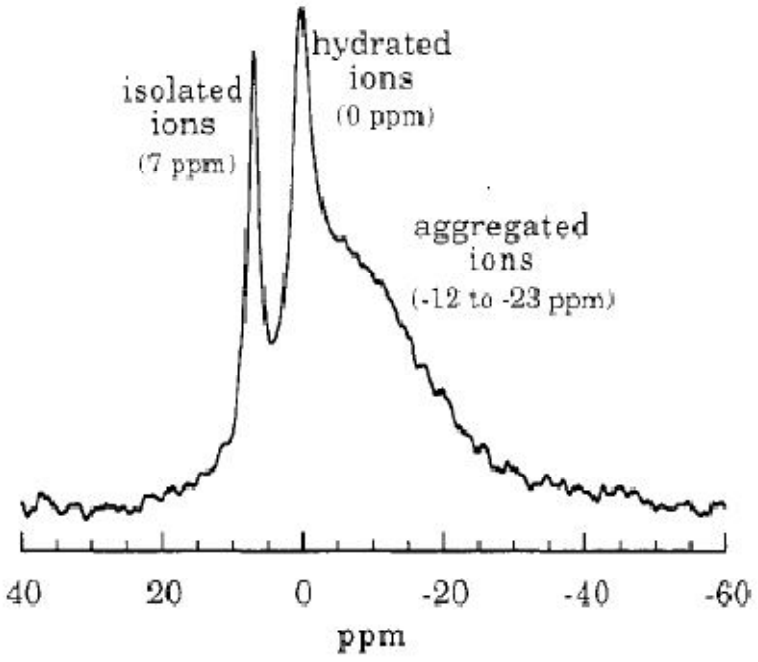

Figure III-14. NMR spectrum of NaSPS at 1.7% sulfonation. The ionomer was exposed to the atmosphere before the experiment. Reprinted from Macromolecules 27(20), 5803. Copyright 1994 American Chemical Society.

Isolated sodium-sulfonate ions were identified at 7 ppm, fully hydrated ion pairs at 0 ppm, and aggregated ions were associated with the peak located between -12 and -23 ppm. The peak determination for the three different types of the sodium-sulfonate ion pairs were developed through the use of model compounds such as NaCl, $NaNO_2$, and Acid Yellow 29. O'Connell and coworkers found that as the degree of ionization was increased within sodium-neutralized polystyrene ionomers that the number of isolated ions decreases. They found that at 6 mol% of sodium sulfonate groups within the ionomer that no isolated ion pairs were identified within the ^{23}Na NMR spectrum. It was also determined that both lone and aggregated ion pairs are readily hydrated as only a single peak is observed at 0 ppm for polystyrene containing 1.7 mol% of sodium-sulfonate groups after humidification at 80°C for 72 hours. It was also shown that as the degree of neutralization of the ionomer increases that there is a broadening and downfield shift of the NMR signal corresponding to aggregated ions suggesting that the ionomer aggregates continue to incorporate sodium into the structure as the degree of neutralization increases. At neutralization levels above 200%, a new peak appears at 0 ppm that is attributed to phase-separated NaOH.

Although the ^{23}Na NMR method does not provide precise ionomer microstructural information it does allow the construction of a qualitative morphological view of the distribution of sulfonate groups within an ionomer to be made. It can be expected that the ratio of isolated to aggregated ion pairs may vary between a random and block ionomer. Therefore, through careful analysis of the ^{23}Na NMR spectra and the center of gravity measurements for a series of copolymers, general trends may be identified that lead to the elucidation of ionomers of different architecture. The ^{23}Na NMR method although rather qualitative in nature when compared to ^{13}C

NMR microstructural determination is advantageous due to that fact the solid ionomers samples can be used to carry out the analysis as opposed to solution samples required for ^{13}C NMR analysis.

The ^{23}Na NMR technique has also been utilized to monitor the dynamic nature of the electrostatic network using sulfonated PET [168] and ethylene-methacrylic acid ionomers [169]. Page and coworkers demonstrated that it is possible for lone sodium-sulfonate ion pairs to be removed from aggregated ion pair structures during the isothermal crystallization process via ^{23}Na NMR analysis. They demonstrated as shown in Figure III-15 of PET containing 5 mol% of dimethyl-5-sodiosulfoisophthalate that although there is still a significantly large peak associated with the presence of aggregated ions within the sulfonated PET ionomer that there is a clear increase the number of isolated pairs present after isothermal crystallization at 200°C for 30 minutes. This data clearly demonstrates the dynamic nature of the electrostatic network within ionomers. This type of experiment is of particular interest in the study of sulfonated syndiotactic polystyrene (SsPS) ionomers prepared from the solution and gel states as it would provide a means to evaluate the effectiveness of the non-random sulfonation method in creating an SsPS ionomer that is able to readily crystallize at higher ion contents.

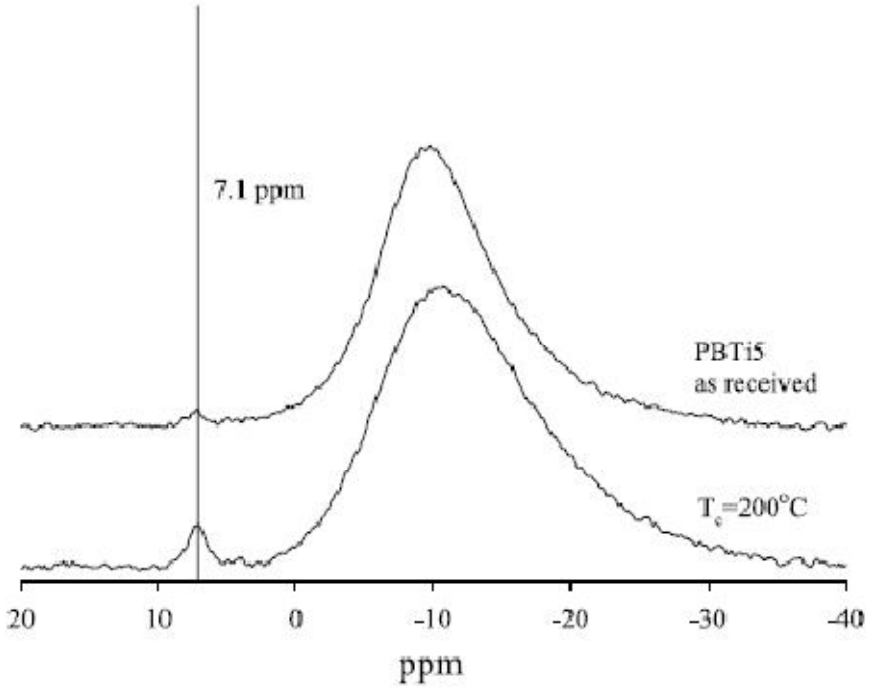

Figure III-15. ^{23}Na NMR for PBTi5 in the as-received state and isothermally crystallized at 200 °C for 30 min. Reprinted from Polymer, Vol 45, Issue 25, Kirt A. Page, Greg D. Schilling and Robert B. Moore, Influence of ionic aggregation on the surface energies of crystallites in poly(butylene terephthalate) ionomers, 8425, Copyright 2004, with permission from Elsevier.

Pyrolysis Gas Chromatography

Pyrolysis Gas Chromatography (Py-GC) utilizes thermal energy to degrade a polymer chain into smaller fragment components such as oligomers, trimers, dimers, and monomeric units [170-173]. These fragmented units are then separated by gas chromatography. The polymeric fragments are then used to construct information about the composition and microstructure of the copolymer. The architecture of the copolymer is elucidated by evaluating the dimer and trimer peaks present within a Py-GC pyrogram. This technique relies upon the idea that the products of pyrolysis reflect and are proportional to the microstructure of the copolymer. This method was recognized in the early 1960's as a potential method to determine the microstructure of polymers [174].

Wang and coworkers utilized the Py-GC method to determine the composition and microstructure of a copolymer of syndiotactic polystyrene and para-methylstyrene [175]. Homogeneous and heterogeneous trimer peak intensities obtained from pyrolysis were used to determine the number average sequence length of the styrene and para-methylstyrene monomers. The number average sequence lengths of both monomers were determined from pyrolysis trimer peak intensities using the same statistical methods used to determine triad sequences via NMR spectroscopy. Combining the homogeneous and heterogeneous trimer units with data from other triad units allowed a construction of the copolymer architecture to be made. The authors determine two quantities using the Py-GC technique, the percent of single units and the percent of desired distributions. The equations for each of the copolymer features are listed below where np is the number-average sequence length of the para-methylstyrene monomer.

$$\%\ single\ units = \frac{2 - n_p}{n_p}\ x\ 100 \tag{3}$$

$$\%\ desired\ distributions = \frac{total\ number\ of\ para-methylstyrene\ blocks}{total\ number\ of\ para-methylstyrene\ units} \tag{4}$$

When all of the para-methylstyrene units are distributed within the copolymer as single-unit blocks, the percent desired distribution is 100%. When half of the para-methylsytrene units are distributed as single unit blocks (the remaining units are present as two-unit blocks), the percent desired sulfonation is 75%.

Py-GC has been employed to determine the microstructure of many different copolymers including styrene-butylacrylate copolymer [176], chlorinated polyethylene [177], styrene-maleic anhydride copolymer [178], styrene-methylmethacrylate copolymer [179-180], and vinyl chloride-vinylidene chloride copolymer [155, 181]. The Py-GC method may be a very attractive alternative to ^{13}C NMR for the determination of copolymer architecture especially for the

microstural determination of ionomers. Solution NMR measurements with ^{13}C NMR are particularly challenging with ionomers due to problems encountered with the aggregation of ionomers in solution [147, 182]. The aggregation of the ionomer leads to line broadening in the NMR spectra which convolutes the integration of peaks and interpretation of the data. The Py-GC method eliminates the problem experienced with the aggregation phenomenon of ionomers in solution as the technique is carried out with solid polymer.

Capillary Electrophoresis

Capillary electrophoresis (CE) has been utilized to study the behavior of both naturally-derived and synthetic charged polymers. Capillary electrophoresis monitors the migration of charged species within an electric field. Unlike size exclusion chromatography which is not an effective technique for discriminating between polymers of the same molecular weight with different compositional arrangements of the charged components, CE provides a high resolution of the charged components with minimal diffusion [183]. Therefore, CE is prime candidate for the evaluation of ionomers and polyelectrolytes [184].

Frontal analysis continuous capillary electrophoresis (FACCE) involves the introduction and separation of the charged polymer into one process which results in the reduction of diffusion broadening effects common in standard CE which thereby allows the quantification of subspecies separated by the electrophoretic process. FACCE has been used to determine copolymer architecture by correlatinf the distribution of electrophoretic chain mobility to the distribution of chains with different acid content. Zhang and coworkers evaluated the compositional heterogeneity of polystyrene sulfonate (PSS) copolymers prepared via the post-polymerization modification of polystyrene and copolymers prepared via the polymerization of

sytrenesulfonate [185]. They found that the FACCE electropherograms of PSS prepared by post-polymerization modification of the PS homopolymer resulted in electropherograms that were quite broad compared to the PSS copolymer prepared via polymerization of sytrenesulfonate. The broadening effect observed in the post-modified PS material was attributed to a non-uniform, incomplete sulfonation of polystyrene. The incomplete sulfonation of the starting PS homopolymer led to compositional heterogeneity resulting from chain-to-chain variations in the degree of sulfonation.

Staggemeier and coworkers utilized FACCE to determine the compositional distribution of copolymers of acrylamide and a charged monomer, 2-(acrylamido)-2-methylpropanesulfonate (AMPS). They compared the electrophoretic behavior of copolymer of varying AMPS content to hyaluronic acid which is homogeneous in terms of composition. Figure III-16 provides the plot of the derivative of absorbance with respect to time versus mobility. The very narrow distribution of the hyaluronic acid is attributed to the homogeneity of the sample. Wide and in some cases multi-modal distributions are observed for the copolymers containing various concentrations of AMPS.

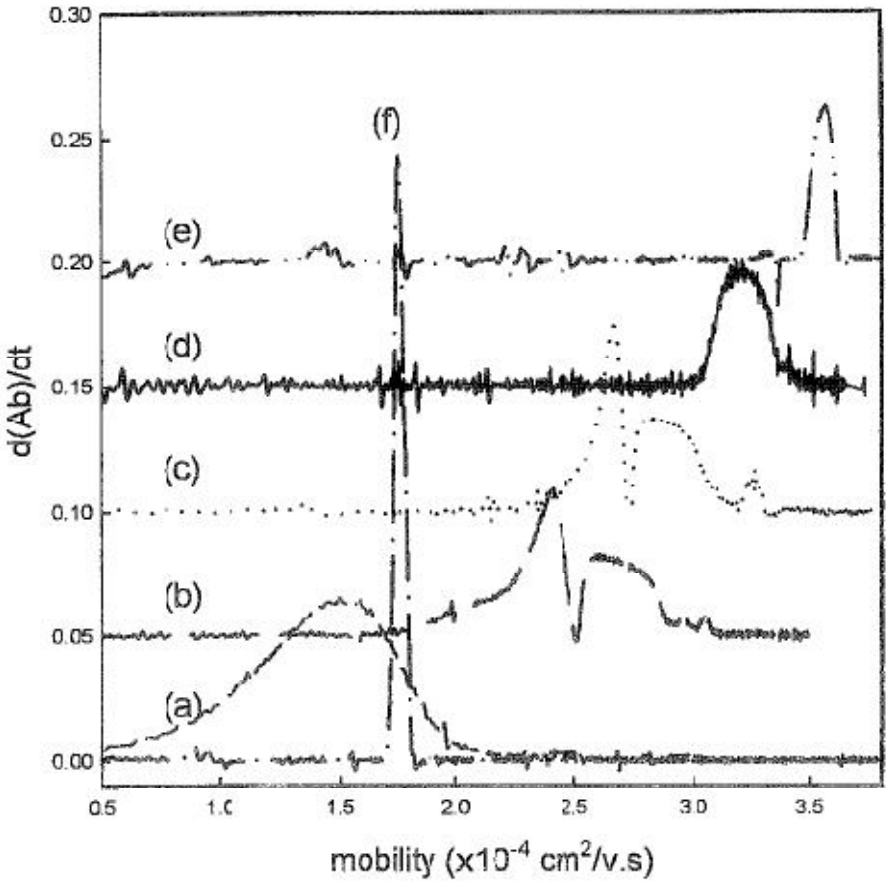

Figure III-16. Mobility distribution obtained by differentiation of the electropherograms of (a) 10% AMPS; (b) 25% AMPS; (c) 30% AMPS; (d) 50% AMPS; (e) pure PAMPS; (f) hyaluronic acid. Reprinted from Analytical Chemistry 72(1), 255. Copyright 1991 American Chemical Society.

FTIR Spectroscopy

The infrared spectra of semicrystalline polymers are sensitive to the physical state of the sample. There are IR bands which are sensitive to the intermolecular forces present within regularly packed arrangements of the polymer and are used to monitor the development and degree of crystallinity [186-188]. There are also IR bands that are sensitive to the intramolecular vibration that occurs within a single polymer chain called helix or regularity bands which are used to monitor the development of specific helical conformations [189-190].

Yoshioka and coworkers have used variable temperature FTIR to monitor the development of crystalline structures of different sequence lengths within syndiotactic polystyrene [191]. The isothermal crystallization at 125 °C of sPS was monitored as shown in Figure III-17 by monitoring the decrease in the IR absorption band at 840 cm^{-1} associated with amorphous sPS and by monitoring the FTIR band located at 1222 cm^{-1} associated with the α-form crystal structure. The band at 1222 cm^{-1} is attributed to polymer chains with critical sequence length of 30–40 monomeric units. The graph in Figure III-17 clearly shows the development of crystalline structure associated with the α-form crystal with a concurrent decrease in the amorphous content. The data was used to identify the induction period – the time prior to the onset of crystallization.

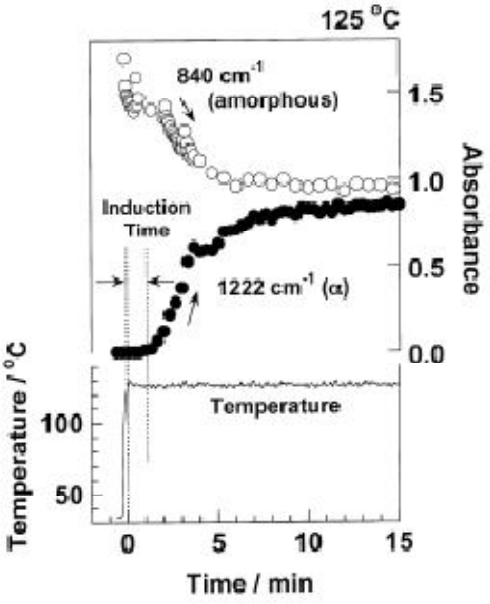

Figure III-17. Dependence of infrared absorbance of the bands characteristic of the amorphous phase (840 cm-1) and the α form (1222 cm-1) measured in the isothermal crystallization at 125 °C. The absorbance of the amorphous band is shifted along the vertical axis for easier comparison. Reprinted from Polymer, Vol 44, Issue 21, Akiko Yoshioka and Kohji Tashiro, Thermally- and solvent-induced crystallization kinetics of syndiotactic polystyrene viewed from time-resolved measurements of infrared spectra at the various temperatures (1) estimation of glass transition temperature shifted by solvent absorption, 6681-6688, Copyright 2003, with permission from Elsevier.

This method may provide a means to monitor the development of crystalline structures within semicrystalline polymers and ionomers that have different microstructures. It may be expected that the differences in the random or blocky placement of functional groups along the polymer backbone may have an effect on the crystallization behavior of the functionalized polymer. Orler and coworkers observed drastic changes in the crystallization behavior for syndiotactic polystyrene functionalized with small concentrations of randomly placed sulfonate groups using DSC [192]. It would be very interesting the monitor the development of crystalline structures of certain sequence length of polymer with different architectures but containing the same concentration of functional groups. Because crystalline conformations of specific sequence lengths can be quantified using this method, it may be possible to utilize FTIR as a means to probe the microstructure of functionalized polymers such as sulfonated syndiotactic polystyrene and other semicrystalline ionomers as well.

REFERENCES

1. Hutchings LR, Narrianen AP, Thompson RL, Clarke N, and Ansari I. Polymer International 2008;57(2):163-170.
2. Khulbe KC, Feng C, and Matsuura T. Journal of Applied Polymer Science 2010;115(2):855-895.
3. Siperko LM and Thomas RR. Journal of Adhesion Science and Technology 1989;3:157-173.
4. Brewis DM and Briggs D. Polymer 1981;22(1):7-16.
5. Wake WC. Polymer 1978;19(3):291-308.
6. Egitto FD and Metizienzo LJ. IBM Journal of Research and Development 1994;38(4).
7. Oosterom R, Ahmed TJ, Poulis JA, and Bersee HEN. Medical engineering & physics 2006;28(4):323-330.
8. Ebdon JR, Hunt BJ, Jones MS, and Thorpe FG. Polymer Degradation and Stability;54(2-3):395-400.
9. Armitage P, Ebdon JR, Hunt BJ, Jones MS, and Thorpe FG. Polymer Degradation and Stability;54(2-3):387-393.
10. Pearce Eli M, Weil Edward D, and Barinov Victor Y. Fire Smart Polymers. Fire and Polymers, vol. 797: American Chemical Society, 2001. pp. 37-48.
11. Lin TK, Wu SJ, Peng CK, and Yeh CH. Polymer International 2009;58(1):46-53.
12. Gibson HW. Polymer 1984;25(1):3-27.
13. Abbasi F, Mirzadeh H, and Katbab AA. Polymer International 2001;50(12):1279-1287.
14. Griesser HJ, Chatelier RC, Gengenbach TR, Vasic ZR, Johnson G, and Steele JG. Polymer International 1992;27(2):109-117.

15. Abbasi F, Mirzadeh H, and Katbab AA. Polymer International 2002;51(10):882-888.

16. Wang S, Cui W, and Bei J. Analytical and Bioanalytical Chemistry 2005;381(3):547-556.

17. Goddard JM and Hotchkiss JH. Progress in Polymer Science 2007;32(7):698-725.

18. Choong C, Griffiths J-P, Moloney MG, Triffitt J, and Swallow D. Reactive and Functional Polymers 2009;69(2):77-85.

19. Awaja F, Gilbert M, Kelly G, Fox B, and Pigram PJ. Progress in Polymer Science 2009;34(9):948-968.

20. Luo S, Van O, and Wim J. Journal of Adhesion Science and Technology 2002;16:1715-1735.

21. Knittel D and Schollmeyer E. Journal of the Textile Institute 2000;91(3):151 - 165.

22. Kesting W, Bahners T, and Schollmeyer E. Applied Surface Science 1990;46(1-4):326-329.

23. Lee JH, Jung HW, Kang I-K, and Lee HB. Biomaterials 1994;15(9):705-711.

24. Kim MS, Khang G, and Lee HB. Progress in Polymer Science 2008;33(1):138-164.

25. Dudek MM, Gandhiraman RP, Volcke C, Cafolla AA, Daniels S, and Killard AJ. Langmuir 2009;25(18):11155-11161.

26. Bhattacharya S, Singh RKR, Mandal S, Ghosh A, Bok S, Korampally V, Gangopadhyay K, and Gangopadhyay S. Journal of Adhesion Science and Technology 2010;24:2707-2739.

27. Katti DS, Vasita R, and Shanmugam K. Current Topics in Medicinal Chemistry 2008;8:341-353.

28. Farris S, Pozzoli S, Biagioni P, Duó L, Mancinelli S, and Piergiovanni L. Polymer 2010;51(16):3591-3605.

29. Song J, Gunst U, Arlinghaus HF, and Vancso GJ. Applied Surface Science 2007;253(24):9489-9499.

30. Song J and Vancso GJ. Langmuir 2008;24(9):4845-4852.

31. Pascual M, Sanchis R, Sanchez L, Garcia D, and Balart R. Journal of Adhesion Science and Technology 2008;22:1425-1442.

32. Brzeziński S, Tracz A, Połowiński S, and Kowalczyk D. Journal of Applied Polymer Science 2010;116(6):3659-3667.

33. Sun C, Zhang D, and Wadsworth LC. Advances in Polymer Technology 1999;18(2):171-180.

34. Koo G-H and Jang J. Fibers and Polymers 2008;9(6):674-678.

35. Eve S and Mohr J. Procedia Engineering 2009;1(1):237-240.

36. Zhu Z and Kelley MJ. Applied Surface Science 2004;236(1-4):416-425.

37. Pfleging W, Torge M, Bruns M, Trouillet V, Welle A, and Wilson S. Applied Surface Science 2009;255(10):5453-5457.

38. Pfleging W, Bruns M, Welle A, and Wilson S. Applied Surface Science 2007;253(23):9177-9184.

39. Youxian D, Griesser HJ, Mau AWH, Schmidt R, and Liesegang J. Polymer 1991;32(6):1126-1130.

40. Bae B, Chun BH, and Kim D. Polymer 2001;42(18):7879-7885.

41. Liston EM, Martinu L, and Wertheimer MR. Journal of Adhesion Science and Technology 1993;7:1091-1127.

42. Chan CM, Ko TM, and Hiraoka H. Surface Science Reports 1996;24(1-2):1-54.

43. Bee TG and McCarthy TJ. Macromolecules 1992;25(8):2093-2098.

44. Lee KT, Goddard JM, and Hotchkiss JH. Packaging Technology and Science 2009;22(3):139-150.

45. Howarter JA and Youngblood JP. Macromolecules 2007;40(4):1128-1132.

46. Gibson HW and Bailey FC. Macromolecules 1980;13(1):34-41.

47. Chen W and McCarthy TJ. Macromolecules 1998;31(11):3648-3655.

48. Phuvanartnuruks V and McCarthy TJ. Macromolecules 1998;31(6):1906-1914.

49. Chen W and McCarthy TJ. Macromolecules 1997;30(1):78-86.

50. Coupe B, Evangelista ME, Yeung RM, and Chen W. Langmuir 2001;17(6):1956-1960.

51. Shoichet MS and McCarthy TJ. Macromolecules 1991;24(6):1441-1442.

52. Tao G, Gong A, Lu J, Sue H-J, and Bergbreiter DE. Macromolecules 2001;34(22):7672-7679.

53. Hu S and Brittain WJ. Macromolecules 2005;38(15):6592-6597.

54. Wu S, Kang ET, Neoh KG, Han HS, and Tan KL. Macromolecules 1998;32(1):186-193.

55. Uyama Y, Kato K, and Ikada Y. Surface Modification of Polymers by Grafting. In: Galina H, Ikada Y, Kato K, Kitamaru R, Lechowicz J, Uyama Y, and Wu C, editors. Grafting/Characterization Techniques/Kinetic Modeling, vol. 137: Springer Berlin / Heidelberg, 1998. pp. 1-39.

56. Zou Y, Kizhakkedathu JN, and Brooks DE. Macromolecules 2009;42(9):3258-3268.

57. Yamamoto K, Tanaka H, Sakaguchi M, and Shimada S. Polymer 2003;44(25):7661-7669.

58. Singh N, Husson SM, Zdyrko B, and Luzinov I. Journal of Membrane Science 2005;262(1-2):81-90.

59. Xiao D, Zhang H, and Wirth M. Langmuir 2002;18(25):9971-9976.

60. Goldmann AS, Walther A, Nebhani L, Joso R, Ernst D, Loos K, Barner-Kowollik C, Barner L, and Mu□ller AHE. Macromolecules 2009;42(11):3707-3714.

61. Kang ET and Zhang Y. Advanced Materials 2000;12(20):1481-1494.

62. Yu WH, Kang ET, and Neoh KG. Langmuir 2004;21(1):450-456.

63. Tu C-Y, Liu Y-L, Lee K-R, and Lai J-Y. Polymer 2005;46(18):6976-6985.

64. Brown SB. Annual Review of Materials Science 1991;21(1):409-435.

65. Eduard VP and Alexandr NZ. Russian Chemical Reviews 2001;70(1):65.

66. Moad G. Progress in Polymer Science 1999;24(1):81-142.

67. Fink JK. Reactive Extrusion. Reactive Polymers Fundamentals and Applications. Norwich, NY: William Andrew Publishing, 2005. pp. 507-530.

68. Wu L, Jia Y, Sun S, Zhang G, Zhao G, and An L. Journal of Materials Processing Technology 2008;199(1-3):56-63.

69. Michaeli W, Grefenstein A, and Frings W. Advances in Polymer Technology 1993;12(1):25-33.

70. Shishuang G, Ying Z, Anna Z, and Xiao H. Polymers for Advanced Technologies 2004;15(4):185-191.

71. Wollny A, Nitz H, Faulhammer H, Hoogen N, and Mülhaupt R. Journal of Applied Polymer Science 2003;90(2):344-351.

72. Michaeli W, Höcker H, Berghaus U, and Frings W. Journal of Applied Polymer Science 1993;48(5):871-886.

73. Jacobsen S, Fritz HG, Degée P, Dubois P, and Jérôme R. Polymer 2000;41(9):3395-3403.

74. Tang W, Murthy NS, Mares F, McDonnell ME, and Curran SA. Journal of Applied Polymer Science 1999;74(7):1858-1867.

75. Jacobsen S, Fritz H-G, Degée P, Dubois P, and Jérôme R. Macromolecular Symposia 2000;153(1):261-273.

76. Du L and Yang G. Journal of Applied Polymer Science 2009;114(5):2662-2672.

77. Shishuang G, Ying Z, Anna Z, and Xiao H. Journal of Applied Polymer Science 2004;91(4):2265-2270.

78. Lambla M. Macromolecular Symposia 1994;83:37-58.

79. Jo WH, Park CD, and Lee MS. Polymer 1996;37(9):1709-1714.

80. Tanaka M, Rastogi A, Toepperwein GN, Riggleman RA, Felix NM, de Pablo JJ, and Ober CK. Chemistry of Materials 2009;21(14):3125-3135.

81. Leitner W. Accounts of Chemical Research 2002;35(9):746-756.

82. Nalawade SP, Picchioni F, and Janssen LPBM. Progress in Polymer Science 2006;31(1):19-43.

83. Kendall JL, Canelas DA, Young JL, and DeSimone JM. Chemical Reviews 1999;99(2):543-564.

84. Fürstner A, Ackermann L, Beck K, Hori H, Koch D, Langemann K, Liebl M, Six C, and Leitner W. Journal of the American Chemical Society 2001;123(37):9000-9006.

85. Kemmere M, van Schilt M, Cleven M, van Herk A, and Keurentjes J. Industrial & Engineering Chemistry Research 2002;41(11):2617-2622.

86. Grignard B, Stassin F, Calberg Cd, Jéro me R, and Jéro me C. Biomacromolecules 2008;9(11):3141-3149.

87. Hayes HJ and McCarthy TJ. Macromolecules 1998;31(15):4813-4819.

88. Jia X and McCarthy TJ. Langmuir 2002;18(3):683-687.

89. Ma X and Tomasko DL. Industrial & Engineering Chemistry Research 1997;36(5):1586-1597.

90. Galia A, De Gregorio R, Spadaro G, Scialdone O, and Filardo G. Macromolecules 2004;37(12):4580-4589.

91. Martinache JD, Royer JR, Siripurapu S, Hénon FE, Genzer J, Khan SA, and Carbonell RG. Industrial & Engineering Chemistry Research 2001;40(23):5570-5577.

92. Stafford CM, Russell TP, and McCarthy TJ. Macromolecules 1999;32(22):7610-7616.

93. Caskey T, Lesser AJ, and McCarthy TJ. Polymer Engineering & Science 2001;41(12):2259-2265.

94. VanHouten DJ and Baird DG. Polymer Engineering & Science 2009;49(1):44-51.

95. Wang Y-M, Wang Y-J, and Lu X-B. Polymer 2008;49(2):474-480.

96. Wang Y-M, Pan Y, Wang Y-L, Wu G-P, Wang Y-J, Nikitin LN, and Lu X-B. The Journal of Supercritical Fluids 2008;44(1):62-70.

97. Hoshi T, Sawaguchi T, Matsuno R, Konno T, Takai M, and Ishihara K. The Journal of Supercritical Fluids 2008;44(3):391-399.

98. http://openlearn.open.ac.uk/mod/oucontent/view.php?id=397881&section=2 accessed February 24, 2011.

99. Gaynor Scott G and Matyjaszewski K. How to Make Polymer Chains of Various Shapes, Compositions, and Functionalities by Atom Transfer Radical Polymerization. Controlled Radical Polymerization, vol. 685: American Chemical Society, 1998. pp. 396-417.

100. Lee SB, Russell AJ, and Matyjaszewski K. Biomacromolecules 2003;4(5):1386-1393.

101. Jeusette M, Leclère P, Lazzaroni R, Simal F, Vaneecke J, Lardot T, and Roose P. Macromolecules 2007;40(4):1055-1065.

102. Tsarevsky Nicolay V and Matyjaszewski K. Controlled Synthesis of Polymers with Ionic or Ionizable Groups Using Atom Transfer Radical Polymerization. Polyelectrolytes and Polyzwitterions, vol. 937: American Chemical Society, 2006. pp. 79-94.

103. Chong YK, Le TPT, Moad G, Rizzardo E, and Thang SH. Macromolecules 1999;32(6):2071-2074.

104. Golas PL, Tsarevsky NV, Sumerlin BS, Walker LM, and Matyjaszewski K. Australian Journal of Chemistry 2007;60(6):400-404.

105. Barner L, Barner-Kowollik C, P. T, and Stenzel MH. Australian Journal of Chemistry 2004;57(1):19-24.

106. Moad G, Rizzardo E, and Thang SH. Australian Journal of Chemistry 2005;58(6):379-410.

107. Moad G, Rizzardo E, and Thang SH. Australian Journal of Chemistry 2006;59(10):669-692.

108. Moad G, Rizzardo E, and Thang SH. Australian Journal of Chemistry 2009;62(11):1402-1472.

109. Hadjichristidis N, Pitsikalis M, Pispas S, and Iatrou H. Chemical Reviews 2001;101(12):3747-3792.

110. Triftaridou AI, Hadjiyannakou SC, Vamvakaki M, and Patrickios CS. Macromolecules 2002;35(7):2506-2513.

111. Webster OW. Journal of Polymer Science Part A: Polymer Chemistry 2000;38(16):2855-2860.

112. Du B, Mei A, Yang Y, Zhang Q, Wang Q, Xu J, and Fan Z. Polymer 2010;51(15):3493-3502.

113. Roy A, Hickner MA, Yu X, Li Y, Glass TE, and McGrath JE. Journal of Polymer Science Part B: Polymer Physics 2006;44(16):2226-2239.

114. Li Y, Roy A, Badami AS, Hill M, Yang J, Dunn S, and McGrath JE. Journal of Power Sources 2007;172(1):30-38.

115. Lee H-S, Badami AS, Roy A, and McGrath JE. Journal of Polymer Science Part A: Polymer Chemistry 2007;45(21):4879-4890.

116. Lee H-S, Roy A, Lane O, Dunn S, and McGrath JE. Polymer 2008;49(3):715-723.

117. Roy A, Lee H-S, and McGrath JE. Polymer 2008;49(23):5037-5044.

118. Lee M, Park JK, Lee H-S, Lane O, Moore RB, McGrath JE, and Baird DG. Polymer 2009;50(25):6129-6138.

119. Makowski HS, Lundberg RD, and Singhal GH. Flexible Polymeric Compositions Comprising a Normally Plastic Polymer Sulfonated To About 0.2 to About 10 Mole% Sulfonate. In: Office USP, editor., vol. 3,870,841. United States: Exxon Research and Engineering Company, 1975.

120. Boris DC and Colby RH. Macromolecules 1998;31(17):5746-5755.

121. Dowling KC and Thomas JK. Macromolecules 1991;24(14):4123-4130.

122. Bakeev KN and MacKnight WJ. Macromolecules 1991;24(16):4578-4582.

123. Weiss RA, Fitzgerald JJ, and Kim D. Macromolecules 1991;24(5):1071-1076.

124. Weiss RA, Fitzgerald JJ, and Kim D. Macromolecules 1991;24(5):1064-1070.

125. Weiss RA and Yu W-C. Macromolecules 2007;40(10):3640-3643.

126. Fan X-D and Bazuin CG. Macromolecules 1995;28(24):8216-8223.

127. Chu B, Wang J, Li Y, and Peiffer DG. Macromolecules 1992;25(16):4229-4231.

128. O'Connell EM, Root TW, and Cooper SL. Macromolecules 1995;28(11):3995-3999.

129. O'Connell EM, Root TW, and Cooper SL. Macromolecules 1995;28(11):4000-4006.

130. O'Connell EM, Peiffer DG, Root TW, and Cooper SL. Macromolecules 1996;29(6):2124-2130.

131. O'Connell EM, Root TW, and Cooper SL. Macromolecules 1994;27(20):5803-5810.

132. Eisenberg A, Hird B, and Moore RB. Macromolecules 1990;23(18):4098-4107.

133. Weiss RA, Lundberg RD, and Turner SR. Journal of Polymer Science: Polymer Chemistry Edition 1985;23(2):549-568.

134. Weiss RA, Turner SR, and Lundberg RD. Journal of Polymer Science: Polymer Chemistry Edition 1985;23(2):525-533.

135. Turner SR, Weiss RA, and Lundberg RD. Journal of Polymer Science: Polymer Chemistry Edition 1985;23(2):535-548.

136. Lundberg RD and Phillips RR. Journal of Polymer Science: Polymer Physics Edition 1982;20(7):1143-1154.

137. Lundberg RD and Makowski HS. Journal of Polymer Science: Polymer Physics Edition 1980;18(8):1821-1836.

138. Coplan MJ and Gotz G. Heterogeneous Sulfonation Process For Difficultly Sulfonatable Poly(ether sulfone). In: Office USP, editor., vol. 4,413,106. United States: Albany International Corp., Albandy, N.Y., 1983.

139. Nolte R, Ledjeff K, Bauer M, and Mülhaupt R. Journal of Membrane Science 1993;83(2):211-220.

140. Borriello A, Lavorgna M, Malagnino N, Mensitieri G, Napoletano T, and Nicolais L. Macromolecular Symposia 2004;218(1):293-302.

141. Lavorgna M, Fusco L, Piscitelli F, Mensitieri G, Agoretti P, Borriello A, and Mascia L. Polymer Engineering & Science 2008;48(12):2389-2399.

142. Borriello A, Agoretti P, Ambrosio L, Fasano G, Pellegrino M, Venditto V, and Guerra G. Chemistry of Materials 2009;21(14):3191-3196.

143. Brar AS and Malhotra M. Macromolecules 1996;29(23):7470-7476.

144. Brar AS and Dutta K. European Polymer Journal 1998;34(11):1585-1597.

145. Brar AS and Hekmatyar SK. Journal of Applied Polymer Science 1999;74(13):3026-3032.

146. Brar AS and Kaur M. Journal of Molecular Structure 2002;606(1-3):231-240.

147. Dickinson LC, Weiss RA, and Wnek GE. Macromolecules 2001;34(9):3108-3110.

148. Skelton R, Dubois F, and Zenobi R. Analytical Chemistry 2000;72(7):1707-1710.

149. Byrd HCM and McEwen CN. Analytical Chemistry 2000;72(19):4568-4576.

150. Räder H and Schrepp W. Acta Polymerica 1998;49(6):272-293.

151. Nielen MWF. Mass Spectrometry Reviews 1999;18(5):309-344.

152. Mirau PA, Tanaka H, and Bovey FA. Macromolecules 1988;21(10):2929-2933.

153. Mirau PA, Heffner SA, Koegler G, and Bovey FA. Polymer International 1991;26(1):29-34.

154. Brar AS, Pradhan DR, and Hooda S. Journal of Applied Polymer Science 2005;96(5):1865-1874.

155. Wang FC-Y and Smith PB. Analytical Chemistry 1996;68(3):425-430.

156. Brar AS, Mukherjee M, and Chatterjee SK. European Polymer Journal 2000;36(1):69-82.

157. Brar AS and Malhotra M. Journal of Applied Polymer Science 1998;67(3):417-426.

158. Brar AS, Singh G, and Shankar R. Polymer 2005;46(18):7164-7175.

159. Brar AS and Thiyagarajan M. Journal of Polymer Science Part A: Polymer Chemistry 1999;37(16):3179-3185.

160. Brar AS, Goyal AK, Hooda S, and Shankar R. Journal of Polymer Science Part A: Polymer Chemistry 2009;47(1):25-37.

161. Brar AS and Markanday M. Polymer 2005;46(25):11527-11539.

162. McManus NT and Penlidis A. Journal of Applied Polymer Science 2007;103(4):2093-2098.

163. Brar AS, Hooda S, and Kumar R. Journal of Polymer Science Part A: Polymer Chemistry 2003;41(2):313-326.

164. Brar AS, Singh G, and Shankar R. Journal of Applied Polymer Science 2006;99(4):1437-1445.

165. Beshah K. Macromolecules 1992;25(21):5597-5600.

166. Sahoo SK, Zhang T, Reddy DV, Rinaldi PL, McIntosh LH, and Quirk RP. Macromolecules 2003;36(11):4017-4028.

167. Liu W, Rinaldi PL, McIntosh LH, and Quirk RP. Macromolecules 2001;34(14):4757-4767.

168. Page KA, Schilling GD, and Moore RB. Polymer 2004;45(25):8425-8434.

169. Jia Y, Kleinhammes A, and Wu Y. Macromolecules 2005;38(7):2781-2785.

170. Wampler TP. Journal of Chromatography A 1999;842(1-2):207-220.

171. Wang FC-Y. Journal of Analytical and Applied Pyrolysis 2004;71(1):83-106.

172. Sobeih KL, Baron M, and Gonzalez-Rodriguez J. Journal of Chromatography A 2008;1186(1-2):51-66.

173. Liebman SA, Wampler TP, and Levy EJ. Journal of High Resolution Chromatography 1984;7(4):172-184.

174. Groten B. Analytical Chemistry 1964;36(7):1206-1212.

175. Wang FCY and Huang YB. Journal of High Resolution Chromatography 1999;22(1):11-16.

176. Wang FC-Y, Gerhart BB, and Smith PB. Analytical Chemistry 1995;67(19):3536-3540.

177. Wang FC-Y and Smith PB. Analytical Chemistry 1997;69(4):618-622.

178. Frank Cheng-Yu W. Journal of Chromatography A 1997;765(2):279-285.

179. Wang FC-Y and Smith PB. Analytical Chemistry 1996;68(17):3033-3037.

180. Tsuge S, Kobayashi T, Nagaya T, and Takeuchi T. Journal of Analytical and Applied Pyrolysis 1979;1(2):133-141.

181. Tsuge S, Okumoto T, and Takeuchi T. Macromolecules 1969;2(3):277-280.

182. Baughman TW, Chan CD, Winey KI, and Wagener KB. Macromolecules 2007;40(18):6564-6571.

183. Staggemeier B, Huang QR, Dubin PL, Morishima Y, and Sato T. Analytical Chemistry 1999;72(1):255-258.

184. Gao JY, Dubin PL, Sato T, and Morishima Y. Journal of Chromatography A 1997;766(1-2):233-236.

185. Zhang B, Hattori T, and Dubin PL. Macromolecules 2001;34(19):6790-6794.

186. Zerbi G, Ciampelli F, and Zamboni V. Journal of Polymer Science Part C: Polymer Symposia 1964;7(1):141-151.

187. Xu H, Ince BS, and Cebe P. Journal of Polymer Science Part B: Polymer Physics 2003;41(23):3026-3036.

188. Filho AR and Vittoria V. Die Makromolekulare Chemie, Rapid Communications 1990;11(5):199-203.

189. Kobayashi M, Akita K, and Tadokoro H. Makromol. Chem. 1968;118:324.

190. Zhang J, Duan Y, Shen D, Yan S, Noda I, and Ozaki Y. Macromolecules 2004;37(9):3292-3298.

191. Yoshioka A and Tashiro K. Polymer 2003;44(21):6681-6688.

192. Orler EB and Moore RB. Macromolecules 1994;27(17):4774-4780.

CHAPTER IV
POLYMER NANOCOMPOSITES: THE PREPARATION AND CHARACTERIZATION OF ENGINEERED NANOSCALE MATERIALS

Hybrid Organic Inorganic Materials

Hybrid organic inorganic materials appear in a number of applications and fields [1-2]. These materials are complex in composition, structure, and function. There has been a surge in the synthesis and characterization of nanostructured hybrid organic inorganic materials with an emphasis on both gaining a fundamental understanding of the behavior of these materials and the potential applications in which these materials may be utilized.

Polymer nanocomposites are a type of hybrid organic inorganic material that has received a significant amount of attention due to significant improvements in the chemical and physical properties of these materials compared to the pristine polymer or microstructured hybrid organic inorganic materials. Polymer nanocomposites are hybrid materials that consist of an organic polymer matrix and secondary guest component that has at least one dimension of the component on the nanometer scale. The tremendous interest in polymer nanocomposites arises from the enhanced chemical and physical properties of these materials compared to conventional polymer composites containing guest structures that are on the micron size scale.

Polymer Nanocomposites

A nanostructured material can have very different properties from a conventional microstructured material of the same composition because there is a change in the physical properties when the secondary guest component has dimensions on the nanoscale. The change in the size of the secondary component within the polymer matrix to the nanoscale results in a larger surface area for a given volume compared to microscale particles. The amount of surface area per volume is inversely proportional to the diameter of the particle. Therefore, a change in the diameter or thickness of the secondary component from the micron to the nanometer scale can result in a change in the amount of surface area per volume by three orders of magnitude.

A number of the enhanced properties of polymer nanocomposites have been attributed to the increased surface area obtained through the use of a nanoscale component within the polymer matrix. Additionally, many of the enhanced properties of polymer nanocomposites have also been attributed to quantum effects that are observed only at the nanoscale. Because many chemical and physical interactions are governed by surfaces and surface properties, the incorporation of nanoscale components within organic polymer matrices is extremely interesting from both fundamental and applied perspectives.

Polymer nanocomposites can be classified according to the geometry of the secondary inorganic component. The secondary inorganic phase can be a particulate spherical nanostructure such as metal nanoparticles such as gold, alumina, CdS, and ZnS, carbon black, and (POSS) [3-6]. Another class of polymer nanocomposites incorporate fibrous nanoscale components such as nanotubes [7-10], nanofibers [11], and nanowhiskers [12-16]. Fibrous

nanoscale components such as nanowhiskers have been prepared from cellulose [17-19] and ZnO [20-21]. Nanotubes have also been incorporated into polymer matrices to form hybrid organic inorganic nanocomposites [22]. Single-wall and multi-wall carbon nanotubes are studied extensively as secondary components to form polymer nanocomposites [23-25]. A third class of polymer nanocomposites are prepared using layered nanostructured materials such as graphene sheets [26-28] and layered clays [29-33].

Hybrid organic-inorganic nanocomposites consisting of layered clay are one of the most extensively studied classes of nanocomposites due to the high aspect ratio of the layered sheets. The aspect ratio of the clay sheets range from 30 – 1000 thereby rendering these inorganic structures as potentially high efficiency reinforcing materials when properly dispersed within a polymer matrix. As with polymer nanocomposites prepared using spherical and fibrous structures, the enhanced performance of polymer nanocomposites derived from layered clays is dependent on the degree of dispersion of the secondary component within the polymer matrix and the nature of the interfacial interactions between the nanoscale component and the polymer matrix.

Polymer Clay Nanocomposites

Polymer nanocomposites derived from layered clays have gained considerable interest in the materials field due to the numerous property enhancements obtained when the clay is properly dispersed within the polymer matrix. Research conducted by Toyota Central Research Laboratories with polymer nanocomposites prepared from nylon 6 and montmorrilonite clay sparked interest in both academic and industrial communities with drastic improvements in the thermal and mechanical properties of nylon 6 with only a small addition of the nanoscale clay

into the polymer matrix [32]. Since that time, a tremendous number of investigations have been carried out to identify methods to both prepare polymer nanocomposites using a wide variety of polymer matrices and to characterize the properties and morphologies of these hybrid materials.

In order to understand the challenges and potential property enhancements that can be achieved by incorporating layered silicate clays into a host polymer matrix, an understanding of the structure and inherent properties of layered silicate clays is essential. Most polymer clay nanocomposites are prepared using layered 2:1 phyllosilicate clays due to their wide availability, low cost, and high aspect ratio. The 2:1 phyllosilicate clays are sheet-like structures composed of two different types of crystalline sheets.

Montmorillonite (MMT) is the most widely studied clay used to prepare polymer nanocomposites due to its very high surface area and high surface reactivity. Montmorillonite clay is composed of an octahedral alumina layer sandwiched between two alumina tetrahedral layers. Each tetrahedral and octahedral layer is 1 nanometer thick with lateral dimensions between 300 Å and tens of microns in length. The lateral dimensions of the clay are related to source of the clay and the method of clay preparation. The length to thickness ratio of MMT clay layers results in high aspect ratio particles with interior specific surface of 750-800 m^2/gram.

Clay Layer Composition

The 2:1 layered structure of MMT is composed of one alumina octahedral sheet and two silica tetrahedral sheets often identified as a TOT (tetrahedral-octahedral-tetrahedral) layer. The central octahedral sheet is connected to the two external silica tetrahedral layers by the oxygen atoms of the octahedral sheet. The octahedral sheet is composed of an aluminum atom

surrounded by eight oxygen atoms while the external tetrahedral sheets are made up of silicon that is surrounded by four oxygen atoms.

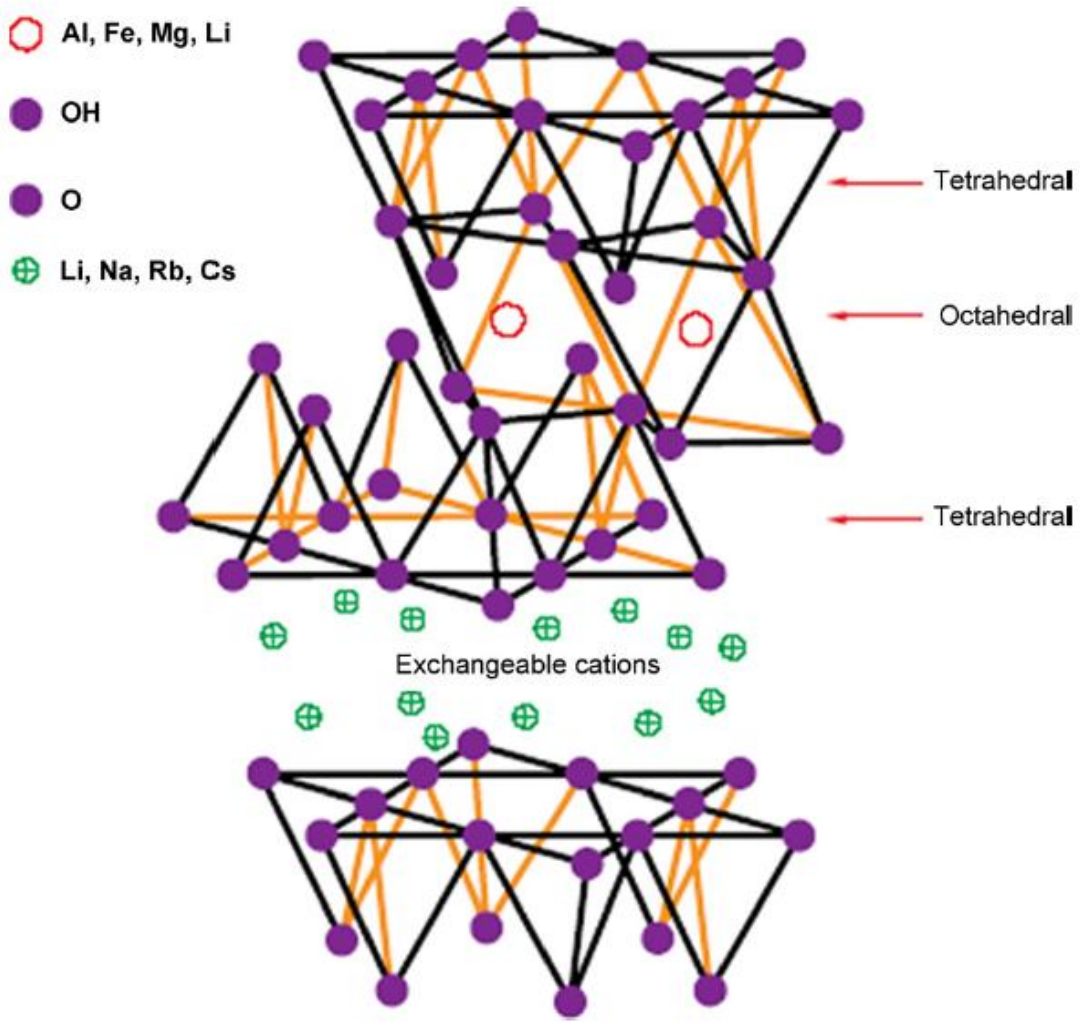

Figure IV-1. The structure of a 2:1 layered silicate. Reprinted from Plastics, Additives and Compounding, Vol 4 Issue 10, Günter Beyer, Nanocomposites: a new class of flame retardants for polymers, 22-28, Copyright 2002, with permission from Elsevier.

The chemical composition of MMT clay is $M_X(Al_{4X}Mg_X)Si_8O_{20}(OH)_4$ where X is the degree of isomorphous substitution. Isomorphous substitution occurs during the formation of the individual clay layers and is a process that results in the replacement or substitution of an atom within the crystalline lattice with an atom of different valence number without a structural change in the crystalline lattice of the clay itself. Isomorphous substitution occurs in both the tetrahedral and the octahedral clay lattices. The replacement of Si^{4+} within the tetrahedral layers with Al^{3+} results in a charge of negative one. The Al^{3+} atom in the octahedral lattice can be replaced with Mg^{2+}, Fe^{2+}, and Zn^{2+} resulting in a charge of negative one as well. As a result of the isomorphous substitution that occurs as the clay is formed in nature, a negative charge density is created. The negative charge generated in each crystalline lattice of the 2:1 MMT layer through isomorphous substitution is counterbalanced by the adsorption of alkali metal cations from the surrounding solution during the clay crystallization process. The majority of the negative charge that occurs through isomorphous substitution occurs on the clay surface, however, substitution of ions also occurs on the edges of the clay as well thus leading to the generation of a negative charge that is balanced by the adsorption of alkali metals on the edges of the clay. Approximately 10-20% of the charge density generated through isomorphous substitution occurs at the edges of the clay sheets. The layer charge density varies between sheets and mean layer charge densities of 0.25 – 0.5 equivalent per mol have been reported for MMT clay. The most common alkali metal cations that neutralize the MMT negative charge created are Na^+ and K^+ ions.

Each TOT layer is separated by a small gap called the interlayer spacing or interlayer gallery. Montmorillonite clay is found in nature as aggregated stacks of TOT layers called tactoids that are held together by electrostatic and van der Waals forces.

Clay Layer Structure and Properties

The naturally occurring MMT clay is not found in nature as individual sheets, but as aggregated stacks of platelets that are on the micron size scale. These MMT clay aggregates are called tactoids and may consist of hundreds of individual clay sheets that are stacked in a face-to-face arrangement with individual clay dimensions of 1 μm x 1 μm X 1 nm.

The size of the interlayer gap between the clay layers within the tactoid is affected by the radius of the adsorbed alkali metal cation and the degree of hydration of the cation. Because the metal cations can absorb water, the clays have the ability to swell in water and other solvents, thereby affecting the size of the clay intergallery region. It is also important to note that the relatively weak intermolecular forces holding the clay layers together can be disrupted releasing the individual clay layers from the tactoid structure.

In order to take advantage of the high aspect ratio of the individual clay layer, the tactoid structure must be peeled apart. The disruption of the aggregated clay layers begins with the outermost layers of the tactoid structure because the inner layers of the tactoid have a higher ionic binding energy than the outer surface layers. A schematic of the ionic binding energy as a function of the location of the clay layer within the tactoid structure is shown in Figure IV-2.

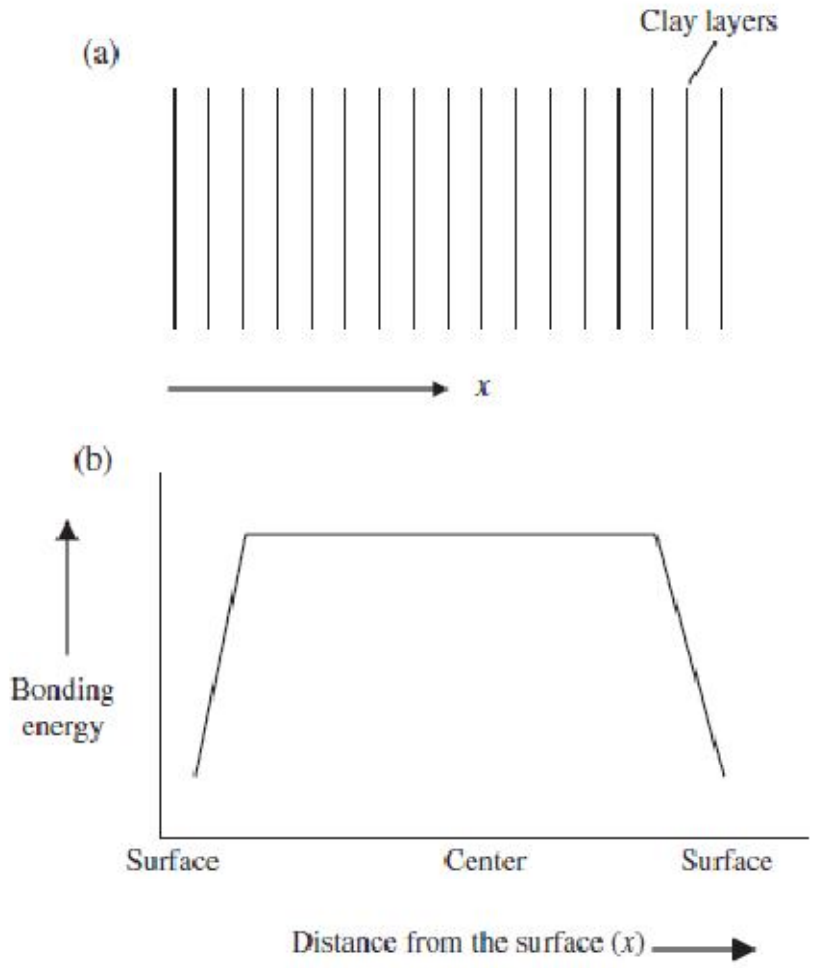

Figure IV-2. Schematic diagram showing the relationship between the ionic bonding energy and the location of the layers in the tactoid. (a) tactoid and (b) variation of bonding energy along the thickness of the tactoid. Reprinted Macromolecules 36(8), 2758. Copyright 2003 American Chemical Society.

Clay Modification

The charged nature of the MMT renders the clay hydrophilic and thus incompatible with most synthetic polymers. Therefore, incorporation of natural MMT into a hydrophobic polymer matrix results in the formation of a phase separated composite containing clay tactoid structures poorly dispersed within the polymer matrix. In order to take advantage of the high aspect ratio

of an individual clay layer that leads to enhanced properties, increased interactions between the clay and polymer must be created. An approach to improve polymer-clay interactions is to replace the alkali metal cations of the clay with organic ions through a cation exchange process. The cation exchange of the alkali metal cations of the clay with organic ions renders the clay hydrophobic and improves the compatibility between the clay and the polymer. Modification of the clay not only renders the clay surface hydrophobic and lowers the surface energy of the clay, but also increases the intergallery height of the clay. Increasing the intergallery height between the clay layers facilitates the delamination process and aids in the entry and penetration of polymer between the clay platelets.

A considerable amount of research has been done to not only understand the effect of clay surface modification on the final properties of the polymer clay nanocomposite [36-45], but to also to understand the effect of the modification agent on the properties of the clay prior to the formation of the polymer clay hybrid [46-51]. The most commonly studied clay surface modification agents have been alkylammonium [52-56] and alkylphosphonium [57-60] cationic surfactants. In addition to the alkylammonium and phosphonim surfactants, sodium montmorillonite clay has been modified with imidazaolium salts [61-62] to produce nanocomposites. Imidazolium-modified montmorillonite dispersed within a polystyrene matrix was shown to produce greater thermal stability than the corresponding polymer nanocomposite prepared with alkylammonium-modified montmorillonite clay [63].

Ionic liquids have also been investigated as MMT clay surface modification agents [64-65]. Kim and coworkers modified the sodium montmorillonite clay surface with three different low molecular weight pyridinium and imidazolium-based ionic liquids [66]. The ionic liquid (IL) -modified clay was used to prepare nanocomposites with polypropylene as the matrix via melt

blending. Wide-angle X-ray diffraction analysis showed only a very minimal increase in the intergallery spacing of the ionic-liquid modified clay in the polypropylene matrix. The small degree of intercalation of polypropylene into the IL-modified clay was ascribed to an insufficient degree of hydrophobicity of the IL-modified clay to lead to increased polymer-clay interactions. Although the IL-modified clay was not effective in producing exfoliated polypropylene nanocomposites, the IL-modified clay exhibited greater thermal stability than MMT modified with alkyammonium surfactants.

The charge density of the clay and structure of the organic cation have a dramatic impact on the manner in which the organic cations are arranged on the clay surface. The charge density of the clay is often discussed in terms of the cation exchange capacity (CEC). The CEC is the capacity for the clay platelets to exchange the clay surface cations with cations from solution. The CEC is often used as a quantitative description of clay surface properties and as a measure of the clay reactivity.

The intergallery height between the clay layers increases with increasing charge density of the clay and increasing surfactant length. Therefore, the size and surface energy of the intergallery height can be manipulated through control of clay surface modification agent. The polar nature of the clay surface is altered when the cationic headgroup of the alkylammonium surfactant is exchanged with the original clay alkali metal ion at the clay surface while the alkyl tail of the surfactant is positioned away from the surface of the clay. The specific arrangement of the tail of the surfactant is highly dependent upon the length of the surfactant and the charge density or CEC of the clay. The organic surfactants can be positioned in many different arragenments on the clay surface as shown in Figure IV-3 such a monolayer, bilayer, pseudo-trilayer, or paraffin structure.

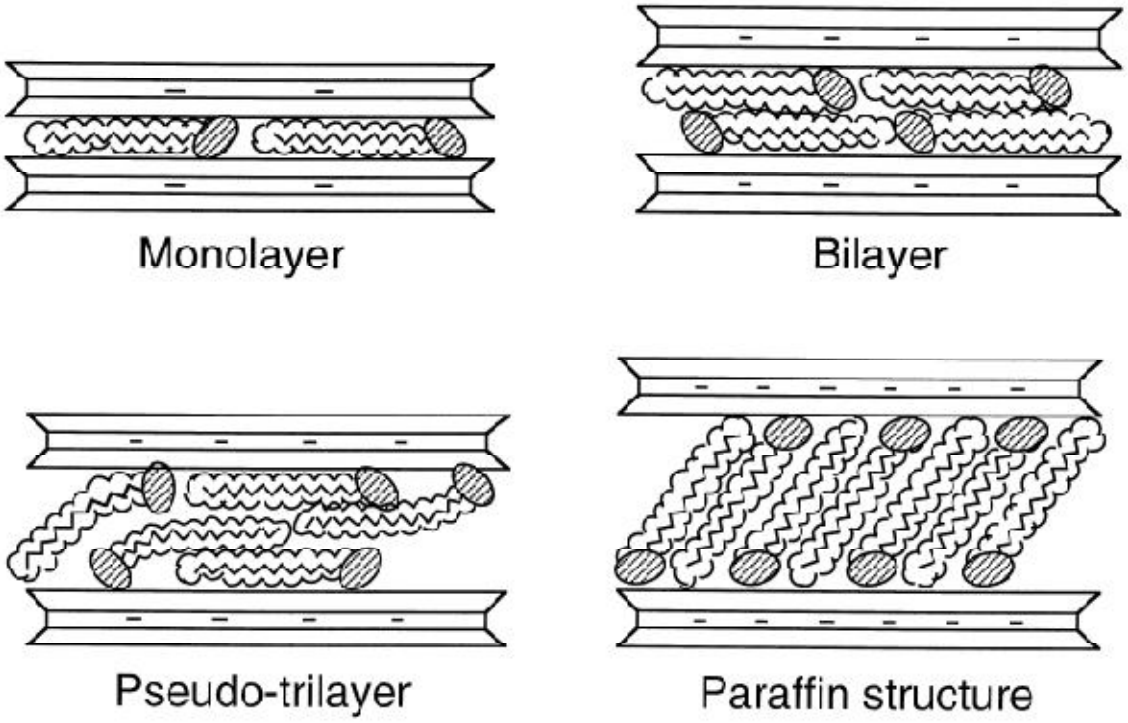

Figure IV-3. Schematic of organic cation arrangement between layered clay sheets. Reprinted from Applied Clay Science, Vol 15 Issues 1-2, Peter C. LeBaron, Zhen Wang and Thomas J. Pinnavaia, Nanocomposites: a new class of flame retardants for polymers, 11-29, Copyright 1999, with permission from Elsevier.

The organic cation can adopt different arrangements and orientations on the clay surface depending on the charge density of the clay and the length of the surfactant. Due to the low charge layer density of MMT clay, there is a larger area per adsorbed cation on the surface of the clay when compared to other layered clays with higher charge densities.

Polymer Clay Nanocomposite Morphology

Polymer clay nanocomposites properties are determined by the size of the reinforcing agent, the properties of the matrix phase, and the degree of mixing between the two component phases. Polymer clay nanocomposites are characterized according to the arrangement of the clay sheets within the polymer matrix. There are three main types of polymer clay nanocomposites:

1. *Phase separated polymer nanocomposites*: Phase separated polymer clay composites are formed when the polymer matrix phase is unable to penetrate the clay intergallery regions. Therefore, the clay remains in micron-sized aggregates throughout the polymer matrix. The properties of phase separated clay composites exhibit properties similar to conventional polymer composites because the clay remains in its native aggregated state and the high surface area of each individual platelets is not accessed .
2. *Intercalated polymer nanocomposites*: Intercalated polymer clay composites are formed when polymer enters the intergallery region of the clay resulting in a well-ordered multilayer arrangement of clay platelets within the polymer matrix. Research has suggested that intercalation occurs when a single or more than one single extended polymer chain is inserted between clay platelets. Although, polymer enters the intergallery region of the clay, the electrostatic forces between the clay platelets are not totally disrupted resulting in a small increase in the clay intergallery height. A periodic registry still remains between the clay platelets within the polymer matrix in an intercalated polymer nanocomposite.

3. *Intercalated and flocculated nanocomposites*: The intercalated and flocculated nanocomposite consists of clay layers that with some degree of polymer inserted between the clay sheets. However, edge-edge clay interactions result in a flocculation of the clay within the clay matrix [68-71].
4. *Exfoliated polymer nanocomposite*s: The exfoliated polymer nanocomposites consists of the clay platelets that are completely delaminated from the original clay aggregate stack and homogenously dispersed throughout the polymer matrix. The clay layers are present as separate, individual layers/sheets throughout the polymer matrix. It is the exfoliated clay platelet that offers approximately 760 m^2/g of surface area allowing these inorganic materials to be effective reinforcements within the polymer matrix.

There is a tremendous challenge in obtaining an intercalated or exfoliated arrangement of clay platelets within a polymer matrix which is critical to producing a hybrid material with significantly enhanced properties. The challenge in producing exfoliated nanocomposites is a two-fold in nature. The layered sheet-like structures utilized to produce polymer clay nanocomposites are composed of a polar alumniosilicate crystalline lattice that is not compatible with organic, nonpolar polymers. The differences in polarity between the clay and polymer lead to the formation of a phase separated composite containing poorly dispersed micron-scale aggregates of clay throughout the polymer matrix. The second challenge encountered in the preparation of exfoliated polymer clay nanocomposites is the delamination of the individual clay sheets from their original tactoid structures of aggregated stacks of clay held together though van der Waals forces.

Polymer Clay Nanocomposite Morphological Characterization

The characterization of polymer clay nanocomposites is essential to determining structure property relationships and evaluating the morphological arrangement of polymer clay nanocomposites within a polymer matrix. Wide-angle x-ray diffraction and transmission electron microscopy are often utilized in combination to characterization the polymer clay nanocomposite morphology as shown in Figure IV-4. The four types of polymer clay nanocomposites that have been observed are characterized by the WAXD profiles and TEM patterns shown in Figure IV-4.

The pristine and organically-modified clay that has not been incorporated into a polymer matrix exhibit strong diffraction peaks due to the inherent stacking of the clay platelets within the aggregated clay tactoid structures. Organically-modified clay exhibits a diffraction peak at a 2θ angle lower than that of the pristine clay due to an increase in gallery height resulting from the organic modification agent. As the clay platelets peel apart within a polymer matrix, there is a shift in the observed WAXD peak to lower 2θ angles indicating an increase in intergallery height. WAXD analysis of exfoliated nanocomposites do not show a diffraction peak attributed to the presence of the clay indicating that there is no long range order due to regularly arranged platelets within the polymer matrix.

TEM is utilized to gain a view of the degree of clay dispersion within the polymer matrix which is essential to constructing structure-property relationships for polymer clay nanocomposites. TEM is very often used as qualitative method to evaluate polymer clay nanocomposite morphology, but research has focused on developing techniques to utilized TEM as a more quantitative tool for characterizing polymer clay nanocomposites [72-74]. Researchers have also investigated SAXS as a means to characterize polymer clay morphology and develop

quantitative methods for determining the degree of clay dispersion within polymer matrices as well [75-77].

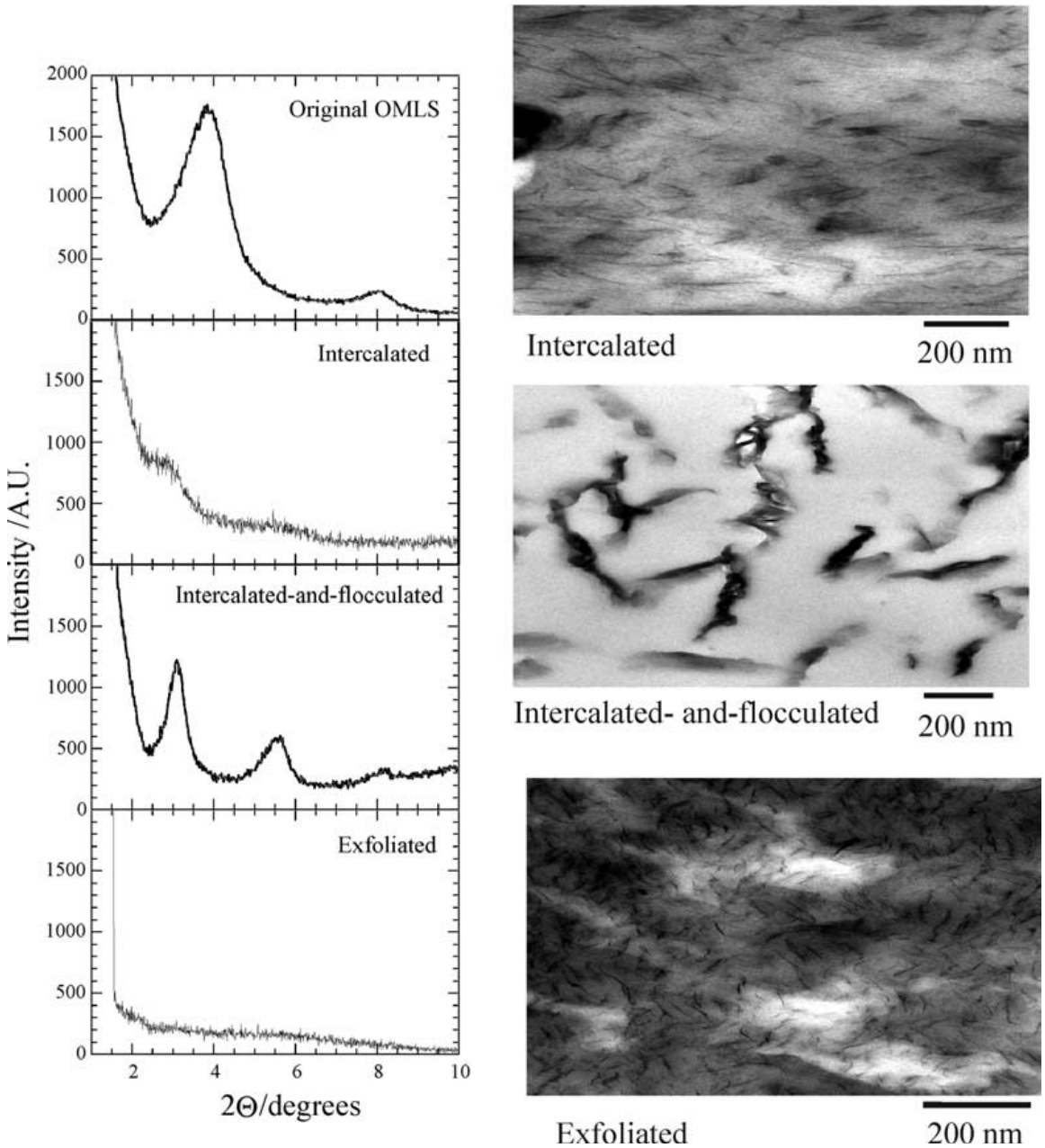

Figure IV-4. WAXD profiles and TEM images of various polymer clay nanocomposite morphological structures. Reprinted from Progress in Polymer Science, Vol 28, Issue 11, Suprakas Sinha Ray and Masami Okamoto, Polymer/layered silicate nanocomposites: a review from preparation to processing, 1539-1641, Copyright 2003, with permission from Elsevier.

Nanocomposite Preparation Methods

Polymer nanocomposites have been prepared via four different techniques. Each of the techniques has been studied extensively and each technique has been used to prepare nanocomposites using many different types of polymer matrices. The five methodologies utilized to prepare polymer nanocomposites are: template synthesis, in-situ intercalative polymerization, solution intercalation or exfoliation-adsorption, melt intercalation, and supercritical carbon dioxide processing.

Template Synthesis Method

The template synthesis method for the formation of polymer nanocomposites involves the synthesis of the inorganic nanoscale particles within the polymer matrix using a self assembly process. The inorganic silicates are formed in situ in a solution containing the polymer and the silicate building blocks. The polymer aids the nucleation and growth of the inorganic silicate crystals and becomes trapped between the inorganic material as it develops. This method is extremely different from the other three nanocomposite fabrication methods in that the inorganic particles are created within the polymer matrix while the other three methods utilize pre-existing inorganic material. Polymer clay nanocomposites using MMT clay have not been prepared using this method, however double layer hydroxide polymer nanocomposites have been created using the template synthesis method [79-81].

In situ Intercalative Polymerization

This technique involves the polymerization of monomer within the clay galleries [82-90]. The layered silicate clay is swollen within the liquid monomer followed by diffusion of an

initiator into the clay galleries. The polymerization of the monomer can occur via heat or radiation. This type of interlamellar polymerization was studied in the 1960s and 1970s. Renewed interest in this method to prepare polymer nanocomposites occurred after the Toyota research group prepared nylon 6 nanocomposites via ring opening polymerization of ε-caprolactam monomer used to swell organically-modified sodium montmorillonite.

Polyolefins are a very important class of polymers that are utilized in many different industries. Due to the very hydrophobic nature of many polyolefins, there has been great difficulty in producing intercalated or exfoliated polymer nanocomposites using these polymers due to the mismatch in hydrophicity of the polymer and the clay. The in situ intercalative technique has been investigated as a means to produce polymer nanocomposites using polyolefins as this method provides a means to polymerize the polyolefin in the presence of clay that has been swollen and modified with catalysts and initiators [91-93].

Additionally, numerous studies have focused on the preparation of thermoset nanocomposites using the in situ intercalative polymerization method [94].

Exfoliation-Adsorption

The exfoliation-adsorption method is a solution based technique that involves combining solvent-swollen clay platelets and soluble polymer to form a polymer nanocomposite. This method is usually a four step method that involves swelling the clay layers in a suitable solvent, dissolving the polymer in an appropriate solvent, combining the clay and polymer solutions, followed by evaporation of the solvent from the polymer-clay mixture. The production of an intercalated or exfoliated polymer nanocomposite is highly dependent upon the choice of the solvent. The solvent must be able to disrupt the native tactoid clay aggregate into single clay

layers or into an intercalated clay structure in order for the macromolecular chains of the polymer solution to penetrate the intergallery spacing of the clay. In many cases the solvent chosen to swell the clay and the polymer is the same, if not the clay solvent and polymer solvent must be miscible. The clay tactoid structure is disrupted by the presence of the solvent because the intermolecular forces holding the individual layers together are weak. Once the clay tactoid is disrupted and the clay layers are delaminated, the polymer can adsorb onto the clay surfaces. After adsorption of the polymer on the clay surface, the solvent is evaporated from the polymer-clay mixture or the polymer-clay mixture is precipitated from the solvent. The result of the exfoliation-adsorption procedure in many causes results in a highly ordered multilayer structure where the polymer is intercalated between the clay sheets. The exfoliation-adsorption method is also referred to as the solution intercalation method due to the fact that many polymer clay hybrids prepared using the exfoliation-adsorption method is comprised of an intercalated morphology. However there are reports of the formation of exfoliated polymer nanocomposite using this technique.

The exfoliation-adsorption technique has been utilized to prepare nanocomposites using water-soluble polymers such as poly(vinyl alcohol) (PVA) [95-99] and poly(ethylene oxide) (PEO) [100-105]. These water-soluble polymers are ideal as the matrix polymers to prepare nanocomposites using pristine sodium montmorillonite clay because the extremely polar clay is easily delaminated in water. Although both the water-soluble polymers and the sodium montmorillonite clay are readily dissolved or swollen in water, respectively, the formation of an exfoliated nanocomposite does not always occur. Often there is a strong interaction between the hydrophilic polymer and the polar clay that triggers the reaggregation of the clay resulting in highly organized, multilayer arrangement of the clay sheets that can be characterized as an

intercalated nanocomposite. The reaggregation of the clay layers using the exfoliation-adsorption method has been observed using PEO and PVPyr as the matrix polymer. In contrast, the swollen clay platelets retain a colloidal distribution upon mixing with PVA. Once the PVA-sodium montmorillonite mixture is dried via evaporation at room temperature, the clay platelets remain unoriented and well-dispersed within the PVA matrix. Upon further drying of the PVA-clay hybrid under vacuum, the clay layers reaggregate to form an intercalated nanocomposite. The study with PVA and sodium montmorillonite to form nanocomposites using the exfoliation-adsorption method demonstrates that many factors including drying conditions have a profound influence on the final morphology of the polymer nanocomposite system.

The exfoliation-adsorption method has been extended to the preparation of polymer clay nanocomposites using hydrophobic polymers. Using this method with hydrophobic polymers requires nonpolar and often very toxic solvents to prepare the polymer solutions and clay dispersions making this method less favorable for adaptation to large scale manufacturing processes. Poly(styrene) [106-107] and poly(ethylene) [108] have been utilized as a matrices to prepare polymer nanocomposites using the exfoliation-adsorption technique. When employing the exfoliation-adsorption to prepare polymer clay nanocomposites with hydrophobic polymers, the sodium montmorillonite clay must be treated to render the clay surface organophilic. Without modification of the highly charged clay surface, the clay tactoids would remain intact and result in the formation of a conventional micro-composite morphology when added to the polymer matrix. Thus, in order for the exfoliation-adsorption method to be an effective in creating an intercalated/exfoliated nanocomposite, the pristine montmorillonite clay must be modified and the polymer and organically-modified clay must be dissolved or swelled, respectively in the same solvent. To facilitate the production of an intercalated/exfoliated

nanocomposite, the hydrophobic polymer is often modified via grafting of acid groups to increase polymer-clay interactions. The modified polymers are then used as the matrix material to prepare polymer nanocomposites using the exfoliation-adsorption method.

The degree and type of mixing has been shown to have a profound influence on the formation of polymer nanocomposites using the exfoliation-adsorption method. Morgan and coworkers [109] reported that supplying high energy mixing though sonication to a polymer-clay mixture of polystyrene and organically-modified montrmorillonite clay. They demonstrated via TEM and WAXD that sonicated polystyrene-organoclay nanocomposites consisted of a higher degree of exfoliation and improved dispersion compared to polystyrene-organoclay mixtures that had not been sonicated.

Melt Intercalation

This method of nanocomposite preparation requires no solvent and utilizes conventional polymer processing equipment to prepare intercalated or exfoliated polymer nanocomposites [94, 110-120]. This method is highly explored because it may be easily adaptable to existing industry-standard polymer processing equipment. The melt intercalation method involves the mixing of the polymer and the layered silicate clay in the molten state. When the polymer and clay are compatible, the molten polymer can penetrate the clay galleries during the extrusion/compounding process resulting in an intercalated or exfoliated nanocomposite. Although the melt intercalation method may be the most readily adaptable method to industry-standard polymer processing environments, there are many different aspects of the melt intercalation preparation method that have a strong influence on the type of nanocomposite that is formed.

A mechanism of clay exfoliation that occurs during the melt intercalation of polymer clay nanocomposites was proposed by Fornes and coworkers [121]. The mechanism is basically a three-step process that involves the breakup of large organoclay structures, clay tactoid breakup, and platelet exfoliation.

Vaia and Giannelis have studied the thermodynamics that drive the insertion of molten polymer chains inside organically-modified layered silicate clay [111]. The polymer intercalation process is governed by enthalpic and entropic forces. Specifically, there is an entropic penalty once the polymer chains are confined upon entering the intergallery spacing of the clay leading to a decrease in the overall entropy of the polymer chains. The entropic penalty that occurs when molten polymer enters the clay galleries is compensated by the increase in conformational freedom gained by the alkylammonium surfactants located on the clay surface as the clay intergallery spacing increases due to the penetration of the clay layers by the polymer.

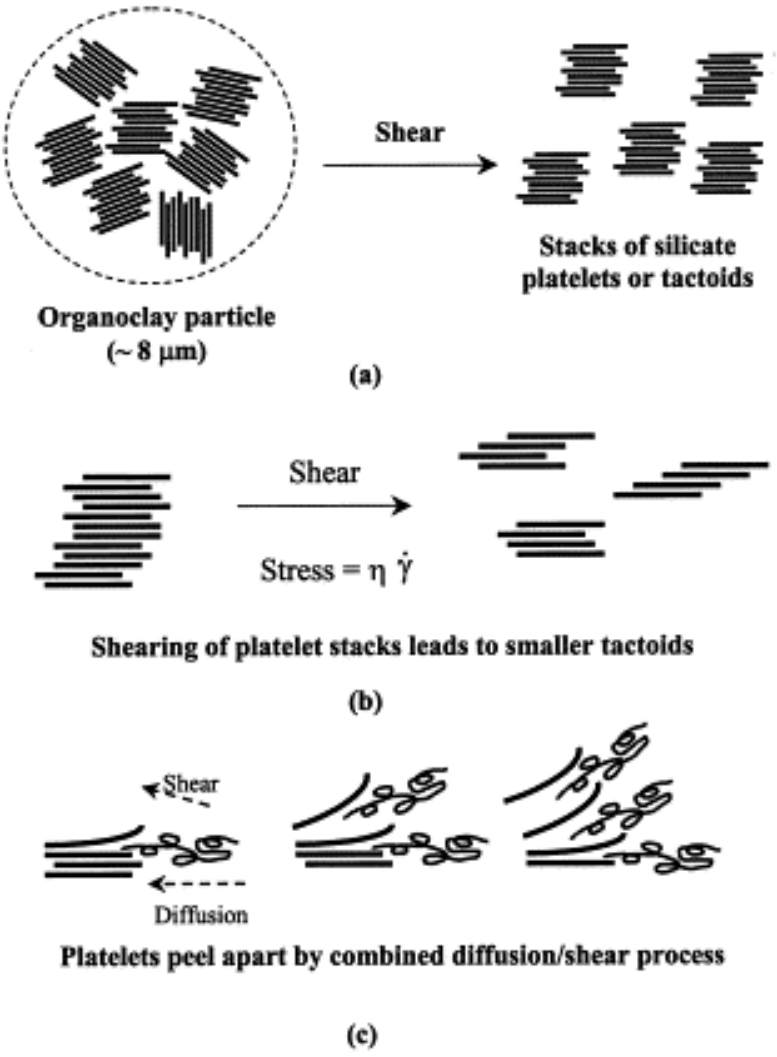

Figure IV-5. Stepwise mechanism of clay platelet exfoliation in the melt compounding of nanocomposites: (a) organoclay particle breakup, (b) clay tactoid breakup, and (c) platelet exfoliation. Reprinted from Polymer Vol 42, Issue 25, T. D. Fornes, P. J. Yoon, H. Keskkula and D. R. Paul, Nylon 6 nanocomposites: the effect of matrix molecular weight, 09929-09940, Copyright 2001, with permission from Elsevier.

The small increase that occurs in the clay gallery spacing when polymer enters the clay gallery does not result in large changes in the total entropy of the system. The intercalation of polymer into the clay galleries is more strongly driven by enthalpic interactions and will be driven by changes in the total enthalpy of the system. Vaia and Giannelis classified the enthalpy of mixing

of polymer and organically-modified clay into two components. The two components considered when studying the enthalpy of mixing between polymer and organically-modified clay are the apolar interacations between the polymer and the apolar, aliphatic portion of the alkylammonium clay surfactant and the polar interactions between the polymer and the clay resulting from the Lewis acid/Lewis base character of the clay interacting with the polymer chain. The organically-modified clay surfactants often contain long alkyl chains which are apolar and therefore, the polymer-surfactant interactions are dominated by dispersion forces. In contrast, there is a favorable decrease in the total enthalpy of the system through favorable polymer-surface interactions which are polar in nature. Therefore, a favorable enthalpy of mixing can be generated by maximizing the number and magnitude of the polymer-surface interactions and minimizing the number and magnitude of polymer-surfactant interactions between the polymer and the long-chain alkyl portion of the surfactant used to modify the clay surface.

Supercritical Carbon Dioxide Processing

Supercritical carbon dioxide ($scCO_2$) has been extensively explored in the field of polymer science research as a means of both synthesizing and processing polymers and polymer composites due to its low toxicity, low cost, and interesting physicochemical properties [122-124]. Researchers have explored $scCO_2$ processing as means to prepare polymer clay nanocomposites with a number of polymer matrices [125-129]. $scCO_2$ exhibits gas-like diffusivity, liquid-like density, low surface tension, and low viscosity which renders $scCO_2$ as excellent choice for synthesizing and processing polymers. $scCO_2$ is often used to prepared polymer nanocomposites by allowing the environmentally-friendly solvent to diffuse into the

clay layers under pressure and then exfoliate the clay tactoids when the reaction vessel is depressurized and the carbon dioxide expands in between the clay layers causing them to expand [126, 130]. $scCO_2$ has proven to be a successful and promising technique to prepare polymer nanocomposite with enhanced properties [131].

Polymer Nanocomposite Properties

The significant improvements in the mechanical properties of nylon 6-clay nanocomposites prepared by Toyota sparked interest in these hybrid materials both in academia and in industry.

Table IV-1 Mechanical and thermal properties of nylon 6 nanocomposite containing 4.7 wt.% MMT and pristine nylon 6
Reprinted from Journal of Materials Research Vol 8, Issue 5, Yoshitsugu Kojima, Arimitsu Usuki, Masaya Kawasumi, Akane Okada, Yoshiaki Fukushima, Toshio Kurauchi and Osami Kamigaito, Nylon 6 nanocomposites: the effect of matrix molecular weight, 1185 Copyright 1993, with permission from Cambridge University Press.

Property	Nylon MMT Nanocomposite	Nylon 6
Tensile modulus (GPa)	1.87	1.11
Tensile strength (MPa)	97.2	68.6
Heat distortion temperature (°C)	152	65
Impact strength (J/m)	18.1	20.6

The significant improvement in the mechanical properties of the nylon 6-clay nanocomposite at low clay content led researchers to study not only the effect of clay incorporation on the mechanical properties of these hybrid materials, but detailed studies have been carried out on the thermal, chemical, and physical properties of these materials as well.

Mechanical Properties

Significant improvements in the mechanical properties of polymer nanocomposites over conventional polymer micro-composites have been reported for a number of polymer matrix materials [133]. The improvements in the mechanical properties have been observed in a wide variety of polymers including both hydrophilic/water-soluble polymers [134] and hydrophobic polymer matrices [135-138]. Polymer nanocomposites with improved mechanical properties have been prepared using the exfoliation-adsorption [139-142], melt intercalation [143-144], in situ intercalative polymerization [86, 145-146], and via supercritical carbon dioxide processing techniques [126-127, 130-131, 147-148]. Regardless of the matrix material or the preparation method, the improvement in the mechanical properties is strongly related to the morphological arrangement of the MMT platelets within the polymer matrix. The enhancement in the mechanical properties of the polymer are realized when the clay platelets are intercalated or exfoliated within the polymer matrix. Generally, as the degree of exfoliation of the clay platelets is increased within the polymer matrix, there is an improvement in the Young's modulus, storage modulus and tensile strength of the hybrid material. However, there is often a corresponding decrease in the impact strength and ductility of the polymer-clay nanocomposite compared to the neat polymer matrix.

Matayabas and Turner provide a thorough review of nanocomposites prepared using poly(ethylene terepthalate) with very a significant amount information provided about the utilization of this polymer as a matrix material [149]. Additionally, poly(ethylene terepthalate) nanocomposites were prepared by Chan and coworkers using organically-modified MMT via the in situ intercalative approach [145]. Table IV-2 summarizes the tensile properties of the PET clay hybrids at different draw ratios. The data within Table IV-2 clearly show that there is a

significant increase in the ultimate tensile strength of PET fibers containing a small weight percent of organically-modified clay at low draw ratios. As the draw ratio increases, the differences between the mechanical property behaviors of the pure PET polymer and the clay-containing hybrid decrease. Chan and coworkers attributed the decrease in the tensile strength at high draw ratios of the pure matrix and PET clay nanocomposites to debonding and the formation of voids during stretching of the materials.

Table IV-2. PET Clay Nanocomposite Tensile Properties
Reprinted from Polymer, Vol 45, Issue 3, Jin-Hae Chang, Sung Jong Kim, Yong Lak Joo and Seungsoon Im, Poly(ethylene terephthalate) nanocomposites by in situ interlayer polymerization: the thermo-mechanical properties and morphology of the hybrid fibers, 919-926, Copyright 2004, with permission from Elsevier.

Organoclay wt.%	Draw Ratio	Ultimate Strength (MPa)	Initial Modulus (GPa)	Elongation at Break (%)
0 (Pure PET)	1	46	2.21	3
	3	47	2.24	3
	10	51	2.28	3
	16	51	2.39	2
1	1	58	2.88	3
	3	56	2.63	3
	10	50	2.51	3
	16	48	2,29	3
2	1	68	3.31	3
	3	55	2.63	3
	10	54	2.51	3
	16	51	2.29	3
3	1	71	4.10	3
	3	68	3.40	3
	10	62	3.12	2
	16	55	3.08	3

Yoon and coworkers [150] evaluated the effect of matrix molecular weight on the degree of MMT clay dispersion and the mechanical properties of polycarbonate nanocomposites. Figure IV-6 contains plots that show the effect of organically-modified clay on various mechanical properties of polycarbonate nanocomposites. There are clear improvements in the tensile modulus, relative modulus, and yield strength of both medium molecular weight and high molecular weight polycarbonate nanocomposites. Similar improvements in mechanical properties have also been reported by the same group with polymer clay nanocomposites prepared using nylon 6 and organically-modified MMT [38, 121]. The improvement in the mechanical properties of the high molecular weight polymer nanocomposites compared to the medium molecular weight polycarbonate nanocomposites was attributed to the higher melt viscosity and the resulting high shear stresses developed during the melt processing of the polymer clay nanocomposites. The higher shear stresses are proposed to lead to improved exfoliation of the clay layers within the polycarbonate matrix. The elongation at break and impact strength properties of the polycarbonate nanocomposites, however, decrease with increasing clay content.

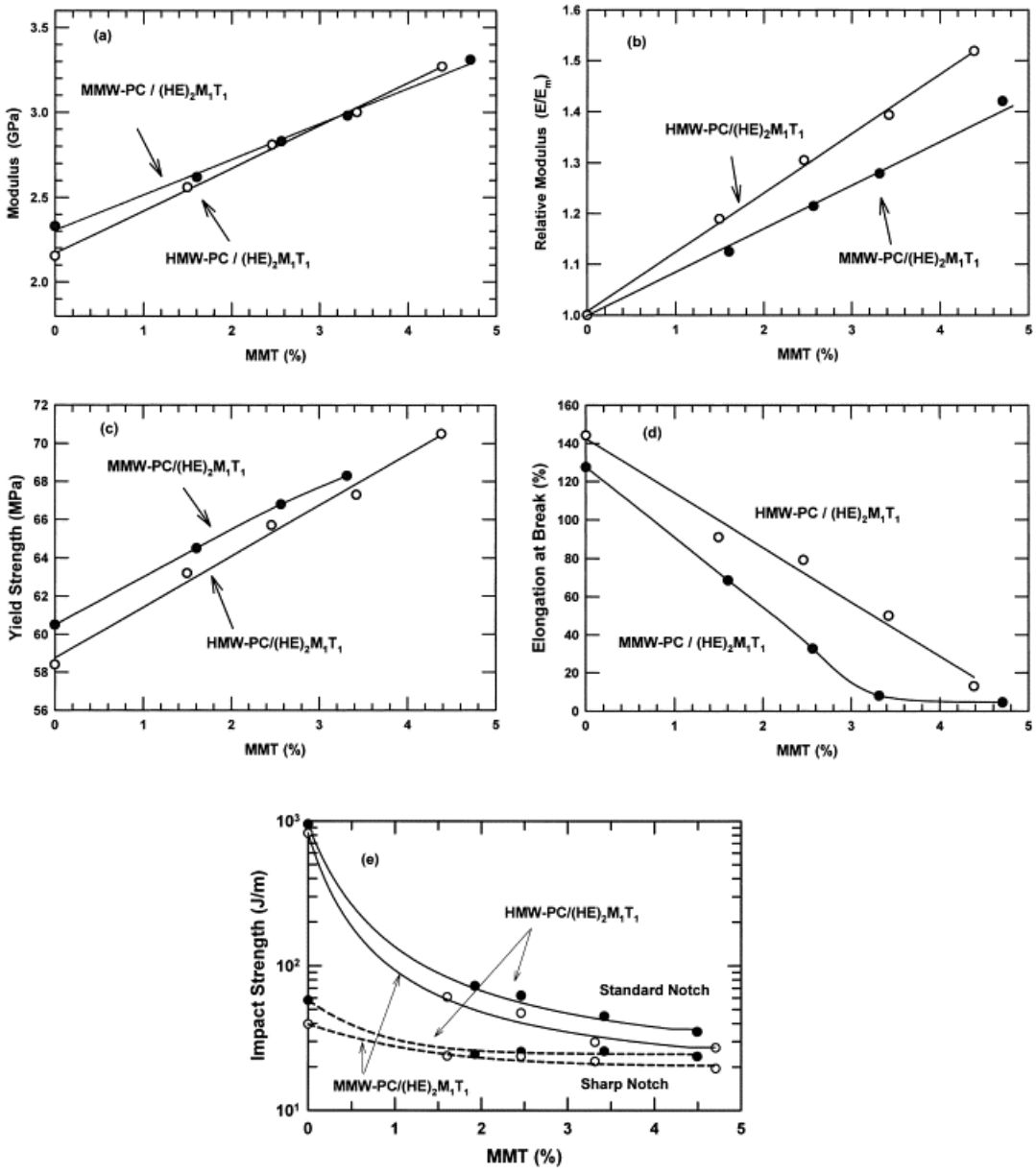

Figure IV-6. (a) Tensile modulus, (b) relative modulus, (c) yield strength, (d) elongation at break, (e) standard and sharp notch impact strength for MMW-PC (●) and HMW-PC (○) based nanocomposites. Reprinted from Polymer, Vol 44, Issue 18, P. J. Yoon, D. L. Hunter and D. R. Paul, Polycarbonate nanocomposites. Part 1. Effect of organoclay structure on morphology and properties, 5323-5339, Copyright 2003, with permission from Elsevier.

Barrier Properties

The improvement in barrier properties observed within polymer clay nanocomposites have been attributed to the presence of the high aspect ratio platelets that alter the diffusion pathway of penetrant molecules. The improvement in the barrier properties of polymer clay nanocomposites is of extreme interest to researchers in a number of fields. The barrier properties of polymer clay hybrids using many matrices have been studied. The impermeable clay layers create a tortuous pathway that decreases the rate of diffusion of penetrant molecules as shown in Figure IV-7.

Experimental data clearly demonstrates the effectiveness of the nanoscale platelets as barriers to the diffusion of penetrates through the polymer matrix. However, there is a need to study the barrier properties of polymer clay nanocomposites using theoretical modeling in order to predict the barrier properties of polymer clay nanocomposites and provide guidelines for the design of polymer clay nanocomposites materials with the required barrier properties for a specific application. Initial investigations into the development of a theoretical model to understand the origin of enhanced barrier properties within polymer clay nanocomposites was conducted by Gusev and Lusti [151]. Their early work utilized finite-element permeability calculations coupled with multi-inclusion computer models containing a random distribution of non-overlapping clay platelets.

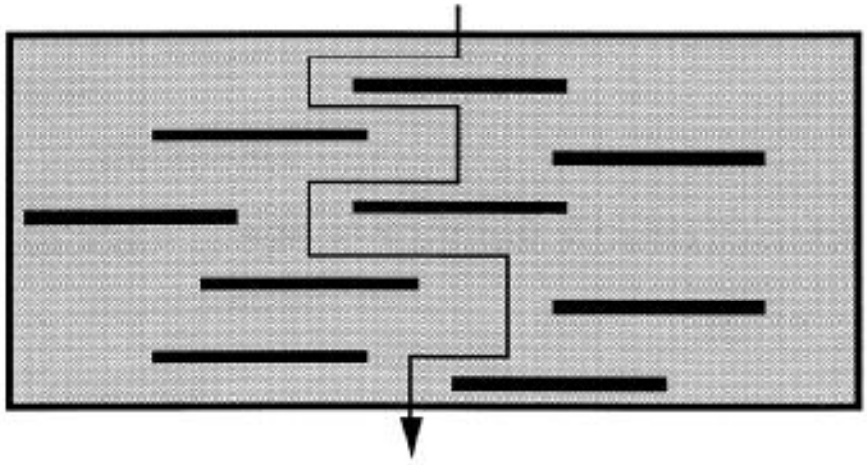

Figure IV-7. Schematic of tortuous pathway created by clay layers within a polymer matrix. Reprinted from Progress in Polymer Science, Vol 26, Issue 6, Peter C. LeBaron, Zhen Wang and Thomas J. Pinnavaia, Polymer-layered silicate nanocomposites: an overview, 11-29, Copyright 1999, with permission from Elsevier.

Xu and coworkers [152] utilized the relative permeability theory and the detour theory to evaluate the effect of layered clay on the barrier properties of a semi-crystalline polymer. Specifically, Xu and coworkers studied the effect of clay dispersion, clay thickness, clay intergallery height, clay layer length, clay volume fraction, and the chain-segment immobility factor on the relative permeability of polymer clay nanocomposites. The theoretical model developed by Xu and coworkers predicts a decrease in the relative permeability of penetrant molecules when the lateral separation of the clay layers is increased. The decrease in relative permeability with increasing lateral separation of the clay layers is even more pronounced with clay layers that are shorter in length. Increasing the volume fraction of clay above 0.05 or increasing the clay layer length above 500 nm does not result in a significant improvement in the barrier properties of polymer clay nanocomposites according to the modeling studies conducted by Xu and coworkers. Their work also showed that intercalated and exfoliated morphologies exhibit improved barrier properties compared to clay tactoid morphologies. Xu and coworkers

also suggested that polymer chain confinement within the clay layers has a role in the reduction of penetrant permeability within polymer clay nanocomposites.

Flammability Properties

Many of the most exciting reports in the enhancements of polymer properties through the incorporation of nanoclay are in the area of reduced flammability [153-157]. There have been reports in significant reductions in the peak heat release rate with the incorporation of very low concentrations of clay into the polymer matrix. The reduced heat release rate is attributed to both physical and chemical processes that occur due to the presence of the clay during the heat-induced decomposition process. It has been proposed that the clay collapses during heating to form a barrier that significantly reduces the pyrolysis of the underlying polymer matrix [154, 158].

Polymer Clay Nanocomposites and Enhanced Crystallization

The incorporation of clay into various semicrystalline polymer matrices has been shown to have an effect on the rate of crystallization [159-166] and the type of crystalline structures formed in the presence of the clay [167-173]. Gopakumar and coworkers studied the effect of the degree of clay exfoliation on the physical properties of montmorillonite/polyethylene composites [143]. They found that the rate of crystallization of polyethylene modified with maleic anhydride containing organically-modified clay was significantly enhanced leading to faster crystallization in the presence of the clay. The enhanced crystallization is attributed to the heterogeneous nucleation mechanism that occurs in the presence of exfoliated clay platelets within the maleic anhydride modified PE matrix. Similar enhancements in the rate of crystallization in the presence of exfoliated clay platelets have been reported for nylon 6 clay nanocomposites [174].

Polymer nanocomposites are interesting hybrid materials that exhibit tremendous property improvements compared to conventional polymer micro-composites. The potential for the utilization of these materials in high performance applications will continue to drive research in this area forward at a rapid rate. Therefore, based on the numerous reports on the enhancement in the rate of polymer crystallization through the incorporation of clay in different polymer matrices, the incorporation of clay into sulfonated syndiotactic polystyrene (SsPS) appears to be a method that must be explored as a means to increase the rate of crystallization of SsPS ionomers.

REFERENCES

1. Gomez-Romero P. Advanced Materials 2001;13(3):163-174.
2. Judeinstein P and Sanchez C. Journal of Materials Chemistry 1996;6(4):511-525.
3. Kannan RY, Salacinski HJ, Butler PE, and Seifalian AM. Accounts of Chemical Research 2005;38(11):879-884.
4. Madbouly SA and Otaigbe JU. Progress in Polymer Science 2009;34(12):1283-1332.
5. Li G and Pittman CU. Polyhedral Oligomeric Silsesquioxane (POSS) Polymers, Copolymers, and Resin Nanocomposites: John Wiley & Sons, Inc., 2005.
6. Iyer P, Iyer G, and Coleman M. Journal of Membrane Science 2010;358(1-2):26-32.
7. Miyagawa H, Misra M, and Mohanty AK. Journal of Nanoscience and Nanotechnology 2005;5:1593-1615.
8. Du F, Scogna RC, Zhou W, Brand S, Fischer JE, and Winey KI. Macromolecules 2004;37(24):9048-9055.
9. Pradhan B, Setyowati K, Liu H, Waldeck DH, and Chen J. Nano Letters 2008;8(4):1142-1146.
10. Xie X-L, Mai Y-W, and Zhou X-P. Materials Science and Engineering: R: Reports 2005;49(4):89-112.
11. Njuguna J, Pielichowski K, and Desai S. Polymers for Advanced Technologies 2008;19(8):947-959.
12. Capadona JR, Shanmuganathan K, Trittschuh S, Seidel S, Rowan SJ, and Weder C. Biomacromolecules 2009;10(4):712-716.
13. Sinha Ray S and Bousmina M. Progress in Materials Science 2005;50(8):962-1079.

14. Garcia de Rodriguez NL, Thielemans W, and Dufresne A. Cellulose 2006;13(3):261-270.

15. Kvien I, Tanem BS, and Oksman K. Biomacromolecules 2005;6(6):3160-3165.

16. Oksman K, Mathew AP, Bondeson D, and Kvien I. Composites Science and Technology 2006;66(15):2776-2784.

17. Ljungberg N, Bonini C, Bortolussi F, Boisson C, Heux L, and Cavaillé. Biomacromolecules 2005;6(5):2732-2739.

18. Braun B and Dorgan JR. Biomacromolecules 2008;10(2):334-341.

19. Petersson L, Mathew AP, and Oksman K. Journal of Applied Polymer Science 2009;112(4):2001-2009.

20. Ma X-Y and Zhang W-D. Polymer Degradation and Stability 2009;94(7):1103-1109.

21. Chung Y-A, Chang Y-C, Lu M-Y, Wang C-Y, and Chen L-J. Journal of The Electrochemical Society 2009;156(5):F75-F79.

22. Frisch HL and Mark JE. Chemistry of Materials 1996;8(8):1735-1738.

23. Moniruzzaman M and Winey KI. Macromolecules 2006;39(16):5194-5205.

24. Thostenson ET, Ren Z, and Chou T-W. Composites Science and Technology 2001;61(13):1899-1912.

25. Coleman JN, Khan U, Blau WJ, and Gun'ko YK. Carbon 2006;44(9):1624-1652.

26. Ramanathan T, Abdala AA, Stankovich S, Dikin DA, Herrera Alonso M, Piner RD, Adamson DH, Schniepp HC, ChenX, Ruoff RS, Nguyen ST, Aksay IA, Prud'Homme RK, and Brinson LC. Nat Nano 2008;3(6):327-331.

27. Jang B and Zhamu A. Journal of Materials Science 2008;43(15):5092-5101.

28. Stankovich S, Dikin DA, Dommett GHB, Kohlhaas KM, Zimney EJ, Stach EA, Piner RD, Nguyen ST, and Ruoff RS. Nature 2006;442(7100):282-286.

29. Pavlidou S and Papaspyrides CD. Progress in Polymer Science 2008;33(12):1119-1198.

30. Usuki A, Hasegawa N, Kato M, and Kobayashi S. Polymer-Clay Nanocomposites. Inorganic Polymeric Nanocomposites and Membranes, vol. 179: Springer Berlin / Heidelberg, 2005. pp. 135-195.

31. Zanetti M, Lomakin S, and Camino G. Macromolecular Materials and Engineering 2000;279(1):1-9.

32. Okada A and Usuki A. Macromolecular Materials and Engineering 2006;291(12):1449-1476.

33. Vermogen A, Masenelli-Varlot K, Séguéla R, Duchet-Rumeau J, Boucard S, and Prele P. Macromolecules 2005;38(23):9661-9669.

34. Beyer G. Plastics, Additives and Compounding 2002;4(10):22-28.

35. Park JH and Jana SC. Macromolecules 2003;36(8):2758-2768.

36. Jash P and Wilkie CA. Polymer Degradation and Stability 2005;88(3):401-406.

37. Mravcáková M, Boukerma K, Omastová M, and Chehimi MM. Materials Science and Engineering: C 2006;26(2-3):306-313.

38. Fornes TD, Yoon PJ, Hunter DL, Keskkula H, and Paul DR. Polymer 2002;43(22):5915-5933.

39. Panek G, Schleidt S, Mao Q, Wolkenhauer M, Spiess HW, and Jeschke G. Macromolecules 2006;39(6):2191-2200.

40. Osman MA, Rupp JEP, and Suter UW. Polymer 2005;46(19):8202-8209.

41. Xie W, Hwu JM, Jiang GJ, Buthelezi TM, and Pan WP. Polymer Engineering & Science 2003;43(1):214-222.

42. Wan C, Qiao X, Zhang Y, and Zhang Y. Polymer Testing 2003;22(4):453-461.

43. Zhang J and Wilkie CA. Polymer 2006;47(16):5736-5743.

44. Chavarria F and Paul DR. Polymer 2006;47(22):7760-7773.

45. Xie W, Gao Z, Liu K, Pan W-P, Vaia R, Hunter D, and Singh A. Thermochimica Acta 2001;367-368:339-350.

46. Prado LASdA, Karthikeyan CS, Schulte K, Nunes SP, and de Torriani IL. Journal of Non-Crystalline Solids 2005;351(12-13):970-975.

47. Beall GW and Goss M. Applied Clay Science 2004;27(3-4):179-186.

48. Kozak M and Domka L. Journal of Physics and Chemistry of Solids 2004;65(2-3):441-445.

49. Marras S, Tsimpliaraki A, Zuburtikudis I, and Panayiotou C. Polymer Engineering & Science 2009;49(6):1206-1217.

50. Pluart LL, Duchet J, Sautereau H, and Gérard JF. The Journal of Adhesion 2002;78(7):645 - 662.

51. Liu P. Applied Clay Science 2007;38(1-2):64-76.

52. Heinz H, Vaia RA, Krishnamoorti R, and Farmer BL. Chemistry of Materials 2006;19(1):59-68.

53. Fornes TD, Hunter DL, and Paul DR. Macromolecules 2004;37(5):1793-1798.

54. Osman MA, Ploetze M, and Skrabal P. The Journal of Physical Chemistry B 2004;108(8):2580-2588.

55. Ranade A, D'Souza NA, and Gnade B. Polymer 2002;43(13):3759-3766.

56. Katti KS, Sikdar D, Katti DR, Ghosh P, and Verma D. Polymer 2006;47(1):403-414.

57. Xie W, Xie R, Pan W-P, Hunter D, Koene B, Tan L-S, and Vaia R. Chemistry of Materials 2002;14(11):4837-4845.

58. Patel HA, Somani RS, Bajaj HC, and Jasra RV. Applied Clay Science 2007;35(3-4):194-200.

59. Calderon JU, Lennox B, and Kamal MR. Applied Clay Science 2008;40(1-4):90-98.

60. Pucciariello R, Villani V, Belviso S, Gorrasi G, Tortora M, and Vittoria V. Journal of Polymer Science Part B: Polymer Physics 2004;42(7):1321-1332.

61. Awad WH, Gilman JW, Nyden M, Harris RH, Sutto TE, Callahan J, Trulove PC, DeLong HC, and Fox DM. Thermochimica Acta 2004;409(1):3-11.

62. Gilman JW, Awad WH, Davis RD, Shields J, Harris RH, Davis C, Morgan AB, Sutto TE, Callahan J, Trulove PC, and DeLong HC. Chemistry of Materials 2002;14(9):3776-3785.

63. Bottino FA, Fabbri E, Fragalà IL, Malandrino G, Orestano A, Pilati F, and Pollicino A. Macromolecular Rapid Communications 2003;24(18):1079-1084.

64. Chigwada G, Wang D, and Wilkie CA. Polymer Degradation and Stability 2006;91(4):848-855.

65. Kim Neung H, Malhotra Sanjay V, and Xanthos M. Ionic Liquids as Modifiers for Cationic and Anionic Nanoclays. Ionic Liquids IV, vol. 975: American Chemical Society, 2007. pp. 234-246.

66. Kim NH, Malhotra SV, and Xanthos M. Microporous and Mesoporous Materials 2006;96(1-3):29-35.

67. LeBaron PC, Wang Z, and Pinnavaia TJ. Applied Clay Science 1999;15(1-2):11-29.

68. Sinha Ray S, Okamoto K, and Okamoto M. Macromolecules 2003;36(7):2355-2367.

69. Sinha Ray S, Yamada K, Okamoto M, Fujimoto Y, Ogami A, and Ueda K. Polymer 2003;44(21):6633-6646.

70. Ray SS and Okamoto M. Macromolecular Rapid Communications 2003;24(14):815-840.

71. Jia Q-X, Wu Y-P, Wang Y-Q, Lu M, Yang J, and Zhang L-Q. Journal of Applied Polymer Science 2007;103(3):1826-1833.

72. Basu SK, Tewari A, Fasulo PD, and Rodgers WR. Applied Physics Letters 2007;91(5):053105.

73. Kim D, Lee JS, Barry CMF, and Mead JL. Microscopy Research and Technique 2007;70(6):539-546.

74. Navarchian AH and Majdzadeh-Ardakani K. Journal of Applied Polymer Science 2009;114(1):531-542.

75. Vermogen A, Masenelli-Varlot K, Vigier G, Sixou B, Thollet G, and Duchet-Rumeau J. Journal of Nanoscience and Nanotechnology 2007;7:3160-3171.

76. Preschilla N, Sivalingam G, Abdul Rasheed AS, Tyagi S, Biswas A, and Bellare JR. Polymer 2008;49(19):4285-4297.

77. Nawani P, Burger C, Rong L, Chu B, Hsiao BS, Tsou AH, and Weng W. Polymer 2010;51(22):5255-5266.

78. Sinha Ray S and Okamoto M. Progress in Polymer Science 2003;28(11):1539-1641.

79. Chen W and Qu B. Chemistry of Materials 2003;15(16):3208-3213.

80. Liao C-S and Ye W-B. Electrochimica Acta 2004;49(27):4993-4998.

81. Leroux F and Besse J-P. Chemistry of Materials 2001;13(10):3507-3515.

82. Bruzaud S and Levesque G. Chemistry of Materials 2002;14(5):2421-2426.

83. Cholli AL, Sahoo SK, Kim DW, Kumar J, and Blumstein A. Formation of Nanocomposites by In Situ Intercalative Polymerization of 2-Ethynylpyrdine in Layered Aluminosilicates: A Solid-State NMR Study. Polymers for Microelectronics and Nanoelectronics, vol. 874: American Chemical Society, 2004. pp. 294-305.

84. Lepoittevin B, Pantoustier N, Devalckenaere M, Alexandre M, Kubies D, Calberg C, Jérôme R, and Dubois P. Macromolecules 2002;35(22):8385-8390.

85. Messersmith PB and Giannelis EP. Chemistry of Materials 1993;5(8):1064-1066.

86. Okamoto M, Morita S, Taguchi H, Kim YH, Kotaka T, and Tateyama H. Polymer 2000;41(10):3887-3890.

87. Paul M-A, Delcourt C, Alexandre M, Degée P, Monteverde F, Rulmont A, and Dubois P. Macromolecular Chemistry and Physics 2005;206(4):484-498.

88. He A, Wang L, Li J, Dong J, and Han CC. Polymer 2006;47(6):1767-1771.

89. Huskic M and Zigon M. European Polymer Journal 2007;43(12):4891-4897.

90. Zeng QH and et al. Nanotechnology 2002;13(5):549.

91. Uthirakumar P, Nahm KS, Hahn YB, and Lee Y-S. European Polymer Journal 2004;40(11):2437-2444.

92. Essawy HA, Badran AS, Youssef AM, and Abd El-Hakim AE-FA. Macromolecular Chemistry and Physics 2004;205(17):2366-2370.

93. Li Y, Zhao B, Xie S, and Zhang S. Polymer International 2003;52(6):892-898.

94. Karger-Kocsis J and Wu CM. Polymer Engineering & Science 2004;44(6):1083-1093.

95. Strawhecker KE and Manias E. Chemistry of Materials 2000;12(10):2943-2949.

96. Carrado KA, Thiyagarajan P, and Elder DL. Clays Clay Mineral. 1996;44(null):506.

97. Chang JH, Jang TG, Ihn KJ, Lee WK, and Sur GS. Journal of Applied Polymer Science 2003;90(12):3208-3214.

98. Ji H, Lee H, Karim M, Cheong I, Bae E, Kim T, Islam M, Ji B, and Yeum J. Colloid & Polymer Science 2009;287(7):751-758.

99. Walther A, Bjurhager I, Malho J-M, Pere J, Ruokolainen J, Berglund LA, and Ikkala O. Nano Letters 2010;10(8):2742-2748.

100. Sengwa RJ, Choudhary S, and Sankhla S. Polymer International 2009;58(7):781-789.

101. Lemmon JP, Wu J, Oriakhi C, and Lerner MM. Electrochimica Acta 1995;40(13-14):2245-2249.

102. Vaia RA, Vasudevan S, Krawiec W, Scanlon LG, and Giannelis EP. Adv. Mater. 1995;7(null):154.

103. Wong S, Vaia RA, Giannelis EP, and Zax DB. Solid State Ionics 1996;86(null):547.

104. Vaia RA, Sauer BB, Tse OK, and Giannelis EP. Journal of Polymer Science Part B: Polymer Physics 1997;35(1):59-67.

105. Hackett E, Manias E, and Giannelis EP. Chemistry of Materials 2000;12(8):2161-2167.

106. Li Y and Ishida H. Polymer 2003;44(21):6571-6577.

107. Li Y and Ishida H. Macromolecules 2005;38(15):6513-6519.

108. Qiu L, Chen W, and Qu B. Polymer 2006;47(3):922-930.

109. Morgan AB and Harris JD. Polymer 2004;45(26):8695-8703.

110. Vaia RA, Jandt KD, Kramer EJ, and Giannelis EP. Chemistry of Materials 1996;8(11):2628-2635.

111. Vaia RA and Giannelis EP. Macromolecules 1997;30(25):8000-8009.

112. Martín Z, Jiménez I, Gómez MAn, Ade H, and Kilcoyne DA. Macromolecules 2009;43(1):448-453.

113. Shen Z, Cheng Y-B, and Simon GP. Macromolecules 2005;38(5):1744-1751.

114. Xu L, Nakajima H, Manias E, and Krishnamoorti R. Macromolecules 2009;42(11):3795-3803.

115. Barick AK and Tripathy DK. Materials Science and Engineering: A 2010;527(3):812-823.

116. Bhiwankar NN and Weiss RA. Polymer 2005;46(18):7246-7254.

117. Bhiwankar NN and Weiss RA. Polymer 2006;47(19):6684-6691.

118. Limpanart S, Khunthon S, Taepaiboon P, Supaphol P, Srikhirin T, Udomkichdecha W, and Boontongkong Y. Materials Letters 2005;59(18):2292-2295.

119. Ma H, Fang Z, and Tong L. Polymer Degradation and Stability 2006;91(9):1972-1979.

120. Meneghetti P and Qutubuddin S. Journal of Colloid and Interface Science 2005;288(2):387-389.

121. Fornes TD, Yoon PJ, Keskkula H, and Paul DR. Polymer 2001;42(25):09929-09940.

122. Nalawade SP, Picchioni F, and Janssen LPBM. Progress in Polymer Science 2006;31(1):19-43.

123. Tomasko DL, Li H, Liu D, Han X, Wingert MJ, Lee LJ, and Koelling KW. Industrial & Engineering Chemistry Research 2003;42(25):6431-6456.

124. Kendall JL, Canelas DA, Young JL, and DeSimone JM. Chemical Reviews 1999;99(2):543-564.

125. Shieh Y-T, Lai J-G, Tang W-L, Yang C-H, and Wang T-L. The Journal of Supercritical Fluids 2009;49(3):385-393.

126. Horsch S, Serhatkulu G, Gulari E, and Kannan RM. Polymer 2006;47(21):7485-7496.

127. Zhao Q and Samulski ET. Polymer 2006;47(2):663-671.

128. Su L, Pei S, Li L, Li H, Zhang Y, Yu W, and Zhou C. International Journal of Hydrogen Energy 2009;34(16):6892-6901.

129. Naveau E, Calberg C, Detrembleur C, Bourbigot S, Jérôme C, and Alexandre M. Polymer 2009;50(6):1438-1446.

130. Nguyen QT and Baird DG. Polymer 2007;48(23):6923-6933.

131. Nguyen QT and Baird DG. Advances in Polymer Technology 2006;25(4):270-285.

132. Yoshitsugu K, Arimitsu U, Masaya K, Akane O, Yoshiaki F, Toshio K, and Osami K. J. Mater. Res. 1993;8(5):1185-1189.

133. Tjong SC. Materials Science and Engineering: R: Reports 2006;53(3-4):73-197.

134. Podsiadlo P, Kaushik AK, Arruda EM, Waas AM, Shim BS, Xu J, Nandivada H, Pumplin BG, Lahann J, Ramamoorthy A, and Kotov NA. Science 2007;318(5847):80-83.

135. Lee H-s, Fasulo PD, Rodgers WR, and Paul DR. Polymer 2005;46(25):11673-11689.

136. Wang KH, Choi MH, Koo CM, Xu M, Chung IJ, Jang MC, Choi SW, and Song HH. Journal of Polymer Science Part B: Polymer Physics 2002;40(14):1454-1463.

137. Ellis TS and D'Angelo JS. Journal of Applied Polymer Science 2003;90(6):1639-1647.

138. Priya L and Jog JP. Journal of Polymer Science Part B: Polymer Physics 2002;40(15):1682-1689.

139. Pramanik M, Srivastava SK, Samantaray BK, and Bhowmick AK. Journal of Applied Polymer Science 2003;87(14):2216-2220.

140. Ratna D, Divekar S, Samui AB, Chakraborty BC, and Banthia AK. Polymer 2006;47(11):4068-4074.

141. Ogata N, Jimenez G, Kawai H, and Ogihara T. Journal of Polymer Science Part B: Polymer Physics 1997;35(2):389-396.

142. Liao M, Zhu J, Xu H, Li Y, and Shan W. Journal of Applied Polymer Science 2004;92(5):3430-3434.

143. Gopakumar TG, Lee JA, Kontopoulou M, and Parent JS. Polymer 2002;43(20):5483-5491.

144. Sinha Ray S, Maiti P, Okamoto M, Yamada K, and Ueda K. Macromolecules 2002;35(8):3104-3110.

145. Chang J-H, Kim SJ, Joo YL, and Im S. Polymer 2004;45(3):919-926.

146. Zeng C and Lee LJ. Macromolecules 2001;34(12):4098-4103.

147. Zerda AS, Caskey TC, and Lesser AJ. Macromolecules 2003;36(5):1603-1608.

148. Manitiu M, Bellair RJ, Horsch S, Gulari E, and Kannan RM. Macromolecules 2008;41(21):8038-8046.

149. Pinnavaia TJ and Beall GW. Polymer-Clay Nanocomposites. In: Pinnavaia TJ and Beall GW, editors. Chichester, West Sussex, England: John Wiley & Sons, Ltd., 2001. pp. 370.

150. Yoon PJ, Hunter DL, and Paul DR. Polymer 2003;44(18):5323-5339.

151. Gusev AA and Lusti HR. Advanced Materials 2001;13(21):1641-1643.

152. Xu B, Zheng Q, Song Y, and Shangguan Y. Polymer 2006;47(8):2904-2910.

153. Gilman JW, Jackson CL, Morgan AB, Harris R, Manias E, Giannelis EP, Wuthenow M, Hilton D, and Phillips SH. Chemistry of Materials 2000;12(7):1866-1873.

154. Morgan AB. Polymers for Advanced Technologies 2006;17(4):206-217.

155. Paul DR and Robeson LM. Polymer 2008;49(15):3187-3204.

156. Zhu J, Morgan AB, Lamelas FJ, and Wilkie CA. Chemistry of Materials 2001;13(10):3774-3780.

157. Cipiriano BH, Kashiwagi T, Raghavan SR, Yang Y, Grulke EA, Yamamoto K, Shields JR, and Douglas JF. Polymer 2007;48(20):6086-6096.

158. Zhu J, Uhl FM, Morgan AB, and Wilkie CA. Chemistry of Materials 2001;13(12):4649-4654.

159. Chisholm BJ, Moore RB, Barber G, Khouri F, Hempstead A, Larsen M, Olson E, Kelley J, Balch G, and Caraher J. Macromolecules 2002;35(14):5508-5516.

160. Barber GD, Calhoun BH, and Moore RB. Polymer 2005;46(17):6706-6714.

161. Xu W, Ge M, and He P. Journal of Polymer Science Part B: Polymer Physics 2002;40(5):408-414.

162. Phang IY, Pramoda KP, Liu T, and He C. Polymer International 2004;53(9):1282-1289.

163. Krikorian V and Pochan DJ. Macromolecules 2004;37(17):6480-6491.

164. Ou C-F. Journal of Polymer Science Part B: Polymer Physics 2003;41(22):2902-2910.

165. Nam JY, Sinha Ray S, and Okamoto M. Macromolecules 2003;36(19):7126-7131.

166. Jog JP. Materials Science and Technology;22:797-806.

167. Pramoda KP, Mohamed A, Yee Phang I, and Liu T. Polymer International 2005;54(1):226-232.

168. Fornes TD and Paul DR. Polymer 2003;44(14):3945-3961.

169. Liu X, Wu Q, and Berglund LA. Polymer 2002;43(18):4967-4972.

170. Hu X and Lesser AJ. Journal of Polymer Science Part B: Polymer Physics 2003;41(19):2275-2289.

171. Zheng W, Lu X, Ling Toh C, Hua Zheng T, and He C. Journal of Polymer Science Part B: Polymer Physics 2004;42(10):1810-1816.

172. Chua YC and Lu X. Langmuir 2007;23(4):1701-1710.

173. Ishisue T, Okamoto M, and Tashiro K. Polymer 2010;51(23):5585-5591.

174. Maiti P and Okamoto M. Macromolecular Materials and Engineering 2003;288(5):440-445.

CHAPTER V
ISOTHERMAL CRYSTALLIZATION OF LIGHTLY-SULFONATED SYNDIOTACTIC POLYSTYRENE/MONTMORILLONITE CLAY NANOCOMPOSITES

ABSTRACT

Lightly sulfonated syndiotactic polystyrene (sPS) nanocomposites were prepared using a solution intercalation technique, and the effect of montmorillonite clay on the crystallization kinetics of sulfonated sPS ionomer nanocomposites was systematically studied. Wide-angle x-ray diffraction (WAXD) and transmission electron microscopy (TEM) were used to evaluate the dispersion of clay platelets within sPS and sulfonated sPS ionomer (SsPS) matrices. Experimental results obtained from WAXD and TEM revealed a predominately exfoliated morphology within the SsPS ionomer containing 5 wt.% of organically-modified clay. The corresponding non-sulfonated sPS control exhibited a mixed morphological structure consisting of intercalated platelets and many platelets that were present as micron-sized agglomerates. Using differential scanning calorimetry (DSC), the Avrami approach was used to elucidate information related to nucleation and growth within the sPS and SsPS systems during the isothermal crystallization process. Pristine and organically-modified clays significantly increased the overall crystallization rate of the SsPS ionomer, while the nanoclays slightly decreased the crystallization rate of the non-ionic sPS. The mechanistic origins of increased crystallization rates within the SsPS ionomer clay nanocomposites were attributed to multiple phenomena including disruption of the ionomer electrostatic network and a nucleating effect due to the presence of well-separated, homogeneously dispersed clay platelets.

INTRODUCTION

Polymer/clay nanocomposites are very important materials from an industrial perspective due to the potential material property enhancements that can be realized with only a small addition of properly dispersed nanoscale clay platelets [1-2]. Therefore, a significant amount of research has been focused on the preparation of polymer/clay nanocomposites using industrially important semicrystalline polymers such as polypropylene [3-4], polyethylene [5-6], polyesters [7-10], and polyamides[11-12]. However, the organophillic character of many industrially important semicrystalline polymers prevents sufficient interaction between the polymer and clay resulting in poor dispersion of the naturally polar aluminosilicate clay within the hydrophobic polymer matrix.

Ion-containing polymers (specifically, ionomers containing less than ca. 10 mol% ionic functionality along the chains) have been investigated as the host matrix for the preparation of polymer/clay nanocomposites [13-14] and as compatibilizers between a host matrix and clay platelets as well [15-17]. The advantage of utilizing ionomers as matrices and compatibilizers in polymer/clay nanocomposites originates from strong specific interactions that can occur between the ionic groups of the ionomer and the highly charged, polar clay surface. The improved interaction between the ion-containing polymer and polar clay through favorable electrostatic interactions may facilitate the development of intercalated and exfoliated morphologies. The resultant intercalated and exfoliated morphologies reveal and expose the high clay surface area necessary to realize enhanced mechanical, thermal, and barrier properties [13-14].

Initial demonstration of the effectiveness of ionomers as host matrices for the preparation of polymer nanocomposites was provided by Chisholm et. al [13]. This study revealed that incorporation of as little as 1.0 mol% -SO_3Na groups onto poly(butylene terepthalate) (PBT) resulted in the formation of an exfoliated morphology of organically-modified montmorillonite clay platelets that were well-dispersed throughout the PBT ionomer matrix. Polyester ionomer clay nanocomposites have also been prepared using poly(ethylene terepthalate) (PET) containing up to 5.8 mol% sodium sulfonate ionic groups [14]. Barber et. al have shown that incorporation of low levels of sodium sulfonate groups into PET along with the utilization of organically-modified montmorillonite clay results in the formation of highly intercalated and exfoliated ionomer clay structures. This study using PET ionomers, supported the previous work completed by Chisholm and coworkers using PBT ionomers and further demonstrated that ionomers may be used as matrices to create intercalated and exfoliated polymer nanocomposites.

Since the initial work of Chisholm et. al, further research has been conducted using ionomers as host matrices for the development of polymer nanocomposites. Nanocomposites have been prepared using ionomers based on polypropylene, polyethylene [18], and polystyrene [19]. Important aspects of ionomer nanocomposite preparation have been investigated such as the effects of ionic functionality on clay platelet dispersion [14], the effects of melt processing on the degree of exfoliation [20], and the effect of surfactant structure [21] on the ionomer nanocomposite morphology. However, in order for semicrystalline ionomer nanocomposites to be effectively used in industrial and commercial applications, a detailed understanding of the effect of clay on the crystallization behavior of the ionomer matrix is of fundamental importance.

Our initial ionomer nanocomposite studies [13-14] provided information on the effect of tactoid, intercalated, and exfoliated morphological clay arrangements on the crystallization

behavior of polyester ionomers. However, conflicting information was obtained from the study of the polyester based ionomer nanocomposites systems based upon poly(ethylene terepthalate) and poly(butylene terepthalate). It was found that the crystallization half-time (the time required for the material to reach 50% crystallinity during isothermal crystallization) slightly increased for PBT ionomer nanocomposites. The increase in crystallization half-time suggested the overall rate of bulk crystallization is decreased and clay did not act as a nucleating agent within the PBT ionomer matrix. Moreover, isothermal crystallization data of PBT ionomer nanocomposites revealed the crystallization half-time was not dependent upon the morphological state of the dispersed clay particles. In contrast, Barber et al [14] found the crystallization behavior of PET ionomer nanocomposites to be dependent upon the degree of clay exfoliation within the ionomer matrix. The crystallization half-time of PET ionomer nanocomposites increased with increasing degree of clay exfoliation indicating the exfoliated nanoscale platelets are less effective nucleants relative to micron-sized clay tactoids.

Due to the contrasting effect of clay on the crystallization kinetics and behavior of semicrystalline PBT and PET ionomers, it necessary to further study the effect of clay on the crystallization behavior and kinetics of a *model* semicrystalline ionomer. Sulfonated syndiotactic polystyrene (SsPS) has been utilized as a model semicrystalline ionomer in fundamental investigations studying the link between ionic aggregation and crystallization behavior of ionomers [22-25]. Since the ionic species of SsPS are incorporated through a post-sulfonation reaction and not through copolymerization (as with previous studies), varying the ionic content does not significantly disrupt the microstructure and molecular weight distribution of the resulting SsPS copolymer. Additionally, a significant advantage of utilizing SsPS as a model semicrystalline ionomer results from the high stereoregularity of sPS, which allows it to

crystallize rapidly from the melt. The wealth of fundamental information on the crystallization behavior of sulfonated sPS provided by these studies renders it a prime candidate for a detailed study of the effect of clay on the crystallization behavior and kinetics of semicrystalline ionomers in general.

In a previous study, the preparation and characterization of SsPS nanocomposite morphology has been reported as a function of ionic content and neutralizing counterion [26]. It was shown that the degree of clay exfoliation increased with increasing ionic content and with increasing size of the neutralizing counterion. This study provided initial qualitative observations on the non-isothermal crystallization behavior of SsPS nanocomposites by monitoring the peak crystallization temperature on cooling from the melt. However, a more detailed quantitative study of the effect of clay on the crystallization behavior and kinetics of SsPS is needed to gain further insight into possible mechanism of crystallization of the SsPS ionomer in the presence of montmorillonite clay.

Thus, the purpose of this study is to determine the effect of pristine and organically-modified clay on the morphology, crystallization behavior, and isothermal crystallization kinetics of SsPS, a model semicrystalline ion-containing polymer.

EXPERIMENTAL

Materials

Syndiotactic polystyrene (Questra 102) MW of 310,000 g/mol was donated by the Dow Chemical Company. Reagent grade chloroform, methanol, sulfuric acid, and potassium monopthalate were obtained from Fisher Scientific. Hexanoic anhydride and cesium hydroxide were received from Sigma Aldrich. Cloisite® Na^+ and Cloisite® 10A were donated by Southern

Clay Products. The clays were used in the received state without additional drying. The cation exchange capacities for Cloisite® Na^+ and Cloisite® 10A are 92.6 and 125 and milliequivalents/100 g, respectively. The organic modification agent for Cloisite® 10A is a quaternary amine salt consisting of a dimethylbenzyl, hydrogenated tallow. The hydrogenated tallow is made up of ~65% C18, ~30% C16, and ~5% C14 chains. Cloisite®10A has been shown to produce intercalated and exfoliated nanostructures in many styrenated polymer matrices [27-31] and is thus a proper choice for enhancing polymer-clay interactions in the sPS matrix. Cloisite® Na^+ and Cloisite® 10A will be identified as Na^+MMT and OMMT respectively. The clay organic modification agent, Arquad DMHTB-80E was donated by Akzo Nobel Surface Chemistry, LLC.

Sulfonation of Syndiotactic Polystyrene

Previous differential scanning calorimetry (DSC) investigations of SsPS ionomers have identified the effect of the degree of sulfonation on the crystallization behavior of SsPS [23]. It has been demonstrated that incorporating greater than 2.0 mol% of ionic content within sPS drastically inhibits the ability of sPS to crystallize. Therefore, we have chosen to lightly sulfonate sPS to yield an ion-containing polymer with 1 mol% sulfonation. By introducing 1 mol% sulfonate groups, the crystallization kinetics of SsPS occurs on a readily observable timescale at crystallization temperatures similar to that of the sPS homopolymer. Thus, direct comparisons between the behavior of the SsPS ionomer and the sPS homopolymer can be made.

The sulfonation agent was prepared according to previously published procedures [23] using chloroform as the solvent. Chloroform (25 mL) was added to a 50 mL volumetric flask containing 0.03 moles of hexanoic anhydride. The chloroform/hexanoic anhydride solution was

cooled in an ice bath for 1 hour, and then 1 mL of concentrated sulfuric acid was added to the chilled solution and shaken vigorously. Additional chloroform was added to the volumetric flask to the 50 mL mark.

sPS was dissolved in chloroform at 100 °C for 1.5 h in a PARR pressure reactor to yield a 2.5% w/v solution. After 1.5 h, the solution was cooled to 70 °C and then transferred to a three-neck round bottom flask. Additional chloroform was added to yield a 1% w/v sPS solution. The sPS solution was allowed to equilibrate at 70 °C under a nitrogen purge. After equilibration, the appropriate amount of sulfonating reagent was added and the reaction was allowed to proceed for 1 hour at 70 °C under a nitrogen purge. After 1 h, 10 mL methanol was added to the solution to terminate the reaction. The solution was poured into a large excess of methanol to precipitate the polymer. The precipitated polymer was filtered and washed with deionized water. The resulting polymer was dried under vacuum at 100 °C for 12 h. The vacuum dried ionomer was redissolved in chloroform using a PARR pressure reactor for 1.5 h at 100 °C and then steam stripped in deionized water to remove residual sulfonating reagent and solvent. The ionomer was then dried in a vacuum oven at 70 °C for 24 h. The degree of sulfonation was determined by nonaqueous titration with methanolic sodium hydroxide. The methanolic sodium hydroxide was standardized using potassium monopthalate.

Neutralization of Sulfonated Syndiotactic Polystyrene

The cesium counterion was chosen as the neutralizing counterion for SsPS within this study of the crystallization behavior and kinetics of SsPS nanocomposites based on previous work by Orler et al [32]. The relatively large cesium counterion yields weaker electrostatic interactions compared to SsPS ionomers neutralized with alkali metals of smaller ionic radii, and

thus leading to enhanced crystallization. Due to the presence of these more thermally-labile ionic aggregates, cesium-neutralized SsPS allows crystallization of chain segments to occur on time-scale similar to the sPS homopolymer. Therefore, cesium-neutralized SsPS was considered to be the most appropriate SsPS ionomer to study the effect of clay on the crystallization behavior and kinetics of the semicrystalline SsPS.

The SsPS ionomer was completely neutralized using 0.1 M cesium hydroxide. The SsPS was dissolved in chloroform using a PARR pressure reactor at 100 °C for 1.5 h. The appropriate amount of 0.1 M CsOH was added to the SsPS solution to obtain a fully neutralized ionomer. The fully cesium-neutralized SsPS 1.0 mol% ionomer was used as the ionomer matrix within this study and will be identified as SsPS.

Nanocomposite Preparation

Nanocomposites were prepared using the solution intercalation method [1-2, 33-34]. Dispersions of Na^+MMT and OMMT (0.5% w/v) were prepared by adding the appropriate amount of clay to chloroform. The respective clay/chloroform mixtures were heated under reflux at 60 °C for 24 h with vigorous stirring. After 24 h, the clay dispersions were sonicated for 2 h.

sPS and SsPS nanocomposites containing 1, 3, and 5% w/w of Na^+MMT and OMMT clays were prepared. Solutions of sPS and SsPS were prepared by dissolving the appropriate amount of the homopolymer or the ionomer in chloroform to yield 1.5% w/v solutions. The sPS homopolymer or SsPS ionomer was dissolved in chloroform using a PARR pressure reactor at 100°C for 1.5 h. The solutions were removed from the reactor upon dissolution and transferred to 50 mL round bottom flasks. The appropriate volume of clay dispersions to yield 1, 3, or 5 % w/w of Na^+MMT or OMMT was taken from the previously prepared 0.5% w/v clay dispersions,

while the mixture was being vigorously stirred to ensure that a homogeneous sample volume was removed. After adding the appropriate amount of clay dispersion to the dissolved polymer, the samples were allowed to mix with vigorous stirring under reflux for 24 h at 60°C. After 24 hours, the mixtures were dried at RT for 5 days to evaporate the solvent followed by drying in a vacuum oven for 24 h at 60 °C.

Sulfonated Syndiotactic Polystyrene Containing Organic Modification Agent

In order to isolate the effect of the organic modification agent on the crystallization behavior of SsPS, the organic modification agent used to render the pristine clay more organophilic, DMHTB, was added to solutions of the SsPS ionomer without any clay present. A solution of DMHTB was prepared by dissolving the surfactant in TCB for 1 hour under reflux conditions. The appropriate amount of the DMHTB solution was added to 1.5% w/v solutions of SsPS ionomer in TCB to yield the amount of DMHTB surfactant that would be present at Cloisite® 10A contents of 1, 3, and 5 wt.%. The SsPS/DMHTB solutions were mixed with vigorous stirring for 1 hour followed by drying in a vacuum oven for 24 hours at 60 °C.

2.6 Transmission Electron Microscopy

Solution-cast samples were prepared for morphological analysis using transmission electron microscopy (TEM) by embedding solution cast sPS and SsPS clay mixtures into epoxy resin. The epoxy resin used was Spurr's Low Viscosity embedding mixture obtained from Electron Microscopy Sciences. The resin was prepared according the supplier's protocol. The resin containing the nanocomposites samples were dried in vacuum oven at 60 °C for 12 h. The samples were microtomed at room temperature with a diamond knife using a Reichart Ultramicrotome in order to obtain 80 nm thick sections. Microtomed sections were transferred

from water onto 200 mesh copper grids and used without staining. The high electron density of the clay platelets provided the necessary contrast for morphological evaluation using TEM. TEM micrographs of solvent-cast sPS and SsPS clay mixtures were obtained using a JEOL 2100 transmission electron microscope operating at 200 kV. The microscope was interfaced with a Gatan camera that was utilized to obtain digital photomicrographs.

Wide Angle X-ray Diffraction

Wide angle x-ray diffraction (WAXD) was used as a quantitative tool to determine the changes in clay platelet intergallery height by following changes in the basal spacing of the clay. Solvent-cast nanocomposite samples were ground into a powder using a mortar and pestle prior to WAXD analysis. A Rigaku Ultima III X-ray Diffractometer using Cu K_α radiation (λ= 1.54 nm) operating at 40 kV and 44 mA was used to obtain nanocomposite WAXD profiles in the 2 theta region from 2θ = 2 - 10°. The WAXD profiles were obtained at a scan rate of 0.1°/min and a step size of 0.05.

Differential scanning calorimetry

Thermal behavior and crystallization kinetics of the polymer clay mixtures were studied using differential scanning calorimetry (DSC). A Perkin-Elmer DSC-7 was used to probe the thermal behavior of the prepared nanocomposites under isothermal crystallization conditions at 240 °C. The weight for each sample was maintained between 6 – 8 mg. The solution cast samples will be identified throughout the paper using the following terminology: sPS XNa^+MMT, sPS XOMMT, SsPS XNa^+MMT and SsPS XOMMT where X will equal 0, 1, 3, or 5 wt.% Na^+MMT or OMMT clay in the sPS homopolymer or the SsPS ionomer.

DSC analysis was performed under a continuous nitrogen flow to minimize sample degradation. The samples were heated to 330 °C and held at that maximum temperature for 5 min to erase previous thermal history and the presence of any persistent nuclei. Following a rapid temperature ramp at -200 °C/min, isothermal crystallization was carried out at 240 °C for 60 min. Pyris Perkin-Elmer software was used to analyze the resulting DSC traces. The crystallization half-time, $t_{½}$, the time at which 50% of the material has crystallized, was obtained from isothermal holds and used as a measure of changes in the bulk crystallization rate of the neat polymers and polymer-clay mixtures.

Polarized Light Microscopy

The determination of the spherulitic growth rates of the pure matrices and clay-containing matrices was carried out using polarized light microscopy. A Nikon LV100 microscope equipped with a Nikon DXM1200 digital camera was used in crossed-polarized configuration to monitor spherulitic growth under isothermal conditions. Images were captured and analyzed using Nikon NIS-Elements BR software. Isothermal crystallization conditions were achieved using a Linkam TMS600 hotstage operated by a Linkam TMS 94 controller and Linkam Linksys32 software. The samples were heated to 330 °C on the Linkam hotstage and held at that maximum temperature for 5 min. Following a rapid temperature ramp at -100 °C/min, isothermal crystallization was carried out at 240 °C with periodic image capture until complete spherulitic impingement occurred.

Small Angle Laser Light Scattering

Small-angle laser light scattering (SALLS) patterns were obtained in H_v mode using a laser light scattering experimental configuration similar to that of Stein and Rhodes [35]. A 3 mW He-Ne laser light of 632.8 nm (Oriel Corporation, Model 6697) was used as the incident light and the H_v patterns were captured using a SenSys 1401E (Photometrics) CCD camera positioned at a sample-to-detector distance of 380 mm. The spherulite diameters of the pristine polymers and polymer/clay mixtures were obtained using volume-filled samples that were isothermally crystallized at 240 °C using a Linkam hotstage according to the heating profile used for the polarized optical microscopy analysis. The H_v patterns were analyzed using POLAR Software (STAR, State University of New York) to obtain the maximum scattering intensity at an azimuthal angle of 45°.

RESULTS AND DISCUSSION

Morphological Characterization of sPS/SsPS Clay Nanocomposites

There are studies of sPS nanocomposites that evaluate the effect of clay on various properties of sPS nanocomposites [30, 36-44]. However, there is only one of the study of SsPS nanocomposites. The morphological and crystallization analysis provided within this work will provide a detailed probe in the effect of clay on the crystallization behavior of SsPS and compare that behavior to that of the non-ionized sPS homopolymer.

WAXD analysis provides insight into the morphological state of polymer clay mixtures through a determination of the degree of periodicity and order present within the dual component system. Figures V-1A and V-1B provide WAXD profiles of solvent-cast sPS and SsPS matrices containing Na^+MMT concentrations of 0, 1, 3, and 5 wt.%. For comparison, the WAXD profile

of pure Na^+MMT is also provided in Figures V-1A and V-1B. The WAXD profile of Na^+MMT contains a peak centered at 7.1° 2θ that corresponds to a basal spacing repeat distance of 1.2 nm of pristine, unmodified clay. Monitoring changes in the position of the Na^+MMT basal reflection provides information regarding changes in the interlayer height of Na^+MMT upon incorporation into the sPS homopolymer and SsPS ionomer matrices.

Figures V-1A and V-1B also contain WAXD profiles of the neat sPS and SsPS matrices. For both the neat sPS and SsPS, the WAXD patterns show a single peak at 8.0° 2θ attributed to the presence of the solvent-induced δ-crystal form of sPS [45-50]. Figure V-1A contains WAXD patterns of sPS Na^+MMT mixtures containing 1, 3, and 5 wt.% Na^+MMT. There are two peaks that can be identified within each sPS Na^+MMT WAXD pattern. The sPS 1 wt.% Na^+MMT WAXD profile, shown in Figure V-2A, reveals the appearance of a peak at 6.7° 2θ upon addition of 1 wt.% Na^+MMT into the sPS matrix. This peak attributed to Na^+MMT has shifted slightly from 7.0° 2θ associated with unintercalated Na^+MMT to 6.7° 2θ in the sPS matrix. This shift in pristine Na^+MMT scattering to a lower angle indicates the interplatelet gallery height has increased slightly from 1.2 nm to 1.31 nm. The slight increase in the gallery height suggests a small portion of sPS chains has entered the interplatelet region resulting in the observed increase in basal spacing.

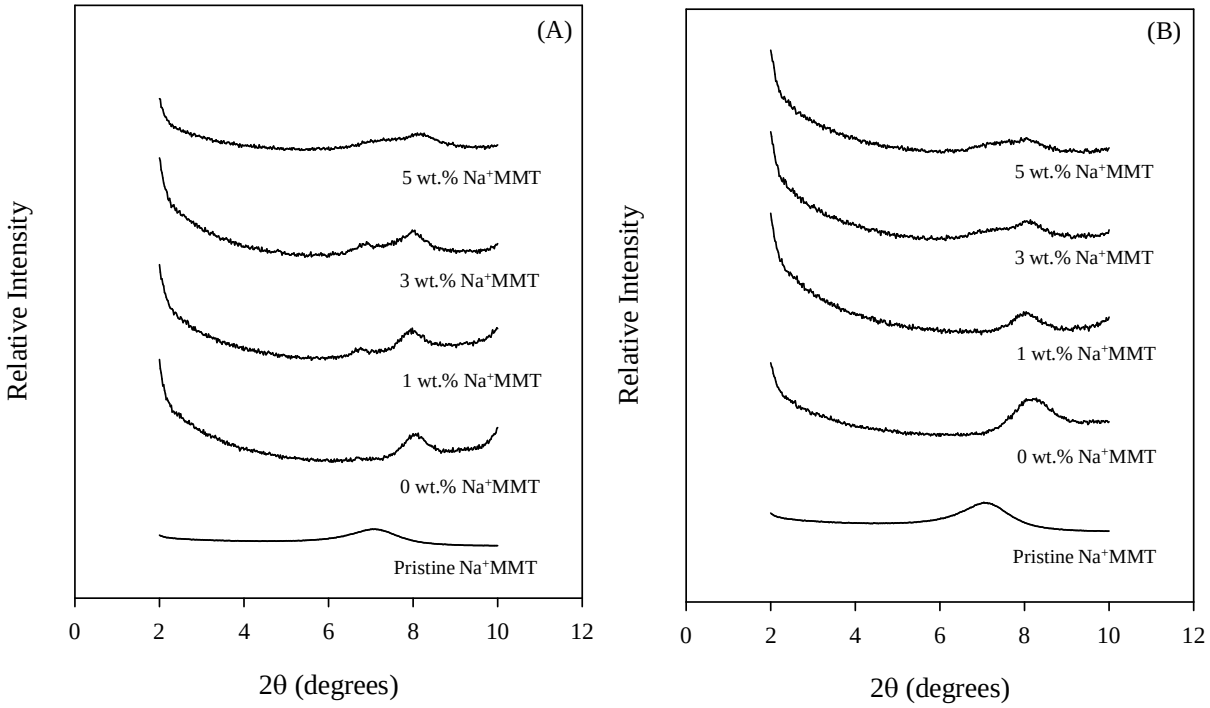

Figure V-1. WAXD patterns in the range of 2θ = 2 - 10° for (A) sPS Na^+MMT mixtures and (B) SsPS Na^+MMT mixtures.

As the concentration of Na^+MMT silicate is increased within the sPS matrix from 1 to 5 wt.% Na^+MMT, three noticeable changes in the WAXD patterns occur as shown in Figure V-1A. The peak attributable to Na^+MMT clay 6.7° 2θ increases in intensity, broadens in peak breadth, and finally merges with the peak corresponding to the sPS δ-crystal form located at 8.0° 2θ. An increase in the breadth of the Na^+MMT peak as shown in Figure V-1A may be ascribed to a wide distribution of platelet intergallery spacings indicative of a heterogeneous arrangement of platelets within the sPS matrix and inherent disordered platelet stacking common to smectite minerals [51-53]. The increase in intensity of the broad peak centered at 6.7° 2θ in WAXD profiles of sPS Na^+MMT composites with increasing clay content is expected based on composition and suggests that there are not sufficient polymer-clay interactions between the hydrophobic sPS homopolymer and the polar aluminosilicate Na^+MMT clay to facilitate significant changes in the inherent tactoid arrangement of Na^+MMT platelets within the sPS homopolymer matrix. Additionally, the peak present at 6.7° 2θ may also be attributed to the sPS β-form polymorph. It has been shown that the incorporation of Na^+MMT clay into the sPS matrix using the solution intercalation induces the formation the β-form polymorph which is usually formed only under melt-processing conditions [27]. The formation of the sPS β-form crystal has been attributed to the crystallization of sPS chain parallel to the clay platelet surface [27].

The WAXD profiles of the ionomeric SsPS Na^+MMT mixtures are provided in Figure V-1B. Upon addition of 1 wt.% Na^+MMT into the ionomer matrix, there are no observable changes in the WAXD profile compared to that of the pure SsPS ionomer as shown in Figure V-1B. The lack of a peak corresponding to Na^+MMT indicates that Na^+MMT platelets do not exhibit a

highly ordered arrangement that can be detected. However, upon addition of 3 wt.% Na^+MMT into the SsPS ionomer matrix as shown in Figure V-1B, a very broad peak appears within the WAXD profile that is centered at 7.0° 2θ corresponding to the basal spacing of Na^+MMT and the presence of the β-form sPS polymorph as well. Because the sPS and SsPS nanocomposites within this study have been prepared under similar conditions, we suggest that the peak in the 6.0 – 6.7° 2θ is also due to the β-crystal polymorph. Further investigation into the polymorphic structure can be obtained by probing higher 2θ angles and by using FTIR [40] to identify the various crystalline chain conformations. However, the scope of this study is not focused on determining the effect of clay on the polymorphic behavior of sPS and SsPS nanocomposites, but on comparing crystallization behavior of the non-ionized polymer and sulfonated material in the presence of the clayAs with the pure sPS matrix, the peak corresponding to Na^+MMT continues to broaden and increase in intensity upon addition of 5 wt.% Na^+MMT into the ionomer matrix. In agreement with our previous work with polyester ionomers [13-14], these data indicate that ionic interactions alone are not sufficient to disrupt the tactoid arrangement of Na^+MMT platelets without organic modification of the clays.

Many investigations into the preparation of polymer nanocomposites have been focused on surfactant modification of the highly charged clay surface in order to render the platelet surface more organophilic and thus aid in the dispersion of the platelets in hydrophobic polymer matrices [54-60]. To facilitate enhanced dispersion of the clay nanoparticles with in the sPS matrix, the natural sodium montmorillonite clay has been chemically-modified via an ion exchange reaction with a quaternary ammonium surfactant. The quaternary ammonium surfactant contains a long chain alkyl portion and a benzyl moiety. The benzyl moiety has been proposed to aid in producing favorable interaction between the clay and styrenated polymers [27,

61-62] . Figures V-2A and V-2B contain WAXD profiles of sPS OMMT and SsPS OMMT respectively. Each figure contains the WAXD profile of the pure OMMT revealing a single peak at 4.7° 2θ attributed to the basal spacing of the platelets in the as-received state. It is important to note that the basal spacing of the montmorillonite clay platelets is significantly increased as a result of organic modification. Comparison of the WAXD profile of Na^{+}MMT in Figure V-1 to the WAXD profile of OMMT in Figure V-2 shows the diffraction peak of the montmorillonite platelets has shifted from 6.7° 2θ to 4.7° 2θ. The intergallery height of the organically modified platelets has increased from 1.2 nm to 1.93 nm. Figures V-2A and V-2B also contain the WAXD profiles of neat sPS and SsPS showing peaks located at 8.0° and 8.2° 2θ, respectively, attributed to the presence of the solvent-induced δ-crystal form of semicrystalline polymer component.

In the WAXD profiles of sPS containing organically modified clay in Figure V-2A, a peak located at 7.0° 2θ attributed to the presence of the β-crystal form in present. This peak increases in intensity with increasing concentration of OMMT. It is extremely important to note the changes in the position and intensity of the peak near 4.7° 2θ attributed to the basal spacing of the organically-modified clay in order to monitor changes in interplatelet gallery height. No observable diffraction peak is present 4.7° 2θ (indicative of periodically arranged platelets) for the sPS 1 wt.% OMMT sample. However, a broad low-intensity peak attributable to OMMT appears in the sPS 3 wt.% OMMT sample, and the peak intensity notably increases for the sPS sample containing 5 wt.% OMMT. The presence of a clear OMMT peak, showing only a minimal increase in the intergallery platelet height, suggests that organic modification of the platelets alone is not sufficient to produce an exfoliated morphology within sPS matrix.

In distinct contrast to the WAXD data of Figures V-1A, V-1B, and V-2A, the WAXD profiles of SsPS OMMT nanocomposites containing OMMT concentrations up to 5 wt% show

only one significantly observable diffraction peak located at 8.2° 2θ corresponding to the solvent-induced δ-crystal form. There is also a very small low intensity, broad peak located at 7.0° 2θ attributed to the presence of the β-form crystal. The most important observation to note is that the WAXD profiles of these ionomer/OMMT composites are featureless in the region characteristic of layered OMMT. The lack of any peak attributable to OMMT suggests that the organically-modified platelets are arranged within the SsPS matrix in such a way that no well-defined order is present and/or the platelet-platelet distance is too large to be detected using WAXD. Therefore, in agreement with our previous studies, we can infer that a considerable degree of SsPS chains may have been inserted into the platelet intergallery region increasing the interplatelet distance and effectively disordering the native, well-defined platelet basal spacing and possibly creating an exfoliated platelet morphology. Chemical modification of both polymer (i.e., ionic functionalization) and clay (i.e., organic modification) appears to be very effective in creating a nanocomposite morphology that may consist of highly disordered platelets within the ionomer matrix.

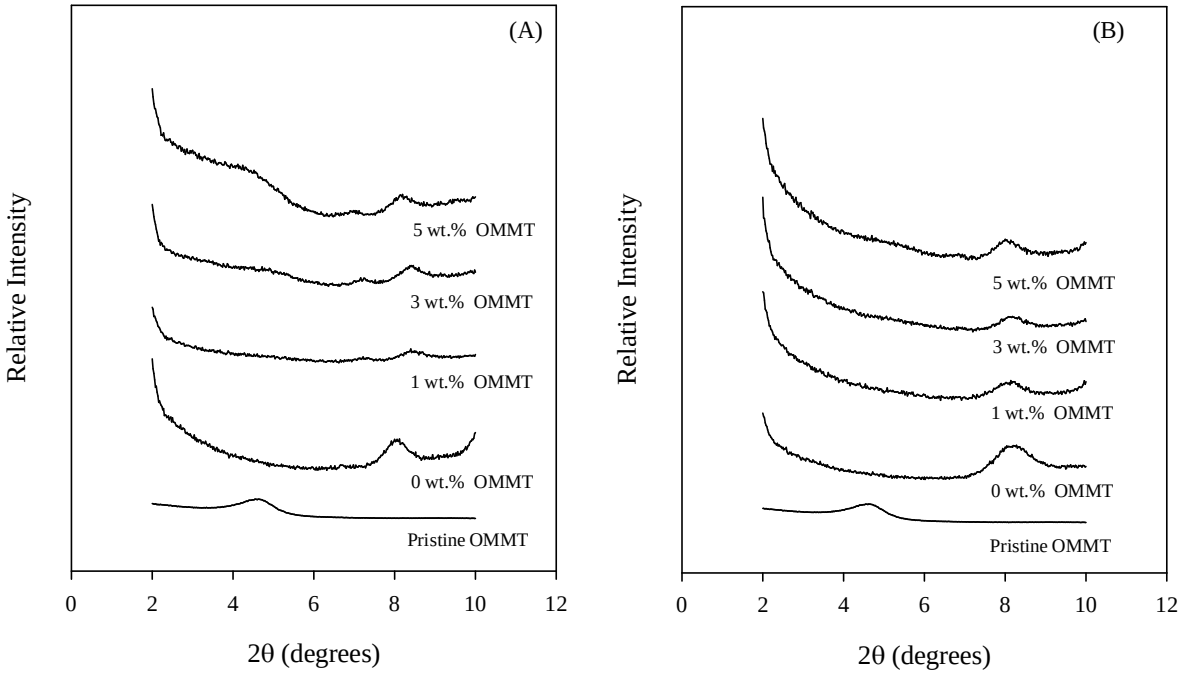

Figure V-2. WAXD patterns in the range of 2θ = 2 - 10° for (A) sPS OMMT mixtures and (B) SsPS OMMT mixtures.

While WAXD is a highly useful technique used to probe the morphology of polymer nanocomposites, WAXD is not sufficient alone to fully characterize the morphology of layered silicate platelets within any polymer matrix. It is often coupled with TEM analysis in order to more fully characterize the state of clay dispersion within the polymeric matrix. Figures V-3A and V-3B contain TEM micrographs of solvent-cast sPS and SsPS matrices containing 5 wt.% Na^+MMT respectively. The TEM micrograph of sPS 5 wt.% Na^+MMT in Figure V-3A reveals a mixed platelet morphology dominated by the presence of large micron-scale clay tactoids. In addition to clay tactoid agglomerates, Figure V-3A of sPS 5 wt.% Na^+MMT also shows platelet structures consisting of tens of platelets and a few single platelet features as well. Figure V-3B provides the TEM micrograph of SsPS containing 5 wt.% Na^+MMT. The presence of micron-sized agglomerates of Na^+MMT platelets within the ionomer matrix are readily visible and the

overall morphology of the SsPS 5 wt.% Na^+MMT mixture is very similar to that of the sPS homopolymer containing 5 wt.% Na^+MMT. In agreement with the WAXD data, this suggests that ionomer- Na^+MMT platelet interactions were not sufficient to result in a highly exfoliated or intercalated platelet morphology using the solution intercalation technique at a concentration of 5 wt.% Na^+MMT in the SsPS ionomer.

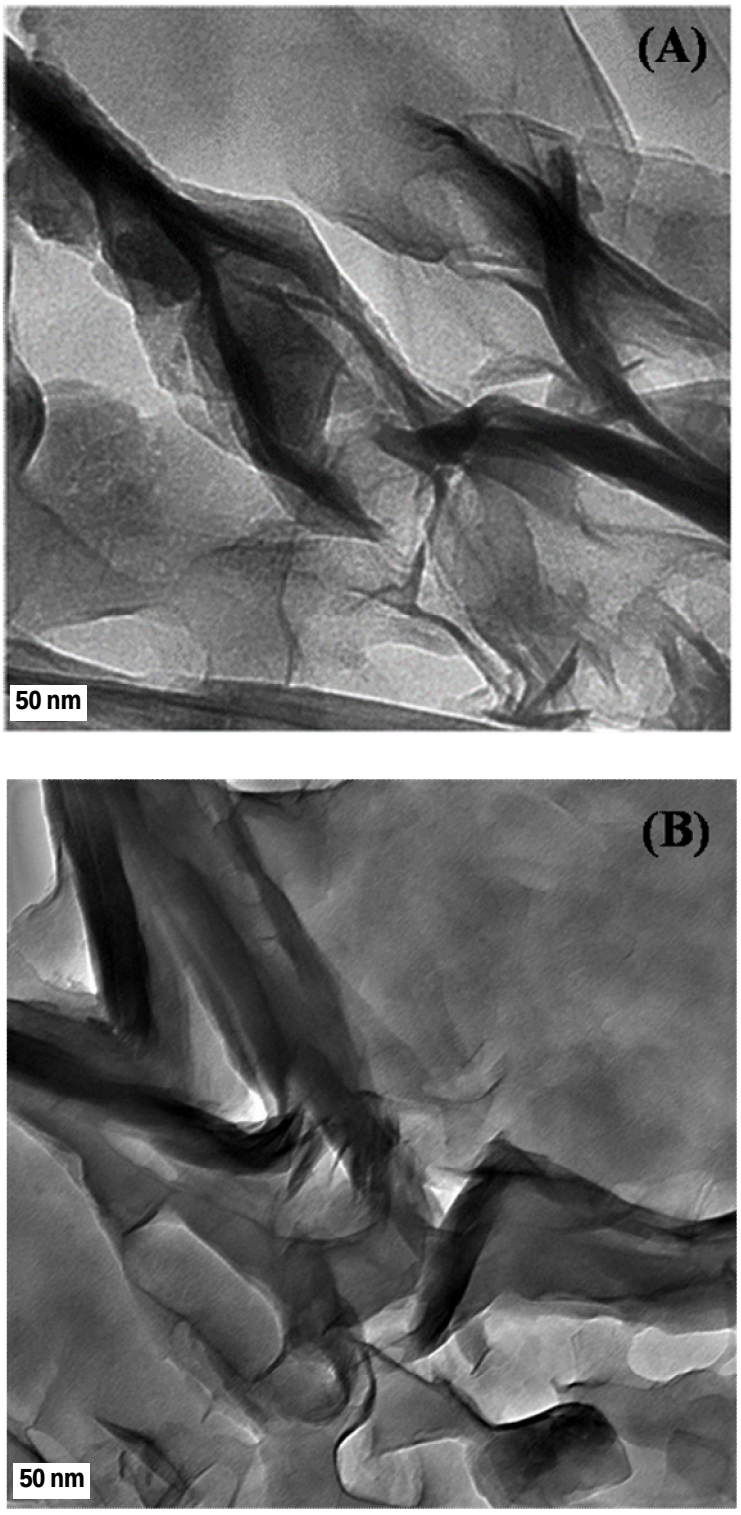

Figure V-3. TEM of (A) sPS 5 wt.% Na^{+}MMT mixtures and (B) SsPS 5 wt.% Na^{+}MMT mixtures. The scale bar in each image is 50 nm.

The morphology of sPS 5 wt.% OMMT as shown in Figure V-4A contains large agglomerates of OMMT platelets on the micron scale. However, there appears to be evidence of intercalated structures within the sPS 5 wt.% OMMT hybrid and relatively more platelet stacks consisting of smaller number of platelets and even single platelet features when compared to sPS 5 wt.% Na^+MMT in Figure V-4A. Coupling TEM micrographs of Figures V-3A and V-4A with WAXD data suggests that sPS hybrids containing 5 wt.% Na^+MMT and OMMT consist of primarily micro-composite features with a relatively small portion of platelets that appear to be dispersed into platelet stacks present on the nanoscale.

However, in contrast, Figure V-4B of SsPS 5 wt.% OMMT reveals a drastically different platelet morphology compared to the SsPS 5 wt.% Na^+MMT hybrid. Figure V-4B shows the presence of OMMT platelet stacks consisting of tens of platelets and single platelet features as well. Furthermore, there are no micron-scale tactoid features present in the SsPS 5 wt.% OMMT nanocomposite. Therefore, based upon TEM and WAXD results, it appears that SsPS-OMMT platelet interactions are sufficient to result in a predominately exfoliated, relatively well-dispersed ionomer-clay nanocomposite.

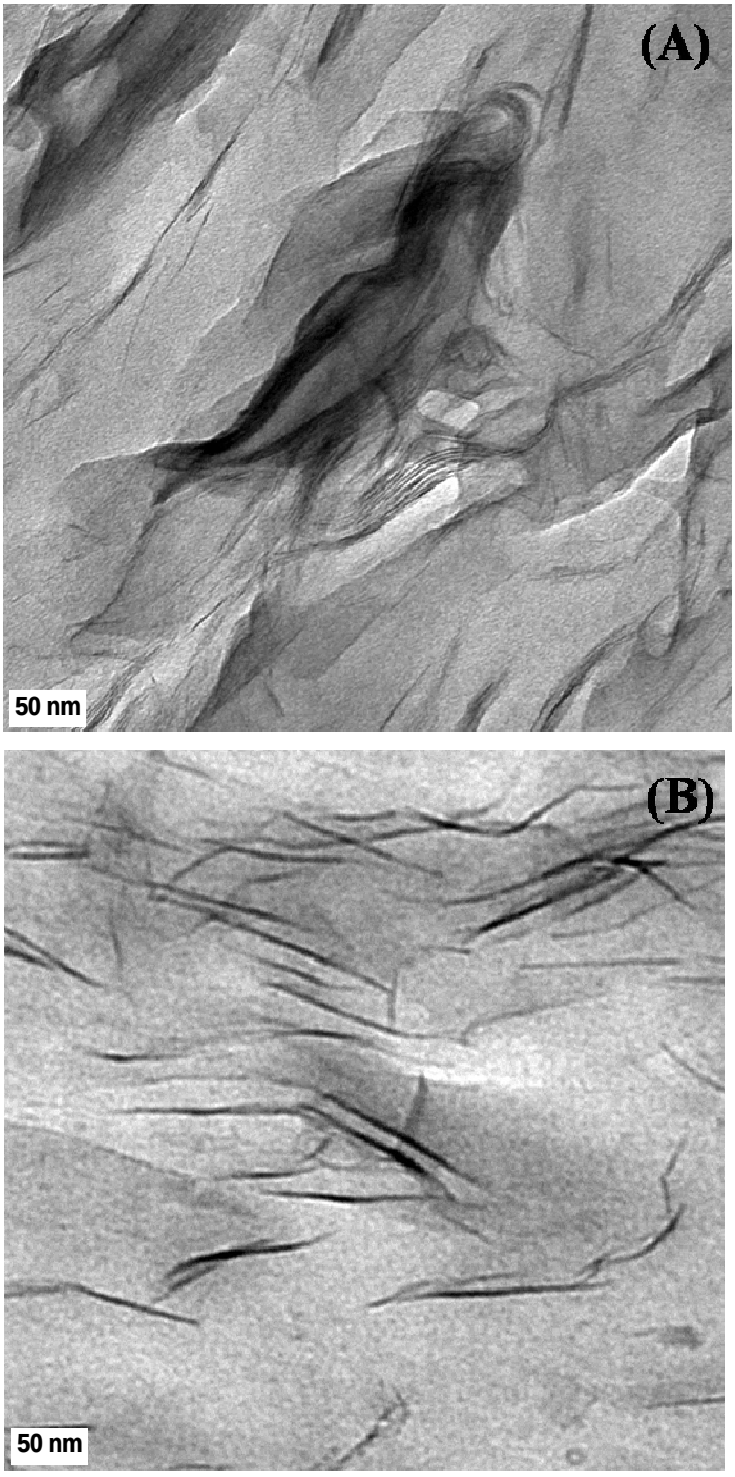

Figure V-4. TEM of (A) sPS 5 wt.% OMMT mixtures and (B) SsPS 5 wt.% OMMT mixtures. The scale bar in each image is 50 nm.

Isothermal Crystallization of sPS/SsPS Clay Nanocomposites

The effect of clay on the crystallization behavior and crystallization kinetics of sPS and SsPS hybrids was monitored via isothermal crystallization experiments using DSC. The development of crystallinity within each polymer clay system was monitored by applying the following relationship:

$$X_c(t) = \frac{\int_0^t \frac{dH}{dT}\,dt}{\int_0^\infty \frac{dH}{dT}\,dt} \qquad (1)$$

The expression given in equation 1 represents the fractional crystallinity of the bulk polymer system, $X_c(t)$, and is equal to the heat evolved during isothermal crystallization at a specific time t divided by the total heat generated during the entire crystallization process. In addition, the crystallization behavior of the different nanocomposite systems was characterized by $t_{½}$ values. The $t_{½}$ values were determined from isothermal crystallization experiments and were used as a measure of the rate of bulk isothermal crystallization.

Figures V-5A and V-5B contain plots of the fraction of material crystallized $X_c(t)$ versus ln time at 240 °C for sPS Na^+MMT and SsPS Na^+MMT mixtures, respectively. As the concentration of Na^+MMT increases from 0 to 5 wt.% Na^+MMT within the sPS matrix as shown in Figure V-5A, each isothermal crystallization curve is shifted to longer times. The increase in the crystallization time with increasing clay content suggests that sPS chain mobility is retarded by the presence of the clay and chains do not have sufficient molecular motion to effectively pack into crystalline structures. In studies of sPS containing organically-modified clay, Wu and coworkers [38] determined that low clay concentrations (less than 1 wt.%) induce heterogeneous nucleation within the sPS matrix and therefore may be considered to be a nucleating agent as the

number of nuclei increases within the clay containing matrix when compared to the pure sPS homopolymer. However, upon addition of increasing concentrations of clay such as 5 wt.% of organically-modified clay Wu and coworkers concluded that higher clay concentrations reduce the mobility of sPS polymer chains during crystallization processes despite the occurrence of more heterogeneous nucleation. The results obtained within our study of sPS nanocomposites is similar to that observed by Wu and coworkers and we also attribute the slight decrease in the rate of crystallization of sPS nanocomposites to a reduction in polymer mobility in the presence of the clay. The reduction in polymer chain mobility may also be due to increased melt viscosity caused by agglomerated micron-sized Na^+MMT platelets. It can also be noted within Figure V-5A that the sigmoidal-shape of each plot does not change upon incorporation of Na^+MMT into the sPS matrix. Moreover, the curves in Figure V-5A appear to be superposable. Similar curve shape and superposability suggest that Na^+MMT clay does not significantly alter the nucleation and growth mechanism within sPS. However, it does appear that the presence of the Na^+MMT retards the rate of bulk isothermal crystallization as observed by the successive shifting of isothermal curves to the longer crystallization times with increasing Na^+MMT concentration.

The chemical modification of sPS through a post-sulfonation reaction has been shown to drastically affect the crystallization behavior of the sPS homopolymer [22-25]. These studies provide a baseline of comparison to aid in monitoring the effect of montmorillonite clay on the crystallization behavior of SsPS ionomers. Govindaiah and coworkers [26] reported qualitative observations on the crystallization behavior of SsPS containing organically-modified clay using the peak crystallization temperature on cooling from the melt using nonisothermal crystallization conditions. Despite these initial qualitative observations made regarding the effect of clay on the crystallization behavior of SsPS, a more detailed analysis of the effect of both pristine Na^+MMT

and OMMT on crystallization behavior of SsPS is necessary to gain insight into changes in crystallization processes that occur upon incorporation of the inorganic clay material into the ionomer matrix.

Figure V-5B provides a plot of $X_c(t)$ versus ln time at 240 °C for SsPS containing 0, 1, 3, and 5 wt.% Na^+MMT. Upon incorporation of 1 and 3 wt.% Na^+MMT, there is a shift of the curves successively to shorter crystallization times. The isothermal crystallization curve corresponding to SsPS 5 wt.% Na^+MMT appears to be superposed onto the plot of SsPS containing 3 wt.% Na^+MMT below approximately $X_c(t) = 0.60$. Above $X_c(t) = 0.60$, the SsPS Na^+MMT hybrid begins to crystallize at a slower rate. The change in the behavior of the SsPS 5 wt.% Na^+MMT mixture above $X_c(t) = 0.60$ suggests changes in crystallization processes may be different from those that occur in the SsPS 3 wt.% Na^+MMT mixture. It is possible that as crystallization proceeds in the SsPS 5 wt.% Na^+MMT mixture that the rate of transport of crystallizable chain segments across the melt/crystal interface is hindered due to rejection of the montmorillonite particles from the melt/crystal interface as crystallization proceeds [63]. The isothermal crystallization behavior of SsPS 5 wt.% Na^+MMT mixture above $X_c(t) = 0.60$ may also suggest that a maximum clay loading limit exists, where ionomer-platelet interactions are maximized and further addition of Na^+MMT platelets may begin to inhibit molecular mobility of crystallizable chain segments.

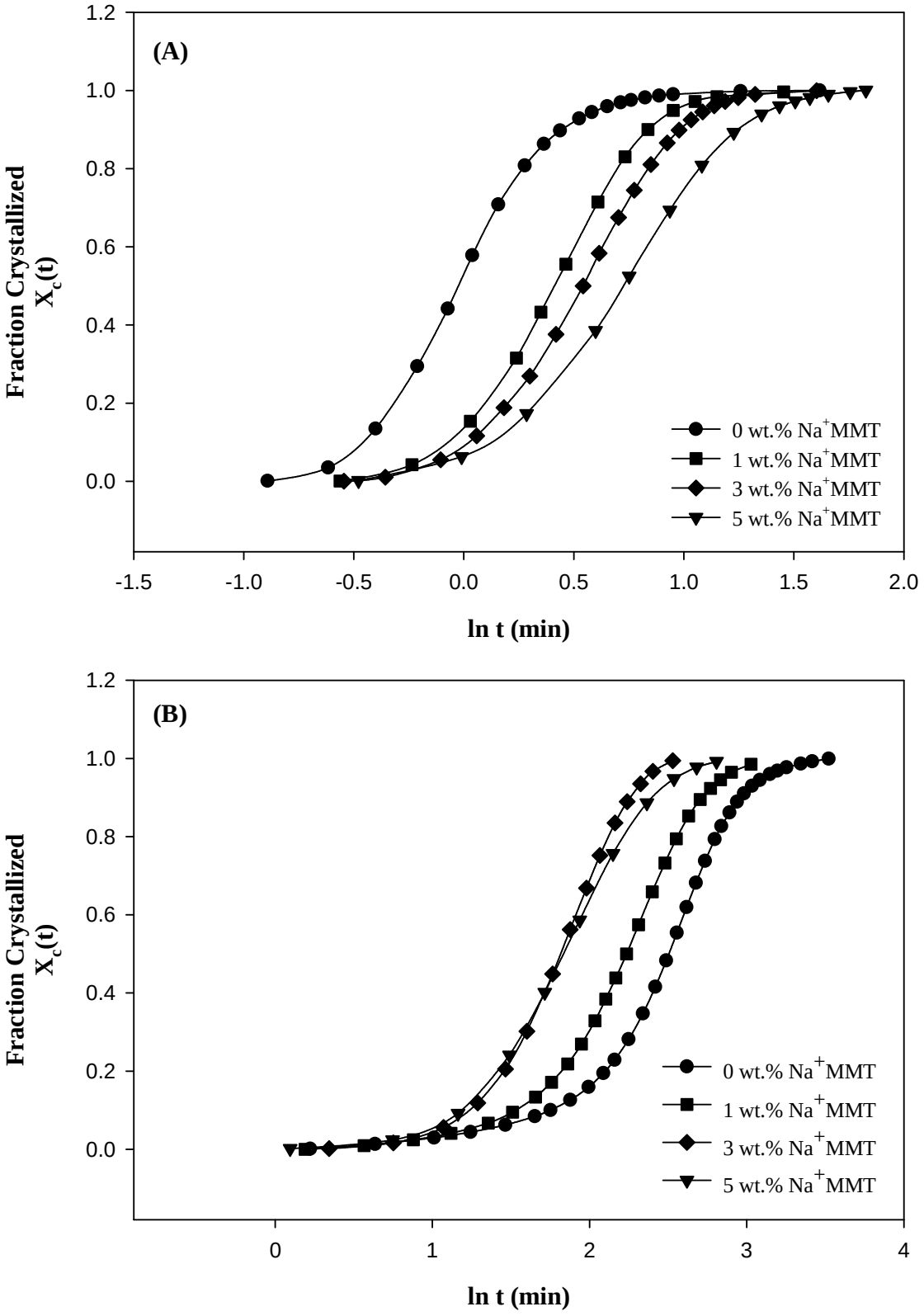

Figure V-5. $X_c(t)$ versus ln time at 240 °C for (A) sPS Na^+MMT mixtures and (B) SsPS Na^+MMT mixtures.

Figure V-6A provides $X_c(t)$ versus ln time at 240 °C for sPS OMMT mixtures. The same general trend of an increase in the time required for crystallization with increasing clay content is observed with sPS OMMT as with sPS Na^+MMT (Figure V-5A). Again, it is highly likely that the increase in the time required for crystallization using the organically modified montmorillonite in the sPS matrix may be attributed to the rejection or occlusion of the OMMT particles from the crystalline domains as crystallization proceeds [63]. As the OMMT content increases within the sPS matrix, the OMMT particle size increases and the ability to act as effective nucleating agent is diminished. The larger sized OMMT particles must then be rejected from the crystal growth front as crystallization proceeds. The rejection of the OMMT particles during crystallization thereby decreases the overall crystallization rate of sPS.

The effect of incorporating organically-modified MMT on the crystallization behavior of SsPS is shown in Figure V-6B. In profound contrast to previous samples, there is a drastic reduction in the time required for the material to crystallize with increasing concentrations of OMMT. Isothermal crystallization curves corresponding to pristine SsPS and SsPS 1 wt.% OMMT appear to be superposable. The similarity in the shape of the isothermal curves for SsPS and SsPS 1 wt.% OMMT suggests that the nucleation and growth mechanism that occur in these materials may be quite similar. However, there is a significant change in the shape of the curves corresponding to SsPS 3 wt.% OMMT and SsPS 5 wt.% OMMT as shown in Figure V-6B. The change in the shape of the curve for the SsPS 3 wt.% OMMT mixture is particularly noticeable when comparing the slope of the linear region of SsPS 3 wt.% OMMT to the isothermal curves of neat SsPS and SsPS 1 wt.% OMMT mixtures. The change in the shapes of the curves suggests

a change in the nucleation and growth of crystalline domains at high concentrations of organically-modified clay within the SsPS matrix.

An additional change in the isothermal crystallization behavior of SsPS containing organically-modified clay is observed upon inspection of the region of the curve associated with the induction period. Figure V-6B containing the isothermal crystallization curve for SsPS 5 wt.% OMMT shows a very small, truncated induction period upon comparison to neat SsPS mixtures that contain lower concentrations of OMMT clay. The shorter induction period for SsPS 5 wt.% OMMT compared to the other materials may occur due to a possible nucleating effect of the well-dispersed organically-modified clay platelets (Figure V-6B) resulting in more rapid crystallization of the SsPS ionomer in the presence of the clay upon cooling from the melt. Further evidence that OMMT platelets may impart a possible nucleating effect during isothermal crystallization of the SsPS mixtures can be seen in the shift of the SsPS isothermal curves to shorter crystallization times with increasing concentrations of organically-modified clay. Coupling this observation with morphological observations from WAXD and TEM analyses, we find that rate of crystallization increases with the degree of exfoliation of clay platelets within the SsPS matrix.

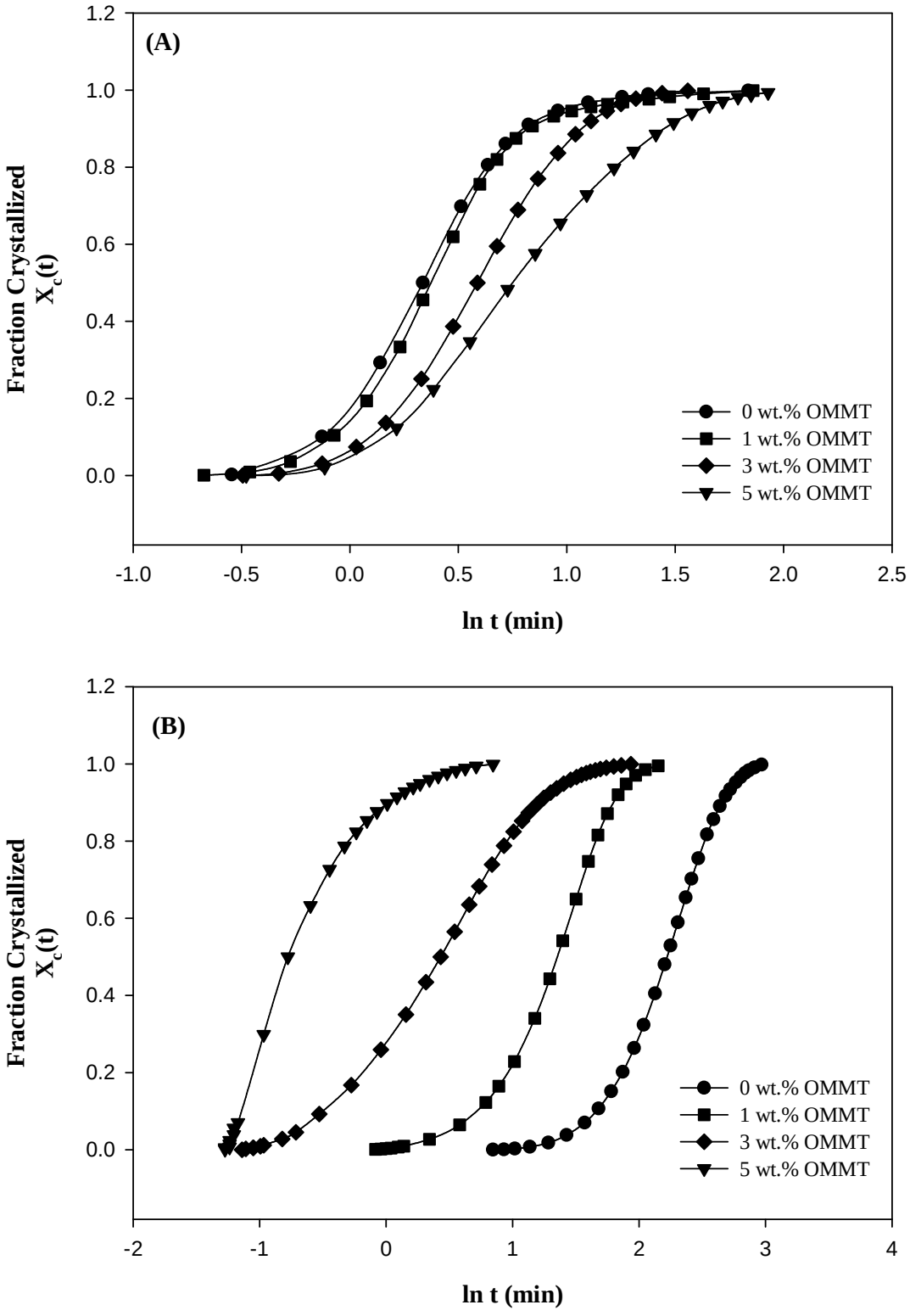

Figure V-6. $X_c(t)$ versus ln time at 240 °C for (A) sPS OMMT mixtures and (B) SsPS OMMT mixtures.

A kinetic evaluation of the crystallization behavior of sPS and SsPS mixtures was completed using the Avrami approach [64-66]. This approach is used extensively in the study of the bulk crystallization of polymers as it provides insight into the nucleation and growth process within the bulk polymer matrix [67-75]. Avrami analysis is utilized extensively to determine the crystallization kinetics of pure polymers and polymer nanocomposites as well. The study of the isothermal crystallization behavior of many differrent polymer nanocomposites has been carried out using this method for several different systems such poly(ε-caprolactone) [76], poly(ethylene terepthalate) [7-8], polyethylene [77-78], poly(trimethylene terepthalate) [79], nylon [80], and poly(3-hydroxybutyrate-co-3-hydroxyvalerate) [81]. The Avrami rate constant K provides a measure of the rate of crystallization for the sPS and SsPS mixtures and is coupled with the crystallization half-times to monitor the rate of crystallization of the pure and clay containing materials The Avrami equation is given in equation 3 and is used to determine the extent of fractional crystallinity, $X_c(t)$ at time t.

$$X_c(t) = 1 - \exp(-Kt)^n \qquad (3)$$

The Avrami rate constant is represented by K and n is the Avrami exponent. The Avrami exponent, n, provides insight into the type of nucleation and growth that occurs within the system. The kinetic analysis of the isothermal crystallization behavior of the polymer clay hybrids is done by taking the double logarithm of the Avrami equation yielding the equation in the following form:

$$\ln[-\ln(1 - X_c(t))] = n \ln t + \ln K \qquad (4)$$

Plots of $\ln[(-\ln(1- X_c(t))]$ versus ln t provide n and K from the slope and intercept, respectively. Linear regression analysis was used to obtain values of n and K for sPS Na^+MMT mixtures as shown in Figure V-7. Table V-1 summarizes the kinetic parameters obtained for isothermal

crystallization processes at 240 °C. For sPS Na^+MMT mixtures, the Avrami exponent n decreases with increasing Na^+MMT concentration. The Avrami exponent remains between values of n = 3.0 - 2.67.

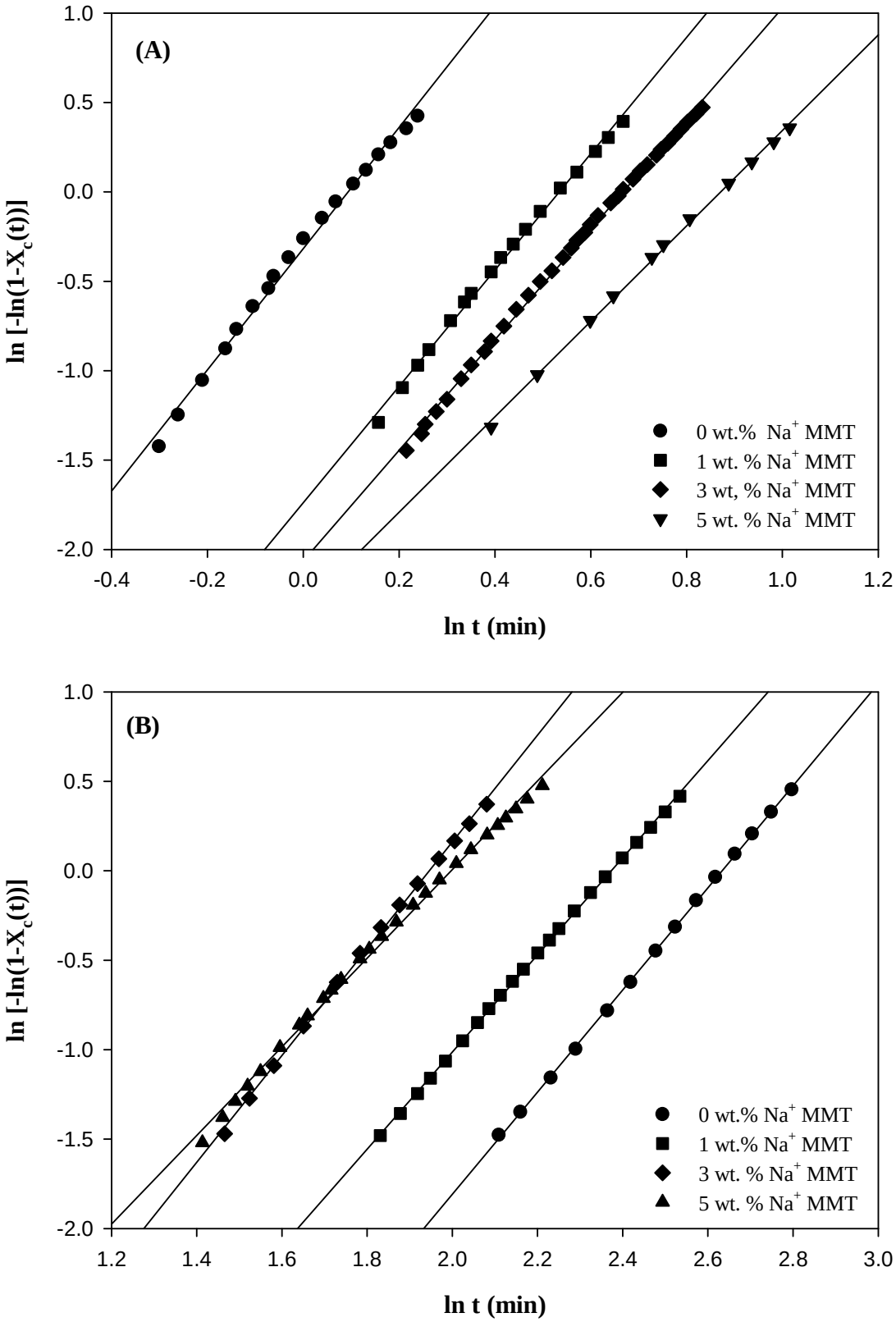

Figure V-7. ln [-ln (1-X_c(t))] versus ln t at 240 °C for (A) sPS Na^+MMT mixtures and (B) SsPS Na^+MMT mixtures.

Since it is most likely that crystalline domains in these materials originate from a heterogeneous nucleation process, Avrami exponents within this range suggest a three dimensional spherical growth process during isothermal crystallization of the sPS Na^+MMT mixtures. A decrease in the n-values of sPS Na^+MMT mixtures with increasing Na^+MMT concentration suggests the growth of the crystalline structures may include geometries that deviate from a three dimensional spherical growth to include more structures that are two dimensional as well. The Avrami rate constant K provided in Table V-1 and $t_{½}$ values as shown in Figure V-9 increase with increasing Na^+MMT concentration in sPS clay mixtures. The decrease in the K and increase in the $t_{½}$ values correspond to slower crystallization rates upon incorporation of increasing amounts of clay into the sPS matrix. This suggests that the poorly dispersed Na^+MMT platelets throughout the sPS matrix are not effective as a nucleating agents, and may inhibit crystal growth due to an increase in melt viscosity [82].

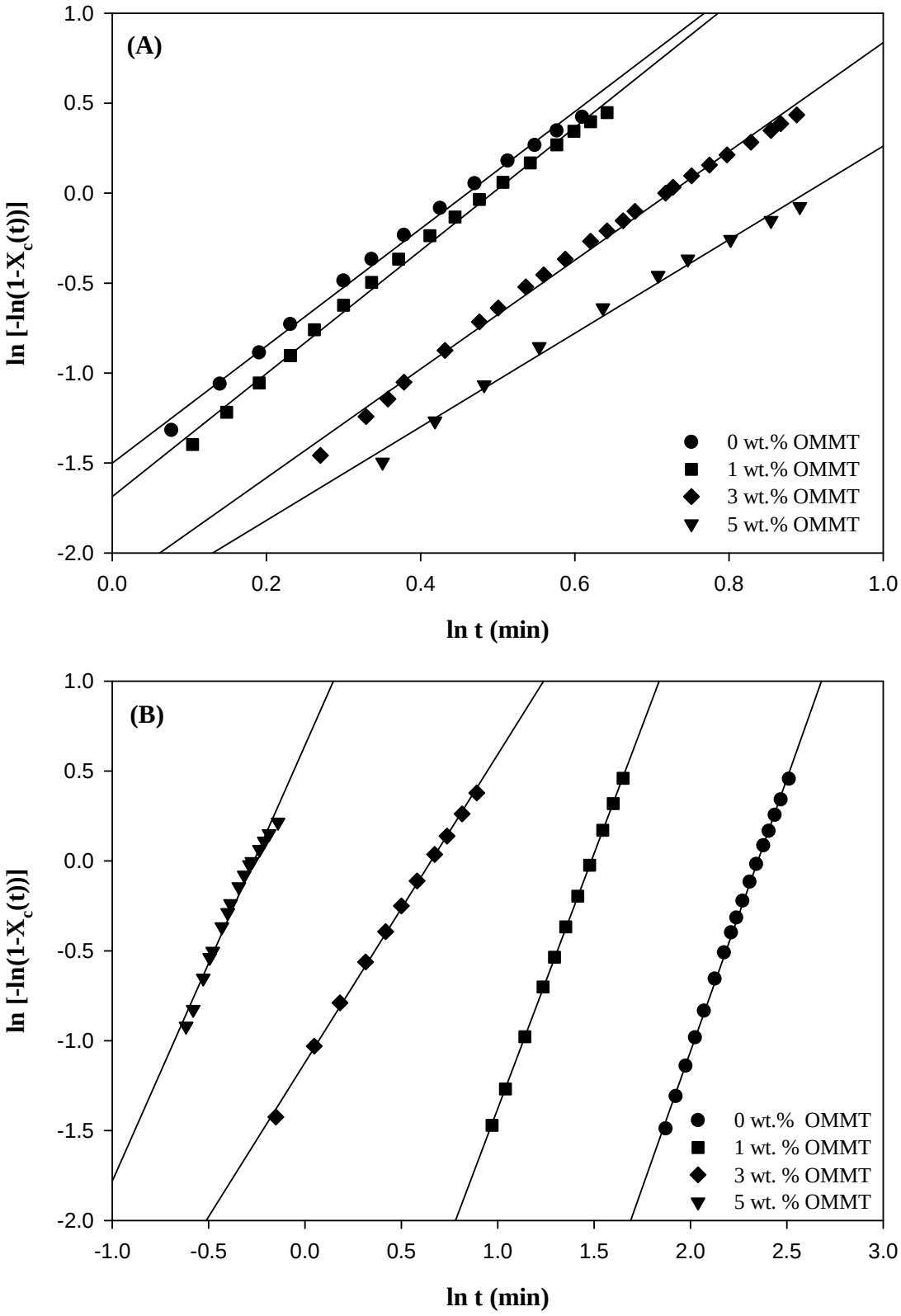

Figure V-8. ln [-ln (1-X_c(t))] versus ln t at 240 °C for (A) sPS OMMT mixtures and (B) SsPS OMMT mixtures.

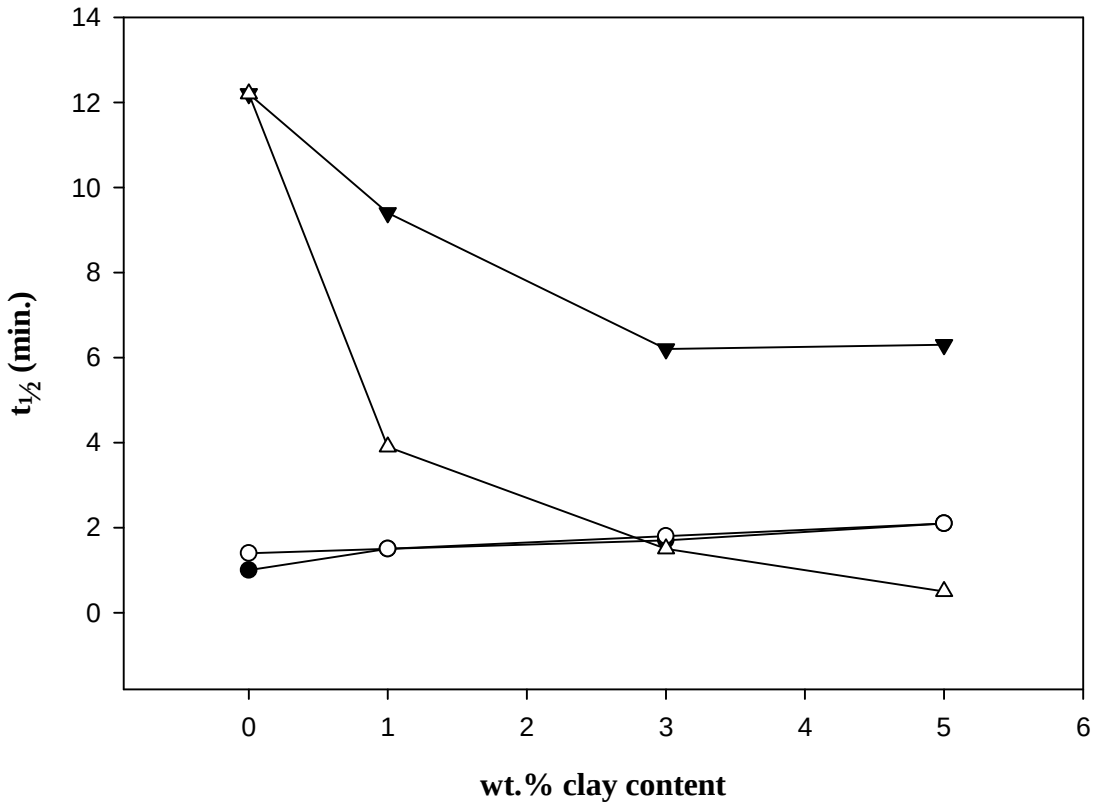

Figure V-9. Crystallization half-time versus wt.% clay content. Closed circles - sPS Na^+MMT, open circles - sPS OMMT, closed triangles – SsPS Na^+MMT, and open triangles – SsPS OMMT.

Table V-1. Avrami parameters for sPS and SsPS Clay Nanocomposites at 240 °C.

Polymer Clay System	n	K (min^{-1})
sPS wt. % Na^+MMT		
0	3.39	7.3×10^{-1}
1	3.25	1.8×10^{-1}
3	3.09	1.3×10^{-1}
5	2.67	9.7×10^{-2}
SsPS wt. % Na^+MMT		
0	3.49	5.4×10^{-4}
1	2.71	1.6×10^{-3}
3	2.96	3.0×10^{-3}
5	3.62	7.1×10^{-3}
sPS wt. % OMMT		
0	3.26	2.2×10^{-1}
1	3.42	1.8×10^{-1}
3	3.02	1.1×10^{-1}
5	2.60	9.7×10^{-2}
SsPS wt. % OMMT		
0	3.03	8.1×10^{-4}
1	2.84	1.5×10^{-2}
3	1.71	3.3×10^{-1}
5	2.42	3.8×10^{-1}

For the SsPS Na^+MMT mixtures (Table V-1), the Avrami exponent n decreases from a value of n = 3.49 for neat SsPS to 2.96 for SsPS containing 3 wt.% Na^+MMT, indicating three dimensional spherical growth during isothermal crystallization at 240 °C. Upon incorporation of 5 wt.% Na^+MMT into the SsPS matrix the n-values increases to 3.62, which slightly is above the n-value for neat SsPS, but still consistent with three-dimensional growth geometry. Therefore, the presence of Na^+MMT does not drastically alter the dimensionality of the crystal growth within the SsPS ionomer. The $t_{½}$ values of SsPS Na^+MMT mixtures as shown in Figure V-7 decrease with increasing Na^+MMT concentration, and the Avrami rate constant K increases

(Table V-1) suggesting that SsPS crystallizable chain segments gain additional mobility as more clay is added to the system, and/or the clay increases nucleation.

The effect of incorporating organically-modified montmorillonite clay on the crystallization behavior of the sPS homopolymer matrix was evaluated using the Avrami approach as well. Table V-1 contains the Avrami parameters for sPS OMMT mixtures, and the value of n decreases from 3.26 to 2.60 as the concentration of OMMT is increased within the sPS matrix. The same general trend of decreasing values of n with increasing clay content is observed in sPS Na^+MMT mixtures as well (Figure V-8A and Table V-1). The changes in the Avrami exponent n to lower values approaching n = 2 in sPS OMMT mixtures is again ascribed to a change from a three dimensional spherical growth process to a crystallization growth process that may occur in a more two-dimensional fashion [83]. Table V-1 also shows the Avrami rate constant K decreases with increasing clay concentration, reflecting slower crystallization.

For SsPS containing organically-modified montmorillonite (Table V-1), there is again a decrease in the Avrami exponents with incorporation of organically-modified clay into the pristine ionomer suggesting a decrease in the dimensionality of the growing crystalline domains. The Avrami rate constant K increases (Table V-1) and $t_{½}$ values for SsPS are reduced upon successive increases in OMMT concentration as shown in Figure V-7, consistent with a profound increase in crystallization rate. It is also important to note that the $t_{½}$ value for SsPS 5 wt.% OMMT is 0.5 min and is now on the same time scale of crystallization as pristine sPS with a $t_{½}$ value of 1.0 min.

The reduction in the crystallization half-time of SsPS clay mixtures is opposite to the behavior displayed by sPS clay mixtures which exhibit increased crystallization half-times upon incorporating clay into sPS homopolymer matrix. The more pronounced changes in the

crystallization behavior of the SsPS ionomer in the presence of the clay are due to chemical modification of the hydrophobic sPS homopolymer. The chemical interactions that occur between the sulfonate groups of the ionomer and the pristine or the organically-modified are significantly improved when compared to the non-ionized sPS homopolymer and the clay. The resulting chemical interactions between the SsPS sulfonate groups and the clay result in the observed changes in the nucleation and crystallization behavior of the SsPS nanocomposites compared to the sPS clay composites. The chemical interactions between the SsPS ionomer sulfonate groups and the clay result in the disruption of the physical crosslinks of the ionic aggregates leading to higher nucleation and more rapid crystallization.

Based upon both the morphological analyses provided from WAXD and TEM in addition to the crystallization studies, we attribute that the enhanced crystallization behavior of SsPS nanocomposites to a number of complex interrelated phenomena including disruption of the ionomer electrostatic network, a plasticization effect by the presence of the clay surfactant in the SsPS OMMT nanocomposites, and a nucleation effect due to exfoliated clay platelets in SsPS OMMT. The mechanistic origins of increased crystallization rates in SsPS ionomer clay nanocomposites is likely the result of multiple phenomena that encompass highly-specific mechanisms that are unique to ionomers and more general behaviors that are observed in many polymer composite systems.

Ionomer properties that may be significantly altered in the presence of aluminosilicate platelets include the stability of ionic aggregates that are formed through electrostatic interactions between dipoles consisting of negatively charged sulfonate groups and positively charged neutralizing cations. A disruption of the electrostatic interactions in these ionomers leads to a destabilization of the electrostatic physically-crosslinked network thereby greatly increasing

the mobility of crystallizable polymer chains that were previously constrained. More specifically, the interaction of ionomer chains with the layered silicate surface may occur in primarily three ways: interaction of the negatively charged sulfonate groups with positively charged edges of clay platelets, cation exchange of ionomer Cs^+ counterions with Na^+ ions of pristine Na^+MMT and quaternary amine counterions of the organically-modified polymer, and possible hydrophobic interactions of ionomer chains with the long chain alkyl moieties provided by the organic modification in the SsPS OMMT nanocomposite through a preferential plasticization mechanism [25].

Chisholm [13] and Barber [14] proposed a two-stage model based on polyester ionomer clay nanocomposites that attributed the formation of highly exfoliated morphologies to the interaction of the negatively charged sulfonate groups with the positively charged edges of the aluminosilicate platelet. This initial site of ionomer attachment to the clay platelet edge thereby facilitates the movement of mobile polymer chains into the intergallery spacing. Although slightly slower crystallization rates were observed for PET ionomer clay containing nanocomposites, this proposed mechanism of ionomer-clay interaction may still provide a plausible mechanism for potential interactions between the SsPS ionomer and montmorillonite clay.

Govindaiah and coworkers [26] suggested, in their study of SsPS nanocomposites, that an increase in the surface energy of sPS through the incorporation of polar entities allows increased interactions between the polymer matrix and the clay surface. However, crystallization data obtained within this study suggests that changes in the surface energy of the polymer alone may not be the sole mechanism by which the crystallization behavior of SsPS is altered. The possibility of a plasticization effect contributed by the clay surfactant must also be considered.

Orler and coworkers [25] studied the incorporation of ionic surfactants and nonpolar plasticizers into lightly sulfonated sPS. A slight increase in the crystallization rate of SsPS was observed when nonpolar plasticizers were added to lightly sulfonated sPS. However, a dramatic increase in the rate of crystallization of SsPS occurred with the incorporation of a polar surfactant into the ionomer matrix. The increase in the rate of crystallization using the polar surfactant was attributed to preferential plasticization of the surfactant into the ionomer aggregate-rich cluster phases and the matrix phase as well [84]. It is therefore possible that the hydrocarbon tail of the OMMT surfactant may effectively plasticize the sPS rich phase thus providing additional molecular mobility to sPS chains within the matrix phase. However, the large reduction in rate of crystallization in SsPS OMMT nanocomposites may be more directly related to potential interaction with the quaternary amine headgroup component of the clay surfactant and the ionomer styrenesulfonate groups. As a control, we have prepared SsPS ionomer mixtures containing an equivalent amount of organic modification agent (DMHTB) that is present in samples containing 1, 3, or 5 wt.% of organically-modified montmorillonite clay. At maximum loading (equivalent to 5 wt.% clay) the crystallization half-time of the SsPS ionomer containing only the DMHTB surfactant decreases by a factor of 2 compared to the pure SsPS ionomer. This reduction in the crystallization half-time is attributed to the preferential plasticization by the clay surfactant resulting in a destabilization of the electrostatic network, and thus greater mobility crystallizable SsPS segments. In contrast, the SsPS ionomer containing the clay that has been organically-modified with the DMHTB surfactant exhibits much smaller $t_{½}$ values that decrease by a factor of 25 relative to the pure SsPS ionomer. Thus, given the relatively minor effect of the free surfactant, these data suggest that the well-exfoliated clay platelets present within the SsPS

ionomer matrix act as nucleation sites and thereby increase the overall rate of bulk crystallization.

Polarized light microscopy was used to investigate the effect of the pristine and organically-modified clay on the spherulitic growth rates of the sPS homopolymer and the SsPS ionomer. Figure 10A shows the plot of spherulite radius versus time for the pure sPS homopolymer and the homopolymer containing 3 wt.% Na^+MMT and OMMT under isothermal crystallization conditions at 240 °C. From this plot, it is clear that the spherulitic growth rate of the sPS homopolymer does not change upon incorporation of clay. The spherulitic growth rate for pure sPS, sPS 3 wt.% Na^+MMT , and sPS 3 wt.% OMMT is 31.5, 31.6, an d 31.7 μm/min, respectively as listed in Table V-2. However, it can be seen from the plot of spherulite radius versus time in Figure V-10B of the pure SsPS ionomer and the SsPS ionomer containing 3 wt.% Na^+MMT that there is a large increase the in spherulitic growth rate of SsPS upon incorporation of 3 wt.% Na^+MMT. The spherulitic growth rate of the pure SsPS ionomer increases from 1.6 μm/min to 10.3 μm/min with the addition of 3 wt.% Na^+MMT. Upon incorporation of 3 wt.% of organically-modified clay, the SsPS spherulitic growth rate is so rapid under isothermal crystallization at 240 °C that a growth rate could not be measured. Such a dramatic increase in the spherulitic growth of SsPS in the presence of both pristine and organically-modified clay strongly suggests that the presence of well-dispersed clay platelets leads to a destabilization of the electrostatic network allowing more rapid nucleation and growth of polymer chains to occur.

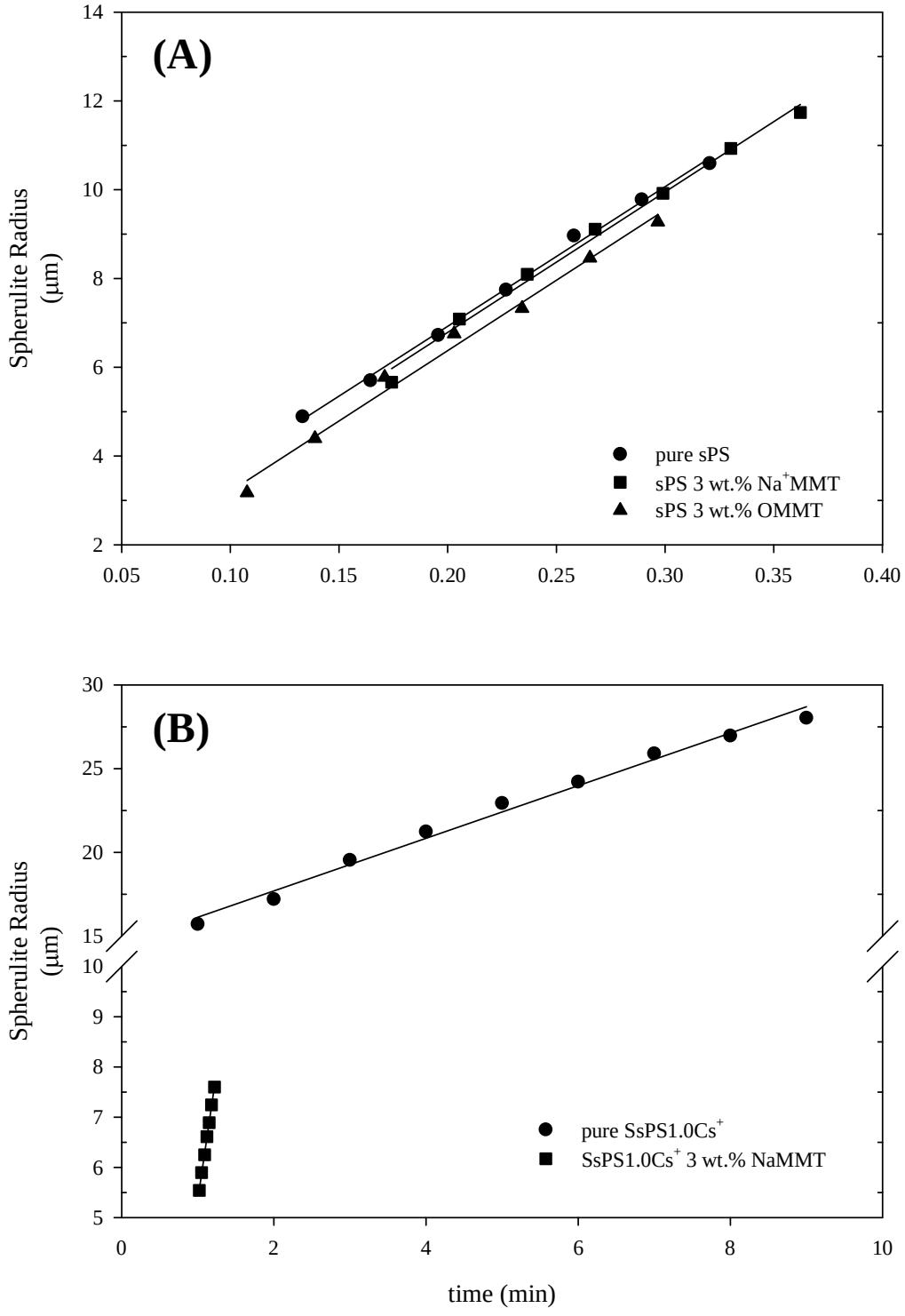

Figure V-10. Spherulite radius versus time of (A) pure sPS and sPS containing 3 wt. % of Na^+MMT and OMMT clay and (B) of pure SsPS and SsPS containing 3 wt.% Na^+MMT.

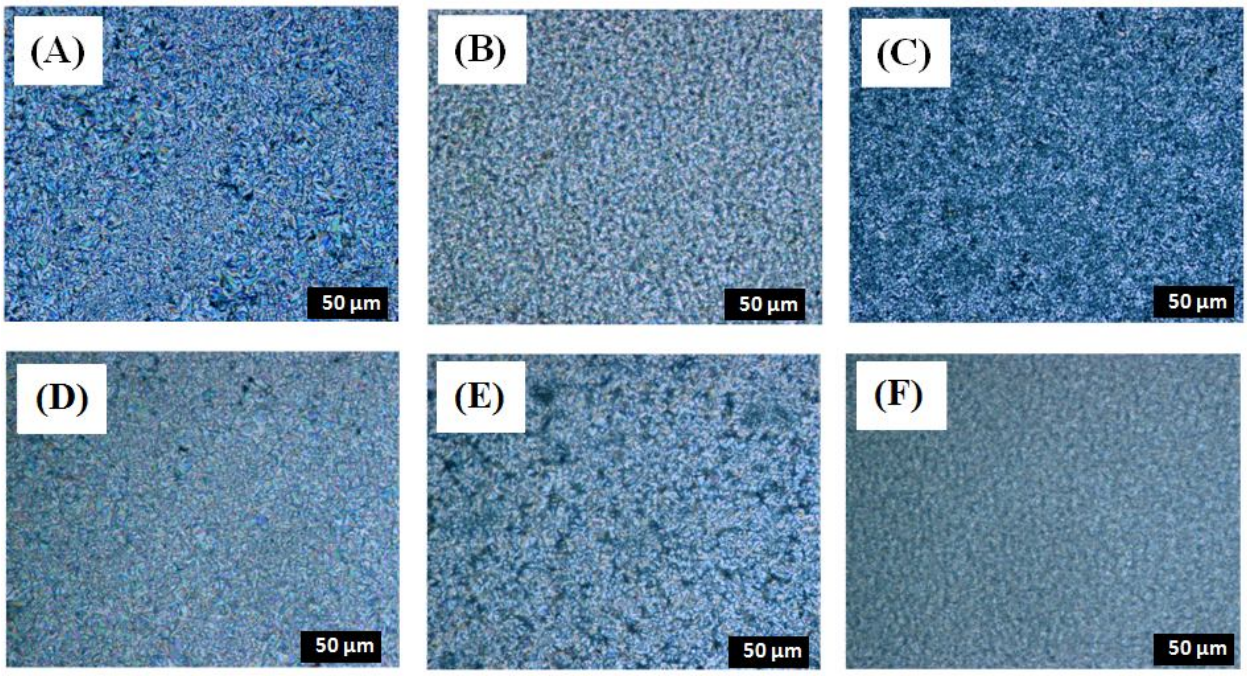

Figure V-11. PLM micrographs of volume filled polymer mixtures after isothermermal crystallization of (A) pure sPS (B) sPS 3 wt. % Na^+MMT (C) sPS 3 wt. %OMMT clay (D) pure SsPS (E) SsPS 3 wt.% Na^+MMT and (F) SsPS 3 wt.% OMMT.

The PLM micrographs shown in Figure V-11 reveal the presence of small spherulites for both the unfilled matrices and the clay containing matrices as well. However, a change in the spherulitic texture is readily observable upon the addition of the pristine and organically-modified clays into the non-ionized and SsPS ionomer matrices. The spherulitic texture becomes finer (smaller spherulites) with the addition of the clay. The shift to smaller spherulite sizes suggests that the nucleation density increases upon incorporation of the clay in both the polymer and ionomer matrices.

Polarized light microscopy provides a very local view of the crystalline structure for a small portion of the sample and may not necessarily be representative of the entire sample. SALLS allows a more global assessment of the crystalline structure to be obtained and an average spherulite size to be determined. Therefore, small-angle laser light scattering was used in order

to determine the effect of incorporation of clay on the spherulite size [85-88] and nucleation density [89-90] of the sPS homopolymer and the SsPS ionomer. Figure V-12A through Figure V-12C shows the SALLS patterns of the sPS homopolymer, sPS 3 wt.% Na^+MMT, and sPS 3 wt.% OMMT, respectively. The average spherulite size was determined using the following relationship [35]:

$$2\pi \frac{D}{\lambda} \sin\frac{\theta}{2} = 4.1 \qquad (5)$$

The spherulite diameter for pure sPS and the sPS mixtures containing 3 wt.% Na^+MMT and 3 wt.% OMMT is provided in Table V-2. The pure sPS spherulitic diameter changes from 98.9 μm to 70.7 μm in the presence of 3 wt.% Na^+MMT, and further decreases to 59.2 μm upon incorporation of the 3 wt.% OMMT. The decrease in sPS spherulite diameter indicates that the nucleation density has increased in the presence of the clay.

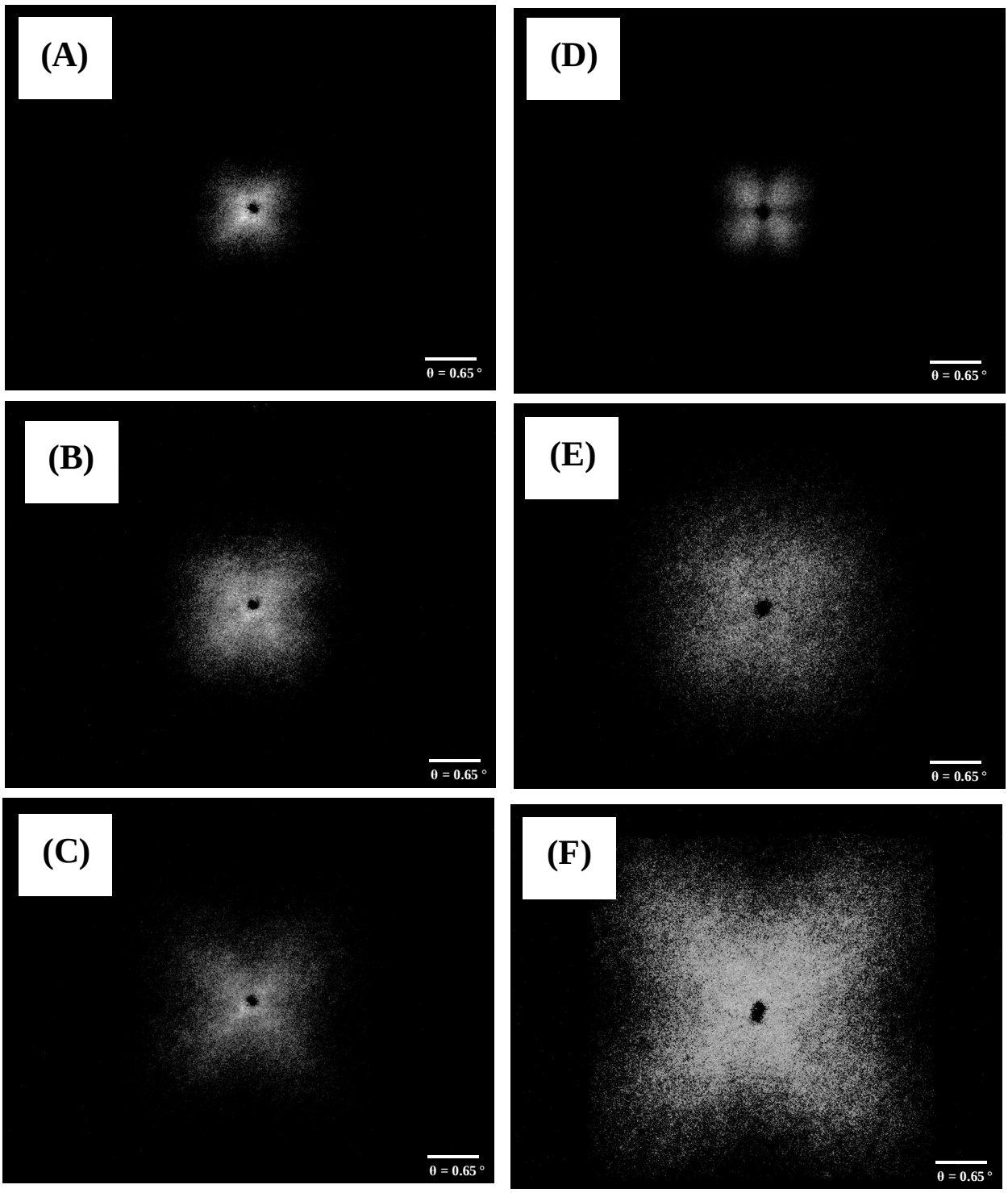

Figure V-12. H_v SALLS patterns of (A) pure sPS (B) sPS 3 wt.% Na^+MMT (C) sPS 3 wt.% OMMT (D) pure SsPS (E) SsPS 3 wt.% Na^+MMT and (F) SsPS 3 wt.% OMMT.

In contrast to the sPS clay-containing mixtures, a further decrease in the spherulite size of the SsPS ionomer is observed upon incorporation of 3 wt.% Na^+MMT or 3 wt.% OMMT. The decrease in the spherulite size upon incorporation the clay is readily observable in Figures V-9D, V-9E, and V-9F. Table V-2 provides the spherulite diameters for SsPS, SsPS 3 wt.% Na^+MMT, and SsPS 3 wt.% OMMT as 71.2, 55.0, and 38.0 μm respectively. The spherulite diameter for SsPS containing 3 wt.% OMMT is nearly 50% smaller than the spherulite diameter of sPS containing 3 wt.% OMMT. Upon comparing the SALLS patterns for the pure sPS and SsPS material it can be seen that the pure matrices reveal well-defined four-leaf clover patterns under Hv mode. However in contrast, the sPS/SsPS nanocomposites reveal diffuse four-leaf-clover patterns compared to the pure matrices. The more diffuse clover-leaf patterns for the clay containing matrices has been attributed to irregular orientation of lamella by the clay particles inside the spherulites. Similar SALLS patterns have been observed for many different polymer-clay nanocomposites systems such as nylon [91], low-density polyethylene [92], polypropylene [93], polylactide [94], PVDF [88], and poly[(butylenes succinate)]-co-adipate] [95]. The significant difference in spherulite diameter between the homopolymer and ionomer matrices may be attributed to the differences in the degree of clay exfoliation. The SsPS ionomer likely contains a more homogenously, well-dispersed, exfoliated clay platelet morphology as supported through WAXD and TEM data than the sPS homopolymer, which act as more effective sites for nucleation.

Table V-2. Spherulite Growth Rate, Spherulite Diameter, and Nucleation Density for sPS and SsPS Clay Mixtures.

Polymer Clay System	**Spherulitic Growth Rate (μm/min)**	**Spherulite Diameter (μm)**	**Nucleation Density (sites/μm^3)**
Pure sPS	32	98.9	1.9×10^{-5}
sPS 3 wt.% Na^+MMT	32	70.7	5.3×10^{-5}
sPS 3 wt.% OMMT	32	59.2	9.1×10^{-5}
Pure SsPS	1.6	71.2	5.2×10^{-5}
SsPS 3 wt.% Na^+MMT	10	55.0	1.1×10^{-4}
SsPS 3 wt.% OMMT	-----	38.0	3.4×10^{-4}

SALLS can also be used to determine the average primary nucleation density, *N*, using equation 6 shown below where D_m is the average diameter of the spherulite prior to impingement.

$$N = \left(\frac{3}{4}\pi\right)\left(\frac{D_m}{2}\right)^{-3} \quad (6)$$

D_m is determined using equation 5. The relationship in equation 6 has been used to estimate the number of nuclei present within a number of polymer clay nanocomposites systems and is thereby a useful method for the determination the effect of clay on the nucleation density of spherulites within sPS and SsPS clay mixtures as well. As shown in Table V-2, the nucleation density for pure sPS, sPS 3 wt. % Na^+MMT, and sPS 3 wt. % OMMT is 1.9×10^{-5}, 5.3×10^{-5}, and 9.1×10^{-5} μm^{-3} respectively. The nucleation density of sPS does exhibit a moderate increase

in the presence of both the pristine and the organically-modified clay. However, there is a more pronounced increase in the nucleation density of the SsPS clay containing mixtures compared to that of the sPS clay containing mixtures. The nucleation densities of SsPS, SsPS 3 wt. % Na^+MMT, and SsPS 3 wt. % OMMT are 5.2 x 10^{-5}, 1.1 x 10^{-4}, and 3.4 x 10^{-4} μm^{-3} respectively as provided in Table V-2. The smaller pure SsPS spherulite size and higher SsPS nucleation density than that of pure sPS may be attributed to the presence of ionic aggregates within SsPS that decrease polymer chain mobility [24]. During the crystallization of SsPS, the dynamic electrostatic networks restricts the mobility of the crystallizable chain segments leading to more effective nucleation, but slower growth. It also important to note that there is an order of magnitude increase the nucleation density of SsPS containing 3 wt.% Na^+MMT and 3 wt. % OMMT while there is only relatively moderate change in the nucleation density of the sPS clay containing mixtures. The drastic increase in the nucleation density of the SsPS clay containing mixtures is attributed to improved exfoliation and dispersion of the clay platelets within the lightly sulfonated sPS ionomer matrix, which disrupts the electrostatic network through enhancement in ionomer/clay interactions. The improved exfoliation and dispersion of clay platelets within the SsPS ionomer compared to that of the pure sPS homopolymer is clearly shown in Figures V-1, V-2, V-3, and V-4.

CONCLUSION

We have utilized the solution intercalation technique in order to prepare polymer clay mixtures using sPS and SsPS. The study shows the significant morphological differences between polymer clay mixtures prepared using the sPS homopolymer and the sulfonated sPS copolymer using WAXD and TEM analyses. The morphology of SsPS OMMT mixtures consist of a well-dispersed, primarily exfoliated morphology exhibiting single platelet features and

platelet aggregates containing stack of tens of platelets. In contrast, sPS OMMT hybrids appeared to consist of a highly mixed morphology dominated by the presence of micron-scale aggregates of clay along with smaller scale morphological features including intercalated platelets and single platelets as well. Both sPS and SsPS MMT hybrids revealed large agglomerates of pristine clay with no evidence of significant degrees of intercalation or exfoliation present. The improvement in the degree of intercalation/exfoliation in both sPS and SsPS OMMT mixtures is attributed to enhanced polymer-clay interactions due to the presence of the clay organic modification agent that imparts hydrophobicity to the inorganic, naturally hydrophilic clay platelets.

Utilization of SsPS as a model ionomer to study the effect of clay on the crystallization behavior semicrystalline ionomers has shown that the rate of crystallization is significantly increased in both tactoid and exfoliated SsPS clay morphologies. The crystallization half-time for the neat SsPS ionomer is 12.2 min, while the $t_{½}$-value decreases to 9.2 and 0.5 min for the SsPS ionomer containing 5 wt.% Na^{+}MMT and OMMT respectively. The crystallization half-time of the SsPS ionomer is reduced to a greater degree in the presence of organically-modified clay versus pristine Na^{+}MMT. It is likely that the more rapid rate of crystallization of SsPS in the presence of OMMT is due to exfoliated, well-dispersed platelets and a complex combination of disruption of the electrostatic network, plasticization effects due the clay surfactant, and nucleation effects due to the presence of the platelets. We have found that unlike sulfonated PBT nanocomposites [13], the rate of crystallization of SsPS nanocomposites may be dependent upon the degree of exfoliation as observed in studies of sulfonated PET nanocomposites [14]. However, the crystallization half-time of SsPS nanocomposites decreases with increasing degree

of exfoliation of clay platelets within the SsPS ionomer matrix rather than increases with increasing degree of exfoliation as observed in sulfonated PBT nanocomposites.

REFERENCES

1. Alexandre M and Dubois P. Materials Science and Engineering: R: Reports 2000;28(1-2):1-63.
2. Sinha Ray S and Okamoto M. Progress in Polymer Science 2003;28(11):1539-1641.
3. Manias E, Touny A, Wu L, Strawhecker K, Lu B, and Chung TC. Chemistry of Materials 2001;13(10):3516-3523.
4. Galgali G, Ramesh C, and Lele A. Macromolecules 2001;34(4):852-858.
5. Wang S, Hu Y, Zhongkai Q, Wang Z, Chen Z, and Fan W. Materials Letters 2003;57(18):2675-2678.
6. Durmus A, Kasgoz A, and Macosko CW. Polymer 2007;48(15):4492-4502.
7. Calcagno CIW, Mariani CM, Teixeira SR, and Mauler RS. Polymer 2007;48(4):966-974.
8. Wan T, Chen L, Chua YC, and Lu X. Journal of Applied Polymer Science 2004;94(4):1381-1388.
9. Acierno D, Scarfato P, Amendola E, Nocerino G, and Costa G. Polymer Engineering and Science 2004;44(6):1012-1018.
10. Li X, Kang T, Cho WJ, Lee JK, and Ha CS. Macromolecular Rapid Communications 2001;22(16):1306-1312.
11. Cho JW and Paul DR. Polymer 2001;42(3):1083-1094.
12. Mathias LJ, Davis RD, and Jarrett WL. Macromolecules 1999;32(23):7958-7960.
13. Chisholm BJ, Moore RB, Barber G, Khouri F, Hempstead A, Larsen M, Olson E, Kelley J, Balch G, and Caraher J. Macromolecules 2002;35(14):5508-5516.
14. Barber GD, Calhoun BH, and Moore RB. Polymer 2005;46(17):6706-6714.

15. Sánchez-Valdes S, López-Quintanilla ML, Ramírez-Vargas E, Medellín-Rodríguez FJ, and Gutierrez-Rodriguez JM. Macromolecular Materials and Engineering 2006;291(2):128-136.
16. Shah RK and Paul DR. Macromolecules 2006;39(9):3327-3336.
17. Bhiwankar NN and Weiss RA. Polymer 2006;47(19):6684-6691.
18. Shah RK and Paul DR. Polymer 2006;47(11):4075-4084.
19. Bhiwankar NN and Weiss RA. Polymer 2005;46(18):7246-7254.
20. Shah RK, Kim DH, and Paul DR. Polymer 2007;48(4):1047-1057.
21. Shah RK, Hunter DL, and Paul DR. Polymer 2005;46(8):2646-2662.
22. Orler EB, Calhoun BH, and Moore RB. Macromolecules 1996;29(18):5965-5971.
23. Orler EB, Yontz DJ, and Moore RB. Macromolecules 1993;26(19):5157-5160.
24. Orler EB and Moore RB. Macromolecules 1994;27(17):4774-4780.
25. Orler EB, Gummaraju RV, Calhoun BH, and Moore RB. Macromolecules 1999;32(4):1180-1188.
26. Govindaiah P, Mallikarjuna SR, and Ramesh C. Macromolecules 2006;39(21):7199-7203.
27. Ghosh AK and Woo EM. Polymer 2004;45(14):4749-4759.
28. Robello DR, Yamaguchi N, Blanton T, and Barnes C. Journal of the American Chemical Society 2004;126(26):8118-8119.
29. Ryu JG, Kim H, and Lee JW. Polymer Engineering and Science 2004;44(7):1198-1204.
30. Sorrentino A, Pantani R, and Brucato V. Polymer Engineering & Science 2006;46(12):1768-1777.

31. Chen K, Wilkie CA, and Vyazovkin S. The Journal of Physical Chemistry B 2007;111(44):12685-12692.

32. Orler EB. The Influence of Electrostatic Interactions on the Crystallization of Sulfonated Syndiotactic Polystyrene Ionomers. Department of Polymer Science, vol. Doctoral. Hattiesburg: University of Southern Mississippi, 1996.

33. LeBaron PC, Wang Z, and Pinnavaia TJ. Applied Clay Science 1999;15(1-2):11-29.

34. Shen Z, Simon GP, and Cheng YB. Polymer 2002;43(15):4251-4260.

35. Stein RS and Rhodes MB. Journal of Applied Physics 1960;31(11):1873-1884.

36. Tseng C-R, Lee H-Y, and Chang F-C. Journal of Polymer Science Part B: Polymer Physics 2001;39(17):2097-2107.

37. Park CI, Choi WM, Kim MH, and Park OO. Journal of Polymer Science Part B: Polymer Physics 2004;42(9):1685-1693.

38. Wu T-M, Hsu S-F, Chien C-F, and Wu J-Y. Polymer Engineering and Science 2004;44(12):2288-2297.

39. Tseng C-R, Wu S-C, Wu J-J, and Chang F-C. Journal of Applied Polymer Science 2002;86(10):2492-2501.

40. Wu H-D, Tseng C-R, and Chang F-C. Macromolecules 2001;34(9):2992-2999.

41. Wu T-M, Hsu S-F, and Wu J-Y. Journal of Polymer Science Part B: Polymer Physics 2003;41(6):560-570.

42. Kim MH, Park CI, Choi WM, Lee JW, Lim JG, Park OO, and Kim JM. Journal of Applied Polymer Science 2004;92(4):2144-2150.

43. Bruzaud S, Grohens Y, Ilinca S, and Carpentier J-F. Macromolecular Materials and Engineering 2005;290(11):1106-1114.

44. Torre L, Lelli G, and Kenny JM. Journal of Applied Polymer Science 2006;100(6):4957-4963.

45. Ray B, Elhasri S, Thierry A, Marie P, and Guenet J-M. Macromolecules 2002;35(26):9730-9736.

46. Vittoria V, De Candia F, Iannelli P, and Immirzi A. Die Makromolekulare Chemie Rapid Communications 1988;9(11):765-769.

47. Vittoria V, Russo R, and de Candia F. Polymer 1991;32(18):3371-3375.

48. De Candia F, Carotenuto M, Guadagno L, and Vittoria V. Journal of Macromolecular Science, Part B: Physics 1996;35(2):265 - 275.

49. Tashiro K and Yoshioka A. Macromolecules 2001;35(2):410-414.

50. Sivakumar M, Yamamoto Y, Amutharani D, Tsujita Y, Yoshimizu H, and Kinoshita T. Macromolecular Rapid Communications 2002;23(1):77-79.

51. Theng BKG. The chemistry of clay-organic reactions. New York: John Wiley & Sons, 1974.

52. Brown G and Nadeau P. Philosophical Transactions of the Royal Society of London. Series A, Mathematical and Physical Sciences 1984;311(1517):221-240.

53. Çapková P and Schenk H. Journal of Inclusion Phenomena and Macrocyclic Chemistry 2003;47(1):1-10.

54. Jeon HS, Rameshwaram JK, Kim G, and Weinkauf DH. Polymer 2003;44(19):5749-5758.

55. Kodgire P, Kalgaonkar R, Hambir S, Bulakh N, and Jog JP. Journal of Applied Polymer Science 2001;81(7):1786-1792.

56. Theng BKG. Formation and Properties of Clay-Polymer Complexes. vol. 9. Amsterdam: Elsevier Scientific Publishing Company, 1979.

57. Moet AS and Akelah A. Materials Letters 1993;18(1-2):97-102.

58. Vaia RA, Ishii H, and Giannelis EP. Chemistry of Materials 1993;5(12):1694-1696.

59. Hasegawa N, Okamoto H, Kawasumi M, Kato M, Tsukigase A, and Usuki A. Macromolecular Materials and Engineering 2000;280-281(1):76-79.

60. Zhang W, Chen D, Zhao Q, and Fang Y. Polymer 2003;44(26):7953-7961.

61. Doh JG and Cho I. Polymer Bulletin 1998;41(5):511-518.

62. Wang D, Zhu J, Yao Q, and Wilkie CA. Chemistry of Materials 2002;14(9):3837-3843.

63. Martuscelli E. Polymer Engineering & Science 1984;24(8):563-586.

64. Avrami M. The Journal of Chemical Physics 1939;7(12):1103-1112.

65. Avrami M. The Journal of Chemical Physics 1940;8(2):212-224.

66. Avrami M. The Journal of Chemical Physics 1941;9(2):177-184.

67. Long Y, Shanks RA, and Stachurski ZH. Progress in Polymer Science 1995;20(4):651-701.

68. Penning JP and St. John Manley R. Macromolecules 1996;29(1):77-83.

69. Ke Y, Long C, and Qi Z. Journal of Applied Polymer Science 1999;71(7):1139-1146.

70. Ma J, Zhang S, Qi Z, Li G, and Hu Y. Journal of Applied Polymer Science 2002;83(9):1978-1985.

71. Yu J and He J. Polymer 2000;41(3):891-898.

72. Lu XF and Hay JN. Polymer 2001;42(23):9423-9431.

73. Loo Y-L, Register RA, Ryan AJ, and Dee GT. Macromolecules 2001;34(26):8968-8977.

74. Grady BP, Pompeo F, Shambaugh RL, and Resasco DE. The Journal of Physical Chemistry B 2002;106(23):5852-5858.

75. Fornes TD and Paul DR. Polymer 2003;44(14):3945-3961.

76. Di Maio E, Iannace S, Sorrentino L, and Nicolais L. Polymer 2004;45(26):8893-8900.

77. Gopakumar TG, Lee JA, Kontopoulou M, and Parent JS. Polymer 2002;43(20):5483-5491.

78. Xu J-T, Zhao Y-Q, Wang Q, and Fan Z-Q. Polymer 2005;46(25):11978-11985.

79. Liu Z, Chen K, and Yan D. European Polymer Journal 2003;39(12):2359-2366.

80. Zhang G and Yan D. Journal of Applied Polymer Science 2003;88(9):2181-2188.

81. Chen GX, Hao GJ, Guo TY, Song MD, and Zhang BH. Journal of Applied Polymer Science 2004;93(2):655-661.

82. Hotta S and Paul DR. Polymer 2004;45(22):7639-7654.

83. Alamo RG and Mandelkern L. Macromolecules 1991;24(24):6480-6493.

84. Kim JS, Roberts SB, Eisenberg A, and Moore RB. Macromolecules 1993;26(19):5256-5258.

85. Ma D, Akpalu YA, Li Y, Siegel RW, and Schadler LS. Journal of Polymer Science Part B: Polymer Physics 2005;43(5):488-497.

86. Filippi S, Marazzato C, Magagnini P, Minkova L, Dintcheva NT, and Mantia FPL. Macromolecular Materials and Engineering 2006;291(10):1208-1225.

87. Famulari A, Arosio P, Filippi S, Marazzato C, Magagnini P, Minkova L, and Meille SV. Journal of Macromolecular Science, Part B: Physics 2007;46(2):355 - 371.

88. Patro TU, Mhalgi MV, Khakhar DV, and Misra A. Polymer 2008;49(16):3486-3499.

89. Maiti P, Nam PH, Okamoto M, Hasegawa N, and Usuki A. Macromolecules 2002;35(6):2042-2049.

90. Sinha Ray S, Yamada K, Okamoto M, Ogami A, and Ueda K. Chemistry of Materials 2003;15(7):1456-1465.

91. Katoh Y and Okamoto M. Polymer 2009;50(19):4718-4726.

92. Xiao Z, Li Y, Ma D, Schadler LS, and Akpalu YA. Journal of Polymer Science Part B: Polymer Physics 2006;44(7):1084-1095.

93. Nam PH, Maiti P, Okamoto M, Kotaka T, Hasegawa N, and Usuki A. Polymer 2001;42(23):9633-9640.

94. Nam JY, Sinha Ray S, and Okamoto M. Macromolecules 2003;36(19):7126-7131.

95. Sinha Ray S, Bandyopadhyay J, and Bousmina M. European Polymer Journal 2008;44(10):3133-3145.

CHAPTER VI

EFFECT OF NEUTRALIZING COUNTERION ON THE CRYSTALLIZATION BEHAVIOR OF LIGHTLY SULFONATED SYNDIOTACTIC POLYSTYRENE CLAY NANOCOMPOSITES

ABSTRACT

Lightly sulfonated syndiotactic polystyrene was neutralized with various alkali metal counterions. The effect of the size of the neutralizing counterion size on the morphology of sulfonated syndiotactic polystyrene nanocomposites was investigated using wide angle X-ray diffraction, transmission electron microscopy, polarized light microscopy, and small angle laser light scattering. The effect of the neutralizing counterion size on the crystallization behavior of sulfonated syndiotactic polystyrene nanocomposites was investigated using differential scanning calorimetry. Exfoliated nanocomposites were obtained for sulfonated syndiotactic polystyrene neutralized with sodium, rubidium, and cesium counterions based upon WAXD and TEM analyses. The cesium-neutralized sulfonated syndiotactic polystyrene nanocomposite crystallized more rapidly than the sodium and rubidium-neutralized nanocomposites over a wide range of isothermal crystallization temperatures. Based upon the morphological and crystallization data, it was determined that the neutralizing counterion strongly affects the crystallization behavior the SsPS ionomer even in the presence of exfoliated clay platelets.

INTRODUCTION

Polymer clay nanocomposites are very important materials that are utilized in a broad range of applications [1-13]. As a result of the research in this area, it has become clear that is often necessary to chemically modify both the polymer matrix and the clay surface in order to improve polymer-clay interactions in order to achieve an intercalated or exfoliated polymer clay morphology [14-15]. There have been many investigations into the use of ionomers as the sole polymer matrix phase in polymer nanocomposites [15-23] and as compatibilizers [24-32] to improve the degree of exfoliation of clay in the presence of hydrophobic polyolefin matrices. The research involving the use of ionomers to prepare polymer nanocomposites has focused on many different aspects of polymer nanocomposite behavior ranging from enhanced rheological properties, flame retardancy, mechanical properties, and crystallization behavior.

The behavior and properties of ionomers have been shown to be significantly affected by the degree and type of neutralizing counterion [33-47]. However, there are only a few studies that focus on understanding the effect of the neutralizing counterion of the ionomer on the formation of properties of polymer nanocomposites [23, 25, 48-49]. Govindaiah and coworkers reported that degree of clay exfoliation increased with increasing size of the neutralizing alkali metal counterion at a constant degree of sulfonation for sulfonated syndiotactic polystyrene nanocomposites. Monitoring the exothermic behavior of SsPS nanocomposites neutralized with different alkali metal counterions using DSC analysis showed that the peak crystallization temperature increased with increasing size of the counterion. Govindaiah and coworkers attributed this behavior to weaker electrostatic interactions within the ionic aggregates with the larger neutralizing counterion.

Monitoring the crystallization behavior of the SsPS nanocomposites from the melt provided qualitative information on the effect of the neutralizing counterion on the crystallization behavior of SsPS nanocomposites. To gain a more in-depth understanding of the effect of the counterion on the crystallization behavior of SsPS nanocomposites, we have conducted a study of the isothermal crystallization behavior to probe the effect of the neutralizing counterion on the preparation and properties of lightly sulfonated syndiotactic polystyrene nanocomposites with specific attention given to the effect of the counterion on the morphology and crystallization kinetics of SsPS nanocomposites.

EXPERIMENTAL

Materials

Syndiotactic polystyrene (Questra 102) MW of 310,000 g/mol was donated by the Dow Chemical Company. Reagent grade chloroform, methanol, sulfuric acid, and potassium monopthalate were obtained from Fisher Scientific. Hexanoic anhydride and cesium hydroxide were received from Sigma Aldrich. Cloisite® Na^+ and Cloisite® 10A were donated by Southern Clay Products. The clays were used in the received state without additional drying. The cation exchange capacities for Cloisite® 10A is 125 and milliequivalents/100 g. The organic modification agent for Cloisite® 10A is a quaternary amine salt consisting of a dimethylbenzyl, hydrogenated tallow. The hydrogenated tallow is made up of ~65% C18, ~30% C16, and ~5% C14 chains. Cloisite®10A has been shown to produce intercalated and exfoliated nanostructures in many styrenated polymer matrices [50-54] and is thus a proper choice for enhancing polymer-clay interactions in the sPS matrix. Cloisite® 10A will be identified as OMMT.

Sulfonation of Syndiotactic Polystyrene

Previous differential scanning calorimetry (DSC) investigations of SsPS ionomers have identified the effect of the degree of sulfonation on the crystallization behavior of SsPS [55]. It has been demonstrated that incorporating greater than 2.0 mol% of ionic content within sPS drastically inhibits the ability of sPS to crystallize. Therefore, we have chosen to lightly sulfonate sPS to yield an ion-containing polymer with 1 mol% sulfonation. By introducing 1 mol% sulfonate groups, the crystallization kinetics of SsPS occurs on a readily observable timescale at crystallization temperatures similar to that of the sPS homopolymer. Thus, direct comparisons between the behavior of the SsPS ionomer and the sPS homopolymer can be made.

The sulfonation agent was prepared according to previously published procedures [55] using chloroform as the solvent. Chloroform (25 mL) was added to a 50 mL volumetric flask containing 0.03 moles of hexanoic anhydride. The chloroform/hexanoic anhydride solution was cooled in an ice bath for 1 hour, and then 1 mL of concentrated sulfuric acid was added to the chilled solution and shaken vigorously. Additional chloroform was added to the volumetric flask to the 50 mL mark.

sPS was dissolved in chloroform at 100 °C for 1.5 h in a PARR pressure reactor to yield a 2.5% w/v solution. After 1.5 h, the solution was cooled to 70 °C and then transferred to a three-neck round bottom flask. Additional chloroform was added to yield a 1% w/v sPS solution. The sPS solution was allowed to equilibrate at 70 °C under a nitrogen purge. After equilibration, the appropriate amount of sulfonating reagent was added and the reaction was allowed to proceed for 1 hour at 70 °C under a nitrogen purge. After 1 h, 10 mL methanol was added to the solution to terminate the reaction. The solution was poured into a large excess of methanol to precipitate the polymer. The precipitated polymer was filtered and washed with deionized water. The resulting

polymer was dried under vacuum at 100 °C for 12 h. The vacuum dried ionomer was redissolved in chloroform using a PARR pressure reactor for 1.5 h at 100 °C and then steam stripped in deionized water to remove residual sulfonating reagent and solvent. The ionomer was then dried in a vacuum oven at 70 °C for 24 h. The degree of sulfonation was determined by nonaqueous titration with methanolic sodium hydroxide. The methanolic sodium hydroxide was standardized using potassium monopthalate.

Neutralization of Sulfonated Syndiotactic Polystyrene

The cesium counterion was chosen as the neutralizing counterion for SsPS within this study of the crystallization behavior and kinetics of SsPS nanocomposites based on previous work by Orler et al [56]. The relatively large cesium counterion yields weaker electrostatic interactions compared to SsPS ionomers neutralized with alkali metals of smaller ionic radii, and thus leading to enhanced crystallization. Due to the presence of these more thermally-labile ionic aggregates, cesium-neutralized SsPS allows crystallization of chain segments to occur on time-scale similar to the sPS homopolymer. Therefore, cesium-neutralized SsPS was considered to be the most appropriate SsPS ionomer to study the effect of clay on the crystallization behavior and kinetics of the semicrystalline SsPS.

The SsPS ionomer was completely neutralized using 0.1 M methanolic sodium, rubidium, or cesium hydroxide. The SsPS was dissolved in chloroform using a PARR pressure reactor at 100 °C for 1.5 h. The appropriate amount of 0.1 M NaOH, RbOH, or CsOH was added to the SsPS solution to obtain a fully neutralized ionomer. The fully neutralized SsPS 1.0 mol% ionomer was used as the ionomer matrix within this study and will be identified as SsPS.

Nanocomposite Preparation

Nanocomposites were prepared using the solution intercalation method [2, 57-59]. Dispersions of Na^{+}MMT and OMMT (0.5% w/v) were prepared by adding the appropriate amount of clay to chloroform. The respective clay/chloroform mixtures were heated under reflux at 60 °C for 24 h with vigorous stirring. After 24 h, the clay dispersions were sonicated for 2 h.

SsPS nanocomposites 5% w/w of OMMT clay was prepared. Solutions of SsPS were prepared by dissolving the appropriate amount of the homopolymer or the ionomer in chloroform to yield 1.5% w/v solutions. The SsPS ionomer was dissolved in chloroform using a PARR pressure reactor at 100°C for 1.5 h. The solutions were removed from the reactor upon dissolution and transferred to 50 mL round bottom flasks. The appropriate volume of clay dispersions to yield 5 % w/w of OMMT was taken from the previously prepared 0.5% w/v clay dispersion, while the mixture was being vigorously stirred to ensure that a homogeneous sample volume was removed. After adding the appropriate amount of clay dispersion to the dissolved polymer, the samples were allowed to mix with vigorous stirring under reflux for 24 h at 60°C. After 24 hours, the mixtures were dried at RT for 5 days to evaporate the solvent followed by drying in a vacuum oven for 24 h at 60 °C.

Transmission Electron Microscopy

Solution-cast samples were prepared for morphological analysis using transmission electron microscopy (TEM) by embedding solution cast sPS and SsPS clay mixtures into epoxy resin. The epoxy resin used was Spurr's Low Viscosity embedding mixture obtained from Electron Microscopy Sciences. The resin was prepared according the supplier's protocol. The resin containing the nanocomposites samples were dried in vacuum oven at 60 °C for 12 h. The

samples were microtomed at room temperature with a diamond knife using a Reichart Ultramicrotome in order to obtain 80 nm thick sections. Microtomed sections were transferred from water onto 200 mesh copper grids and used without staining. The high electron density of the clay platelets provided the necessary contrast for morphological evaluation using TEM. TEM micrographs of solvent-cast SsPS clay mixtures were obtained using a JEOL 2100 transmission electron microscope operating at 200 kV. The microscope was interfaced with a Gatan camera that was utilized to obtain digital photomicrographs.

Wide Angle X-ray Diffraction

Wide angle x-ray diffraction (WAXD) was used as a quantitative tool to determine the changes in clay platelet intergallery height by following changes in the basal spacing of the clay. Solvent-cast nanocomposite samples were ground into a powder using a mortar and pestle prior to WAXD analysis. A Rigaku Ultima III X-ray Diffractometer using Cu K_α radiation (λ= 1.54 nm) operating at 40 kV and 44 mA was used to obtain nanocomposite WAXD profiles in the 2 theta region from 2θ = 2 - 10°. The WAXD profiles were obtained at a scan rate of 0.1°/min and a step size of 0.05.

Differential scanning calorimetry

Thermal behavior and crystallization kinetics of the polymer clay mixtures were studied using differential scanning calorimetry (DSC). A TA Instruments Q2000 DSC was used to probe the thermal behavior of the prepared nanocomposites under isothermal crystallization conditions at 235, 240, 245, 250, and 255 °C. The weight for each sample was maintained between 6 – 8

mg. The solution cast samples will be identified using the following terminology: SsPS XOMMT where X will equal 5 wt.% OMMT clay in the SsPS ionomer.

DSC analysis was performed under a continuous nitrogen flow to minimize sample degradation. The samples were heated to 330 °C and held at that maximum temperature for 5 min to erase previous thermal history and the presence of any persistent nuclei. Following a rapid temperature ramp at -200 °C/min, isothermal crystallization was carried out at 235, 240, 245, 250, and 255 °C. TA Instruments Universal Analysis software was used to analyze the resulting DSC traces. The crystallization half-time, $t_{½}$, the time at which 50% of the material has crystallized, was obtained from isothermal holds and used as a measure of changes in the bulk crystallization rate of the neat polymers and polymer-clay mixtures.

Polarized Light Microscopy

The determination of the spherulitic growth rates of the pure matrices and clay-containing matrices was carried out using polarized light microscopy. A Nikon LV100 microscope equipped with a Nikon DXM1200 digital camera was used in crossed-polarized configuration to monitor spherulitic growth under isothermal conditions. Images were captured and analyzed using Nikon NIS-Elements BR software. Isothermal crystallization conditions were achieved using a Linkam TMS600 hotstage operated by a Linkam TMS 94 controller and Linkam Linksys32 software. The samples were heated to 330 °C on the Linkam hotstage and held at that maximum temperature for 5 min. Following a rapid temperature ramp at -100 °C/min, isothermal crystallization was carried out at 240 °C with periodic image capture until complete spherulitic impingement occurred. Fast Fourier Transform analysis was performed on polarized light microscopy (PLM) images using Image J software (National Institutes of Health) to obtain

Small Angle Laser Light Scattering

Small-angle laser light scattering (SALLS) patterns were obtained in H_v mode using a laser light scattering experimental configuration similar to that of Stein and Rhodes [60]. A 3 mW He-Ne laser light of 632.8 nm (Oriel Corporation, Model 6697) was used as the incident light and the H_v patterns were captured using a SenSys 1401E (Photometrics) CCD camera positioned at a sample-to-detector distance of 380 mm. The spherulite diameters of the pristine polymers and polymer/clay mixtures were obtained using volume-filled samples that were isothermally crystallized at 240 °C using a Linkam hotstage according to the heating profile used for the polarized optical microscopy analysis. The H_v patterns were analyzed using POLAR Software (STAR, State University of New York) to obtain the maximum scattering intensity at an azimuthal angle of 45°.

RESULTS AND DISCUSSION

The degree of clay exfoliation clay within SsPS neutralized with various counterions containing 5 wt.% OMMT is shown in Figure VI-1. The WAXD profile of the organically modified clay is included in Figure VI-1 for comparison. The peak centered at 4.67° 2θ is attributed to unintercalated organically-modified clay. Monitoring the change in peak position, intensity, and breadth of the as-received OMMT clay peak provides information regarding the periodicity of the clay platelets within the SsPS matrix. It can be seen in Figure VI-1 that for each SsPS nanocomposites that there is one prominent, observable peak located at approximately 8.0° 2θ is attributed to the δ-crystal polymorph of the semicrystalline component of the ionomer. The position of the δ-form peak does not shift as a function of the neutralizing counterion size. The most significant observation from the WAXD profiles of the SsPS 5 wt.% OMMT

nanocomposites is that there is no prominent peak present in the region of 4.67° 2θ. Upon close inspection of the SsPS 5 wt.% OMMT WAXD profiles of the alkali-metal neutralized ionomers, there appears to be a very broad, extremely low intensity peak in the region attributable to OMMT clay. The lack of an intense peak or the presence of a very broad, low intensity peak in the clay region suggests that the SsPS1Na^+, SsPS1Na^+Rb^+, and SsPS1Cs^+ 5 wt.% OMMT hybrids are likely exfoliated or highly intercalated nanocomposites.

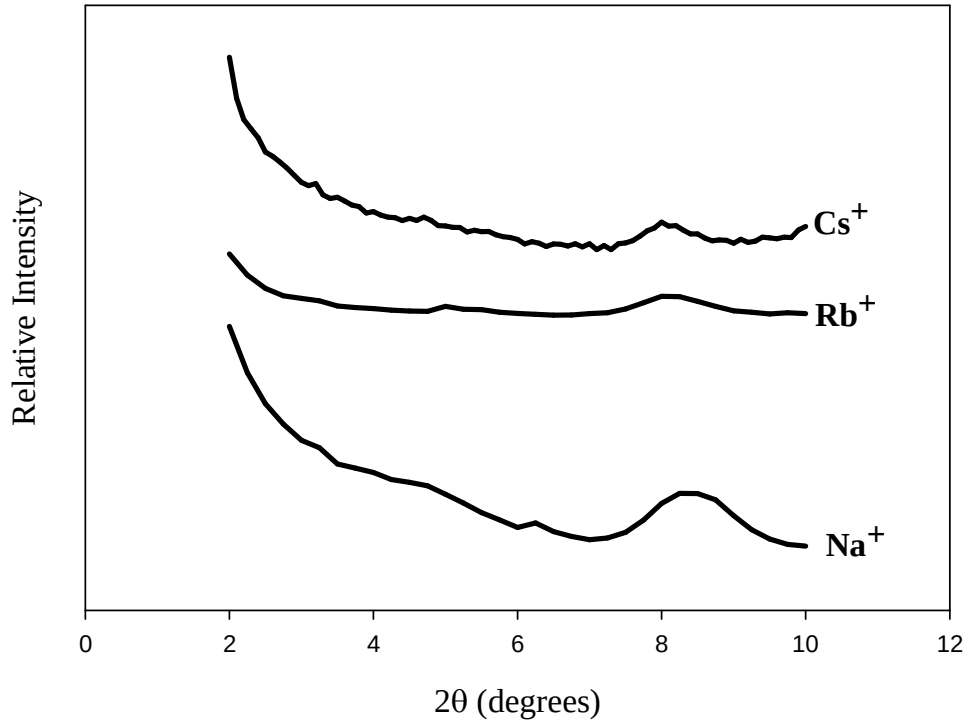

Figure VI-1. Relative intensity versus 2θ for SsPS1.0X^+ 5 wt.% OMMT nanocomposites solution cast from chloroform.

WAXD provides are global assessment of the degree of periodicity within the various SsPS ionomer matrices while TEM provides are local assessment of the arrangement of clay

within ionomer matrix. Figure VI-2 contains the TEM micrographs of SsPS1Cs^+ and SsPS1Na^+containing 5 wt.% OMMT.

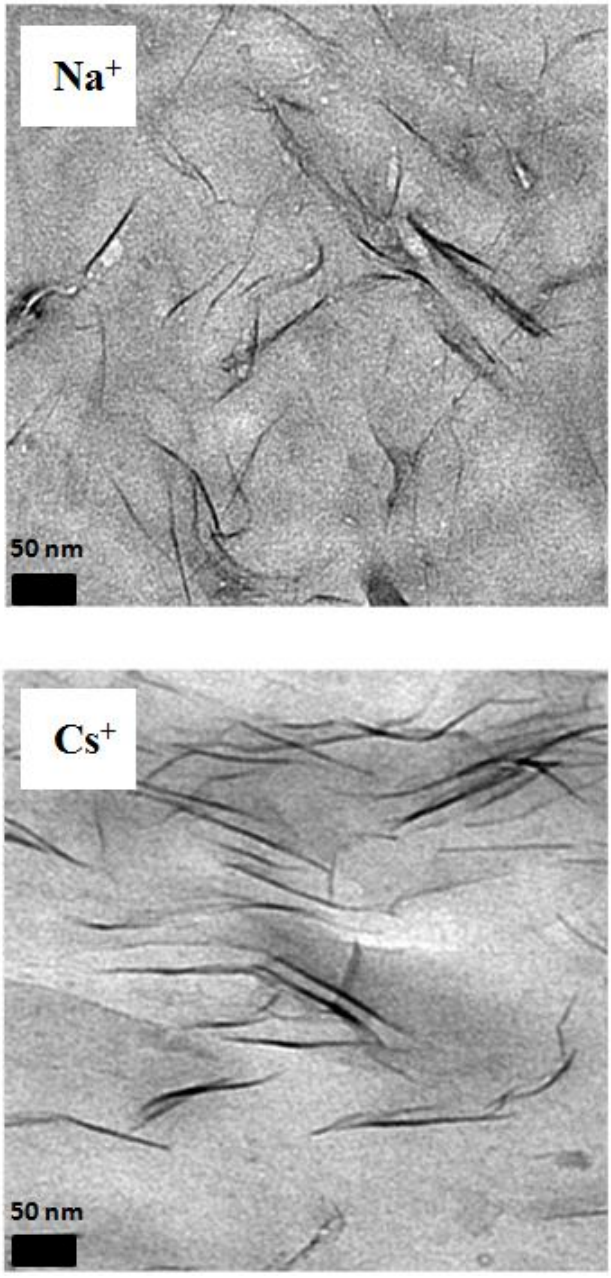

Figure VI-2. Transmission electron micrographs of solvent-cast SsPS1.0Na^+ 5 wt.% OMMT and SsPS1.0Cs^+ 5 wt.% OMMT.

The arrangement of clay platelets within both SsPS matrices is similar. Both SsPS nanocomposites contain single clay platelets along with very small clay platelet stacks. There are no micron-sized tactoid agglomerates of OMMT clay that are observed within either SsPS ionomer matrix. Based upon the WAXD profiles and TEM micrographs, it can be concluded the SsPS1.0Na^+, SsPS1.0Rb^+, and SsPS1.0Cs^+ 5 wt.% OMMT are exfoliated nanocomposites. Regardless of the size of the alkali metal used to neutralize SsPS1.0H^+, an exfoliated nanocomposite is obtained using the solution intercalation technique. This behavior is different from SsPS nanocomposite behavior reported by Govindaiah and coworkers. In their study of SsPS nanocomposites they report that the degree of clay is a function of the size of the neutralizing alkali metal counterion. Govindaiah reported that the degree of clay exfoliation increased with increasing neutralizing alkali metal size. The WAXD profiles and TEM micrographs provided in Figures VI-1 and VI-2 of this study do not show a strong counterion size dependence on the degree of exfoliation of clay platelets within the SsPS matrix. It appears that 1 mol% of sulfonate groups is sufficient to lead to enhanced interactions with the organically-modified clay platelets regardless of the size of the neutralizing counterion.

The crystallization behavior of SsPS1.0Na^+, SsPS1.0Rb^+, and SsPS1.0Cs^+ 5 wt.% OMMT nanocomposites was studied over a wide temperature range in order to investigate the effect of size of the neutralizing alkali metal counterion on the crystallization of the SsPS ionomer in the presence of the clay.

The development of crystallinity within SsPS nanocomposite was monitored by applying the following relationship:

$$X_c(t) = \frac{\int_0^t \frac{dH}{dT} dt}{\int_0^\infty \frac{dH}{dT} dt} \quad (1)$$

The expression given in equation 1 represents the fractional crystallinity of the bulk polymer system, $X_c(t)$, and is equal to the heat evolved during isothermal crystallization at a specific time t divided by the total heat generated during the entire crystallization process. In addition, the crystallization behavior of the different nanocomposite systems was characterized by $t_{½}$ values. The $t_{½}$ values were determined from isothermal crystallization experiments and were used as a measure of the rate of bulk isothermal crystallization.

A kinetic evaluation of the crystallization behavior of the SsPS nanocomposites was completed using the Avrami approach [61-63]. This approach is used extensively in the study of the bulk crystallization of polymers as it provides insight into the nucleation and growth process within the bulk polymer matrix [64-72]. The Avrami equation is given in equation 3 and is used to determine the extent of fractional crystallinity, $X_c(t)$ at time t.

$$X_c(t) = 1 - \exp(-Kt)^n \quad (3)$$

The Avrami rate constant is represented by K and n is the Avrami exponent. The Avrami exponent, n, provides insight into the type of nucleation and growth that occurs within the system. The kinetic analysis of the isothermal crystallization behavior of the polymer clay hybrids is done by taking the double logarithm of the Avrami equation yielding the equation in the following form:

$$\ln[-\ln(1 - X_c(t))] = n \ln t + \ln K \quad (4)$$

Plots of $\ln[(-\ln(1- X_c(t))]$ versus ln t provide n and K from the slope and intercept, respectively.

Figures VI-3, VI-4, VI-5, VI-6, and VI-7 contain the fraction of material crystallized versus ln time and the ln time versus time at 235, 240, 245, 250, and 255 °C.

The crystallization half-time, $t_{½}$, can be extracted from the $X_c(t)$ versus ln t graphs by determining the time at which $X_c(t)$ equals 0.50. Figure VI-8 provides a plot of the crystallization half-time of SsPS1.0X^+ 5 wt.% nanocomposites versus the ionic radius of the neutralizing counterion. The crystallization half-time for the SsPS nanocomposites decreases with increasing counterion size over the entire crystallization range studied. Also, it is clear that the crystallization half-time increases as the isothermal crystallization temperature increases. The trend of increasing crystallization half-time with increasing isothermal crystallization temperature can be explained is attributed to the change in the degree of supercooling experienced by the SsPS nanocomposites at each isothermal crystallization temperature. At larger degrees of supercooling, the crystallization half-time is shorter because the polymer chains have less molecular mobility the further away the crystallization temperature is from the equilibrium melting temperature of the polymer. As the crystallization temperature approaches the melting temperature of the polymer, the crystallization half-time increases because the polymer chains retain more molecular mobility due to the larger amount of thermal energy present at the higher temperature and the reduced ability of the polymer chains to pack into crystalline structures as the crystallization temperature approaches the melting point of the polymer.

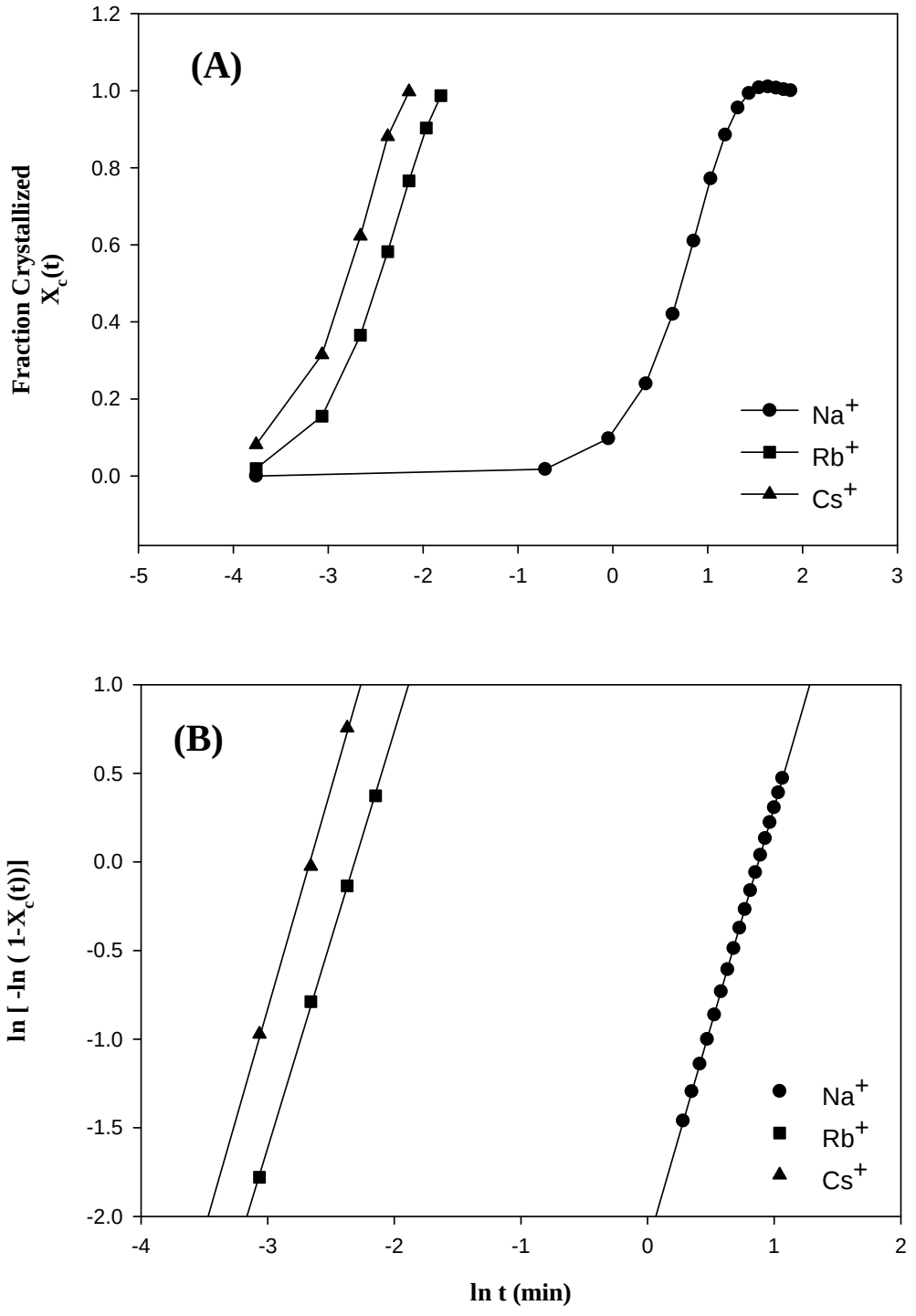

Figure VI-3. (A) $X_c(t)$ versus ln time at 235 °C and (B) ln [-ln(1-$X_c(t)$)] for SsPS1.0X^+ 5 wt.% OMMT where X = Na^+, Rb^+, and Cs^+.

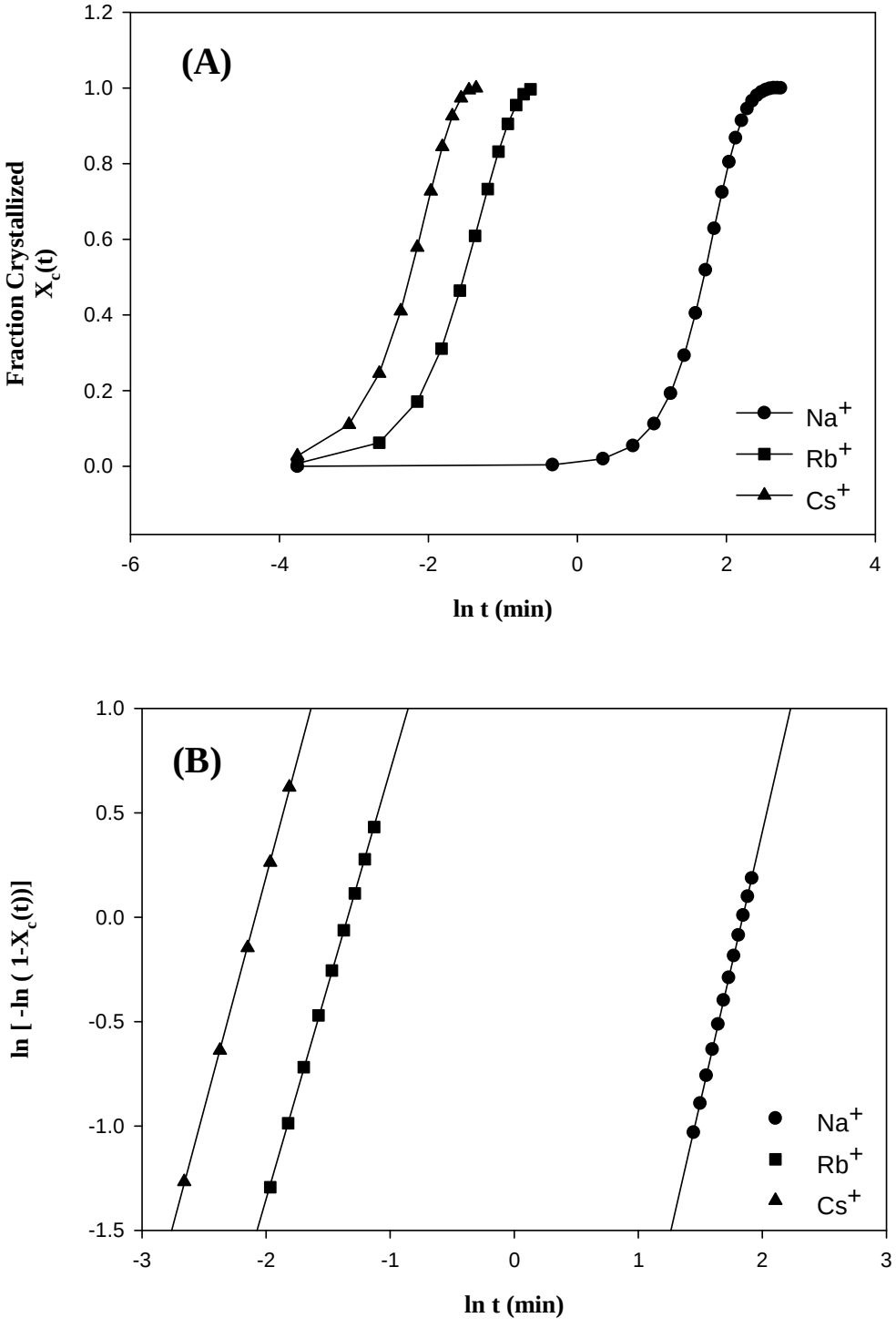

Figure VI-4. (A) $X_c(t)$ versus ln time at 240 °C and (B) ln [-ln(1-$X_c(t)$)] for SsPS1.0X^+ 5 wt.% OMMT where X = Na^+, Rb^+, and Cs^+.

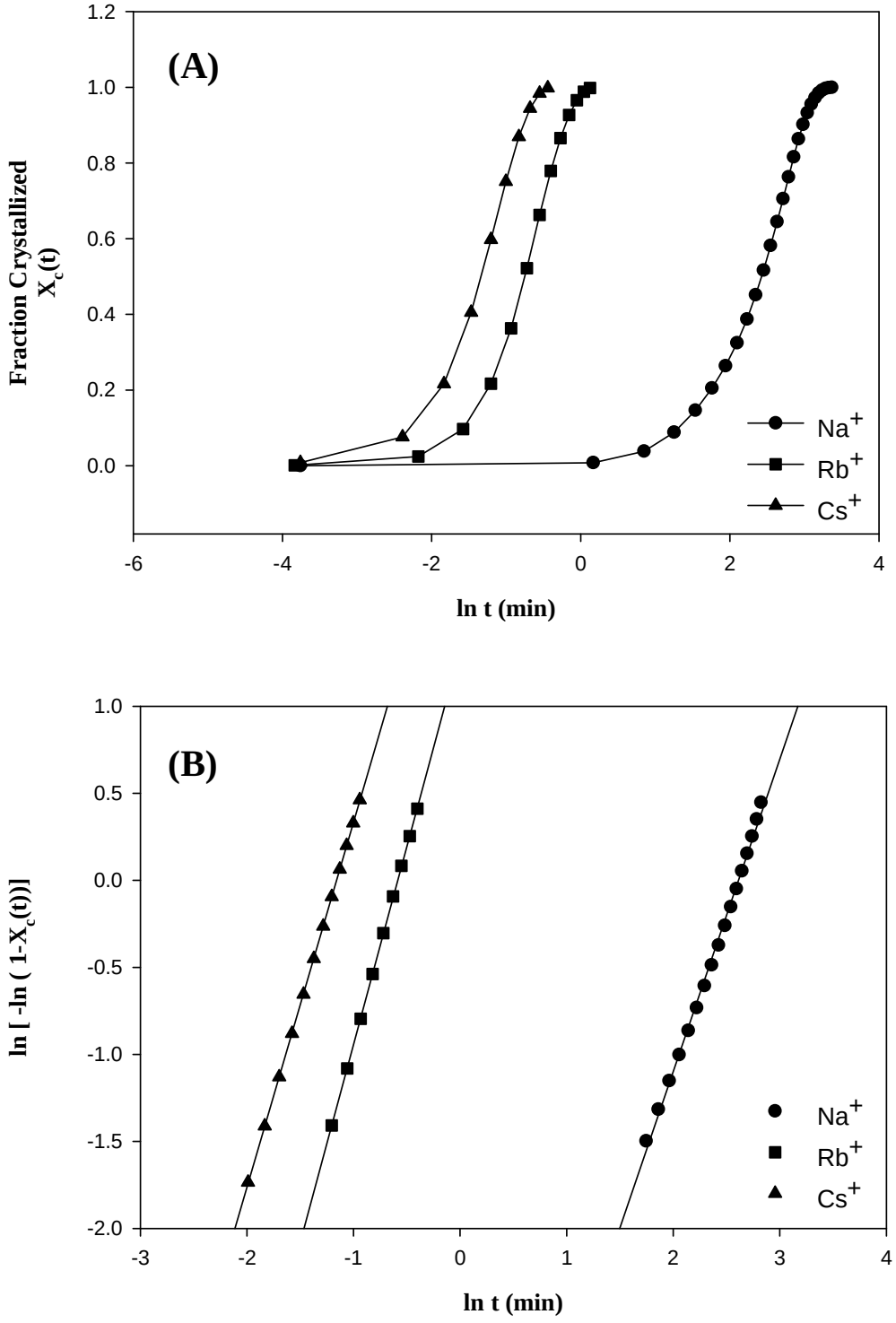

Figure VI-5. (A) $X_c(t)$ versus ln time at 245 °C and (B) ln [-ln(1-$X_c(t)$)] for SsPS1.0X^+ 5 wt.% OMMT where X = Na^+, Rb^+, and Cs^+.

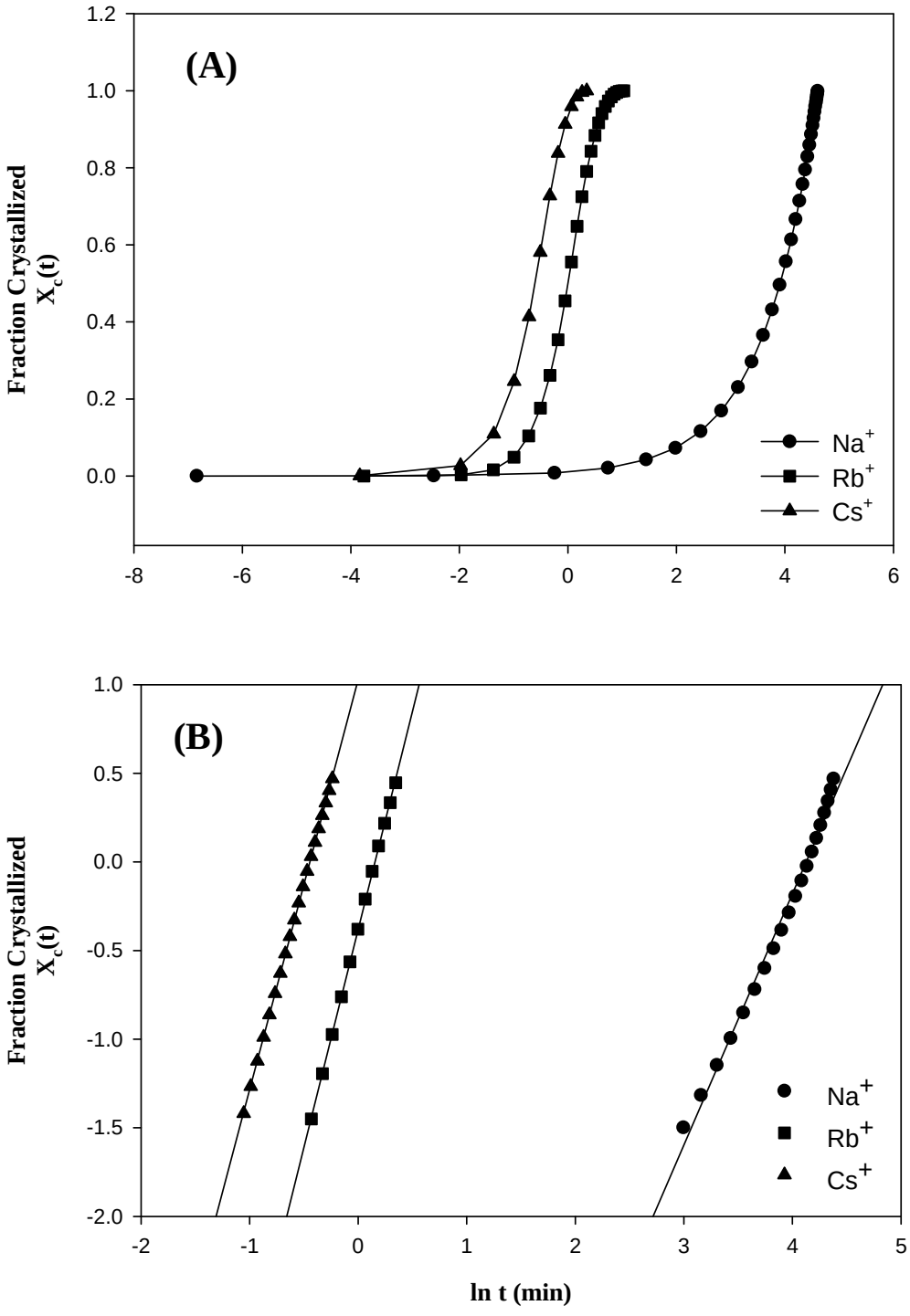

Figure VI-6. (A) $X_c(t)$ versus ln time at 250 °C and (B) ln [-ln(1-$X_c(t)$)] for SsPS1.0X^+ 5 wt.% OMMT where X = Na^+, Rb^+, and Cs^+.

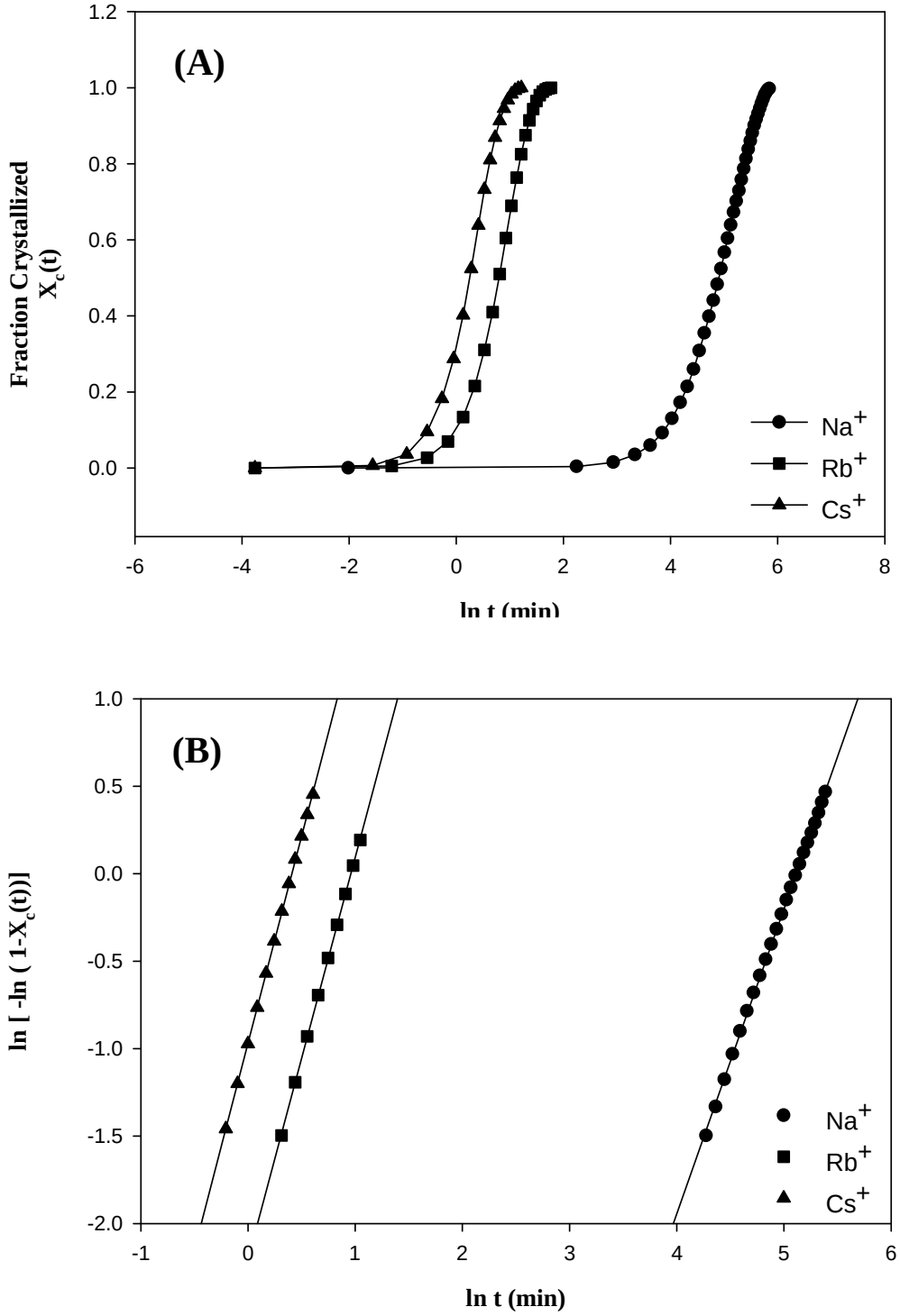

Figure VI-7. (A) $X_c(t)$ versus ln time at 255 °C and (B) ln [-ln(1-$X_c(t)$)] for SsPS1.0X^+ 5 wt.% OMMT where X = Na^+, Rb^+, and Cs^+.

The parameters for the SsPS nanocomposites obtained from the Avrami analysis are provided in Table VI-1. 235°C

Table VI-1. Avrami parameters for SsPS1.0X^+ 5 wt.% OMMT nanocomposites at various isothermal crystallization temperatures where X = Na^+, Rb^+, and Cs^+.

SsPS1.0X^+ 5 wt.% OMMT	**K (min^{-1})**	**N**
235°C		
Na^+	1.2 x 10^{-1}	2.47
Rb^+	228	2.39
Cs^+	757	2.49
240°C		
Na^+	8.40 x 10^{-3}	2.6
Rb^+	16	2.05
Cs^+	104	2.22
245°C		
Na^+	9.20 x 10^{-3}	1.79
Rb^+	3.78	2.27
Cs^+	11	2.09
250°C		
Na^+	2.9 x 10^{-3}	1.42
Rb^+	6.8 x 10^{-1}	2.46
Cs^+	2.8	2.32
255°C		
Na^+	1.4 x 10^{-4}	1.74
Rb^+	1.1 x 10^{-4}	2.3
Cs^+	3.8 x 10^{-1}	2.4

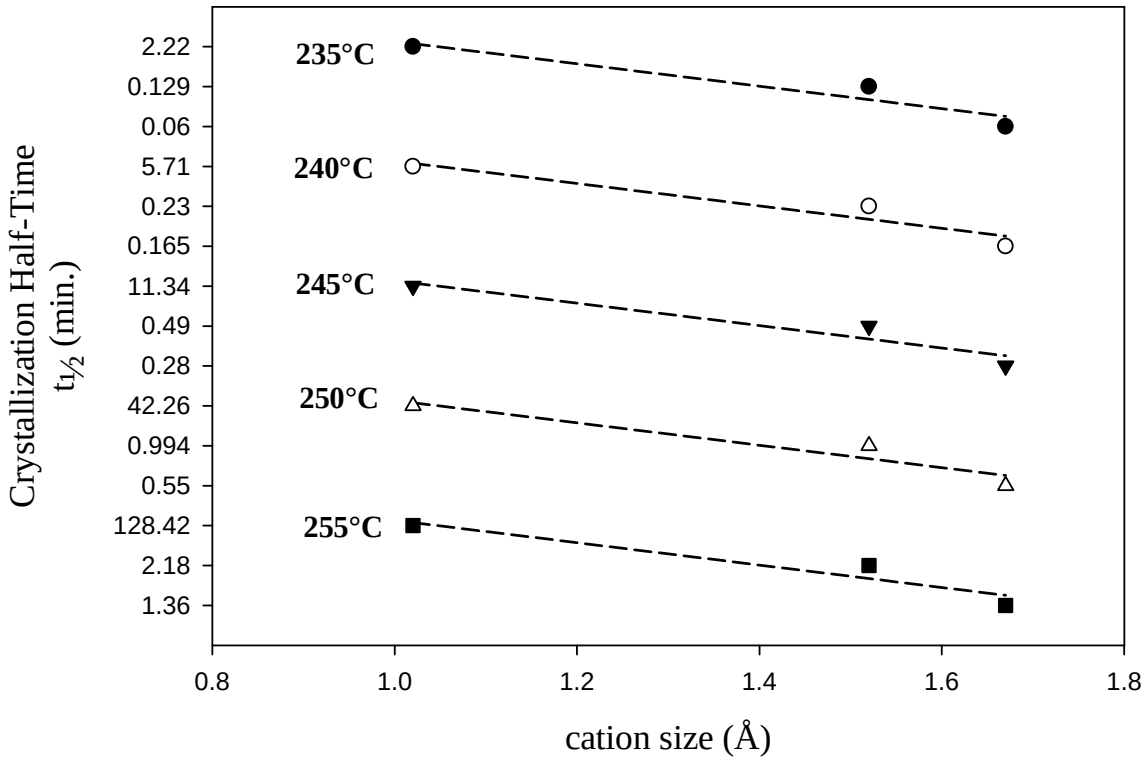

Figure VI-8. Crystallization half-time versus cation size of SsPS1.0Na^+, SsPS1.0Rb^+, and SsPS1.0Cs^+, containing 5 wt.% OMMT clay. The cation size of Na^+, Rb^+, and Cs^+ is 1.02, 1.52, and 1.67 Å, respectively.

The size of the neutralizing counterion has a significant effect on the crystallization half-time of SsPS nanocomposites containing 5 wt.% OMMT clay. The crystallization half-time, $t_{½}$, is a bulk measure of the rate of crystallization of the polymer. Figure VI-8 contains plots of the crystallization half-time versus cation size. It can be seen that over a wide temperature from 235 to 255 °C, that the rate of crystallization decreases within increasing cation size. The decrease in the crystallization half-time value with increasing counterion size can be attributed to an increasing destabilization of the electrostatic network as the size of the neutralizing counterion increases.

The activation energy for crystallization of the SsPS ionomers in the presence of the clay can be determined using the following equation

$$\frac{1}{n}(\ln K) = \ln k_0 - \frac{\Delta E}{RT} \qquad (5)$$

where is a temperature-independent pre-exponential factor, R is the universal gas constant, T is the temperature in Kelvin at which crystallization occurred. ΔE is the total activation energy which consists of the transport activation energy ΔE^* and the nucleation activation energy ΔF. The total activation energy, ΔE, is the energy required to transport molecular segments across the phase boundary to the crystallization surface and ΔF is the free energy of formation of the crystal nuclei of critical size at a specific crystallization temperature.

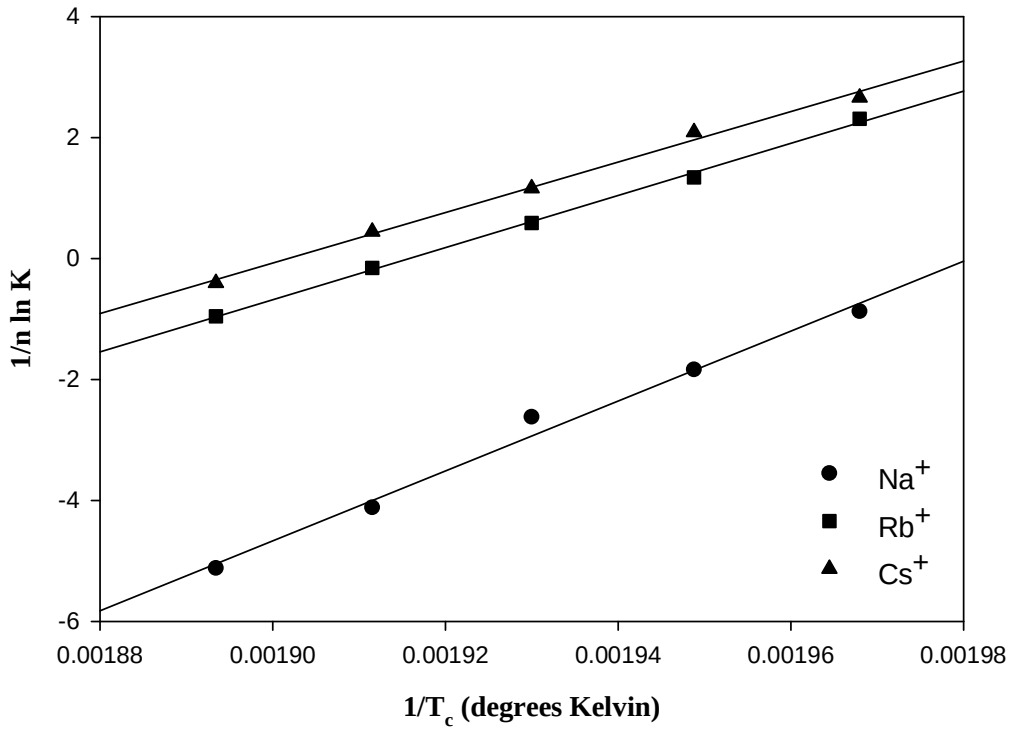

Figure VI-9. Arrhenius plots of 1/n ln K versus $1/T_c$ for SsPS1.0X^+ 5 wt.% OMMT where X = Na^+, Rb^+, and Cs^+.

The activation energy for crystallization to occur within the SsPS ionomer nanocomposites can be determined from the slope of the Arrhenius plots shown in Figure VI-8. The energy of activation for the Na^+, Rb^+, and Cs^+ neutralized SsPS ionomers containing 5 wt.% OMMT is 947, 690, and 656 J/mol, respectively. The activation energy for crystallization to occur for SsPS 5 wt.% OMMT decreases with increasing counterion size. The activation energy for crystallization to occur is lowered due to the increased weakening of the electrostatic network as the size of the neutralizing counterion increases. As the size of the counterion increases, there strength of the electrostatic interaction between the negatively charged sulfonate group and the positively charged alkali metal counterion decreases according the relationship below:

The isothermal crystallization data provided in Figure VI-3 through Figure VI-8 strongly suggests that the size of the neutralizing counterion has a profound effect on the crystallization behavior of the SsPS nanocomposites. Moreover, the neutralizing counterion appears to continue to exert a profound effect on the crystallization behavior of SsPS even in the presence of clay. Based upon our SsPS nanocomposite studies, we have determined that clay disrupts the electrostatic network of the SsPS allowing more rapid crystallization to occur. However, by systematically changing the size of the neutralizing counterion, it can be seen that the electrostatic network may still be present even in the presence of well-exfoliated clay that act as sites for heterogeneous nucleation. The exfoliated clay platelets may disrupt larger ionic aggregates, but the presence of smaller ionomer aggregates or lone ion pairs may still be present. As the size of the neutralizing counterion increases, it is easier to disrupt the electrostatic network because the strength of the dipole-dipole interaction between the negatively charged sulfonate group and the positively charged counterion has decreased in the presence of the clay.

The thermal properties of sPS homopolymer and SsPS ionomer were monitored as function. Figure VI-9 shows a plot after isothermal crystallization at 240 °C for 60 minutes. sPS exhibits a complex polymorphic behavior that is highly dependent upon whether the polymer is thermally crystallized or crystallized from solution. Thermally-induced crystallization leads to the formation of the α or β-crystal forms of sPS. The development of specific sPS polymorphic crystal forms via melt crystallization is affected by the original crystalline form of sPS prior to melting and crystallization, the maximum melting temperature, residence time in the melt, crystallization temperature, and cooling rate from the melt [73]. These factors will determine if the sPS chains crystallize into a mixture of both the α- and β-crystal forms together or if the chains will crystallize into pure α or pure β-crystal forms.

sPS has been shown to exhibit multiple melting endotherms following thermally-induced crystallization. Figure VI-9 shows the melting behavior of sPS after isothermal crystallization at 240 °C for 60 minutes. Three endothermic peaks are present in both the pure sPS and sPS containing 5 wt.% OMMT. The position of the endothermic peaks of sPS did not shift upon adding organically-modified clay to the sPS homopolymer matrix. The low intensity peak located at 245.6 °C is attributed to the formation of small crystals during annealing. In addition to the small endothermic peak at 245.6 °C, both sPS and sPS 5 wt.% OMMT both exhibits two distinct melting events at 259.8 and 269.4 °C. It is not possible to attribute these melting events to a specific crystalline form without detailed WAXD analysis. However, it is known that sPS exhibits contains both the α and β-crystal forms when crystallized at intermediate temperatures between 230 - 260 °C.

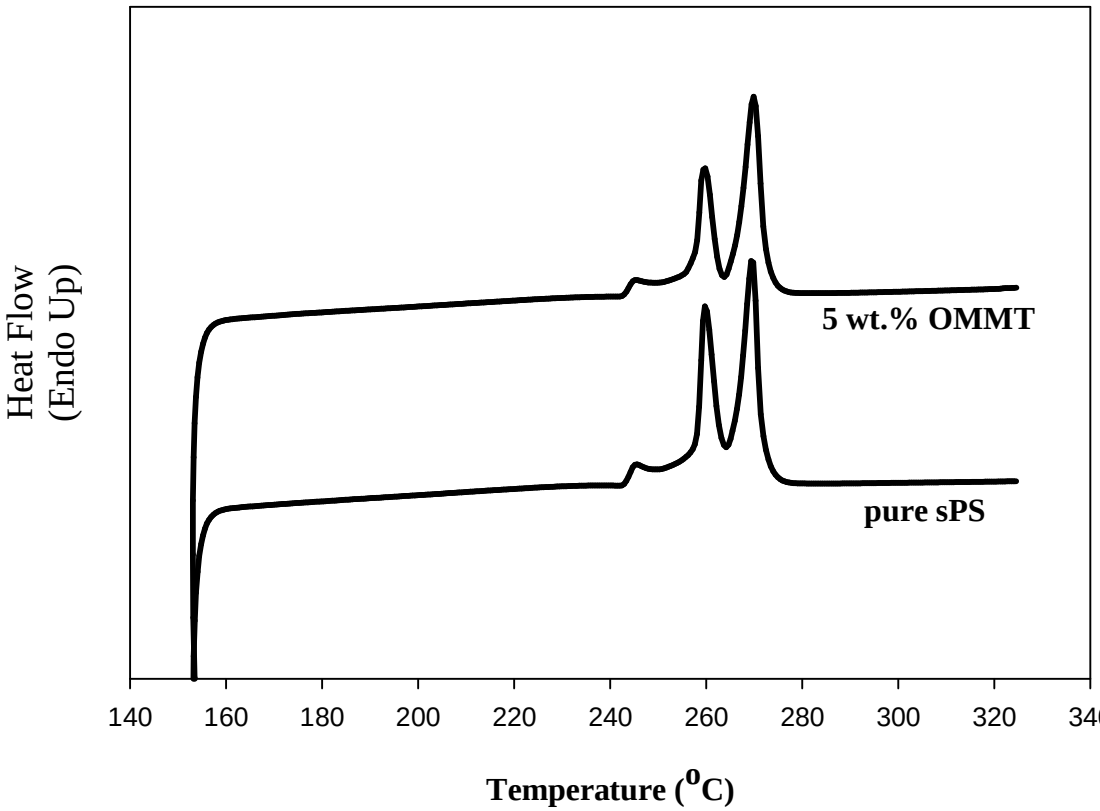

Figure VI-10. Heat flow versus temperature for pure sPS and sPS 5 wt.% OMMT after isothermal crystallization at 240 °C for 60 minutes.

The ΔH_f values for pure sPS and sPS 5 wt.% OMMT after isothermal crystallization at 240 °C for 60 minutes are 31.7 and 32.5 J/g, respectively. The degree of crystallinity for the sPS homopolymer and the sPS clay-containing hybrid was determined using the relationship below. A ΔH^o_f value of 82.6 J/g was used to determine X_c .

$$X_c = \frac{\Delta H_f}{\Delta H_f^o} \, x \, 100 \qquad (6)$$

Based upon these ΔH_f values, the degree of crystallinity for pure sPS and sPS 5 wt.% OMMT are 38.4 and 39.6%, respectively. There is no significant increase in the degree of crystallinity of the sPS homopolymer upon adding the organically-modified clay to the sPS homopolymer matrix. This may suggest that the clay platelets do not act as nucleation agents within the sPS homopolymer matrix. WAXD, TEM, PLM, and SALLS data reported by Benson and Moore show that the organically-modified clay platelets are present within the sPS matrix primarily as micron-size tactoids and therefore do not act as nucleation agents [17].

The melting behavior of SsPS1.0Cs^+ without organically-modified clay and SsPS1.0X^+ 5 wt.% OMMT where $X^+ = Na^+$, Rb^+, and Cs^+ after isothermal crystallization at 240 °C is shown in Figure VI-10. There is one primary melting peak at 262 °C in pure SsPS1.0Cs^+ and each of the clay containing ionomers with different neutralizing counterion. This primary melting at 262 °C cannot be attributed to a particular crystal form without in-depth WAXD/FTIR analysis. However, it can be seen that the breadth of the peak increases with increasing counterion size for the clay containing SsPS ionomers without any change in the position of the melting peak. An increase in the breadth of the melting peak suggests that there is an increase in the distribution of sizes of crystallites that melt near 262 °C. It may also be that the crystallites located that are melting at 262 °C are the same crystalline polymorph. There are also small shoulders present within the SsSP1.0X^+ 5 wt.% OMMT nanocomposites. These shoulders may be due to the development of small crystallites that developed during the isothermal crystallization process or the small melting endothermic peaks present as small shoulder in the DSC thermogram may represent the melting of different crystalline forms. Further structural investigation via WAXD, SAXS, and FTIR are required to identify the polymorphic structures developed during the melt crystallization of pure and clay-containing SsPS ionomers.

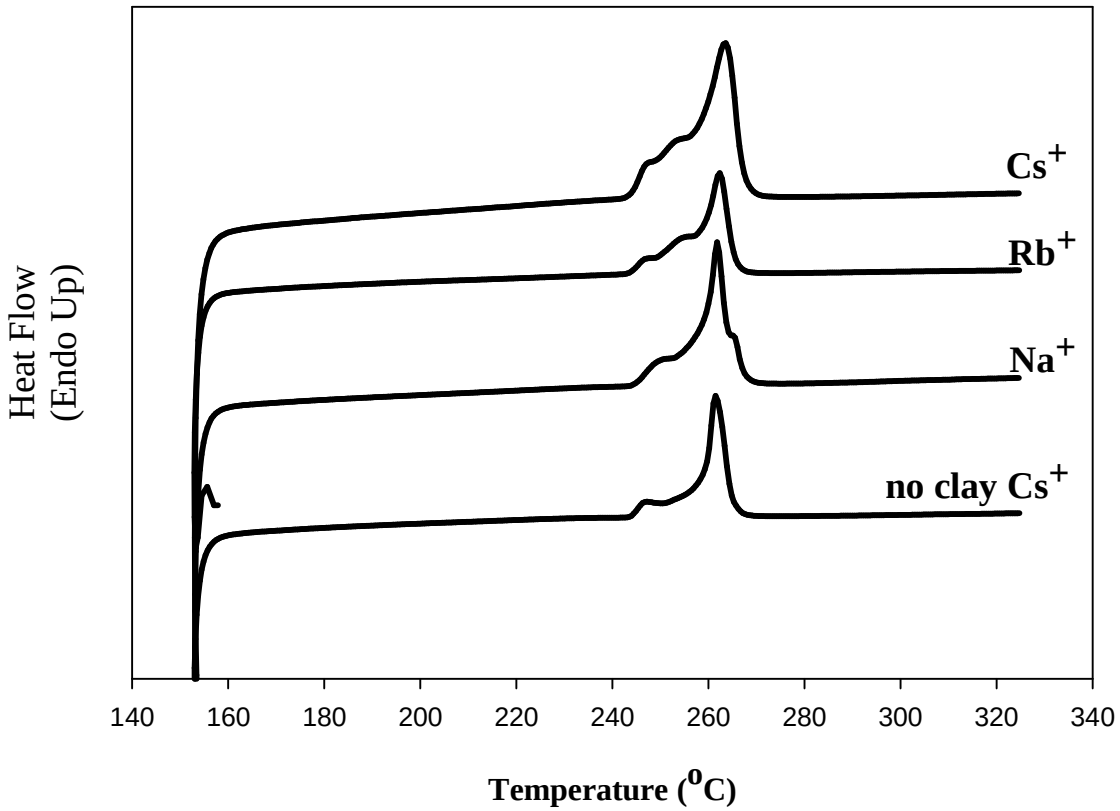

Figure VI-11. Heat flow versus temperature after isothermal crystallization at 240 °C for 60 minutes of SsPS1.0X^+ 5 wt.% OMMT where X^+ = Na^+, Rb^+, or Cs^+. Pristine SsPS1.0Cs^+ without clay is included for comparison.

3.5 SsPS Nanocomposite Supramolecular Structure via Polarized Light Microscopy

The supramolecular crystalline structure of the SsPS1.0X^+ 5 wt.% OMMT nanocomposites was evaluated using polarized light microscopy. The volume-filled morphology of SsPS1.0X^+ OMMT samples isothermally crystallized at 240 °C is shown in Figure VI-9. Due to the high nucleation density and small size of the spherulites, it is difficult to observe fine texture of the crystalline suprastructures of these materials. However, it is clear that the overall spherulitic texture of the SsPS nanocomposites becomes finer as the size of the neutralizing counterion increases from 1.02, 1.52, to 1.67 Å for Na^+, Rb^+, Cs^+, respectively.

In order to gain further insight into the crystalline suprastructure of the SsPS nanocomposites neutralized with different counterions, Fast Fourier Transform (FFT) was completed on phase contrast microscopy (PCM) images. The FFT images obtained from the treatment of the PCM digital photographs are shown in Figure VI-10. The histograms of the FFT images are provided in Figure VI-11. It can be seen that as the size of the counterion increases that there is a shift in the frequency of entities detected in the FFT images. The count at each frequency maximum also increases as the size of the neutralizing counterion increases as well. This data suggest that the number of crystalline entities detected via FFT of SsPS nanocomposite PCM images increases as the size of the neutralizing counterion increases. The increase in the frequency of crystalline entities detected indicates that the nucleation density within the SsPS1.0X^+ nanocomposites increases as the size of the neutralizing counterion increases from Na^+, Rb^+ to Cs^+.

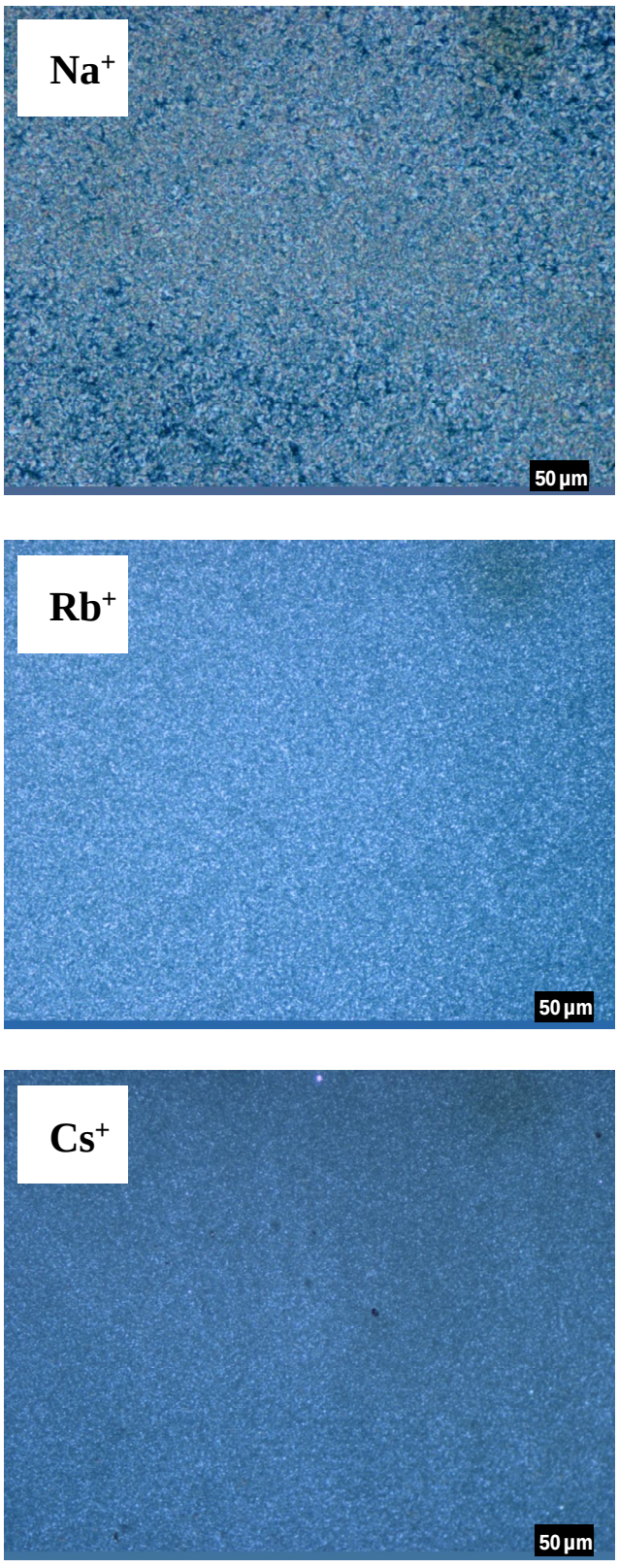

Figure VI-12. PLM images SsPS1.0X^{+} 5 wt.% OMMT nanocomposites where X = Na^{+}, Rb^{+}, and Cs^{+}.

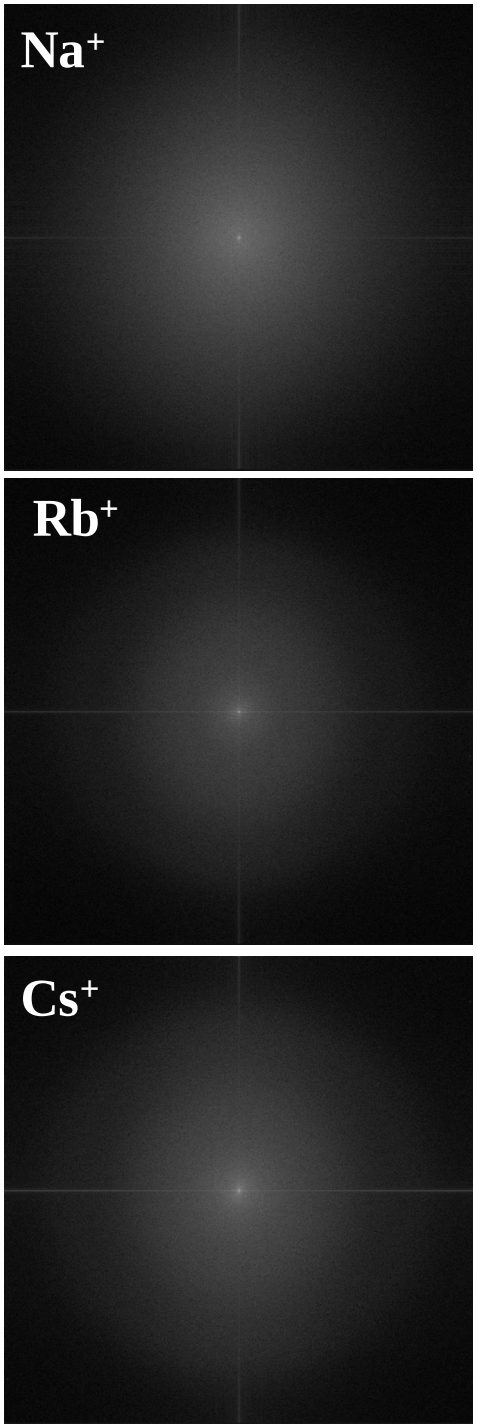

Figure VI-13. FFT of SsPS1.0X$^+$ 5 wt.% OMMT nanocomposite PLM images obtained after isothermal crystallization at 240 °C where X = Na^+, Rb^+, and Cs^+ .

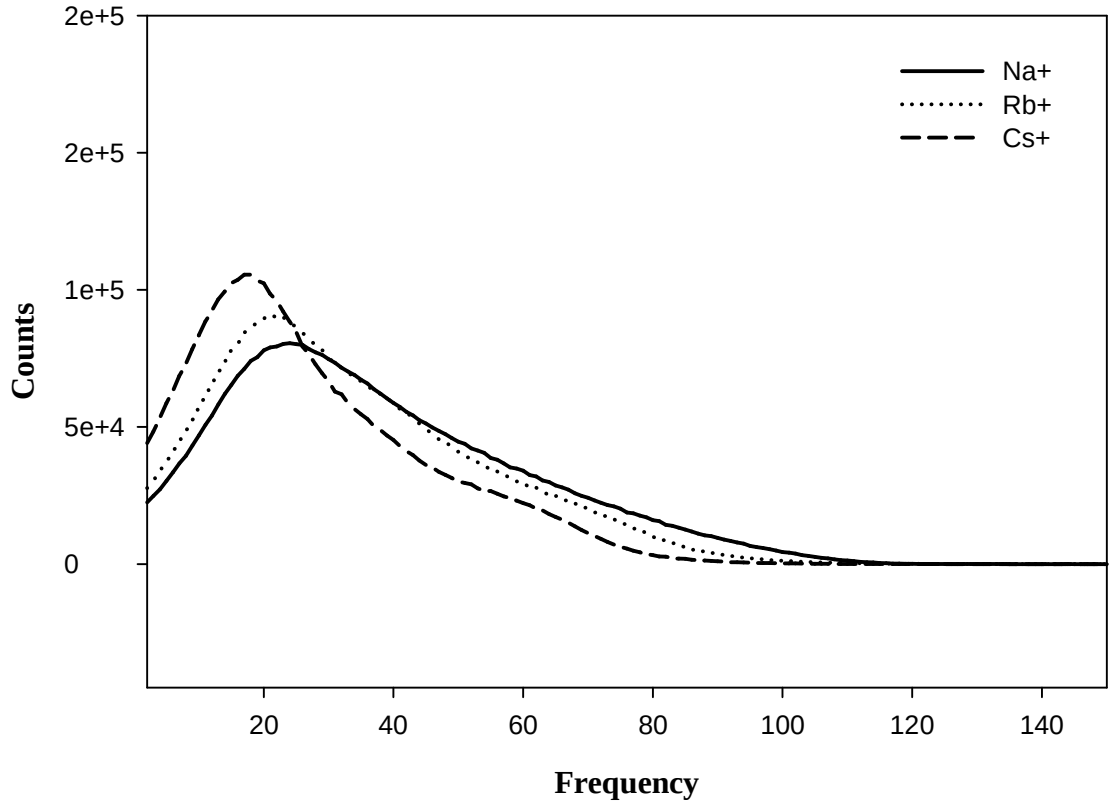

Figure VI-14. FFT histograms of SsPS1.0X$^+$ 5 wt.% OMMT nanocomposite PLM images obtained after isothermal crystallization at 240 °C where X = Na^+, Rb^+, and Cs^+ .

3.4 SsPS Nanocomposite Supramolecular Structure via Small Angle Laser Light Scattering

Polarized light microscopy is a useful tool to observe the crystalline suprastructure of the SsPS nanocomposites on a local level. It can be used to view the structural nature of the crystallites, the size of micron-sized crystalline structure, and the nucleation density of crystallites present. However, it is difficult to use PLM microscopy to determine the size and nucleation density of the crystalline structures when the dimensions of the crystalline entities are smaller than ten microns. Therefore, SALLS was used to determine the average size of the spherulites.

$$2\pi \frac{D}{\lambda} \sin\frac{\theta}{2} = 4.1 \quad (6)$$

The nucleation density of crystalline structures of SsPS1.0X$^+$ 5 wt.% OMMT nanocomposites. The equation provided below was used to determine the nucleation density of the SsPS nanocomposites

$$N = \left(\frac{3}{4}\pi\right)\left(\frac{D_m}{2}\right)^{-3} \quad (7)$$

Figure VI-12 shows the SALLS patterns of volume-filled SsPS1.0X$^+$ OMMT after isothermal crystallization at 240 °C. Using equation 6 the size of the spherulites for SsPS SsPS1.0Na$^+$ 5 wt.% OMMT and SsPS1.0Rb$^+$ 5 wt.% OMMT was 39.3 and 29.2 μm, respectively. The size of the spherulites for the SsPS1.0Cs$^+$ 5 wt.% OMMT were too small to be detected using SALLS at the sample-to-detector distance of 381 mm used to obtain the SALLS patterns of the SsPS1.0Na$^+$ 5 wt.% OMMT and SsPS1.0Rb$^+$ 5 wt.% OMMT nanocomposites. The SALLS pattern of the SsPS1.0Cs$^+$ 3 wt.% OMMT nanocomposites is provided for reference at the same sample-to-detector distance of 381 mm used to obtain the sodium and rubidium neutralized nanocomposites. The average spherulite size for the SsPS1.0Cs$^+$ 3 wt.% OMMT nanocomposite is 38.0 μm. Based upon this measurement, it can be expected that the size of the SsPS1.0Cs$^+$ 5 wt.% OMMT is smaller than 38.0 μm due to the higher clay content which may provide a higher number of nucleation sites. The nucleation densities of the SsPS1.0Na$^+$ 5 wt.% OMMT, SsPS1.0Rb$^+$ 5 wt.% OMMT, and SsPS1.0Cs$^+$ 3 wt.% OMMT are 3.1 x 10^{-4} μm^{-3}, 7.6 x 10^{-4} μm$^-$3, and 3.4 x 10^{-4} μm^{-3}, respectively. It is interesting to note that the nucleation density differs by an order of magnitude between the SsPS nanocomposites containing 3 wt.% and 5 wt.% organically-modified clay.

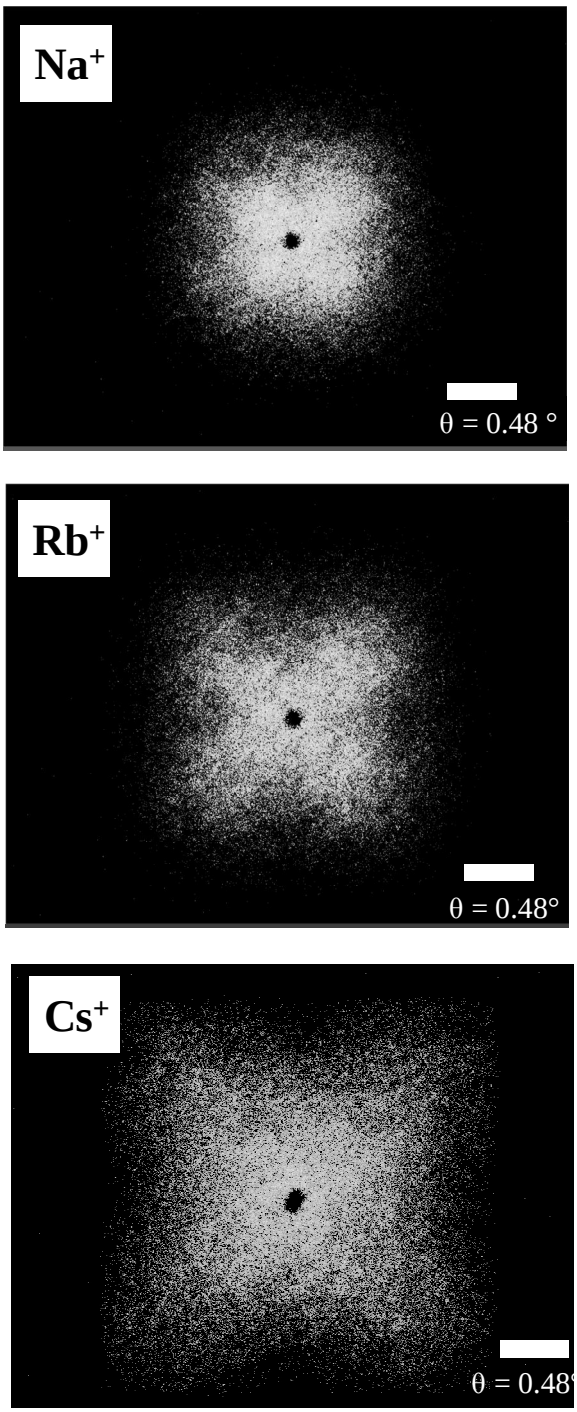

Figure VI-15. SALLS patterns of SsPS1.0Na^+ 5 wt.% OMMT, SsPS1. 0Rb^+ 5 wt.% OMMT, and SsPS1.0Cs^+ 3 wt.% OMMT nanocomposites isothermally crystallized at 240 °C until volume-filled.

CONCLUSION

WAXD and TEM micrographs reveal that the organically-modified clay platelets are present within the SsPS ionomer matrix in an exfoliated manner regardless of the counterion size. Therefore, it appears that a low ionic content and 5 wt.% OMMT, that the size of the alkali metal counterion does not have a prominent effect on the degree of exfoliation of the clay platelets. It can be inferred based upon this observation that the presence of the sulfonate groups has the more prominent effect on the degree of dispersion of the clay platelets within the polymer matrix. PLM microscopy shows the very small birefringent crystalline suprastructures observed within the SsPS nanocomposites. Although the crystalline suprastructures were too small to be measured using PLM microscopy, SALLS was used to determine the average size of the spherulites. It was found that size of the spherulites of the SsPS ionomer nanocomposites decreased with increasing counterion size due to an increase in the nucleation density. The size of the neutralizing counterion has a dramatic effect on the crystallization behavior of lightly sulfonated SsPS containing 5 wt.% of organically-modified clay. As the size of the alkali metal counterion increases in atomic radius from the small Na^+ to the larger Cs^+, the rate of crystallization increases.

REFERENCES

1. Godovsky D. Device Applications of Polymer-Nanocomposites. Biopolymers · PVA Hydrogels, Anionic Polymerisation Nanocomposites, vol. 153: Springer Berlin / Heidelberg, 2000. pp. 163-205.
2. Alexandre M and Dubois P. Materials Science and Engineering: R: Reports 2000;28(1-2):1-63.
3. Fischer H. Materials Science and Engineering: C 2003;23(6-8):763-772.
4. Avella M, De Vlieger JJ, Errico ME, Fischer S, Vacca P, and Volpe MG. Food Chemistry 2005;93(3):467-474.
5. Fei Fang F, Jin Choi H, and Joo J. Journal of Nanoscience and Nanotechnology 2008;8:1559-1581.
6. Usuki A, Hasegawa N, Kato M, and Kobayashi S. Polymer-Clay Nanocomposites. Inorganic Polymeric Nanocomposites and Membranes, vol. 179: Springer Berlin / Heidelberg, 2005. pp. 135-195.
7. Garcés JM, Moll DJ, Bicerano J, Fibiger R, and McLeod DG. Advanced Materials 2000;12(23):1835-1839.
8. Ahmadi SJ, Huang YD, and Li W. Journal of Materials Science 2004;39(6):1919-1925.
9. Okada A and Usuki A. Macromolecular Materials and Engineering 2006;291(12):1449-1476.
10. Aranda P, Darder M, Fernández-Saavedra R, López-Blanco M, and Ruiz-Hitzky E. Thin Solid Films 2006;495(1-2):104-112.

11. Uyama H, Kuwabara M, Tsujimoto T, Nakano M, Usuki A, and Kobayashi S. Chemistry of Materials 2003;15(13):2492-2494.

12. Paquette JW, Kim KJ, Nam J-D, and Tak YS. Journal of Intelligent Material Systems and Structures 2003;14(10):633-642.

13. Njuguna J and Pielichowski K. Advanced Engineering Materials 2004;6(4):193-203.

14. Chisholm BJ, Moore RB, Barber G, Khouri F, Hempstead A, Larsen M, Olson E, Kelley J, Balch G, and Caraher J. Macromolecules 2002;35(14):5508-5516.

15. Lee JA, Kontopoulou M, and Parent JS. Polymer 2005;46(14):5040-5049.

16. Barber GD, Calhoun BH, and Moore RB. Polymer 2005;46(17):6706-6714.

17. Benson SD and Moore RB. Polymer 2010;51(23):5462-5472.

18. Filippi S, Marazzato C, Magagnini P, Minkova L, Dintcheva NT, and La Mantia FP. Macromolecular Materials and Engineering 2006;291(10):1208-1225.

19. Li Y, Ma J, Wang Y, and Liang B. Journal of Applied Polymer Science 2005;98(3):1150-1156.

20. Yoo Y, Shah RK, and Paul DR. Polymer 2007;48(16):4867-4873.

21. Nguyen VK and Yoo Y. Sensors and Actuators B: Chemical 2007;123(1):183-190.

22. Peneva Y, Tashev E, and Minkova L. European Polymer Journal 2006;42(10):2228-2235.

23. Govindaiah P, Mallikarjuna SR, and Ramesh C. Macromolecules 2006;39(21):7199-7203.

24. Shah RK, Krishnaswamy RK, Takahashi S, and Paul DR. Polymer 2006;47(17):6187-6201.

25. Bhiwankar NN and Weiss RA. Polymer 2006;47(19):6684-6691.

26. Vidotti SE, Chinellato AC, Hu G-H, and Pessan LA. Journal of Polymer Science Part B: Polymer Physics 2007;45(22):3084-3091.

27. Artzi N, Nir Y, Narkis M, and Siegmann A. Polymer Composites 2003;24(5):627-639.

28. Ammala A, Bell C, and Dean K. Composites Science and Technology 2008;68(6):1328-1337.

29. Marazzato C, Peneva Y, Lefterova E, Filippi S, and Minkova L. Polymer Testing 2007;26(4):526-536.

30. Lee JA, Kontopoulou M, and Parent JS. Macromolecular Rapid Communications 2007;28(2):210-214.

31. Liu H, Tag Lim H, Hyun Ahn K, and Jong Lee S. Journal of Applied Polymer Science 2007;104(6):4024-4034.

32. Lee HS, Fishman D, Kim B, and Weiss RA. Polymer 2004;45(23):7807-7811.

33. Hara M, Jar P, and Sauer JA. Macromolecules 1990;23(20):4465-4469.

34. Hara M, Wu J, and Lee AH. Macromolecules 1989;22(2):754-757.

35. Tsujita Y, Yasuda M, Takei M, Kinoshita T, Takizawa A, and Yoshimizu H. Macromolecules 2001;34(7):2220-2224.

36. Kim J-S and Eisenberg A. Journal of Polymer Science Part B: Polymer Physics 1995;33(2):197-209.

37. Tachino H, Hara H, Hirasawa E, Kutsumizu S, Tadano K, and Yano S. Macromolecules 1993;26(4):752-757.

38. Kirkmeyer BP, Weiss RA, and Winey KI. Journal of Polymer Science Part B: Polymer Physics 2001;39(5):477-483.

39. Hirasawa E, Yamamoto Y, Tadano K, and Yano S. Macromolecules 1989;22(6):2776-2780.

40. Orler EB and Moore RB. Macromolecules 1994;27(17):4774-4780.

41. Register RA, Foucart M, Jerome R, Ding YS, and Cooper SL. Macromolecules 1988;21(4):1009-1015.

42. Moore RB, Cable KM, and Croley TL. Journal of Membrane Science 1992;75(1-2):7-14.

43. Hourston DJ, Williams GD, Satguru R, Padget JC, and Pears D. Journal of Applied Polymer Science 1999;74(3):556-566.

44. Cable KM, Mauritz KA, and Moore RB. Journal of Polymer Science Part B: Polymer Physics 1995;33(7):1065-1072.

45. Visser SA and Cooper SL. Polymer 1992;33(5):920-929.

46. Li C, Register RA, and Cooper SL. Polymer 1989;30(7):1227-1233.

47. Fan X-D and Bazuin CG. Macromolecules 1995;28(24):8209-8215.

48. Cui L, Troeltzsch C, Yoon PJ, and Paul DR. Macromolecules 2009;42(7):2599-2608.

49. Shah RK and Paul DR. Macromolecules 2006;39(9):3327-3336.

50. Ghosh AK and Woo EM. Polymer 2004;45(14):4749-4759.

51. Robello DR, Yamaguchi N, Blanton T, and Barnes C. Journal of the American Chemical Society 2004;126(26):8118-8119.

52. Ryu JG, Kim H, and Lee JW. Polymer Engineering and Science 2004;44(7):1198-1204.

53. Sorrentino A, Pantani R, and Brucato V. Polymer Engineering & Science 2006;46(12):1768-1777.

54. Chen K, Wilkie CA, and Vyazovkin S. The Journal of Physical Chemistry B 2007;111(44):12685-12692.

55. Orler EB, Yontz DJ, and Moore RB. Macromolecules 1993;26(19):5157-5160.

56. Orler EB. The Influence of Electrostatic Interactions on the Crystallization of Sulfonated Syndiotactic Polystyrene Ionomers. Department of Polymer Science, vol. Doctoral. Hattiesburg: University of Southern Mississippi, 1996.

57. LeBaron PC, Wang Z, and Pinnavaia TJ. Applied Clay Science 1999;15(1-2):11-29.

58. Sinha Ray S and Okamoto M. Progress in Polymer Science 2003;28(11):1539-1641.

59. Shen Z, Simon GP, and Cheng Y-B. Polymer 2002;43(15):4251-4260.

60. Stein RS and Rhodes MB. Journal of Applied Physics 1960;31(11):1873-1884.

61. Avrami M. The Journal of Chemical Physics 1939;7(12):1103-1112.

62. Avrami M. The Journal of Chemical Physics 1940;8(2):212-224.

63. Avrami M. The Journal of Chemical Physics 1941;9(2):177-184.

64. Long Y, Shanks RA, and Stachurski ZH. Progress in Polymer Science 1995;20(4):651-701.

65. Penning JP and St. John Manley R. Macromolecules 1996;29(1):77-83.

66. Ke Y, Long C, and Qi Z. Journal of Applied Polymer Science 1999;71(7):1139-1146.

67. Ma J, Zhang S, Qi Z, Li G, and Hu Y. Journal of Applied Polymer Science 2002;83(9):1978-1985.

68. Yu J and He J. Polymer 2000;41(3):891-898.

69. Lu XF and Hay JN. Polymer 2001;42(23):9423-9431.

70. Loo Y-L, Register RA, Ryan AJ, and Dee GT. Macromolecules 2001;34(26):8968-8977.

71. Grady BP, Pompeo F, Shambaugh RL, and Resasco DE. The Journal of Physical Chemistry B 2002;106(23):5852-5858.

72. Fornes TD and Paul DR. Polymer 2003;44(14):3945-3961.

73. Woo EM, Sun YS, and Yang CP. Progress in Polymer Science 2001;26(6):945-983.

CHAPTER VII

NON-RANDOM SULFONATION OF SYNDIOTACTIC POLYSTYRENE: A FACILE ROUTE TO CONTROLLED IONOMER ARCHITECTURE VIA POST-POLYMERIZATION MODIFICATION

ABSTRACT

Sulfonated syndiotactic polystyrene (SsPS) ionomers were produced using two different post-polymerization modification techniques to create random and non-random ionomer architectures. The thermal properties and crystallization behavior of the two different SsPS ionomers containing 3 and 9 mol% sulfonic acid groups were investigated using differential scanning calorimetry (DSC). The morphologies of the random and non-random SsPS ionomers were probed using Small-angle X-ray scattering (SAXS). The higher melting point and faster crystallization rate of the non-random SsPS compared to the random SsPS ionomer containing the same ion content indicates the architectures of the two materials are different. SAXS patterns confirm the architectural differences between the randomly and non-randomly sulfonated SsPS and allows the construction of a morphological model that attributes the difference in the thermal properties and crystallization behavior of the non-random SsPS ionomers as compared to random SsPS ionomers to the presence of ionic aggregates that are well-separated from the crystalline component.

INTRODUCTION

Ionomers are polymers that contain less than 15 mol% of ionic content incorporated into a hydrophobic polymer backbone through copolymerization or post-polymerization modification of a homopolymer [1-3]. Due to the interesting properties of these materials great attention has been given to understanding the effect of ionic content on the thermal, mechanical, solution, and morphological properties of these materials.

Sulfonated atatic polystyrene has been one of the most widely studied ionomers. Numerous studies have been done on the thermal [4-11], mechanical [12-17], solution [18-25], and morphological [26-38] properties of SaPS. SaPS ionomers have been prepared via copolymerization of styrene with sodium styrene sulfonate and by post polymerization modification of preformed PS homopolymer. Weiss and coworkers conducted studies that compared the properties of SaPS prepared via emulsion copolymerization and post polymerization modification [39-40]. They attributed differences in the thermal and solution properties of SaPS prepared by these two methods to differences in the distribution of sulfonate groups along the hydrocarbon backbone. Based upon differences in the glass transitions of the materials, Weiss and coworkers suggested that copolymerization of styrene and sodium styrene sulfonate resulted in the incorporation of the sulfonated comonomer as blocks of sulfonate groups along the polymer backbone rather than a random placement of the sulfonate groups along the polymer backbone for the SaPS ionomer prepared by post polymerization modification.

Although SaPS, an amorphous ionomer, has been studied in great detail, many of the industrially important ionomers such as Nafion® and Surlyn® are semicrystalline in nature and

the morphologies of semicrystalline ionomers are complex three-phase systems made up of an ion rich phase, crystalline domains, and an amorphous hydrocarbon phase. It is likely that the process of ionic aggregation influences the crystallization process of these semicrystalline ionomers as one polymer chain may traverse all three phases of the semicrystalline ionomer.

Although Nafion® and Surlyn® are used many technological applications, it is difficult to study the link between ionic aggregation and crystallization in these systems because the molecular weight distribution of these ionomers may change considerably with ion content as these ionomers are produced through copolymerization methods. It is also difficult to use Nafion® and Surlyn® to study the link between ionic aggregation and crystallization because of the low degree of crystallinity of these ionomers that is also difficult to quantify especially in the case of Nafion®.

Orler and coworkers utilized sulfonated syndiotactic polystyrene as a model semicrystalline ionomer [41-44] to study the link between ionic aggregation and crystallization. Orler successfully sulfonated syndiotactic polystyrene by modifying a mild post-polymerization sulfonation procedure developed by Makowski to sulfonate aPS [45]. This sulfonation procedure maintains the molecular weight distribution and microstructure of the homopolymer while introducing ionic functionality to the nonpolar sPS homopolymer. Therefore, Orler and coworkers were able to conducte a systematic study of the effect of ion content [42], neutralizing counterion [41, 43], and the effect of plasticizers [44] on the crystallization behavior of SsPS.

It was found that incorporation of as little as 2 mol% of sulfonate groups onto sPS significantly decreased the ability of SsPS to crystallize in the ionized form. Such a pronounced decrease in the ability of the polymer to crystallize at low ion contents may be a challenge in utilizing SsPS in applications where high ion content and high degree of crystallinity are desired

membrane properties. For example, a proton exchange membrane for fuel cell applications requires high ion content for the transport of water and ions through the membrane [46-49]. A proton exchange membrane must also possess mechanical stability to withstand harsh fuel cell operation conditions and low solvent swelling behavior [50]. The mechanical integrity necessary for operation in harsh environments such as elevated temperature with low swelling may be derived from a membrane containing a substantial crystalline component [51]. Consequently, it would be desirable to produce a semicrystalline ionomer with a degree of sulfonation required to successfully conduct protons and a high degree of crystallinity to provide mechanical stability [52]. Crystallinity has been linked to improved barrier properties and decreased membrane swelling in the presence of solvents [53]. Crystalline domains have also been proposed to act as physical crosslinks that enhance mechanical properties [54].

We have utilized a post-polymerization method to sulfonate syndiotactic polystyrene to yield a non-random, blocky distribution of the sulfonate groups along the homopolymer backbone. The method is based upon conducting the sulfonation process while sPS in the physical gel state. The sPS gel consists of both amorphous and crystalline domains. The sulfonating reagent is excluded from the crystalline domains and only penetrates the amorphous regions thereby maintaining long sequences of unsulfonated sPS homopolymer. Borriello and coworkers conducted sorption and diffusivity studies of SsPS prepared via post-polymerization of the sPS homopolymer in the solid state [55]. They proposed that a uniform sulfonation of the phenyl rings of the amorphous phase is obtained when the sulfonation of sPS in performed in the solid state while the crystalline phase of the sPS homopolymer is not sulfonated. Our current study is focused on comparing the thermal properties and crystallization behavior sPS sulfonated in the physical gel state to sPS sulfonated while in a homogeneous solution state to understand the

effect of ionomer architecture (the placement of sulfonate groups) on the thermal properties of SsPS ionomers.

EXPERIMENTAL

Materials

Syndiotactic polystyrene (Questra 102) MW of 310,000 g/mol was donated by the Dow Chemical Company. Reagent grade 1,2,4-trichlorobenze (TCB), methanol, sulfuric acid, potassium monopthalate were obtained from Fisher Scientific. Hexanoic anhydride, benzyltrimethylammoniuim hydroxide, and benzoic acid were received from Sigma Aldrich.

Preparation of Sulfonation Agent

The sulfonation agent was prepared according to previously published procedures using TCB as the solvent. TCB (25 mL) was added to a 50 mL volumetric flask containing 0.03 moles of hexanoic anhydride. The TCB/hexanoic anhydride solution was cooled in an ice bath for 1 hour, and then 1 mL of concentrated sulfuric acid was added to the chilled solution and shaken vigorously. Additional TCB was added to the volumetric flask to the 50 mL mark.

Random Sulfonation of Syndiotactic Polystyrene

sPS was dissolved in TCB under reflux for 1.5 h to yield a 10% w/v solution. After 1.5 h, the solution was cooled to 70 °C and then additional TCB was added to yield a 1% w/v sPS solution. The sPS solution was allowed to equilibrate at 70 °C under a nitrogen purge for 1.5 hr. After equilibration, the appropriate amount of sulfonating reagent was added and the reaction was allowed to proceed for 1 hour at 70 °C under a nitrogen purge. After 1 h, 10 mL methanol was

added to the solution to terminate the reaction. The solution was poured into a large excess of methanol to precipitate the ionomer. The precipitated ionomer was filtered and washed with deionized water.

Non-Random Sulfonation of Syndiotactic Polystyrene

Syndiotactic polystyrene was dissolved in TCB under reflux for 1.5 h to yield a 10% w/v solution. After 1.5 h, the solution was cooled to room temperature. Upon cooling, the 10% w/v sPS solution and allowed to remain at room temperature for 24 hours. Upon, the sPS solution crystallizes and forms a physical gel. The solid gel was manually broken in small, micron particles using a spatula. The sPS gel particles were resuspended in additional TCB to yield a 1% w/v sPS solution. The sPS gel-particle dispersion was allowed to equilibrate at 70 °C under a nitrogen purge for 1.5 hr. After equilibration, the appropriate amount of sulfonating reagent was added and the reaction was allowed to proceed for 1 hour at 70 °C under a nitrogen purge. After 1 h, 10 mL methanol was added to the dispersion to terminate the reaction. The dispersion was poured into a large excess of methanol. The SsPS ionomer particles were filtered and washed with deionized water. The resulting ionomer was dried under vacuum at 100 °C for 12 h.

Determination of Degree of Sulfonation

The randomly and non-randomly sulfonated SsPS ionomers were redissolved in 90/10 v/v TCB/methanol for 1.5 h to a yield 0.5% w/v solution. The 0.5% w/v solution was used to determine the degree of sulfonation via non aqueous titration with methanolic benzyltrimethylammonium hydroxide. The benzyltrimethylammonium hydroxide was standardized using benzoic acid. SsPS ionomers of low ion content and high ion content were

prepared. Low ion content SsPS ionomers containing 3.2 mol% sulfonate groups are identified as SsPS3.2H^+R and SsPS3.2H^+NR where the H^+ denotes the ionomers are in the acid-form. The R and NR nomenclature denotes the SsPS random and the SsPS non-random ionomer respectively.

Neutralization of Sulfonated Syndiotactic Polystyrene

The SsPS ionomer was completely neutralized using 0.1 M methanolic sodium hydroxide. The SsPS was dissolved in chloroform using a PARR pressure reactor at 100 °C for 1.5 h. The appropriate amount of 0.1 M NaOH was added to the SsPS solution to obtain a fully neutralized ionomer. The fully neutralized SsPS 1.0 mol% ionomer was used as the ionomer matrix within this study and will be identified as SsPS.

Differential Scanning Calorimetry

Thermal behavior and crystallization kinetics of the SsPS ionomers were studied using differential scanning calorimetry (DSC). A TA Instruments Q2000 DSC was used to probe the thermal behavior of the SsPS ionomers. Samples were prepared by thermally pressing each ionomer at 200 °C at 3000 psi for 3 min using a Carver Laboratory Press. The SsPS ionomers films were allowed to cool to RT under ambient conditions after removal from the press. Samples from the thermally pressed films were die cut and placed within aluminum DSC pans. The weight for each sample was maintained between 6 – 8 mg.

DSC analysis was performed under a continuous nitrogen flow to minimize sample degradation. The samples were heated to 330 °C at 20 °C/min from 50 °C and held at that maximum temperature for 5 min to erase previous thermal history and the presence of any persistent nuclei. Samples were then rapidly quench to 50 °C at -100 °C/min and then heated to

330 °C at 20 °C/min. The glass transition, crystallization temperature, and melting temperatures of the SsPS3.2H^+R and SsPS3.2H^+NR ionomers were determined from the second DSC scan after erasing the thermal history using TA Instruments Universal Analysis Software. Isothermal crystallization was carried out at 220, 225, 230, and 235 °C for 60 min for the low ion content SsPS ionomers. TA Instruments Universal Analysis software was used to analyze the resulting DSC traces. The $t_{½}$, the time at which 50% of the material has crystallized, was obtained from isothermal holds at various temperatures and used as a measure of changes in the crystallization behavior of the randomly sulfonated non-randomly sulfonated SsPS ionomers. High ion content SsPS ionomers were heated from 50 °C to 330 °C at 20 °C/min and held at 330 °C for 5 min. The ionomers were rapidly cooled to 200 °C at -100 °C/min and held at 200 °C for 2 hr. After isothermal crystallization at 200 °C, the sample was cooled to 150 °C at -100 °C/min and then heated to 330 °C at 20 °C/min. The thermal transitions of the high ion content ionomers were evaluated from the DSC heating scan post isothermal crystallization.

RESULTS AND DISCUSSION

The strategy for producing a non-random ionomer SsPS architecture is depicted in Figure VII-1.

A homogenous solution of sPS will crystallize upon cooling the solution from elevated temperature to room temperature. Over time the number and size of the crystalline domains increase until a physical gel is formed from the initial homogenous solution. Physical gelation of the polymer chains occurs as the chains organize and pack into crystalline structure. The presence of the crystalline domains that form the gel provide a means by which to preserve the sequences of unsulfonated material when the sulfonation process is conducted while sPS is in the physical gel state. When conducting the sulfonation process while sPS in the gel state, the

sulfonation reagent represent by the red circles in Figure VII-1 is not able to penetrate the crystalline regions. The sulfonation reagent can only penetrate the amorphous region leaving long sequences of unsulfonated sPS homopolymer. In contrast, it can be seen in Figure VII-1 that conducting the sulfonation process while sPS is a homogenous solution leads to a random placement of sulfonate groups along the polymer backbone with comparatively shorter sequences of unsulfonated material. The aforementioned method of sulfonating sPS while in the physical gel state provides a very simple post-polymerization modification approach to creating a pseudo-blocky, non-random placement of sulfonate groups along the polymer backbone. The thermal properties, crystallization behavior, and morphologies of these materials are investigated to elucidate the effect of these sulfonation methods on ionomer architecture and properties.

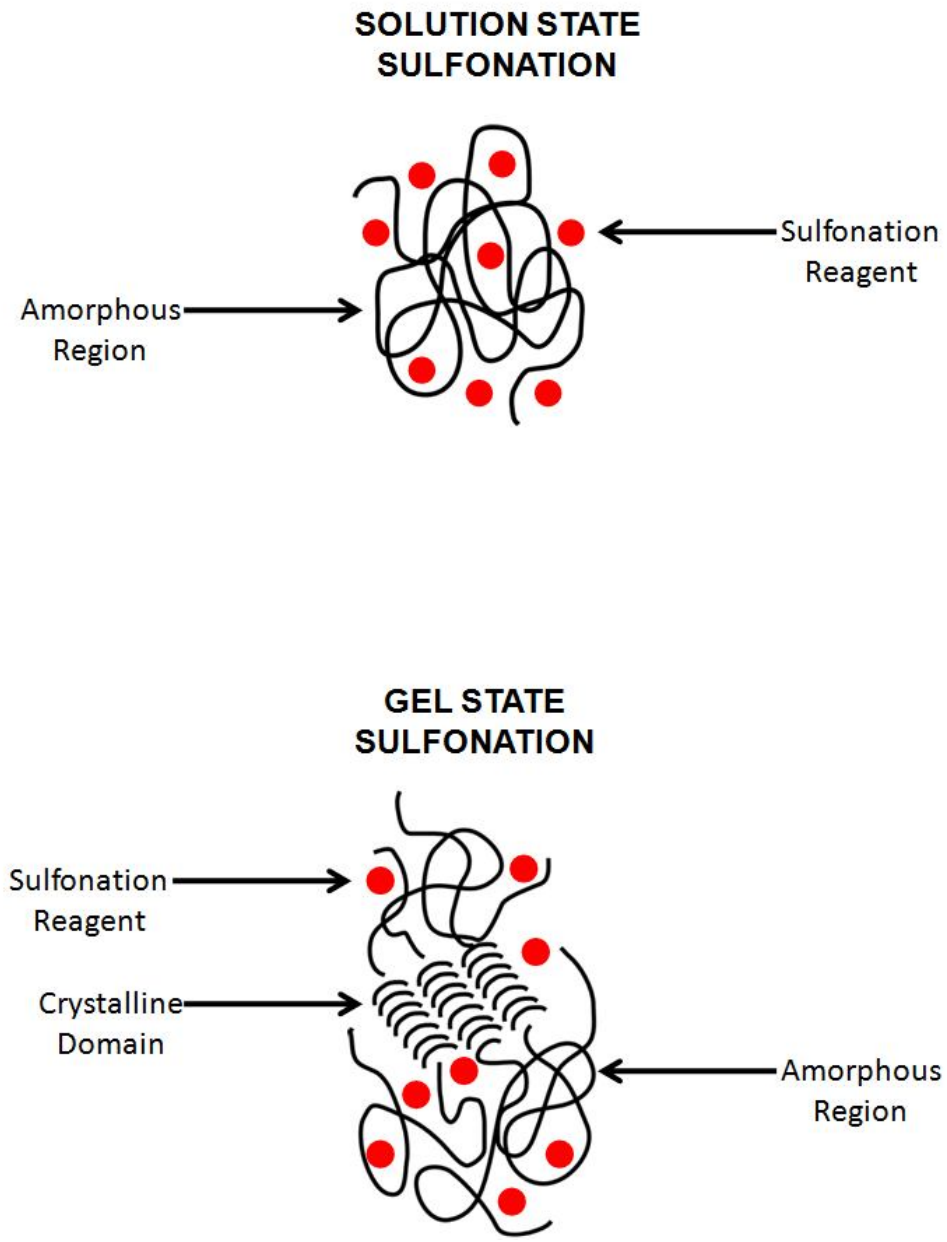

Figure VII-1. Diagram of solution state and gel state sulfonation post-polymerization methods.

The thermal behavior of low ion content SsPS ionomers is shown in Figure VII-2 which provides the DSC thermogram of relative heat flow versus temperature for SsPS3.2H^+R, SsPS3.2H^+NR, and the sPS homopolymer.

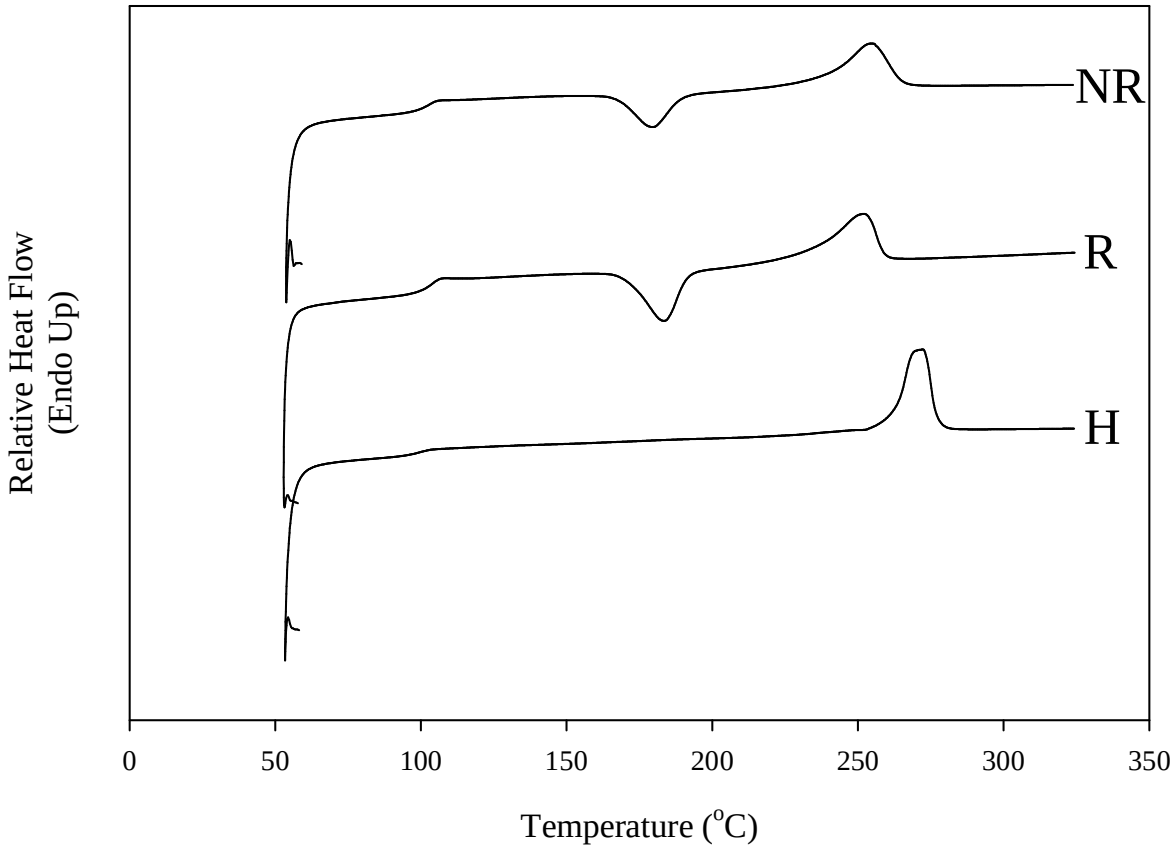

Figure VII-2. Relative heat flow versus temperature of sPS homopolymer (H), SsPS3.2H$^+$R (R), and SsPS3.2H$^+$NR (NR).

The thermogram for the sPS homopolymer contains two visible thermal transitions, the glass transition and melting temperature of sPS, located at 99 and 270 °C respectively. Upon incorporation of the sulfonate groups onto the sPS homopolymer an increase in the glass transition and a decrease in the melting temperature are expected based upon previous work by Orler [42]. This behavior is observed for both the SsPS3.2H$^+$R and SsPS3.2H$^+$NR ionomers as shown in Figure VII-2. The glass transitions for the SsPS3.2H$^+$R and SsPS3.2H$^+$NR ionomers

increased from 99 °C from the unsulfonated material to 104 and 102°C respectively for the different ionomers. The glass transition temperature for the randomly sulfonated ionomer is slightly higher than that of the randomly sulfonated ionomer containing the same ion content. The slight difference in glass transition temperature between the ionomers suggests that polymer chains in the SsPS3.2H$^+$R ionomer experience more restricted mobility requiring a greater thermal energy input for the onset of long-range molecular mobility to occur.

The two SsPS ionomers both exhibit crystallization exotherms as shown in Figure VII-2 in contrast to the sPS homopolymer. The sPS homopolymer does not exhibit a crystallization exotherm because all of the crystallizable chain segments have sufficient molecular mobility to pack into crystalline structures on the cool down during the rapid quench of the material from the melt. However, as seen in Figure VII-2, crystallization exotherms are present for SsPS3.2H$^+$R and SsPS3.2H$^+$NR at 183 and 180 °C respectively. The difference in the crystallization temperatures for the two different ionomers can be attributed to differences in chain mobility. During heating, the polymer chains within the SsPS3.2H$^+$R may be more restricted than polymer chains of the SsPS3.2H$^+$NR ionomer. The restricted chain mobility that does not allow the crystallizable chain segments of the both SsPS ionomers to completely pack into crystalline structures during the quench is due to the presence of ionic aggregates formed through the aggregation of sulfonate groups along the polymer backbone. The aggregation of these sulfonate groups via strong electrostatic interactions limits the mobility of the polymer chains and retards their motion. Randomly distributed sulfonate groups would likely result in a homogenous distribution of ionic aggregates throughout the polymer matrix that have a more pronounced effect on chain dynamics because more of the polymer chains would experience hindered molecular mobility due to the presence of a homogenously dispersed electrostatic network. The

non-random ionomer likely consists of ionic aggregates heterogeneously distributed within the polymer matrix and possibly exist as blocks of sulfonate groups that creates a small, isolated an electrostatic network that does not restricts a significantly smaller portion of the polymer chains of the ionomer. Less polymer chain restriction leads to high molecular mobility and the corresponding lower crystallization exotherm observed for the SsPS3.2H^+NR ionomer compared to the randomly sulfonated ionomer containing the same ion content.

The melting point for both ionomers as shown in Figure VII-2 has decreased from 270 °C to 252 and 255°C for the SsPS3.2H^+R and SsPS3.2H^+NR ionomers respectively. The higher melting point for the SsPS3.2H^+NR ionomer is attributed to maintaining longer sequences of unsulfonated sPS homopolymer via the non-random sulfonation technique that are able to crystallize into larger crystallites requiring a larger amount of heat input to destroy their crystalline order.

The differences in the thermal properties of the SsPS3.2H^+R and SsPS3.2H^+NR ionomers as compared to the sPS homopolymer are attributed to the presence of an electrostatic network created by ionic aggregates of sulfonate groups. These ionic aggregates restrict polymer chain mobility leading to the increased glass transition temperature and lower melting point temperature of both SsPS ionomers when compared to the sPS homopolymer. The different placement of the sulfonate groups along polymer backbone within the SsPS3.2H^+R and SsPS3.2H^+NR ionomers possibly creates a different ionomer architecture which creates different ionomer morphologies containing homogenous or heterogeneous distributions of ionic aggregates throughout the matrices. It is very reasonable to observe small differences in the thermal transitions the SsPS3.2H^+R and SsPS3.2H^+NR ionomers at this low ion content. At low ion content, it is likely that the sequence of unsulfonated sPS homopolymer would be very

similar for both ionomers leading to similar crystallization and thermal behavior for the crystallizable component of each ionomer. Therefore, it is expected that large differences in the crystallization and thermal behavior of randomly sulfonated and non-randomly SsPS would be observed at higher ion content.

Previous studies by Orler and coworkers showed that ion contents above 3 mol% for randomly sulfonated sPS eliminated the ability of the polymer to crystallize. Therefore, it is of significant interest to sulfonate sPS at elevated ion contents using the non-random sulfonation method to determine if longer sequences of unsulfonated material are maintained that have the ability to pack into crystalline domains in the presence of an electrostatic network created via ionic aggregates. We have prepared high ion content SsPS ionomers that have been sulfonated via the random and non-random post-polymerization methods containing 9.2 and 9.8 mol% sulfonate groups respectively. Figure VII-3 contains the DSC thermogram of relative heat flow versus temperature for the sPS homopolymer, SsPSR9.2H^+R and SsPSNR9.8H^+NR. The glass transition and melting temperature for the sPS homopolymer are 99 and 270 °C respectively. The only thermal transition present for the SsPSR9.2H^+R ionomer is the glass transition located at 109 °C. In contrast, three thermal transitions are observed in the DSC heating scan of SsPSNR9.8H^+NR. The glass transition, crystallization temperature, and melting temperature of SsPSNR9.8H^+NR are 104, 195, and 248 °C respectively. The lack of a crystallization exotherm and melting endotherm in the SsPSR9.2H^+R ionomer suggests that the presence of the electrostatic network diminishes polymer chain molecular mobility under the time scale of the DSC experiment.

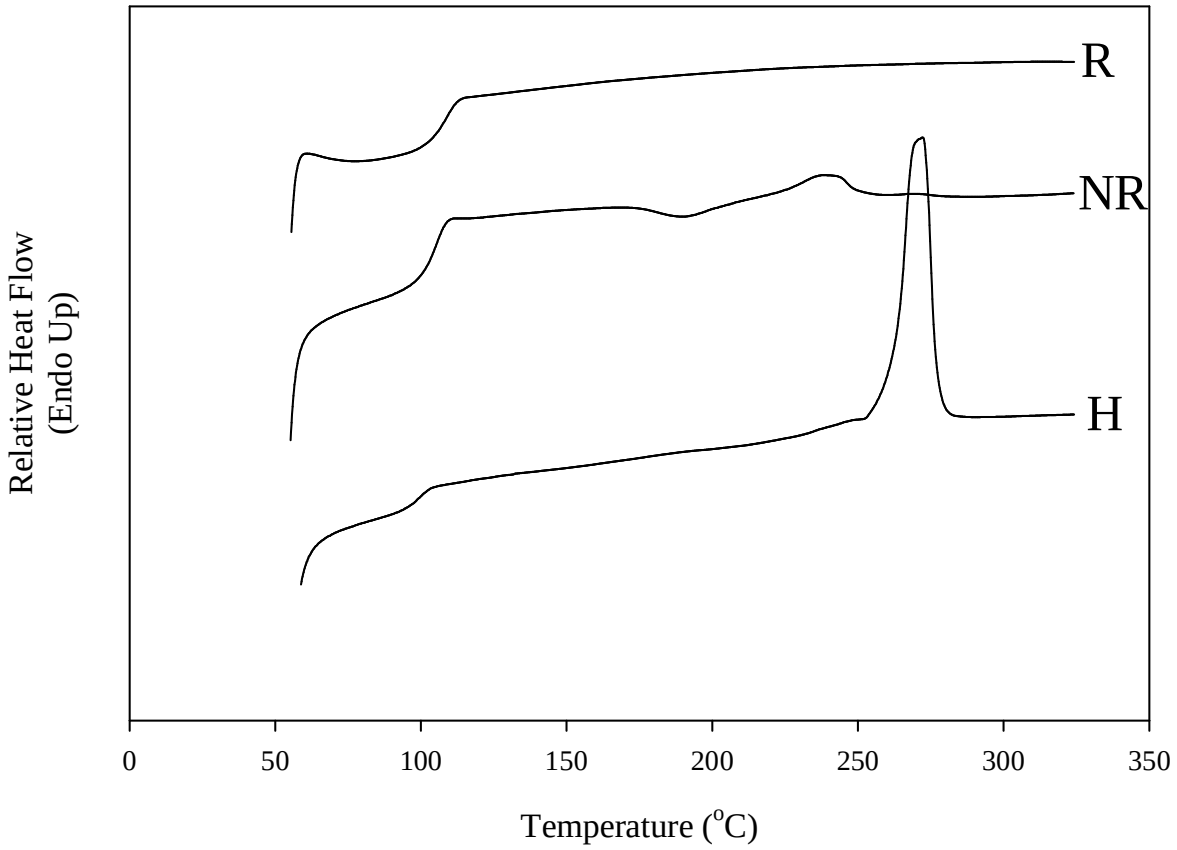

Figure VII-3. Relative heat flow versus temperature of sPS homopolymer (H), SsPS9.8H^+NR (NR), and SsPSN9.2H^+R (R).

However, in strong contrast to the randomly sulfonated ionomer, the non-randomly sulfonated sPS ionomer shows three distinct thermal transitions which demonstrates that a significant portion of polymer chains have the ability to pack into crystalline structures even in the presence of an electrostatic network created through aggregation of the sulfonate groups. The tremendous differences in the thermal transitions of SsPSR9.2H^+R and SsPSNR9.8H^+NR can be attributed to two different ionomer architectures that result in different ionomer morphologies as suggested for the low ion content SsPS ionomers. However, at higher ion content, a more pronounced effect of the placement of sulfonate groups along the polymer

backbone can be expected. The SsPSNR9.8H^+NR ionomer may consist of ionic aggregates that are present as isolated domains within the polymer matrix due to longer sequences of unsulfonated material that have been maintained via the non-random post-polymerization sulfonation technique. The SsPSNR9.2H^+R ionomer is likely to have shorter segments of unsulfonated sPS homopolymer due to the random placement of sulfonate groups along the polymer backbone.

Semicrystalline polymers may be subjected to thermal annealing as a means to increase the degree of crystalline order within crystalline domains and the overall degree of crystallinity within the material. Thermal energy supplied to the polymer increases chain mobility and can lead to enhanced crystalline organization. The SsPSR9.2H^+R and SsPSNR9.8H^+NR ionomers were thermally annealed at 200 °C for 2 hours. Figure VII-4 provides the DSC thermogram of relative heat flow versus temperature for SsPSR9.2H^+R and SsPSNR9.8H^+NR after thermal annealing. It is clear from this thermogram that even after thermal annealing that the SsPSR9.2H^+R has not crystallized under the time scale of the experiment. The lack of the development of crystallinity for the SsPSR9.2H^+R ionomer even with extended thermal annealing strongly suggests that the electrostatic network created via ionomer multiplets completely diminishes the ability of the polymer chains to crystallize. In contrast, there is a large melting endotherm present for the SsPSNR9.8H^+NR ionomer located at 258 °C. The increase in the melting temperature of SsPSNR9.8H^+NR from 248 °C in the second DSC heating scan as shown in Figure VII-3 to 258 °C as shown in Figure 4 after thermal annealing indicates that size of the crystallites have increased under thermal annealing conditions requiring greater thermal input to destroy the crystalline structure.

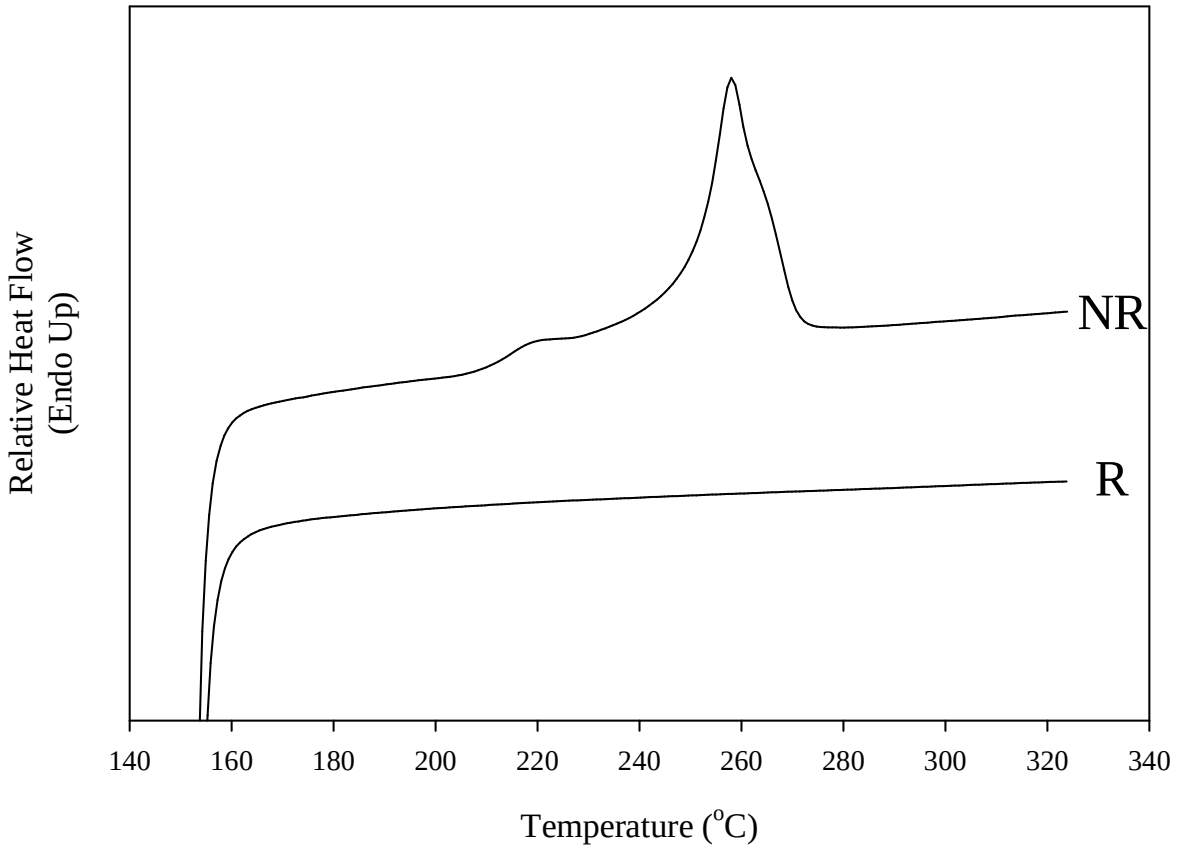

Figure VII-4. Relative heat flow versus temperature of SsPS9.2H$^+$R (R), and SsPS9.8H$^+$NR (NR) post-isothermal crystallization at 200°C for 2 hours.

There is a small endothermic transition present in the SsPSNR9.8H$^+$NR thermogram within Figure VII-4. The small melting transition located at 219 °C is attributed to the melting of smaller crystallites that have developed during the thermal annealing process. The development of small crystallites during thermal annealing is a very common phenomenon for semicrystalline polymers. It is also important to note the degree of crystallinity of the SsPSNR9.8H$^+$NR. The area under the melting endotherm of SsPSNR9.8H$^+$NR was used to determine the overall degree of crystallinity,χ_c, for the ionomer using the following relationship:

$$\chi_c = \frac{\Delta H_f}{\Delta H_f^o} \quad (1)$$

The value of ΔH_f^o for sPS is 82.6 J/g. The ΔH_f value for SsPSNR9.8H$^+$NR after isothermal crystallization at 200 °C for 2 hours was 20.7 J/g leading to a χ_c of 25%. An overall degree of crystallinity of 25% for an SsPS ionomer containing 9.8 mol% sulfonate groups is tremendously large and strongly indicative of long sequences of unsulfonated material that have sufficient molecular mobility to organize into crystalline structures.

The effect of ionomer architecture via the placement of the sulfonate groups on crystallization behavior of sPS was monitored via DSC isothermal crystallization experiments. The development of crystallinity within SsPS3.2H$^+$R and SsPS3.2H$^+$NR was monitored by applying the following relationship:

$$X_c(t) = \frac{\int_0^t \frac{dH}{dT} dt}{\int_0^\infty \frac{dH}{dT} dt} \quad (2)$$

The expression given in equation 2 represents the fractional crystallinity of the bulk ionomer system,$X_c(t)$ and is equal to the heat evolved during isothermal crystallization at a specific time t divided by the total heat generated during the entire crystallization process. Figure VII-5 contains the plot of $X_c(t)$ versus ln time at 220, 225, 230, and 235 °C for SsPS3.2H$^+$R and SsPS3.2H$^+$NR. It can be seen that the shape of the sigmoidal curves within Figure VII-5A and VII-5B for SsPS3.2H$^+$R and SsPS3.2H$^+$NR respectively are similar. This suggests that the induction period prior to the onset of polymer crystallization, primary crystallization, and secondary crystallization processes that occur within the SsPS3.2H$^+$R and SsPS3.2H$^+$NR may occur by the same mechanisms.

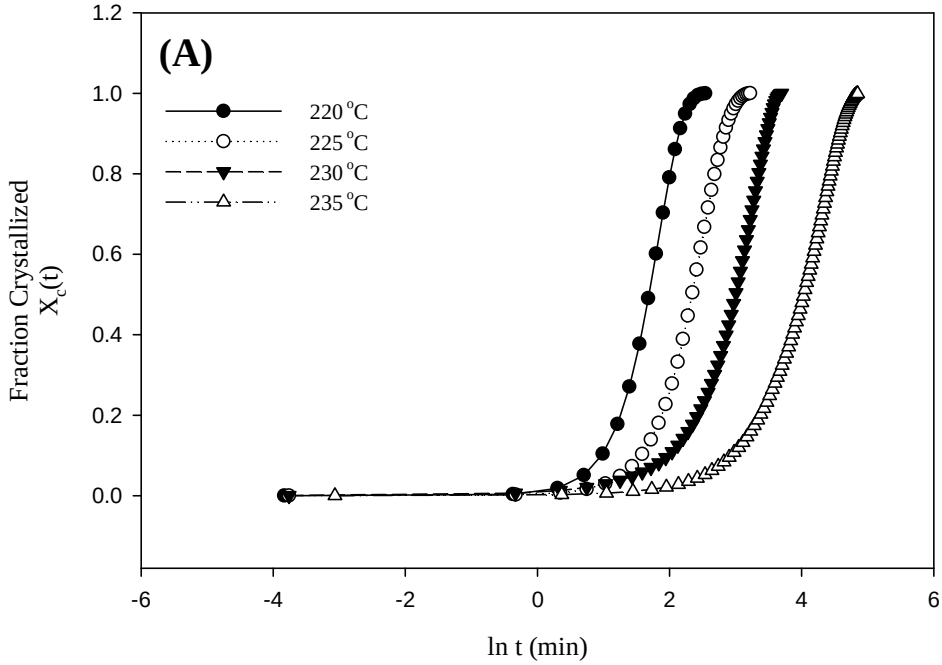

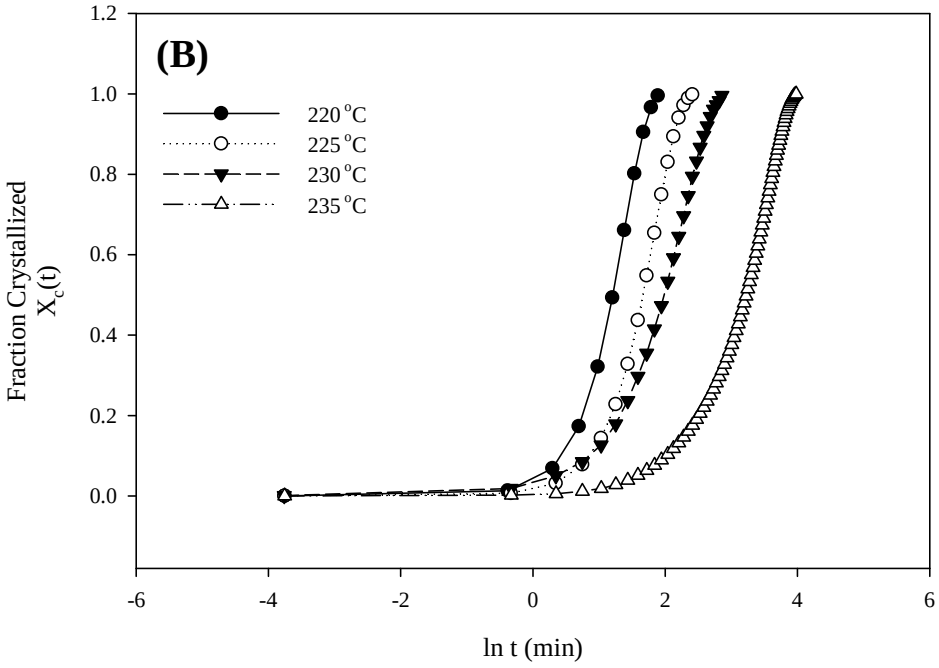

Figure VII-5. $X_c(t)$ versus ln time at 220, 225, 230, and 235 °C for (A) SsPS3.2H$^+$R and (B) SsPS3.2H$^+$NR.

More detailed information regarding the mechanisms for nucleation and growth within SsPS3.2H$^+$R and SsPS3.2H$^+$NR was determined using the Avrami approach. The Avrami method allows a quantitative kinetic evaluation of the crystallization behavior of the ionomers to be constructed. This approach is used extensively in the study of the bulk crystallization of polymers as it provides insight into the nucleation and growth process within the bulk polymer matrix. The Avrami equation is given in equation 3 and is used to determine the extent of fractional crystallinity, $X_c(t)$ at time t.

$$X_c(t) = 1 - \exp(-Kt)^n \quad (3)$$

The Avrami rate constant is represented by K and n is the Avrami exponent. The Avrami exponent, n, provides insight into the type of nucleation and growth that occurs within the system. The kinetic analysis of the isothermal crystallization behavior of the polymer clay hybrids is done by taking the double logarithm of the Avrami equation yielding the equation in the following form:

$$\ln[-\ln(1 - X_c(t))] = n \ln t + \ln K \quad (4)$$

Plots of ln[(-ln(1- $X_c(t)$)] versus ln t provide n and K from the slope and intercept respectively. Figure VII-6A and VII-6B contain plots of ln[(-ln(1- $X_c(t)$)] versus ln t for SsPS3.2H$^+$R and SsPS3.2H$^+$NR respectively. The Avrami exponents indicating the type of nucleation and growth mechanism that occurs during primary crystallization for SsPS3.2H$^+$R at 220, 225, 230, and 235 °C are 2.89, 2.48, 2.08, and 1.78 respectively and are listed in Table VII-1.

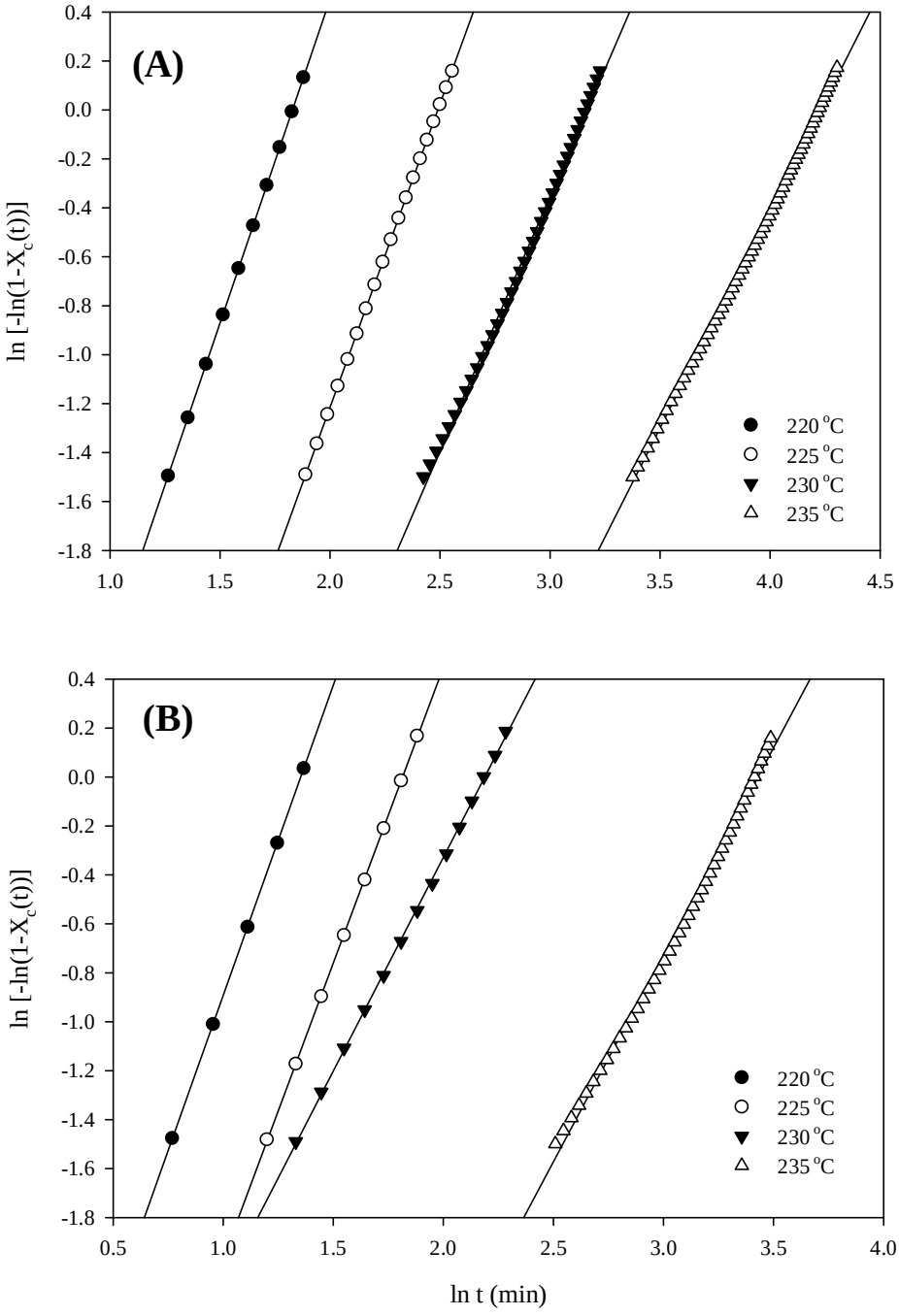

Figure VII-6. ln [-ln (1-Xc(t))] versus ln t at 220, 225, 230, and 235 °C for (A) SsPS3.2H^{+}R and (B) SsPS3.2H^{+}NR.

The non-integer values suggest that nucleation and growth occur by more than one mechanism and the dimensionality of the crystallites are mixed as well. The Avrami exponent, n, does appear to decrease within increasing crystallization temperature suggesting that the growth mechanism may be changing from a three-dimensional spherulitic structure to a more two-dimensional disc-like geometry.

Table VII-1. Kinetic parameters at 220, 225, 230 and 235 °C for SsPS3.2H$^+$R and SsPS3.2H$^+$ NR**.**

SsPS Kinetic Parameter	220 °C	225 °C	230 °C	235 °C
SsPS3.2H$^+$R				
t½ (min)	2.89	4.57	7.16	36.45
n	2.65	2.48	2.08	1.78
K (min^{-1})	7.9 x 10^{-3}	2.1 x 10^{-3}	1.4 x 10^{-3}	5.4 x 10^{-3}
SsPS3.2H$^+$NR				
t½ (min)	4.64	9.56	32.51	65.99
n	2.53	2.41	1.74	1.69
K (min^{-1})	3.2 x 10^{-2}	2.2 x 10^{-2}	1.3 x 10^{-2}	3.1 x 10^{-3}

The Avrami rate constant, K, which is a measure of the rate of crystallization can be extracted from ln[(-ln(1- $X_c(t)$)] versus ln t plots for SsPS3.2H$^+$R at various crystallization temperatures. The values are listed in Table VII-1. There is an increase in the Avrami rate constant K with increasing crystallization temperature from 7.9 to 5.4 x 10^{-3} min^{-1}. The increase in K within increasing crystallization temperature may be attributed to the lower degree of supercooling experienced by the polymer. As the crystallization temperature approaches the melting temperature of the polymer, the polymer chains retain more molecular mobility and are not able to crystallize due to their enhanced molecular motion.

A detailed kinetic analysis was completed for the SsPS3.2H$^+$NR as well as shown in Figure VII-6B. The Avrami exponent, n, does exhibit a decrease in value with increasing crystallization temperature as observed for the SsPS3.2H$^+$R ionomer. The n-values for SsPS3.2H$^+$NR at 220, 225, 230, and 235 °C are 2.89, 2.48, 2.08, and 1.78. The change in the Avrami exponent from a value approaching 3 of 2.89 to 1.78 with increasing crystallization temperature may indicate a change in the dimensionality crystalline superstructures from a three-dimensional spherical geometry to a two-dimensional disk-like geometry under these crystallization conditions. The Avrami rate constants, K, for SsPS3.2H$^+$NR are also listed in Table VII-1. There Avrami rate constant, K, decreases from 3.2 x 10^{-3} at 220 °C to 3.1 x 10^{-2} at 235 °C. The increase in the rate of crystallization for SsPS3.2H$^+$NR is attributed to the lower degree of supercooling experienced at higher crystallization temperatures similar to the SsPS3.2H$^+$R ionomer. The Avrami analyses of the SsPS3.2H$^+$R and SsPS3.2H$^+$NR ionomers suggests that the crystallizable components of the two different ionomers may pack into similar crystalline geometries under similar growth mechanisms.

The rate of crystallization of semicrystalline polymers is often measured by determining the crystallization half-time, $t_{½}$. The $t_{½}$-value is the time at which 50% of the material and is indicative of the bulk rate of crystalline of the polymer. The $t_{½}$ values can be extracted from plots of $X_c(t)$ versus ln time when $X_c(t)$ is equal to 0.50. The plot of crystallization half-time versus crystallization temperature is provided in Figure VII-7 for SsPS3.2H$^+$R and SsPS3.2H$^+$NR. The $t_{½}$-values for the two SsPS ionomers are summarized in Table VII-1.

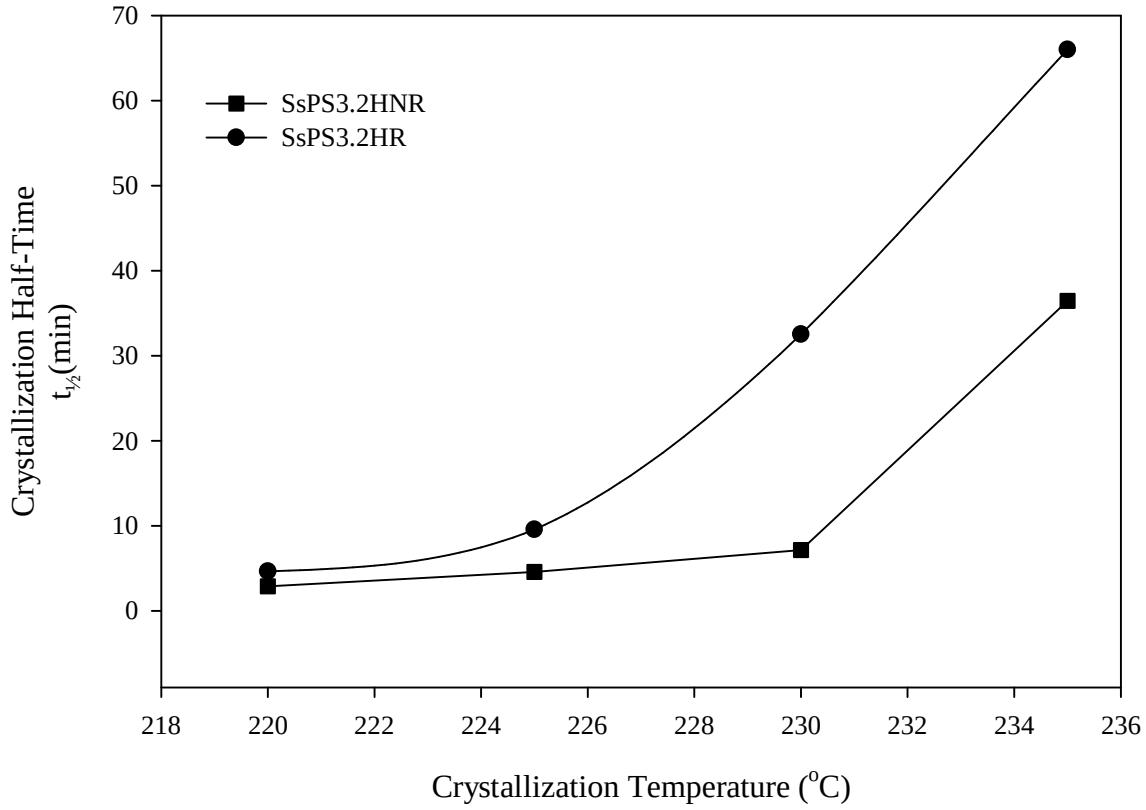

Figure VII-7. Crystallization half-time versus crystallization temperature for SsPSR3.2H^{+}R and SsPS3.2H^{+}NR.

It is clear from this graph that the crystallization half-time is much faster for the non-randomly sulfonated sPS ionomer than the randomly sulfonated sPS ionomer containing the same ion content. The faster crystallization half-time of SPS3.2H^{+}NR can be attributed to both longer sequences of unsulfonated material that are able to pack more readily into crystalline structures when compared to the randomly sulfonated SsPS ionomer that is likely to more frequently encounter an ionic aggregate during the crystallization process that must be rejected from the growing crystallite. Upon cooling from the melt, as the polymer chains attempt to pack into crystalline structures, ionic aggregates act as defects in the polymer chain and must be rejected from the growing crystalline/melt interface. Rejection of the encountered defects

increases the time required for crystallization to occur and leads to longer crystallization half-times as observed for the SsPS3.2H^+R ionomer.

The Hoffman-Weeks approach was utilized to determine the equilibrium melting point of the random and non-random SsPS ionomers. Figure VII-8 contains plots of the melting temperature versus the crystallization temperature for the SsPS ionomers. The solid line represents the plot of the $T_m = T_c$. Extrapolation of the experimental data to $T_m = T_c$ yield equilibrium melting temperatures, T_m^o, of 279 and 267 °C for the non-random and random SsPS ionomers, respectively.

The equilibrium melting point can be expressed in terms of changes in the enthalpy and entropy upon cooling of the ionomers from melt as shown in equation

$$T_m^o = \frac{\Delta H_f^o}{\Delta S_f^o} \quad (5)$$

The higher equilibrium melting point for the non-random ionomer is attributed to a relatively lower degree in the change in entropy upon cooling of the ionomer from the melt compared to the random SsPS when the change in the enthalpic interactions upon cooling from the melt are considered to be the same for the two different SsPS ionomers.

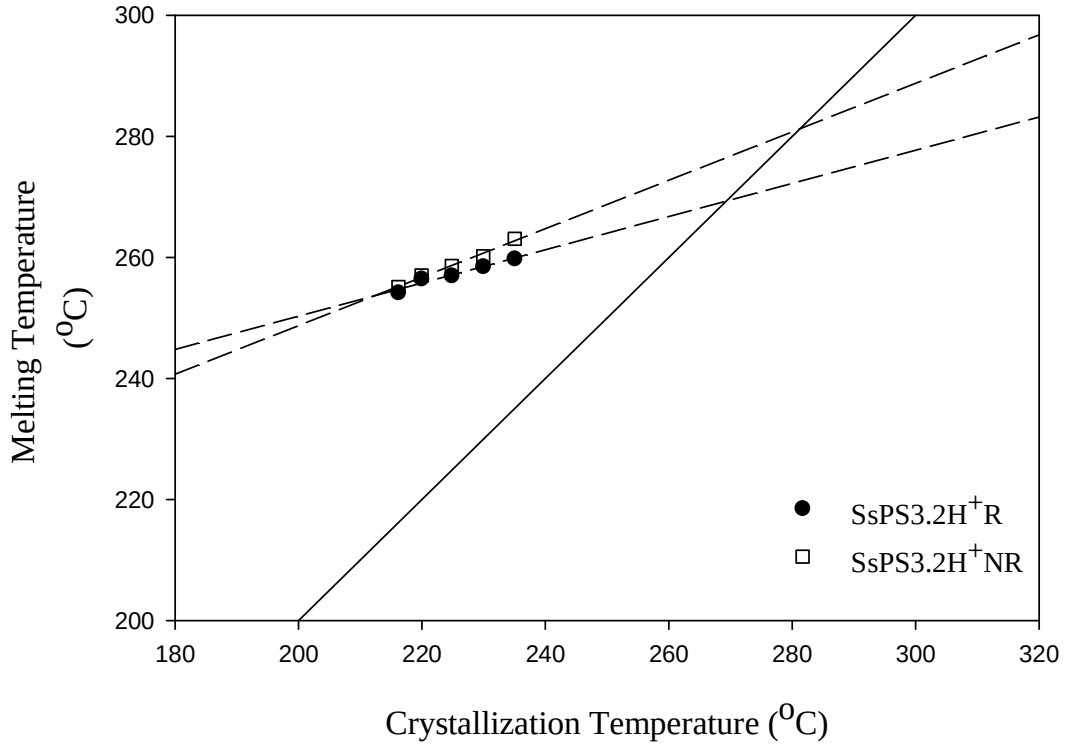

Figure VII-8. Melting temperature versus crystallization temperature for SsPSR3.2H$^+$R and SsPS3.2H$^+$NR.

The thermal transitions of the low and high ion content ionomers that have been randomly and non-randomly sulfonated suggest that the two ionomer architectures are extremely different. Additional evidence indicating that the architectures and morphologies of these two materials are different is provided in the plot of glass transition temperature versus mol% sulfonation provided in Figure VII-9.

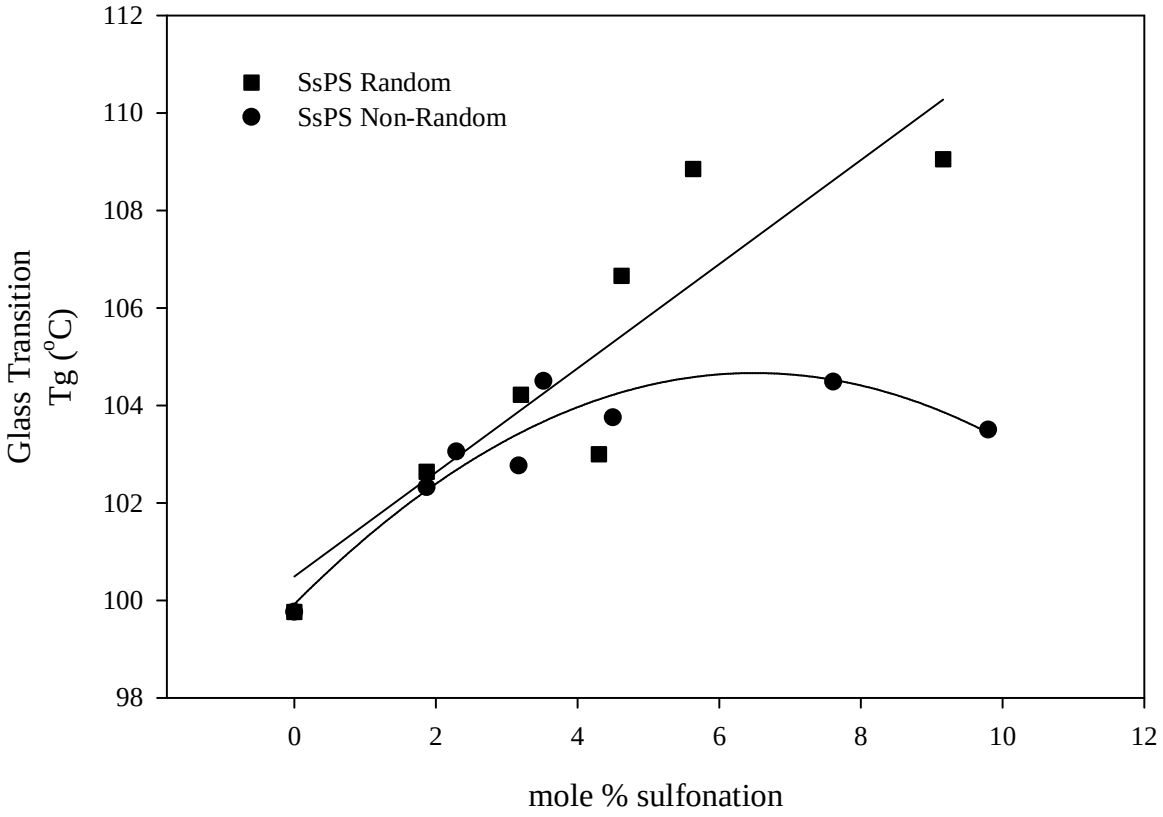

Figure VII-9. Glass transition temperature versus mole % sulfonation of SsPS random and SsPS non-Random ionomers.

There is a linear increase in the glass transition temperature with increasing degree of sulfonation for the randomly sulfonated SsPS ionomer. This suggests that the presence of ionic aggregates throughout the ionomer matrix drastically restrict the molecular mobility of polymer chains. However, the glass transition temperature for the non-randomly sulfonated material does not continue to increase with increasing mol% sulfonation as observed for randomly sulfonated sPS. The glass transition temperature for non-randomly sulfonated sPS reaches at maximum at 104 °C at 4 mol% sulfonation and does not continue to increase upon increasing the concentration of sulfonic acid groups. This data indicates that the ionic aggregates are isolated from the crystallizable chain segments and are not able to impart a strong influence on the chain

mobility of the segments during the crystallization process. This data strongly compliments and supports previous work completed by Weiss and coworkers. Weiss and coworkers prepared sulfonated atactic polystyrene (SaPS) of two different architectures. Emulsion copolymerization of styrene and sodium styrene sulfonate was used to synthesize SaPS that was proposed consist of a blocky ionomer architecture and post-polymerization sulfonation of atactic polystyrene was conducted to produce randomly sulfonated SaPS. DSC thermograms of glass transition versus mol% of sulfonate for the SaPS ionomers produced via copolymerization and post-polymerization sulfonation exhibited the same increases in glass transition temperature with ion content as observed for non-randomly sulfonated sPS and randomly sulfonated sPS respectively within this study. Weiss and coworkers suggested the differences in T_g for the two SaPS ionomers was due to fundamental differences in the structure of the two ionomers. The data provided in Figure VII-9 for SsPS ionomers strongly suggests fundamental differences in the structure of the SsPS ionomers as well.

Small-angle X-ray scattering is a powerful tool used to characterize the morphology of polymeric materials. There are many reports on the use of this technique to construct morphological models of ionomer structure. Figure VII-10A and VII-10B contain two-dimensional SAXS images of SsPS3.2H^+R and SsPS3.2H^+NR respectively. It is clear that there is the presence of higher contrast scattering in Figure VII-10A of SsPS3.2H^+R compared to that of SsPS3.2H^+NR in Figure VII-10B. The origin of the increased contrast for SsPS3.2H^+R as seen in Figure 9A is due to the homogenous distribution of higher electron density ionic aggregates distributed throughout the low electron density amorphous phase of the SsPS3.2H^+R ionomer. The homogeneous distribution of the ionic aggregates throughout the SsPS3.2H^+R

matrix results in a more intense scattering pattern. However, it is can be readily observed that there is significantly less scattering present in Figure VII-10B of the SsPS3.2H^+NR ionomer.

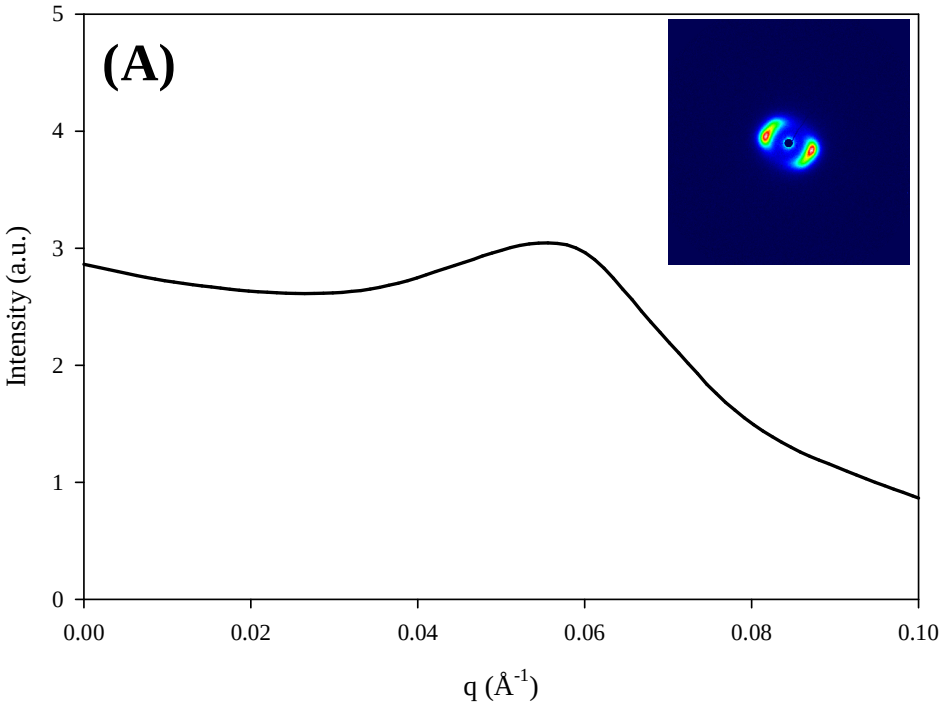

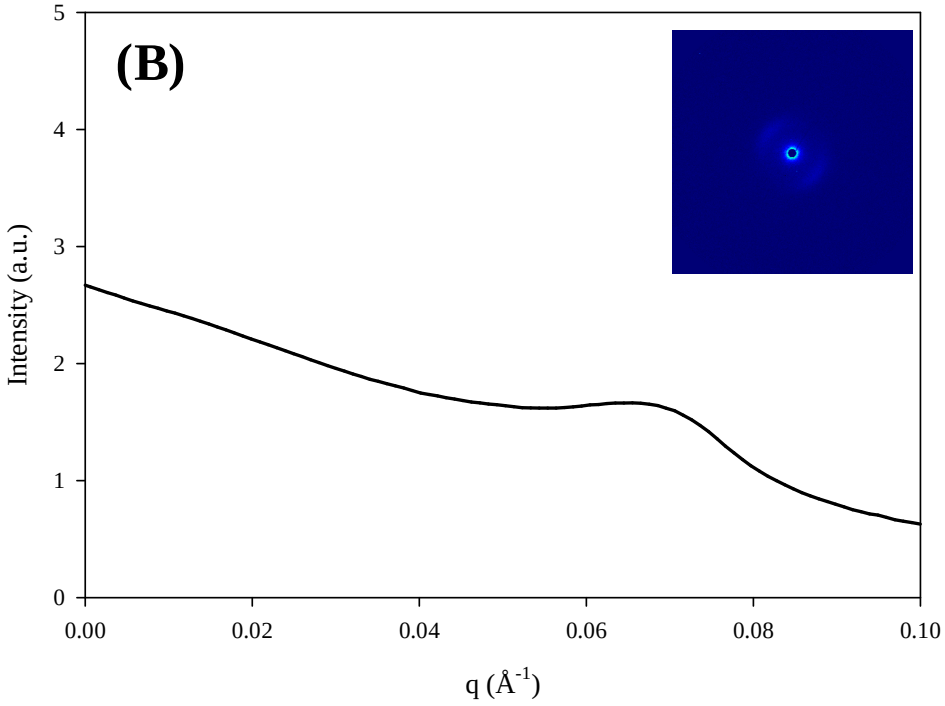

Figure VII-10. SAXS 2D patterns of (A) SsPSR3.2H^{+}R and (B) SsPS3.2H^{+}NR.

The origin of the less intense two-dimensional scattering pattern for the randomly sulfonated ionomer is attributed the presence of a lower density amorphous phase that does not contain a large amount of scattering centers such as ionic aggregates distributed throughout the ionomer matrix. Figure VII-11A and VII-11B contain schematics of the two different ionomer morphologies that have been constructed based upon the two-dimensional scattering patterns and crystallization behavior these materials.

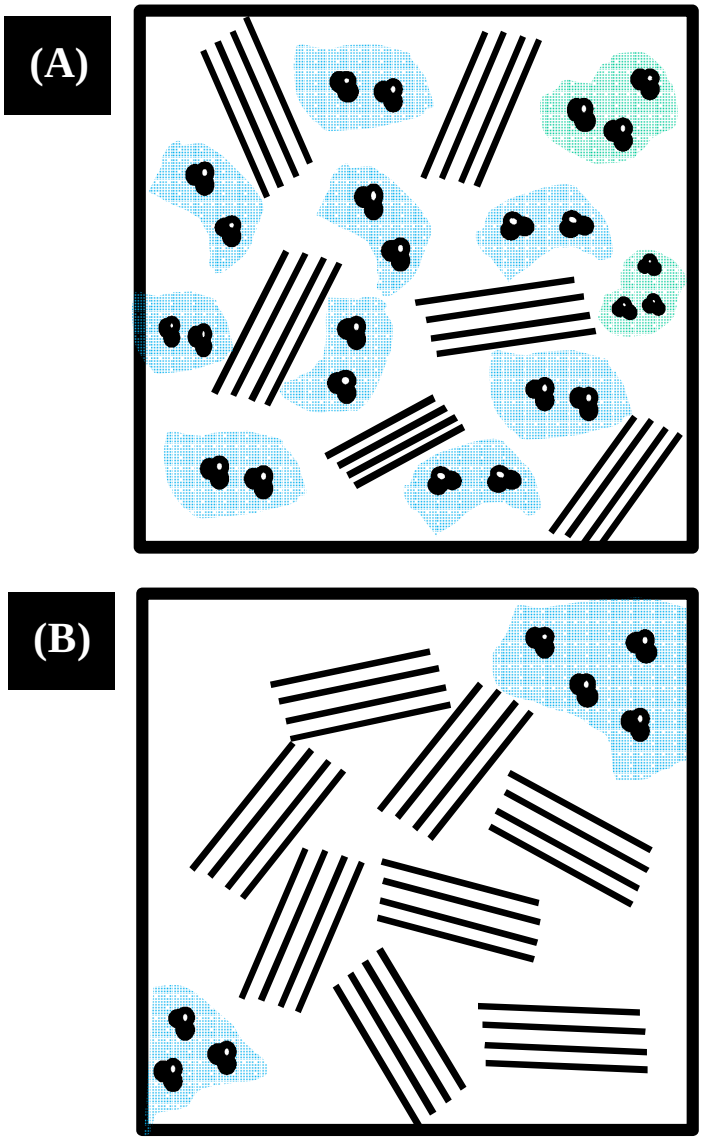

Figure VII-11. Schematic of SsPS ionomer morphology based upon SAXS data for (A) SsPSR3.2H^+R and (B) SsPS3.2H^+NR.

Figure VII-10A representing randomly sulfonated sPS shows the presence of ionic aggregates distributed homogenously throughout the matrix. This homogenous distribution of ionic aggregates leads to the increased scattering as observed in the 2D SAXS patterns and the greater degree of restricted chain mobility observed within the crystallization kinetic studies of SsPS3.2H^+R and SsPS9.2H^+R ionomers. The morphological model constructed for non-randomly sulfonated sPS ionomers, SsPS3.2H^+NR and SsPS9.8H^+NR, shown in Figure VII-11B is based upon the 2D SAXS pattern in Figure VII-10B and the crystallization and thermal data is provided in Figures 2 through 8. The ionic aggregates are well isolated from the crystalline domains of the non-randomly sulfonated matrix due to the non-random placement of the sulfonate groups along the polymer backbone. Isolation of the unsulfonated sequences of sPS allows for more rapid crystallization of the crystallizable component of the ionomer because the chains are less restricted by the electrostatic network of ionic aggregates.

Neutralization has a considerable effect on the rate of crystallization within semicrystalline ionomers. Figure VII-12 shows the plots of crystallization half-time versus crystallization temperature for the random and non-random SsPS ionomers containing 1.9 mol% sulfonate groups fully-neutralized with sodium counterions. Even at a lower degree of sulfonation, there is a very profound difference in the rate of crystallization of the different ionomers in the presence of the neutralized SsPS ionomers. The rate of crystallization for the SsPS1.9Na^+R ionomer was so slow at crystallization temperatures above 230 °C that the ability of the polymer chain to crystallization was essentially eliminated.

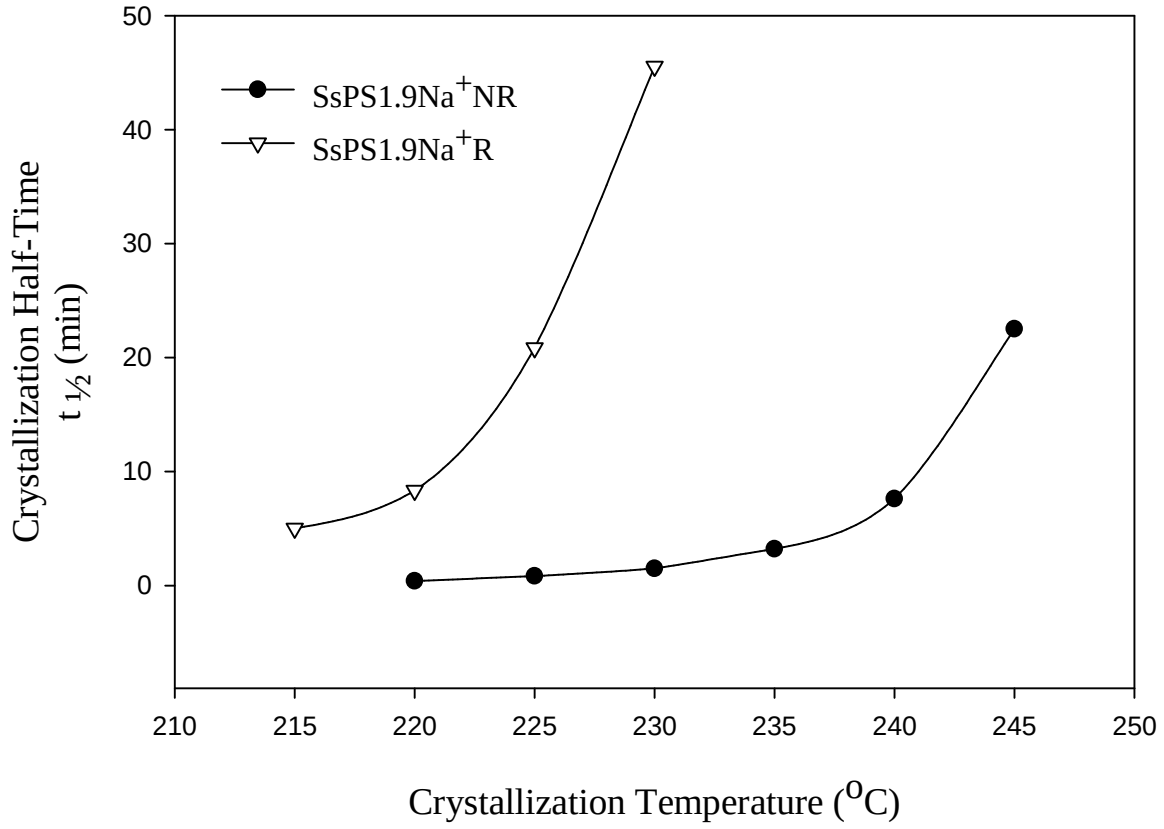

Figure VII-12. Crystallization half-time versus crystallization temperature for SsPS1.9Na$^+$R and SsPS1.9Na$^+$NR.

CONCLUSION

We have utilized a very simple post-polymerization method to non-randomly sulfonate sPS to yield an ionomer architecture that contains longer sequences of unsulfonated sPS homopolymer. The longer sequences of unsulfonated material of the non-random SsPS are able to pack much more quickly into crystalline structures than the randomly sulfonated sPS ionomer at an ion content of 3.2 mol%. At high ion contents approaching that of 10 mol%, the randomly sulfonated ionomer is not able to crystallize under the time scale of the experiment due to the tremendous restriction of the electrostatic network of ionic aggregates on polymer chain

mobility. However, in contrast the SsPS9.8H^+NR ionomer retains the ability to crystallize rapidly from the melt and exhibits both a crystallization exotherm and melting endotherm under the same experimental conditions of that of the sPS homopolymer. The SsPS9.8H^+NR exhibits enhanced crystallization behavior in response to thermal annealing as well while the SsPS9.2H^+R ionomer does not crystallize even in the presence of the additional heat input supplied via thermal annealing. SAXS data also suggests that the morphologies of these two ionomers are different and that the differences in the thermal properties and crystallization behavior can be attributed to the method of placement of the sulfonate group along the polymer backbone.

.

REFERENCES

1. Eisenberg A and King M. Ion-containing polymers : physical properties and structure Polymer physics, vol. 2. New York: Academic Press, 1977.
2. Eisenberg A and Pineri M. Structure and properties of ionomers. Norwell: Kluwer Academic Publishers, 1987.
3. Eisenberg A and Kim J-S. Introduction to ionomers. New York: Wiley, 1998.
4. Yang S, Sun K, and Jr. WMR. Journal of Polymer Science Part B: Polymer Physics 1990;28(10):1685-1697.
5. Weiss RA, Agarwal PK, and Lundberg RD. Journal of Applied Polymer Science 1984;29(9):2719-2734.
6. Mattera Jr. VD and Risen Jr. WM. Journal of Polymer Science Part B: Polymer Physics 1986;24(4):753-760.
7. Kim J-S, Yoshikawa K, and Eisenberg A. Macromolecules 1994;27(22):6347-6357.
8. Wallace RA. Journal of Polymer Science Part A-2: Polymer Physics 1971;9(7):1325-1332.
9. Bazuin CG and Eisenberg A. Journal of Polymer Science Part B: Polymer Physics 1986;24(5):1137-1153.
10. Atorngitjawat P and Runt J. Macromolecules 2007;40(4):991-996.
11. Smith P and Eisenberg A. Journal of Polymer Science Part B: Polymer Physics 1988;26(3):569-580.
12. Bellinger M, Sauer JA, and Hara M. Macromolecules 1994;27(6):1407-1412.
13. Hara M and Jar PY. Macromolecules 1988;21(11):3187-3190.
14. Hara M, Jar PY, and Sauer JA. Macromolecules 1988;21(11):3183-3186.

15. Fan X-D and Bazuin CG. Macromolecules 1995;28(24):8216-8223.

16. Cánovas MJ, Sobrados I, Sanz J, Acosta JL, and Linares A. Journal of Membrane Science 2006;280(1-2):461-469.

17. Atorngitjawat P, Klein RJ, and Runt J. Macromolecules 2006;39(5):1815-1820.

18. Boris DC and Colby RH. Macromolecules 1998;31(17):5746-5755.

19. Lundberg RD and Phillips RR. Journal of Polymer Science: Polymer Physics Edition 1982;20(7):1143-1154.

20. Young AM, Higgins JS, Peiffer DG, and Rennie AR. Polymer 1995;36(4):691-697.

21. Pedley AM, Higgins JS, Peiffer DG, and Burchard W. Macromolecules 1990;23(5):1434-1437.

22. Fitzgerald JJ and Weiss RA. Cation-Anion and Cation-Cation Interactions in Sulfonated Polystyrene Ionomers. Coulombic Interactions in Macromolecular Systems, vol. 302: American Chemical Society, 1986. pp. 35-53.

23. Lantman CW, MacKnight WJ, Higgins JS, Peiffer DG, Sinha SK, and Lundberg RD. Macromolecules 1988;21(5):1339-1343.

24. Bodycomb J and Hara M. Macromolecules 1994;27(25):7369-7377.

25. Bodycomb J and Hara M. Macromolecules 1995;28(24):8190-8197.

26. O'Connell EM, Root TW, and Cooper SL. Macromolecules 1995;28(11):4000-4006.

27. Galambos AF, Stockton WB, Koberstein JT, Sen A, Weiss RA, and Russell TP. Macromolecules 1987;20(12):3091-3094.

28. Eisenberg A, Hird B, and Moore RB. Macromolecules 1990;23(18):4098-4107.

29. Lefelar JA and Weiss RA. Macromolecules 1984;17(6):1145-1148.

30. O'Connell EM, Root TW, and Cooper SL. Macromolecules 1994;27(20):5803-5810.

31. O'Connell EM, Root TW, and Cooper SL. Macromolecules 1995;28(11):3995-3999.

32. O'Connell EM, Peiffer DG, Root TW, and Cooper SL. Macromolecules 1996;29(6):2124-2130.

33. Kirkmeyer BP, Weiss RA, and Winey KI. Journal of Polymer Science Part B: Polymer Physics 2001;39(5):477-483.

34. Ding YS, Yarusso DJ, Pan HKD, and Cooper SL. Journal of Applied Physics 1984;56(9):2396-2403.

35. Register RA, Sen A, Weiss RA, and Cooper SL. Macromolecules 1989;22(5):2224-2229.

36. Toriumi H, Weiss RA, and Frank HA. Macromolecules 1984;17(10):2104-2107.

37. Kim JS, Roberts SB, Eisenberg A, and Moore RB. Macromolecules 1993;26(19):5256-5258.

38. Chu B, Wang J, Li Y, and Peiffer DG. Macromolecules 1992;25(16):4229-4231.

39. Weiss RA, Lundberg RD, and Turner SR. Journal of Polymer Science: Polymer Chemistry Edition 1985;23(2):549-568.

40. Weiss RA, Turner SR, and Lundberg RD. Journal of Polymer Science: Polymer Chemistry Edition 1985;23(2):525-533.

41. Orler EB, Calhoun BH, and Moore RB. Macromolecules 1996;29(18):5965-5971.

42. Orler EB, Yontz DJ, and Moore RB. Macromolecules 1993;26(19):5157-5160.

43. Orler EB and Moore RB. Macromolecules 1994;27(17):4774-4780.

44. Orler EB, Gummaraju RV, Calhoun BH, and Moore RB. Macromolecules 1999;32(4):1180-1188.

45. Makowski HS, Lundberg RD, and Singhal GH. Flexible Polymeric Compositions Comprising a Normally Plastic Polymer Sulfonated To About 0.2 to About 10 Mole%

Sulfonate. In: Office USP, editor., vol. 3,870,841. United States: Exxon Research and Engineering Company, 1975.

46. Hickner MA, Fujimoto CH, and Cornelius CJ. Polymer 2006;47(11):4238-4244.

47. Shi Z and Holdcroft S. Macromolecules 2005;38(10):4193-4201.

48. Carretta N, Tricoli V, and Picchioni F. Journal of Membrane Science 2000;166(2):189-197.

49. Wang F, Hickner M, Kim YS, Zawodzinski TA, and McGrath JE. Journal of Membrane Science 2002;197(1-2):231-242.

50. Hickner MA, Ghassemi H, Kim YS, Einsla BR, and McGrath JE. Chemical Reviews 2004;104(10):4587-4612.

51. Yeo RS and Cheng C-H. Journal of Applied Polymer Science 1986;32(7):5733-5741.

52. Doyle M, Lewittes ME, Roelofs MG, and Perusich SA. The Journal of Physical Chemistry B 2001;105(39):9387-9394.

53. Peterlin A. Journal of Macromolecular Science, Part B: Physics 1975;11(1):57 - 87.

54. Yeo RS. Polymer 1980;21(4):432-435.

55. Borriello A, Agoretti P, Ambrosio L, Fasano G, Pellegrino M, Venditto V, and Guerra G. Chemistry of Materials 2009;21(14):3191-3196.

CHAPTER VIII

NON-ISOTHERMAL CRYSTALLIZATION BEHAVIOR OF RANDOM AND NON-RANDOM SULFONATED SYNDIOTACTIC POLYSTYRENE

ABSTRACT

Lightly sulfonated ionomers were prepared through the post-polymerization modification of syndiotactic polystyrene in the solution state and physical gel state resulting in the placement of sulfonate groups randomly and non-randomly along the homopolymer backbone, respectively. The non-isothermal crystallization behavior of syndiotactic polystyrene ionomers (SsPS) prepared through the sulfonation of syndiotactic polystyrene in the solution state and physical gel state was monitored using differential scanning calorimetry. It was found that the peak crystallization temperature was higher for the SsPS ionomers prepared in the physical gel state than the SsPS ionomer through the sulfonation of sPS in the solution state. The breadth of the crystallization exotherm for the SsPS ionomer prepared through sulfonation of the sPS physical gel was broader than the crystallization exotherm of the solution state ionomer. The differences in the non-isothermal crystallization behaviors of the two different ionomers are attributed to the differences in the placement of the sulfonate groups along the homopolymer backbone.

INTRODUCTION

A number of fundamental studies of polymer crystallization are carried out under ideal conditions where the experimental conditions such as crystallization temperature and are held constant such as in isothermal crystallization studies [1]. However, the study of non-isothermal crystallization processes within semicrystalline polymers is extremely important from an industrial perspective as the non-isothermal crystallization process may more closely approximate the conditions associated with many industrial polymer processing techniques [1]. Therefore, studies of the non-isothermal crystallization behavior of polymer and polymer composites are of considerable interest in terms of understanding fundamental crystallization processes and improving industrial processes [2].

There are several models that have been developed to analyze and interpret the non-isothermal crystallization process including the Ozawa [3], Ziabicki [4-5], and Nakamura [6-7] methods. Many of the aforementioned models have not been successful in describing the non-isothermal crystallization of many pristine polymers and polymer-filled systems [8] or have been found to be successful only under certain conditions such as at low cooling rates [9-11]. Nevertheless, there are basic fundamental parameters that can be extracted from a study of the non-isothermal crystallization of polymers via differential scanning calorimetry. By simply evaluating the crystallization exotherm produced during non-isothermal crystallization, basic parameters such as the onset time of crystallization, the time required for the sample to crystallize, and the breadth of the exothermic crystallization event may provide insight into the crystallization behavior of polymeric materials.

Therefore, an investigation into the non-isothermal crystallization behavior of SsPS ionomers sulfonated in the solution and physical gel states may provide insight into the effect of the placement of the ionic group on the crystallization behavior of the ionomer.

EXPERIMENTAL

Materials

Syndiotactic polystyrene (Questra 102) MW of 310,000 g/mol was donated by the Dow Chemical Company. Reagent grade 1,2,4-trichlorobenze (TCB), methanol, sulfuric acid, potassium monopthalate were obtained from Fisher Scientific. Hexanoic anhydride, benzyltrimethylammoniuim hydroxide, and benzoic acid were received from Sigma Aldrich.

Preparation of Sulfonation Agent

The sulfonation agent was prepared according to previously published procedures using TCB as the solvent. TCB (25 mL) was added to a 50 mL volumetric flask containing 0.03 moles of hexanoic anhydride. The TCB/hexanoic anhydride solution was cooled in an ice bath for 1 hour, and then 1 mL of concentrated sulfuric acid was added to the chilled solution and shaken vigorously. Additional TCB was added to the volumetric flask to the 50 mL mark.

Random Sulfonation of Syndiotactic Polystyrene

sPS was dissolved in TCB under reflux for 1.5 h to yield a 10% w/v solution. After 1.5 h, the solution was cooled to 70 °C and then additional TCB was added to yield a 1% w/v sPS solution. The sPS solution was allowed to equilibrate at 70 °C under a nitrogen purge for 1.5 hr. After equilibration, the appropriate amount of sulfonation reagent was added and the reaction was allowed to proceed for 1 hour at 70 °C under a nitrogen purge. After 1 h, 10 mL methanol was

added to the solution to terminate the reaction. The solution was poured into a large excess of methanol to precipitate the ionomer. The precipitated ionomer was filtered and washed with deionized water.

Non-Random Sulfonation of Syndiotactic Polystyrene

Syndiotactic polystyrene was dissolved in TCB under reflux for 1.5 h to yield a 10% w/v solution. After 1.5 h, the solution was cooled to room temperature. Upon cooling, the 10% w/v sPS solution and allowed to remain at room temperature for 24 hours. Upon, the sPS solution crystallizes and forms a physical gel. The solid gel was manually broken in small, micron particles using a spatula. The sPS gel particles were resuspended in additional TCB to yield a 1% w/v sPS solution. The sPS gel-particle dispersion was allowed to equilibrate at 70 °C under a nitrogen purge for 1.5 hr. After equilibration, the appropriate amount of sulfonation reagent was added and the reaction was allowed to proceed for 1 hour at 70 °C under a nitrogen purge. After 1 h, 10 mL methanol was added to the dispersion to terminate the reaction. The dispersion was poured into a large excess of methanol. The SsPS ionomer particles were filtered and washed with deionized water. The resulting ionomer was dried under vacuum at 100 °C for 12 h.

Determination of Degree of Sulfonation

The randomly and non-randomly sulfonated SsPS ionomers were redissolved in 90/10 v/v TCB/methanol for 1.5 h to a yield 0.5% w/v solution. The 0.5% w/v solution was used to determine the degree of sulfonation via non aqueous titration with methanolic benzyltrimethylammonium hydroxide. The benzyltrimethylammonium hydroxide was standardized using benzoic acid. SsPS ionomers of low ion content and high ion content were

prepared. Low ion content SsPS ionomers containing 3.2 mol% sulfonate groups are identified as SsPS3.2H^+R and SsPS3.2H^+NR where the H^+ denotes the ionomers are in the acid-form. The R and NR nomenclature denotes the SsPS random and the SsPS non-random ionomer respectively.

Differential Scanning Calorimetry

Thermal behavior and crystallization kinetics of the SsPS ionomers were studied using differential scanning calorimetry (DSC). A TA Instruments Q2000 DSC was used to probe the thermal behavior of the SsPS ionomers. Samples were prepared by thermally pressing each ionomer at 200 °C at 3000 psi for 3 min using a Carver Laboratory Press. The SsPS ionomers films were allowed to cool to RT under ambient conditions after removal from the press. Samples from the thermally pressed films were die cut and placed within aluminum DSC pans. The weight for each sample was maintained between 6 – 8 mg.

DSC analysis was performed under a continuous nitrogen flow to minimize sample degradation. The samples were heated to 330 °C at 20 °C/min from 50 °C and held at that maximum temperature for 5 min to erase previous thermal history and the presence of any persistent nuclei. Samples were then cooled to 50 °C at the following cooling rates -100, -50, -20, -10, and -5 °C/min and then heated to 330 °C at 20 °C/min. The glass transition, crystallization temperature, and melting temperatures of the SsPS3.2H^+R and SsPS3.2H^+NR ionomers were determined from the second DSC scan after erasing the thermal history using TA Instruments Universal Analysis Software. TA Instruments Universal Analysis software was used to analyze the resulting DSC traces.

RESULTS AND DISCUSSION

The preparation of block copolymers is often accomplished by utilizing various copolymerization techniques that are often complex and require stringent conditions or specialized reaction apparatus making many methods of copolymerization not highly suited for rapid introduction into industrial environments. The post-polymerization modification of polymers is often explored as a facile method to prepare functionalized polymers, but modification of a polymer after it has been polymerized often leads to a random placement of functional groups along the homopolymer backbone. In cases where block copolymer architecture is desired, copolymerization has been the primary method primary choice to prepare a copolymer with controlled architecture. However, a method to prepare a blocky placement of functional groups along the backbone of a semicrystalline polymer such as sPS may be possible by taking advantage of the innate morphology of the homopolymer. Figure VIII-1 contains a depiction of the sulfonation process that occurs in a homogenous solution of sPS and the sulfonation process that occurs when sPS has formed a physical gel upon cooling from the solution state that consists of crystalline and amorphous domains. When the sulfonation process is conducted while sPS is in the solution state, the sulfonate groups are randomly placed along the polymer backbone. However, when sulfonation occurs while sPS is in the physical gel state, the sulfonation reagent is excluded from the crystalline domains and is only able to penetrate the amorphous regions.

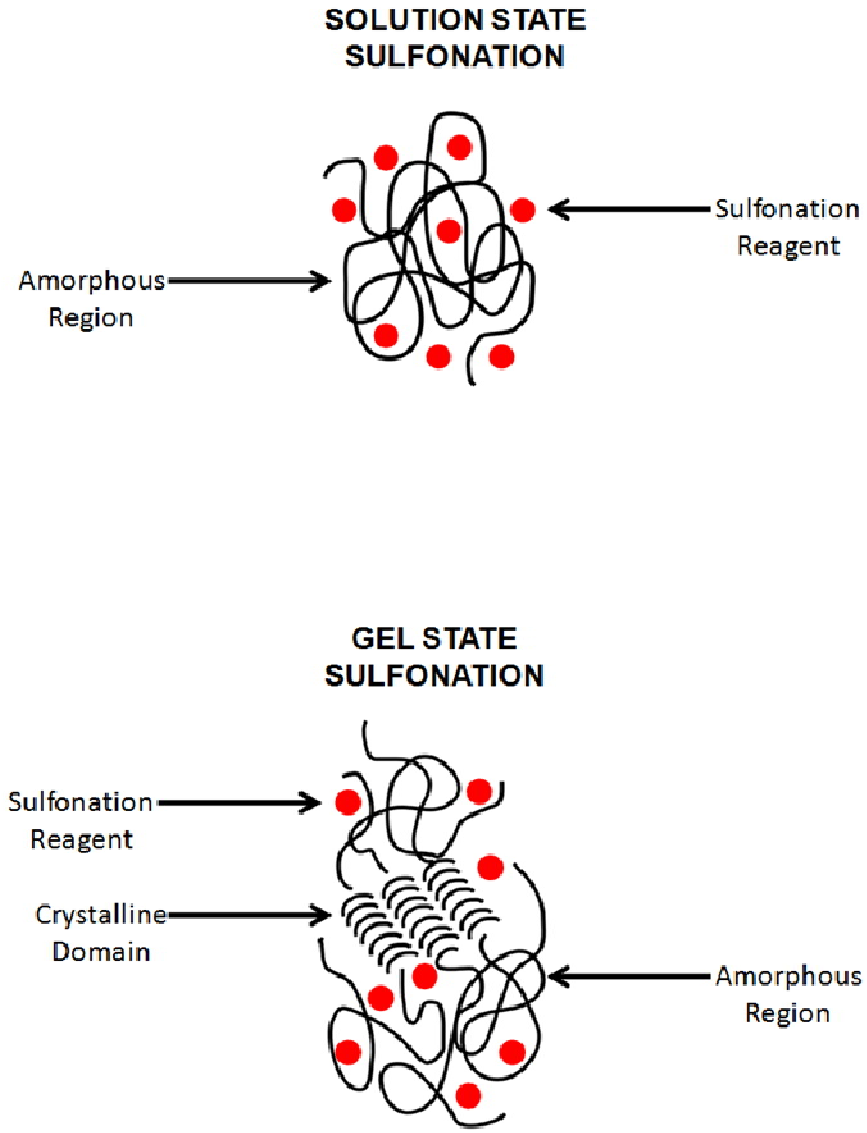

Figure VIII-1. Diagram of solution state and gel state sulfonation post-polymerization methods.

Therefore, sulfonation in the physical gel state is likely to result in considerable longer sequences of unsulfonated sPS homopolymer than sPS that has been sulfonated in the solution state. The resulting SsPS ionomers from each method of sulfonation are likely to have different morphologies in the solid state which are depicted in Figure VIII-2. The random SsPS ionomer is likely to consist of phase separated ionic domains that are homogeneously distributed

throughout the ionomer matrix due to random placement of the sulfonate groups along the polymer backbone.

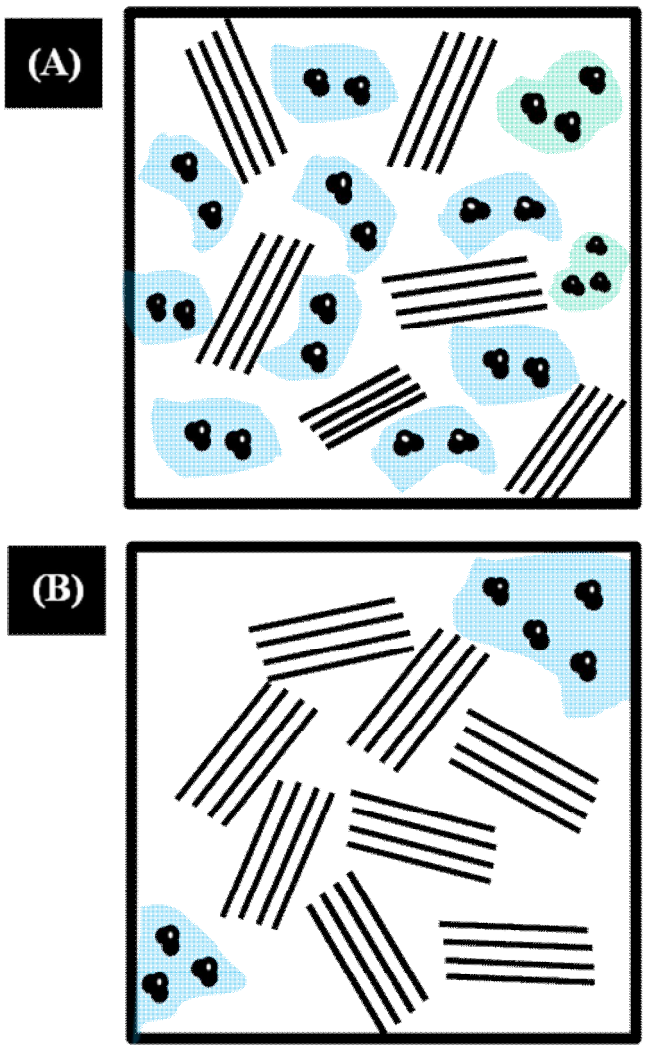

Figure VIII-2. Schematic of proposed SsPS ionomer morphology a for (A) randomly sulfonated sPS and (B) non-randomly sulfonated sPS.

In contrast, the SsPS ionomer sulfonated in the physical gel state likely consists of a more phase separated morphology where a larger portion of the crystalline domains are present with a greater degree of separation between the ionic and crystalline regions overall.

Previous studies on the crystallization behavior syndiotactic polystyrene under non-isothermal crystallization conditions has shown that the cooling rate has a significant effect of

the crystallization rate, crystallization mechanism, and development of different polymorphic structures [12-15]. Therefore, it is of primary interest to also evaluate the effect of the incorporation of sulfonate groups on the non-isothermal crystallization behavior of SsPS ionomer with random and non-random architectures.

Figure VIII-3 contains a plot of the heat evolved during crystallization versus temperature for SsPS3.2H^+R at various cooling rates from the melt. The general trend observed in this plot is that as the cooling rate decreases there is a shift in the peak crystallization temperature to higher temperatures. There is also a very prominent crystallization exotherm that is observed for the SsPS3.2H^+R ionomer cooled from the melt at 20 °C/min. The shift in the peak crystallization temperature to higher temperature and the increase in the amount of heat evolved during crystallization as the cooling rate decreases may be attributed to the increase in time available for the crystallizable chain segments of the SsPS3.2H^+R ionomer to organize and pack into crystalline structures as the rate of cooling from the melt state decreases. At higher rates of crystallization there is less time for the crystallizable chain segments to pack into crystalline structures under rapid cooling from the melt resulting in less heat evolved during crystallization.

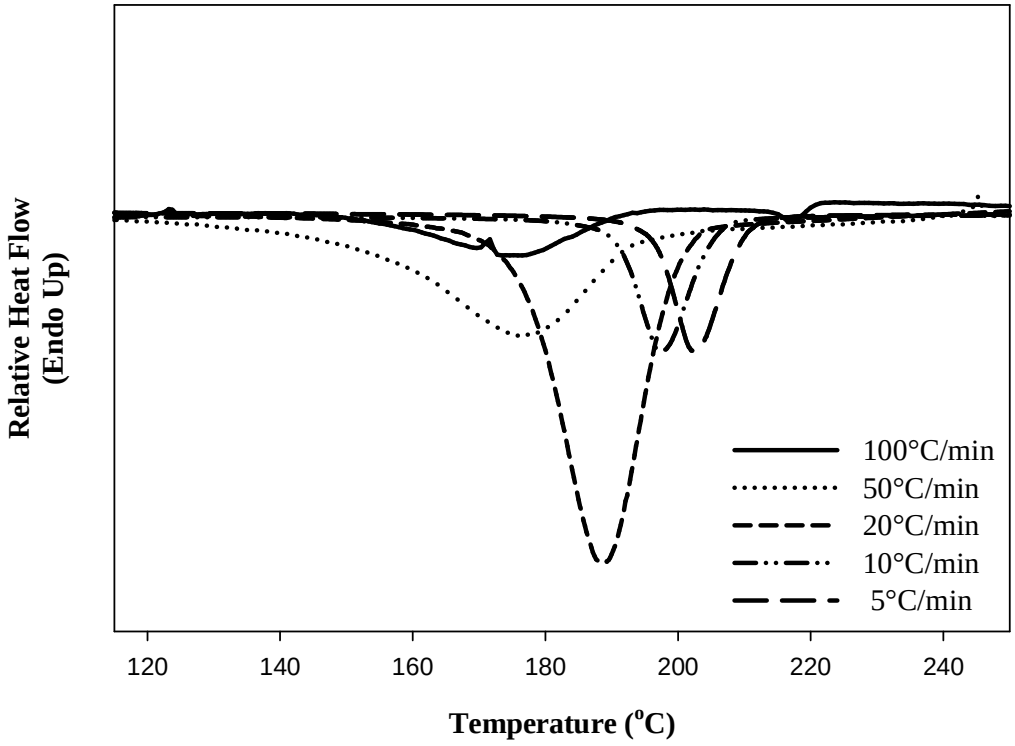

Figure VIII-3. Heat flow versus temperature (°C) for SsPS3.2H$^+$R at various cooling rates.

Figure VIII-3 shows a maximum amount of heat evolved during crystallization at a cooling rate of 20 °C/min. At cooling rates below 20 °C/min, the amount heat evolved during crystallization decreases, but the peak crystallization temperature continues to increase. The decrease in the heat evolved at lower cooling rates may also be attributed to the lack of a driving force to initiate polymer crystallization at temperatures close to the melting temperature of the ionomer. It is well known that the degree of supercooling has a significant impact on the rate of polymer crystallization. As the degree of supercooling increases by shifting towards temperatures further away from the melting temperature, the driving force for crystallization increases. However, at low degrees of supercooling the rate of polymer crystallization is slow due to the enhanced mobility of chains at the higher temperatures. A decrease in the heat

evolved at cooling rates below 20 °C/min may also suggest that different polymorphic crystal structures may form under different cooling rates. Previous research has shown that the α-crystal is the kinetically-favored polymorphic structure formed during melt crystallization, while the β-crystal of sPS is the more thermodynamically stable crystal structure and has been shown to develop at long isothermal crystallization times. It may be possible that at 20 °C/min, the formation of the sPS α-crystal is favored with rapid nucleation and growth occurring at 20 °C/min followed by a change in the mechanism of crystal nucleation and growth at lower cooling rates that may favor the formation β -crystal of sPS.

The heat evolved during exothermic crystallization under various cooling rates for the SsPS3.2H^+NR ionomer is shown in Figure VIII-4. The same general trends are observed for the SsPS3.2H^+NR ionomer as seen for the randomly sulfonated SsPS ionomer containing the same mol% of sulfonate groups. There is an increase in the peak crystallization temperature with decreasing cooling rates. The shift in the peak crystallization temperature may also be attributed to the increase in the amount of time given to the crystallizable chain segments to organize and pack into crystalline structures at higher temperatures. The same possible origins for the observed changes in the heat evolved during the crystallization of SsPS3.2H^+R may also be applied for the behavior observed in the SsPS3.2H^+NR ionomer. Changes in the degree of supercooling and potential changes in the type of polymorphic structure may contribute to the manifestation of the crystallization behavior observed in Figure VIII-4.

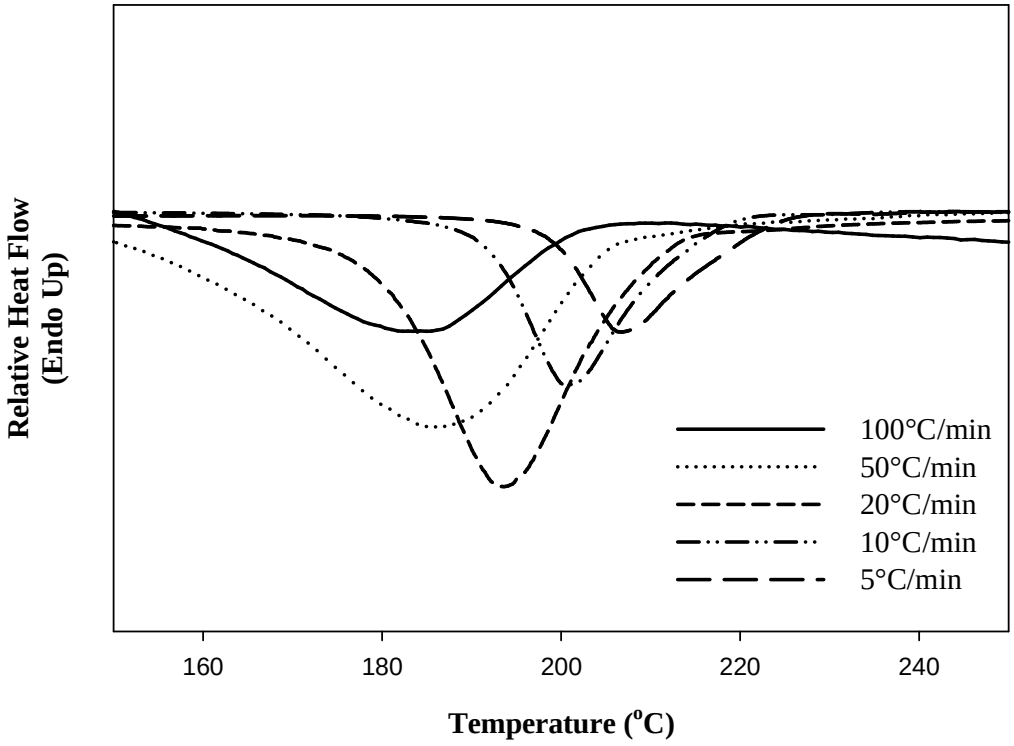

Figure VIII-4. Heat flow versus temperature (°C) for SsPS3.2H$^+$NR at various cooling rates.

It is also interesting to note that the breadths of the exothermic peaks for the SsPS3.2H$^+$R and SsPS3.2H$^+$NR ionomers are different as shown in Figure VIII-3 and Figure VIII-4, respectively. The exothermic peak breadths of the SsPS3.2H$^+$NR ionomer at various cooling rates are broader than the peak breadths of the randomly sulfonated SsPS ionomer. The narrower peak breadth for the SsPS3.2H$^+$R ionomer may be attributed to a more pronounced effect of ionic aggregates on the development of crystalline structures from the crystallizable component of the ionomer.

It is suggested that the ionic aggregates of the randomly sulfonated ionomer are homogeneously distributed throughout the polymer matrix (Figure VIII-2) and therefore have the potential to restrict the movement of polymer chains to a greater degree than ionic aggregates

that may be heterogeneously distributed throughout the polymer matrix or present as more isolated ionic domains due to a pseudo-blocky placement of the sulfonate groups along the polymer backbone. A greater restrictive motion of polymer chains in the random SsPS ionomer due to the homogeneity of ionic groups throughout the matrix (Figure VIII-2) would lead to the development of thinner crystallites and a smaller distribution of crystallite thickness which could be detected within the DSC thermogram as a narrower exothermic peak.

The broader exothermic peak of the non-randomly sulfonated ionomer as seen in Figure VIII-4 may be attributed to the pseudo-blocky placement of sulfonate groups along the polymer backbone. The sulfonation reagent is excluded from the crystalline domains and therefore only penetrates the amorphous regions where a random sulfonation of the polymer chains occurs as shown in Figure VIII-1. Therefore upon cooling from the melt, the portions of the polymer chains that were a part of the crystalline domain during the sulfonation process are able to more readily crystallize because there are no sulfonated sPS units that must be excluded from the crystalline lattice and also because the ionic domains have less of an influence on the crystallization process because there is likely a greater degree of separation between the crystalline and ionic components as shown in the schematic diagram of Figure VIII-2.

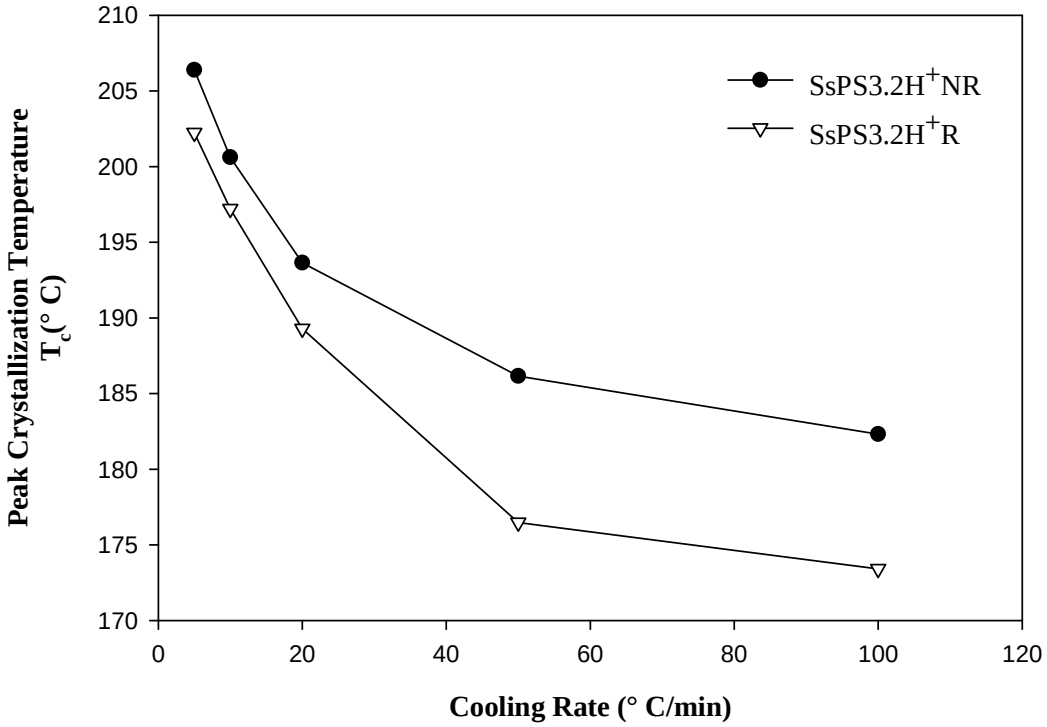

Figure VIII-5. Peak crystallization temperature (°C) for SsPS3.2H$^+$R and SsPS3.2H$^+$NR at various cooling rates.

.

The changes in the crystallization exotherms for the random and non-random SsPS ionomers are summarized in Figure VIII-5 and Figure VIII-6 which plot the changes in the peak exothermic crystallization temperatures and the amount of heat evolved during crystallization, respectively.

Figure VIII-6 shows a plot of the heat evolved during crystallization for the random and non-random SsPS ionomer containing 3 mol% sulfonate groups. At rapid crystallization rates, the difference in the amount of heat evolved during crystallization from the melt for the two systems is small. However, as the cooling rate decreases, the difference between the heats evolved during crystallization becomes greater for the non-random SsPS ionomer.

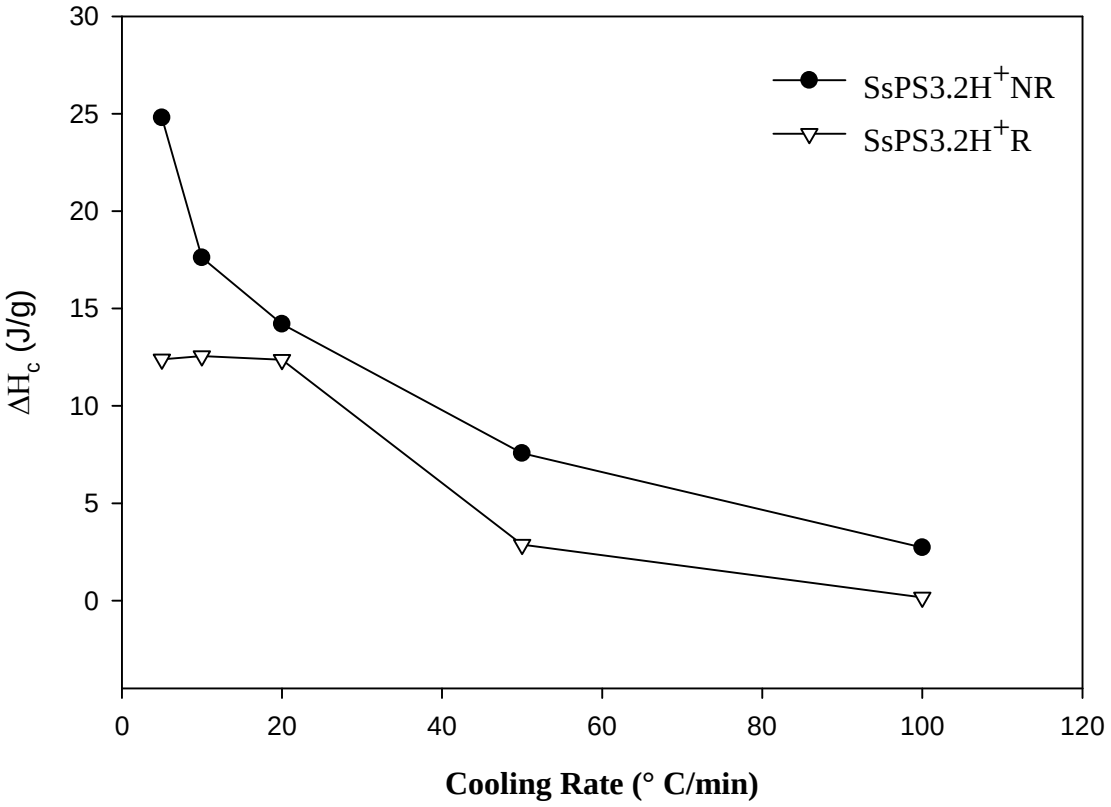

Figure VIII-6. ΔH_c versus cooling rate for (closed circles) SsPS3.2H$^+$R and (open triangles) SsPS3.2H$^+$NR at various cooling rates.

This trend may suggest that the non-random SsPS ionomer has greater chain mobility at the lower cooling rates than the random SsPS ionomer. The greater chain mobility may be the result of few encountered defects in the form of the pendant sulfonate groups during crystallization from the melt.

The melting transitions of the random and non-random SsPS ionomers were determined after cooling to 30 °C at various cooling rates. After cooling to 30 °C, the ionomers were

heated to 330 °C at a heating rate of 20 °C/min. Figure VIII-7 contains the plots of melting temperature versus cooling rate for the two different ionomers. The melting temperature of the SsPS3.2H^+NR ionomer remains higher than that of the randomly sulfonated system after isothermal crystallization at every cooling rate. There is a maximum melting temperature for both SsPS ionomers after cooling to 30 °C at 20 °C/min. The maximum melting temperature observed at this cooling rate may be attributed crystallization phenomenon associated with supercooling and molecular mobility or may be the result of the preferential formation of one sPS crystalline polymorph over another. The equilibrium melting temperature of the β-crystal has been reported to be higher than that of the α-crystal [16-18] and this maximum melting temperature may indicate that slow cooling from the melt at 20 °C/min may induce the formation of the β-crystal polymorph through the presence of a maximum melting temperature at 20 °C/min. A more complete investigation of the crystallization mechanisms occurring during the non-isothermal crystallization of SsPS ionomers must include WAXD and FTIR studies in order to determine the nature of the polymorphic structure of the different ionomers [17, 19-25].

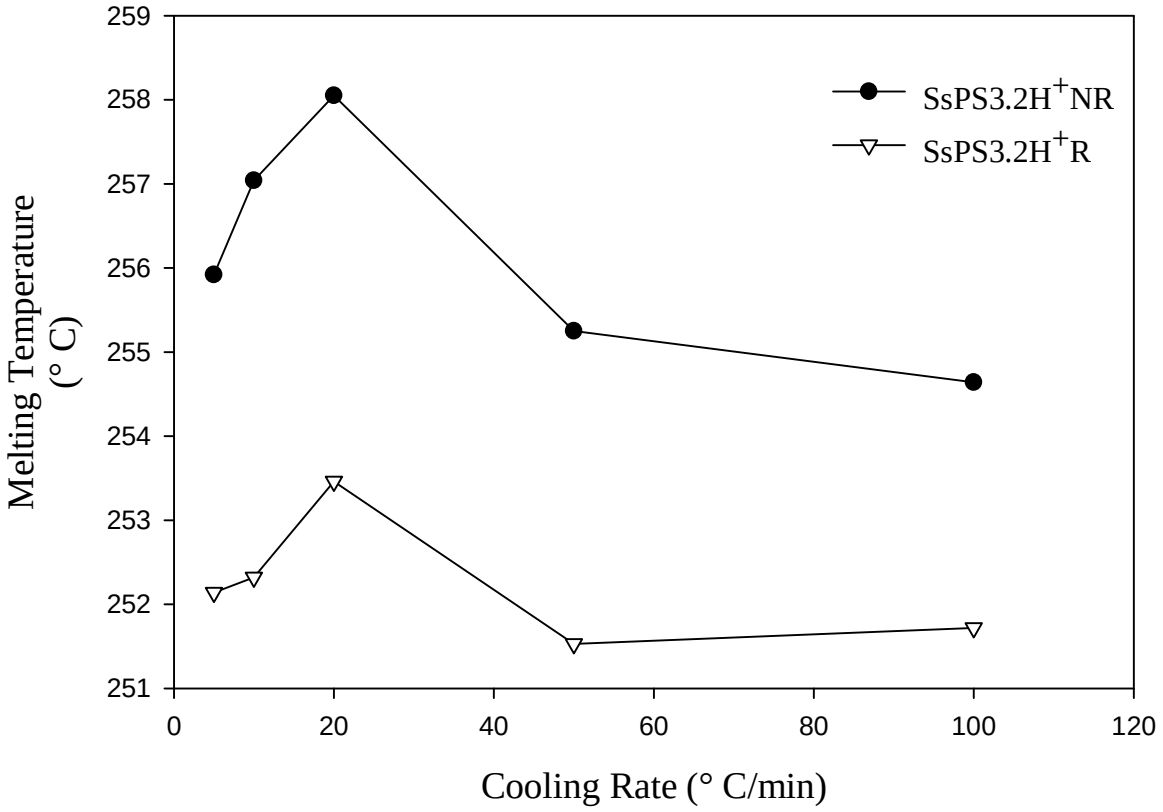

Figure VIII-7. Melting temperature versus cooling rate for (closed circles) SsPS3.2H$^+$R and (open triangles) SsPS3.2H$^+$NR at various cooling rates. The melting temperatures were taken after non-isothermal crystallization to 30 °C and a scan rate of 20 °C/min to 330 °C.

The kinetics of the non-isothermal crystallization process was monitored by following changes in the relative crystallinity as a function of temperature at different cooling rates. The plots of relative crystallinity versus temperature for the SsPS3.2H$^+$R and SsPS3.2H$^+$NR ionomers are shown in Figures VIII-8 and VIII-9, respectively.

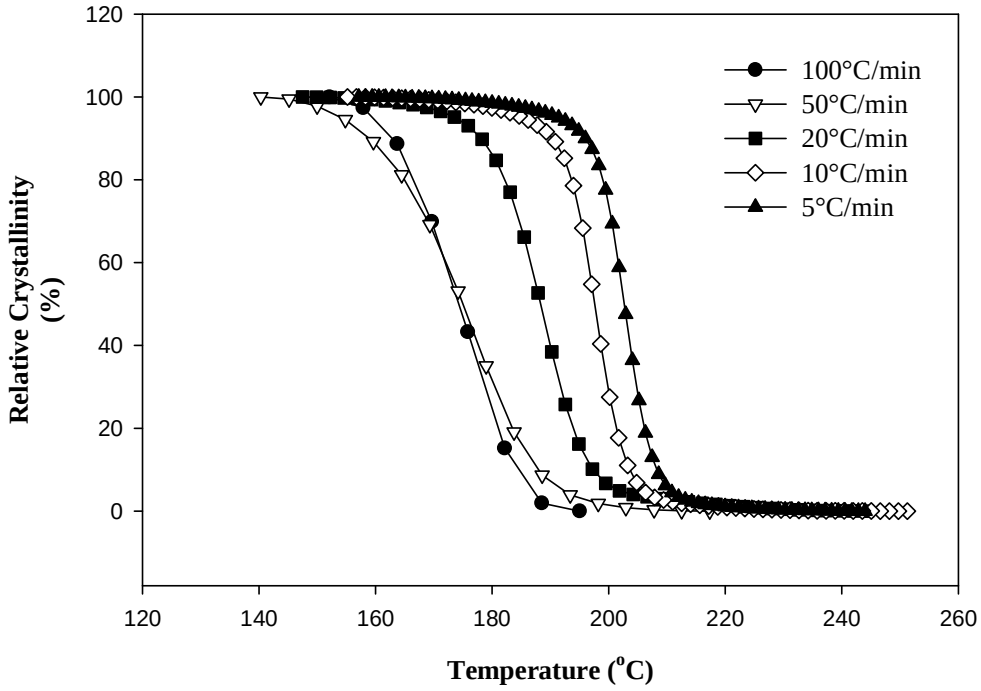

Figure VIII-8. Relative crystallinity versus time for SsPS3.2H^{+}R at various cooling rates.

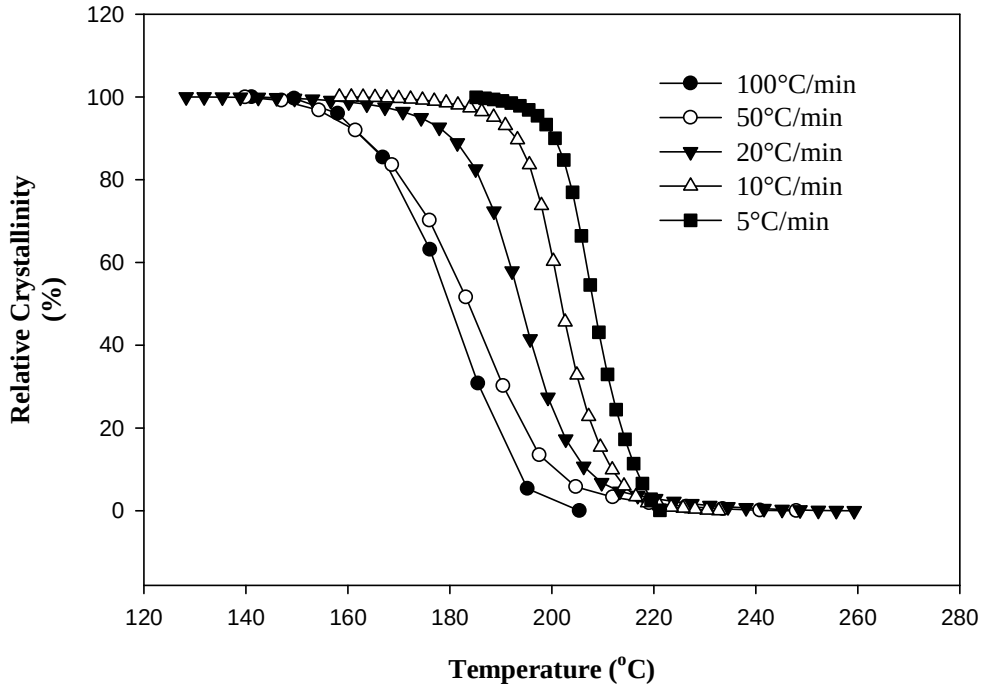

Figure VIII-9. Relative crystallinity versus temperature for SsPS3.2H^{+}NR at various cooling rates.

The plots of relative crystallinity versus temperature can be transformed into plots of relative crystallinity versus time by using the following relationship between crystallization temperature and time:

$$t = \frac{|T - T_0|}{\Phi} \quad (1)$$

T is the temperature at which crystallization begins which is taken to be *t* = 0. The plots of relative crystallinity versus ln t obtained after utilizing equation 1 for the SsPS3.2H$^+$R and SsPS3.2H$^+$NR ionomers are shown in Figures VIII-10 and VIII-11, respectively.

It can be seen in the plots of relative crystallinity versus ln t for both SsPS ionomers that as the rate of cooling decreases that the plots of relative crystallinity shift to longer times.

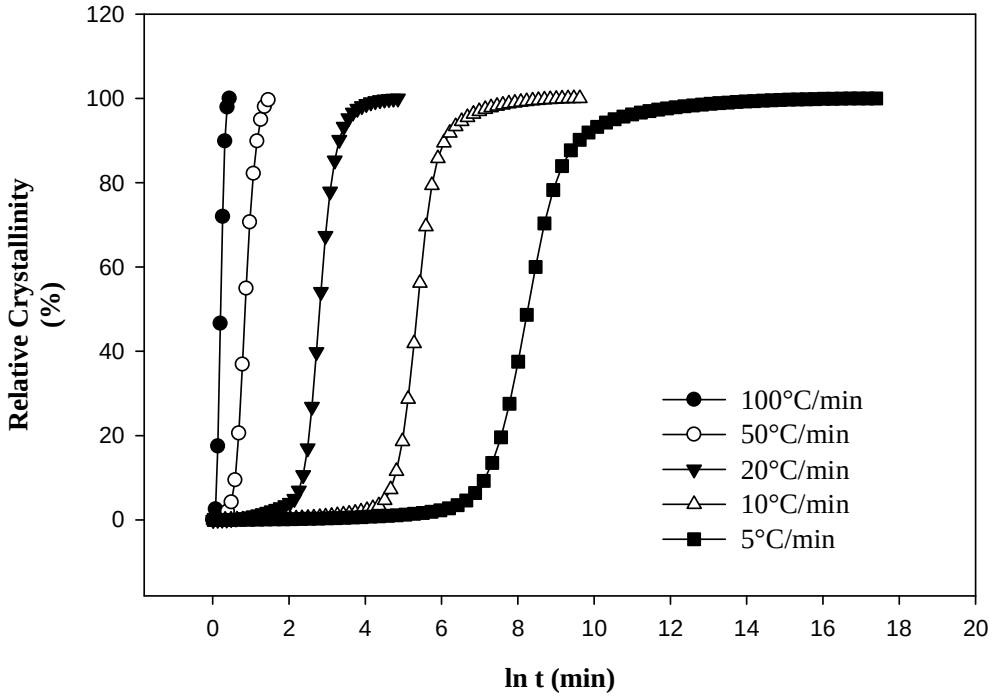

Figure VIII-10. Relative crystallinity versus ln time for SsPS3.2H$^+$R at various cooling rates.

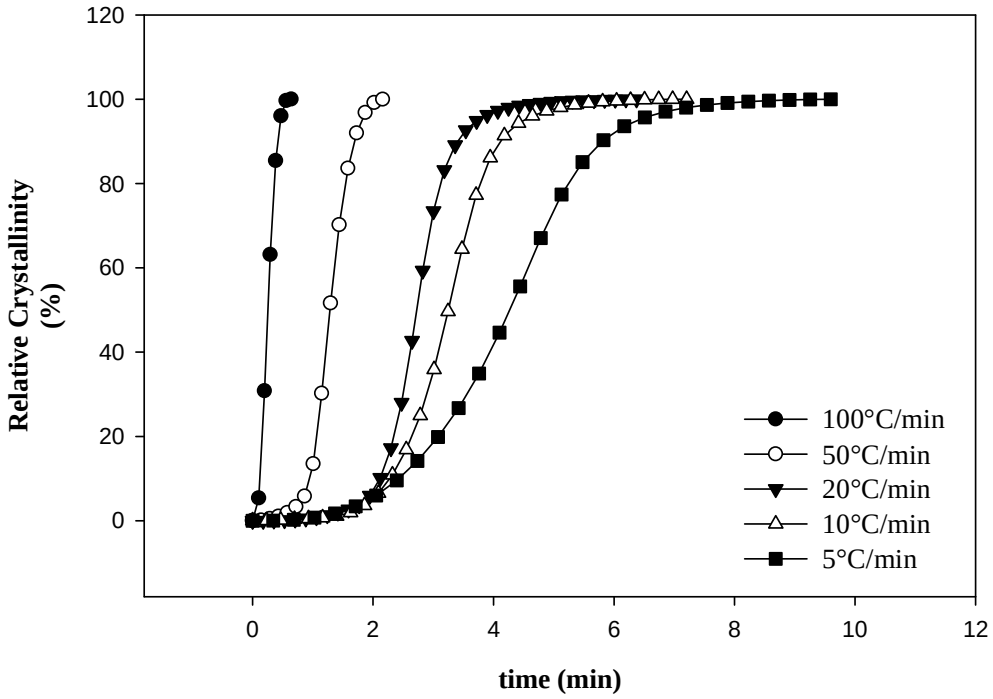

Figure VIII-11. Relative crystallinity versus ln time for SsPS3.2H$^+$ NR at various cooling rates.

A measure of the rate of bulk crystallization may be determined using the crystallization half-time which is the time which 50% of the crystalline fraction has crystallized which can be obtained from the plots of relative crystallinity versus time for both SsPS ionomers. Figure VIII-12 shows the plots of the crystallization half-time versus cooling rate for the two different ionomers. It can be seen that at rapid cooling rates such as 100 and 50 °C/min, that the crystallization half-times of both ionomers are very close. At 20 °C/min, the crystallization half-time for the SsPS3.2H$^+$ R ionomer is slightly lower than the crystallization half-time value for the SsPS3.2H$^+$ NR ionomer. This indicates that the random SsPS ionomer may be crystallizing more rapidly at this cooling rate, but it is also likely that the half-times can be considered to be essentially the same as the difference between the half-time values is less than one minute.

However, there is a strong difference in the crystallization rate of the random and non-random ionomers at slow cooling rates as shown in Figure VIII-12. The crystallization half-time value for the random SsPS ionomer is almost double that of the non-random SsPS at cooling rates of 10 and 5 °C/min from the melt.

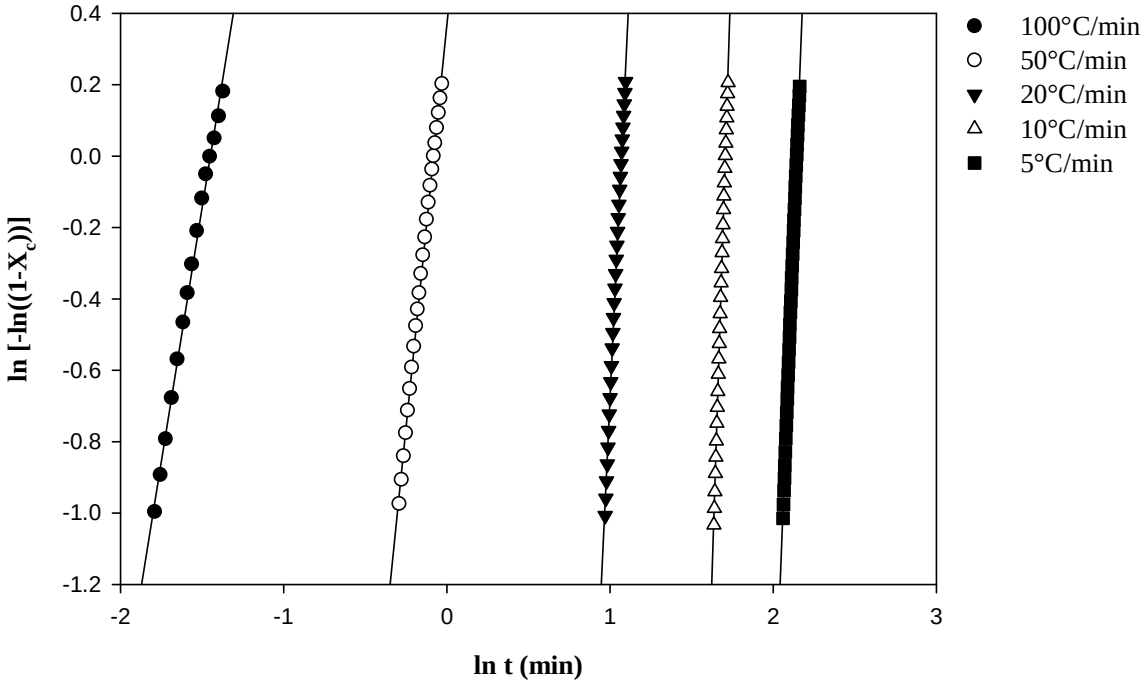

Figure VIII-12. ln [-ln(1-X_c(t))]versus ln time for SsPS3.2H^+ R at various cooling rates.

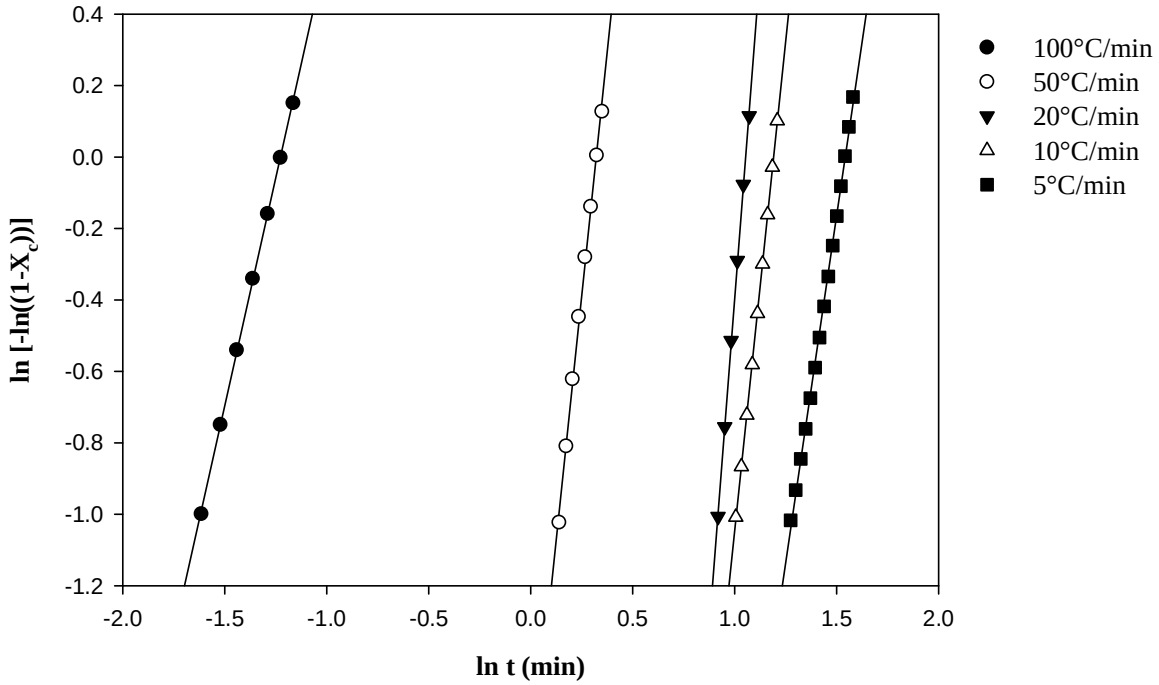

Figure VIII-13. ln [-ln(1-X_c(t))]versus ln time for SsPS3.2H$^+$ NR at various cooling rates.

Table VIII-1. Avrami kinetic parameters for SsPS3.2H$^+$R and SsPS3.2H$^+$R.

SsPS 3.2H$^+$R Cooling Rate (C/min)	**n**	**K (min^{-1})**
100	2.2	48
50	4.5	14
20	9.7	3.1 x 10^{-5}
10	14.4	6.2 x 10^{-11}
5	11.9	8.7 x 10^{-12}
SsPS 3.2H$^+$NR Cooling Rate (C/min)	**n**	**K (min^{-1})**
100	2.6	23
50	5.5	1.7 x 10^{-1}
20	7.4	4.2 x 10^{-4}
10	5.5	1.5 x 10^{-3}
5	3.9	3.1 x 10^{-3}

The value of n for the Avrami rate exponent does not represent the dimensionality of the crystalline structures developed during the non-isothermal crystallization process, but the rate of crystallization obtained from the Avrami analysis has been utilized to describe the rate of crystallization for semicrystalline polymers during a non-isothermal crystallization process. As seen in Table VIII-1, the rate of crystallization K for the non-random SsPS ionomer is significantly faster than the non-random SsPS ionomer. This behavior is attributed to longer sequences of unsulfonated material that are able to organize and pack into crystalline structures more quickly in the non-random SsPS 3.2H^+NR than the randomly sulfonated SsPS 3.2H^+R ionomer. It is likely that few sulfonate groups which act as defects are encountered during the crystallization of the non-random SsPS ionomer than the SsPS ionomer consisting of a random architecture.

CONCLUSION

The non-isothermal crystallization behavior of syndiotactic polystyrene sulfonated in the solution and physical gel states were studied using DSC analysis. The non-random SsPS peak exothermic crystallization temperature, T_p, is higher than the T_p for the random SsPS ionomer and the breadth of the entire exothermic peak of the non-random SsPS ionomer is broader than the exothermic peak for the random SsPS ionomer as well. The crystallization half-time obtained from plots of relative crystallinity versus time for the SsPS ionomers revealed that he crystallization half-times were essentially the same at very rapid to moderate cooling rates, but the non-random SsPS ionomer crystallized more rapidly at lower cooling rates than the random SsPS ionomer. The rate of crystallization determined by using the Avrami analysis also showed similar behavior with the rate of crystallization of the non-random SsPS ionomer being significantly higher than the randomly sulfonated material.

These differences in the crystallization trends observed during the non-isothermal crystallization of the two SsPS ionomers are attributed to differences in the placement of the sulfonate group along the polymer backbone. Further investigation and modeling of the non-isothermal crystallization behavior of these two ionomers using non-isothermal crystallization model such as the Ozawa model are of fundamental interest.

REFERENCES

1. Di Lorenzo ML and Silvestre C. Progress in Polymer Science 1999;24(6):917-950.
2. Martins JA and Cruz Pinto JJC. Polymer 2000;41(18):6875-6884.
3. Ozawa T. Polymer 1971;12(3):150-158.
4. Ziabicki A and Jarecki L. Colloid & Polymer Science 1978;256(4):332-342.
5. Ziabicki A. Colloid & Polymer Science 1974;252(3):207-221.
6. Nakamura K, Watanabe T, Katayama K, and Amano T. Journal of Applied Polymer Science 1972;16(5):1077-1091.
7. Nakamura K, Katayama K, and Amano T. Journal of Applied Polymer Science 1973;17(4):1031-1041.
8. Hu X and Lesser AJ. Macromolecular Chemistry and Physics 2004;205(5):574-580.
9. Sajkiewicz P, Carpaneto L, and Wasiak A. Polymer 2001;42(12):5365-5370.
10. Ray SS and Bousmina M. Macromolecular Chemistry and Physics 2006;207(14):1207-1219.
11. Alvarez VA, Stefani PM, and Vázquez A. Journal of Thermal Analysis and Calorimetry 2005;79(1):187-193.
12. Chen Q, Yu Y, Na T, Zhang H, and Mo Z. Journal of Applied Polymer Science 2002;83(12):2528-2538.
13. Wesson RD. Polymer Engineering & Science 1994;34(14):1157-1160.
14. Yuan Z, Song R, and Shen D. Polymer International 2000;49(11):1377-1382.
15. Bu W, Li Y, He J, and Zeng J. Macromolecules 1999;32(21):7224-7225.
16. Wang C, Hsu YC, and Lo CF. Polymer 2001;42(20):8447-8460.

17. Ho R-M, Lin C-P, Tsai H-Y, and Woo E-M. Macromolecules 2000;33(17):6517-6526.

18. Lawrence SS and Shinozaki DM. Polymer Engineering & Science 1997;37(11):1825-1832.

19. Musto P, Tavone S, Guerra G, and De Rosa C. Journal of Polymer Science Part B: Polymer Physics 1997;35(7):1055-1066.

20. Lin RH and Woo EM. Polymer 2000;41(1):121-131.

21. Kobayashi M, Nakaoki T, and Ishihara N. Macromolecules 1989;22(11):4377-4382.

22. Wu S-C and Chang F-C. Polymer 2004;45(3):733-738.

23. Guerra G, Musto P, Karasz FE, and MacKnight WJ. Die Makromolekulare Chemie 1990;191(9):2111-2119.

24. Sun YS, Woo EM, Wu MC, and Ho R-M. Macromolecules 2003;36(22):8415-8425.

25. Sorrentino A, Pantani R, and Titomanlio G. Journal of Polymer Science Part B: Polymer Physics 2007;45(2):196-207.

CHAPTER IX

SPHERULITIC GROWTH OF RANDOM AND NON-RANDOM SULFONATED SYNDIOTACTIC POLYSTYRENE IONOMERS

ABSTRACT

The spherulitic growth rates of random and non-random sulfonated syndiotactic polystyrene (SsPS) ionomers containing 3 mol% sulfonic acid groups were measuring using polarized light microscopy. The rate of spherulitic growth was more rapid in the non-random sulfonated syndiotactic polystyrene ionomer than the random ionomer. There was also a significant difference between the spherulitic textures of the non-random and random SsPS ionomers. The spherulites of the non-random SsPS ionomer were larger and appeared to be than the spherulites random SsPS ionomer upon solidification over a wide range of isothermal crystallization temperatures. The nucleation density of the random SsPS ionomer was higher than the non-random ionomer which contributed to the development of smaller spherulites during isothermal crystallization. The differences in the spherulitic growth rate and morphology of the two ionomers are attributed to the differences in the distribution of the sulfonate groups along the sPS homopolymer backbone using two different post-polymerization modification techniques. The non-random SsPS ionomer likely consists of blocky type of architecture with longer sequences of unsulfonated material that more readily crystallizes from the melt.

INTRODUCTION

The crystallization and morphological behavior of syndiotactic polystyrene has been studied in detail due to many of the very interesting properties that the polymer displays such as high melting temperature, rapid crystallization rate, and good electrical properties. Researchers have characterized the crystallization behavior of sPS under isothermal, non-isothermal, and cold crystallization conditions and have found that the rate of crystallization and the formation of the resulting crystalline suprastructures are heavily influenced by a number of parameters including maximum melting temperature, residence time in the melt, cooling rate, and crystallization temperature [1-6].

Changes in the crystallization behavior and crystalline suprastructure of sPS has been investigated by studying blends of sPS with other polymers and have found the blending sPS with other polymers significantly alters both the rate of crystallization and the particular sPS crystal polymorph that is formed [7-15]. Many of the sPS blend studies focus on the conditions under which the blend components are miscible and the differences in the thermal properties, but little information is available on the effect of the additional polymer on the spherulitic growth rate and overall crystalline suprastructure. However, Cimmino and coworkers studied the change in the thermal properties and spherulitic growth rate in addition to changes in spherulitic texture in the presence of an additional polymer [16]. They prepared blends of sPS and poly(vinyl methyl ether) (PVME) and blends of sPS and poly(2,6-dimethyl-1,4diphenylene oxide) (PPO). They observed a decrease in the spherulitic growth rate of sPS when PPO was

added, but an increase in the spherulitic growth rate of sPS upon addition of PVME to sPS. They attributed the increase in the spherulitic growth rate of sPS /PVME blends to a decrease in the glass transition of the sPS-rich phase which lowered the energy required for the transport of crystalline segments in the melt according to kinetic theories of crystallization [17-19]. The increase in the spherulitic growth rate of sPS/PPO blends was decreased due to the increase in the glass transition temperature of sPS in the presence of PPO which increased the energy required for the transport of polymer segments across the melt/crystal interface.

Copolymers of syndiotactic polystyrene have been produced via copolymerization and post-polymerization modification of the sPS homopolymer [20-26] but there is very limited information of the effect of comonomer incorporation on the spherulitic growth rate spherulitic and morphology of sPS copolymers. Orler and coworkers prepared random sulfonated syndiotactic polystyrene ionomers via post-polymerization sulfonation of sPS in solution [27-29]. They found that the spherulites of lightly sulfonated sPS were much smaller than the spherulites of the sPS homopolymer under the same isothermal crystallization conditions using small angle laser light scattering studies of volume-filled polymer films [28]. They attributed the decrease in the size of the SsPS ionomer spherulites to increased nucleation density and a retarded spherulitic growth rate. The increase in nucleation density was due to the presence of ionic aggregates distributed throughout the random SsPS ionomer matrix which acted as nucleation sites. Although, there was a high nucleation density for the SsPS ionomer compared to the sPS homopolymer, the ionic aggregates restricted the mobility of the polymer chains and additionally contributed to the formation of smaller spherulites.

The aim of this study is to further investigate the effect of the incorporation of sulfonic acid groups on the spherulitic growth rate and spherulitic morphology of sulfonated syndiotactic

polystyrene (SsPS) ionomers. To the knowledge of the author, this will be the first report of the spherulitic morphology of SsPS ionomers using a combination of polarized light microscopy and small angle laser light scattering.

EXPERIMENTAL

Materials

Syndiotactic polystyrene (Questra 102) MW of 310,000 g/mol was donated by the Dow Chemical Company. Reagent grade 1,2,4-trichlorobenze (TCB), methanol, sulfuric acid, potassium monopthalate were obtained from Fisher Scientific. Hexanoic anhydride, benzyltrimethylammoniuim hydroxide, and benzoic acid were received from Sigma Aldrich.

Preparation of Sulfonation Agent

The sulfonation agent was prepared according to previously published procedures using TCB as the solvent. TCB (25 mL) was added to a 50 mL volumetric flask containing 0.03 moles of hexanoic anhydride. The TCB/hexanoic anhydride solution was cooled in an ice bath for 1 hour, and then 1 mL of concentrated sulfuric acid was added to the chilled solution and shaken vigorously. Additional TCB was added to the volumetric flask to the 50 mL mark.

Random Sulfonation of Syndiotactic Polystyrene

sPS was dissolved in TCB under reflux for 1.5 h to yield a 10% w/v solution. After 1.5 h, the solution was cooled to 70 °C and then additional TCB was added to yield a 1% w/v sPS solution. The sPS solution was allowed to equilibrate at 70 °C under a nitrogen purge for 1.5 hr. After equilibration, the appropriate amount of sulfonation reagent was added and the reaction was allowed to proceed for 1 hour at 70 °C under a nitrogen purge. After 1 h, 10 mL methanol was

added to the solution to terminate the reaction. The solution was poured into a large excess of methanol to precipitate the ionomer. The precipitated ionomer was filtered and washed with deionized water.

Non-Random Sulfonation of Syndiotactic Polystyrene

Syndiotactic polystyrene was dissolved in TCB under reflux for 1.5 h to yield a 10% w/v solution. After 1.5 h, the solution was cooled to room temperature. Upon cooling, the 10% w/v sPS solution and allowed to remain at room temperature for 24 hours. Upon, the sPS solution crystallizes and forms a physical gel. The solid gel was manually broken in small, micron particles using a spatula. The sPS gel particles were resuspended in additional TCB to yield a 1% w/v sPS solution. The sPS gel-particle dispersion was allowed to equilibrate at 70 °C under a nitrogen purge for 1.5 hr. After equilibration, the appropriate amount of sulfonation reagent was added and the reaction was allowed to proceed for 1 hour at 70 °C under a nitrogen purge. After 1 h, 10 mL methanol was added to the dispersion to terminate the reaction. The dispersion was poured into a large excess of methanol. The SsPS ionomer particles were filtered and washed with deionized water. The resulting ionomer was dried under vacuum at 100 °C for 12 h.

Determination of Degree of Sulfonation

The randomly and non-randomly sulfonated SsPS ionomers were redissolved in 90/10 v/v TCB/methanol for 1.5 h to a yield 0.5% w/v solution. The 0.5% w/v solution was used to determine the degree of sulfonation via non aqueous titration with methanolic benzyltrimethylammonium hydroxide. The benzyltrimethylammonium hydroxide was standardized using benzoic acid. SsPS ionomers of low ion content and high ion content were

prepared. Low ion content SsPS ionomers containing 3.2 mol% sulfonate groups are identified as SsPS3.2H^+R and SsPS3.2H^+NR where the H^+ denotes the ionomers are in the acid-form. The R and NR nomenclature denotes the SsPS random and the SsPS non-random ionomer respectively.

Polarized Light Microscopy

The determination of the spherulitic growth rates of the pure matrices and clay-containing matrices was carried out using polarized light microscopy. A Nikon LV100 microscope equipped with a Nikon DXM1200 digital camera was used in crossed-polarized configuration to monitor spherulitic growth under isothermal conditions. Images were captured and analyzed using Nikon NIS-Elements BR software. Isothermal crystallization conditions were achieved using a Linkam TMS600 hotstage operated by a Linkam TMS 94 controller and Linkam Linksys32 software. The samples were heated to 330 °C on the Linkam hotstage and held at that maximum temperature for 5 min. Following a rapid temperature ramp at -100 °C/min, isothermal crystallization was carried out at 220, 225, 230, 235, and 240 °C with periodic image capture until complete spherulitic impingement occurred.

Small Angle Laser Light Scattering

Small-angle laser light scattering (SALLS) patterns were obtained in H_v mode using a laser light scattering experimental configuration similar to that of Stein and Rhodes [30]. A 3 mW He-Ne laser light of 632.8 nm (Oriel Corporation, Model 6697) was used as the incident light and the H_v patterns were captured using a SenSys 1401E (Photometrics) CCD camera positioned at a sample-to-detector distance of 380 mm. The spherulite diameters of the pristine

polymers and polymer/clay mixtures were obtained using volume-filled samples that were isothermally crystallized at 220, 225, 230, 235, and 240 °C using a Linkam hotstage according to the heating profile used for the polarized optical microscopy analysis. The H_v patterns were processed using ImageJ software (National Institute of Health).

RESULTS AND DISCUSSION

The effect of the controlled placement of comonomers within a copolymer is very interesting. Research has shown that polymer properties are influenced by the architecture of the polymer system. The synthesis and preparation of copolymers of varying architecture such as block copolymers containing polar functional groups is often accomplished using complex synthetic procedures which often require the use of harsh solvents and specialized reaction equipment and vessels. Therefore, it is of considerable interest to develop methods to prepare functionalized copolymers with controlled architectures.

The post-polymerization functionalization of syndiotactic polystyrene using acetyl sulfate has been done while the sPS homopolymer was in the solution state resulting in an ionomer containing a random placement of the sulfonic acid groups along the polymer backbone [27-29, 31-33]. However, it is proposed that conducting the sulfonation of sPS while the polymer is in the physical gel state would result in a non-random placement of the sulfonic acid groups along the polymer backbone. When in the physical gel state, the sulfonation reagent is not able to penetrate the crystalline domains of the sPS polymer which make up the physical gel. The sulfonation reagent would penetrate or reside in the amorphous domains of the gel resulting in the sulfonation of only the amorphous regions. A schematic of the sulfonation process in the solution and physical gel states and the resulting ionomer architectures is shown in Figure IX-1.

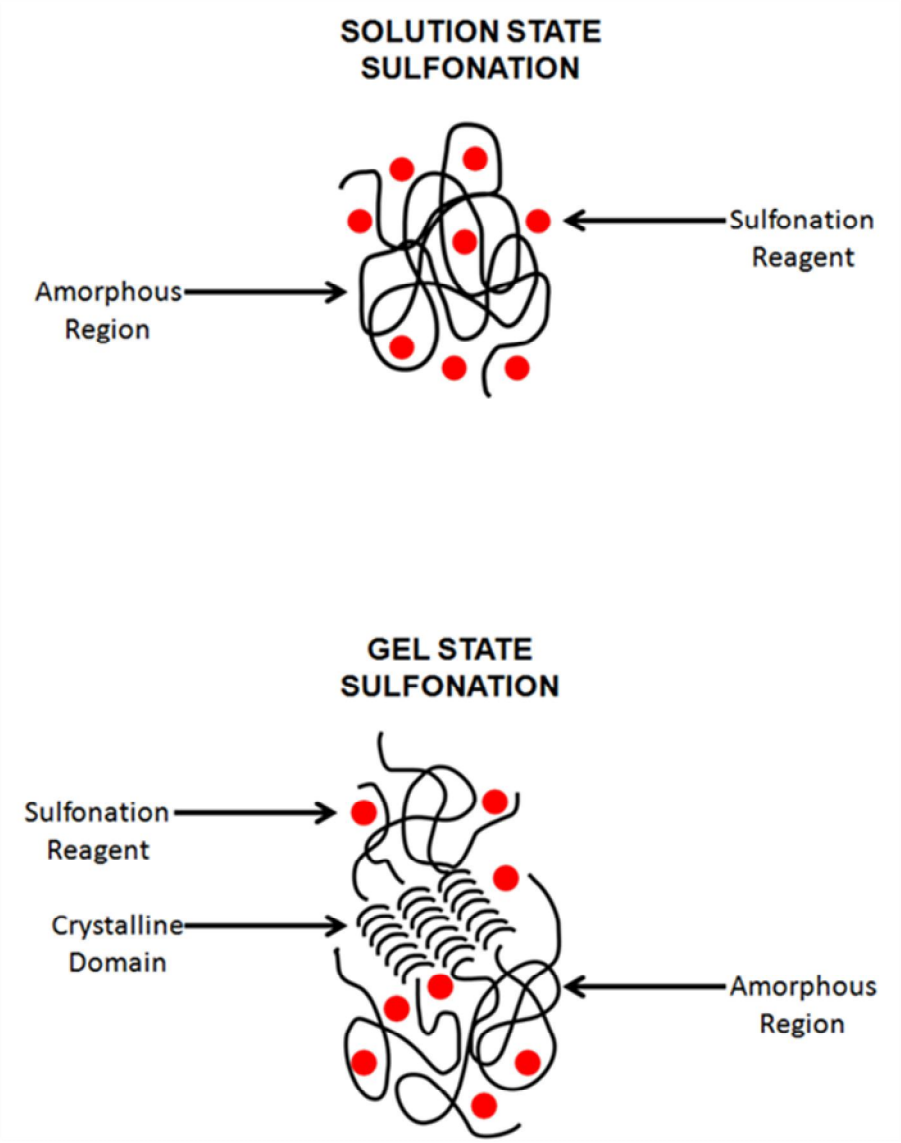

Figure IX-1. Diagram of solution state and gel state sulfonation post-polymerization methods.

As can be seen in Figure IX-1, the sulfonation of sPS in the physical gel state is likely to maintain longer sequences of unsulfonated sPS homopolymer compared to the SsPS ionomer prepared via sulfonation of sPS in solution. It is expected that differences in the placement of the sulfonic acid groups along the polymer backbone leading to random and non-random (pseudo-

blocky) ionomer architectures would exhibit differences in the spherulitic growth rates of the non-random and random SsPS ionomers.

Figure IX-2 through Figure IX-6 contains plots of the spherulite radius versus time for the SsPS3.2H$^+$NR (Non-Random or NR) and SsPS3.2H$^+$R (Random or R) at different isothermal crystallization temperatures. Both SsPS ionomers exhibit linear growth of the entire temperature range studied from 220 to 240 °C. The slopes of the lines obtained via linear regression analysis from the plots of spherulite radius versus time were used to determine the spherulitic growth rates of the non-random and random SsPS ionomers.

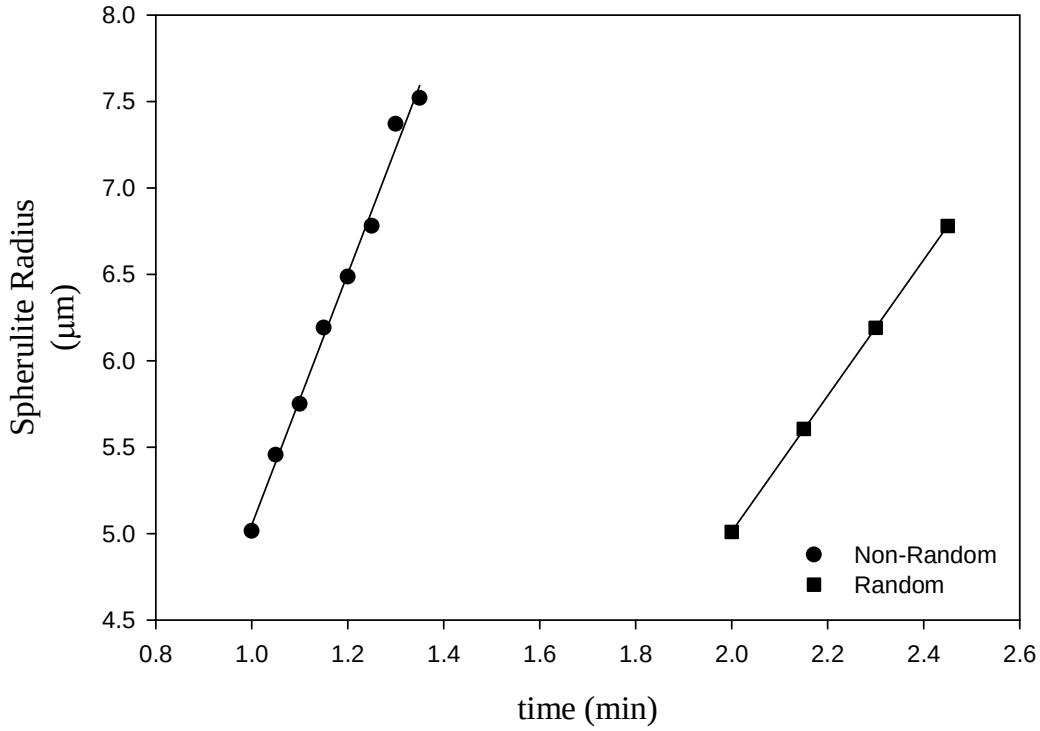

Figure IX-2. Spherulitic radius versus time for SsPS3.2H$^+$R and SsPS3.2H$^+$NR during isothermal crystallization at 220 °C.

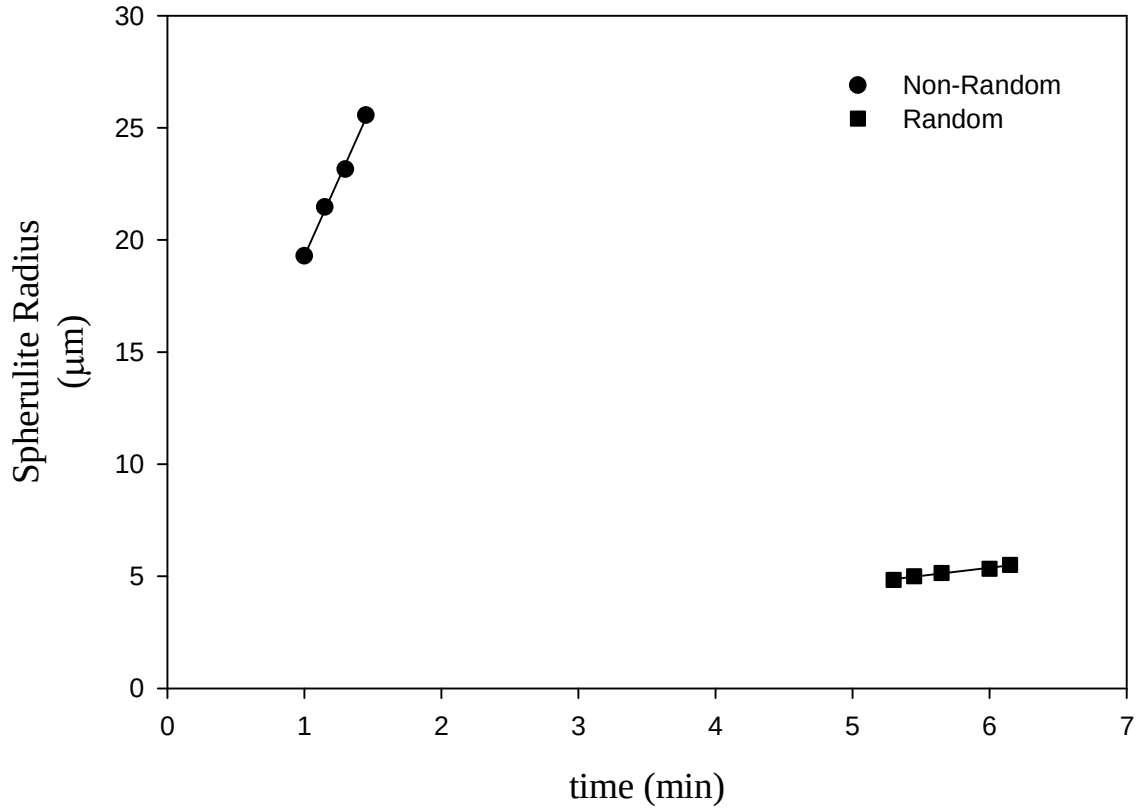

Figure IX-3. Spherulitic radius versus time for SsPS3.2H^{+}R and SsPS3.2H^{+}NR during isothermal crystallization at 225 °C.

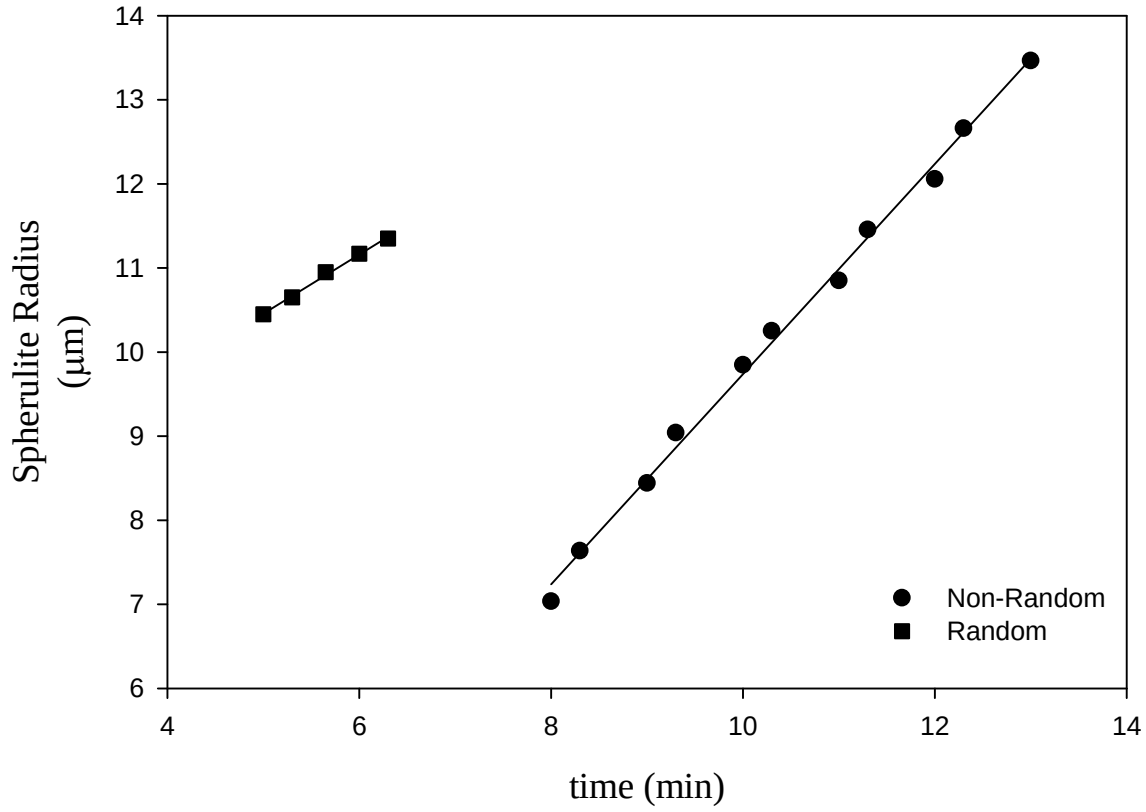

Figure IX-4. Spherulitic radius versus time for SsPS3.2H^{+}R and SsPS3.2H^{+}NR during isothermal crystallization at 230 °C.

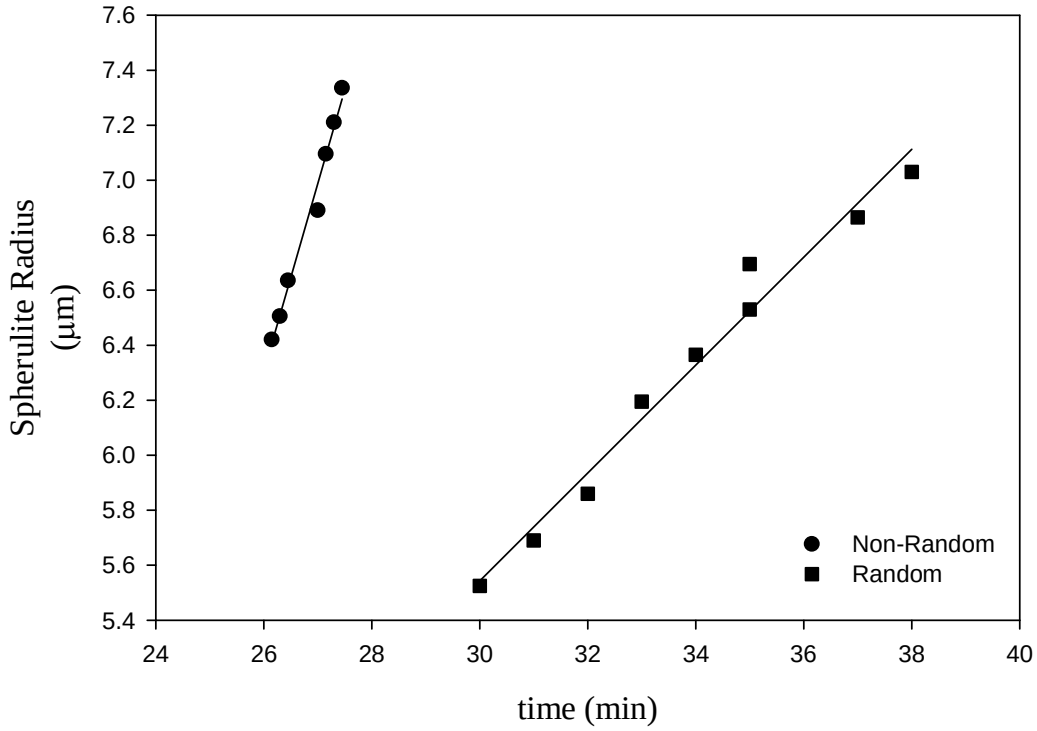

Figure IX-5. Spherulitic radius versus time for SsPS3.2H^{+}R and SsPS3.2H^{+}NR during isothermal crystallization at 235 °C.

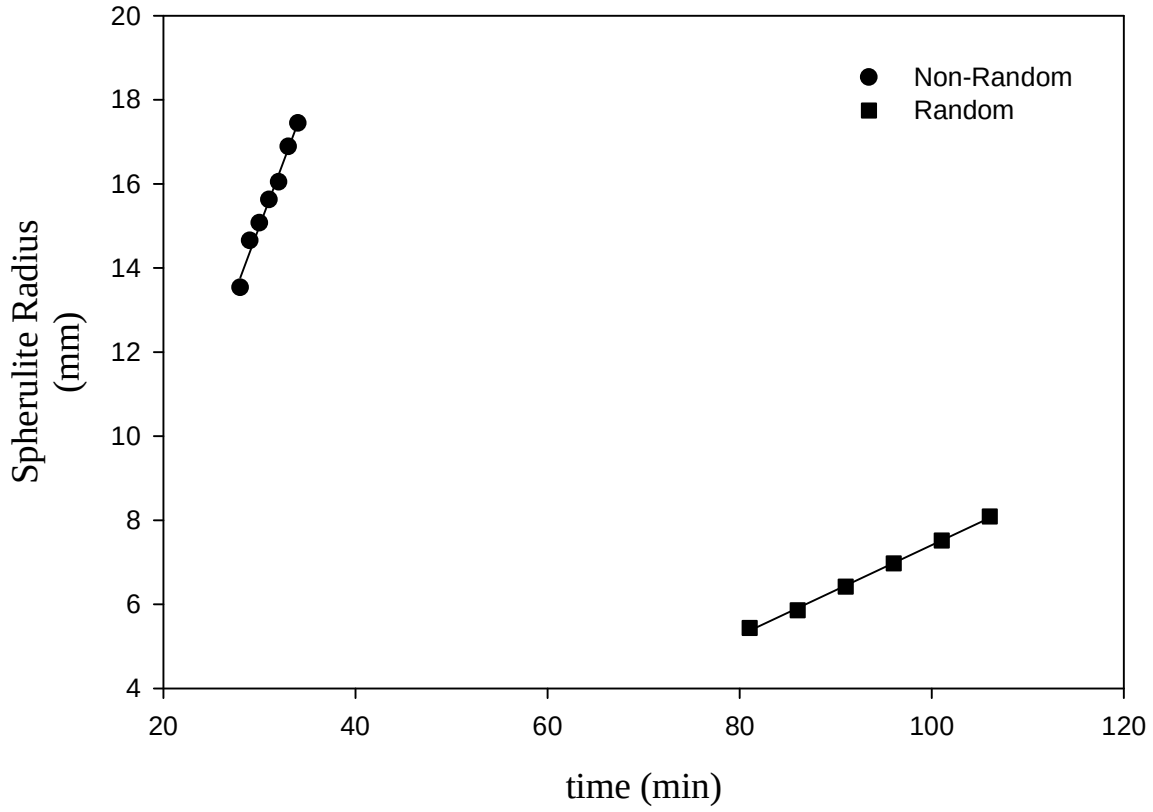

Figure IX-6. Spherulitic radius versus time for SsPS3.2H^{+}R and SsPS3.2H^{+}NR during isothermal crystallization at 240 °C.

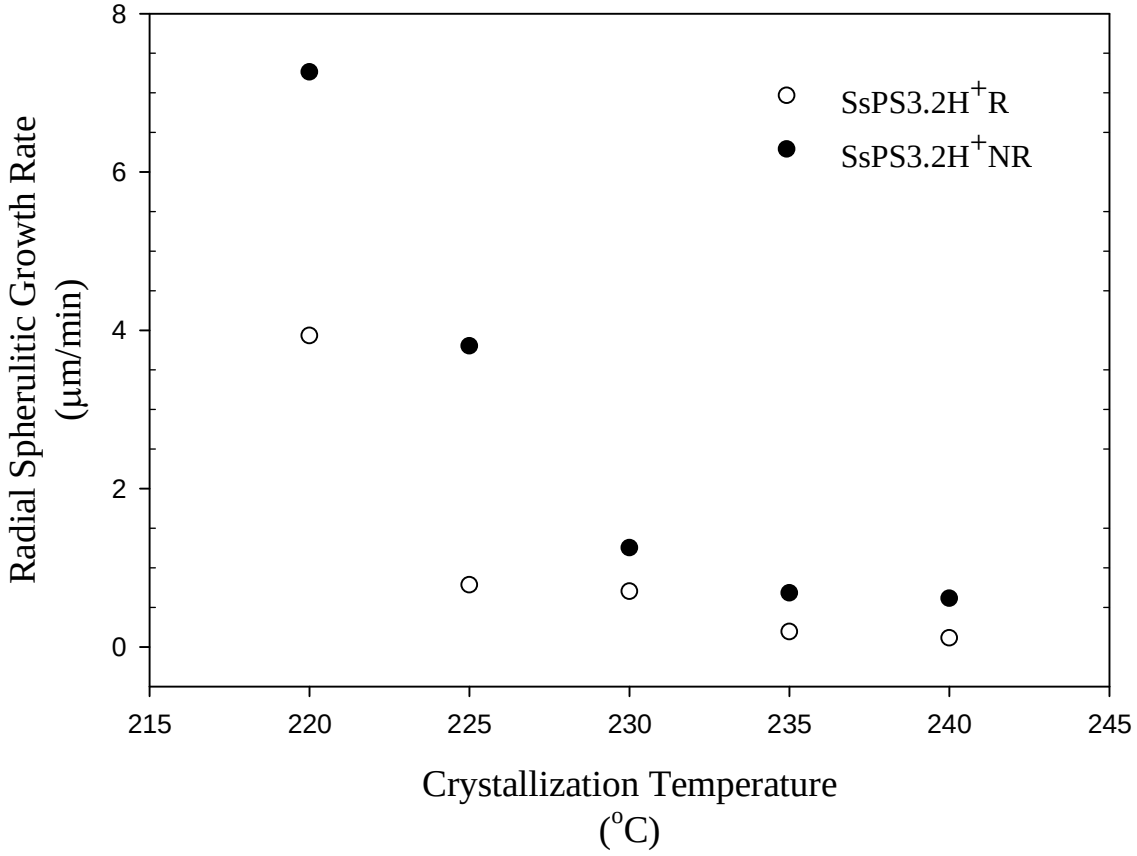

Figure IX- 7. Spherulitic growth rate versus crystallization temperature for SsPS3.2H$^+$NR and SsPS3.2H$^+$R.

It can be seen in Figure IX-7 that the rate of spherulitic growth of the non-random SsPS ionomer is higher than that of the random SsPS ionomer at every isothermal crystallization temperature. The more rapid rate of growth for the non-random SsPS ionomer is attributed to longer sequences of unsulfonated material that may organize more rapidly into spherulitic structures. The polymer chains of the random SsPS ionomer most likely encounter a greater number of defects (sulfonic acid groups) during the crystallization process that must be rejected from the crystalline/melt interface leading to retardation in the rate of spherulitic growth.

The spherulitic growth rate at any given crystallization temperature according to Lauritzen-Hoffman theory is affected by the energy required for the formation of a nucleus of critical size and the energy required for the transport of chains across the melt/crystal interface. Even though the nucleation density is higher for the random SsPS ionomer and as a result it may be possible that the energy required for the formation of a critical nucleus may be lower than that of the of corresponding non-random SsPS ionomer, the energy required for the transport of crystalline segments is higher for the random SsPS ionomer than the non-random ionomer. The presence of homogeneously distributed ionic aggregates throughout the polymer matrix for the random SsPS ionomer would likely more greatly restrict the movement of polymer chains leading to higher energy required for the transport of chain in the melt. In contrast, the non-random SsPS ionomer likely consist of ionic aggregates that are well-separated from the crystalline regions resulting in less restricted movement of crystallizable chain segments and lower required to transport chains from the melt to the crystalline phase.

Figure XI-8 through Figure XI-12 contains PLM images of the SsPS3.2H^+R and SsPS3.2H^+NR ionomers after impingement at isothermal crystallization temperatures of 220, 225, 230, 235, and 240 °C. The most pronounced difference between the non-random and random SsPS ionomers is in the size of the non-random SsPS spherulites. The sizes of the non-random SsPS spherulites are clearly larger than the random SsPS ionomer at every isothermal crystallization temperature. There also appears to be considerable differences in not only the size of the spherulites, but also differences in the texture of the spherulitic structures. The crystalline suprastructure for the random SsPS ionomer appears to be axialitic while the non-random SsPS ionomer exhibits more spherulitic structures. Crystalline suprastructures called axialites were first reported for solution grown polyethylene crystals which appeared to grow as

multilayers that splayed from a common axis [34]. Axialiatic structures have also been reported for polymers crystallized from the melt which are often referred to as hedrites [35-38]. Olley and Bassett suggested that the development of axialitic and spherulitic structures for a given polymer is due to differences in the randomization in the growth direction and out of the plane of the growing crystalline structures with incomplete randomization leading to the development of axialitic structures [39]. Researchers have also suggested that axialites are immature spherulites that may develop into spherulitic structures upon crystallization over long time periods. Syndiotactic polystyrene has been reported to form both spherulitic and axialitic crystalline suprastructures. Therefore, it is reasonable to expect to observe both axialitic and spherulitic structures within SsPS ionomers. More detailed studies are required to investigate the effect of comonomer placement of the development of specific types of spherulites within SsPS ionomers.

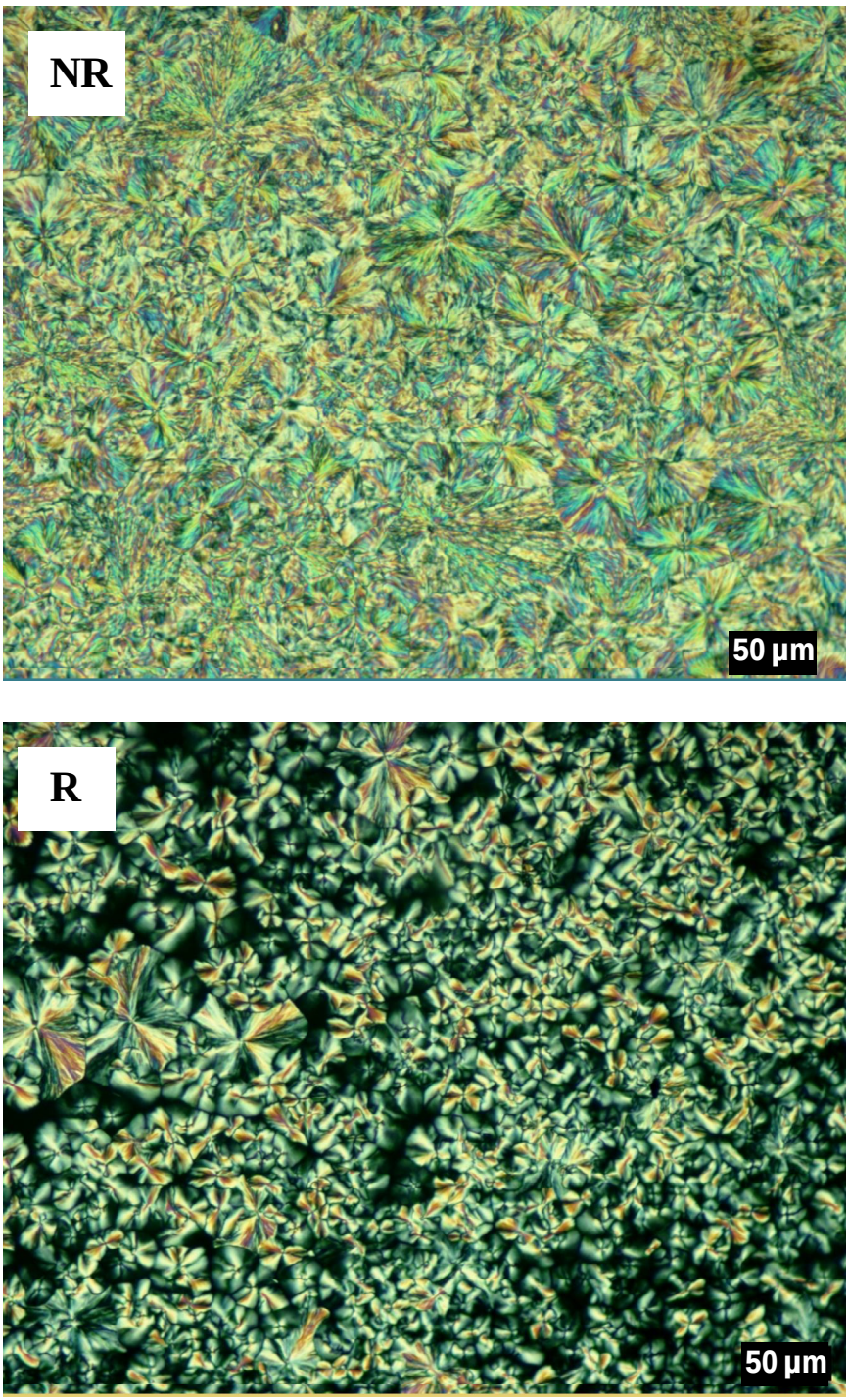

Figure IX-8. PLM images of the spherulitic structures of SsPS3.2H^{+}R and SsPS3.2H^{+}NR upon impingement after isothermal crystallization at 220 °C.

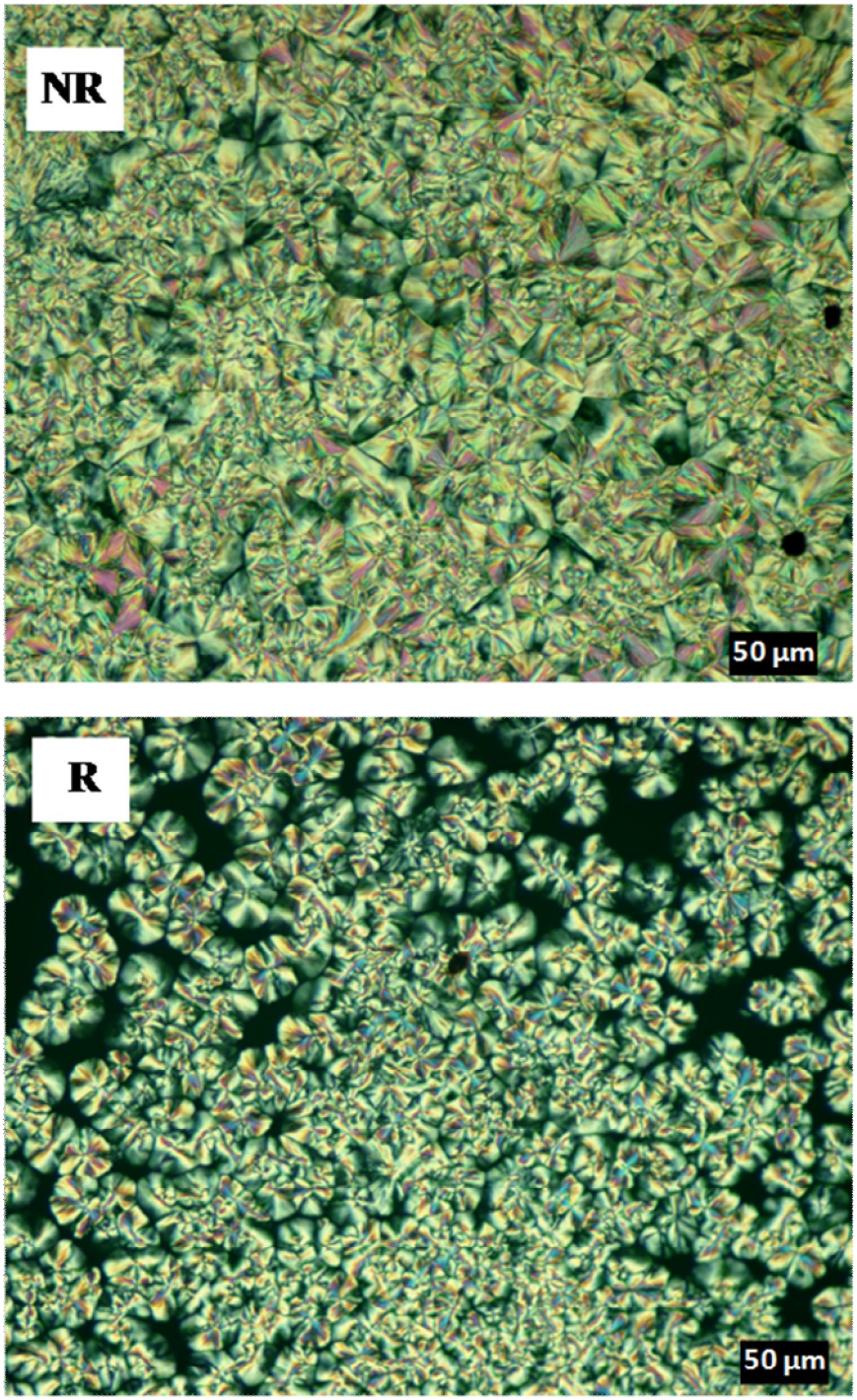

Figure IX-9. PLM images of the spherulitic structures of SsPS3.2H$^+$R and SsPS3.2H$^+$NR upon impingement after isothermal crystallization at 225 °C.

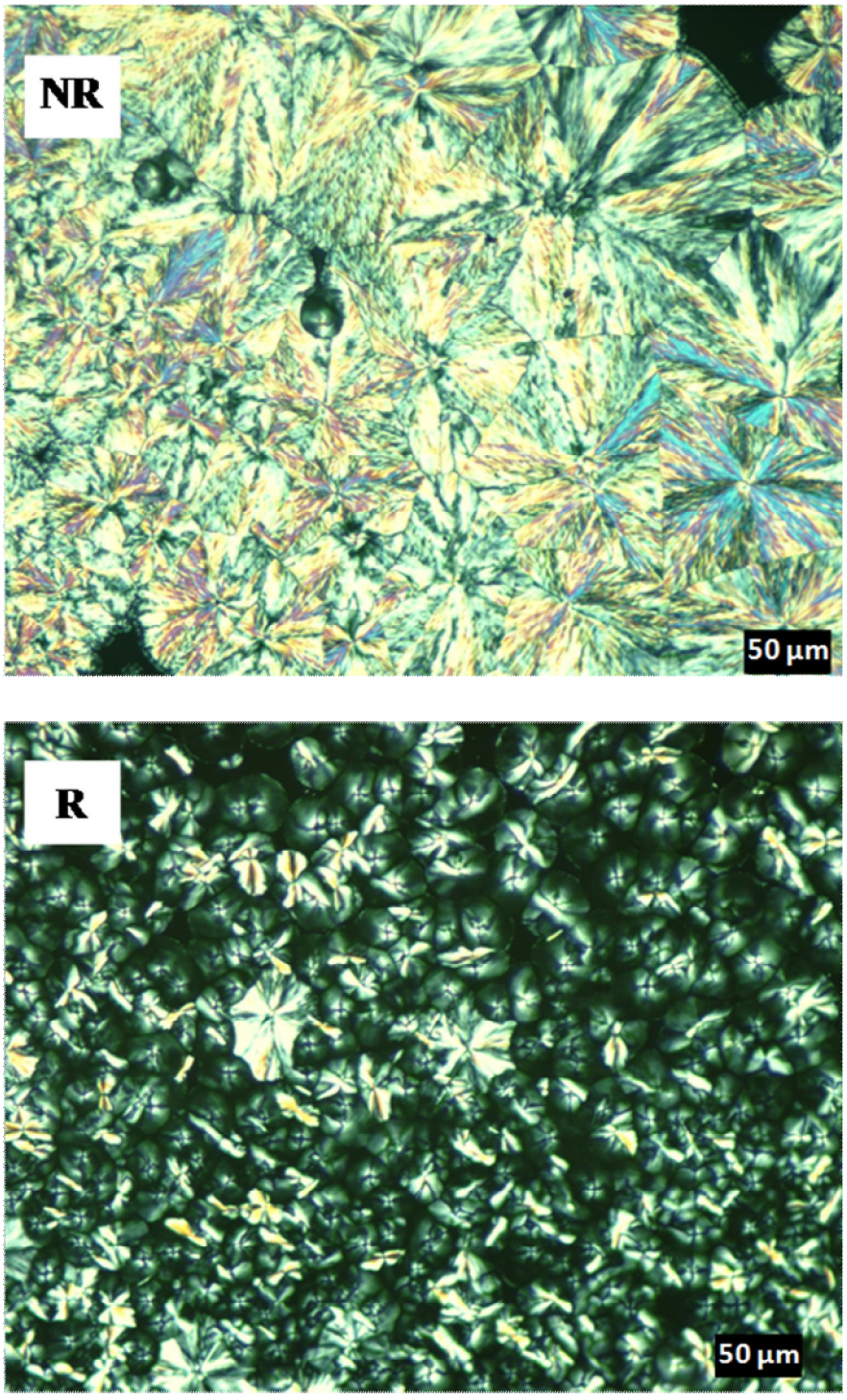

Figure IX-10. PLM images of the spherulitic structures of SsPS3.2H$^+$R and SsPS3.2H$^+$NR upon impingement after isothermal crystallization at 230 °C.

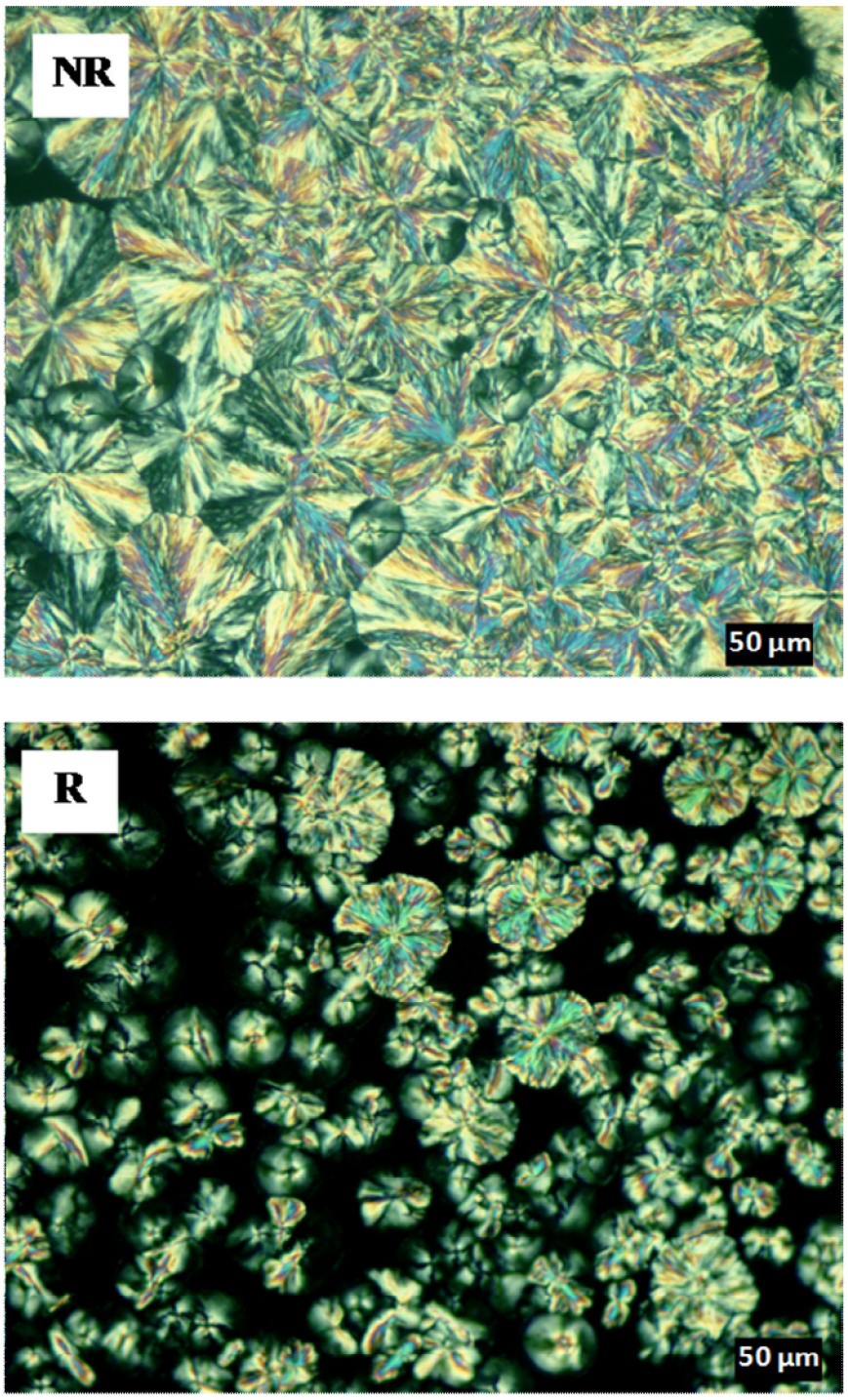

Figure IX-11. PLM images of the spherulitic structures of SsPS3.2H$^+$R and SsPS3.2H$^+$NR upon impingement after isothermal crystallization at 235 °C.

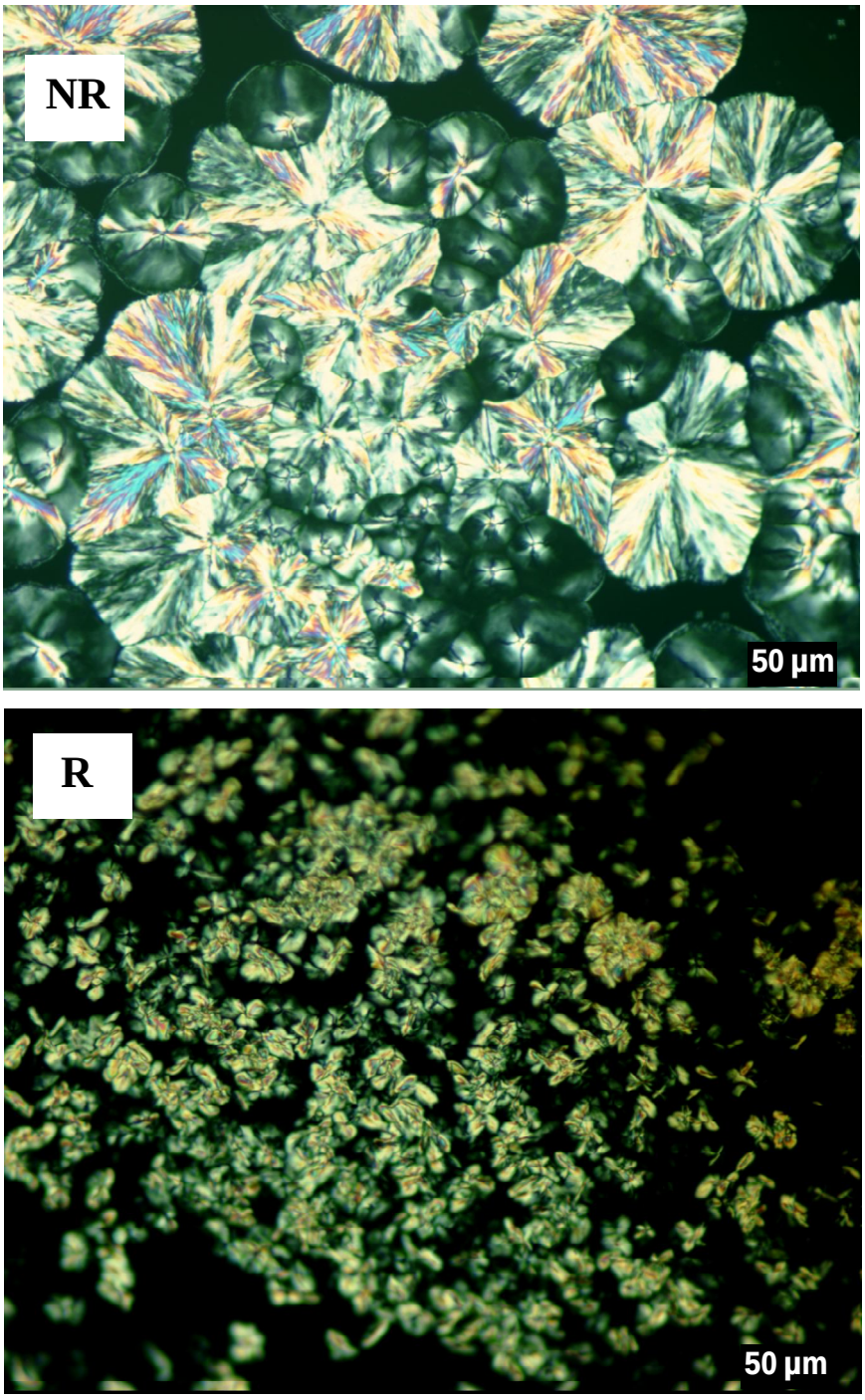

Figure IX-12. PLM images of the spherulitic structures of SsPS3.2H$^+$R and SsPS3.2H$^+$NR upon impingement after isothermal crystallization at 240 °C.

Polarized light microscopy provides a local view of the spherulite structure of the SsPS ionomer. SALLS analysis provides a more global assessment of the volume-filled SsPS ionomer samples. The SALLS patterns for volume-filled SsPS3.2H^+NR and SsPS3.2H^+R ionomers are shown in Figure IX-13 through Figure IX-17 after isothermal crystallization at 220, 225, 230, 235, and 240 °C. Since the distance between the sample and detector was constant for each sample studied, the SALLS patterns obtained for the different SsPS ionomers at different isothermal crystallization temperatures can be compared to each other.

There is a reciprocal relationship between the size of the four-leaf clover SALLS pattern and the size of the spherulites in real space. A small SALLS pattern in reciprocal space indicates a large spherulite size in real space. The SALLS patterns of the SsPS3.2H^+NR and SsPS3.2H^+R ionomers can be qualitatively compared to each other based upon the aforementioned relationship. It can be seen that at every isothermal crystallization temperature that the size of the non-random SsPS spherulites are larger than those of the random SsPS ionomer.

Future studies of the morphological structures of the SsPS3.2H^+NR and SsPS3.2H^+R ionomers should be completed using SEM, TEM, an AFM to obtain a higher resolution of the spherulites and also a view of the crystalline lamella using the higher resolution techniques.

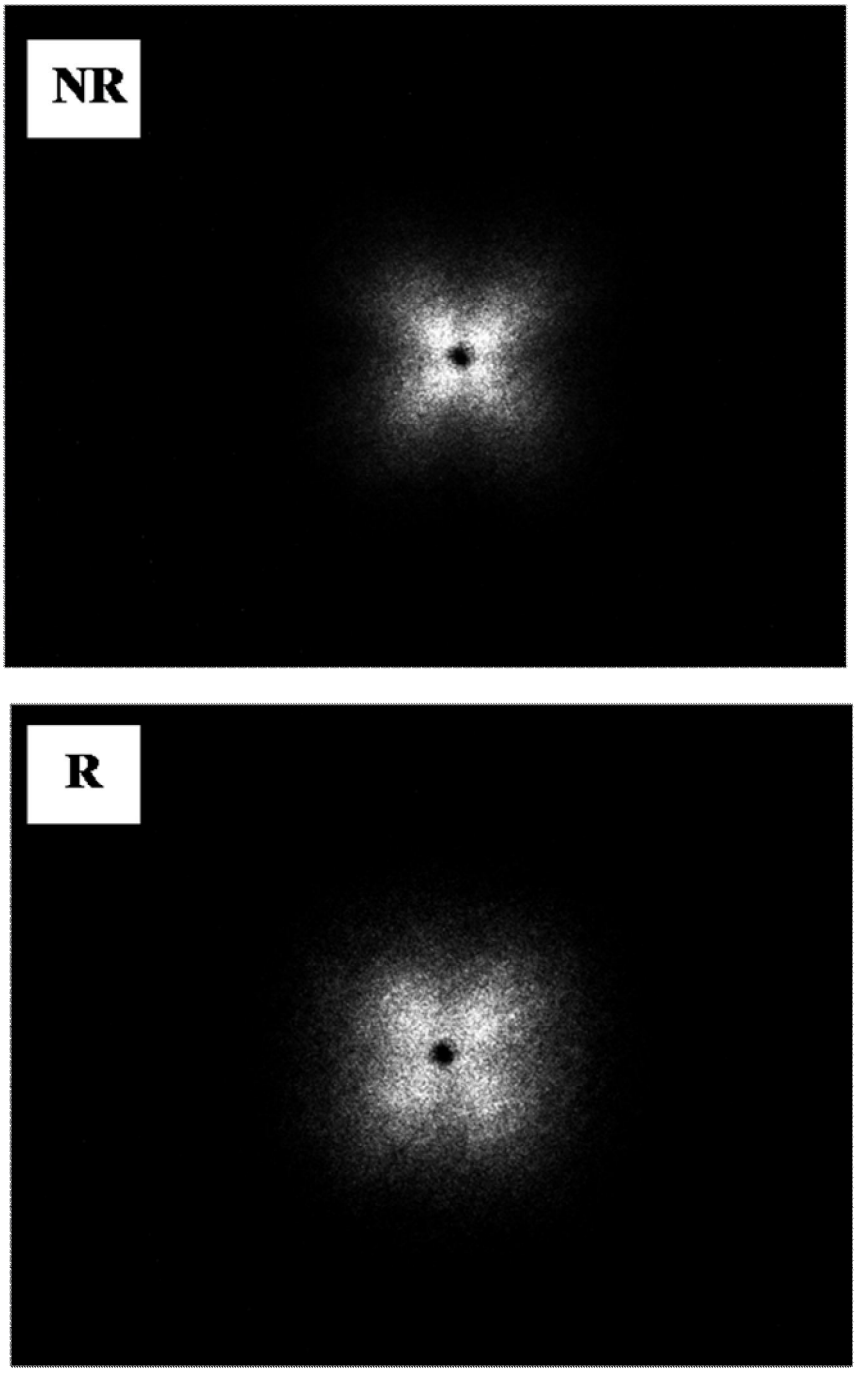

Figure IX-13. H_v SALLS patterns of SsPS3.2H^+R and SsPS3.2H^+NR upon impingement after isothermal crystallization at 220 °C.

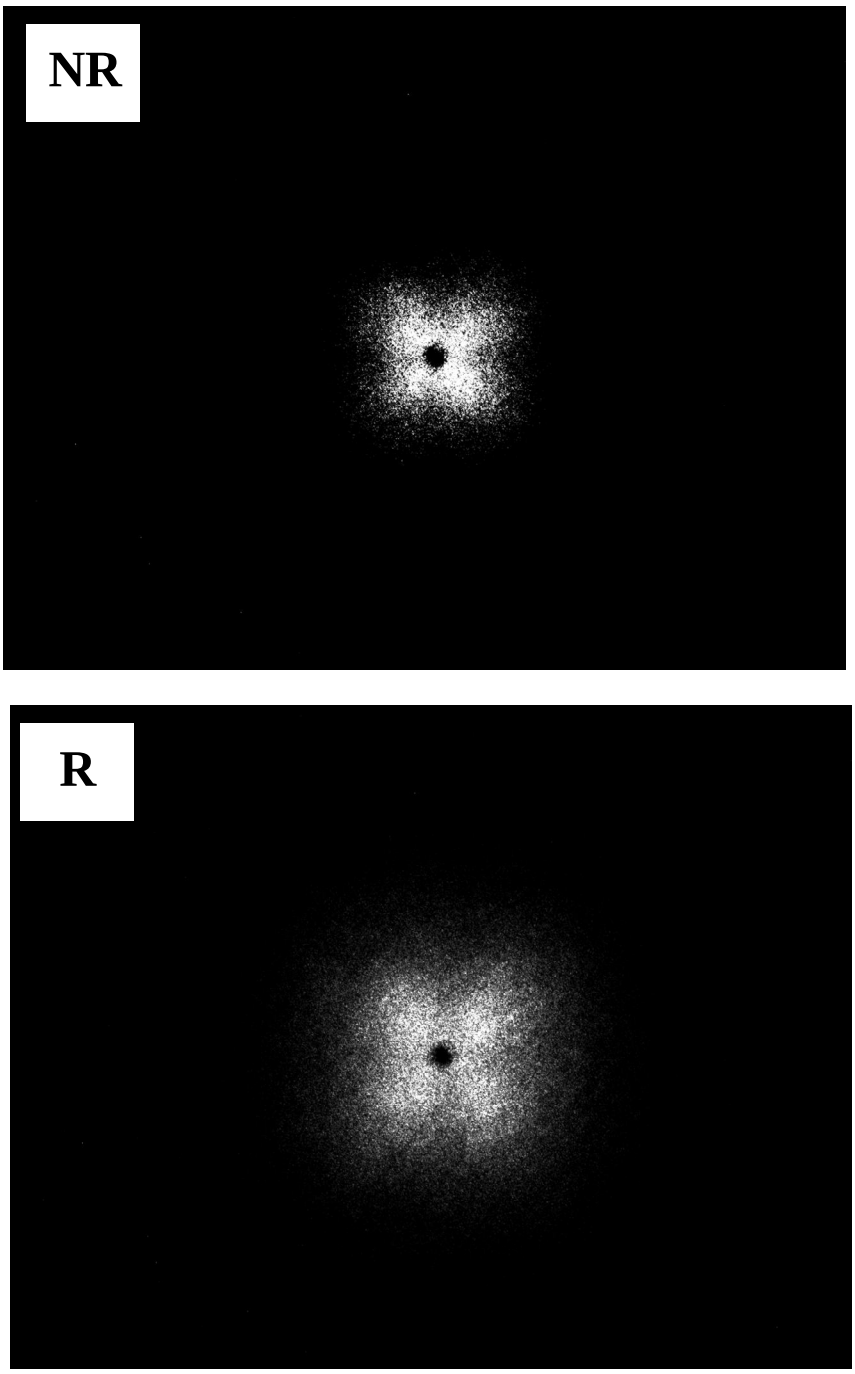

Figure IX-14. H_v SALLS patterns of SsPS3.2H^+R and SsPS3.2H^+NR upon impingement after isothermal crystallization at 225 °C.

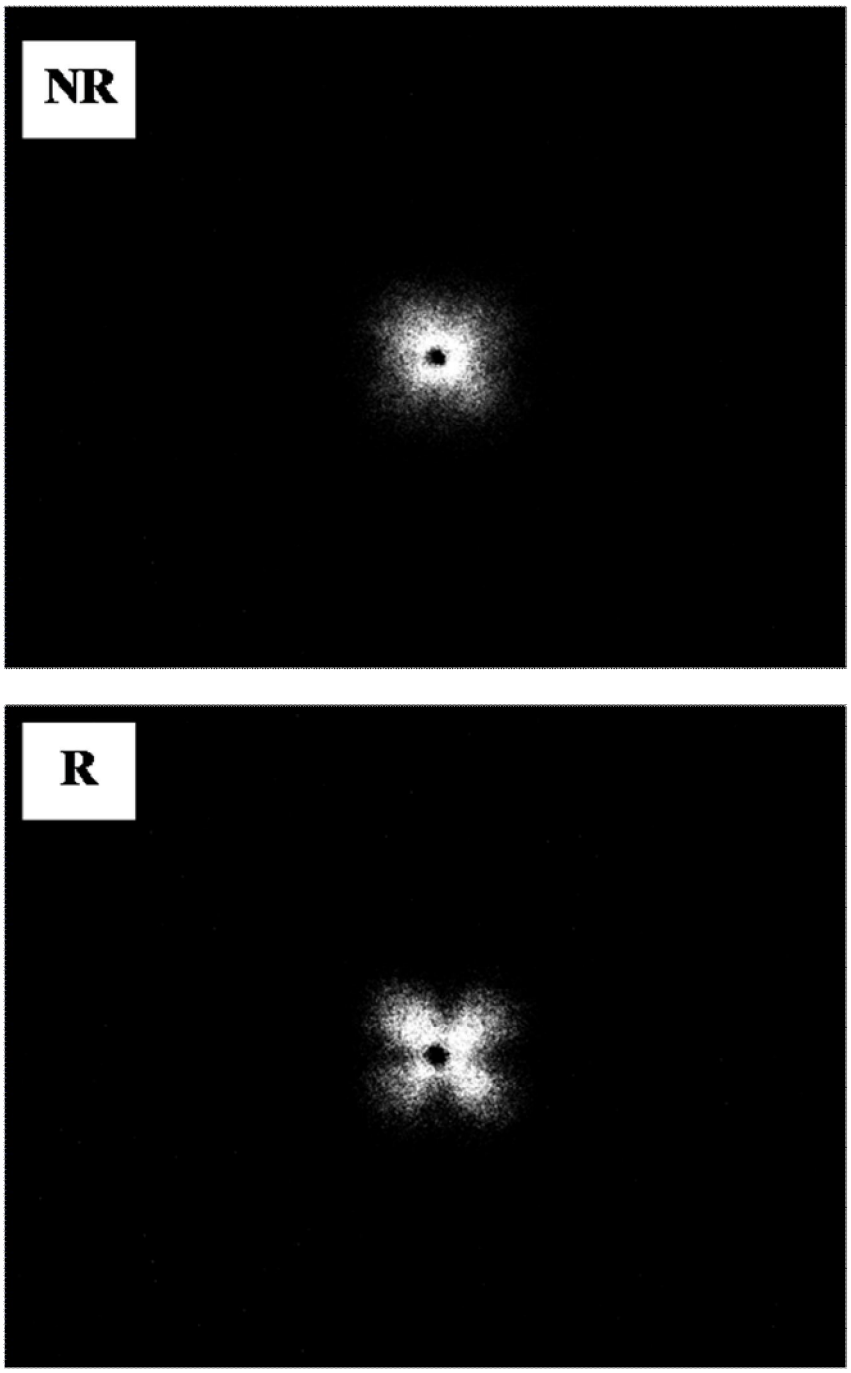

Figure IX-15. H_v SALLS patterns of SsPS3.2H^+R and SsPS3.2H^+NR upon impingement after isothermal crystallization at 230 °C.

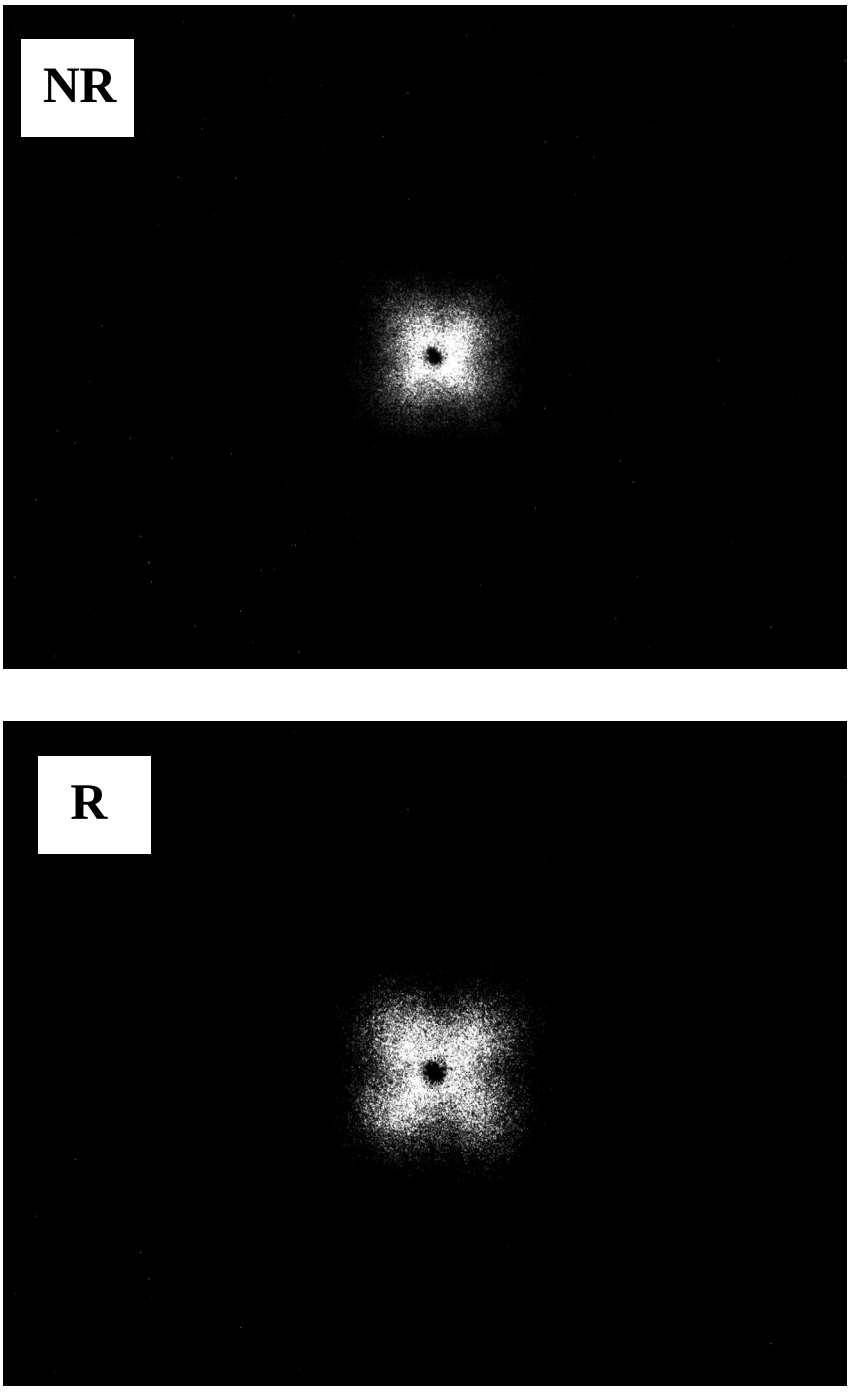

Figure IX-16. H_v SALLS patterns of SsPS3.2H^+R and SsPS3.2H^+NR upon impingement after isothermal crystallization at 235 °C.

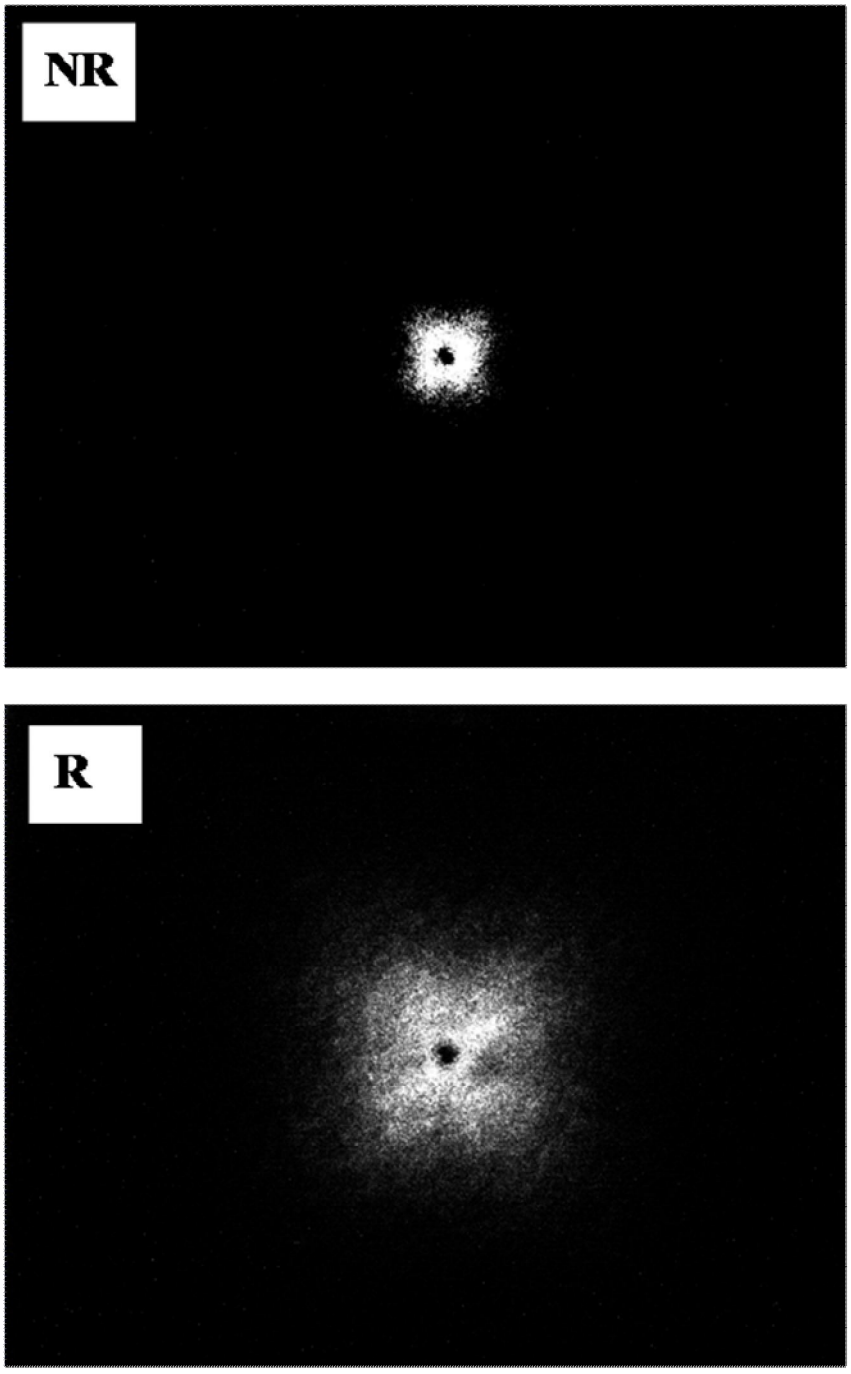

Figure IX-17. H_v SALLS patterns of SsPS3.2H^+R and SsPS3.2H^+NR upon impingement after isothermal crystallization at 240 °C.

CONCLUSION

The spherulitic growth rates and spherulitic morphologies of the SsPS3.2H^+NR and SsPS3.2H^+R ionomers are considerably different over a wide crystallization range. The spherulitic growth rate of the SsPS3.2H^+NR ionomer is faster than the growth rate of the corresponding random SsPS ionomer. These behaviors are attributed to the differences between the placement of the sulfonic acid groups along the polymer backbone. It is likely that the non-random SsPS ionomer contains long sequences of unsulfonated sPS that are able to organize more rapidly into spherulitic structures. It is also likely that the energy of activation for the transport of chains across the melt/crystal interface is lower for the non-random SsPS ionomer.

REFERENCES

1. Lu H and Nutt S. Journal of Applied Polymer Science 2003;89(13):3464-3470.
2. Woo EM, Sun YS, and Yang CP. Progress in Polymer Science 2001;26(6):945-983.
3. Wang C, Lin C-C, and Chu C-P. Polymer 2005;46(26):12595-12606.
4. Woo EM, Sun YS, and Lee ML. Polymer 1999;40(15):4425-4429.
5. Tseng C-R, Wu S-C, Wu J-J, and Chang F-C. Journal of Applied Polymer Science 2002;86(10):2492-2501.
6. Su CH, Jeng U, Chen SH, Lin SJ, Wu WR, Chuang WT, Tsai JC, and Su AC. Macromolecules 2009;42(17):6656-6664.
7. Wang C, Lin C-C, and Tseng L-C. Polymer 2006;47(1):390-402.
8. Guerra G, De Rosa C, Vitagliano VM, Petraccone V, and Corradini P. Journal of Polymer Science Part B: Polymer Physics 1991;29(3):265-271.
9. Wang C, Lin C-C, and Chu C-P. Macromolecules 1999;39(26):9267-9277.
10. Dutt G and Kit KM. Journal of Applied Polymer Science 2003;87(12):1975-1983.
11. Hong BK, Jo WH, Lee SC, and Kim J. Polymer 1998;39(10):1793-1797.
12. Mandal TK and Woo EM. Polymer 1999;40(10):2813-2820.
13. Wang C, Liao W-P, Wang M-L, and Lin C-C. Polymer 2004;45(3):973-981.
14. Wu FS and Woo EM. Polymer Engineering & Science 1999;39(5):825-832.
15. Dutt G and Kit KM. Journal of Applied Polymer Science 2003;87(12):1984-1994.
16. Cimmino S, Di Pace E, Martuscelli E, and Silvestre C. Polymer 1993;34(13):2799-2803.
17. Mandelkern L. Crystallization of Polymers. New York: McGraw-Hill 1964.
18. Wunderlich B. Macromolecular Physics. vol. II. New York: Academic Press, 1976.

19. Hoffman JD, Davis GT, and Lauritzen JI. Treatise on Solid State Chemistry. In: Hannay NB, editor. Crystalline and Non-Crystalline Solids, vol. 3. New York: Plenum Press, 1976.

20. Yan RJ, Ajji A, and Shinozaki DM. Polymer Engineering & Science 2001;41(10):1674-1682.

21. De Rosa C, Buono A, Ricci A, De Luca F, and Caporaso L. Macromolecules 2003;36(17):6389-6400.

22. Soga K, Nakatani H, and Monoi T. Macromolecules 1990;23(4):953-957.

23. Liu S and Sen A. Macromolecules 2000;33(14):5106-5110.

24. Grassi A, Caprio M, Zambelli A, and Bowen DE. Macromolecules 2000;33(22):8130-8135.

25. Xu G and Chung TC. Macromolecules 1999;32(25):8689-8692.

26. Zinck P, Bonnet F, Mortreux A, and Visseaux M. Progress in Polymer Science 2009;34(4):369-392.

27. Orler EB, Gummaraju RV, Calhoun BH, and Moore RB. Macromolecules 1999;32(4):1180-1188.

28. Orler EB and Moore RB. Macromolecules 1994;27(17):4774-4780.

29. Orler EB, Yontz DJ, and Moore RB. Macromolecules 1993;26(19):5157-5160.

30. Stein RS and Rhodes MB. Journal of Applied Physics 1960;31(11):1873-1884.

31. Orler EB, Calhoun BH, and Moore RB. Macromolecules 1996;29(18):5965-5971.

32. Su Z, Hsu SL, and Li X. Macromolecules 1994;27(1):287-291.

33. Li H-M, Liu J-C, Zhu F-M, and Lin S-A. Polymer International 2001;50(4):421-428.

34. Bassett DC, Keller A, and Mitsuhashi S. Journal of Polymer Science Part A: General Papers 1963;1(2):763-788.

35. Haeringen DT-V, Varga J, Ehrenstein GW, and Vancso GJ. Journal of Polymer Science Part B: Polymer Physics 2000;38(5):672-681.

36. Geil PH. Polymer Single Crystals. New York:Wiley, 1963. pp. 189-221.

37. Varga J and Ehrenstein G. Colloid & Polymer Science 1997;275(6):511-519.

38. Lopez JMR and Gedde UW. Polymer 1988;29(6):1037-1044.

39. Olley RH and Bassett DC. Polymer 1989;30(3):399-409.

CHAPTER X

FUTURE WORK

FUNDAMENTAL INVESTIGATIONS AND APPLIED EXPLORATORY STUDIES OF SULFONATED SYNDIOTACTIC POLYSTYRENES

FUNDAMENTAL INVESTIGATIVE STUDIES

Preparation of Ionomer Nanocomposites using SsPS Neutralized with Organic Alkyl Ammonium Cations

SsPS montmorillonite nanocomposites prepared with lightly sulfonated cesium-neutralized sPS revealed that the presence of the ionic content improved polymer-clay interactions even at 1 mol% sulfonate groups over the unsulfonated polymer. SsPS nanocomposites prepared with the pristine Na^+MMT clay exhibited a moderate decrease in the crystallization half-time, while SsPS NCs prepared using organically-modified clay displayed a drastic decrease in the crystallization half-time when compared to the crystallization half-time of the unmodified SsPS ionomer. In fact, SsPS1.0Cs+ containing 5 wt.% OMMT crystallized faster than the sPS homopolymer containing 5 wt.% of organically-modified clay.

Based on the observation that there is improved interaction between the lightly sulfonated sPS and organically-modified clay, it may be beneficial to neutralize SsPS with organic alkyl ammonium cations. Neutralization of SsPS with alkylammonium cations may further improve interactions between SsPS and organically-modified. It would also be of particular interest to investigate the effectiveness of SsPS neutralized with organic alkylammonium cations in

producing intercalated or exfoliate ionomer/clay nanocomposites with pristine, unmodified Na^+MMT. Bhiwankar prepared intercalated nanocomposites using sulfonated atatic polystyrene that had neutralized with various alkylamines and quarternized ammonium salts and pristine Na^+MMT via melt intercalation [1]. Melt intercalation was also used by Ports to prepare polymer nanocomposites composed of poly(ethylene-co-ran-acrylic acid) and sodium montmorillonite in the presence of various alkylammonium salts [2]. A similar one-pot preparation method was utilized by Alexandre and coworkers to prepare nanocomposites from pristine sodium montmorillonite and ethylene−vinyl acetate copolymer in the presence of dimethyldioctadecylammonium bromide [3].

The melt intercalation methods utilized by Bhiwankar, Ports, and Alexandre although more readily similar to industrial polymer processing techniques than the solution intercalation method of preparing nanocomposites may lead to breaking of the clay platelets as a result of the high shear conditions employed within the melt intercalation method. The high shear conditions that are common within extrusion and batch mixing processes may reduce the length of the clay platelets and potentially reduce the barrier and mechanical properties of the resulting composites. It would therefore be extremely beneficial to prepare nanocomposites using SsPS neutralized with alkyammonium salts and pristine, unmodified Na^+MMT clay using the solution intercalation technique. In addition to potentially maintaining the length of the clay platelet via the solution intercalation method which applies less shear the polymer-clay system, it may also be possible to further manipulate polymer-clay interactions via solvent selection. Several studies could be carried out that varied the ion content of the SsPS ionomer, the type and concentration of alkylammonium cation, and the nature of the solvent used for solution intercalation. Solvent selection may play an extremely critical role in creating enhanced ionomer-clay interactions as a

function of the hydrophobicity of the neutralizing cation as the solubility characteristics of the SsPS ionomer may change drastically as the neutralizing cation changes. Even with the additional level of complexity that proper solvent choice may pose, an investigation of the role of neutralizing counterion on the nature of polymer-clay interactions would provide additional insight to field of polymer-clay nanocomposites.

The Effect of Montmorillonite Clay on the Polymorphic Behavior of Sulfonated Syndiotactic Polystyrene Nanocomposites

Montmorillonite clay has been shown to induce changes in the polymorphic behavior of syndiotactic polystyrene [4-8]. It would be of interest to study the effect of clay on the development of specific polymorphic structures within the SsPS ionomers also. Detailed investigations of the crystallization behavior in the presence of clay can be carried out using a combination of DSC, FTIR, and WAXD.

Determination of the type and relative percentage of a certain polymorphic crystal are extremely important in constructing structure-property relationships and identifying processing conditions that lead to the formation of specific crystalline structures as the mechanical properties of sPS have been shown to be dependent upon the crystalline structure [9].

.

The Effect of Molecular Weight of the Base Homopolymer on the Preparation of Non-Random SsPS Ionomers

The thermal properties and crystallization behavior of sPS sulfonated in the solution state and physical gel states have been shown to be significantly different. The more rapid rate of crystallization of the non-random SsPS is attributed to longer sequences of unsulfonated material that are able to more readily organize and pack into crystalline structures.

It is likely that the influence of the placement of the ionic group would be more pronounced at lower homopolymer molecular weights in both the non-random and random SsPS ionomers. In the sulfonation of low molecular weight sPS in the solution state, there may be a greater chance of creating a more blocky architecture because there are fewer sites available for sulfonation. When conducting the sulfonation of sPS in the physical gel state, lower molecular weight may also favor the formation of an ionomer with a higher degree of blockiness because at lower molecular weight, the sPS chains would likely be able to crystallize to an overall higher degree of crystallinity because of greater chain mobility (less chain entanglement at lower molecular weight). A higher degree of crystallinity would mean that less of the polymer chains are in an amorphous state where the actual sulfonation process occurs and therefore longer sequences of unsulfonated material may be formed. Also, if a smaller fraction of polymer is in the amorphous phase, it may be possible that at higher degrees of sulfonation, the amorphous phase may be sulfonated in a blockier manner as well.

Characterization of Random and Non-Random SsPS Ionomer Architectures

Characterization of the different ionomer architectures is critical to gaining more insight into the morphology and placement of the sulfonate group along the polymer backbone. Chapter III of this document on the chemical modification of polymers covers various potential methods that could be utilized to characterize the nature of the placement of the sulfonic acid groups along the sPS homopolymer backbone. Characterization of the SsPS ionomers using ^{23}Na NMR would be a useful method to characterize the architectural differences between the two ionomers for a number of reasons.

^{23}Na NMR provides information about the state of ionic aggregation within sodium-neutralized ionomers. O'Connell and coworkers completed a series of studies that investigated the effect of a number of parameters such as polydispersity, humidification, degree of sulfonation, and neutralization on the number of lone ion pairs and aggregated ion pairs within sulfonated atactic polystyrene ionomers [10-13]. The position, shape, and intensity of the NMR peak can be utilized to gather information on the state of ionic aggregation within SsPS ionomers of differing architecture as well.

Cold Crystallization Behavior of Random and Non-Random SsPS Ionomers

The isothermal and non-isothermal crystallization behavior of SsPS ionomers produced from solution state and physical gel state sulfonation processes were investigated in detail. Additional investigation into the mechanism of cold crystallization within these two ionomers may provide further insight into the effect of architecture on the development of crystalline structures in the presence of ionic aggregates. Because the cold crystallization process occurs

from the glassy state under conditions were the molecular mobility of the polymer chains are much more limited compared to crystallization from the melt, there may be significant differences in the rate and mechanisms of crystallization for the non-random and random SsPS ionomers. Figure X-1 contains plots of relative heat flow versus temperature for sPS homopolymer and random and non-random SsPS ionomers containing 4 mol% sulfonate groups. Each material was placed into DSC pans as amorphous films prepared by melt pressing the materials and quenching the polymers in liquid nitrogen. The sPS homopolymer and the two ionomers were confirmed to be completely amorphous via WAXD (not shown). The amorphous films were heated at 20 °C/min. It can be seen that there is no crystallization exotherm for the non-random ionomer under these conditions. However, both the sPS homopolymer and the non-random SsPS ionomer readily crystallization at the heating rate utilized. The peak exothermic crystallization temperature for sPS and the non-random SsPS ionomer was 168 and 175 °C, respectively. Further investigations into the mechanisms of crystallization that occur during cold crystallization should be carried out using DSC, WAXD, SAXS, SALLS, and PLM. Valuable information can be obtained about the mobility and organization of polymer chains in the presence of ionic aggregates from the glassy state would be very interesting.

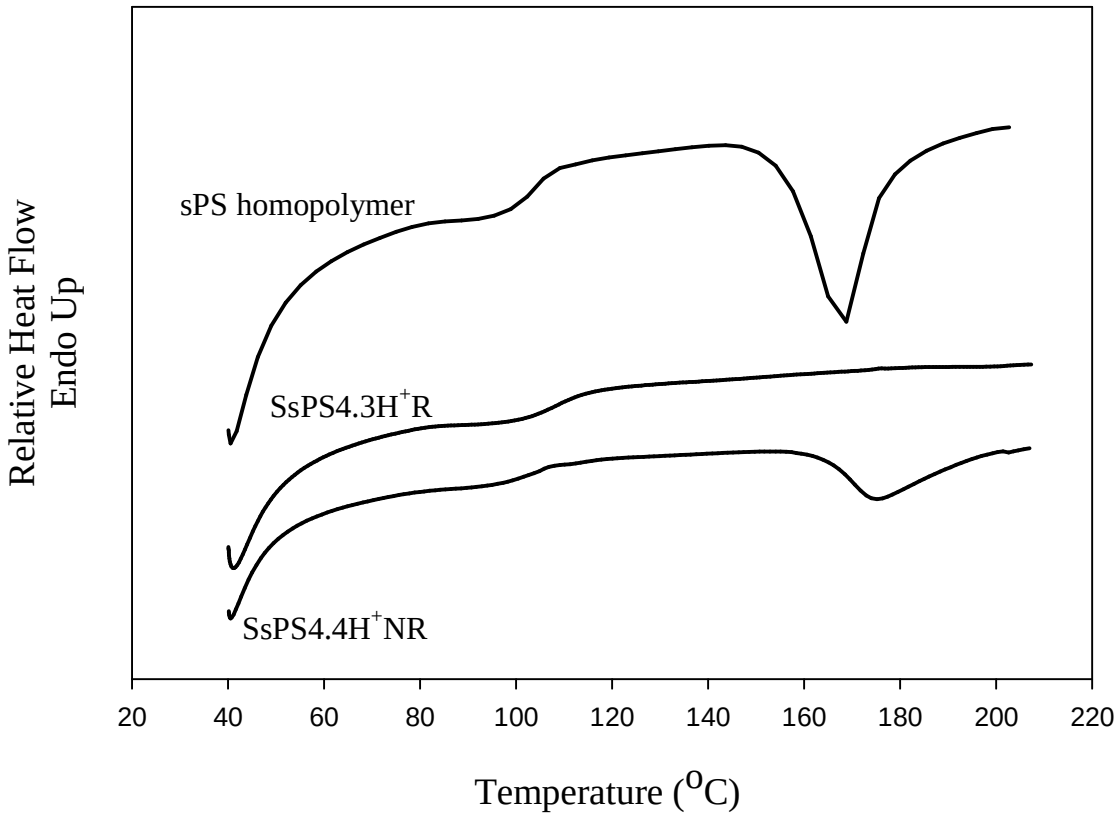

Figure X-1. Relative heat flow versus temperature for sPS homopolymer, SsPS4.3H$^+$R and SsPS4.3H$^+$NR.

The Effect of Architecture of the Solvent-Induced Crystallization Behavior of SsPS Ionomers

Syndiotactic polystyrene crystallizes into helical structures during solvent-induced crystallization. The helical structures transform into the planar, all-trans crystalline forms upon heating. These structural changes have been monitored within sPS using WAXD, DSC, and FTIR. The incorporation of sulfonate groups may affect the development of these structures.

Figure X-2 contains a plot of pure sPS homopolymer sPS containing 3.2 mol% sulfonate groups that has been sulfonated in the solution and physical gel states to yield random and non-

random SsPS ionomers, respectively. sPS-R and sPS-NR are pure sPS homopolymers that were treated to the same sulfonation procedures as their ionomeric counterparts without adding the sulfuric acid to the sulfonation reagent mixture. The sPS-R and sPS-NR homopolymers are included in the DSC analysis as controls. The hompolymers and ionomers were cast from 0.5 wt% solutions of 90/10 1,1,2,2-tetrachloroethane/methanol.

The thermal transition located at approximately 200 °C for each material is attributed to the transition of the solvent-induced γ-crystal form to the α/β-crystal forms. It is clear that the magnitude of the transition that occurs for the random SsPS is much greater than the transition for the homopolymer and non-random ionomer. This data suggests placement of the ionic groups has an effect on the structural transitions from the helical form to the all-trans, planar forms. The study of the structural change can be done quite readily via FTIR analysis. Monitoring the changes in IR peaks associated with different crystal structures as a function of ion content, counterion, architecture, solvent, and heating rate would be interesting.

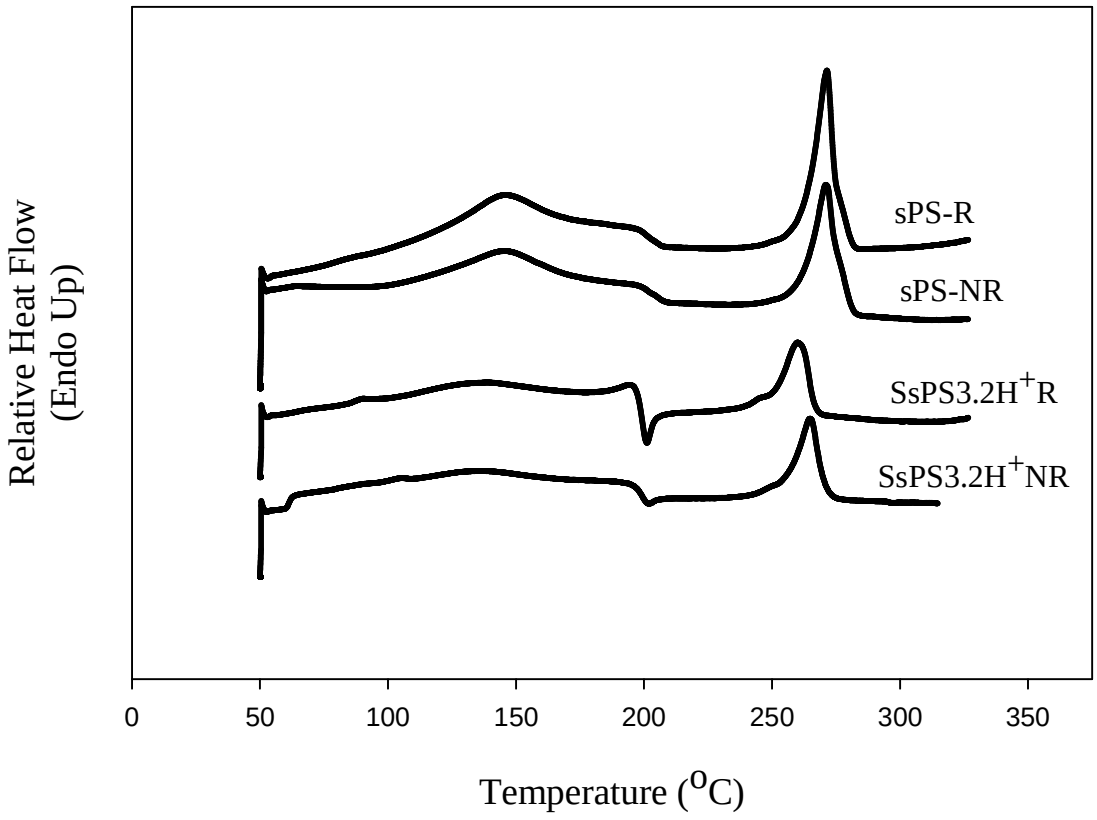

Figure X-2. Relative heat flow versus temperature for sPS-R, sPS-NR, SsPS3.2H$^+$R, and SsPS3.2H$^+$NR.

Blends of Sulfonated Syndiotactic Polystyrene and Syndiotactic Poly(p-fluoro-styrene)

Syndiotactic poly(p-fluoro-styrene) (s-PPFS) has been reported to have a melting temperature of 321 °C [14] which is significantly higher than the melting temperature of syndiotactic polystyrene at 270 °C. s-PPFS was also reported to have exhibit a complex polymorphic behavior similar to that of sPS [14]. It would be interesting to prepare blends of sulfonated syndiotactic polystyrene and s-PPFS and evaluate the miscibility of the two components and as a function of ionic content and neutralizing counterion. Studies of blends of

Nafion® and PVDF by Landis and Moore showed that the degree of miscibility between the two components was enhanced by utilizing large alkylammonium counterions to neutralize the ionomer component [15].

APPLICATION –FOCUSED INVESTIGATIVE STUDIES

Effect of Ionomer Architecture and Crystallinity on the Behavior of SsPS Ionomers as Proton Exchange Membranes

There is a great amount of interest in preparing low cost, high performance proton exchange membranes (PEMs) for fuel cell applications. The benchmark material, Nafion® is relatively costly and much about the morphological structure of this ionomer is still under a considerable amount of debate. Therefore, utilizing a low cost material such as SsPS as a model semicrystalline ionomer with a more easily characterized morphological structure to prepare a PEM is ideal. Also, by preparing SsPS ionomers via the solution state and physical gel state methods, it would be possible to evaluate the effect of ionomer architecture on various properties of PEMs such as water uptake and degree of swelling in addition to proton conductivity.

Preparation of Ionic Polymer Metal Composites using Random and Non-Random SsPS Ionomers

Ionic polymer metal composites (IPMCs) are interesting hybrid materials with a great deal of focus on using these materials as artificial muscles. Nafion® is o the benchmark material for IPMCs. Utilization of SsPS as a model semicrystalline ionomer would be of consideration interest for similar reasons as previously noted for the study of proton exchange membranes. Also, because sPS and its copolymers such as SsPS are much stiffer materials than Nafion®, it

possible that higher bending forces would be produced in IPMCs prepared from SsPS which may be desirable for particular applications.

REFERENCES

1. Bhiwankar, N.N. and R.A. Weiss. Polymer 2006. 4719: 6684-91.
2. Ports, B.F. and R.A. Weiss. Industrial & Engineering Chemistry Research 2010: null-null.
3. Alexandre, M., G. Beyer, C. Henrist, R. Cloots, A. Rulmont, R. Jérôme, and P. Dubois. Chemistry of Materials 2001. 1311: 3830-2.
4. Wu, H.-D., C.-R. Tseng, and F.-C. Chang. Macromolecules 2001. 349: 2992-9.
5. Wu, T.-M., S.-F. Hsu, and J.-Y. Wu. Journal of Polymer Science Part B: Polymer Physics 2002. 408: 736-46.
6. Ghosh, A.K. and E.M. Woo. Polymer 2004. 4514: 4749-59.
7. Wu, T.-M., S.-F. Hsu, and J.-Y. Wu. Journal of Polymer Science Part B: Polymer Physics 2003. 416: 560-70.
8. Wu, T.-M., S.-F. Hsu, and J.-Y. Wu. Journal of Polymer Science Part B: Polymer Physics 2003. 4114: 1730-8.
9. D'Aniello, C., P. Rizzo, and G. Guerra. Polymer 2005. 4625: 11435-41.
10. O'Connell, E.M., T.W. Root, and S.L. Cooper. Macromolecules 1995. 2811: 3995-9.
11. O'Connell, E.M., T.W. Root, and S.L. Cooper. Macromolecules 1995. 2811: 4000-6.
12. O'Connell, E.M., D.G. Peiffer, T.W. Root, and S.L. Cooper. Macromolecules 1996. 296: 2124-30.
13. O'Connell, E.M., T.W. Root, and S.L. Cooper. Macromolecules 1994. 2720: 5803-10.
14. Galdi, N., A.R. Albunia, L. Oliva, and G. Guerra. Polymer 2009. 508: 1901-7.
15. Landis, F.A. and R.B. Moore. Macromolecules 2000. 3316: 6031-41.